NASA Conference Publication 3332
Volume II

Thirteenth Workshop for Computational Fluid Dynamic Applications in Rocket Propulsion and Launch Vehicle Technology

R.W. Williams, Compiler

Proceedings of a workshop held at
Huntsville, Alabama
April 25–27, 1995

March 1996

NASA Conference Publication 3332
Volume II

Thirteenth Workshop for Computational Fluid Dynamic Applications in Rocket Propulsion and Launch Vehicle Technology

R.W. Williams, Compiler
Marshall Space Flight Center • MSFC, Alabama

Proceedings of a workshop held at
Huntsville, Alabama
April 25–27, 1995

National Aeronautics and Space Administration
Marshall Space Flight Center • MSFC, Alabama 35812

March 1996

THIRTEENTH WORKSHOP FOR COMPUTATIONAL FLUID DYNAMIC APPLICATIONS IN ROCKET PROPULSION AND LAUNCH VEHICLE TECHNOLOGY – VOLUME I

TABLE OF CONTENTS

TABLE OF CONTENTS (Continued)

THIRTEENTH WORKSHOP FOR COMPUTATIONAL FLUID DYNAMIC APPLICATIONS IN ROCKET PROPULSION AND LAUNCH VEHICLE TECHNOLOGY – VOLUME II

TABLE OF CONTENTS

TABLE OF CONTENTS (Continued)

S1-25
51376
130097
18p

Combustion Zone Characterization of GO_2/GH_2 Rocket Using Laser-Induced Fluorescence of OH.

M. D. Moser and R. J. Santoro

Propulsion Engineering Research Center
and
Department of Mechanical Engineering
The Pennsylvania State University
University Park, PA 16802

With recent interest in gas/gas injectors for use in rocket combustors, there is a critical need for experiments that address this combustion process in terms of detailed flowfield measurements. Such measurements would also serve as a data base for validating computational fluid dynamic (CFD) computer codes. A series of studies have been undertaken at the Propulsion Engineering Research Center (PERC) at the Pennsylvania State University to measure various parameters such as velocity, species concentration , and temperature downstream of a shear coaxial injector in an optically accessible uni-element rocket chamber. Techniques applied to this study to date include the following: laser Doppler velocimetry (LDV) for velocity; laser light scattering (LLS) for flow visualization and estimating mixture fraction and density; laser-induced fluorescence (LIF) of hydroxyl radicals (OH) to determine the characteristics and extent of the reaction zone; and Raman spectroscopy to measure major species concentrations and temperature. The results of the LIF studies are presented here.

The OH molecule is a key intermediate in hydrocarbon and hydrogen combustion. High OH concentration, indicated by high fluorescence intensity, mark the location of the primary reaction zone where the oxidizer to fuel ratio is nearly stoichiometric. Two-dimensional imaging of LIF near the injector face provides a qualitative view of the reaction zone structure. Two-dimensional LIF was limited to qualitative measurements near the injector face due to poor signal to noise ratio with the present experimental setup.

One-dimensional measurements of LIF, which provide a radial profile of relative OH concentration, have been made at several axial locations in the combustion chamber. Results from multiple images, typically 120, have been averaged to yield average OH profiles at each axial location probed. Probability density functions (PDF) of OH peak widths and locations show that the reaction zone is thin near the injector face as expected and remains thin as the flow progresses downstream. Also, the increase in widths of the average OH peaks as the flow progresses downstream is due to movement of the thin reaction zone rather than an increase in individual OH peaks. This analysis indicates the flame is a wrinkled laminar flame front in the region probed.

COMBUSTION ZONE CHARACTERIZATION OF GO_2/ GH_2 ROCKET USING LASER-INDUCED FLUORESCENCE OF OH

PENNSTATE

1855

Marlow D. Moser
and
Robert J. Santoro

13th Workshop for CFD Applications in Rocket Propulsion

Marshall Space Flight Center

April 25-27, 1995

MOTIVATION

Need For *Low Cost, Reusable,* and *Reliable* Propulsion Systems Require Detailed Understanding Of Combustion Phenomena

- Full Scale Tests Are Expensive
- Computer Technology Enables Detailed Modeling
- Advances In Optical Diagnostic Techniques Enhance Measurement Capabilities

OBJECTIVE

- Apply Laser-Based Diagnostics To Study Flowfield Of Gas/Gas Coaxial Injector
  - – Laser Doppler Velocimetry
  - ✓Laser-Induced Fluorescence of OH
  - – Laser Light Scattering From Tracer Particles
  - – Raman Spectroscopy
- Obtain Data Where Boundary Conditions Are Well Specified And Provide To Rocket Research Community

IMPACT

- Gain Insight in Gas/Gas Injector Design
- Obtain Data Base for CFD Code Validation
- Extend Application of Laser Based Diagnostics to High Pressure & Reynold's Number Flows

CRYOGENIC COMBUSTION LABORATORY

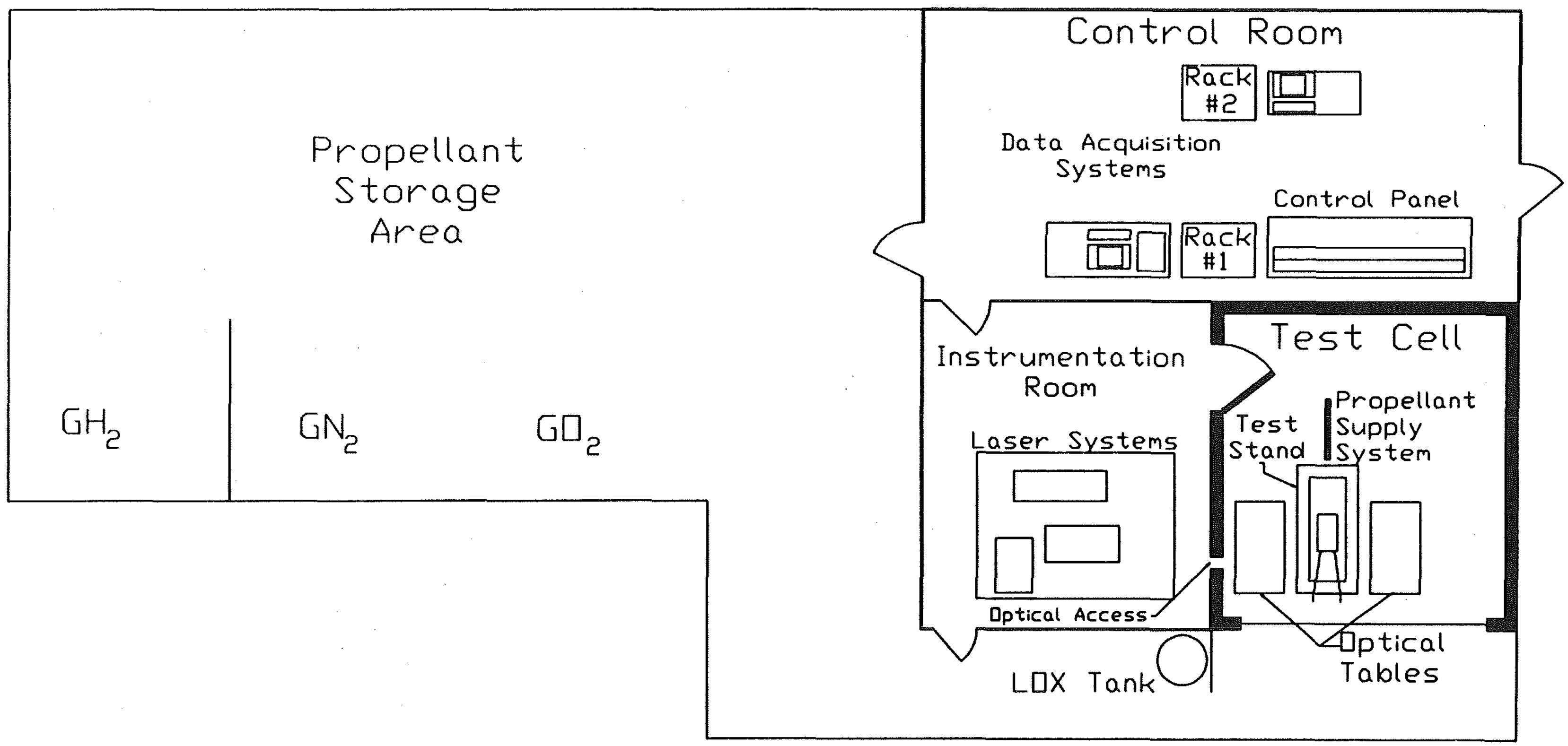

OPTICALLY-ACCESSIBLE ROCKET CHAMBER

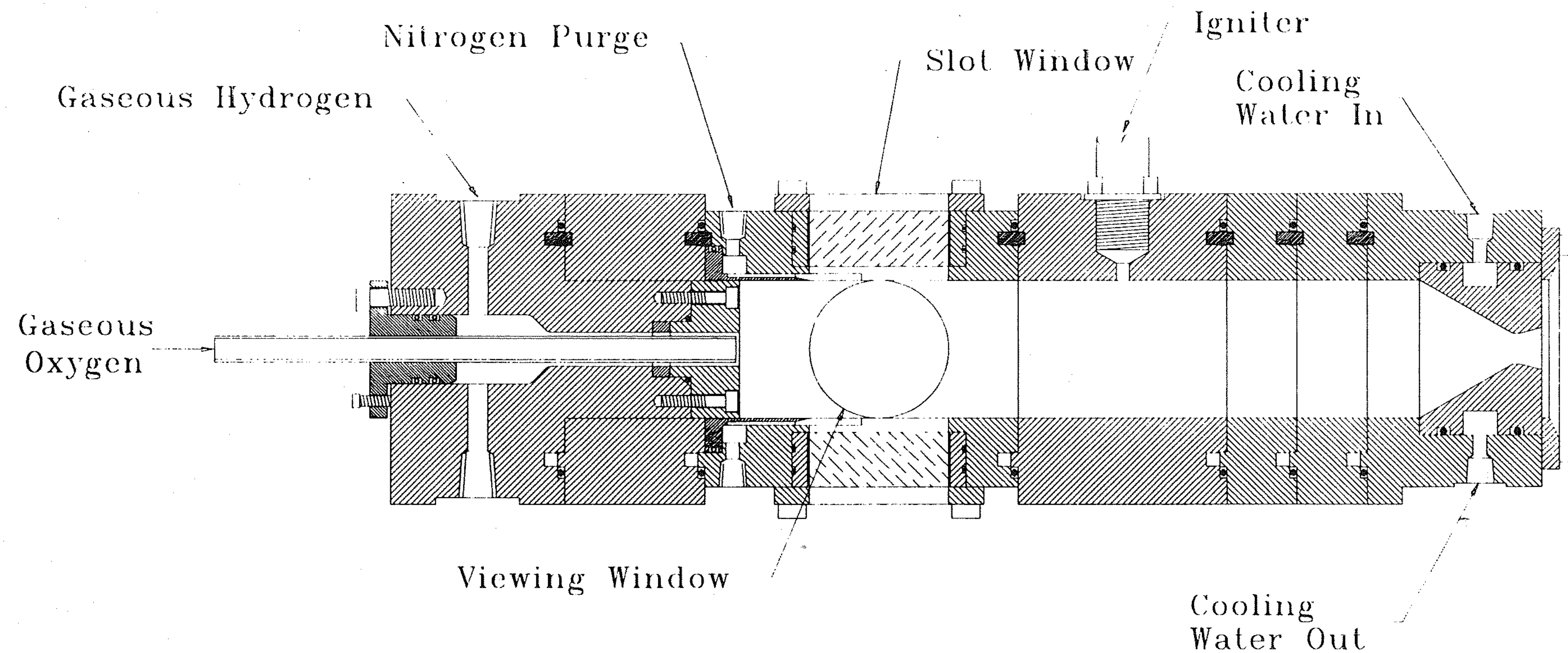

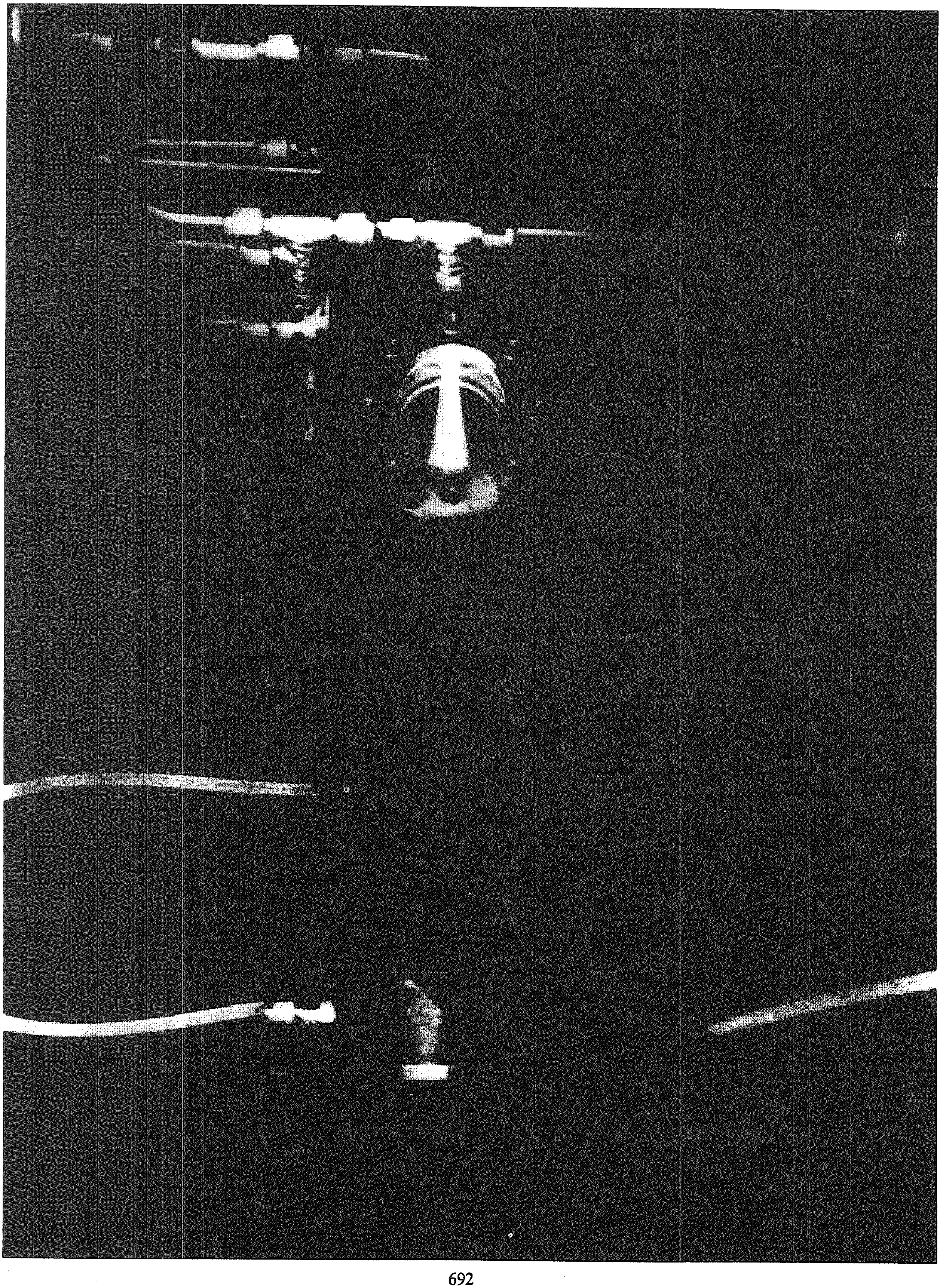

TEST CONDITIONS

GH_2 Mass Flow Rate kg/s (lbm/s)	0.010 (0.022)
GO_2 Mass Flow Rate kg/s (lbm/s)	0.042 (0.093)
GO_2/GH_2 Mass Flow Ratio	4.2
Chamber Pressure MPa (psia)	1.31 (191)
Annulus Reynolds Number	6×10^4
Post Reynolds Number	3×10^5

LASER-INDUCED FLUORESCENCE OF OH

- Hydroxyl-Radicals (OH) Are a Key Intermediate
- Relatively Simple Technique
- Indicates Reaction Zone Location and Structure

LASER-INDUCED FLUORESCENCE OF OH

- Excite (1,0) Band of OH
- Collect Fluorescence from (1,1) and (0,0) Band
- Two-Dimensional Images
  - Laser Beam Formed into Sheet
  - Laser Tuned to $Q_1(9)$ and $Q_2(8)$ Lines at 283.92 nm
- One-Dimensional Images
  - Laser Beam Focused
  - Laser Tuned to $P_2(8)$ Line at 285.98 nm or to $S_{21}(8)$ Line at 278.83 nm

LASER-INDUCED FLUORESCENCE
Experimental Setup

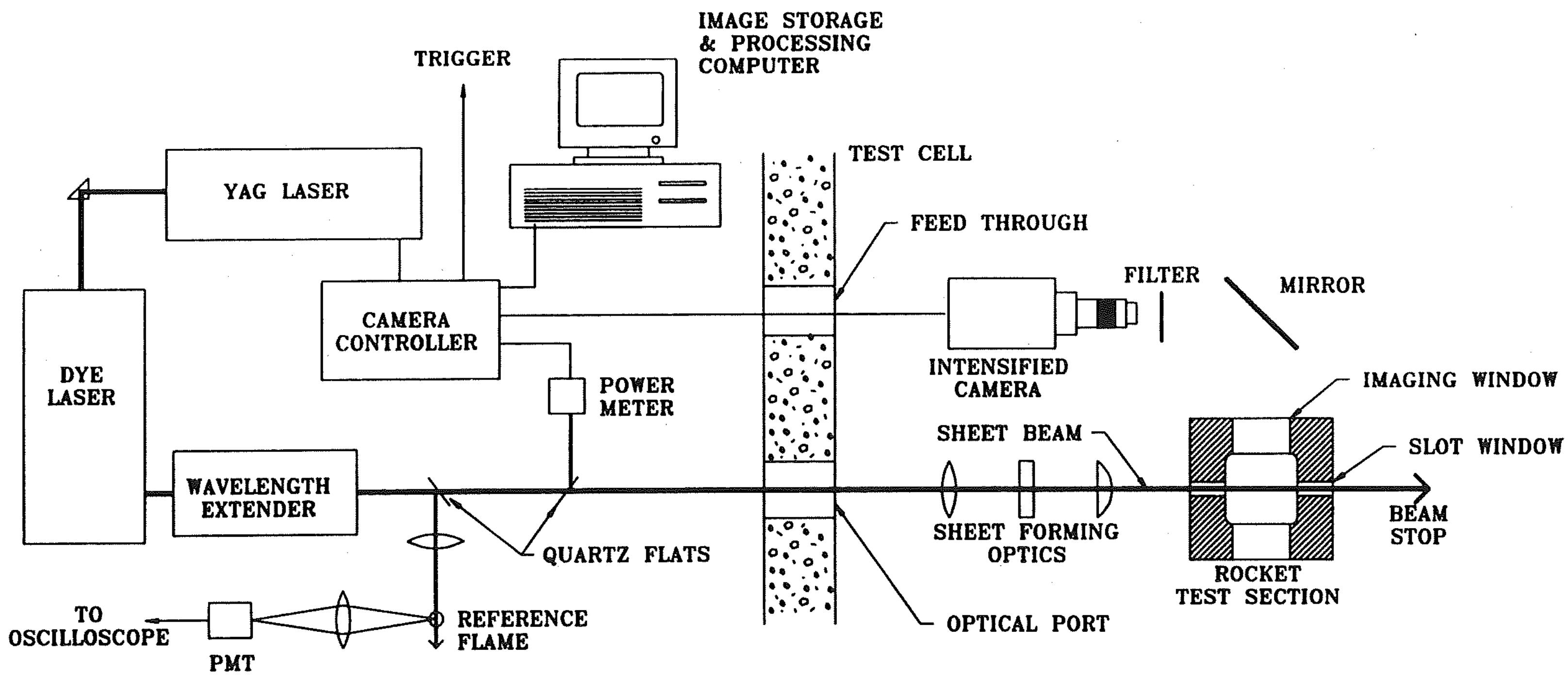

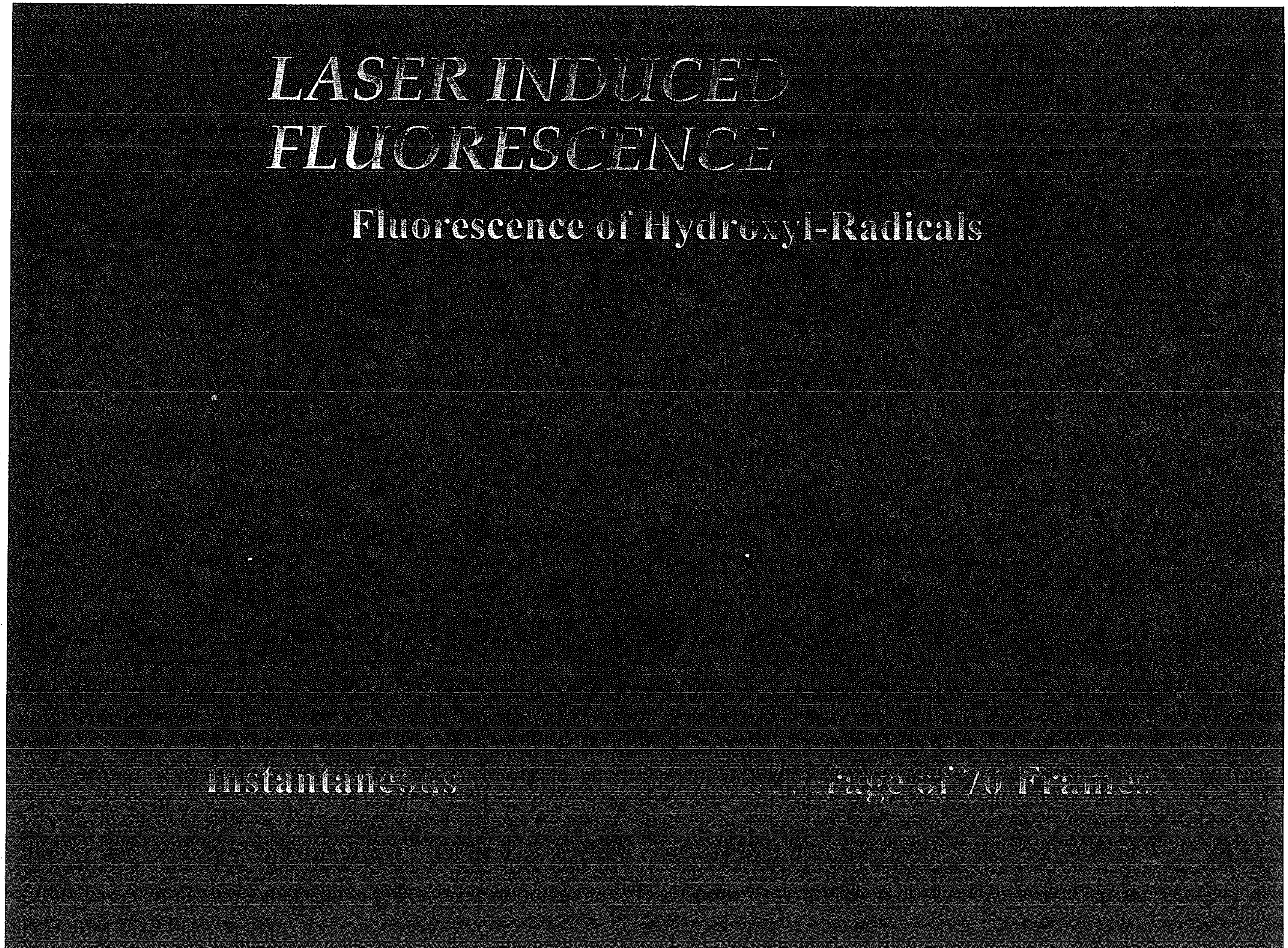
LASER INDUCED
FLUORESCENCE
Fluorescence of Hydroxyl-Radicals
Instantaneous
erage of 76 Frames

AVERAGE LIF PROFILES

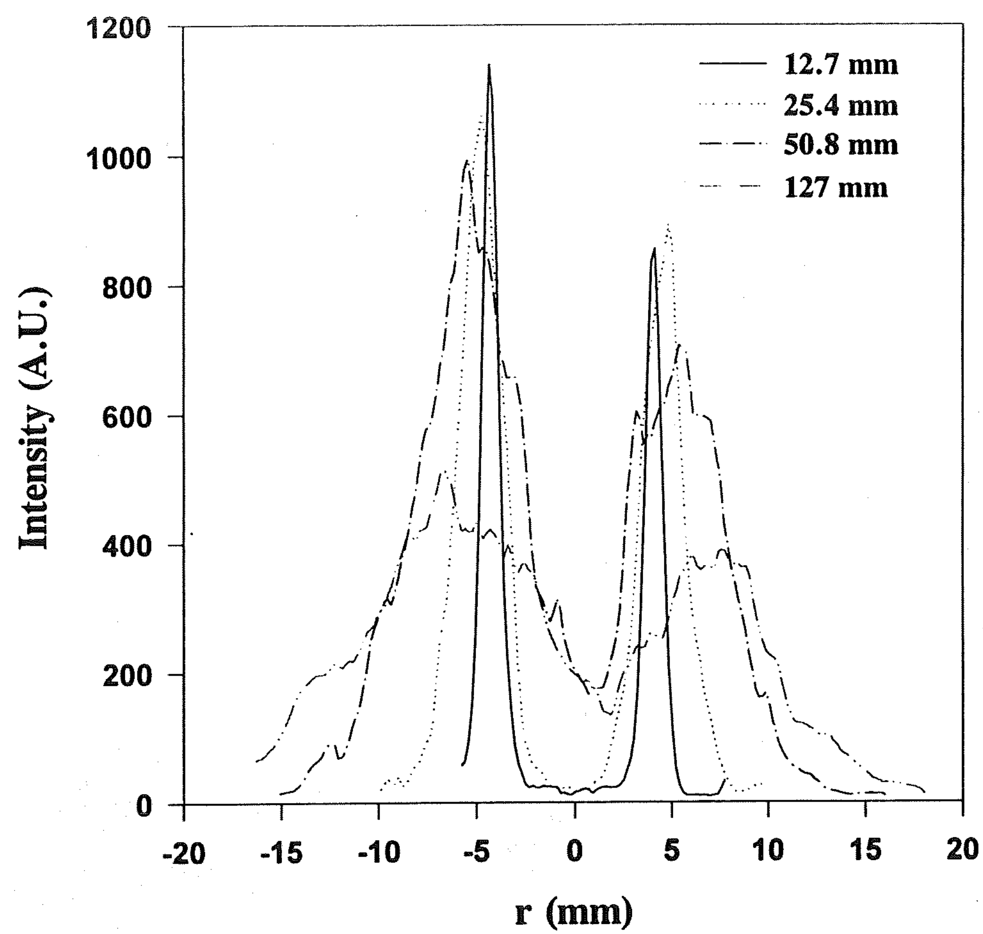

PEAK WIDTH PDFs

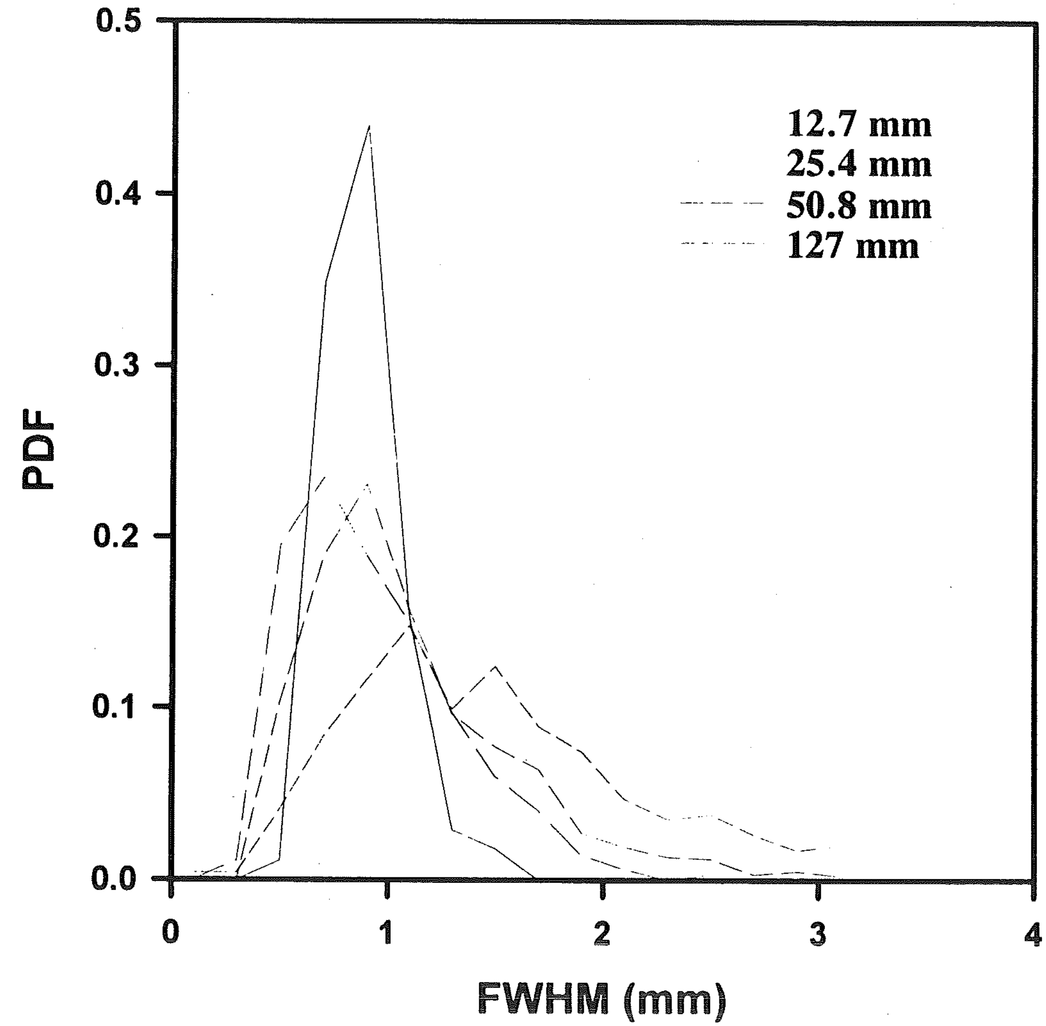

PEAK POSITION PDFs & LIF PROFILES

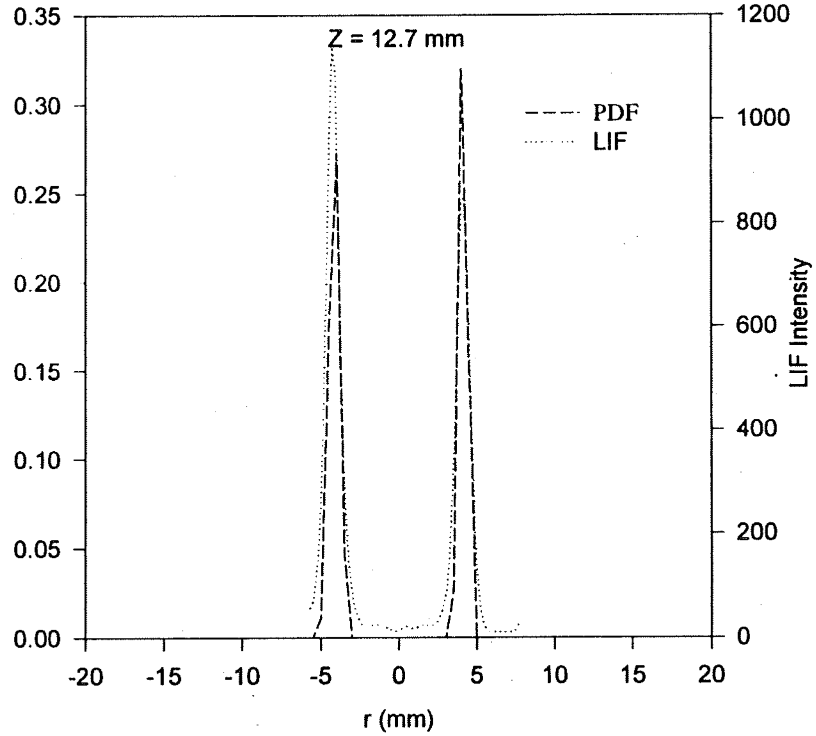

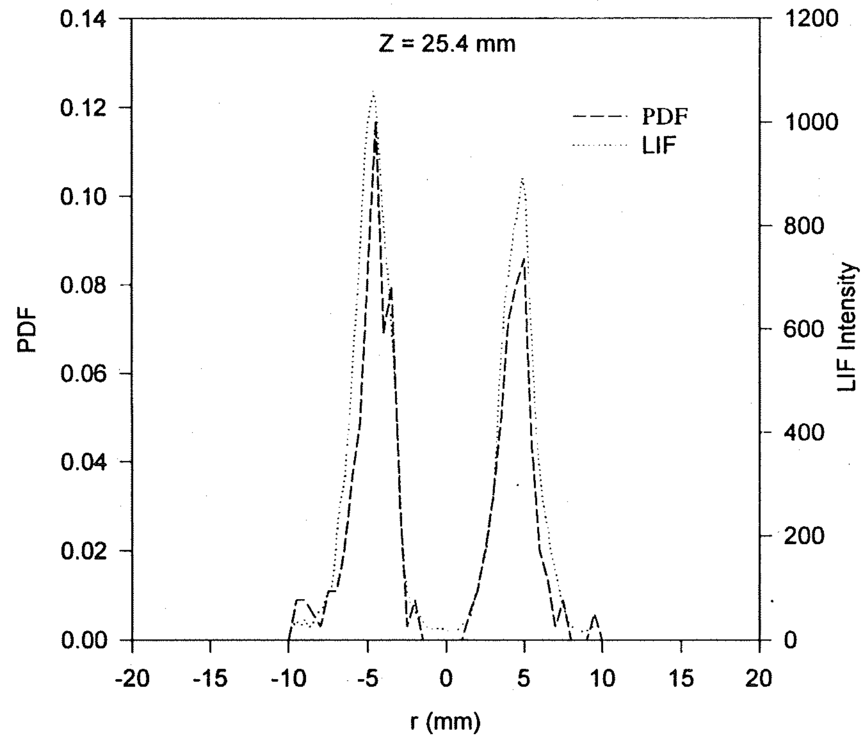

PEAK POSITION PDFs & LIF PROFILES

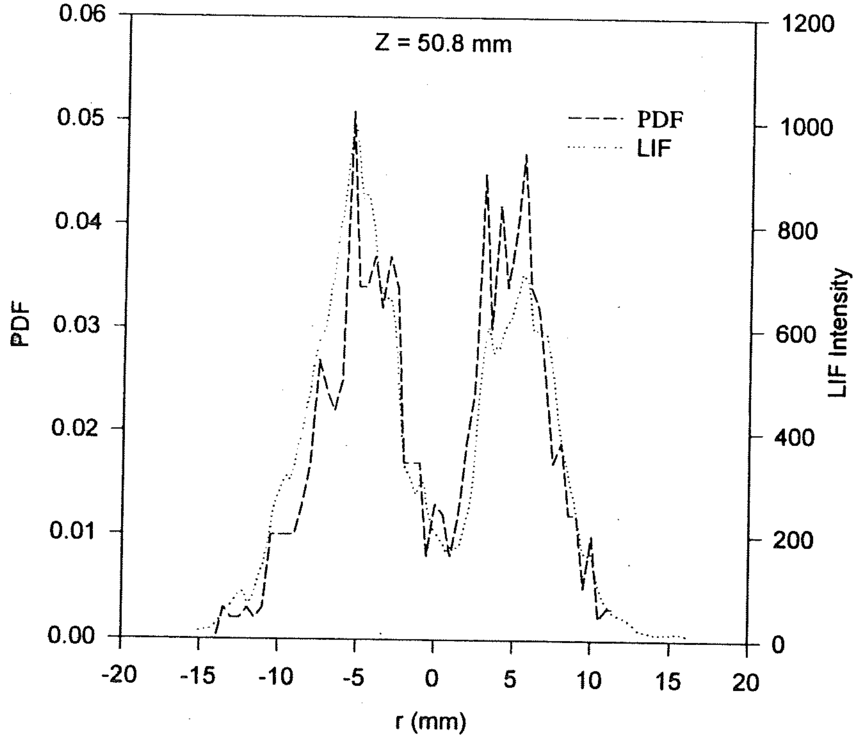

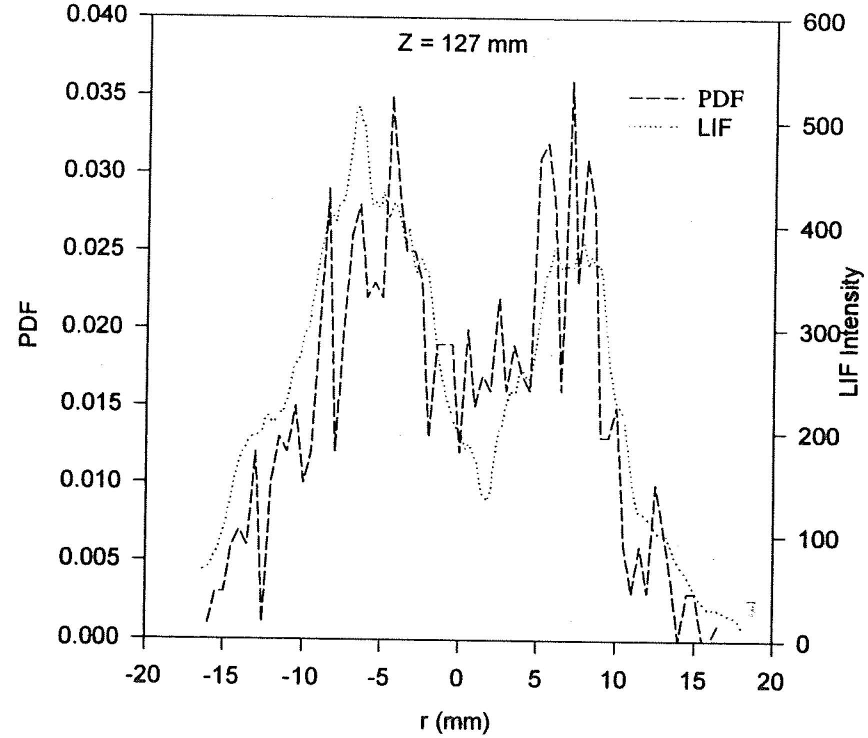

SUMMARY/CONCLUSIONS

- Gas/Gas Shear Coaxial Injector Exhibits Poor Mixing Characteristics
- Reaction Zone has Characteristics of Thin Wrinkled Laminar Flame Front
  - Reacting Flowfield Dominated by Large Scale Turbulence
- Data Available To Rocket Research Community
  - Average LIF Profiles Useful for General Profile Shape and Location Comparisons
  - Velocity and Light Scattering Data Also Available

52-25
57377
132098
20p

Spatially Resolved Species Measurements in a GO_2/GH_2 Propellant Rocket

M.J. Foust, T. Ni and R.J. Santoro

Propulsion Engineering Research Center
and
Department of Mechanical Engineering
The Pennsylvania State University
University Park, PA 16802

Statement of Problem

Local species concentration and temperature are among the most important parameters to characterize in a combustion system. However, the harsh environment in rocket chambers under hot-fire conditions limits the applicability of conventional probing methods for the acquisition of this information. Laser-based diagnostic methods show great promise for achieving this goal by providing instantaneous images of species concentrations and temperature.

Objective of Work

The objective of the current work is to develop a non-intrusive technique to experimentally determine the major species and temperature field in the combustion chamber of an uni-element rocket for a GO_2/GH_2 propellant combination.

Approach

The experiments were conducted at the Cryogenic Combustion Laboratory at Penn State University. The uni-element rocket chamber used is modular in design and is easily configured to provide optical access along the chamber length. A shear coaxial injector was used to introduce GO_2 and GH_2 into the combustion chamber. The nominal flow rates of GO_2 and GH_2 are 0.1 lb/s and 0.025 lb/s, respectively, resulting in an O/F ratio of four. The experiments were for a chamber pressure of 190 psia.

One-dimensional profiles of species concentrations and temperature were measured by using laser-induced spontaneous Raman spectroscopy. The Raman system consists of a flash pumped dye laser operating at 10 Hz and an intensified CCD camera. The dye laser has a typical pulse energy of 2 J at 511 nm and a pulse duration of 5 μs. The Raman emission was detected at a right angle to the laser beam. A narrow band interference filter was placed in front of the camera to selectively measure the number density of the species. For each rocket firing, 50 single-shot Raman images and 50 background images were captured. By using different optical filters, Raman images of oxygen, hydrogen, water and nitrogen (used for window cooling) were obtained. Measurements were conducted at 1, 2, and 5 inch downstream of the injector face. The ratio of the signal to background level for hydrogen and oxygen Raman images at 1 inch downstream is about 10. Further downstream, the background luminosity increases significantly. Thus, the species concentration can only be determined from averaged Raman images. The temperature profiles were calculated from averaged data of total species number density using the ideal gas law. Since the Raman signal is stronger in lower temperature regions, the averaged temperature generally underestimates the temperature in regions where temperature fluctuates highly.

Conclusions

Single-shot and averaged profiles of species concentration have been measured under combusting conditions. These results demonstrate that the laser-based technique can be effectively applied for in-situ measurements in a rocket chamber. Experiments with an improved detection system for obtaining images of instantaneous and simultaneous multi-species concentration and temperature are underway.

SPATIALLY RESOLVED SPECIES MEASUREMENTS IN A GO_2/GH_2 PROPELLANT ROCKET

M. J. Foust, T. Ni and R. J. Santoro

13th Workshop for CFD Applications in Rocket Propulsion
NASA/Marshall Space Flight Center

April 25-27, 1995

PENNSTATE

Propulsion Engineering Research Center

OVERVIEW

- Demonstrate Application of Raman Spectroscopy
- Present Measurements Using 2 Techniques
  - Optical Bandpass Filters
    - Good Light Collection for Obtaining Single Species
    - Cannot Assess Flame Luminosity Contribution
    - Simultaneous Species Measurements Require Multiple Detectors
  - Spectrometer
    - Provides Simultaneous Species Measurements Using Single Detector
    - Assessment of Flame Background
    - Needs Wide Dynamic Range
- Summarize Raman Experiments

MOTIVATION

- Improved Fundamental Understanding of Combustion-Driven Flows
- Combusting Flowfield Measurements used for CFD Code Validation
- Performance Assessment for Candidate Gas/Gas Injectors in Reusable Launch Vehicle Program

APPROACH

- **Experiments in a Uni-Element Rocket**
- **Apply Laser-Based Diagnostic Techniques**
  - ❑ **Laser Doppler Velocimetry**
  - ❑ **Laser-Induced Fluorescence of OH**
  - ❑ **Laser Light Scattering from Tracer Particles**
  - ✓ **Laser-Induced Raman Spectroscopy**

OPTICALLY-ACCESSIBLE ROCKET CHAMBER

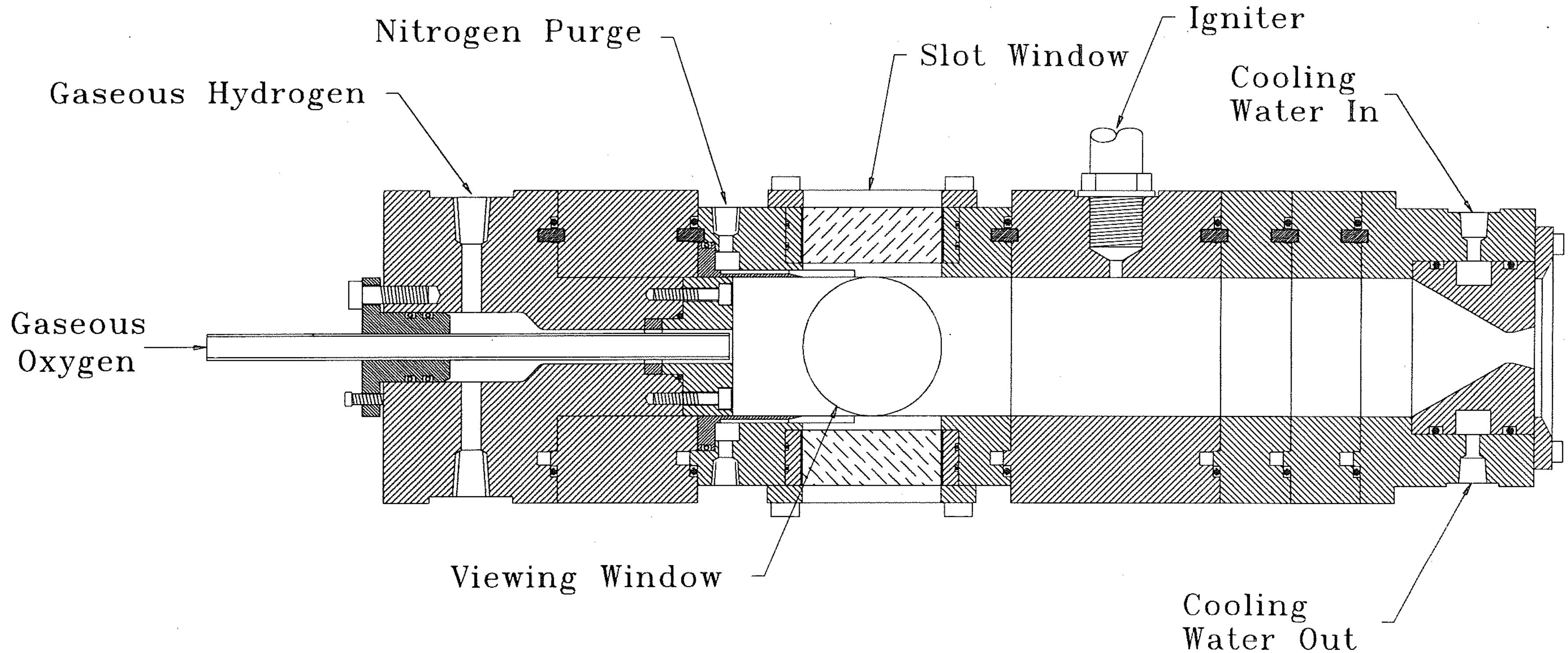

PENNSTATE

1855

Propulsion Engineering Research Center

GO_2/GH_2 ROCKET TEST CONDITIONS

Shear Coaxial Injector

GH_2 Mass Flow Rate kg/s (lbm/s)	0.010 (0.023)
GO_2 Mass Flow Rate kg/s (lbm/s)	0.042 (0.092)
GN_2 Mass Flow Rate kg/s (lbm/s)	0.010 (0.022)
GO_2/GH_2 Mixture Ratio	4.0
Chamber Pressure MPa (psia)	1.29 (187)

PENNSTATE

Propulsion Engineering Research Center

RAMAN SPECTROSCOPY

Stokes Vibrational Shift

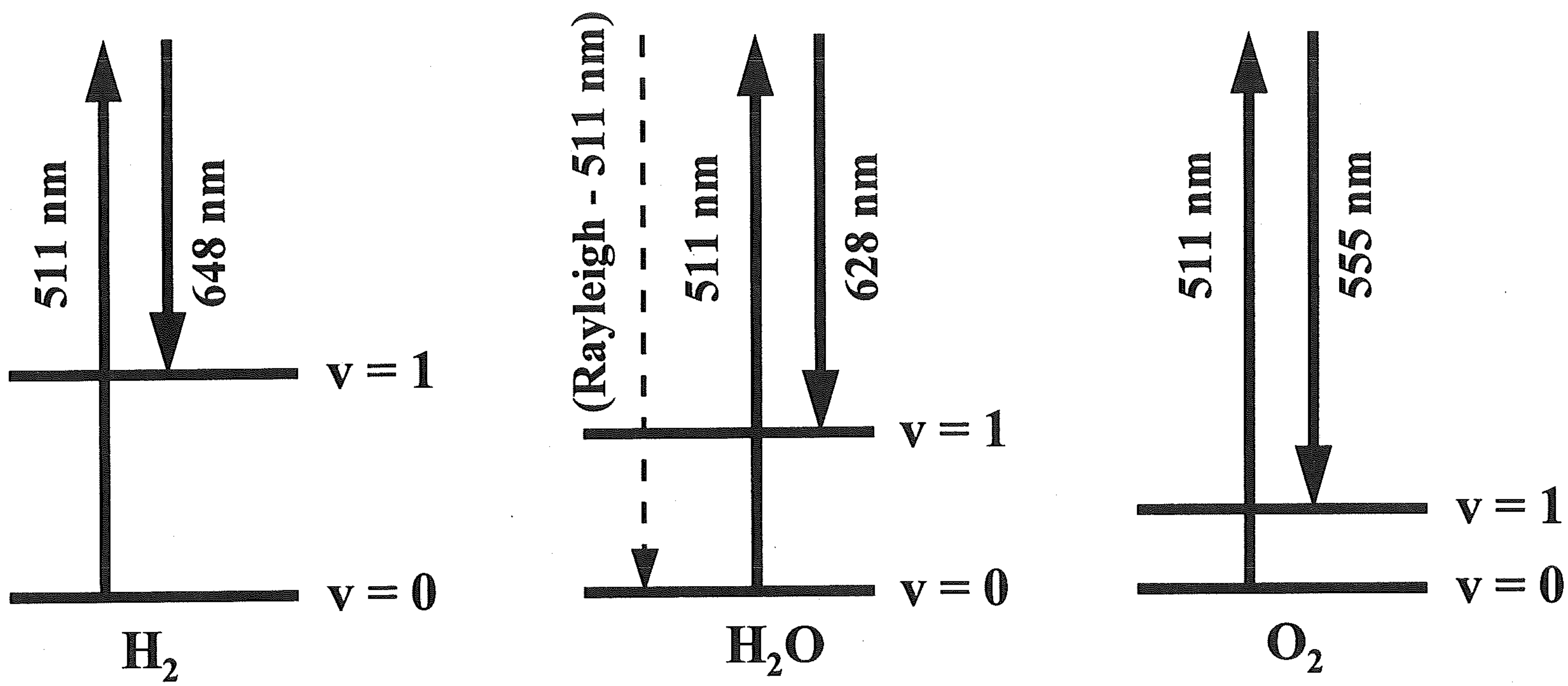

- **Raman Signal Specific to Each Species**
- **Linearly Proportional to Species Number Density**
- **$1 / \lambda^4$ Wavelength Dependence**

PENNSTATE

Propulsion Engineering Research Center

EXPERIMENTAL SETUP

- **Optimized System for Collecting Weak Raman Signal**

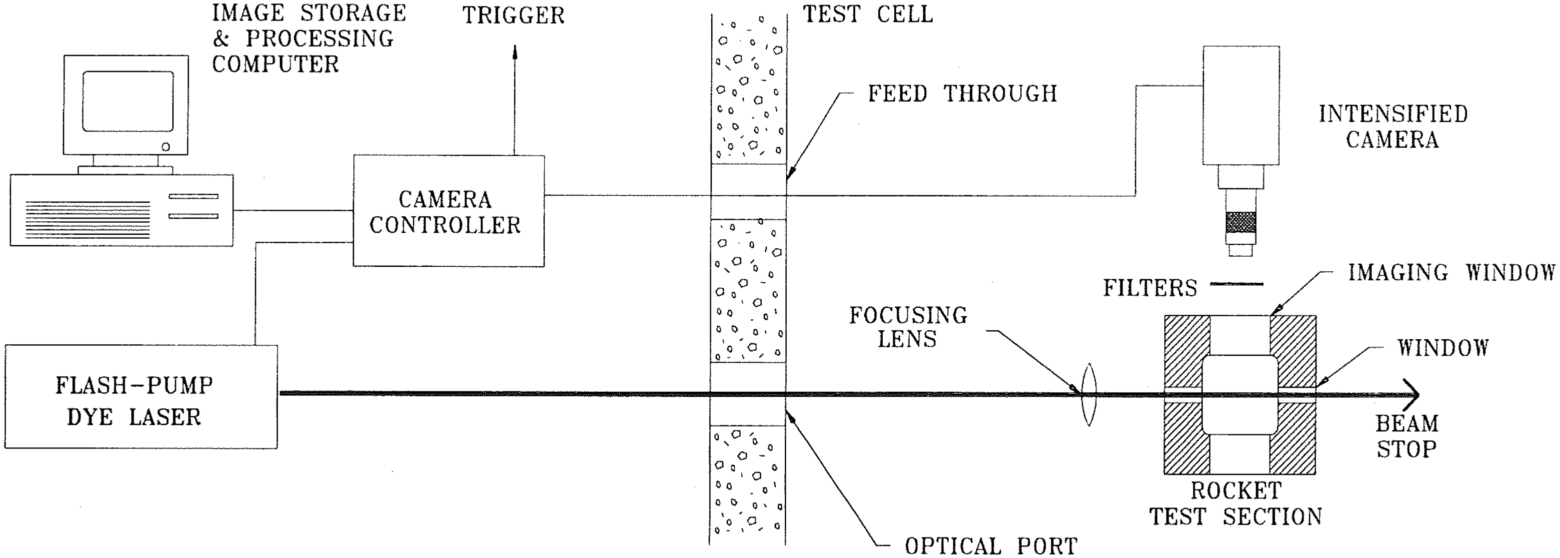

SPECIES MEASUREMENTS IN GO_2/GH_2 Rocket

- **Obtained 35 Instantaneous Line Images Individually for Each Species (GO_2, GH_2, H_2O and GN_2 - Purge) During 4 sec. Rocket Firings**
- **Calibrated Measurements for Each Species Using Pure Gas Concentration**
- **Extracted Average Species Mole Fractions from 100 Images**

PENNSTATE

Propulsion Engineering Research Center

INSTANTANEOUS RAMAN IMAGES

Shear Coaxial Injector

25.4 mm from Injector Face

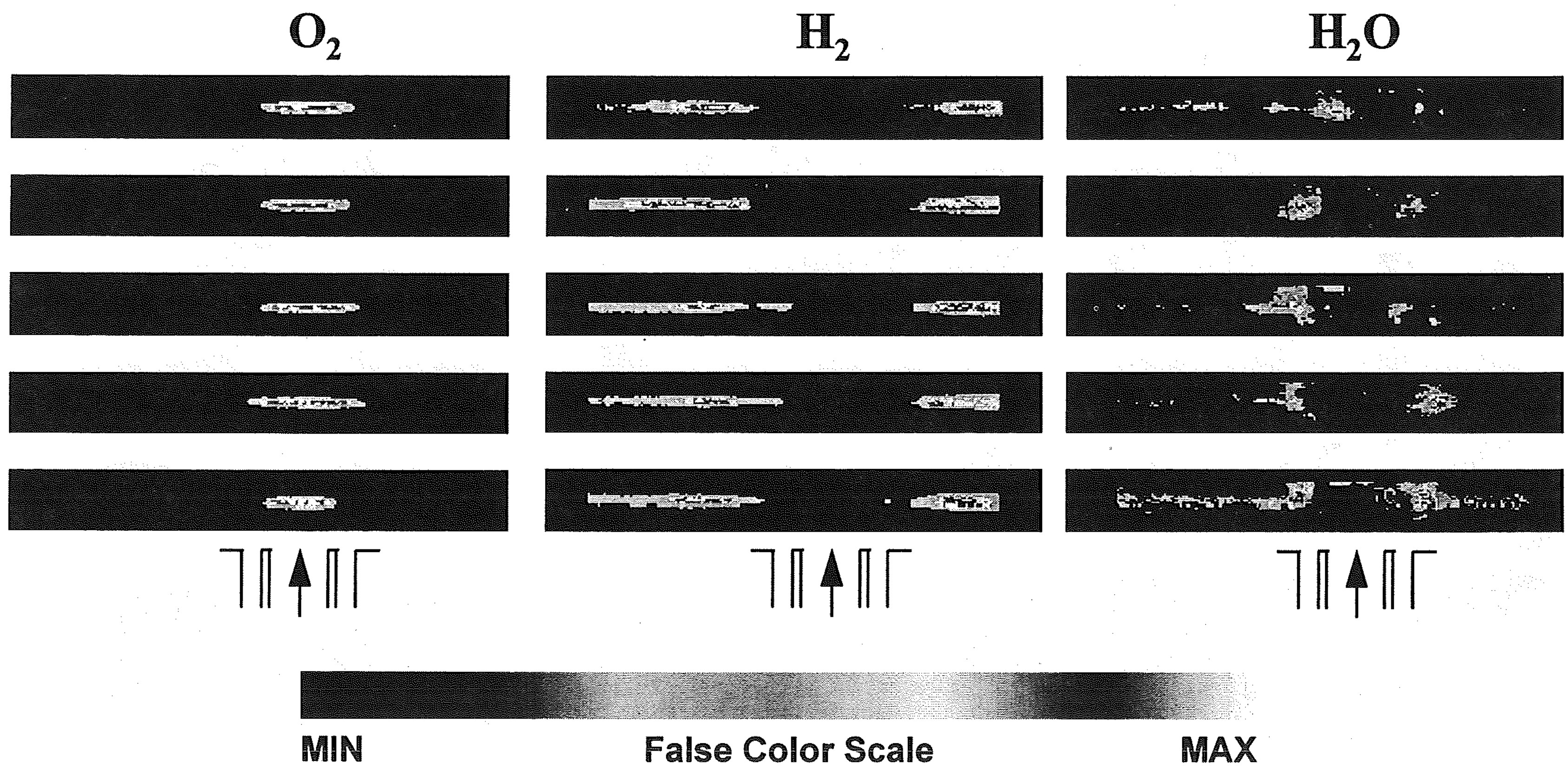

PENNSTATE

1855

Propulsion Engineering Research Center

MEAN RAMAN IMAGES

Shear Coaxial Injector

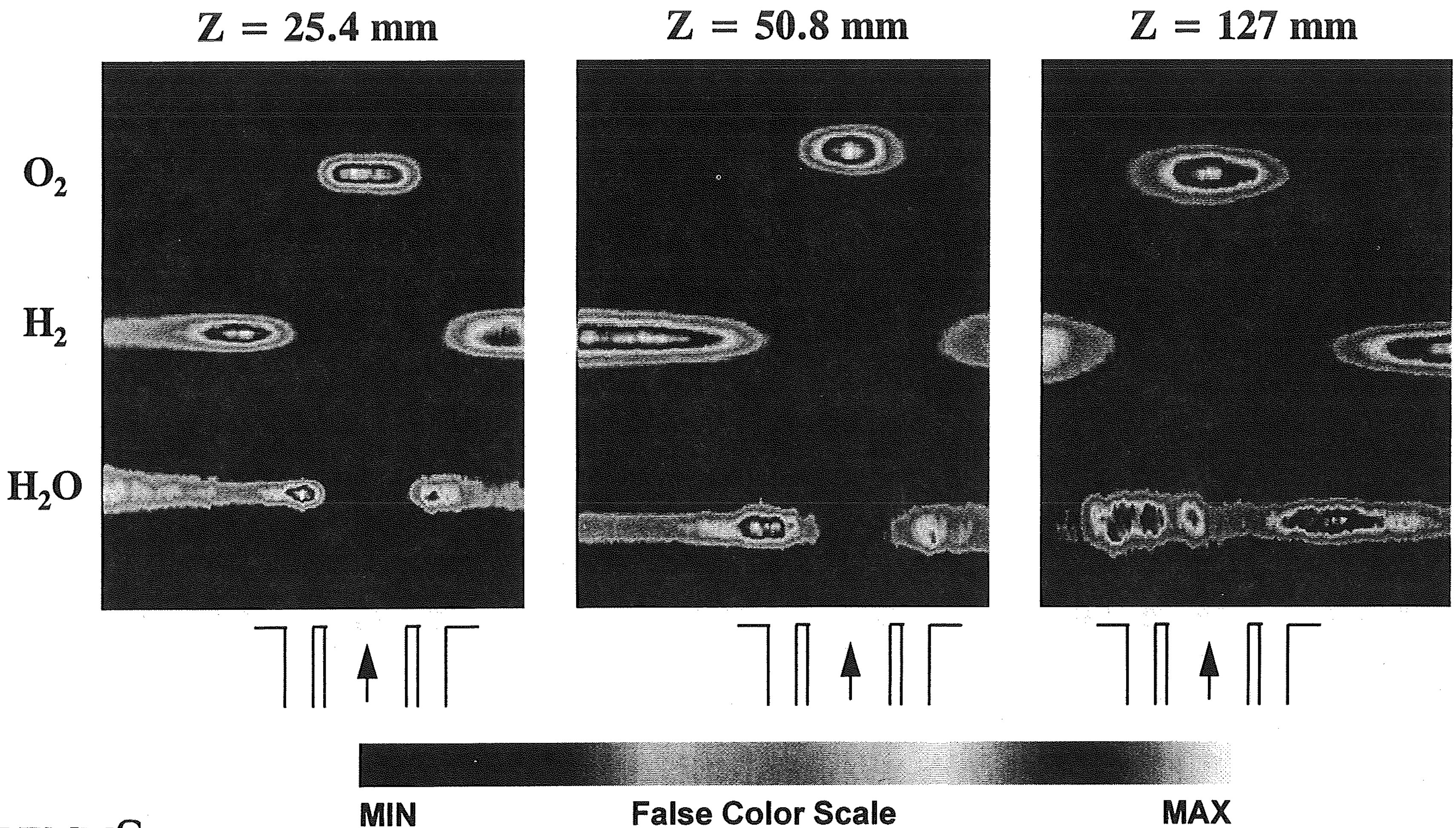

PENNSTATE

Propulsion Engineering Research Center

SPECIES MEASUREMENTS

Radial Profiles of Species Mole Fractions

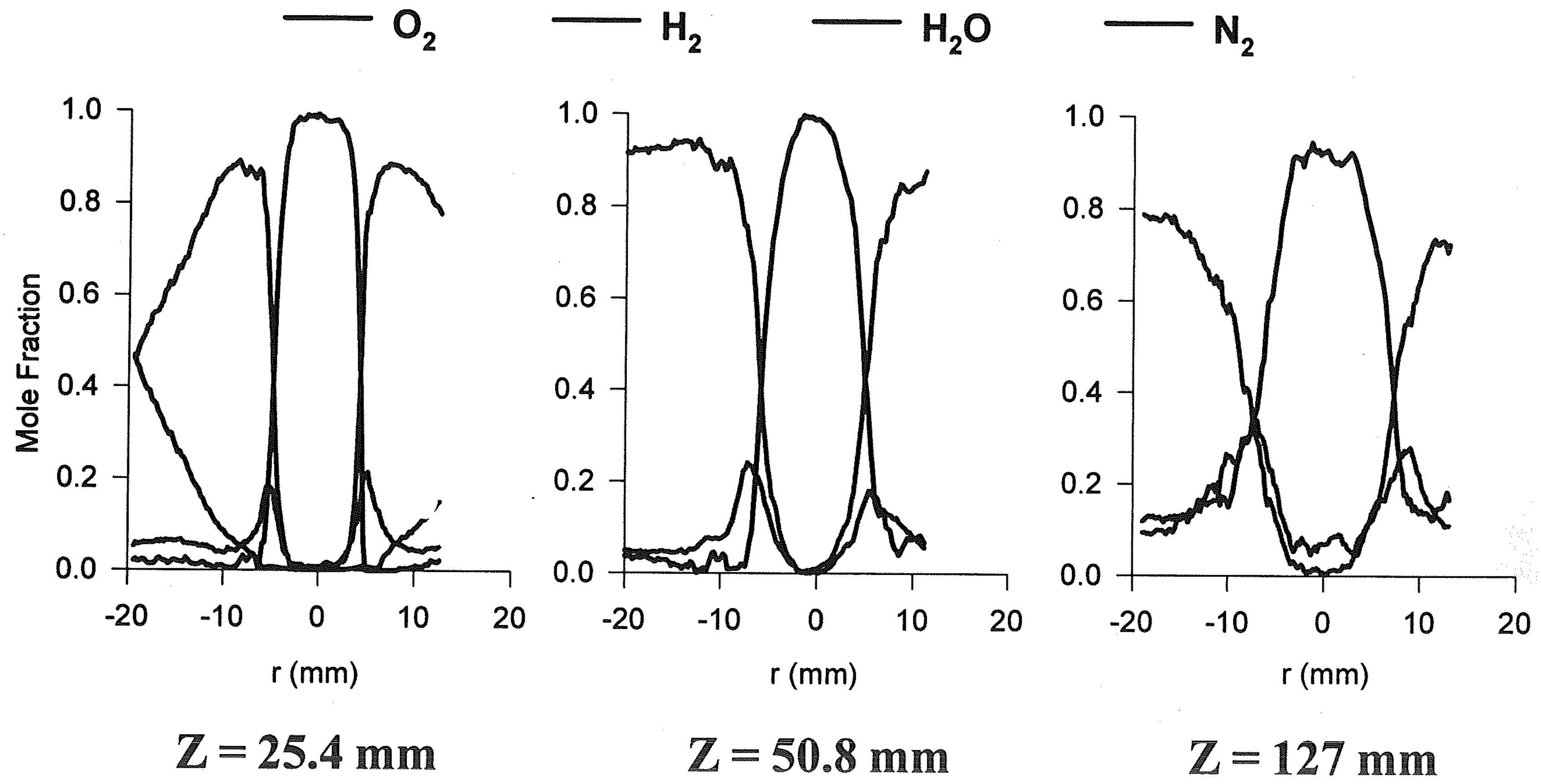

PENNSTATE

Propulsion Engineering Research Center

EXPERIMENTAL MEASUREMENTS

Mean Density Comparisons @ 25.4 mm from Injector Face

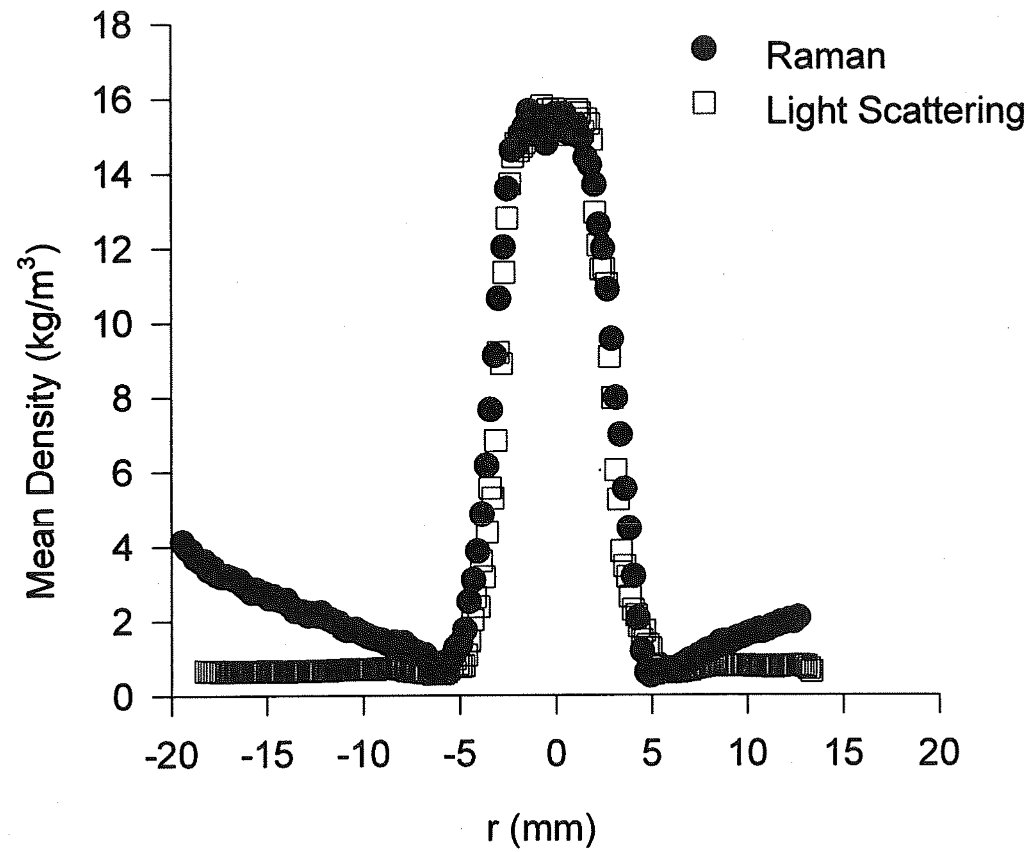

PENNSTATE

Propulsion Engineering Research Center

GO_2/GH_2 ROCKET
Oxygen Mole Fraction Comparisons

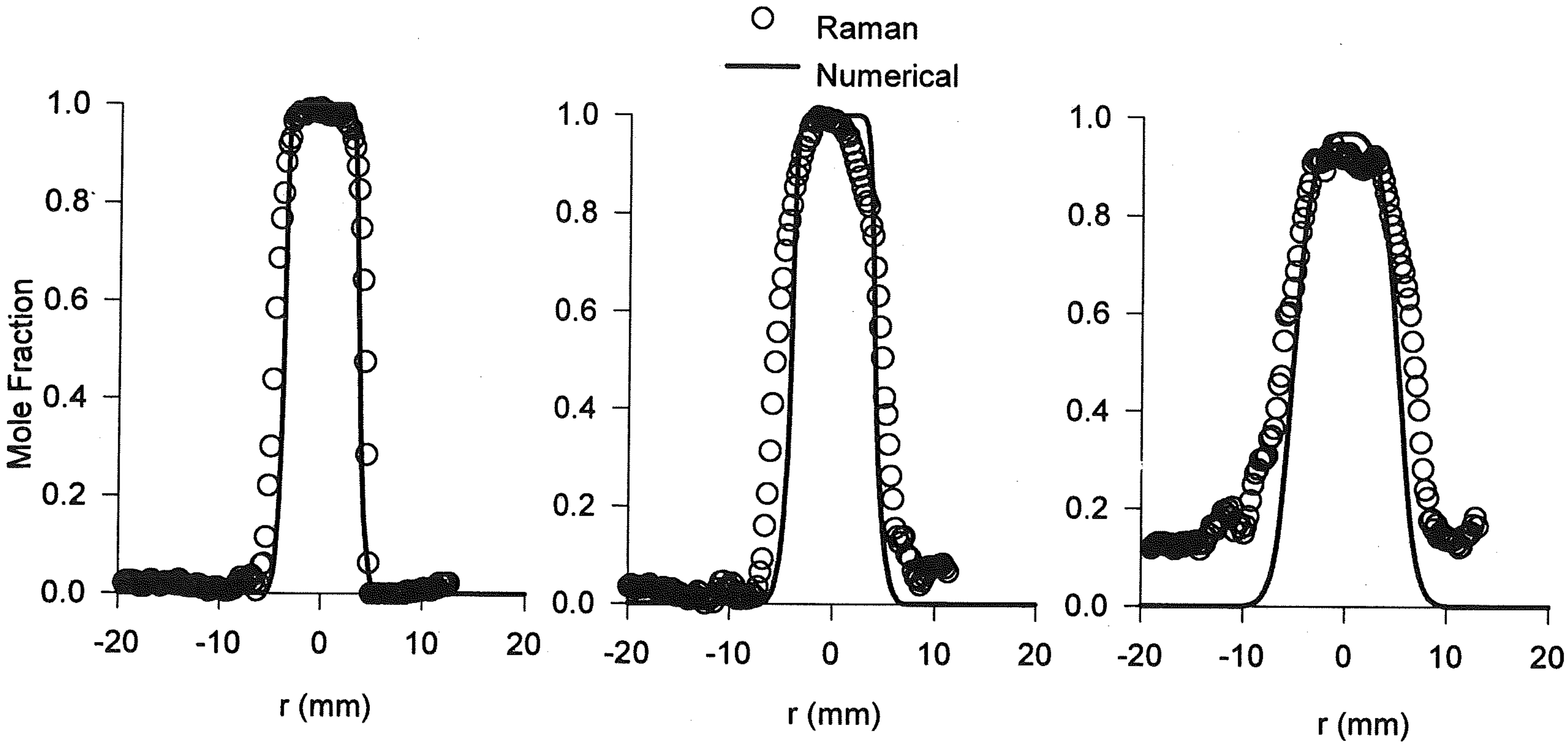

Z = 25.4 mm **Z = 50.8 mm** **Z = 127 mm**

- **Computation Predicts Faster Combustion Rates**

PENNSTATE

Propulsion Engineering Research Center

SINGLE-SHOT MULTI-SPECIES DETECTION
(Recent Development)

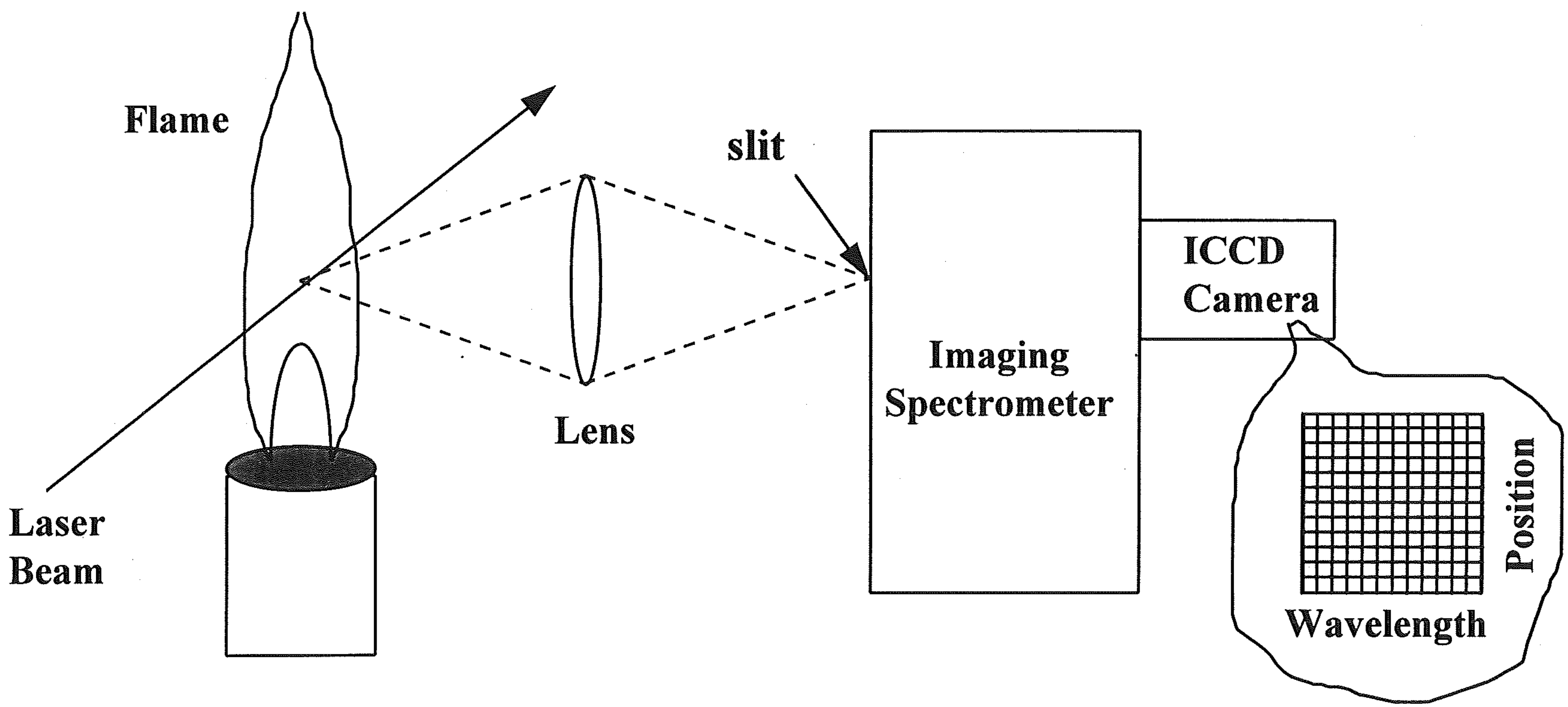

PENNSTATE

1855

Propulsion Engineering Research Center

SIMULTANEOUS SPECIES MEASUREMENTS
25.4 mm from Injector Face

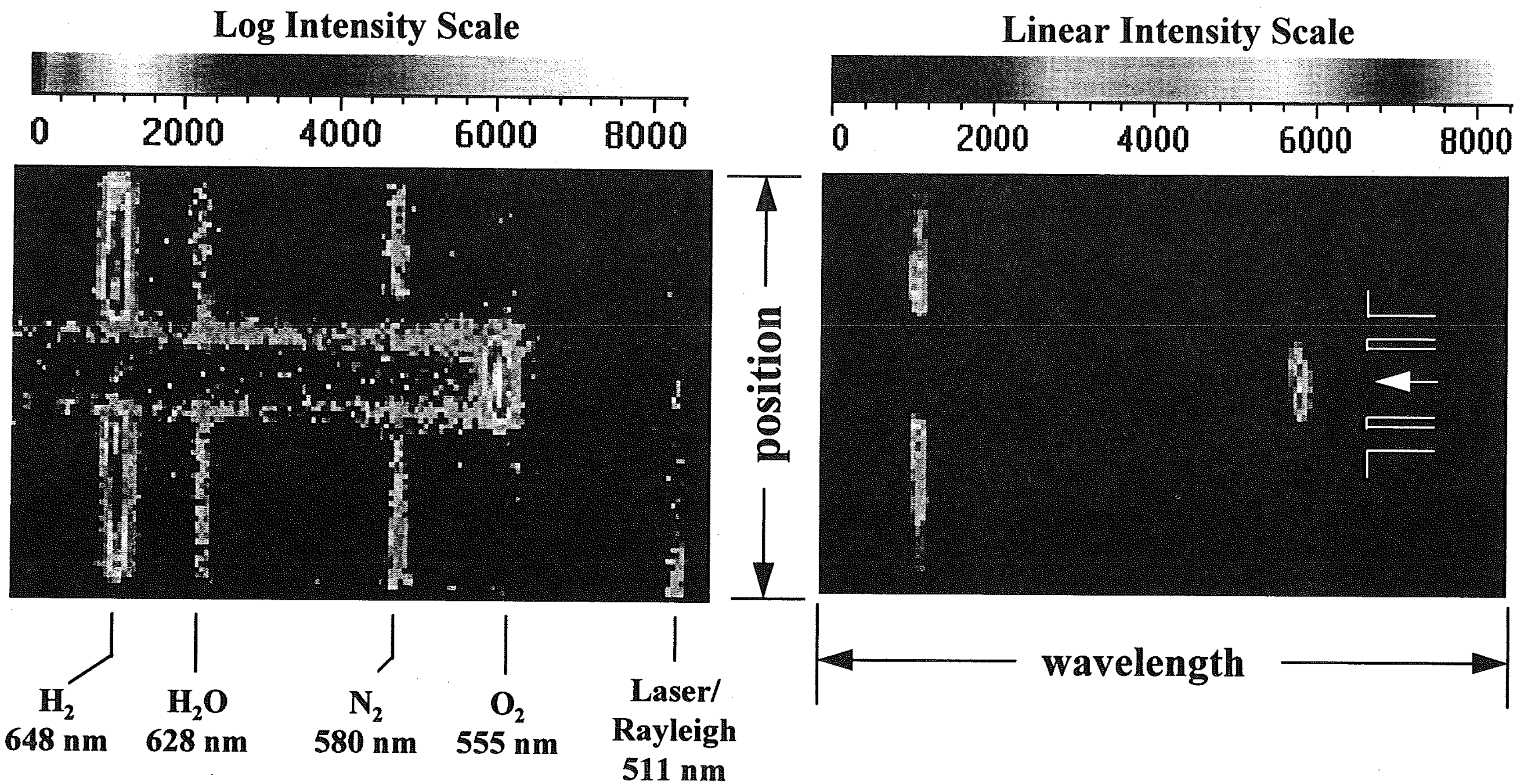

PENNSTATE

Propulsion Engineering Research Center

SUMMARY/CONCLUSIONS

- 2 Techniques for Raman Species Detection
  - Optical Bandpass Filters
    - Single-Shot Measurements for a Single Species
    - Spatially Resolved Average Species Mole Fractions
    - Feasible in Relatively Low Flame Background
  - Spectrometer
    - Single-Shot Multiple Species Measurements
    - Possible Method for Subtracting Flame Background Luminosity
- Shear Coaxial Injector Exhibits Poor Mixing
  - GO_2 Core Region Extends Beyond Mid-Chamber
  - H_2O Mole Fraction Levels Low

ACKNOWLEDGEMENTS

- **Funding by NASA/Marshall Space Flight Center Under Contract NAS-8-38862 is Gratefully Acknowledged**

53-34
51378
132099
22 p

Fluctuating Pressure Analysis of a 2-D SSME Nozzle Air Flow Test

Darren Reed
Induced Environments Branch
NASA Marshall Space Flight Center, Huntsville, Alabama 35812

Homero Hidalgo
SSME Assurance Office
NASA Marshall Space Flight Center, Huntsville, Alabama 35812

Abstract

To better understand the SSME startup/shutdown transients, an airflow test of a 2-D nozzle was conducted at MSFC's Trisonic wind tunnel. Photographic and other instrumentation show during a SSME start large nozzle shell distortions occur as the Mach disk is passing through the nozzle. During the earlier development of the SSME, this startup transient resulted in a low cycle fatigue failure of one of the LH_2 feedlines. The 2-D SSME nozzle test was designed to measure the static and fluctuating pressure environment and color schlieren video during the startup and shutdown phases of the run profile.

The model consisted of two identical blocks having the same inner contour of the SSME nozzle. The sides of the nozzle were made of glass for schlieren photography. The upper block was instrumented for static pressure measurements. The lower block was instrumented with thirteen Entron fluctuating pressure transducers. Steady state and slow sweep flows were tested for three back pressure conditions (0.5-2.0 psi, 7 psi, 14 psi.) The static pressure data was acquired by a scanning pressure system. The fluctuating pressure data was recorded onto a VHS analog tape recorder. The video, static pressure, and fluctuating pressure data were time synchronized for data correlation.

The shlieren video clearly shows a lambda (λ) shock foot moving down the throat during the slow sweep. The fluctuating pressure RMS time histories show the levels increase as the downstream foot of the lambda shock approaches. When the shock foot is directly above the transducer, levels decrease about 50%. When the upstream leg of the lambda shock approaches the transducer the level quickly jumps up to twice the downstream leg values. After the upstream leg of the lambda shock passes the transducer, the level falls down to the noise floor of the measurement.

Schlieren video, model configuration, fluctuating pressure time histories, power spectrum densities of the test will be shown. Future 2-D nozzle tests and plans for a 3-D nozzle facility will be addressed.

Fluctuating Pressure Analysis of a 2-D Space Shuttle Main Engine (SSME) Nozzle Air Flow Test

Darren Reed
Homero Hidalgo
NASA / MSFC

Workshop for Computational Fluid Dynamic Applications
in Rocket Propulsion and Launch Vehicle Technology
Huntsville, Alabama
26 April 1995

Fluctuating Pressure Analysis of a 2-D SSME Nozzle Air Flow Test

Marshall Space Flight Center
Homero Hidalgo / CR55
Darren Reed / ED33

Introduction / History

- **SSME Nozzles are subjected to significant unsteady aerodynamic forces during engine start and shutdown transients**
- **High loads are associated with the start / shutdown nozzle transients**
  - » **High Stress in Nozzle Aft Region (Excitation of nozzle flexural modes)**
  - » **Actuator Sideloads**
- **These transients were severe enough to cause two major test failures of the large coolant supply tubes, downcomers (steerhorn failures)**
  - » **First failure: Test 750-041 (14 May 1979) Engine E0201**
    - fatigue load failure
    - resolved by increasing steerhorn thickness
  - » **Second failure: Test SF6-03 (4 Nov 1979) Engine E2002**
    - incorrect weld material
    - resolved by adding nickel plating to tee weld joints, added steam loop to coolant line

SSME COMBUSTION DEVICES

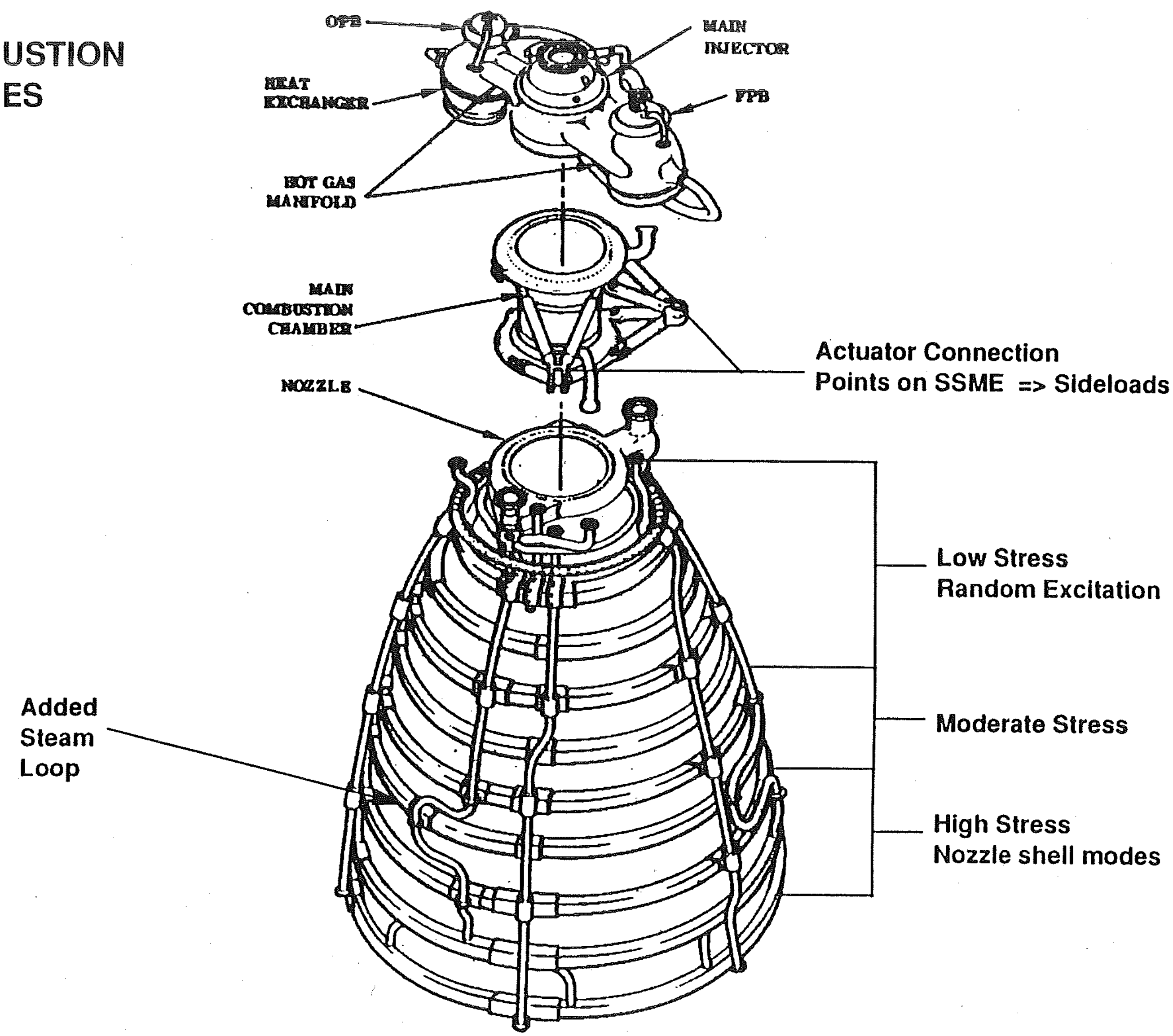

Fluctuating Pressure Analysis of a 2-D SSME Nozzle Air Flow Test

Marshall Space Flight Center
Homero Hidalgo / CR55
Darren Reed / ED33

Test Objectives

- To better understand the unsteady nozzle flows, a wind tunnel experiment using a scaled 2-D (planar) contour model of the SSME nozzle was run
- Tests were conducted at MSFC's 14 inch Trisonic Wind Tunnel facility
- Model was instrumented to measure static, fluctuating pressures, and coloured schlieren videotapes
  - » Recording schlieren video of the shock structure as it move out of the nozzle during startup and back in during shutdown was one of the main objectives
  - » The static pressure ports would help define the relative strength of the shocks
  - » The fluctuating pressure transducers were used to measure the unsteady levels and the show the spectrum shape

Marshall Space Flight Center
Homero Hidalgo / CR55
Darren Reed / ED33

Model and Test Descriptions

- 2-D SSME contour shape
  - » Area Ratio = 8.8:1
  - » Nozzle Length = 11 inches (6.8 inches from throat to exit)
  - » Nozzle Width = 5.0 inches
  - » Nozzle Exit Height = 5.0 inches
  - » Throat Height = 0.568 inches
- Model Instrumentation
  - » 18 Ports - 12 Fluctuating Pressure Transducers Recorded (Lower Block)
  - » 18 Static Pressure Ports (Top Block)
- Facility Measurements
  - » Total Pressure, Total Temperature, and Static Pressure at Nozzle Exit
  - » Schlieren Video
- Test Conditions
  - » 3 Nozzle exit pressure conditions (2 psia, 7 psia, and atmospheric)
  - » Slow sweep runs
  - » 5 steady state runs at predetermined shock locations

NOZZLE BLOCK MODEL AND PRESSURE PORT LOCATIONS

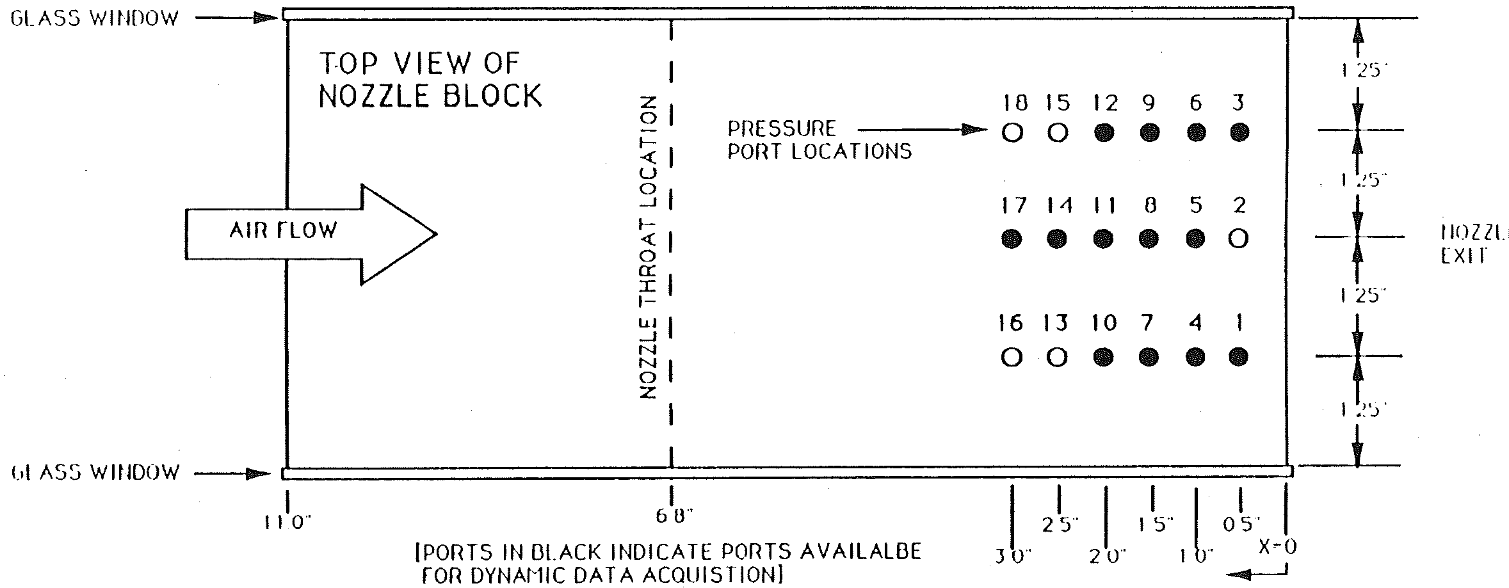

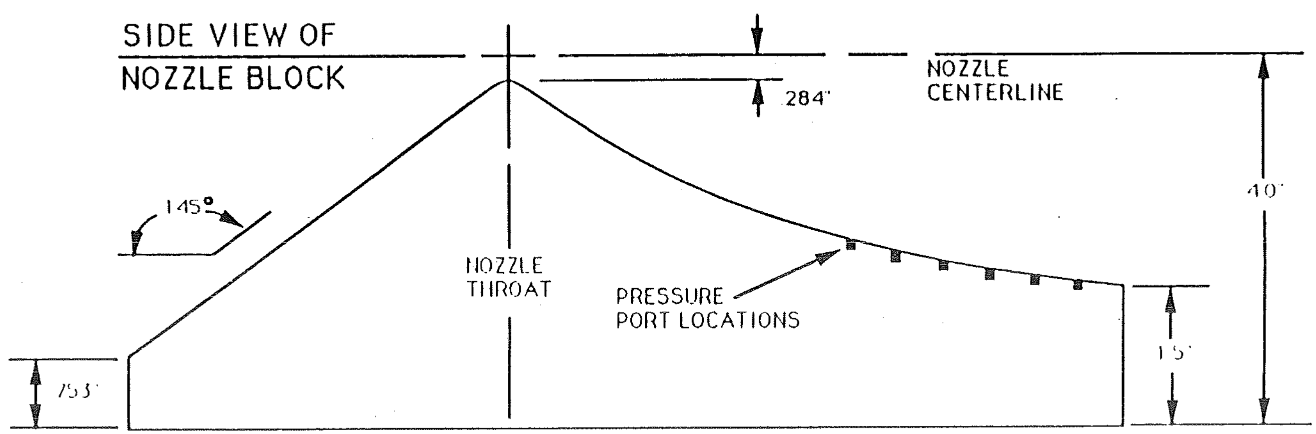

George C. Marshall Space Flight Center
Science and Engineering Directorate

Structures and Dynamics Laboratory
Aerophysics Division
Induced Environments Branch ED33

National Aeronautics and Space Administration

Test Section With 2-D SSME Nozzle Contour Model Installed

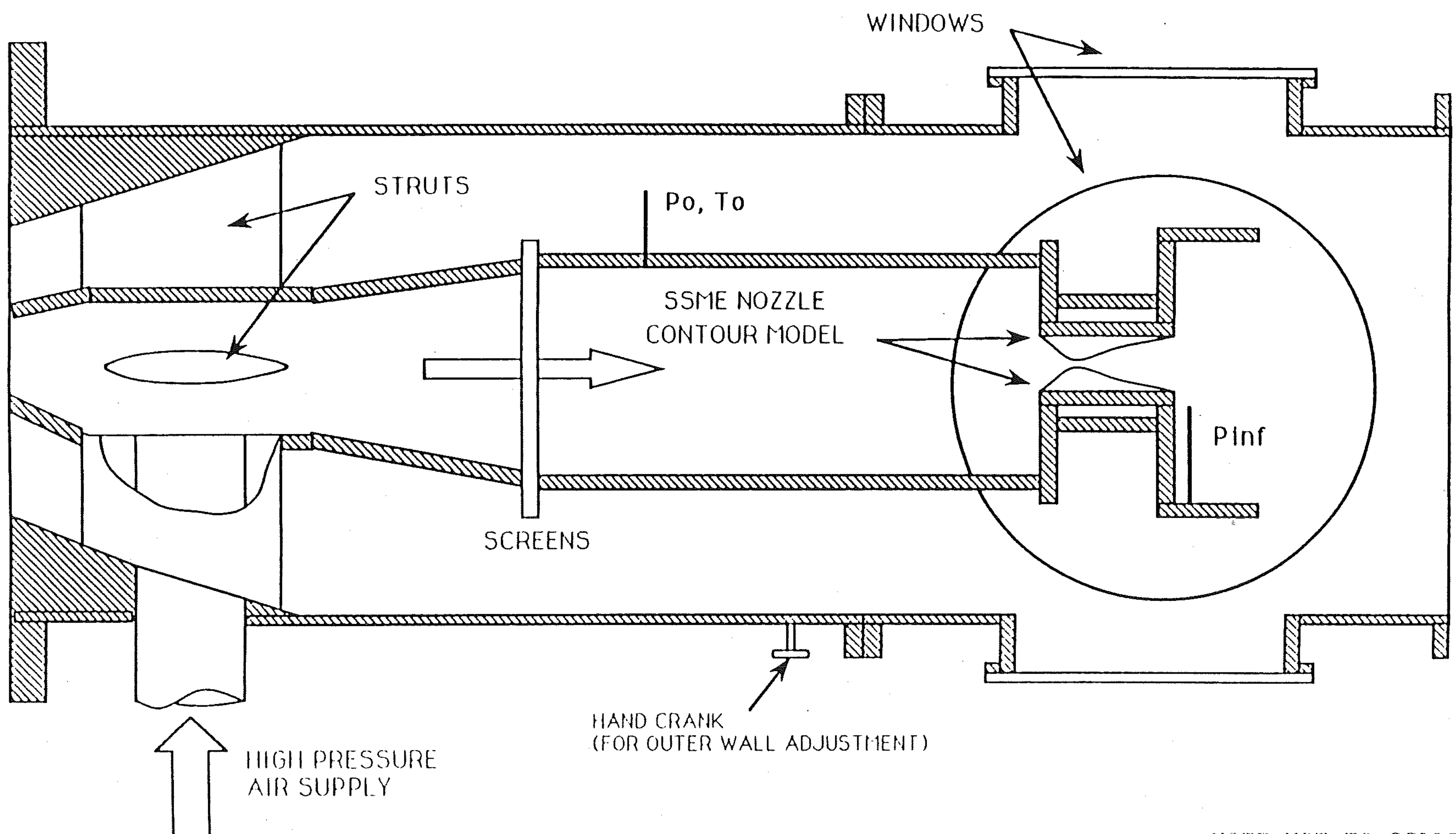

NOTE: NOT TO SCALE

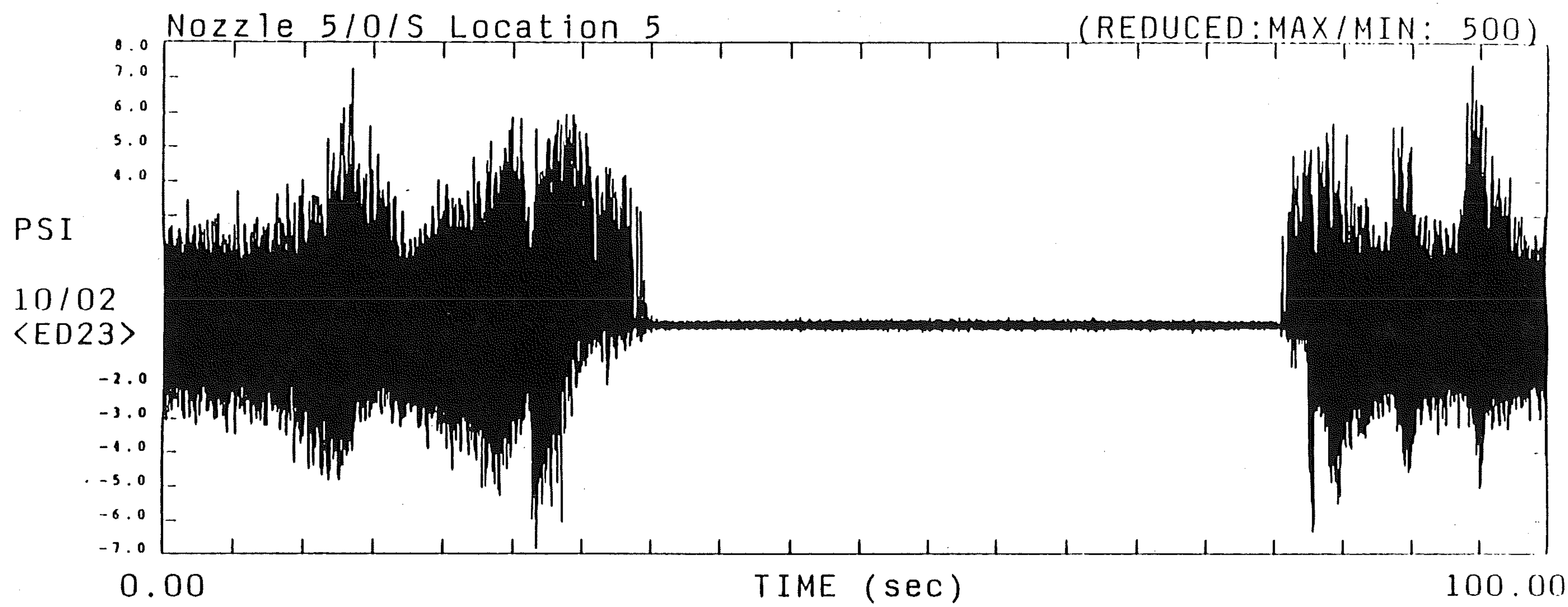
Nozzle 5/O/S Location 5
(REDUCED:MAX/MIN: 500)
8.0
7.0
6.0
5.0
4.0
PSI
10/02
<ED23>
-2.0
-3.0
-4.0
-5.0
-6.0
-7.0
0.00
TIME (sec)
100.00

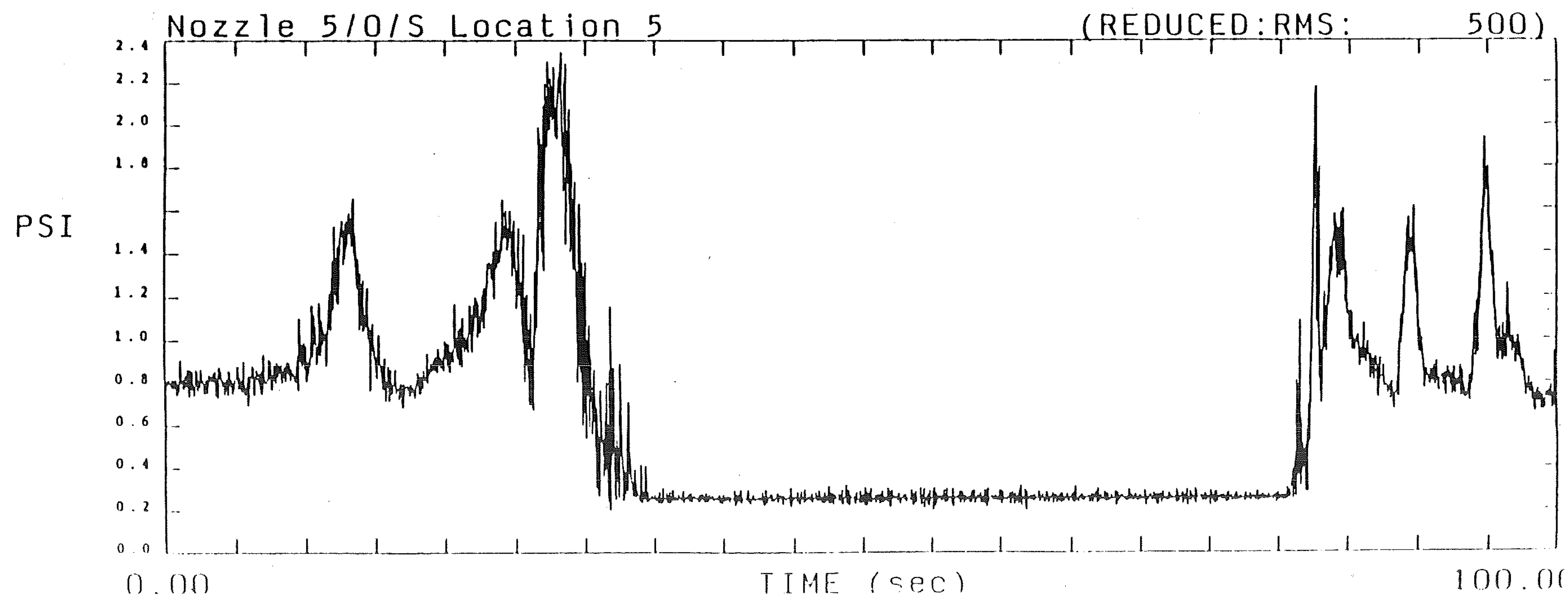
Nozzle 5/O/S Location 5
(REDUCED:RMS: 500)
2.4
2.2
2.0
1.8
PSI
1.4
1.2
1.0
0.8
0.6
0.4
0.2
0.0
0.00
TIME (sec)
100.00

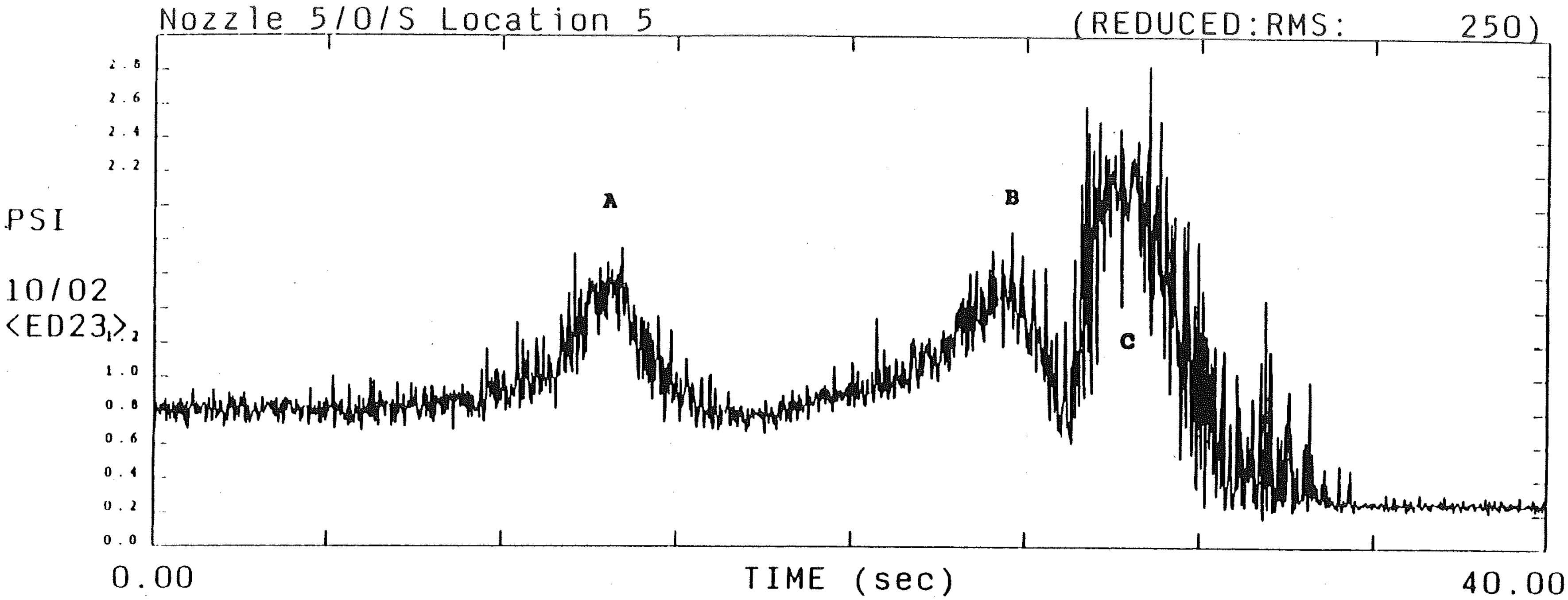
Nozzle 5/0/S Location 5
(REDUCED:RMS: 250)
PSI
10/02
<ED23>
2.8
2.6
2.4
2.2
1.0
0.8
0.6
0.4
0.2
0.0
A
B
C
0.00
TIME (sec)
40.00

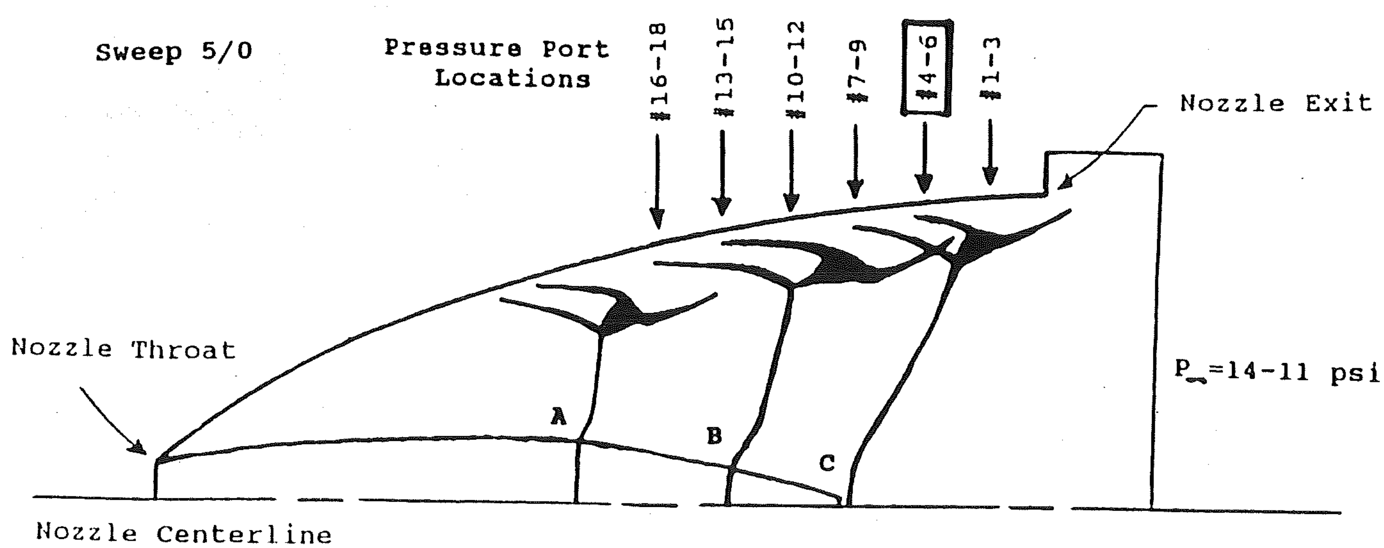
Sweep 5/0
Pressure Port Locations
#16-18
#13-15
#10-12
#7-9
#4-6
#1-3
Nozzle Exit
Nozzle Throat
P_∞=14-11 psi
A
B
C
Nozzle Centerline

Nozzle 5/0/S Location 5 S+ 11.00

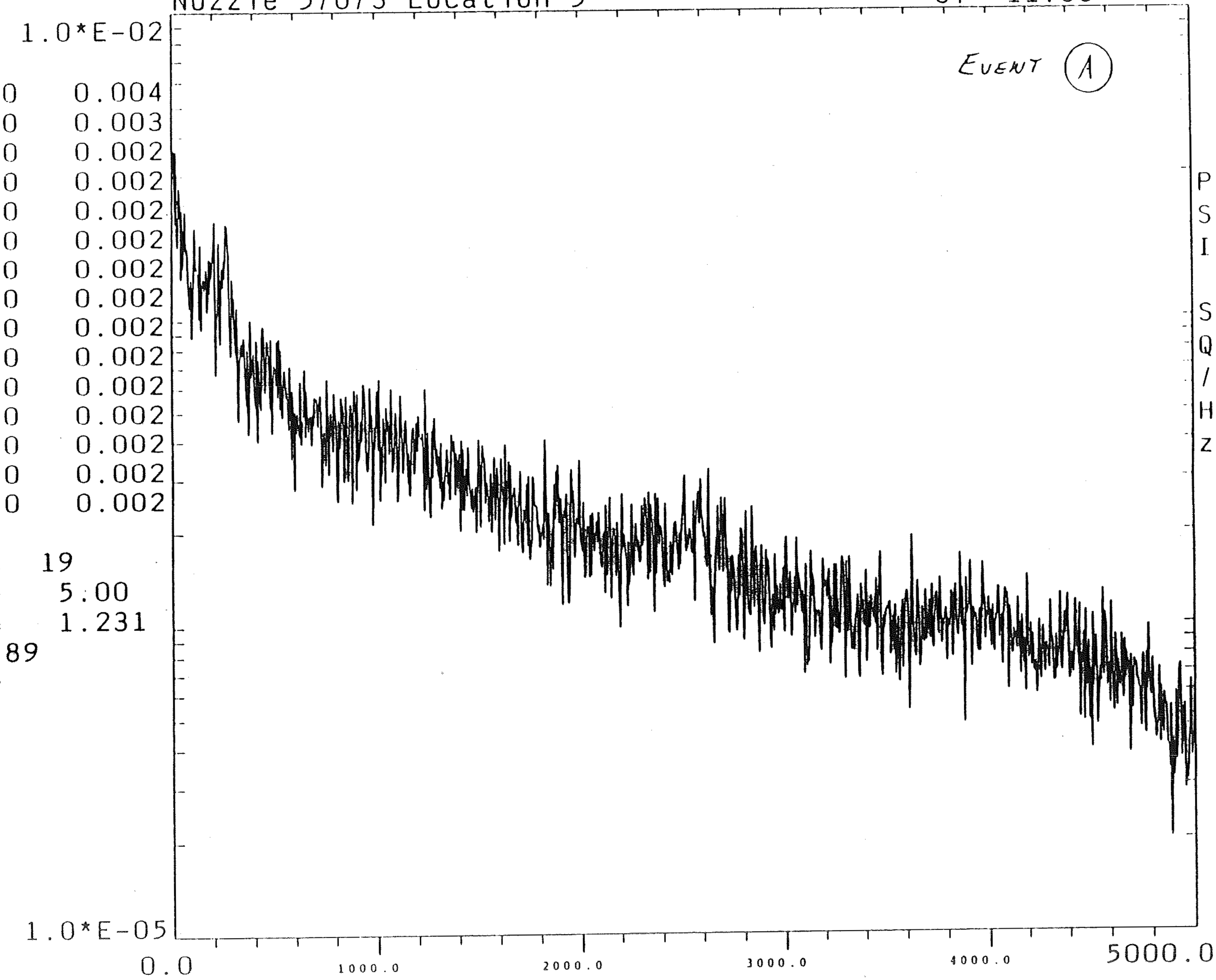

20.0	0.004
35.0	0.003
50.0	0.002
65.0	0.002
210.0	0.002
265.0	0.002
110.0	0.002
230.0	0.002
140.0	0.002
75.0	0.002
180.0	0.002
190.0	0.002
255.0	0.002
120.0	0.002
245.0	0.002

#AVGS= 19
BW= 5.00
COMP= 1.231
10/02/89
<ED23>

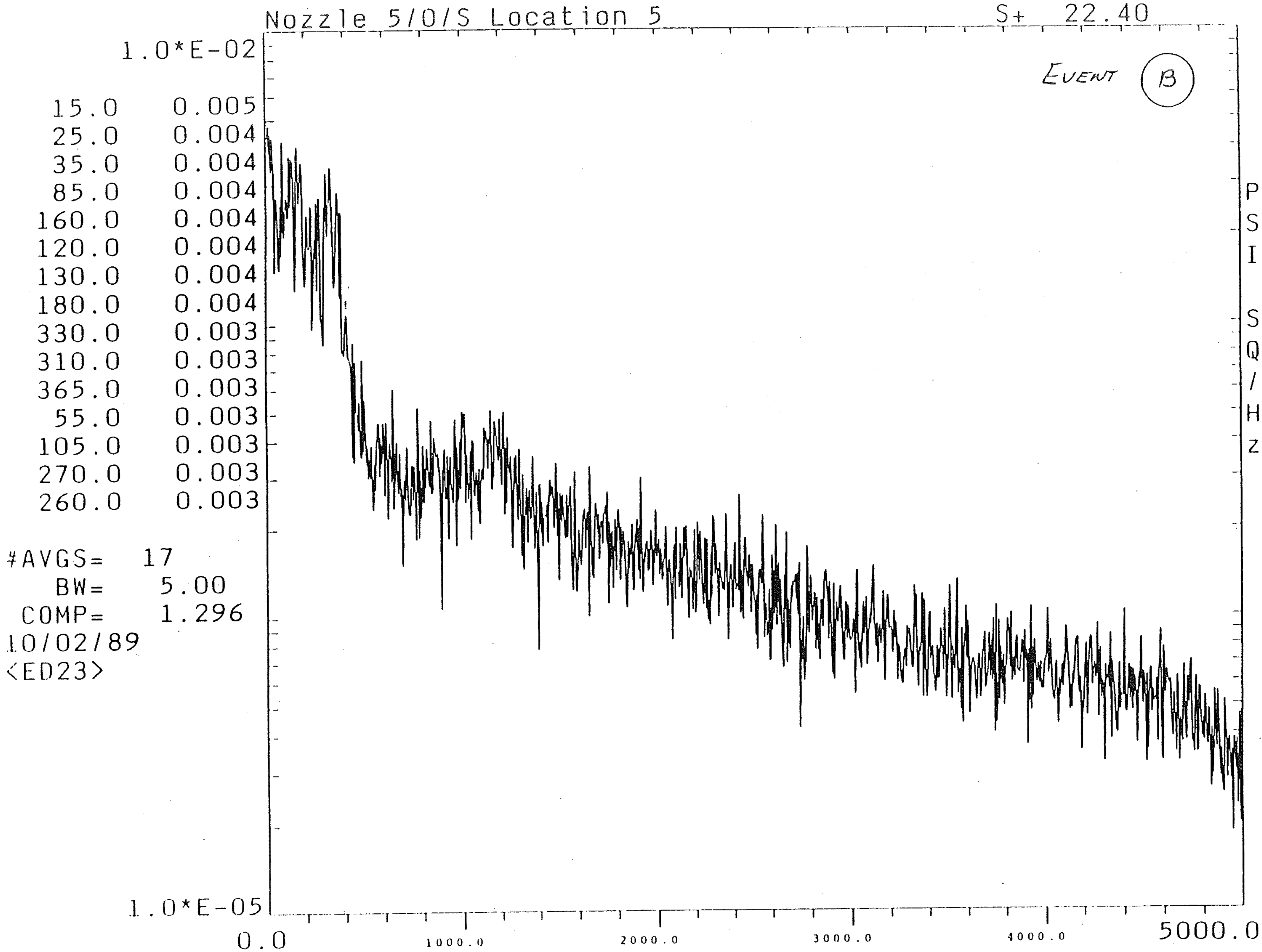
Nozzle 5/0/S Location 5
S+ 22.40
EVENT
B
1.0*E-02
15.0 0.005
25.0 0.004
35.0 0.004
85.0 0.004
160.0 0.004
120.0 0.004
130.0 0.004
180.0 0.004
330.0 0.003
310.0 0.003
365.0 0.003
55.0 0.003
105.0 0.003
270.0 0.003
260.0 0.003
#AVGS= 17
BW= 5.00
COMP= 1.296
10/02/89
<ED23>
1.0*E-05
0.0
1000.0
2000.0
3000.0
4000.0
5000.0
PSI SQ/HZ

Nozzle 5/0/S Location 5 S+ 25.60

1.0*E-01

35.0	0.018
25.0	0.018
270.0	0.011
45.0	0.009
110.0	0.008
280.0	0.007
95.0	0.007
65.0	0.006
230.0	0.006
170.0	0.006
75.0	0.005
290.0	0.005
195.0	0.005
130.0	0.005
150.0	0.005

#AVGS= 26
BW= 5.00
COMP= 1.524
10/02/89
<ED23>

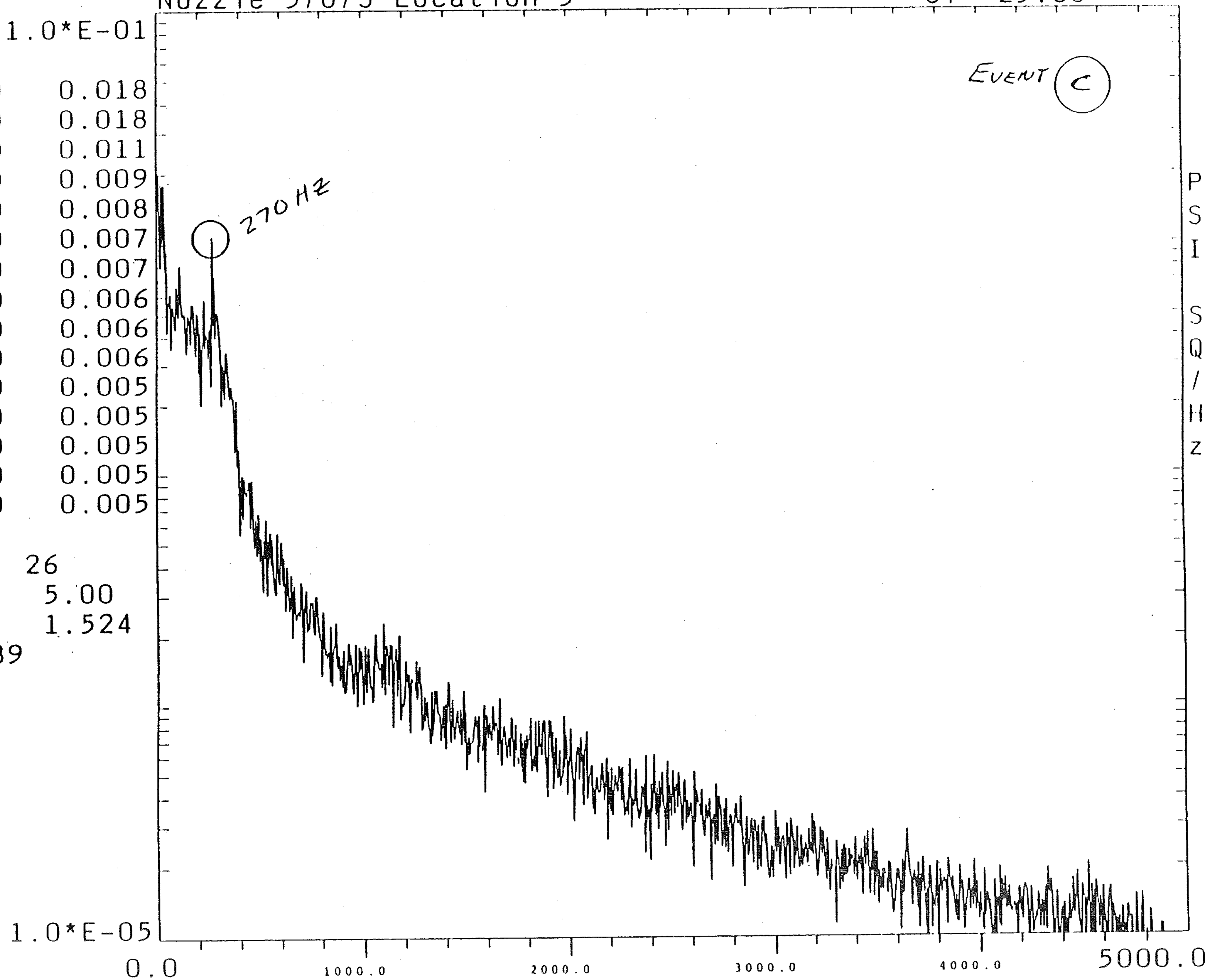

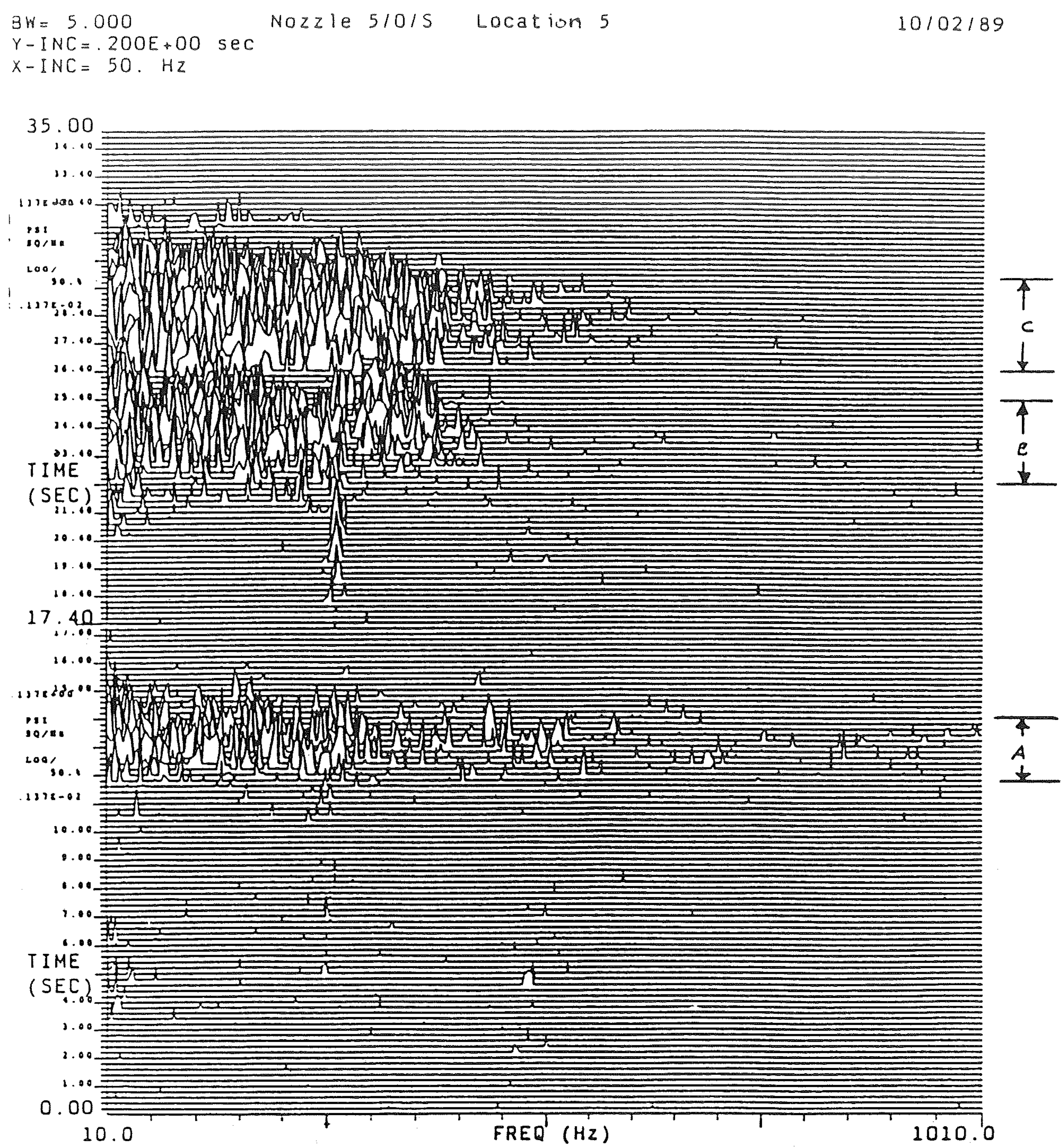
BW= 5.000
Y-INC=.200E+00 sec
X-INC= 50. Hz
Nozzle 5/0/S
Location 5
10/02/89
35.00
17.40
0.00
TIME (SEC)
TIME (SEC)
10.0
FREQ (Hz)
1010.0
c
e
A

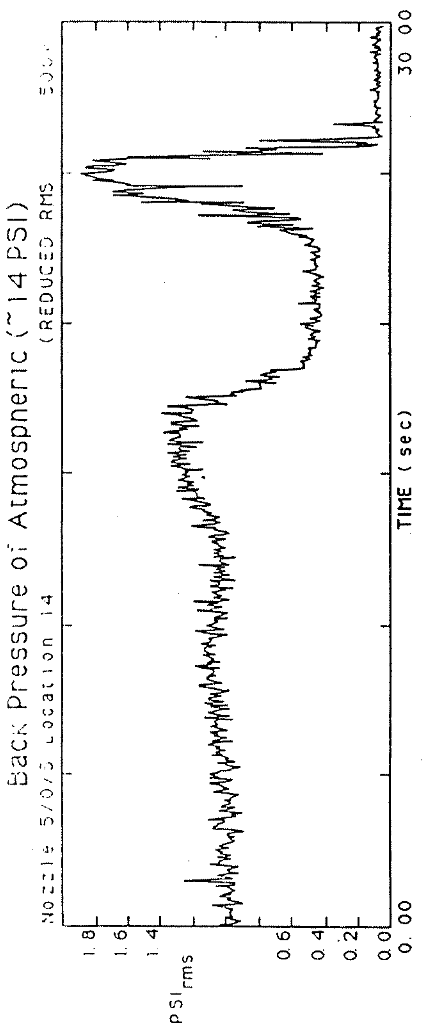
Back Pressure of Atmospheric (~14 PSI)
(REDUCED RMS
Nozzle 5/0/5 Location 14
PSI_rms
1.8
1.6
1.4
0.6
0.4
0.2
0.0
0.00
30.00
500
TIME (sec)

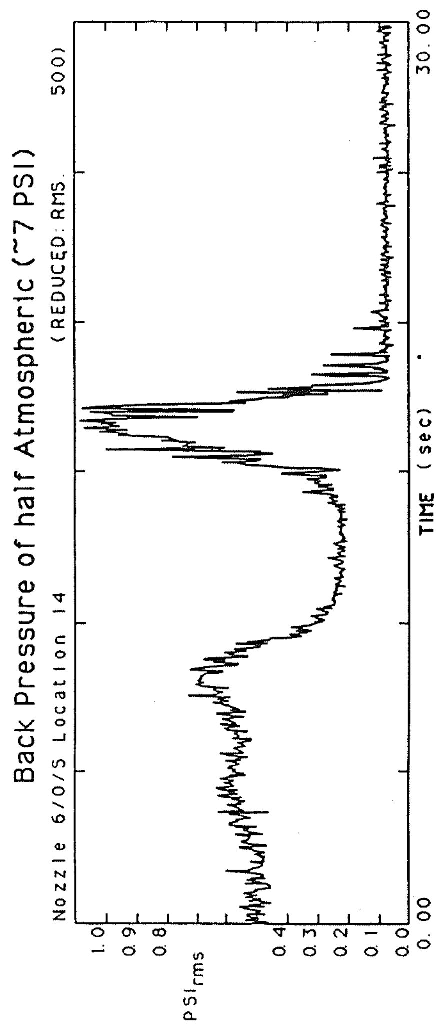
Back Pressure of half Atmospheric (~7 PSI)
(REDUCED: RMS.
Nozzle 6/0/5 Location 14
PSI_rms
1.0
0.9
0.8
0.4
0.3
0.2
0.1
0.0
0.00
30.00
500)
TIME (sec)

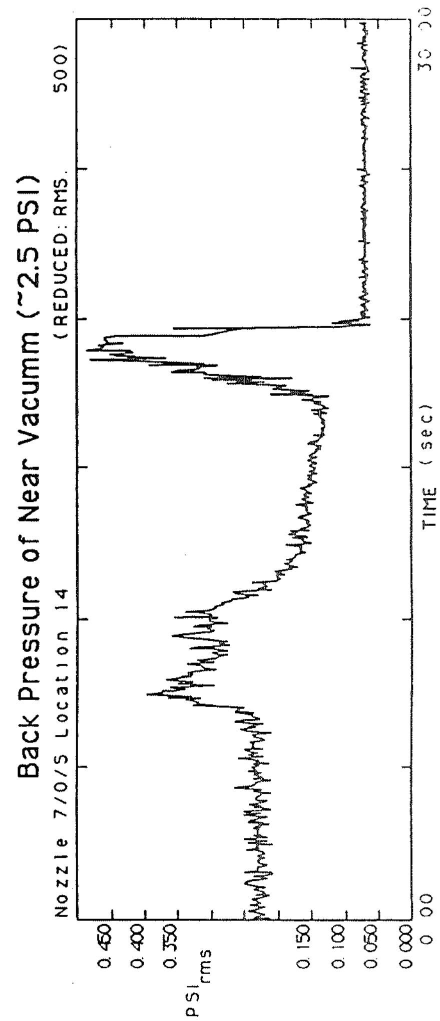
Back Pressure of Near Vacumm (~2.5 PSI)
(REDUCED: RMS.
Nozzle 7/0/5 Location 14
PSI_rms
0.450
0.400
0.350
0.150
0.100
0.050
0.000
0.00
500)
TIME (sec)

SSME NOZZLE SHELL
SHOCK WAVE LOCATION

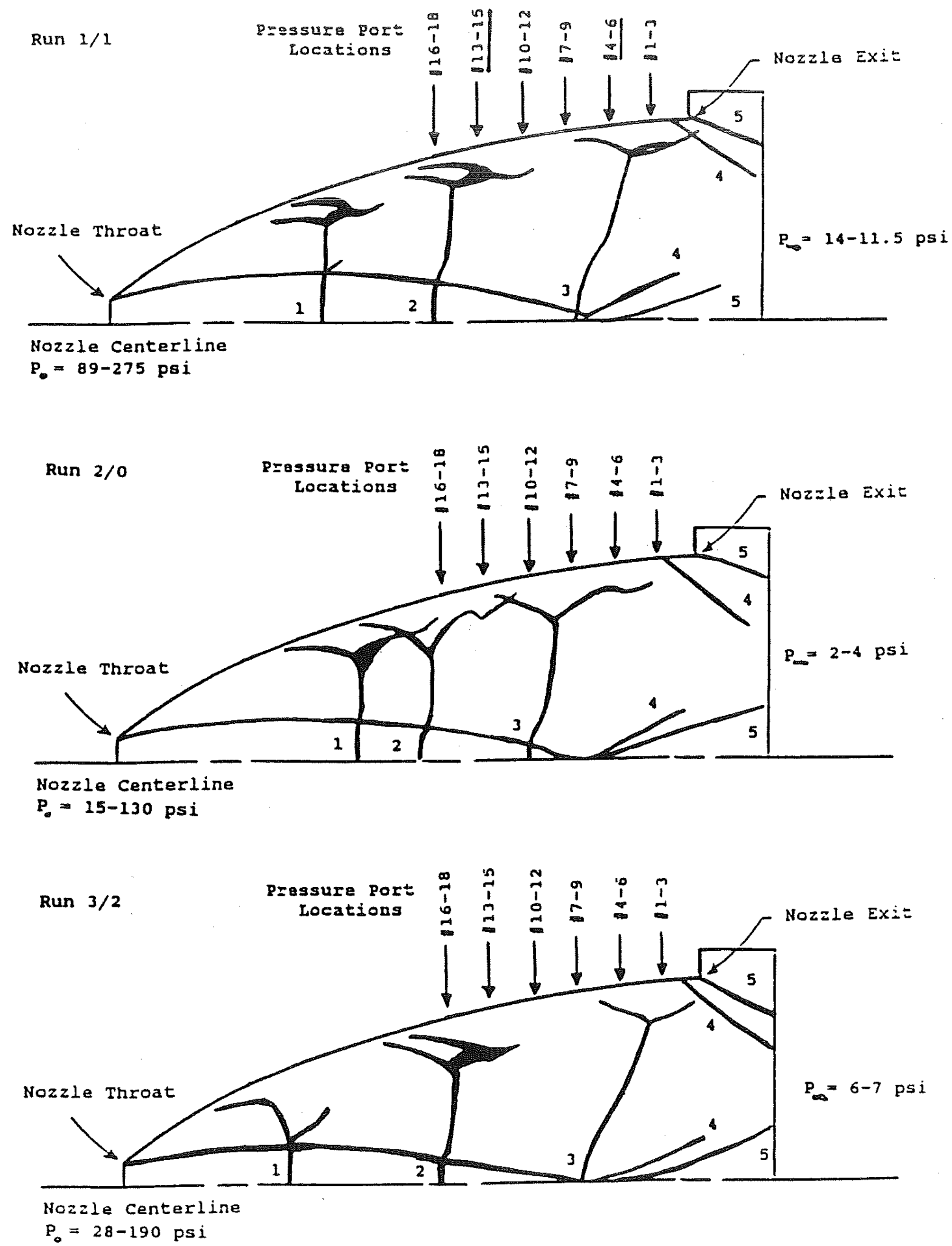

Marshall Space Flight Center
Homero Hidalgo / CR55
Darren Reed / ED33

Conclusions

- Fluctuating Pressures are highest at the upstream edge of the lambda shock
- Fluctuating pressure levels decrease “inside” the shock foot
- Spectrum shapes show mostly low frequency energy - this is consistent with similar flow conditions (external bow shock impingement)
- Nondimensional amplitude, ΔCp, levels are similar to external flow conditions
- The plane flow nozzle with side windows is a good method to observe the shock wave patterns
- Data from this experiment have helped describe the unsteady aerodynamic forces a nozzle experiences during startup and shutdown

Marshall Space Flight Center
Homero Hidalgo / CR55
Darren Reed / ED33

Future Fluctuating Pressure Analyses of Nozzle Transients

- The Fluid Dynamics Division has developed plans for 3-D subscale nozzles with the following capabilities:

» Maximum test pressure		350 psi (nitrogen)
» Maximum flow rate	primary	12 lb/s @ 810 °
	secondary	50 lb/s
» Minimum back pressure		0.05 psia
» Maximum run duration		360 sec. @ 12 lb/s
» Maximum supply temperature		350 °F
» Maximum testable area ratio		230
» Test Cabin Size		3 ft diameter x 5 ft

- Two different nozzle contours are to be tested in the Trisonic wind tunnel special test section this July
- The new nozzles will be instrumented and tested similar to the SSME nozzle

Fluctuating Pressure Analysis of a 2-D SSME Nozzle Air Flow Test

Marshall Space Flight Center
Homero Hidalgo / CR55
Darren Reed / ED33

Fluid Dynamics Division's 3-D Nozzle Test Facility

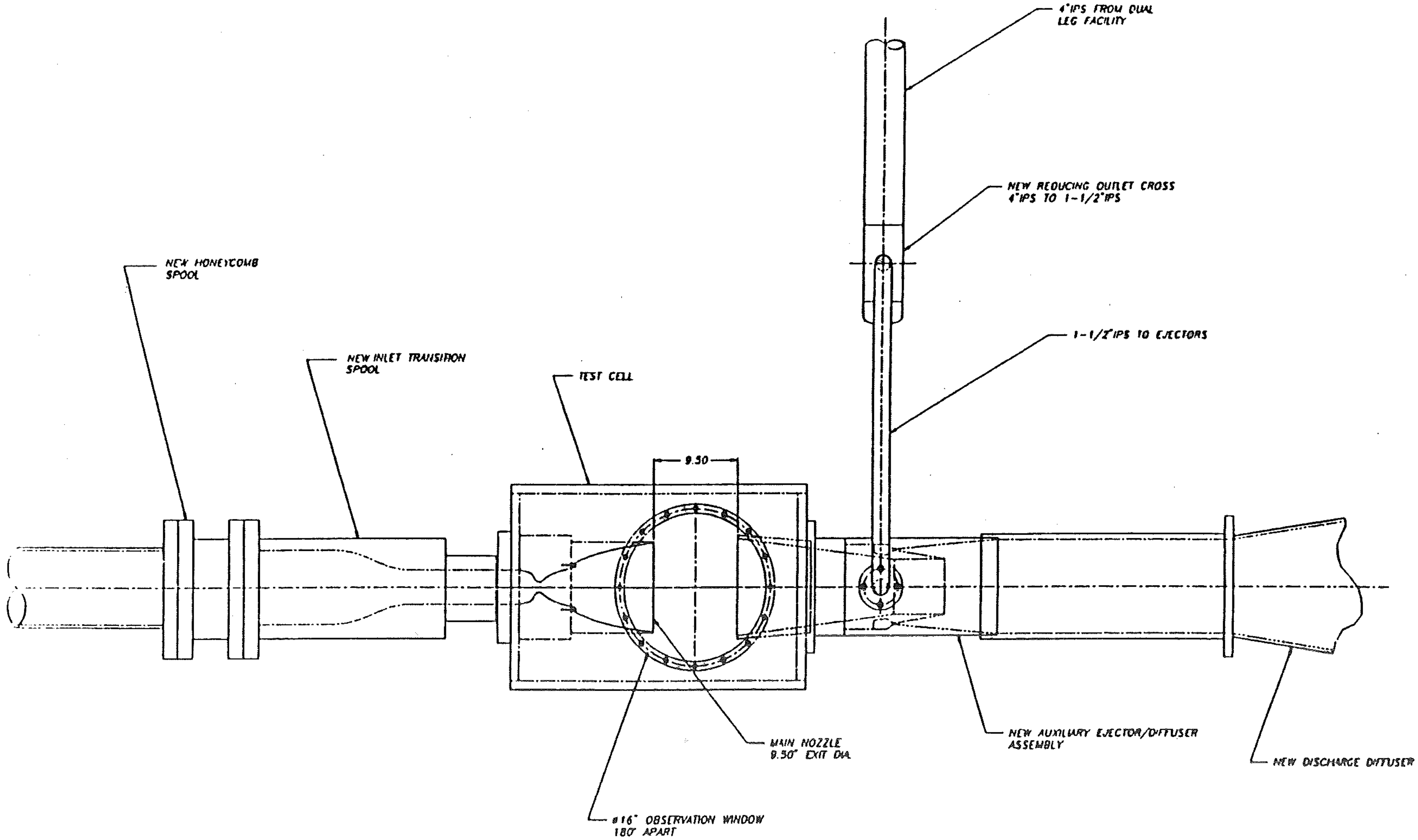

Marshall Space Flight Center
Homero Hidalgo / CR55
Darren Reed / ED33

Rocketdyne Tripropellant Nozzle Contour

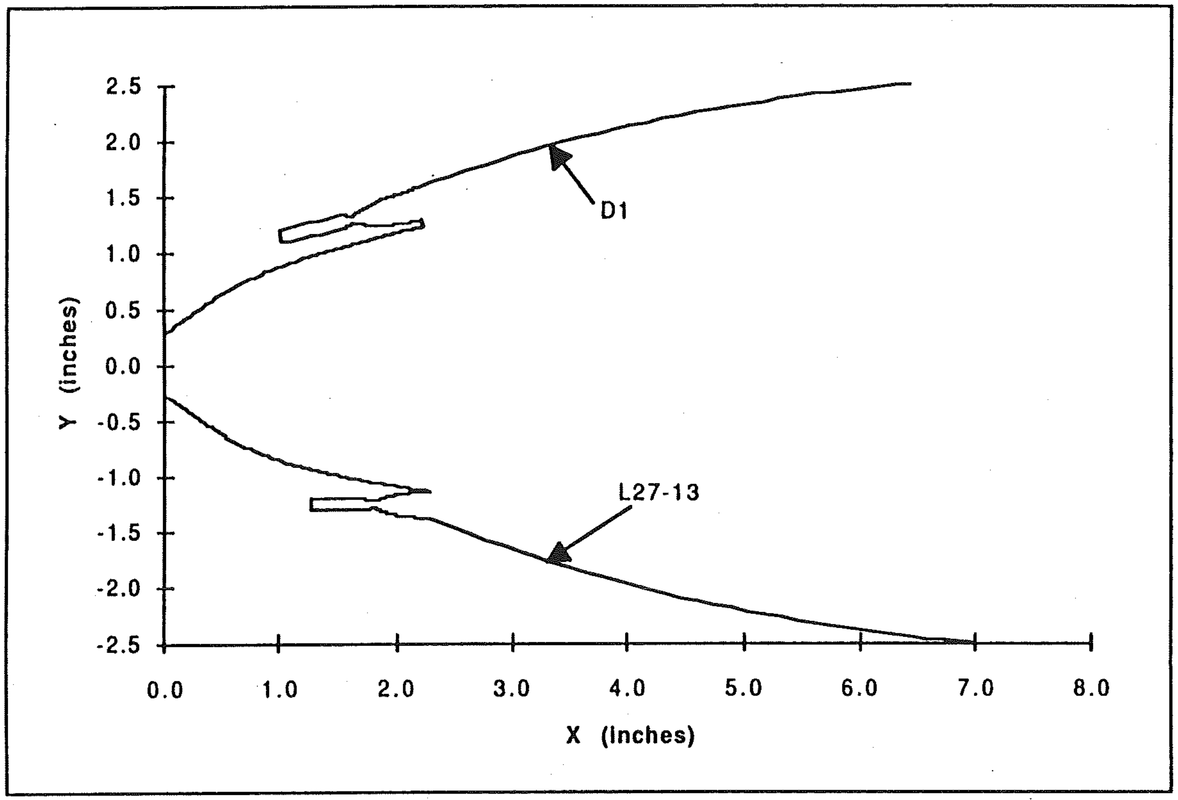

LMS 2/23/95

Marshall Space Flight Center
Homero Hidalgo / CR55
Darren Reed / ED33

Dual Bell Concept Nozzle Contour

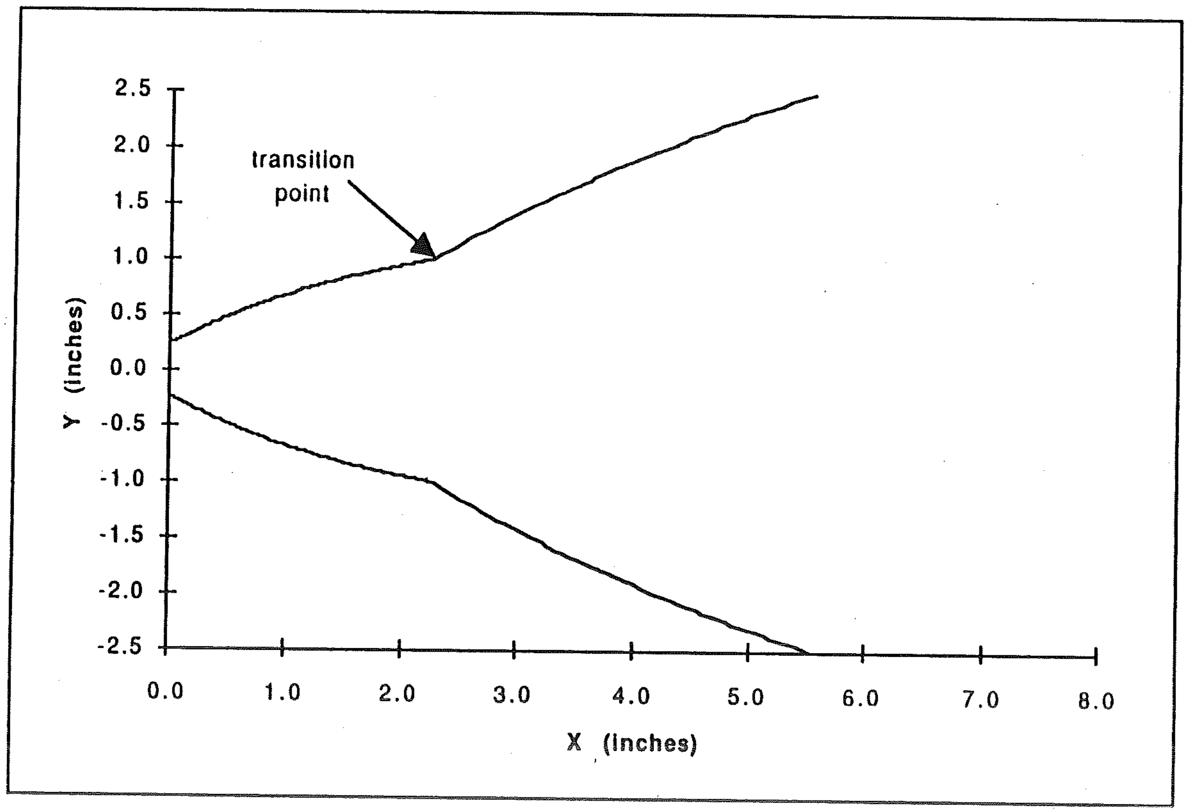

LMS 2/23/95

EXPERIMENTAL INVESTIGATION OF THE EFFECTS OF ACCELERATION ON HEAT TRANSFER IN THE TURBULENT BOUNDARY LAYER

Walid M. Chakroun
and
Robert P. Taylor

Department of Mechanical Engineering
Mississippi State University
Mississippi State, MS 39762

Abstract

Rocket propulsion system components such as turbines/pumps and nozzles often have aerodynamically-rough surfaces or surfaces which become rough during operation. Also, these surfaces are often in regions of accelerating flow. The interaction between surface roughness and acceleration is complicated and not predicted by a simple superposition of flat-plate rough-wall correlations and smooth-wall acceleration effects.

For the smooth wall, acceleration causes a decrease in the Stanton number when compared with equivalent unaccelerated flow. When the acceleration is strong enough, the turbulent boundary-layer heat transfer rates will approach those of a laminar flow and the boundary layer is said to have relaminarized. Under proper conditions, rough-wall accelerated flow can have the opposite behavior with increasing Stanton numbers and hence much larger heat transfer rates.

The objective of this research was to experimentally investigate the combined effects of freestream acceleration and surface roughness on heat transfer and fluid flow in the turbulent boundary layer. The experiments included a variety of flow conditions ranging from aerodynamically-smooth to transitionally-rough to fully-rough boundary layers with accelerations ranging from moderate to moderately strong. The test surfaces used were a smooth-wall test surface and two rough-wall test surfaces which were roughened with 1.27 mm diameter hemispheres spaced 2 and 4 base diameters apart in a staggered array. The experiments were conducted in the Turbulent Heat Transfer Test Facility in the mechanical engineering laboratories at Mississippi State University. The measurements consisted of Stanton number distributions, mean-temperature profiles, skin-friction distributions, mean-velocity profiles, turbulence-intensity profiles, and Reynolds-stress profiles.

The Stanton numbers for the rough-wall experiments increased with acceleration. For aerodynamically-smooth and transitionally-rough boundary layers, the effect of the roughness is not seen immediately at the beginning of the accelerated region as it is for fully-rough boundary layers; however, as the boundary layer thins under acceleration, the surface becomes relatively rougher resulting in a sharp increase in Stanton number.

EXPERIMENTAL INVESTIGATION OF THE EFFECTS OF ACCELERATION ON HEAT TRANSFER IN THE TURBULENT BOUNDARY LAYER

by
Walid M. Chakroun
and
Robert P. Taylor

Department of Mechanical Engineering
Mississippi State University

April 26, 1995

Mississippi State University

BACKGROUND

- Acceleration effects on smooth-wall boundary layers--strong accelerations cause sharp decrease in the Stanton number

$$K = \frac{\nu}{U_e^2} \frac{dU_e}{dx}$$

$K > 3.0 \times 10^{-6}$ relaminarization

- Fully-rough boundary layers react to acceleration in the opposite way--Stanton number increases under acceleration.

Mississippi State University

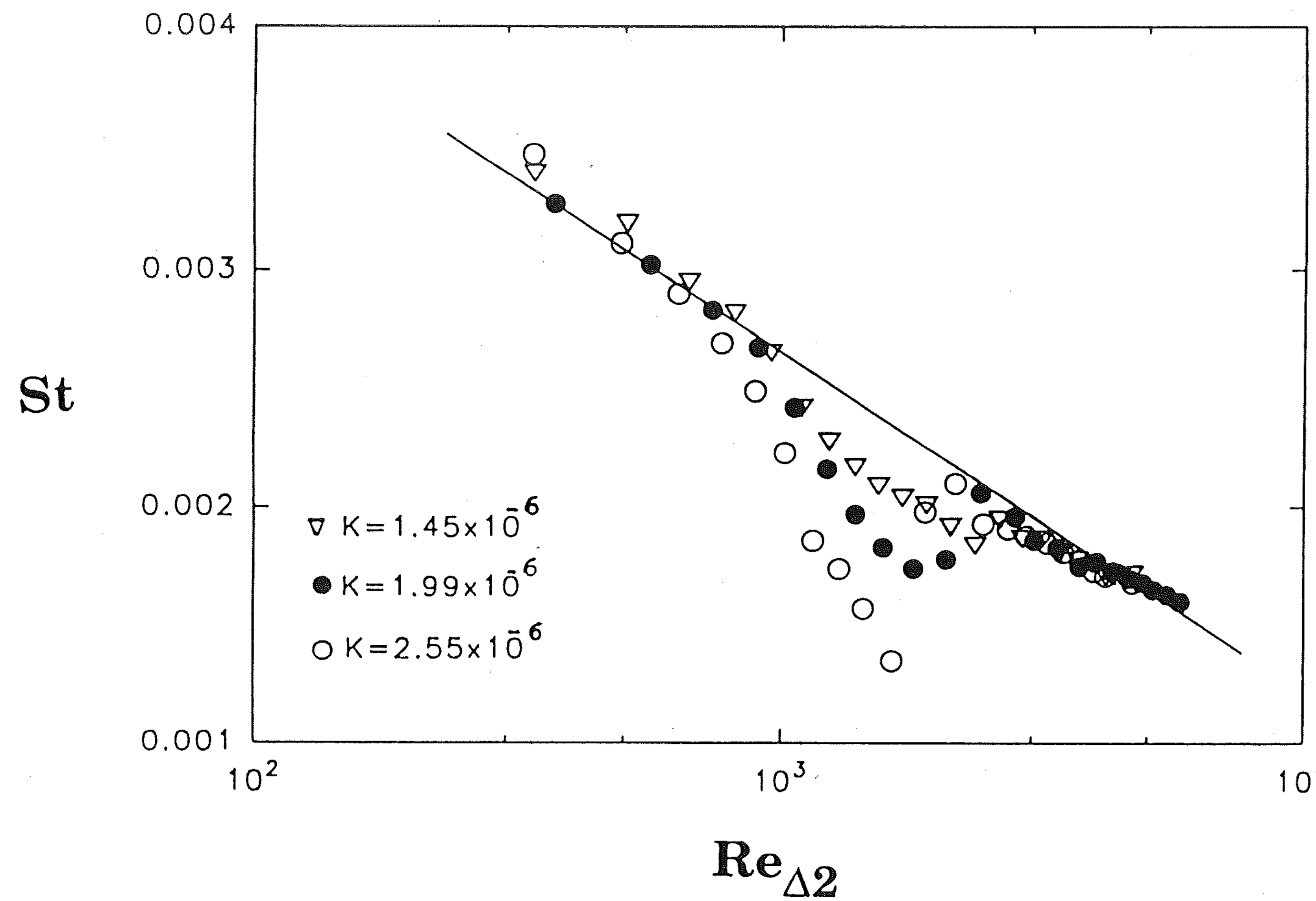

Effects of acceleration on smooth-wall turbulent Stanton numbers, from Kays and Moffat (1975)

Mississippi State University

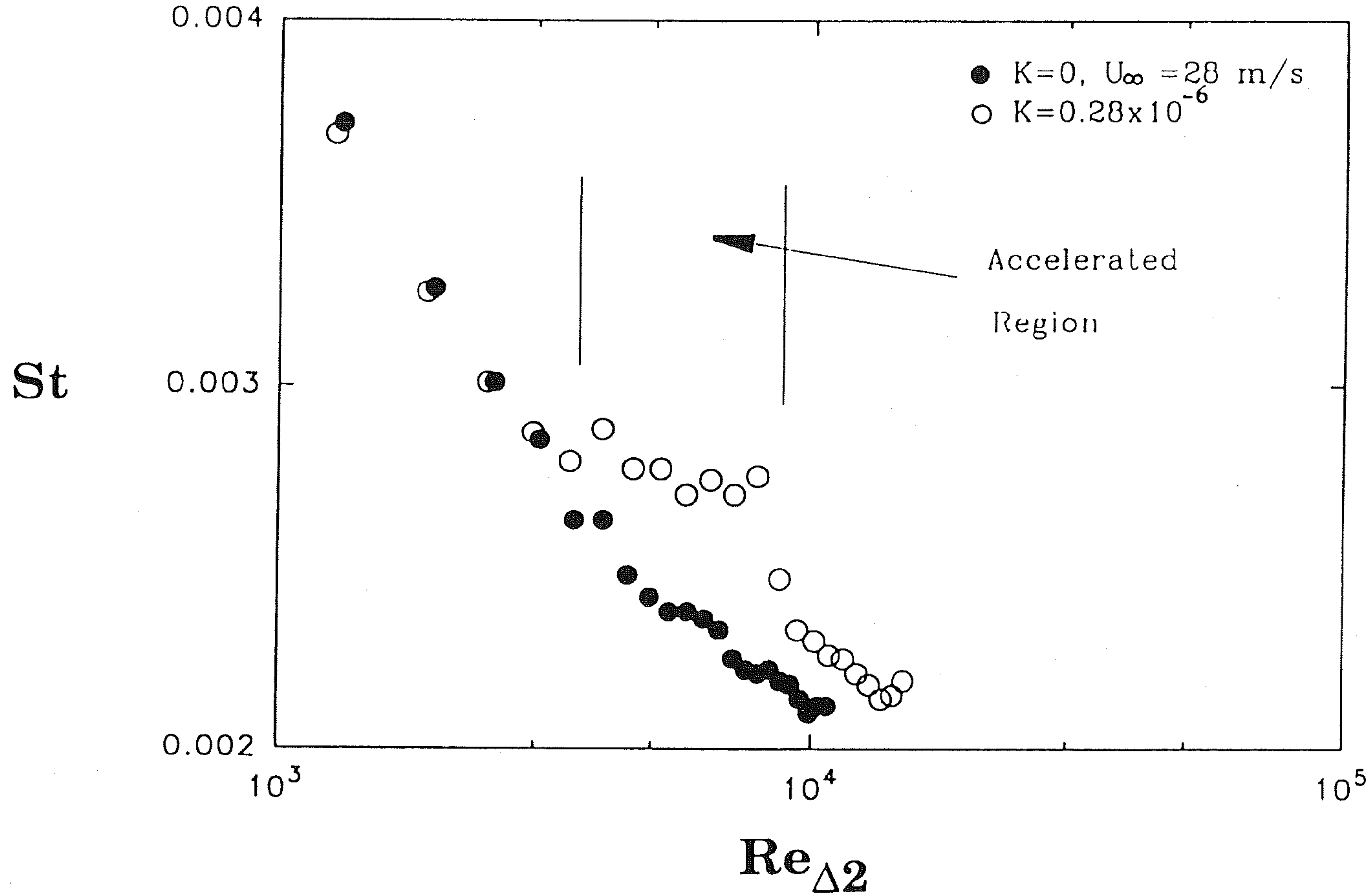

Effects of acceleration on full-rough turbulent Stanton numbers, from Coleman (1976)

- In a smooth-wall boundary layer, acceleration stretches the eddies **reducing the trans-boundary-layer diffusion**, decreases the boundary-layer thickness, **increases the viscous sublayer thickness**, and ***reduces the Stanton number***.

- In a **fully-rough** boundary layer, acceleration stretches the eddies reducing the trans-boundary-layer diffusion, **decreases the boundary-layer thickness**, **increases the nondimensional size of the roughness elements**, and ***increases the Stanton number***.

Mississippi State University

OBJECTIVES OF THIS WORK

- Experimentally investigate the effects of freestream acceleration on heat transfer in the turbulent rough-wall boundary layer.

- Investigate a variety of flow conditions ranging from aerodynamically-smooth to fully-rough boundary layers.

Mississippi State University

EXPERIMENTS

- Closed-loop boundary-layer wind tunnel with 2.5-m long test section.
- Flexible top wall to adjust edge velocity.
- Rough-wall boundary-layer thickness of about 5 cm.
- Roughness made with 1.27-mm diameter hemispheres spaced 2 and 4 diameters apart.
- Stanton numbers determined form energy balance on individual plates.
- Velocity and turbulence profiles measured with hot-wire anemometry.

Mississippi State UNIVERSITY

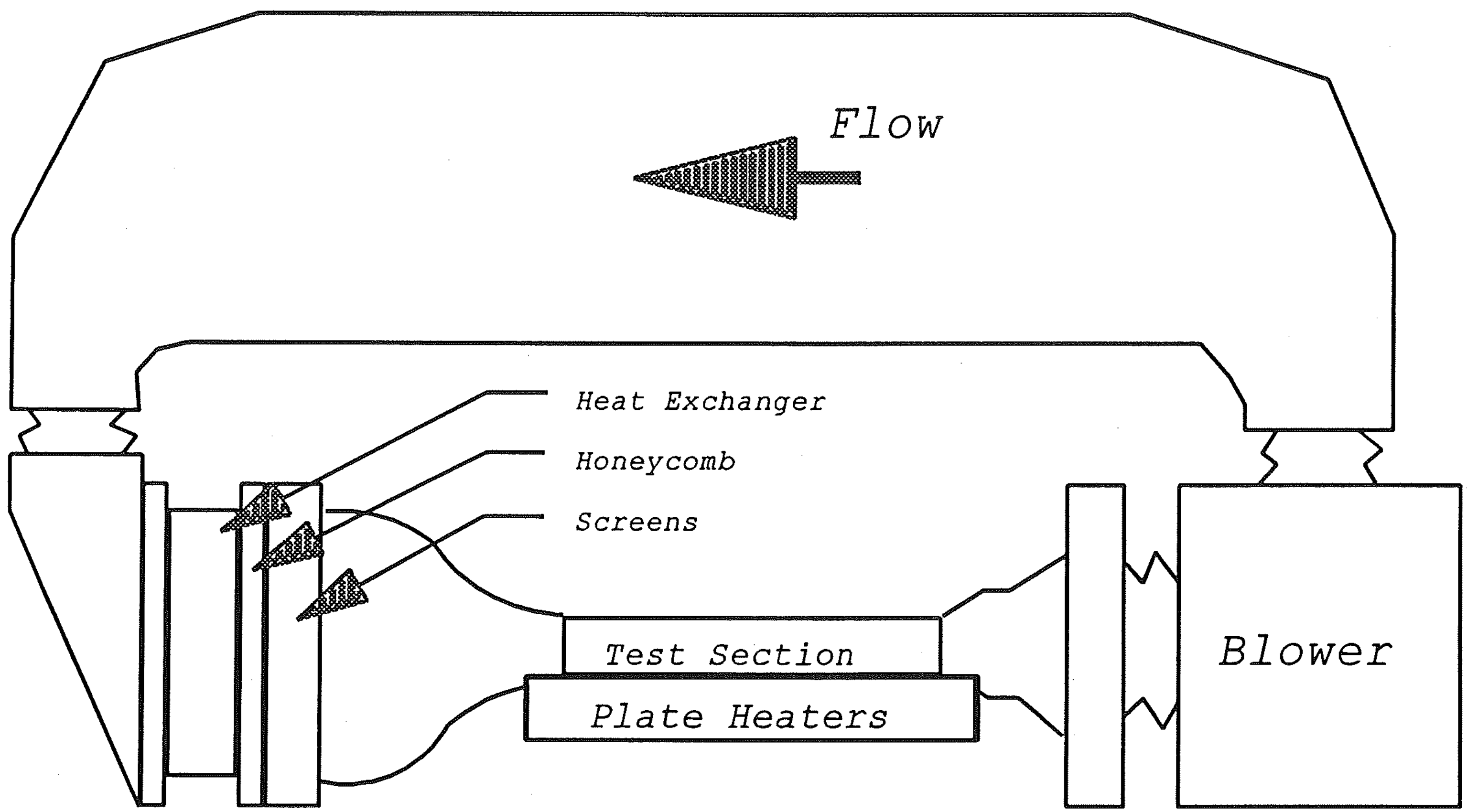

Turbulent heat transfer test facility

Mississippi State University

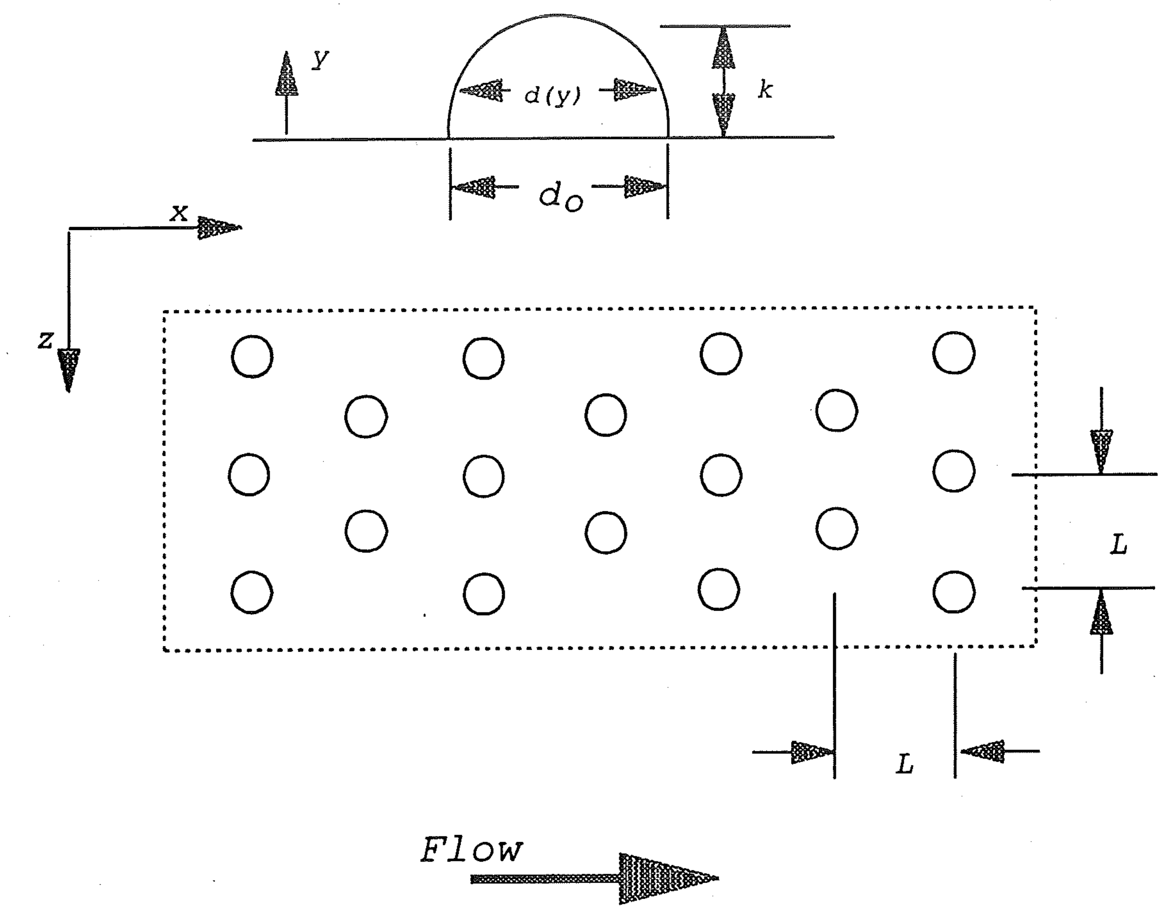

Surface roughness description

Mississippi State University

HEAT TRANSFER DATA

$K \times 10^6$	U_∞ m/s	$L/d_o = 2$	$L/d_o = 4$
0.3	28	fully rough	fully rough
0.6	12	fully rough	tran'ly rough
0.9	8	tran'ly rough	tran'ly rough
1.4	5	aero'ly smooth	aero'ly smooth

Roughness state based on the boundary layer conditions just upstream of the accelerated region.

Mississippi State University

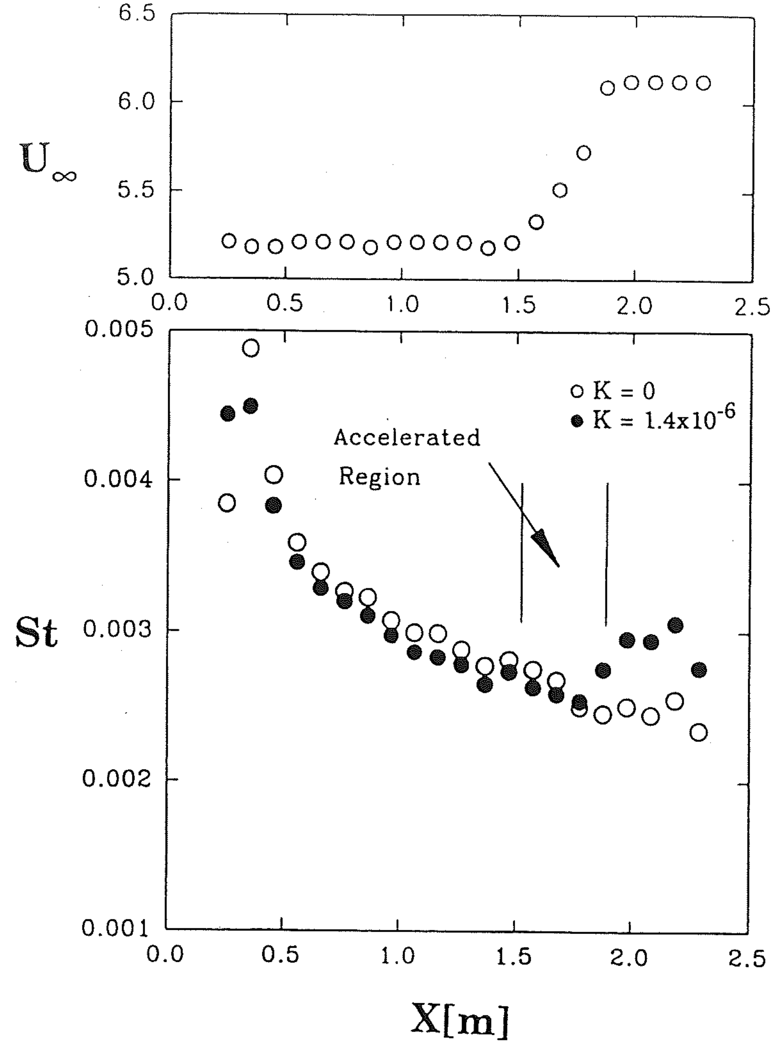

$K = 1.4 \times 10^{-6}$, $L/d_o = 2$, aerodynamically-smooth approaching flow

Mississippi State University

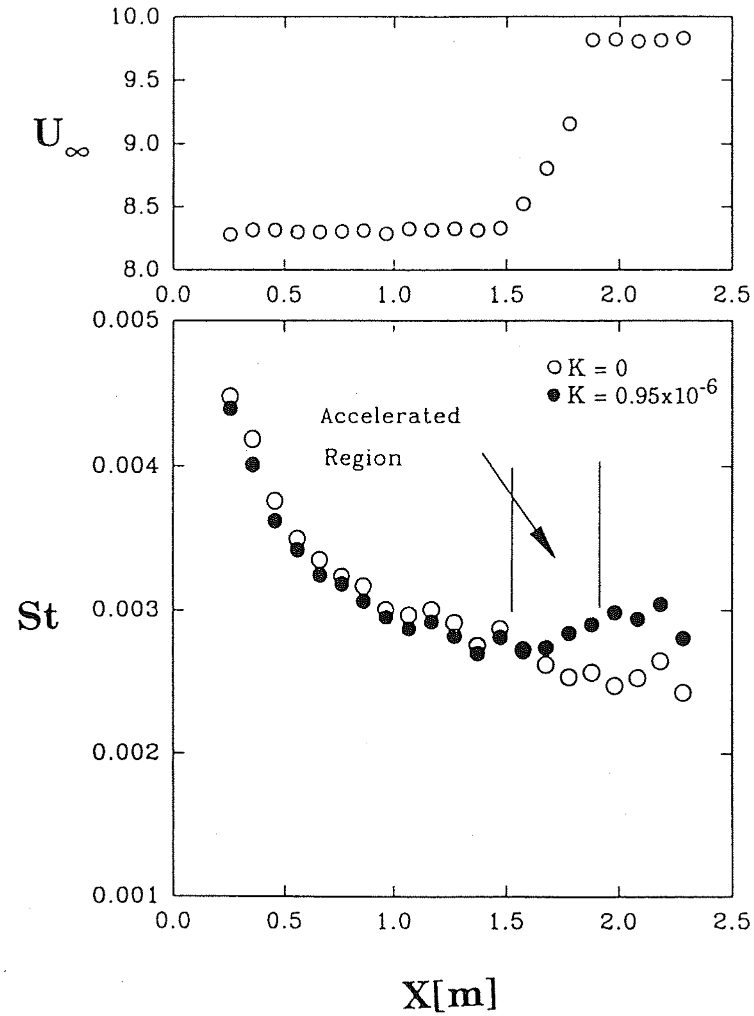

$K = 0.95 \times 10^{-6}$, $L/d_o = 2$, transitionally-rough approaching flow

Mississippi State University

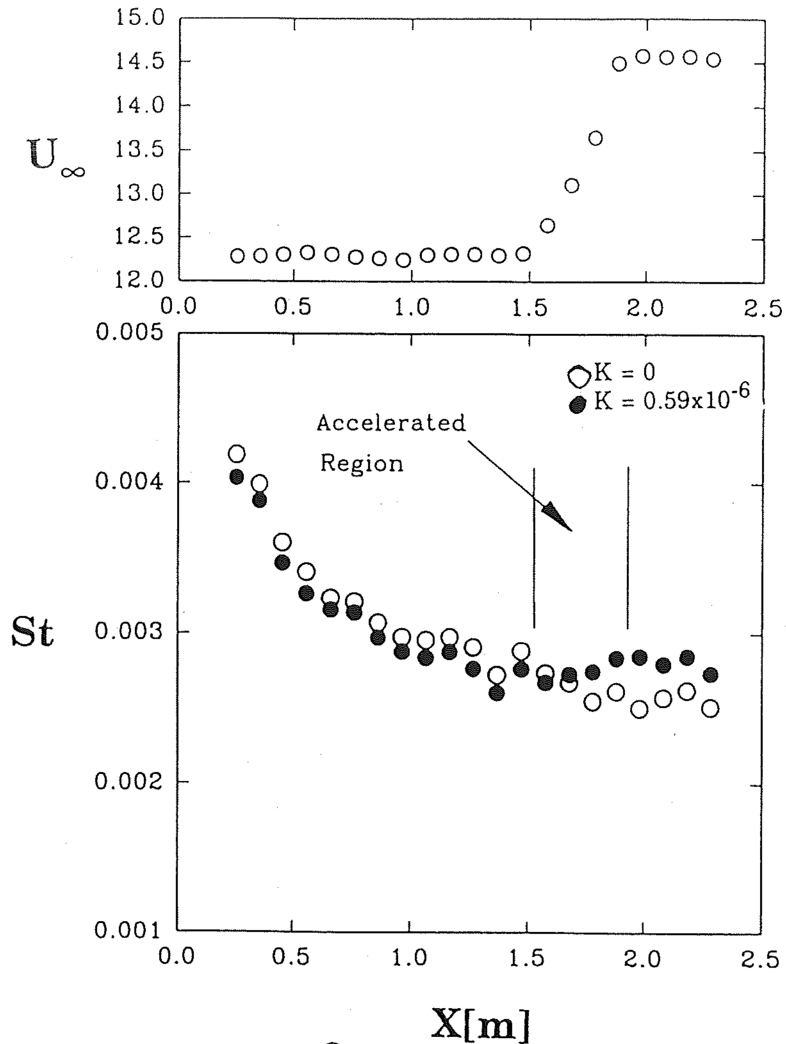

K = 0.59 X 10^{-6}, L/d_o = 2, fully-rough approaching flow

Mississippi State University

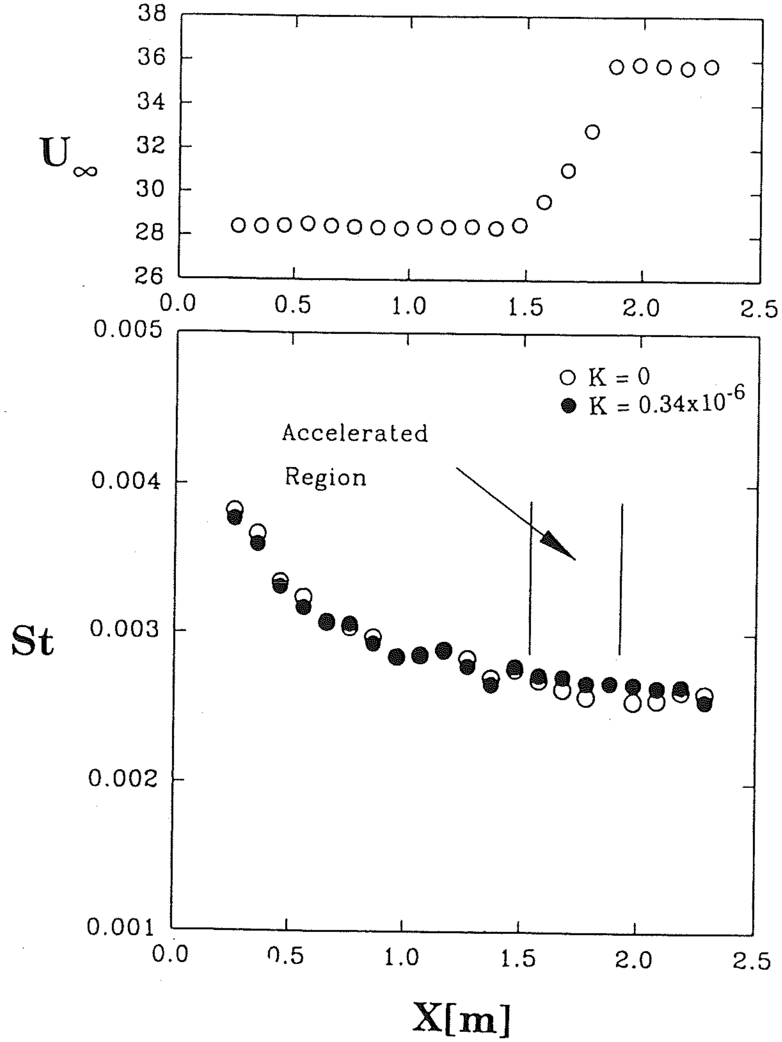

$K = 0.34 \times 10^{-6}$, $L/d_o = 2$, fully-rough approaching flow

Mississippi State University

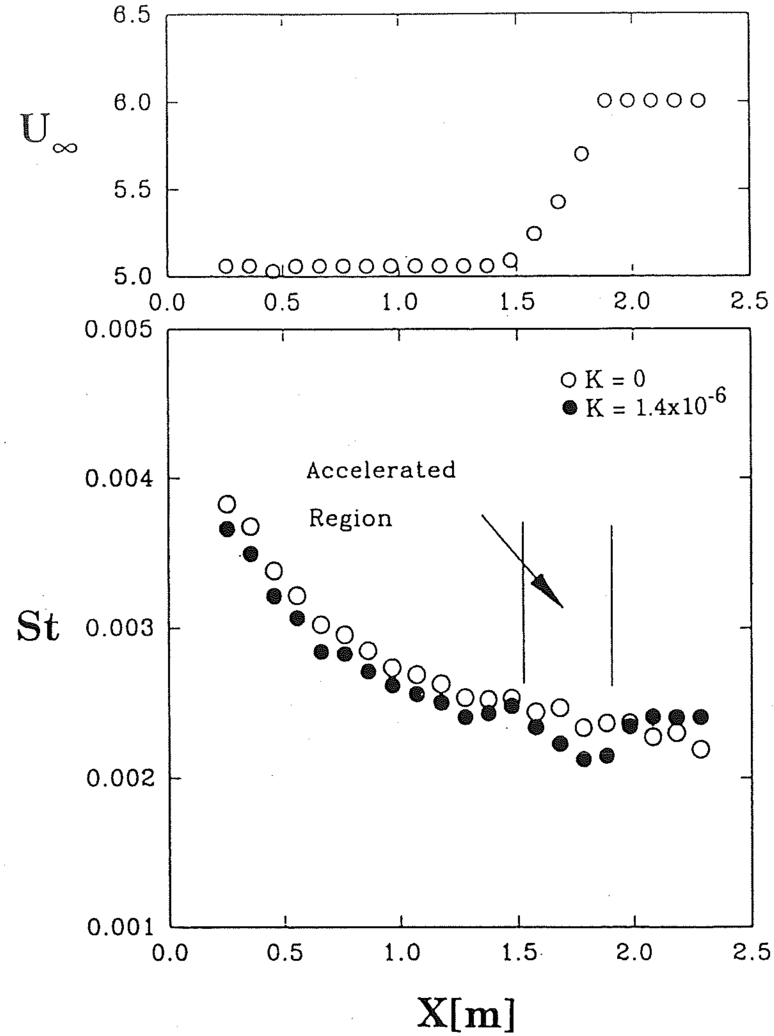

$K = 1.4 \times 10^{-6}$, $L/d_o = 4$, aerodynamically-smooth approaching flow

Mississippi State University

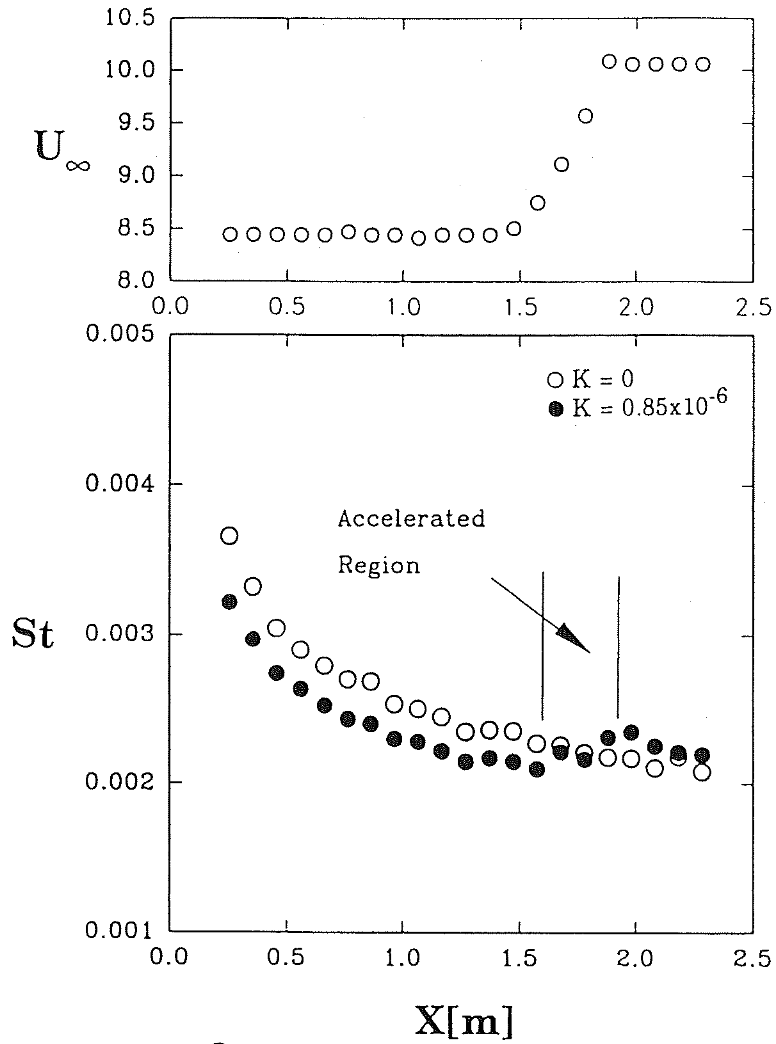

$K = 0.85 \times 10^{-6}$, $L/d_o = 4$, transitionally-rough approaching flow

Mississippi State University

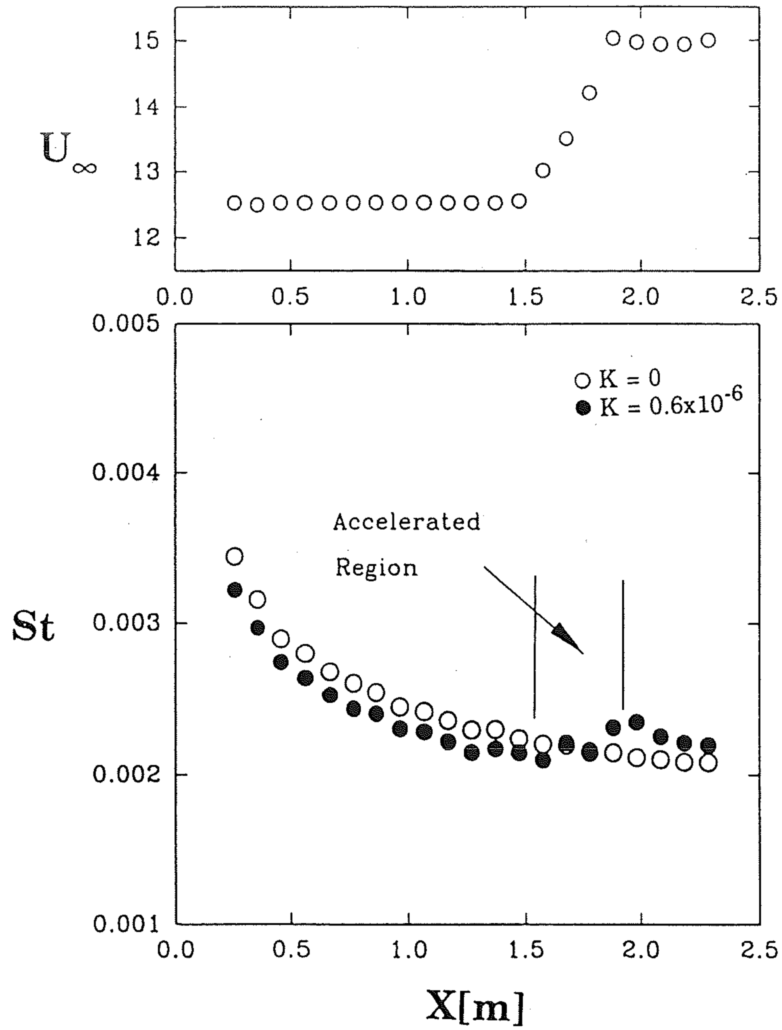

K = 0.6 X 10^{-6}, L/d_o = 4, transitionally-rough approaching flow

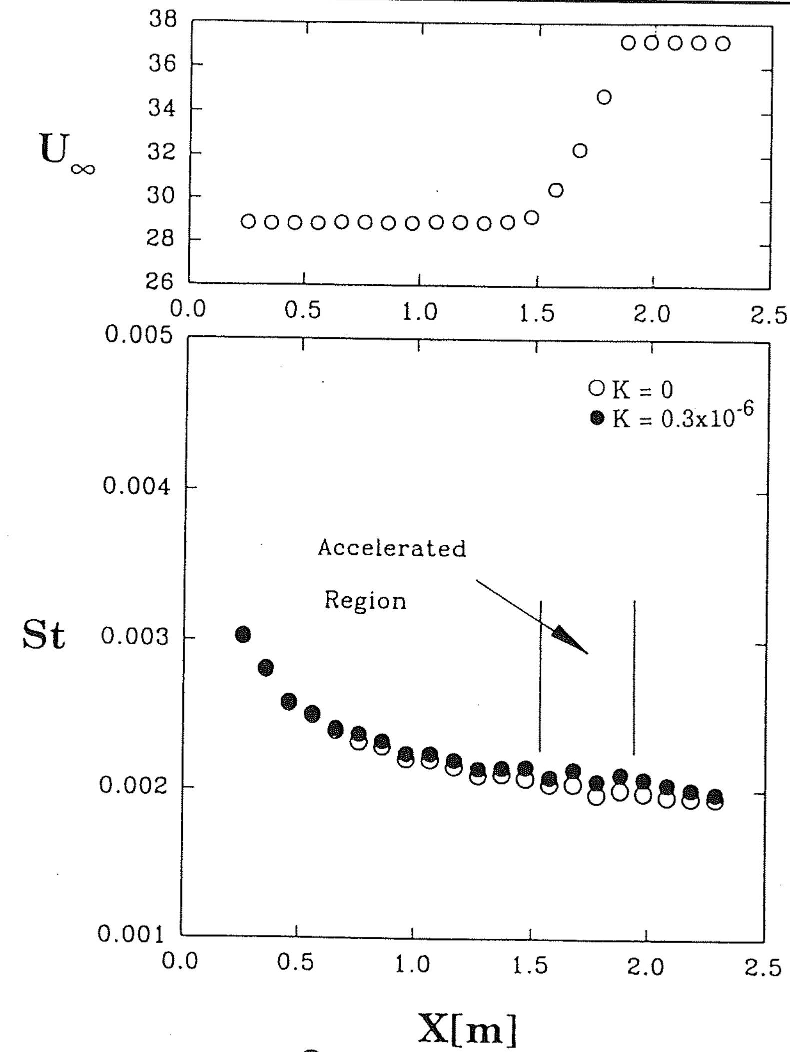

$K = 0.31 \times 10^{-6}$, $L/d_o = 4$, fully-rough approaching flow

Mississippi State University

FLUID-FLOW DATA

K X 10^6	U_∞ m/s	$L/d_o = 2$	$L/d_o = 4$
0.3	28	fully rough	fully rough
1.4	5	aero'ly smooth	aero'ly smooth

Roughness state based on the boundary layer conditions just upstream of the accelerated region.

Mississippi State UNIVERSITY

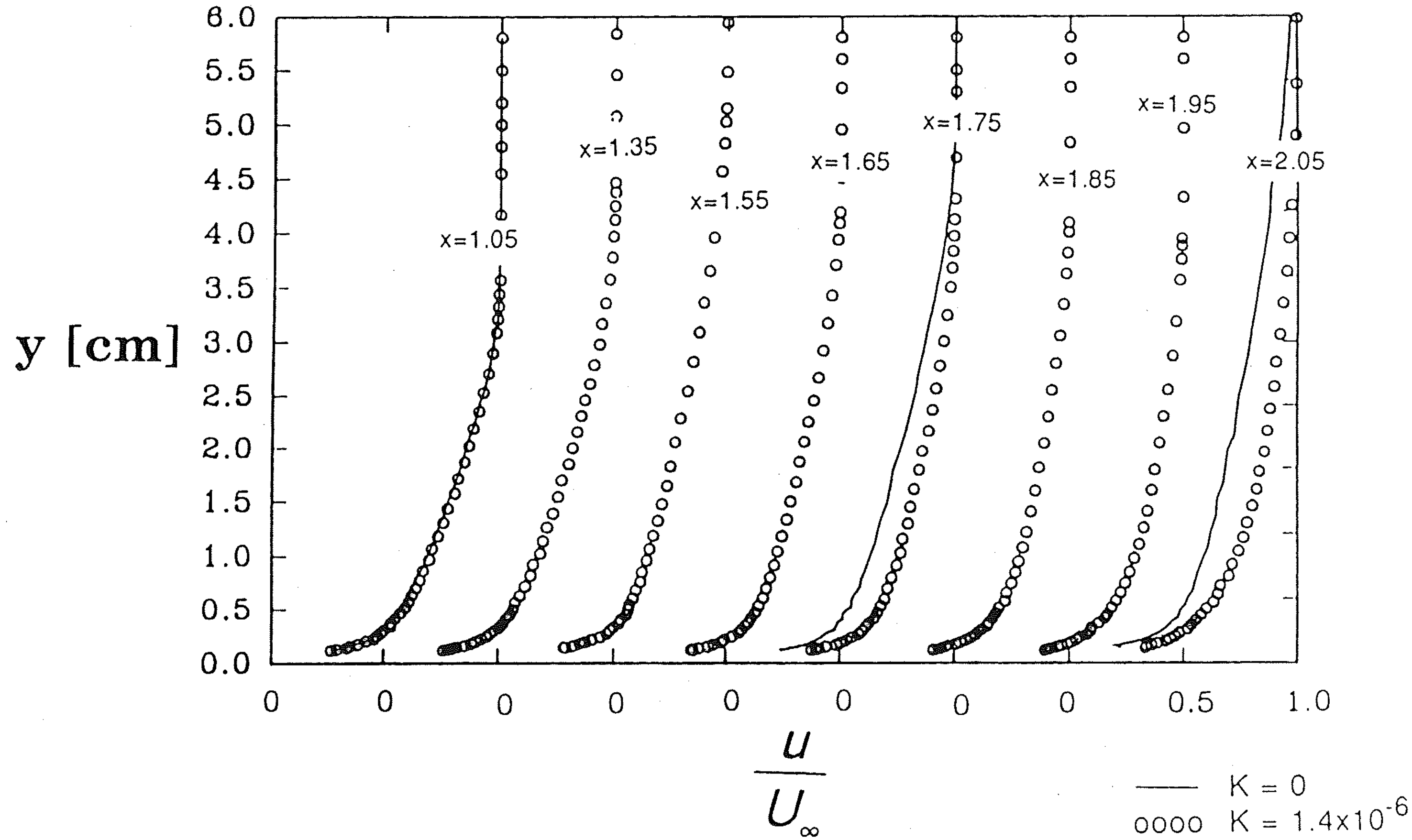

K = 1.4 X 10^{-6}, L/d_o = 2, aerodynamically-smooth approaching boundary layer

Mississippi State UNIVERSITY

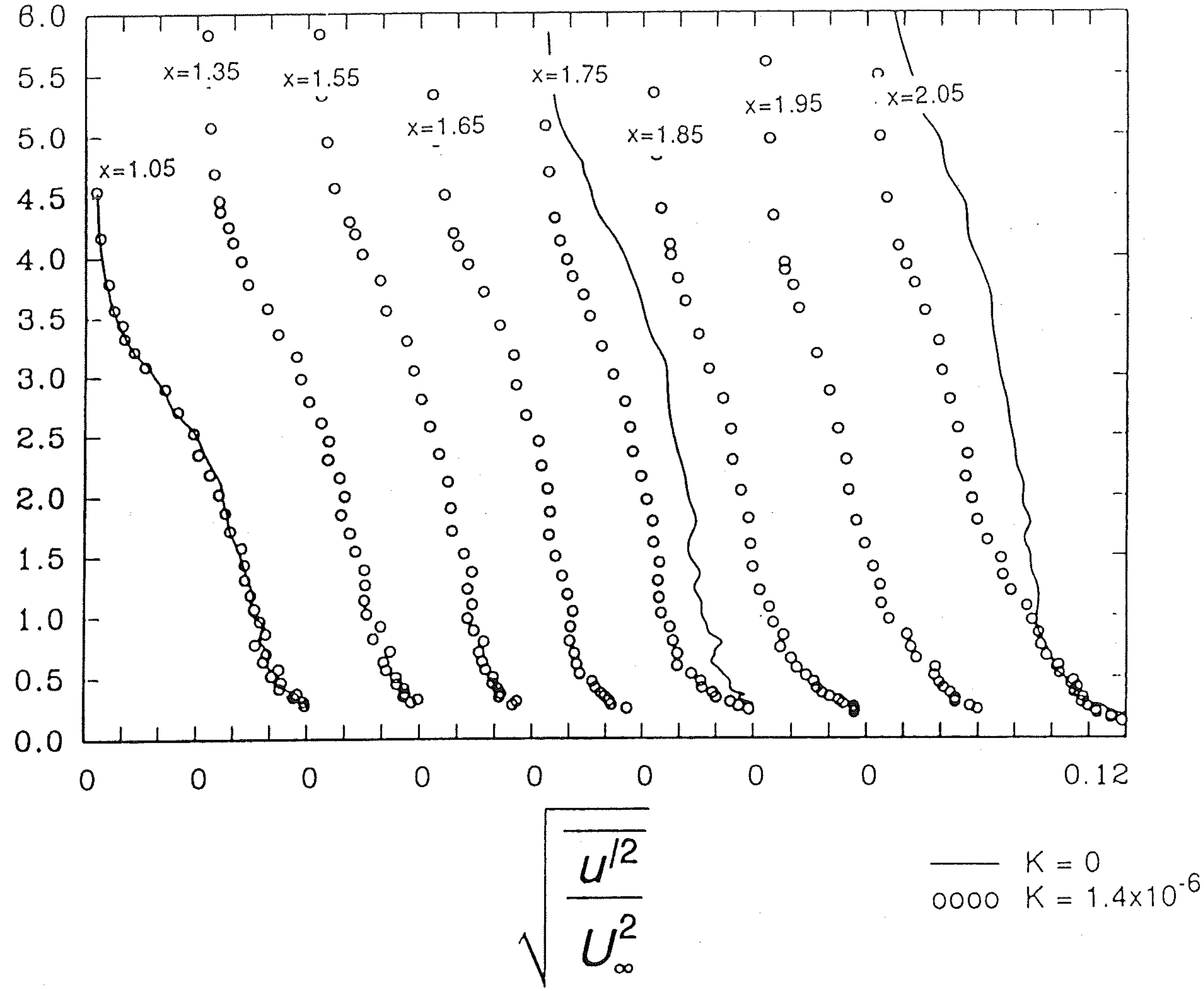

K = 1.4 X 10^{-6}, L/d$_o$ = 2, aerodynamically-smooth approaching boundary layer

Mississippi State University

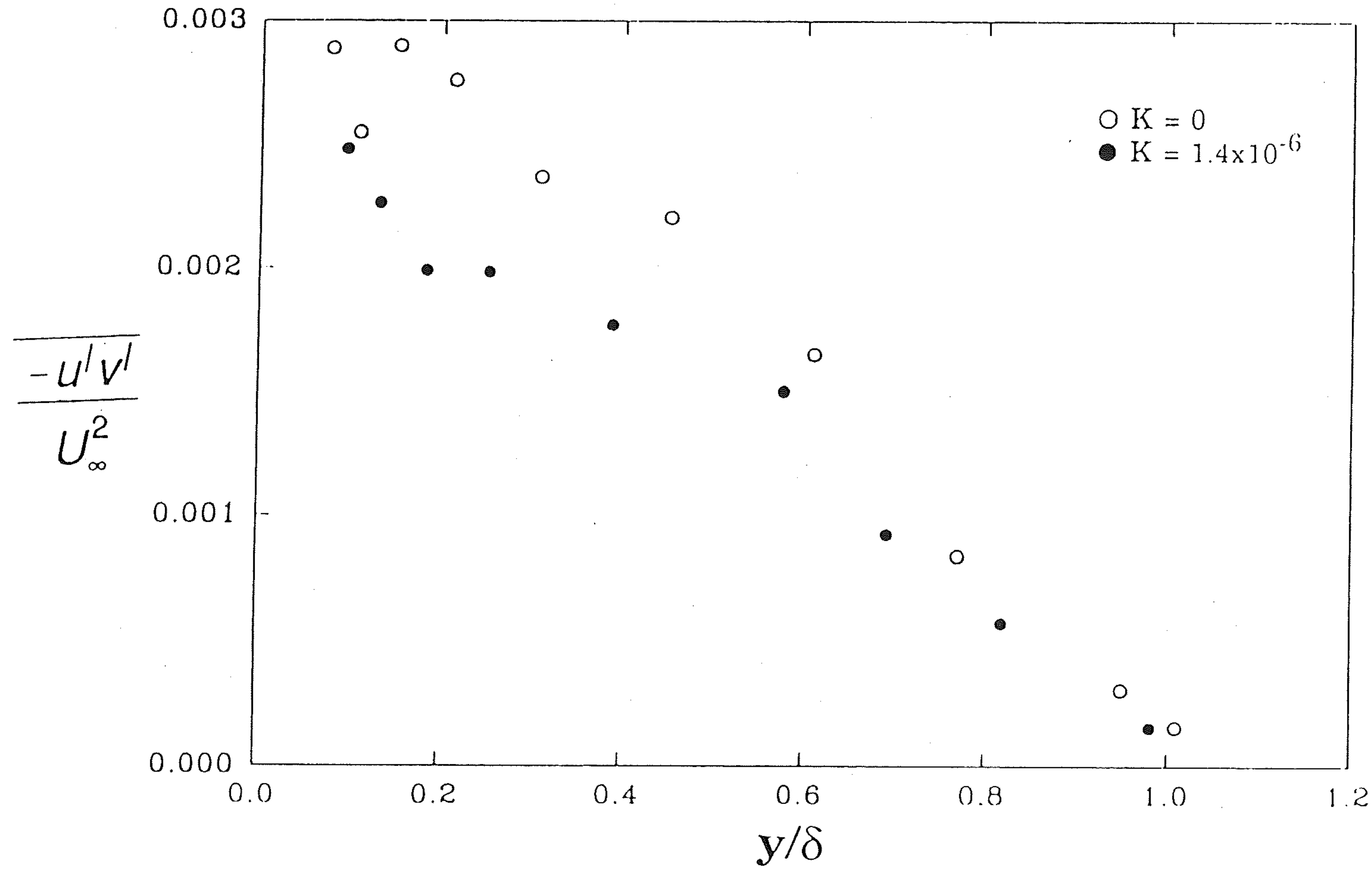

K = 1.4 X 10^{-6}, L/d$_o$ = 2, aerodynamically-smooth approaching boundary layer

Mississippi State University

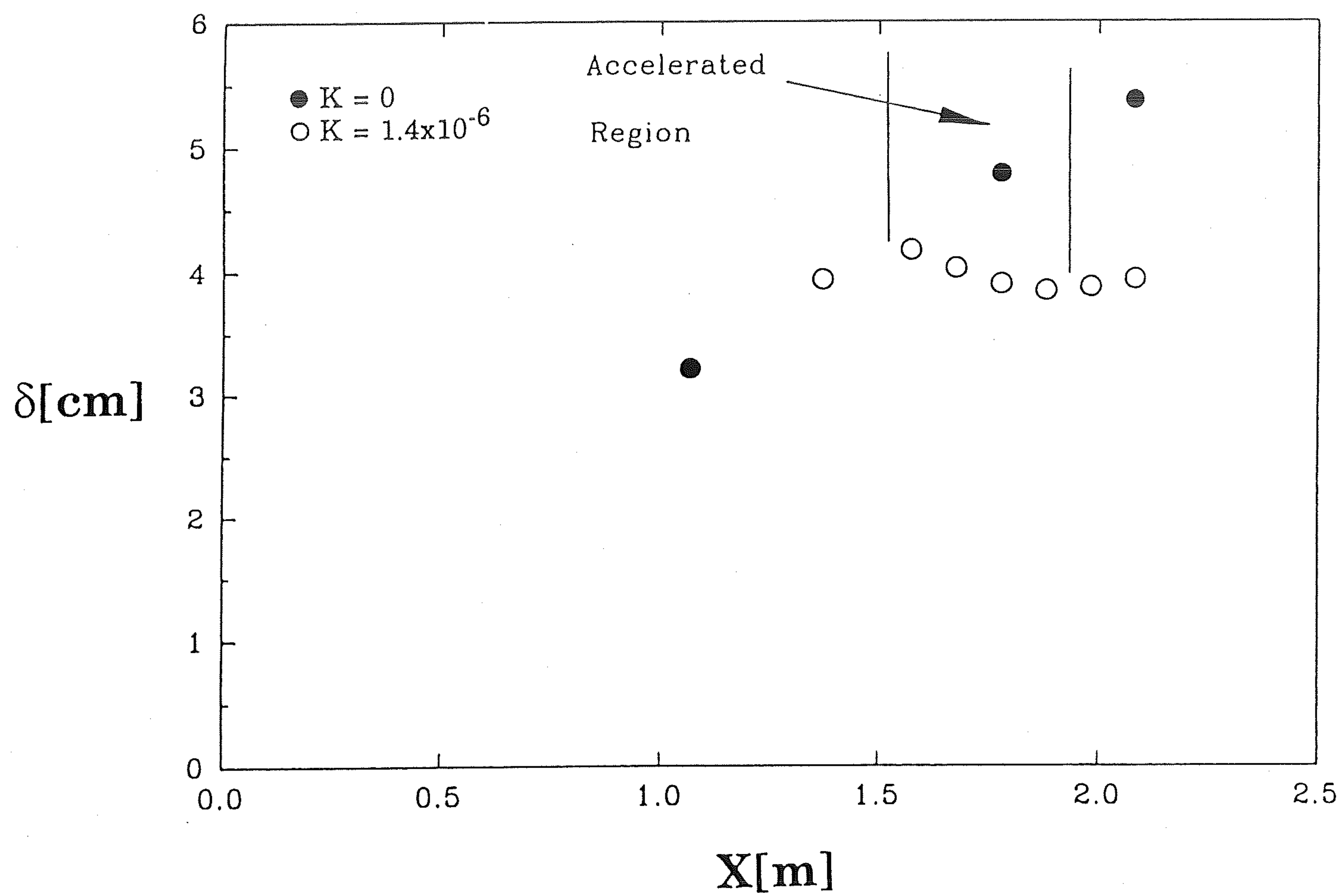

$K = 1.4 \times 10^{-6}$, $L/d_o = 2$, aerodynamically-smooth approaching boundary layer

Mississippi State University

CONCLUSIONS

- Stanton numbers for fully-rough boundary layers increase with acceleration compared to zero-pressure gradient boundary layers.
- For the flows considered, roughness effects increased in the region of acceleration, indicating flow regime trend toward a rougher state when accelerated.
- For aerodynamically-smooth and transitionally-rough flows the effect of acceleration is not seen immediately at the beginning of the accelerated region as it is for fully-rough flows; however, as the boundary layer thins under acceleration, the surface becomes relatively rougher resulting in a sharp increase in Stanton number.

Mississippi State University

CONCLUSIONS (Continued)

- After the acceleration, Stanton numbers return to the $K=0$ baseline case only for the fully-rough boundary layers. For the others, the Stanton numbers show a distinct shift indicating different roughness states upstream and down stream of the acceleration.

- Acceleration decreases the turbulent kinetic energy throughout the boundary layer for both the smooth and rough walls.

Mississippi State UNIVERSITY

REFERENCES

Chakroun, W., 1992, "Experimental Investigation of the Effects of Acceleration on Flow and Heat Transfer in the Turbulent Rough-Wall Boundary Layer," Ph. D. Dissertation, Department of Mechanical Engineering, Mississippi State University.

Coleman, H. W., 1976, "Momentum and Energy Transport in the Accelerated Fully Rough Turbulent Boundary Layer," Ph. D. Dissertation, Mechanical Engineering Department, Stanford University.

Kays, W. M. and Moffat, R. J., 1975, "The Behavior of Transpired Turbulent Boundary Layers," Report No. HMT-20, Thermosciences Division, Mechanical Engineering Department, Stanford University.

Mississippi State University

55-20
51380
132102
18p

Computational and Experimental Efforts in Gravity Probe B Microthruster Analysis

Gravity Probe B, an experiment to test the theory of relativity, will be launched near the turn of the millennium. Due to the precise pointing requirements needed to successfully carry out this experiment, the satellite will use sixteen proportionally controlled microthrusters as a main component of the attitude control system. These microthrusters use the helium boil-off from the on-board dewar as propellant.

Marshall Space Flight Center, overseeing the project, verified the design of the thruster flow path by both computational and experimental methods. The flow performance of the thruster has been adequately characterized. Graphs show specific impulse, thrust coefficient, discharge coefficient, and mass flow rate trends. Value was added to the program through gained confidence in the design of the thruster and through evaluation of some design trade-offs.

This work may be valuable in the future due to the possible need of small thrusters on spacecraft that have precise pointing requirements.

Computational and Experimental Efforts in Gravity Probe B Microthruster Analysis

Alan Droege and Andrew Smith
NASA/MSFC

James Carter
Dynamic Engineering, Inc.

April 26, 1995

Presented at Workshop for Computational
Fluid Dynamic Applications in Rocket Propulsion
and Launch Vehicle Technology

Computational and Experimental Efforts in GPB Microthruster Analysis

Background

- **Gravity Probe B (GPB)**
  - A satellite borne relativity experiment
  - Requires precise pointing control and acceleration free environment to be provided by attitude control system

- **Microthrusters**
  - Helium gas from dewar boiloff used as propellant
  - Sixteen microthrusters on spacecraft; used for orbit trim, spin-up, spin-down, and attitude control
  - Concerns about mission lifetime and control saturation

Objectives

- **Verify design of microthruster**
  - Thrust
  - Specific Impulse
- **Gain knowledge about the physics of rarefied thruster flows**
  - In the future, this size of thruster may become more common on spacecraft, due to:
    - » extremely tight spacecraft attitude control requirements
    - » use of large liquid helium dewars

Method

Direct Simulation Monte Carlo (DSMC):

Limits on areas of application

Slow - not useful for large parametric studies

Works well for low Reynolds number flows, costly to use for higher Reynolds number flows

Gives good characterization of the flowfield

Experiment:

Covers all of the flowfield

Very fast once hardware is in place useful for parametric studies, useful for assessment of configuration change

Possible data scatter at low Reynolds numbers, but works well for higher Reynolds number flows

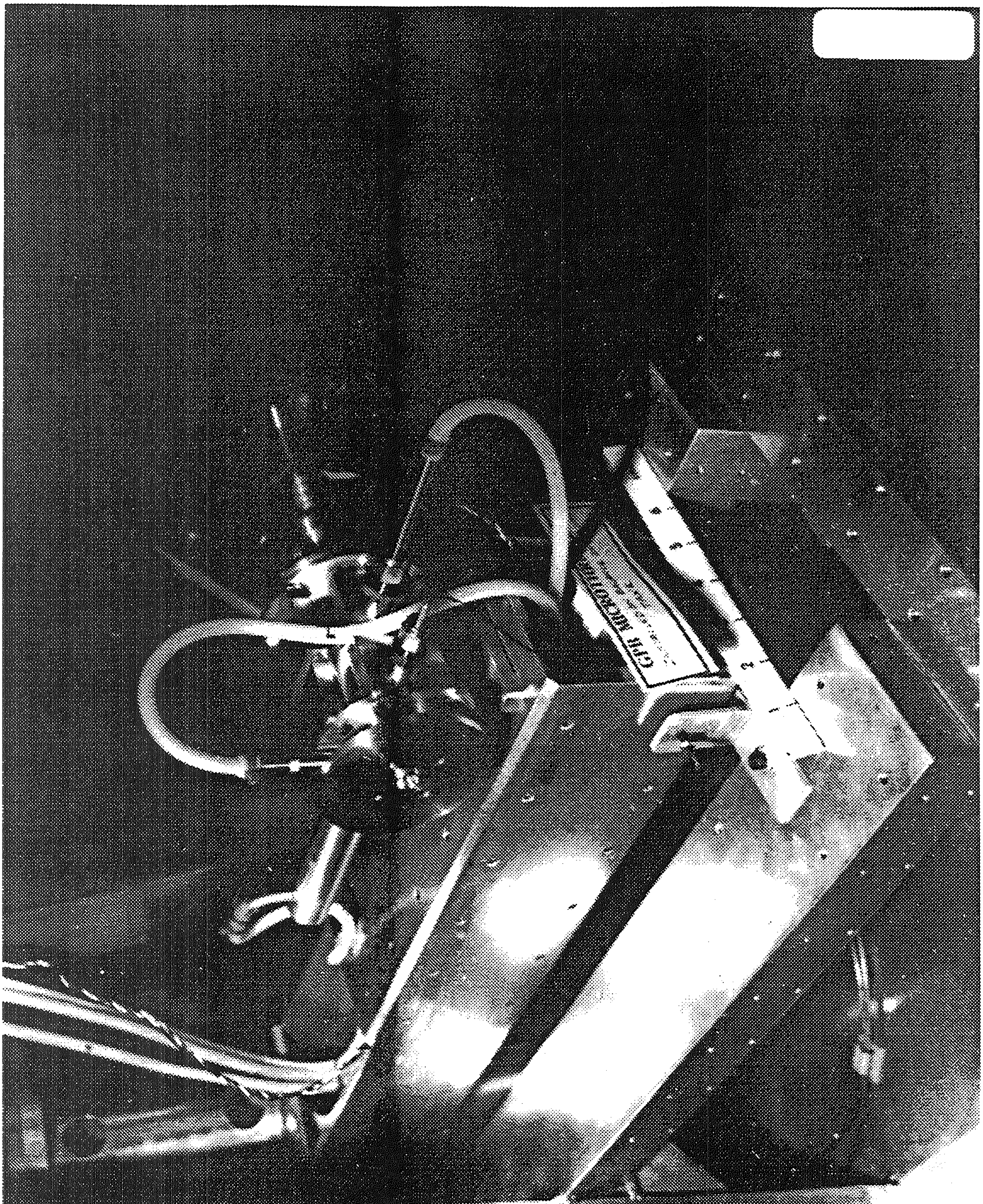

Results

- **Requirements:**
  - Thrust $\geq$ 8 mN at $P_{inlet} \geq$ 9.7torr and mass flow $\leq$ 1.52E-05 lbm/s
  - Thrust $\leq$ 0.05 mN at $P_{inlet} \leq$ 12.5 torr and mass flow $\leq$ 9.48E-07 lbm/s
  - Thrust $\geq$ 2.55 mN at $P_{inlet} \geq$ 4.2 torr and mass flow $\leq$ 4.85E-06 lbm/s

- **Microthruster Characterization**
  - Thrust
  - I_{sp}

- **Added Value**
  - Conical Nozzle vs. Sharp Edged Orifice
  - Analysis of change in piston and valve seat design

National Aeronautics and
Space Administration

Computational and Experimental Efforts in GPB Microthruster Analysis

Computational Fluid Dynamics Branch
Fluid Dynamics Division
Structures and Dynamics Laboratory
George C. Marshall Space Flight Center

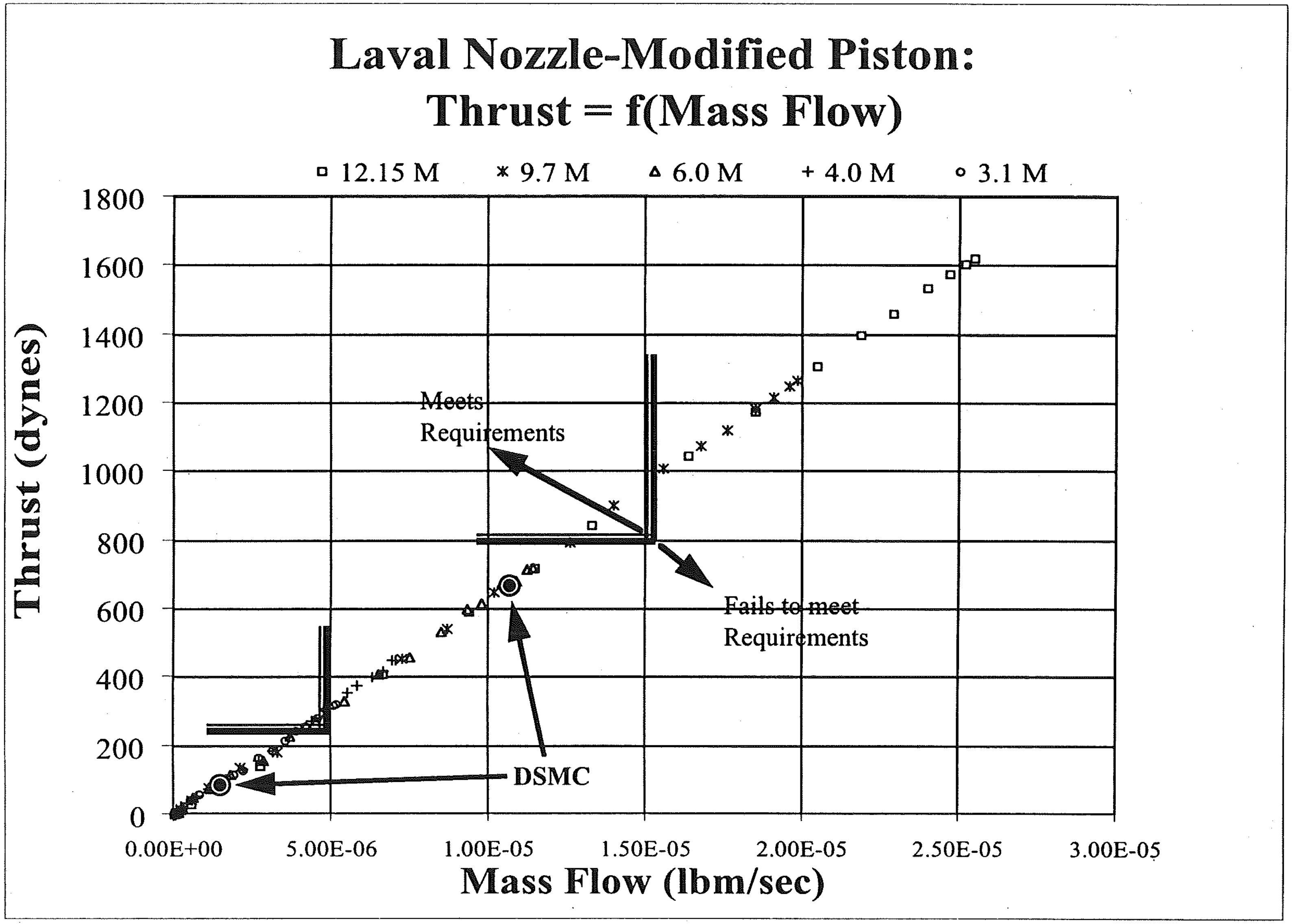

National Aeronautics and
Space Administration

Computational and Experimental Efforts in GPB Microthruster Analysis

Computational Fluid Dynamics Branch
Fluid Dynamics Division
Structures and Dynamics Laboratory
George C. Marshall Space Flight Center

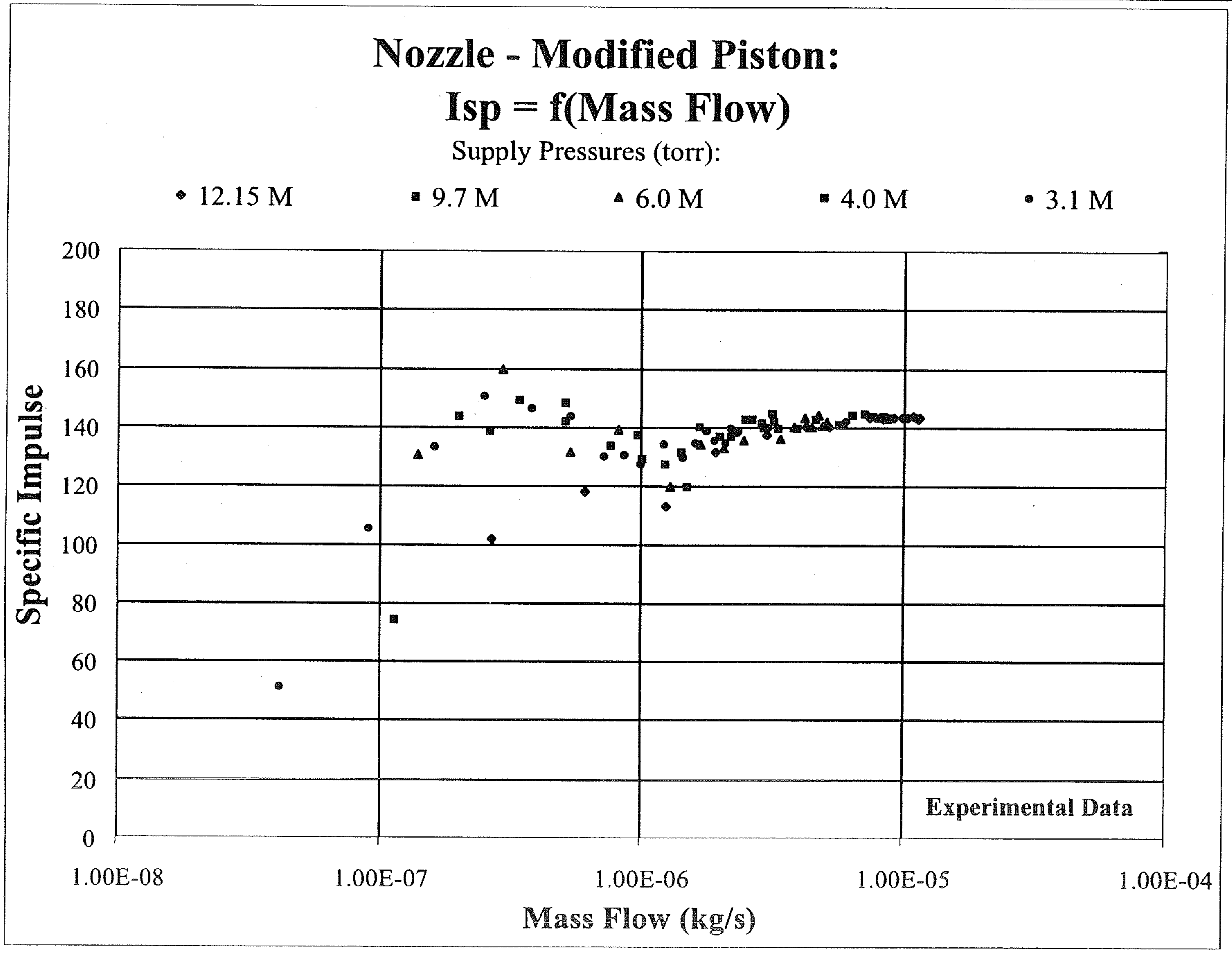

DSMC Calculation of Specific Impulse

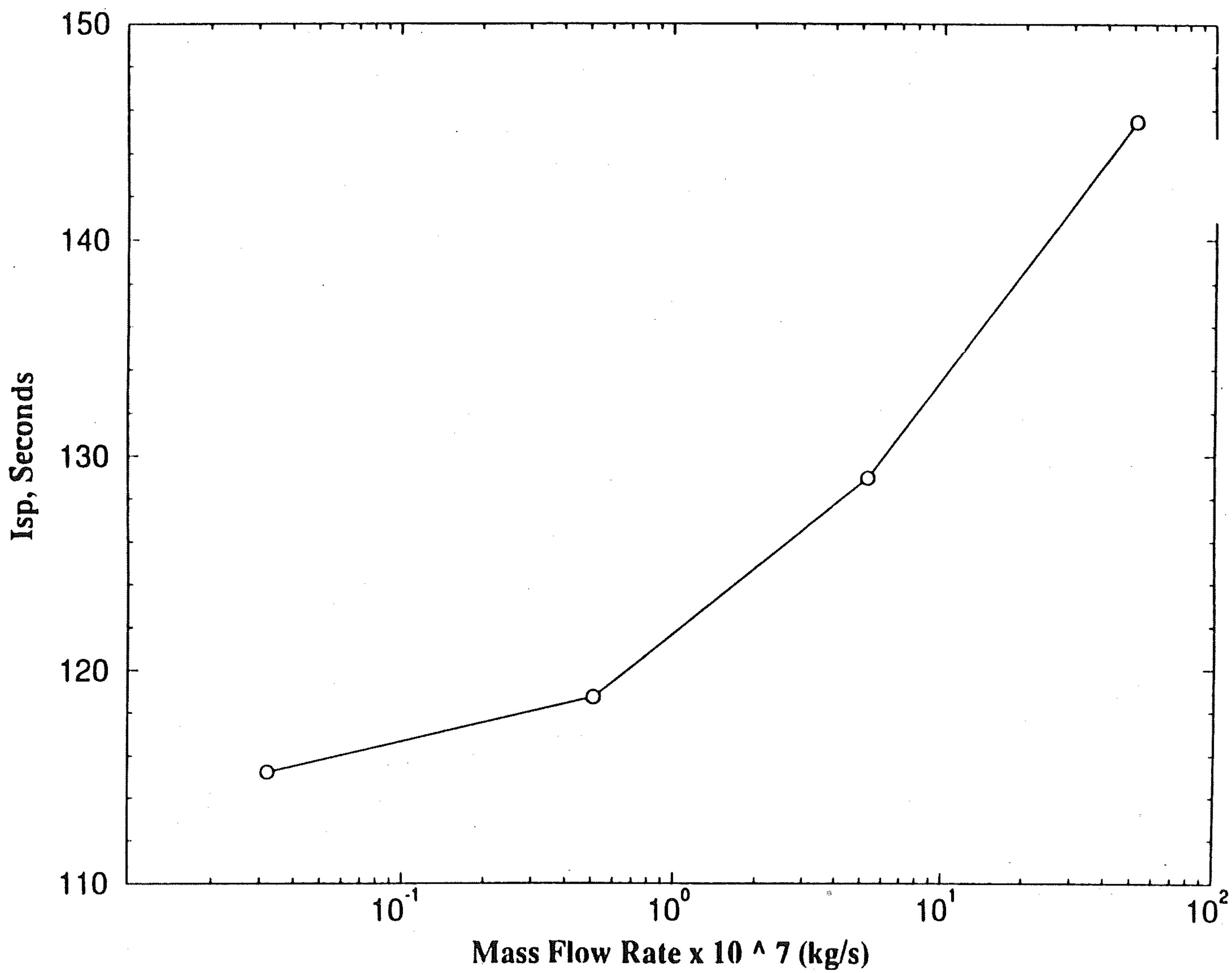

National Aeronautics and Space Administration

Computational and Experimental Efforts in GPB Microthruster Analysis

Computational Fluid Dynamics Branch
Fluid Dynamics Division
Structures and Dynamics Laboratory
George C. Marshall Space Flight Center

Grid for Stanford Nozzle

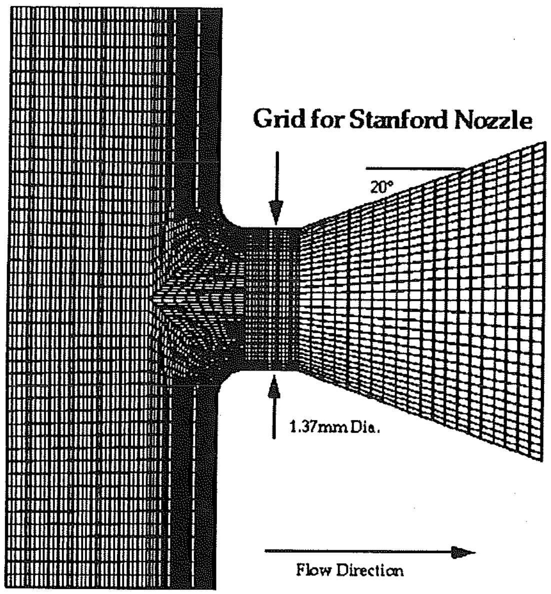

Typical Grid for MSFC A2 Nozzle

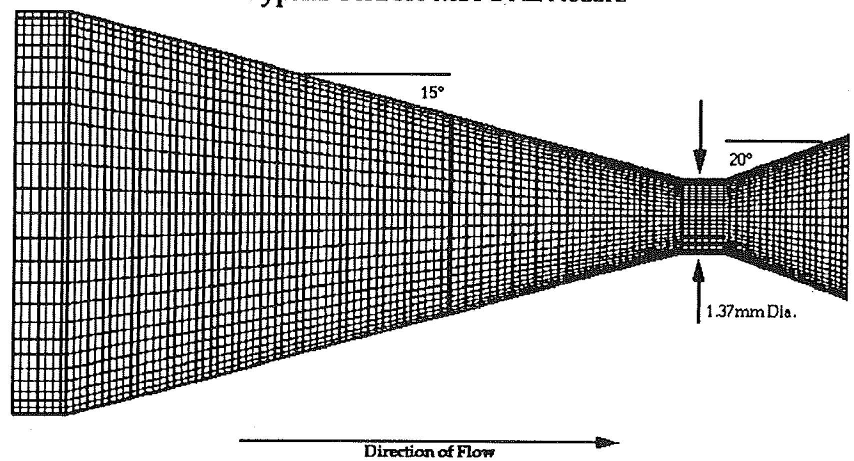

Note: Grids are not on the same scale

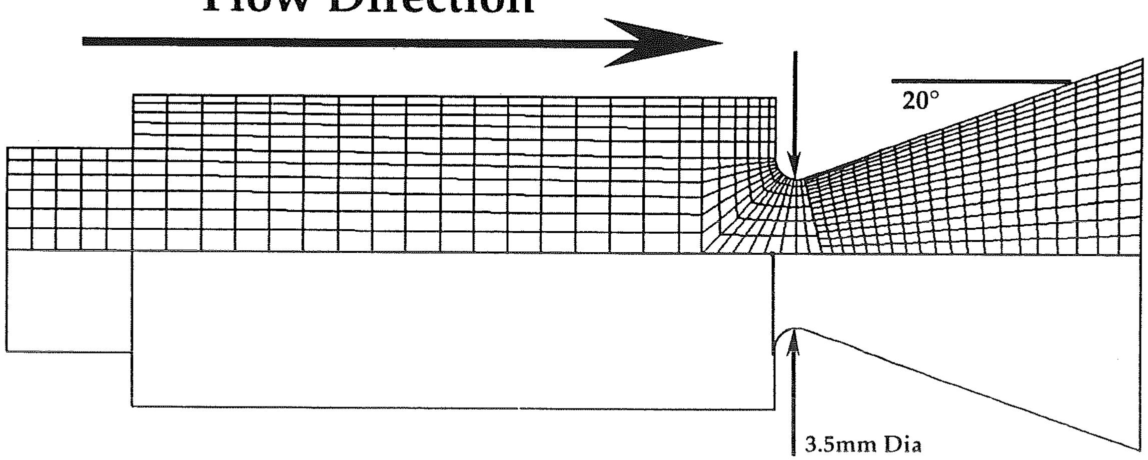

Grid / Geometry for Flight Nozzle

GP-B MODEL INSTRUMENTATION

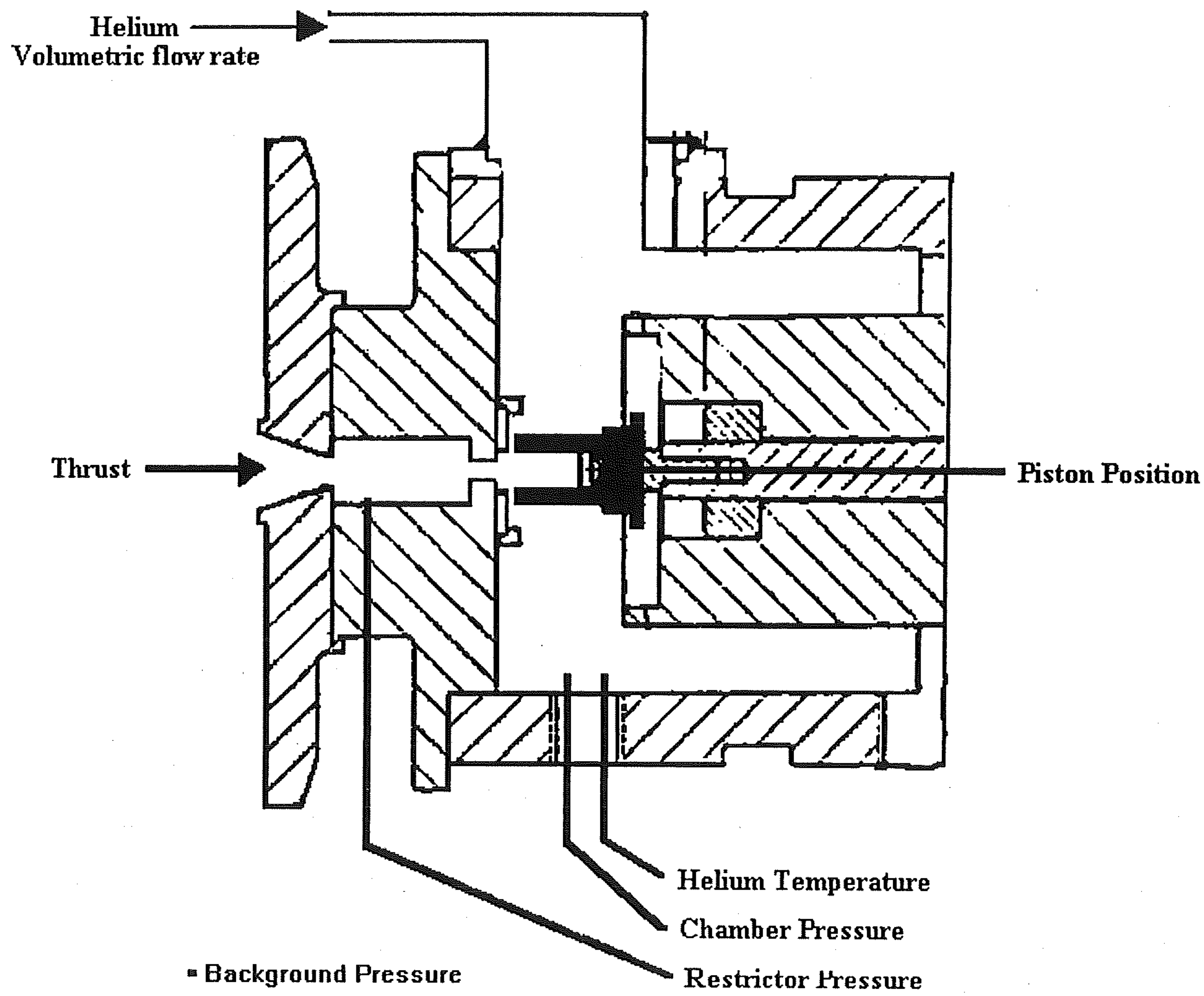

National Aeronautics and
Space Administration

Computational and Experimental Efforts in GPB Microthruster Analysis

Computational Fluid Dynamics Branch
Fluid Dynamics Division
Structures and Dynamics Laboratory
George C. Marshall Space Flight Center

Contributions of the Nozzle Bell and the Cylindrical Throat to the MSFC A2 Configuration Total Thrust

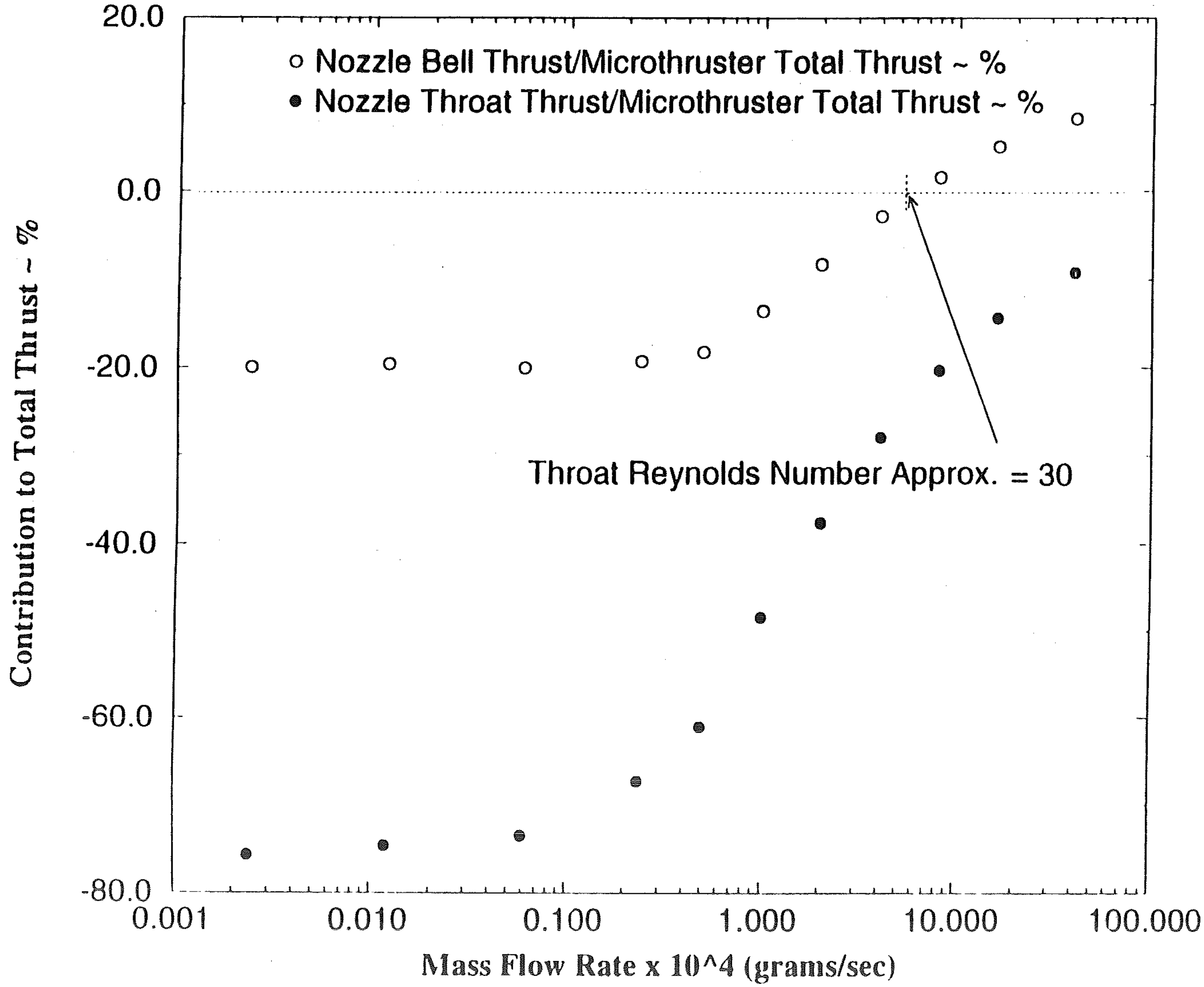

Computational and Experimental Efforts in GPB Microthruster Analysis

Computational Fluid Dynamics Branch
Fluid Dynamics Division
Structures and Dynamics Laboratory
George C. Marshall Space Flight Center

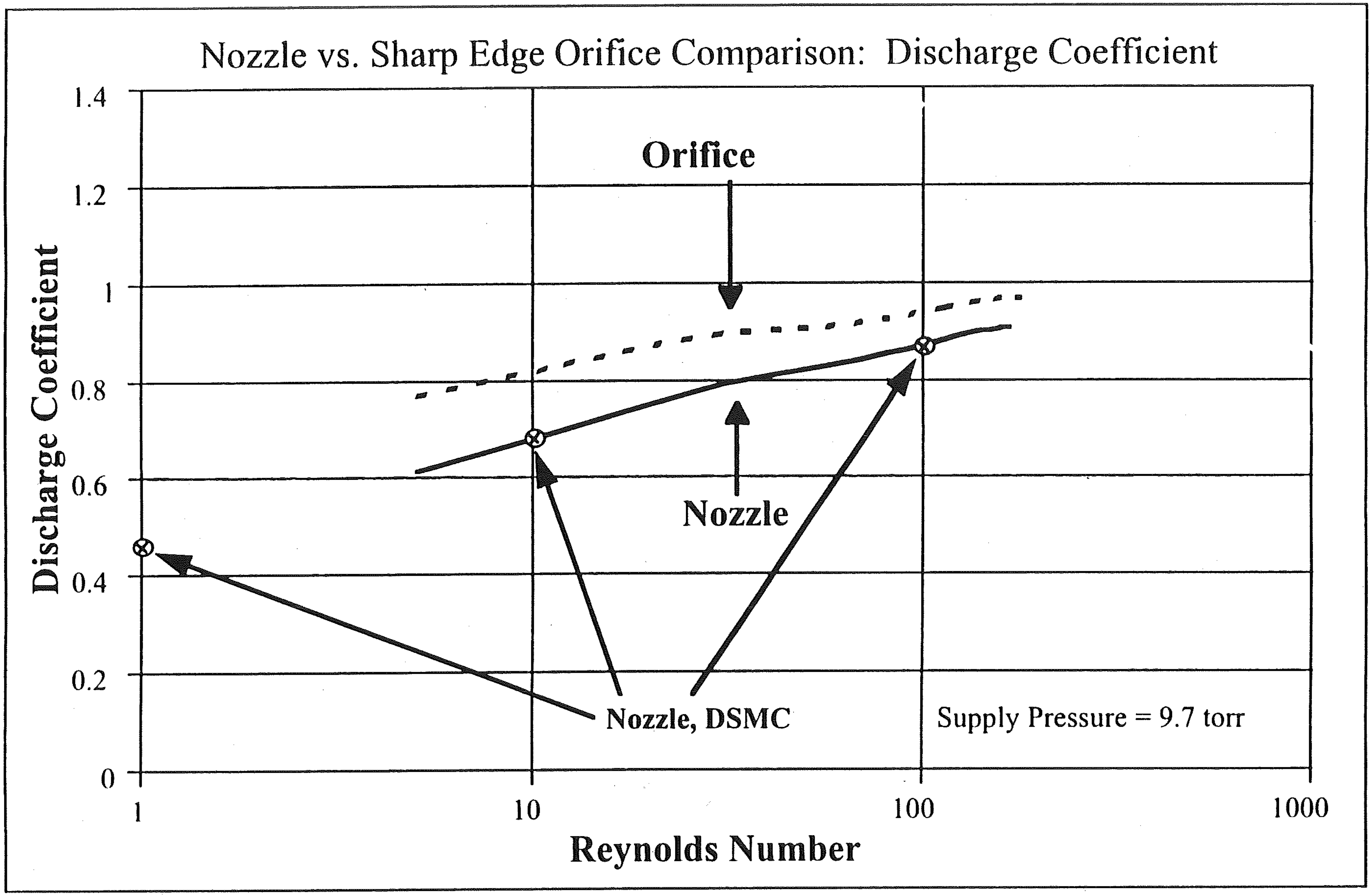

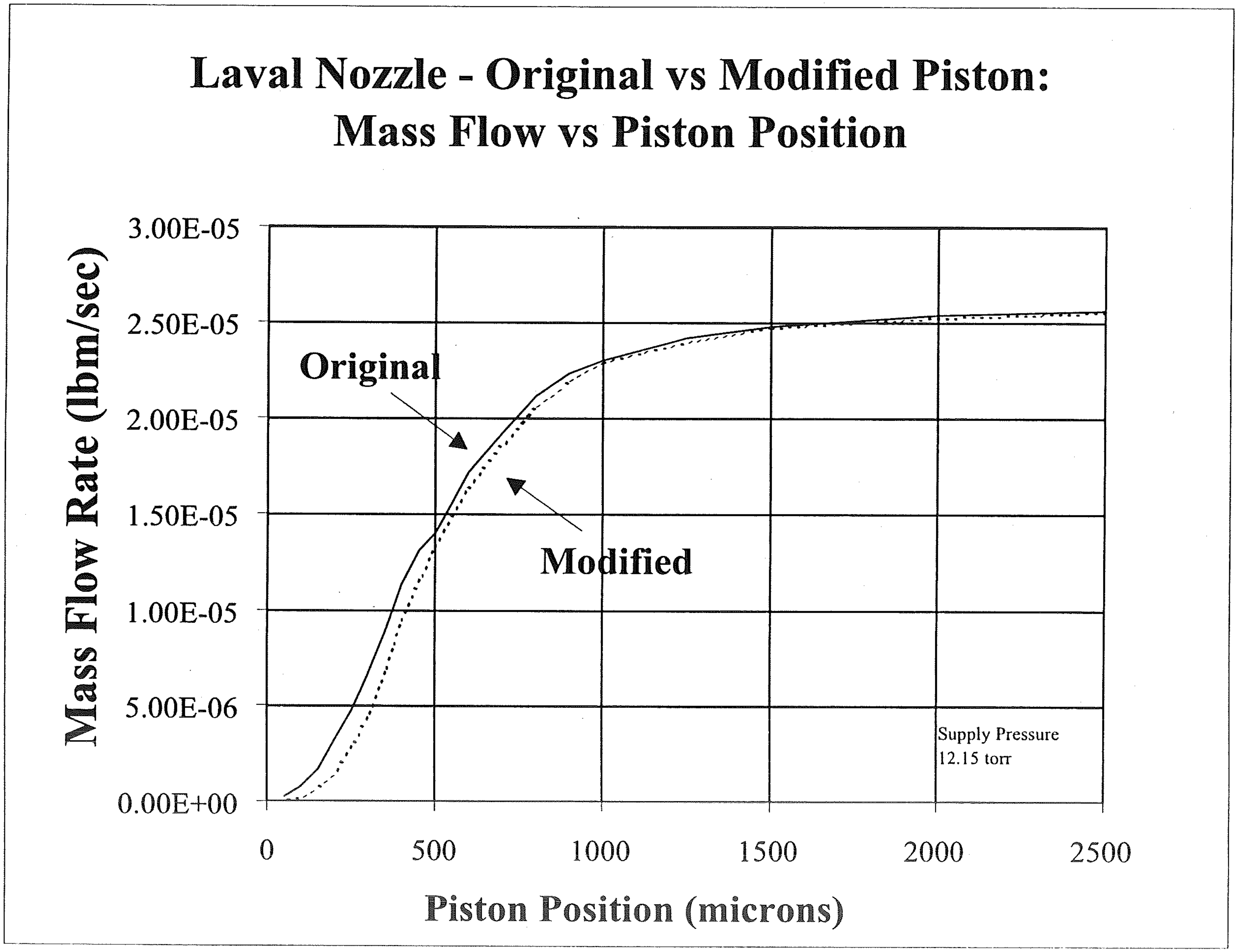
Laval Nozzle - Original vs Modified Piston:
Mass Flow vs Piston Position
Mass Flow Rate (lbm/sec)
3.00E-05
2.50E-05
2.00E-05
1.50E-05
1.00E-05
5.00E-06
0.00E+00
Original
Modified
Supply Pressure
12.15 torr
0
500
1000
1500
2000
2500
Piston Position (microns)

Computational and Experimental Efforts in GPB Microthruster Analysis

Computational Fluid Dynamics Branch
Fluid Dynamics Division
Structures and Dynamics Laboratory
George C. Marshall Space Flight Center

Nozzle vs. Sharp Edge Orifice Comparison: Thrust Coefficient

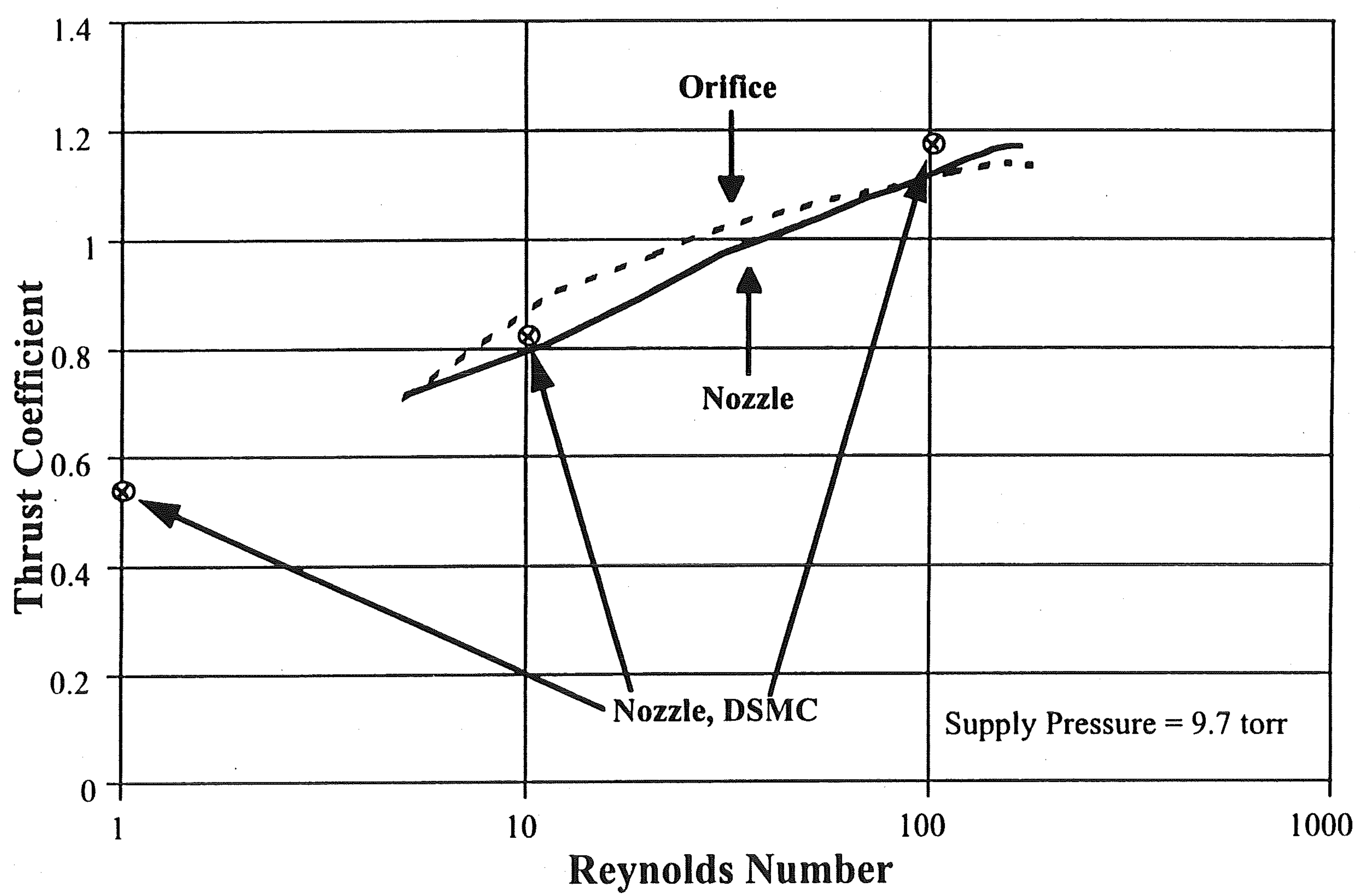

Conclusions

- Thruster meets or exceeds requirements
- Specific Impulse varies over operating range
- Current nozzle design is adequate throughout operating range
- Change in piston/valve seat increased flow resistance through the thruster

Future Work

- **DSMC**
  - Plume characterization and comparison with experiment
  - Plume impingement on spacecraft
- **Experimental**
  - Possible re-run of experiment with highly sensitive force balance in order to eliminate data scatter at low Reynolds numbers
- **Both**
  - Write detailed NASA Tecnical Memos or Technical Papers

56-34
57381
22p
132103

Subject: A parametric study of a plug nozzle, using the Liquid Propellant Program (LPP) Code

By: Stuart S Dunn, Douglas E Coats, Software and Engineering Associates, Inc.

Abstract

The Liquid Propellant Program (LPP) computer code is a super-set of the industry standard Two Dimensional Kinetics (TDK) computer code, which has been developed by Software and Engineering Associates, Inc. (SEA, Inc.) over the past twelve years. The TDK code uses a Two-Dimensional Method of Characteristics solution with fully coupled finite rate kinetics for axially symmetric nozzles. The chemical reactions are modeled with a generalized reaction package that includes 3rd body efficiencies and four reaction rate forms. The code performs optional solutions for frozen or equilibrium flow. TDK evaluates discrete shocks, both attached or induced. The Transonic module models variable mixture ratio profiles from the combustion chamber injector. The Mass Addition Boundary Layer module (MABL) calculates the boundary parameters with the same chemistry options, and includes transpiration or tangential slot injection of gas at the wall.

The LPP upgrades include: planar nozzles, scarfed nozzles, plug nozzles, and scramjet nozzle configurations. The code evaluates both upper and lower wall flow simulation, and includes the interaction with the external flow. The MABL module evaluates equilibrium radiation heat transfer for both upper and lower walls. In addition, the LPP code models combustion effects due to injector inefficiencies with the Spray Combustion Analysis Program (SCAP) module. The LPP package provides extensive post plotting capabilities for flow visualization. The LPP is sufficiently fast and robust to provide performance predictions for extensive parametric studies and sufficiently accurate to provide flow field and performance solutions for detailed studies.

The evaluation of a planar or axially symmetric plug nozzle has received recent interest due to the SSTO studies. The LPP code allows easy modeling of a plug nozzle configuration, since the user is allowed to input an arbitrary inner and outer wall geometry (referred to as the plug and the cowl). The transonic analysis models both planar or axially symmetric annular flow, including straited and variable mixture ratio profiles. When the internal flow reaches the exit of the outer wall, a Prandtl-Meyer fan allows the flow to expand to the external pressure. At this point, a pressure boundary condition is applied for either quiescent sub-sonic, or super-sonic external flow. The MABL analyses is subsequently performed to evaluate the boundary layer losses for both the inner and outer walls. Following JANNAF standard procedures, the characteristic analysis is automatically repeated with the boundary layer compensated wall geometry.

The above procedure was employed to parametrically evaluate the performance of several plug nozzle configurations at different flight conditions. The altitude compensating effects are evaluated and related to ideal conventional nozzle performance. An optimization technique is presented, which includes chemistry, divergence, and boundary layer effects. Graphical output includes flow field contours, and wall property profiles.

Plug Nozzle Parametric Study Using The Liquid Performance Program (LPP)

Stuart S. Dunn and Douglas E. Coats

Software and Engineering Associates, Inc.
333 S. Carson Meadows, Suite 44
Carson City, NV 89701
702-882-1966

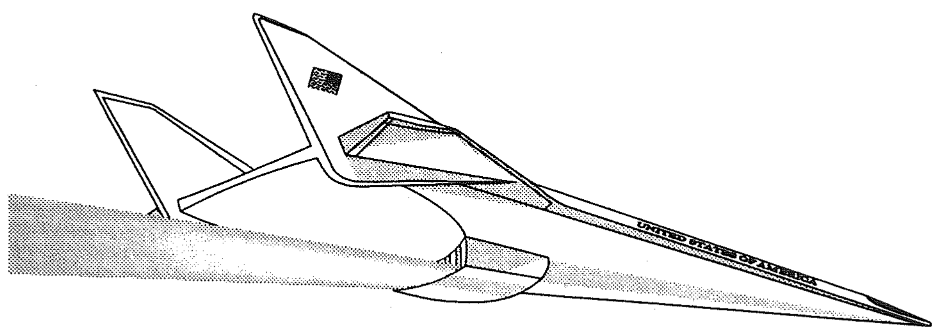

OUTLINE

- WHAT IS LPP
- PLUG NOZZLE DESCRIPTION
- LPP PLUG NOZZLE CAPABILITY
- EFFECT OF INLET AND COWL GEOMETRY ON PERFORMANCE

WHAT IS LPP?

The Liquid Performance Program (LPP) is a Super Set of the JANNAF TDK Code.

- Liquid Rocket Engine Performance
- Scramjets
- Plug and Aerospike Nozzles
- Efficient MOC Solver, Can Model Actual or Boundary Layer Displaced Walls Automatically
- Finite Rate and Equilibrium Chemistry
  - 3 different types of reactions including a global first order type
  - generalize symbolic reactions

WHAT IS LPP? (Continued)

- Mass Addition Boundary Layer
  - Models Wall Equilibrium Radiation Heat Transfer
  - Calculates Boundary Layers On Both Upper and Lower Walls
  - Tangential Slot Injection or Transpiration Cooling
- Planar and Axisymmetric Flow
  - Handles External Flow Interactions

WHAT IS LPP? (Continued)

- Spray Combustion Module
- Standard Plume Flowfield (SPF) and Rao Optimum Nozzle Linkage
- Pre and Post Processors

Plug Nozzles

- Characteristics
  - Center Body
  - Short Nozzle Configuration
  - Automatic Altitude Compensating
  - Complex Structure
  - Difficult To Cool

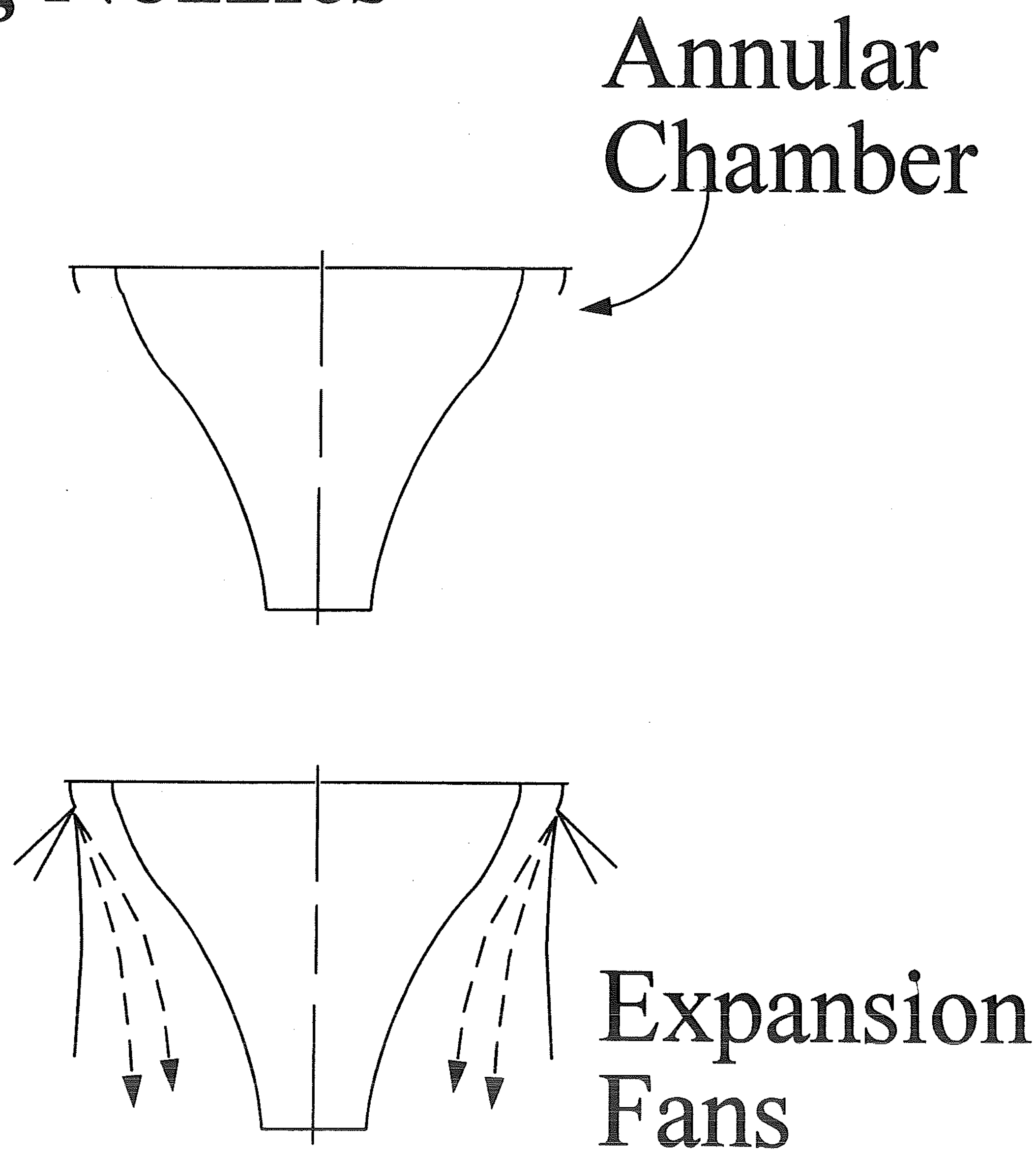

Flow Characteristics

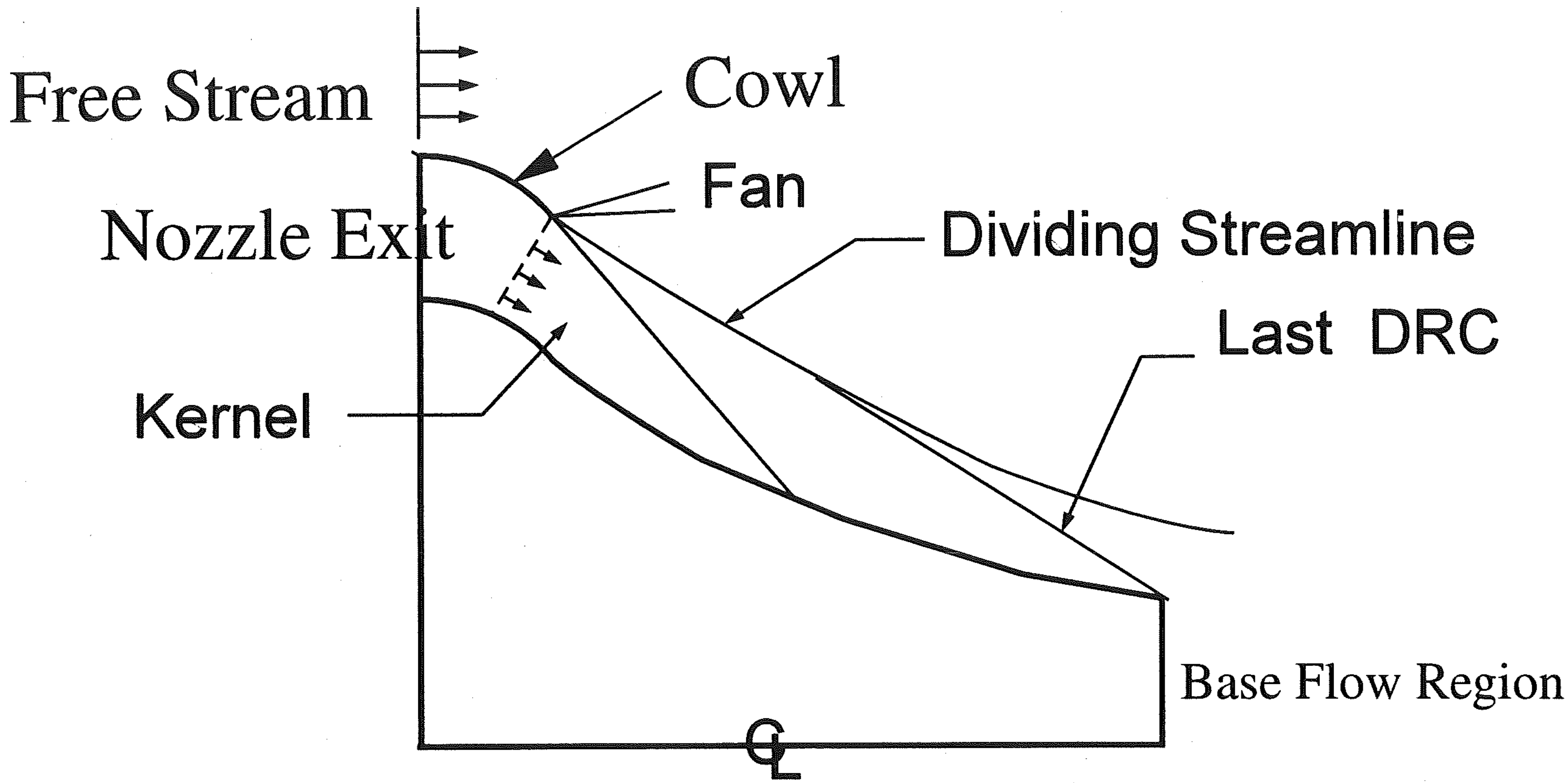

LPP Plug Nozzle Capability

- 2D or Axisymmetric Flow
- External Flow Modeled With Newtonian Pressure Boundary
- Boundary Layer Computed On Both Upper and Lower Walls
- Base Flow Region Not Modeled

SSTO Base Line Plug Nozzle

- 1,000,000 lbf Thrust Class
- 2630 psia Chamber Pressure
- Annular Nozzle With 50 psia Exit Pressure and Mach 3 Flow
- L H2 - L O2 Propellants at an O/F=6

Isp Variation With Inlet Angle

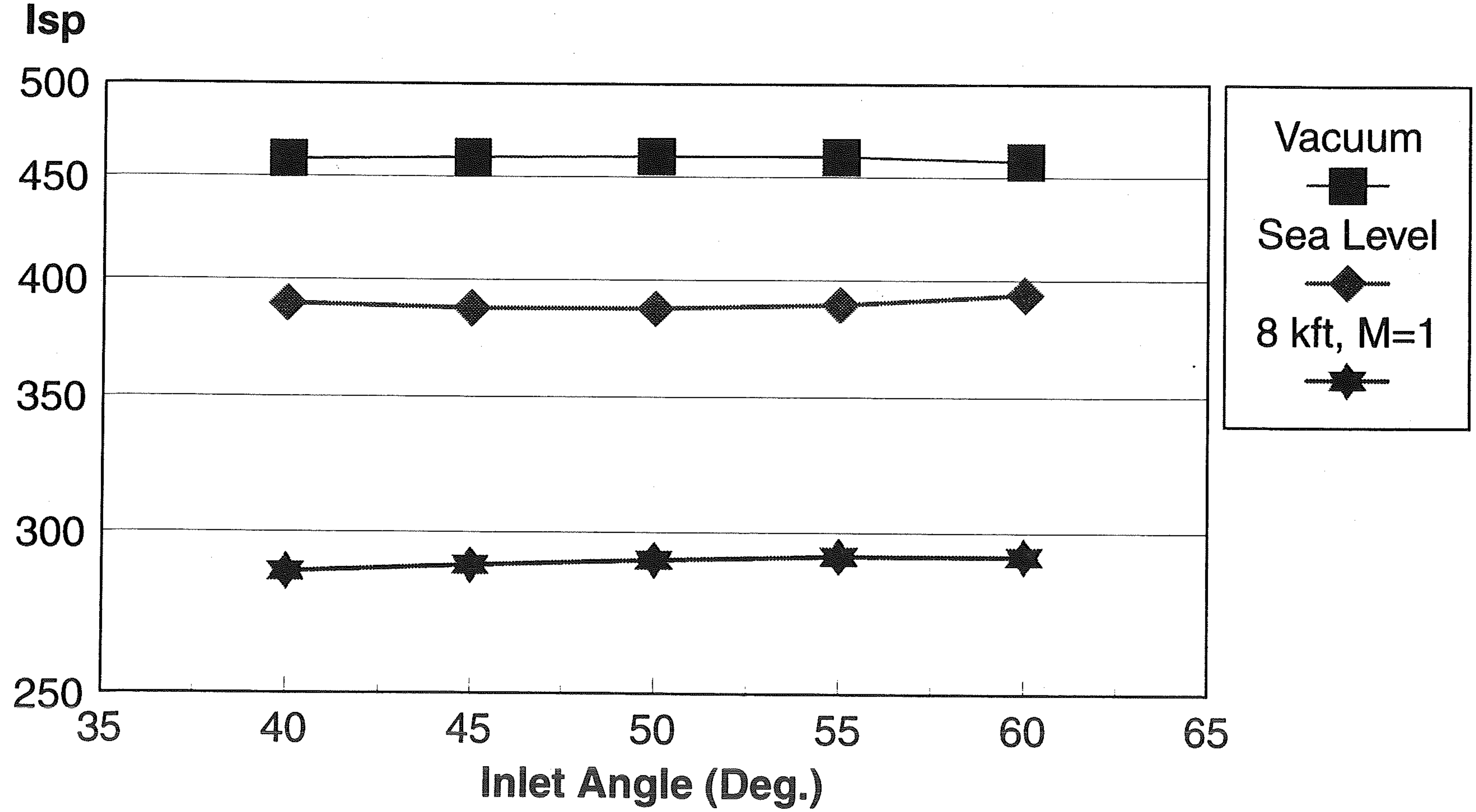

SEA 4-26-95/13 th Propulsion CFD Workshop

Isp Variation With Cowl Length

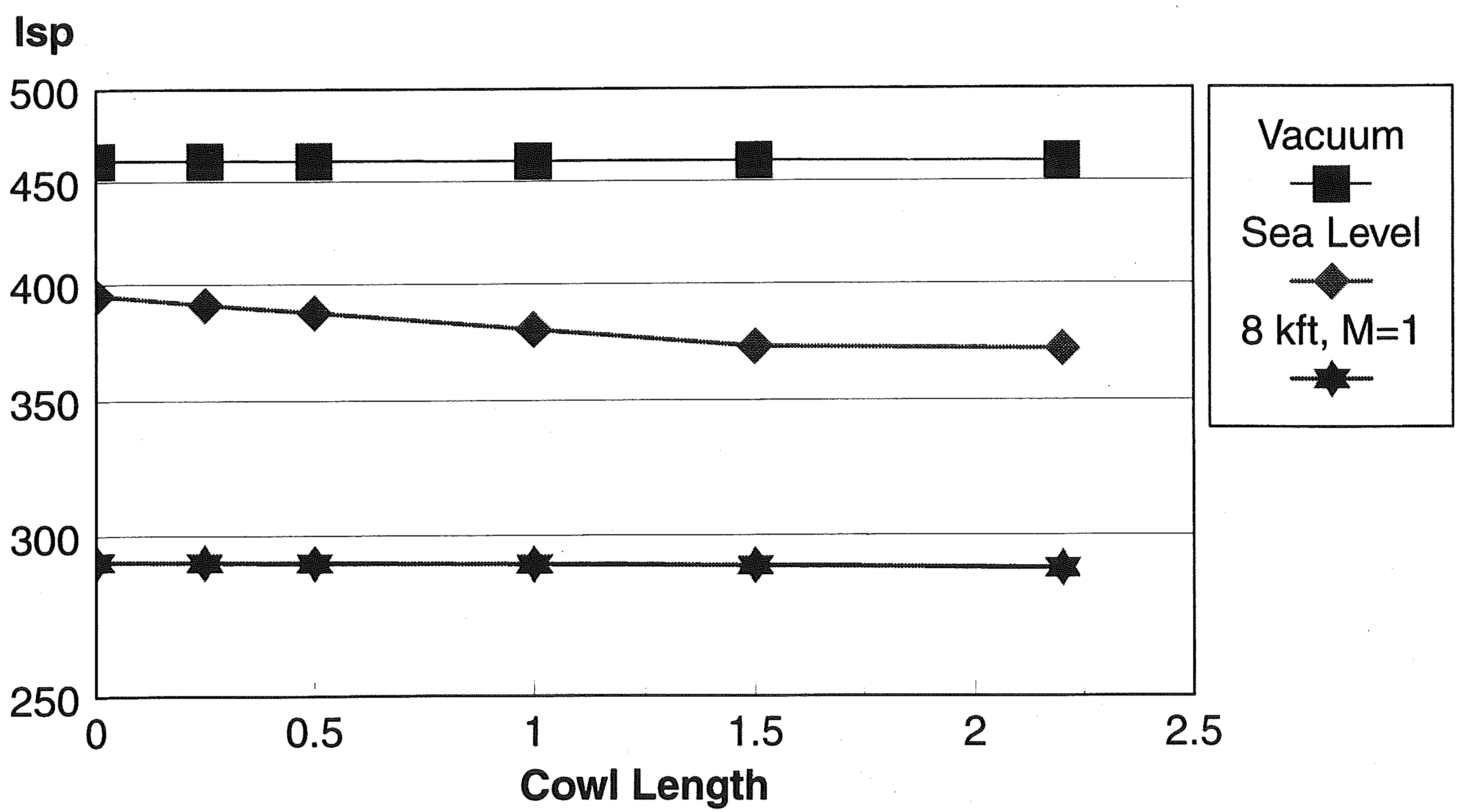

SEA 4-26-95/13 th Propulsion CFD Workshop

SSTØ H2/02 PLUG NØZZLE ... MACH 1 AIR AT 8 KFT : PRESSURE

LEGEND	Ø) 2.275	1) 2.926	2) 3.763
3) 4.839	4) 6.223	5) 8.002	6) 10.29
7) 13.23	8) 17.02	9) 21.89	10) 28.15
11) 36.19	12) 46.55	X) 59.86	

21 APR 95 16:53:18

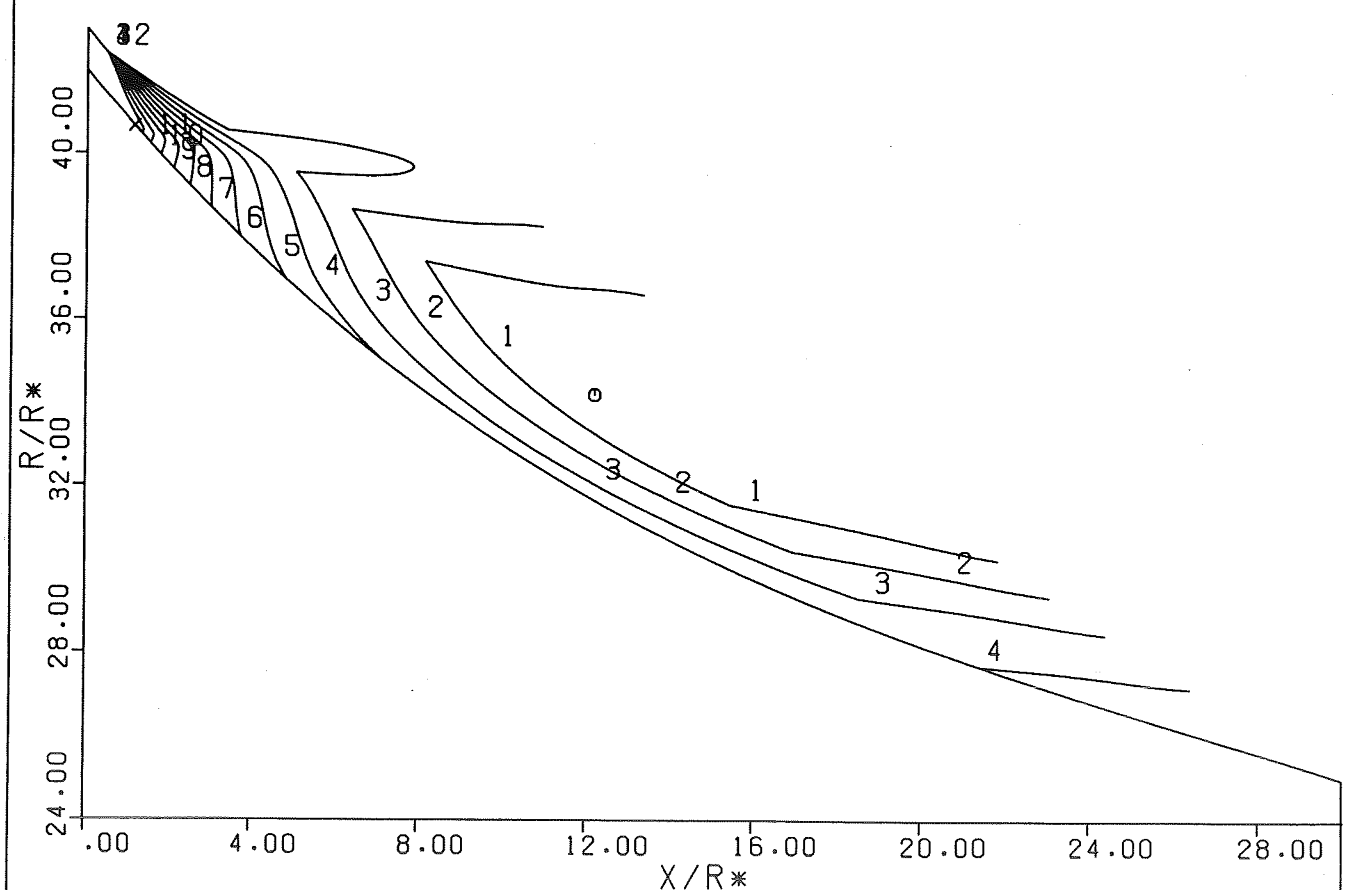

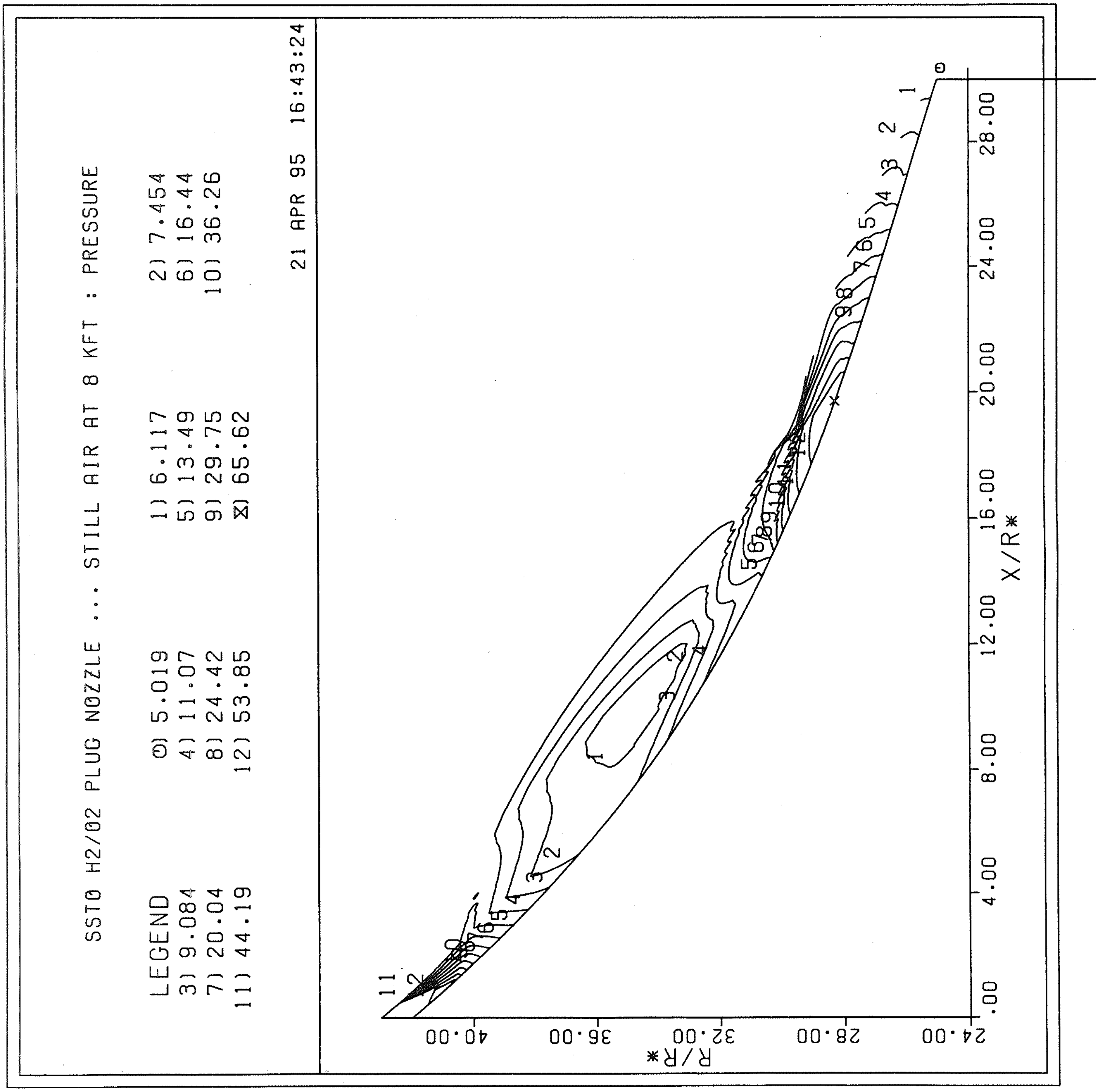
SSTO H2/O2 PLUG NOZZLE ... STILL AIR AT 8 KFT : PRESSURE
LEGEND
0) 5.019
1) 6.117
2) 7.454
3) 9.084
4) 11.07
5) 13.49
6) 16.44
7) 20.04
8) 24.42
9) 29.75
10) 36.26
11) 44.19
12) 53.85
X) 65.62
21 APR 95 16:43:24
X/R*
R/R*
.00
4.00
8.00
12.00
16.00
20.00
24.00
28.00
32.00
36.00
40.00

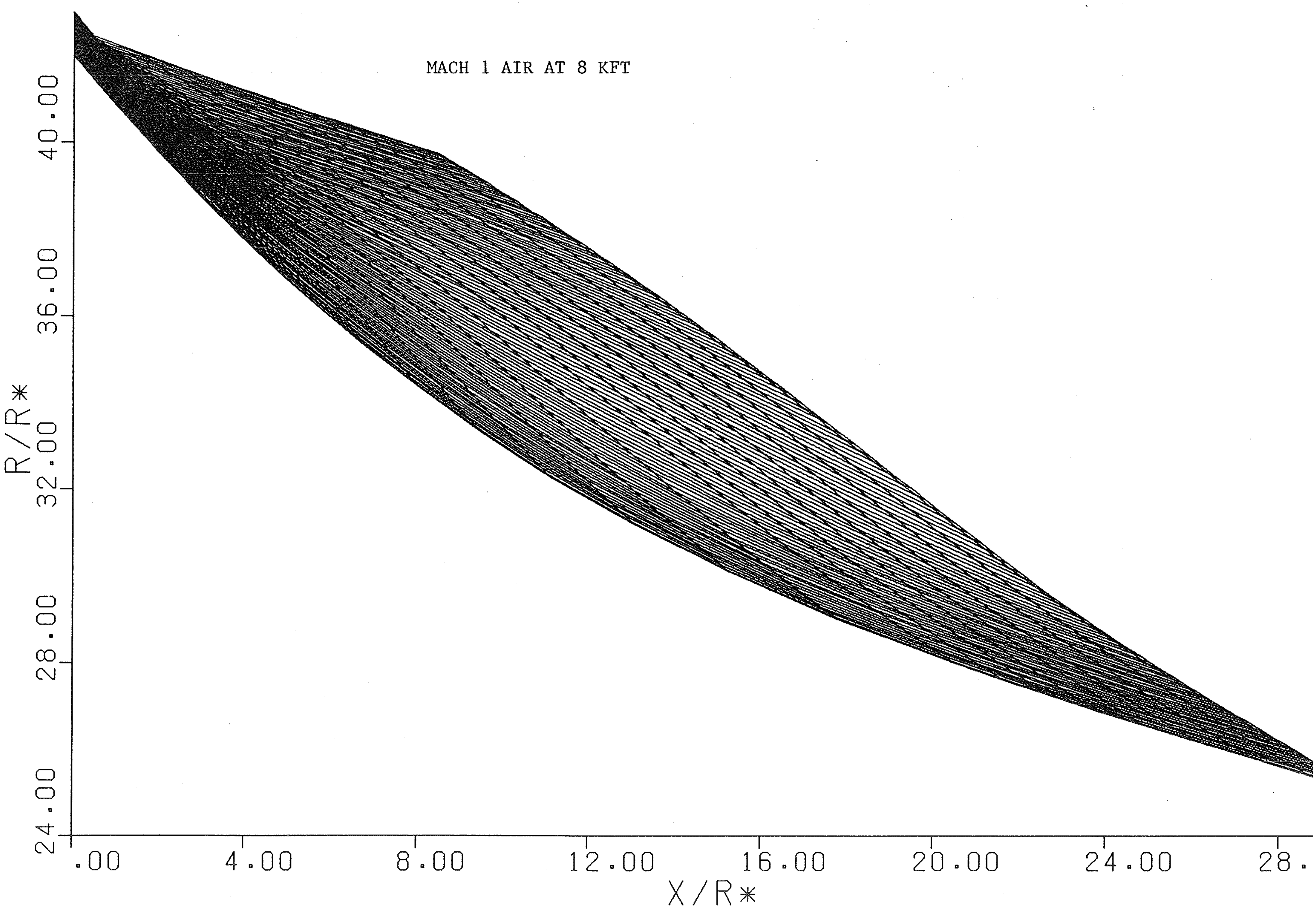
MACH 1 AIR AT 8 KFT
R/R*
40.00
36.00
32.00
28.00
24.00
.00
4.00
8.00
12.00
16.00
20.00
24.00
28.
X/R*

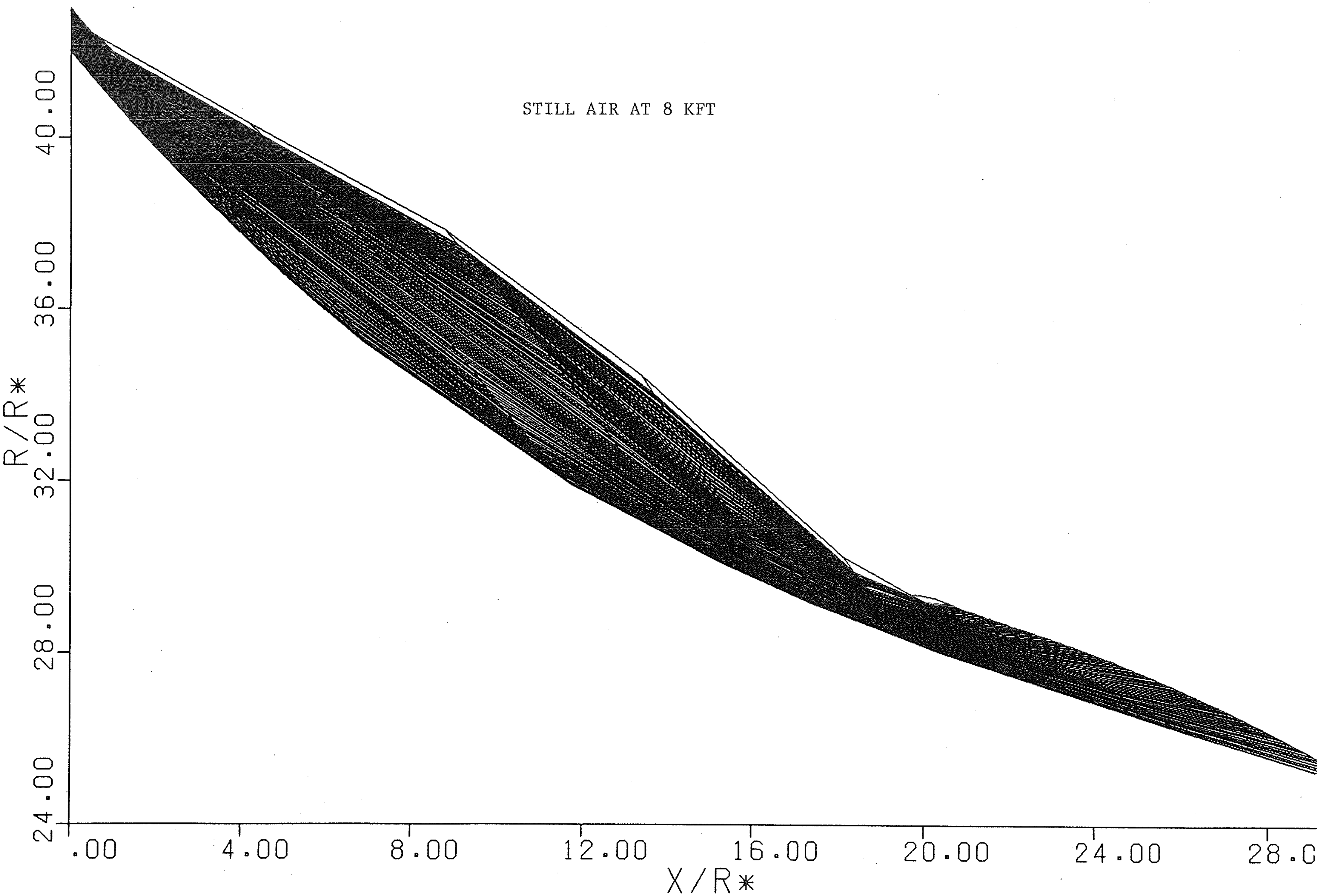

STILL AIR AT 8 KFT
40.00
36.00
32.00
28.00
24.00
R/R*
.00
4.00
8.00
12.00
16.00
20.00
24.00
28.0
X/R*

MACH 1 AIR AT 8KFT

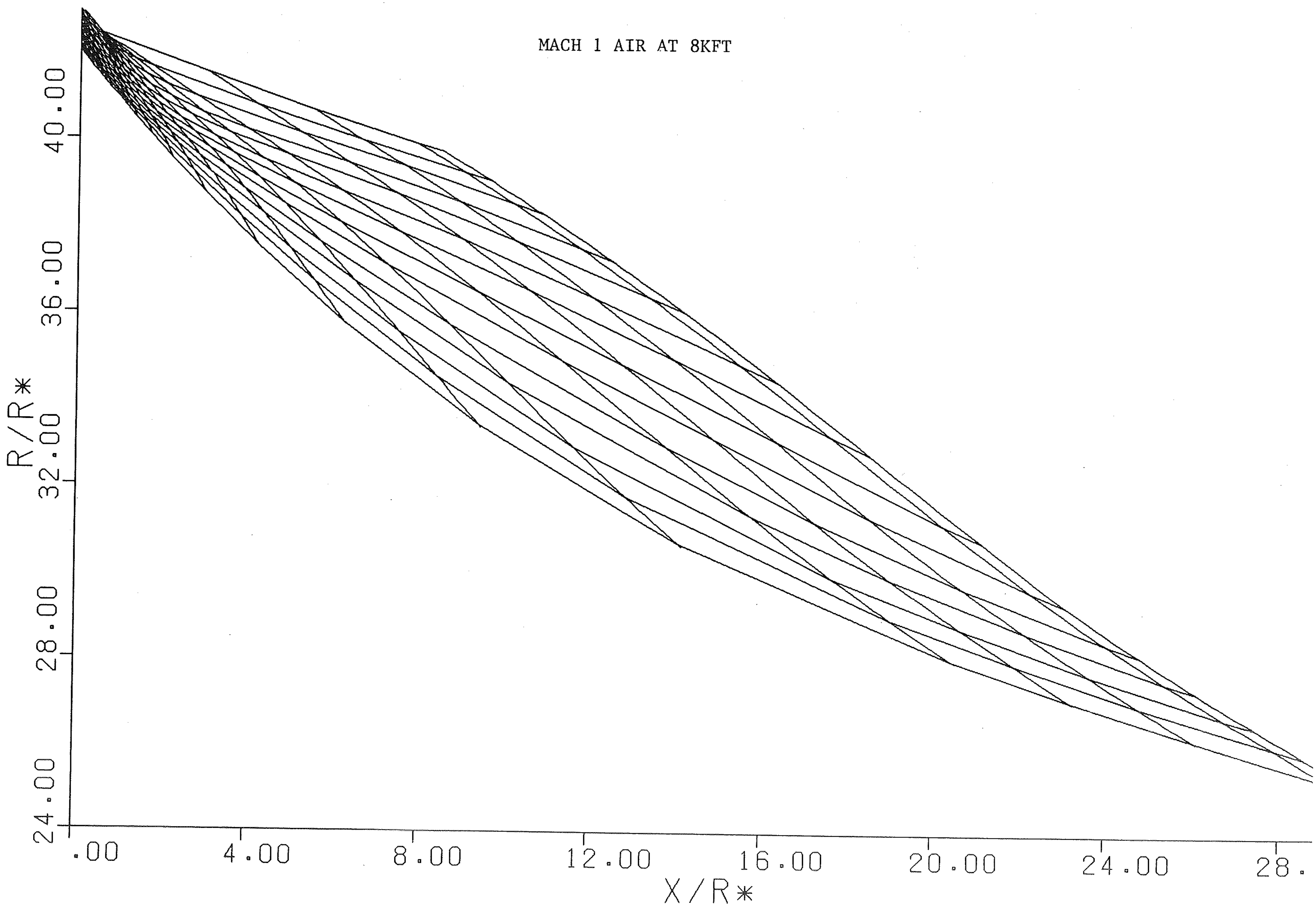

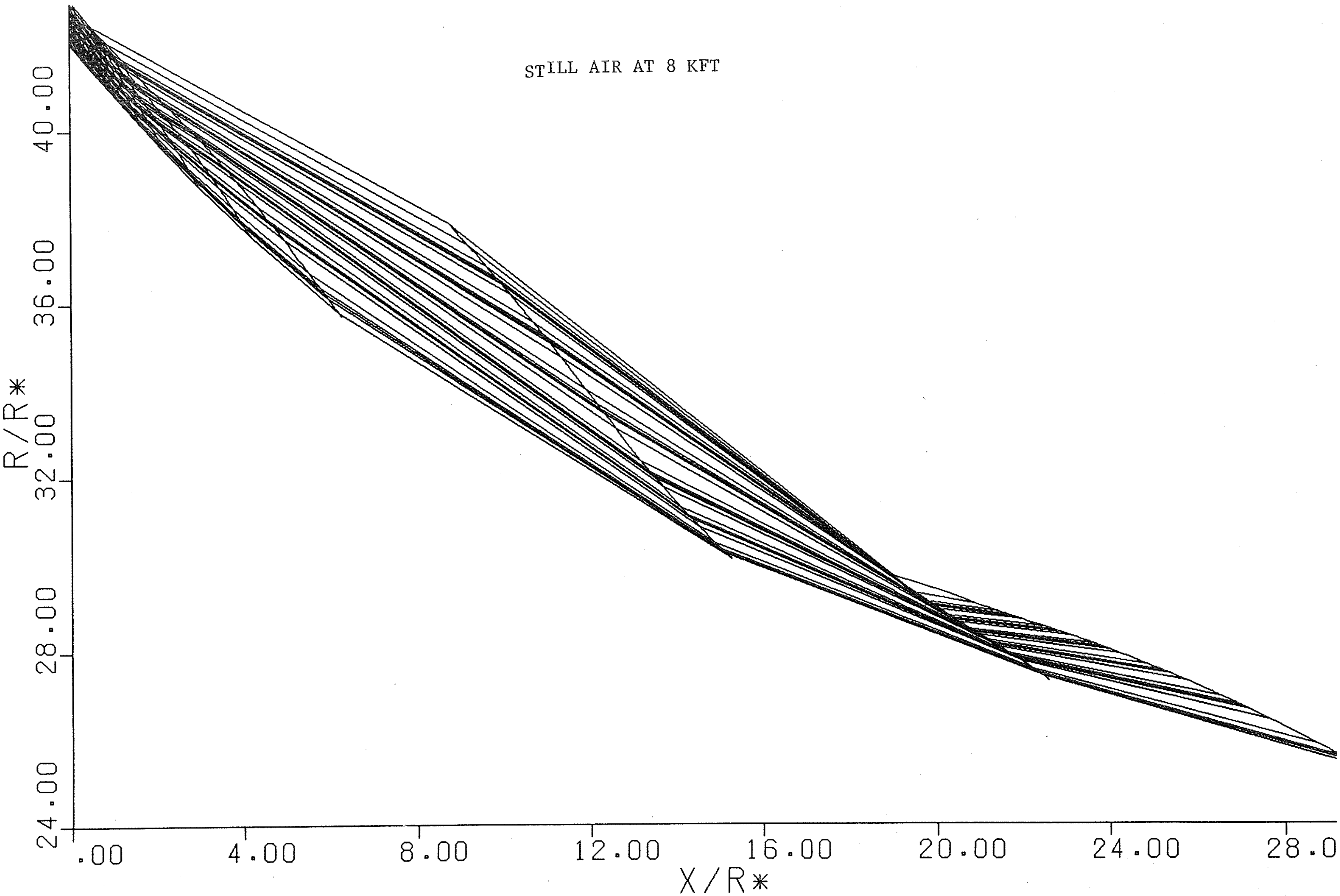
STILL AIR AT 8 KFT
R/R*
40.00
36.00
32.00
28.00
24.00
.00
4.00
8.00
12.00
16.00
20.00
24.00
28.0
X/R*

Isp vs. Area Ratio For an SSME Type Engine (Pc=2630psia)

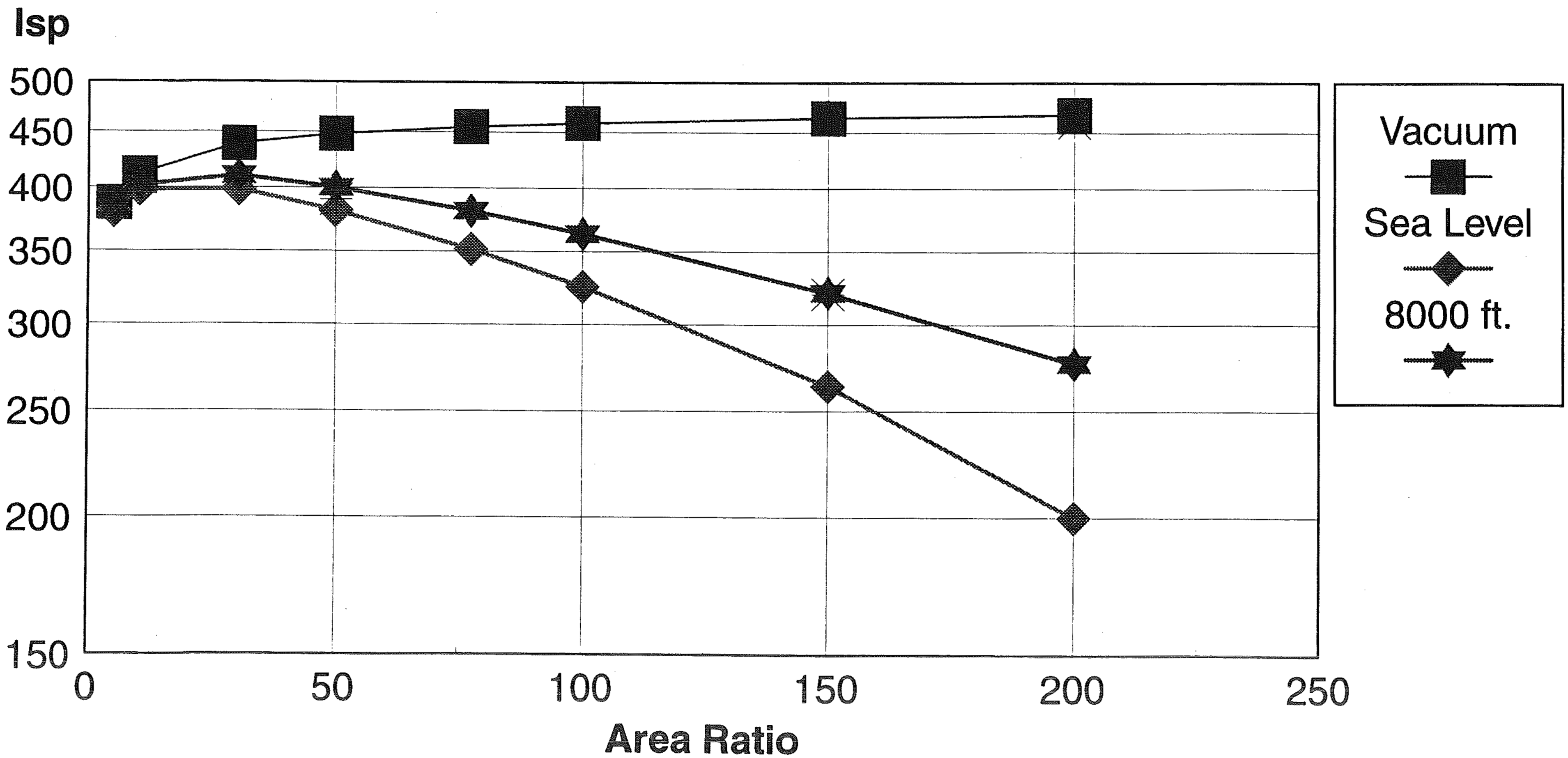

Isp Variation With Pressure Ratio

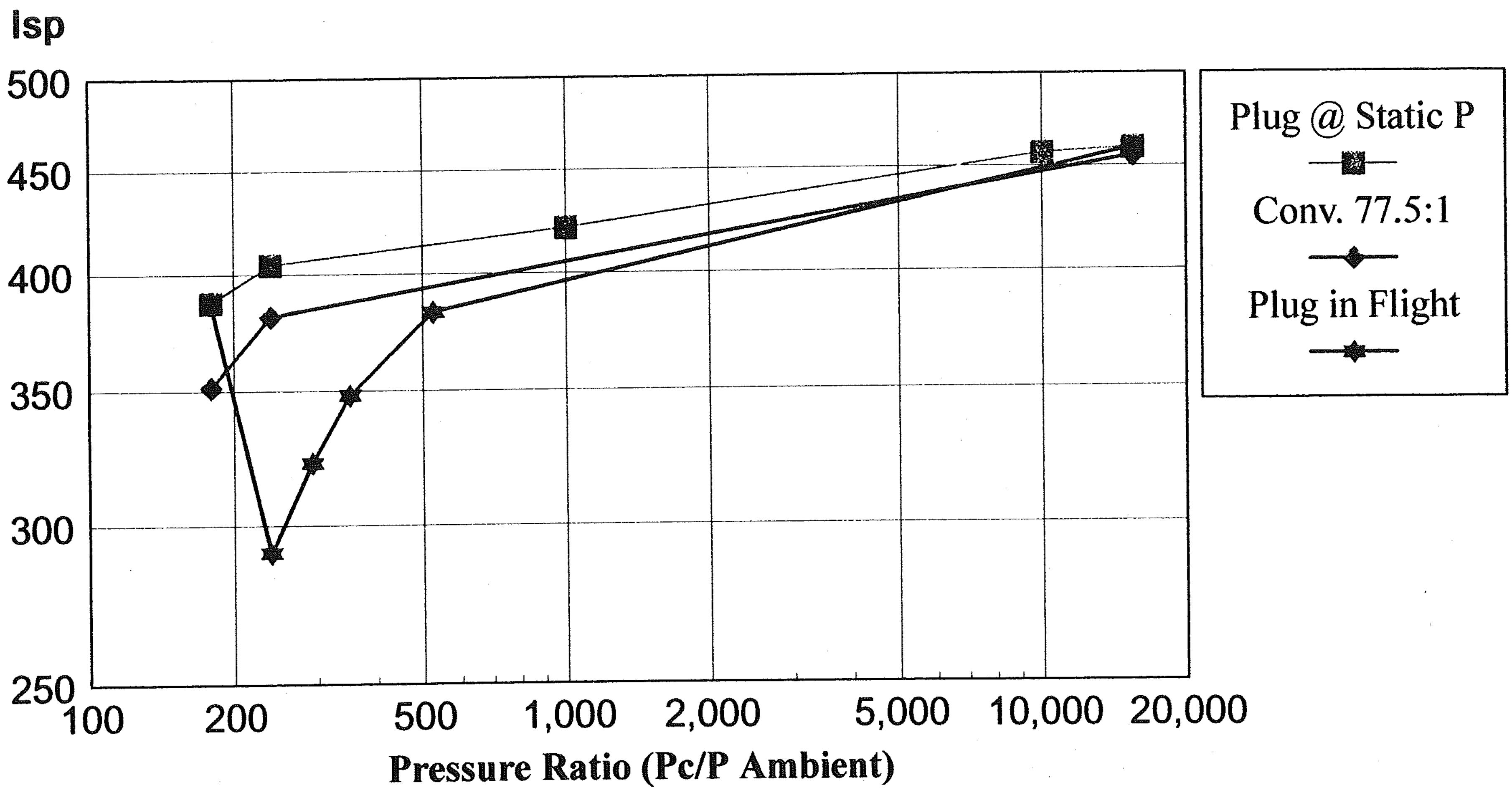

SEA 4-26-95/13 th Propulsion CFD Workshop

CONCLUSIONS

- Demonstrated The Ability Of LPP To Compute Performance of Plug Nozzles
- Performance Is Best With Short Cowls
- Performance Is Improved When The Flow Is Channeled Parallel To The Plug
- Showed That The Altitude Compensation Of Plug Nozzles Is Highly Dependent On The Flight Trajectory

RECOMMENDATIONS

- That An Automatic Trajectory Option Be Added To LPP
- That A Simple Base Flow Model Be Added To LPP

57-34
57382
132104
16p

CFD ANALYSIS OF MODULAR THRUSTERS PERFORMANCE

Ronald J. Ungewitter, James Beck, Andrew Ketchum
Rocketdyne Division, Rockwell International
Mail Code IB39, 6633 Canoga Avenue
Canoga Park, CA 91303

ABSTRACT

The effective performance of modular thrusters in an aerospike configuration is difficult to determine. Standard analytical tools are applicable to conventional nozzle shapes, but are limited when applied to an aerospike nozzle (An aerospike nozzle is an altitude compensating external nozzle). Three baseline nozzle shapes are derived using standard analytical procedures. The baseline nozzles sizes are restricted to fill a volume envelope. The three shapes are an axi-symmetric round nozzle, a 2D planar square exit nozzle, and a super elliptic round to nearly square nozzle. The integrated (thruster /aerospike) performance of the three nozzles is determined through the use of 3-D viscous CFD calculations where complex features of the flowfield can be accurately captured. The resulting installed performance is then used to evaluate the efficiency of these nozzle shapes for aerospike applications.

The determination of effective performance of a thruster nozzle integrated into an aerospike nozzle requires the solution of the three dimensional turbulent Navier-Stokes equations. The model used in this study consisted of two zones; one of the upstream thruster cowl surface so freestream conditions can be accurately predicted, and two, the aerospike surface beginning with with thruster outflow and extending to the end of the aerospike surface. The numerical grid consisted of over 120,000 nodes and used symmetry on the thruster centerline and edge. A two species non-reacting chemistry model was used to capture the variation of fluid properties between the hot plume gas and freestream air.

From the results of the three baseline nozzle aerospike calculations, the effective performance of the nozzle was determined. The flowfield of these calculations do show some variation between the cases. Recirculation zones on the cowl surface is predicted for the 2D planar nozzle and a smaller one for the super elliptic nozzle. The recirculation is caused by the strong pressure gradient between the plume and freestream flows. The axi-symmetric nozzle results indicates recirculation zones on the thruster face. These recirculation zones smooth the pressure gradient between the plume and freestream flow limiting the formation of recirculation on the cowl surface. Thruster to thruster interaction is evident for the axi-symmetric and super elliptic calculation while the 2D planar nozzle did not have any lateral expansion in the nozzle so thruster to thruster interaction is limited. The integrated performance results, at the altitude choosen, shows very little variation between the three thruster shapes. This result allows for nozzle shape determination to based on additional considerations (thermal, structural, weight) besides performance.

CFD ANALYSIS OF MODULAR THRUSTERS PERFORMANCE

CFD WORKSHOP
MARSHALL SPACE FLIGHT CENTER
HUNTSVILLE, AL

APRIL 25-27, 1995

Ronald J. Ungewitter
CFD Technology Center

James Beck and Andrew Ketchum
Performance Analysis and Applied Fluid Dynamics

Rockwell Aerospace
Rocketdyne

CFD Technology Center

CFD 95-016-001/D1/RJU

BASELINE COMPARISONS

- **GOAL**
  - TO EVALUATE THE PERFORMANCE OF THREE BASELINE NOZZLE SHAPES INDIVIDUALLY AND INTEGRATED INTO AEROSPIKE

- **APPROACH**
  - USE MOC AND CFD CODES TO DETERMINE THE Isp OF THE INDIVIDUAL BASELINE NOZZLES
  - COMPARE THE MOC AND CFD RESULTS FOR CONSISTENCY
  - USE 3D CFD MODEL TO DETERMINE THE INSTALLED BASELINE NOZZLE / AEROSPIKE PERFORMANCE

BASELINE NOZZLE DEFINITIONS

- **3 UNIQUE SHAPES**
  - AXISYMMETRIC
  - 2-D PLANAR
  - 3-D SUPER-ELLIPSE
- **CONSTRAINTS**
  - SAME NOZZLE LENGTH
  - SQUARE EXIT
  - SAME MASS FLOW (THROAT AREA)
- **EACH SHAPE OPTIMIZED FOR Isp**

BASELINE NOZZLE DESIGNS

Baseline Thrust Cell Nozzle	Schematic	Throat Area (in2)	Nozzle Length (in)	Exit Dimension (in)	Nozzle Area Ratio
Axisymmetric	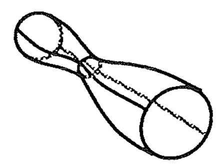	3.7688	11.585	D = 7.519	11.8
2-D Planar	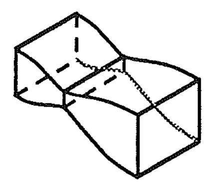	3.7688	11.585	H = W = 7.519	15.0
3-D Super-Elliptic	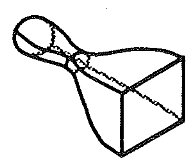	3.7688	11.585	H = W = 7.519	14.8

Rockwell Aerospace
Rocketdyne

BASELINE COMPARISONS

BASELINE NOZZLE AND ANALYTICAL METHOD COMPARISON

- MOC AND CFD CALCULATIONS WERE MADE OF EACH BASELINE NOZZLE SHAPE

NOZZLE SHAPE	EXIT AREA RATIO	MOC INVISCID	CFD INVISCID	CFD VISCOUS
AXISYMMETRIC	11.8:1	409.0	410.6	406.1
2-D PLANAR	15.0:1	414.2	417.0	411.4
3-D SUPER ELLIPTIC	14.8:1	412.9	414.6	409.1*

* VALUE BASED ON LAMINAR CFD PREDICTION WITH SKIN FRICTION ESTIMATED BASED ON PREVIOUS CALCULATIONS AND WETTED SURFACE AREA

- **CONCLUSIONS:**
  - MOC AND CFD PREDICT CONSISTENT RESULTS
  - MOC CODES PROVIDE RAPID ANALYSIS CAPABILITY
  - CFD CODE PROVIDES RANGE OF ANALYSIS OPTIONS

Rockwell Aerospace
Rocketdyne

CFD-95-009-002/D1/BJH

BASELINE COMPARISONS
3-D CFD MODEL

- FULL NAVIER-STOKES SOLUTIONS
- BALDWIN-LOMAX TURBULENCE MODEL
- TWO SPECIES (FREESTREAM, PLUME) NONREACTING CHEMISTRY MODEL
- TWO ZONE, 125,350 NODE GRID
  - ZONE ONE INCLUDES FLOW OVER COWL
  - ZONE TWO SIMULATES INFINITE ARRAY OF THRUSTERS AND AEROSPIKE SURFACE
- FREESTREAM INLET CONDITIONS AT 50,000 FT (MACH NUMBER = 1.83), REPRESENTATIVE OF MIDPOINT OF FLIGHT ENVELOPE

Rockwell Aerospace
Rocketdyne

CFD-95-009-003/D1/RJU

GEOMETRY OF INTEGRATED THRUST CELL MODEL

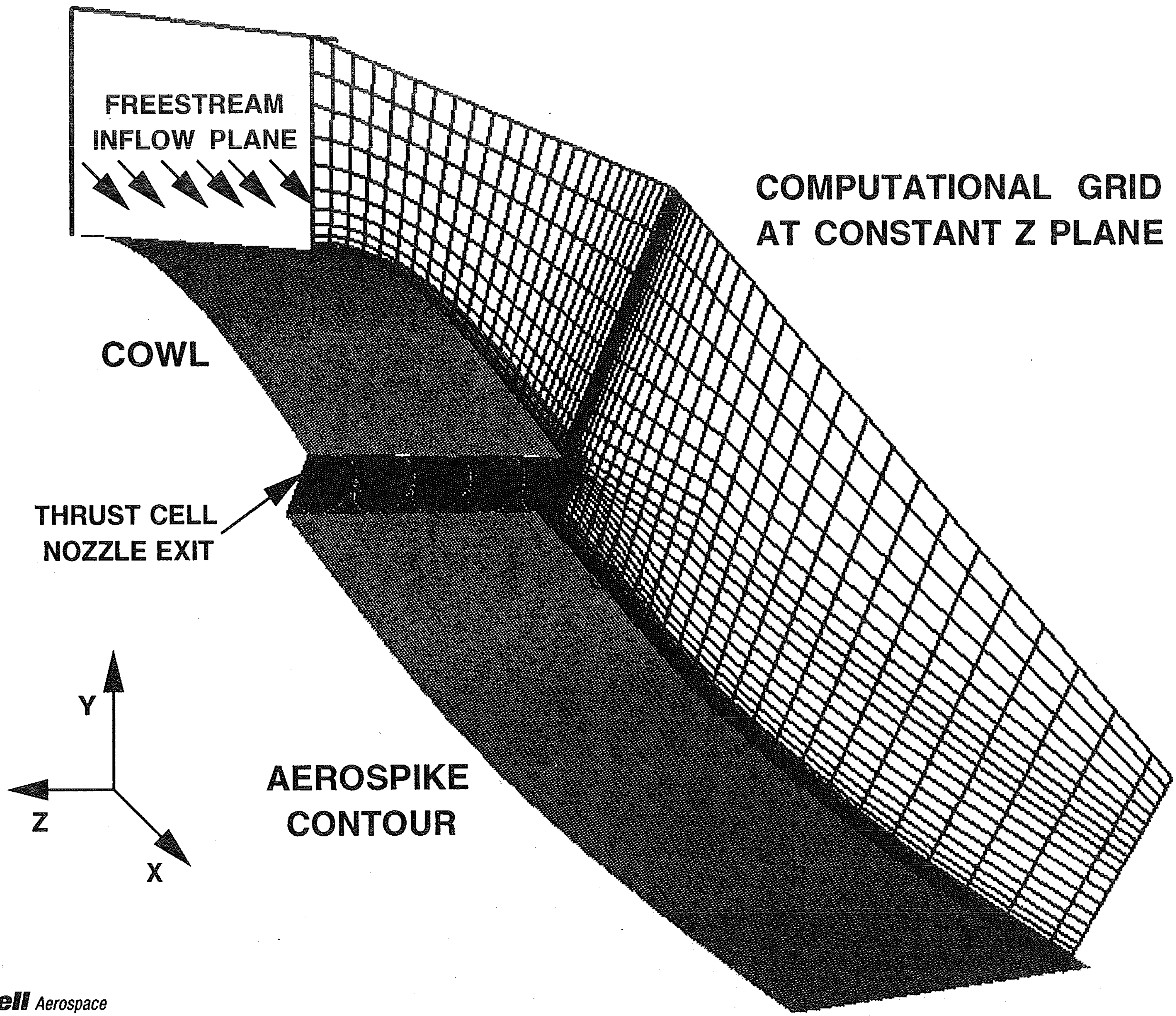

CFD-95-009-004/D1/RJU

BASELINE COMPARISONS
FLOW FEATURES COMMON TO ALL SOLUTIONS

- NORMAL SHOCK UPSTREAM OF THRUSTERS ON COWL SURFACE, DECREASING IN STRENGTH FROM COWL SURFACE
- MODULE TO MODULE INTERACTION CAUSES THREE DIMENSIONAL PLUME SHAPE
- RECIRCULATION REGIONS ON COWL SURFACE AND/OR ON THRUSTER FACE
- MODULE TO MODULE INTERACTIONS ON AEROSPIKE SURFACE
- AEROSPIKE EXPANDS FLOW TO SIMILAR PRESSURE VALUES

THRUST CELL TECHNOLOGIES: INTEGRATED THRUST CELL / AEROSPIKE ANALYSIS

BASELINE INTEGRATED SUPER ELLIPTIC NOZZLE RESULTS:

MACH NUMBER CONTOURS IN THE CROSS PLANES

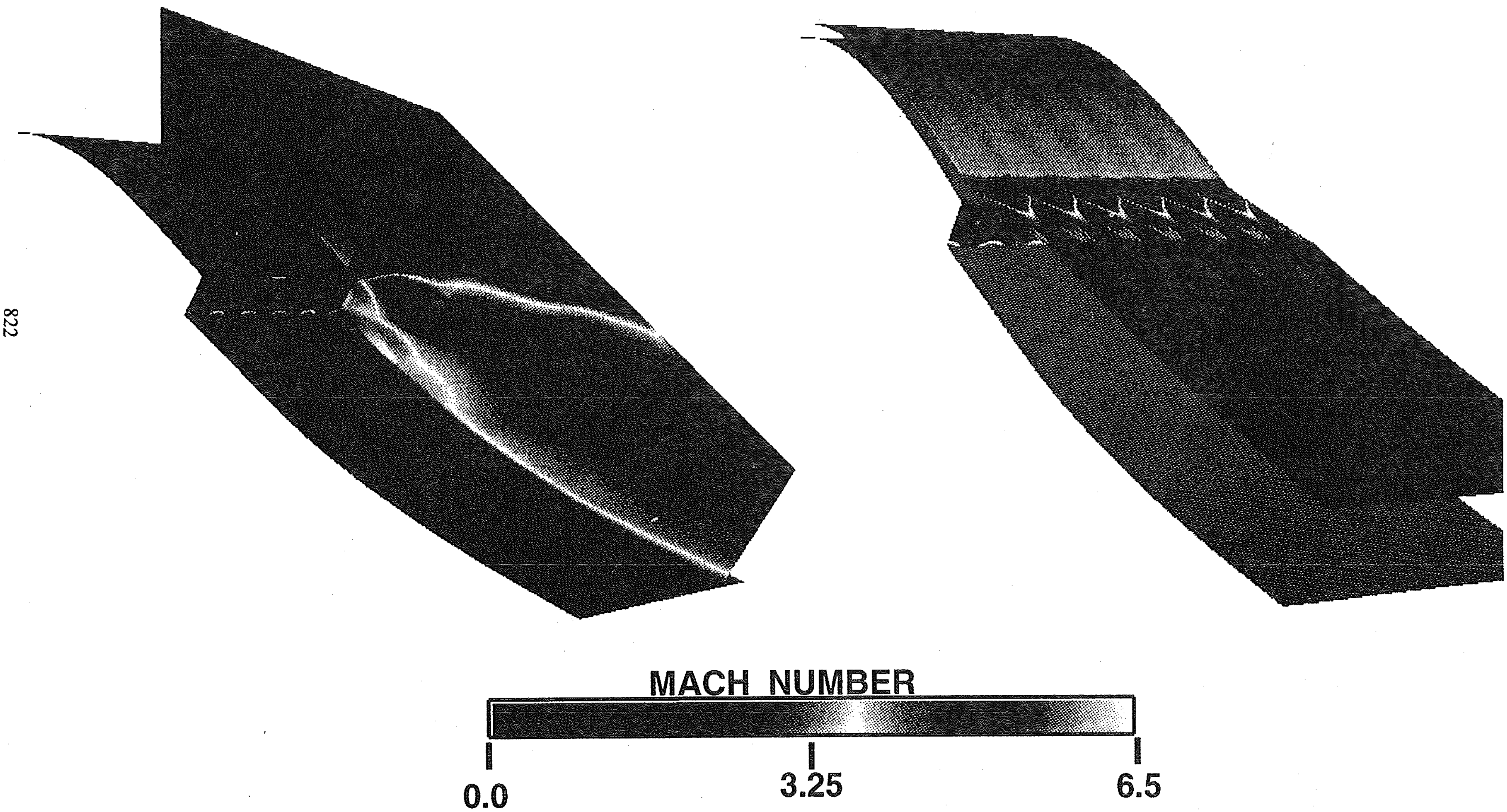

THRUST CELL TECHNOLOGIES: INTEGRATED THRUST CELL / AEROSPIKE ANALYSIS
BASELINE NOZZLE COMPARISON

PARTICLE TRACES

2D PLANAR THRUSTERS

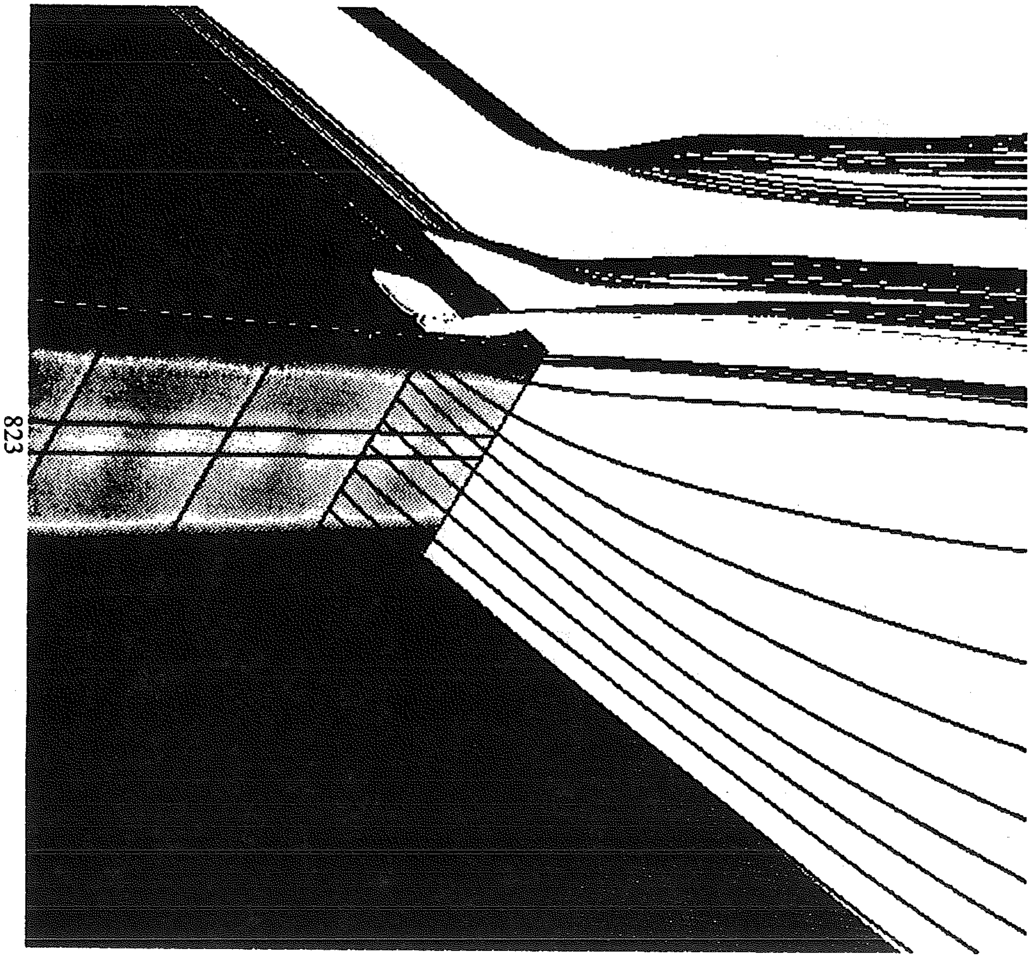

AXISYMMETRIC THRUSTERS

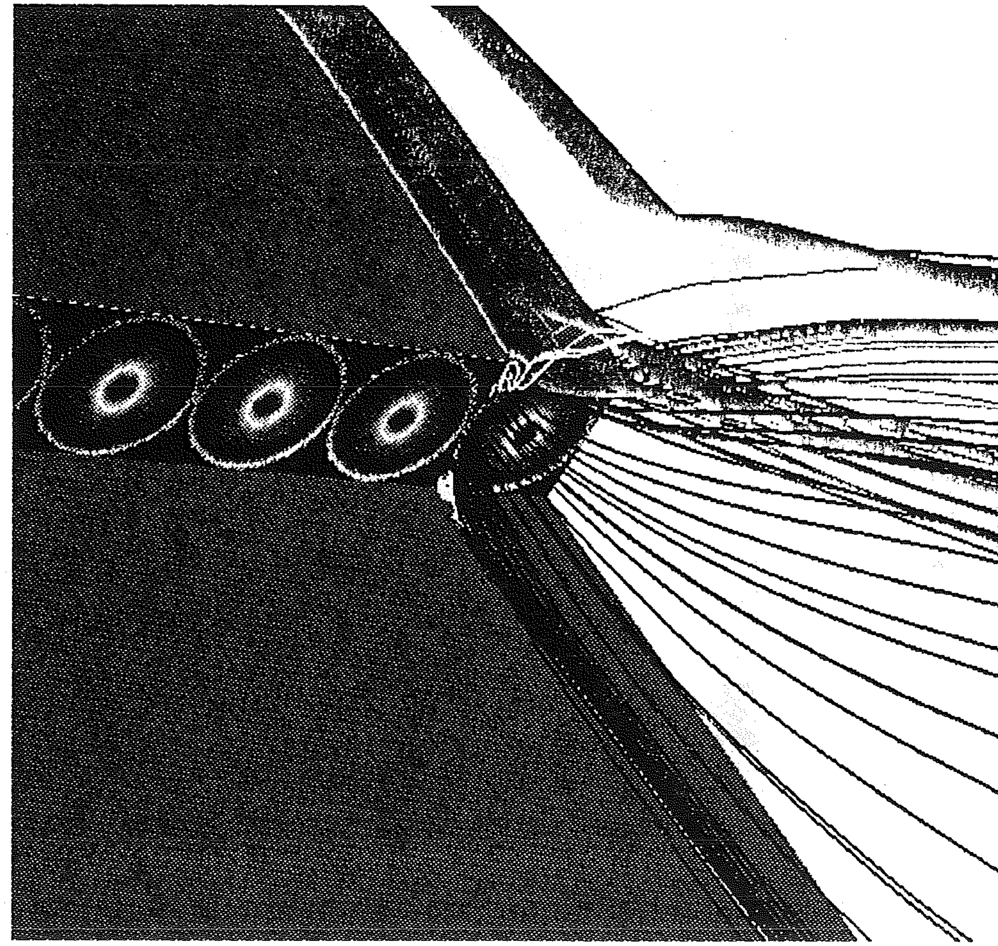

RED: PLUME FLOW

LIGHT BLUE: FREESTREAM FLOW

: RECIRCULATION FLOW

Rockwell Aerospace
Rocketdyne

CFD-95-009-007/D1/RJU

THRUST CELL TECHNOLOGIES: INTEGRATED THRUST CELL / AEROSPIKE ANALYSIS
BASELINE NOZZLE COMPARISON

PRESSURE CONTOURS ALONG AEROSPIKE SURFACE

2D PLANAR THRUSTERS

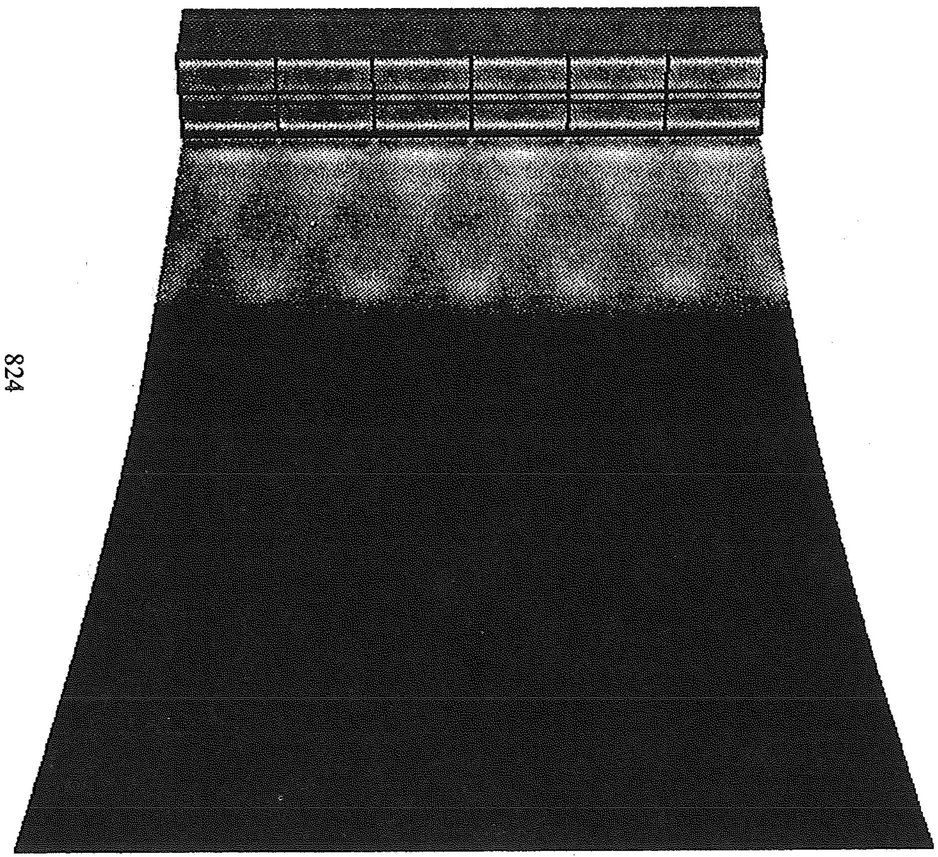

AXISYMMETRIC THRUSTERS

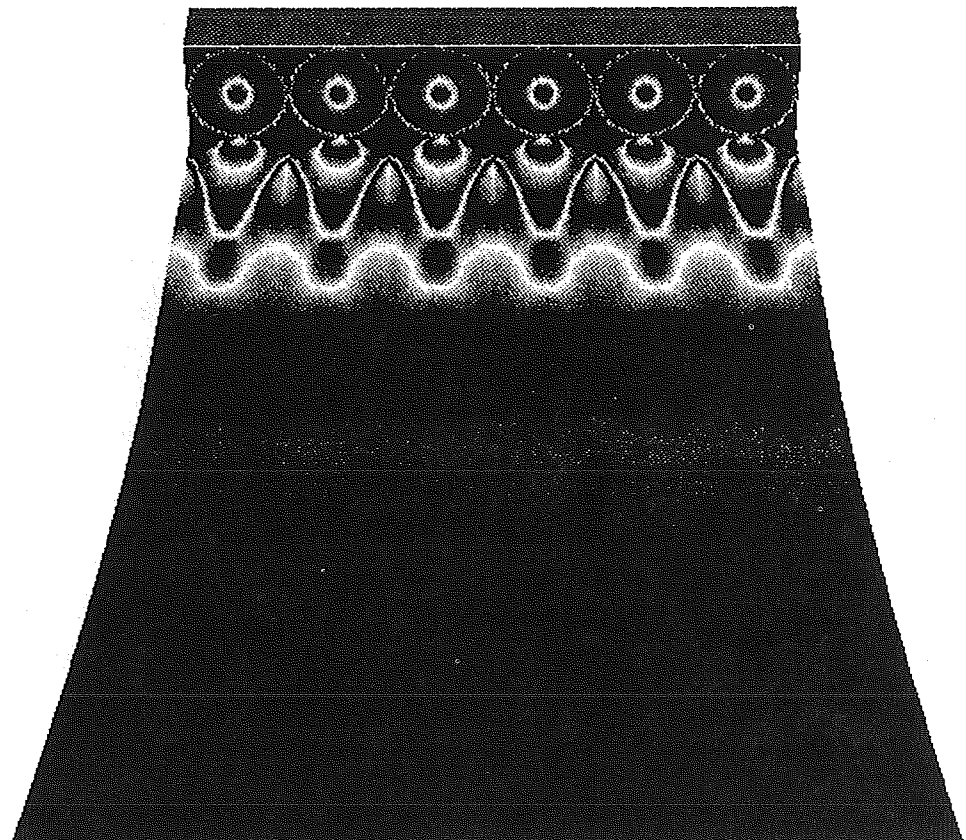

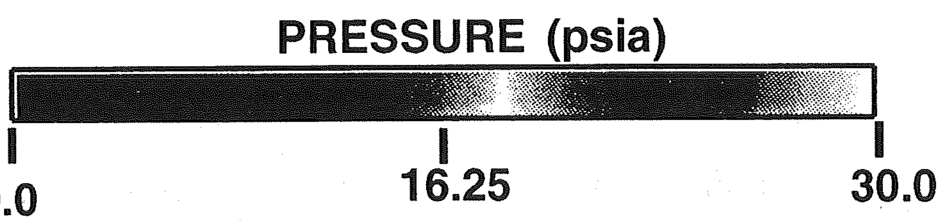

Rockwell Aerospace

CFD-95-009-008/D1/RJU

BASELINE NOZZLE COMPARISON

PRESSURE PROFILES ALONG AEROSPIKE SURFACE

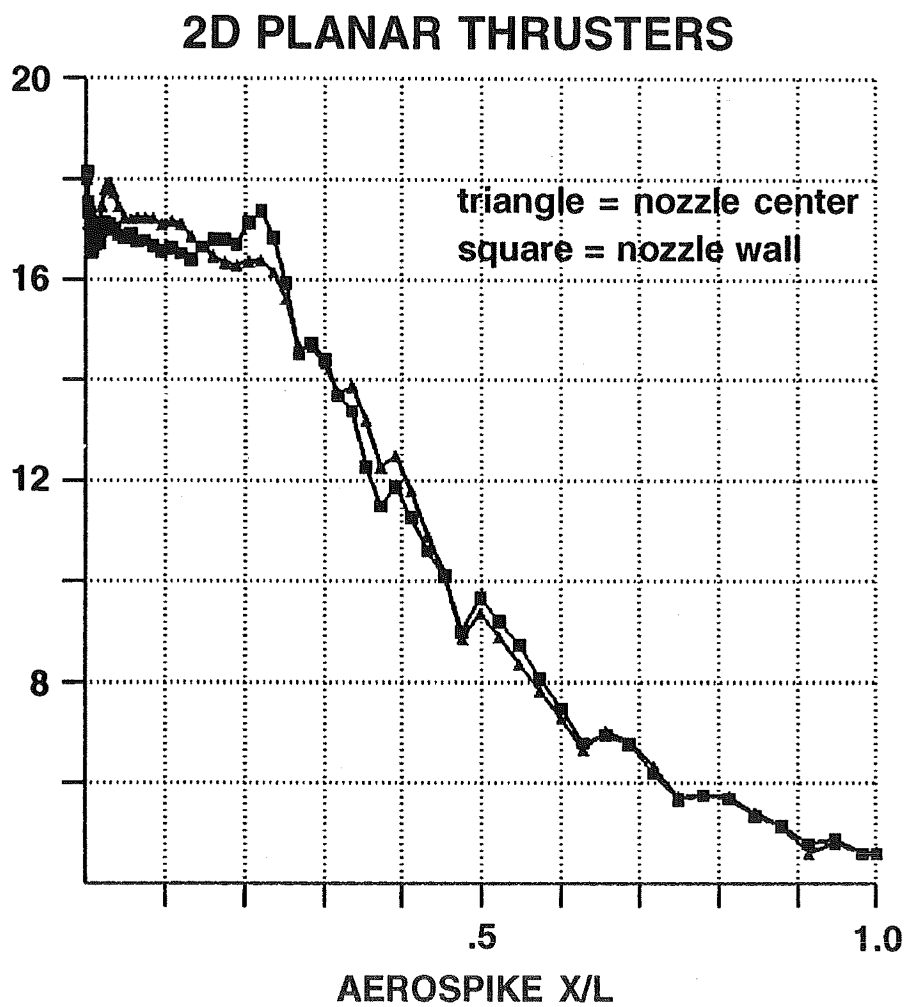

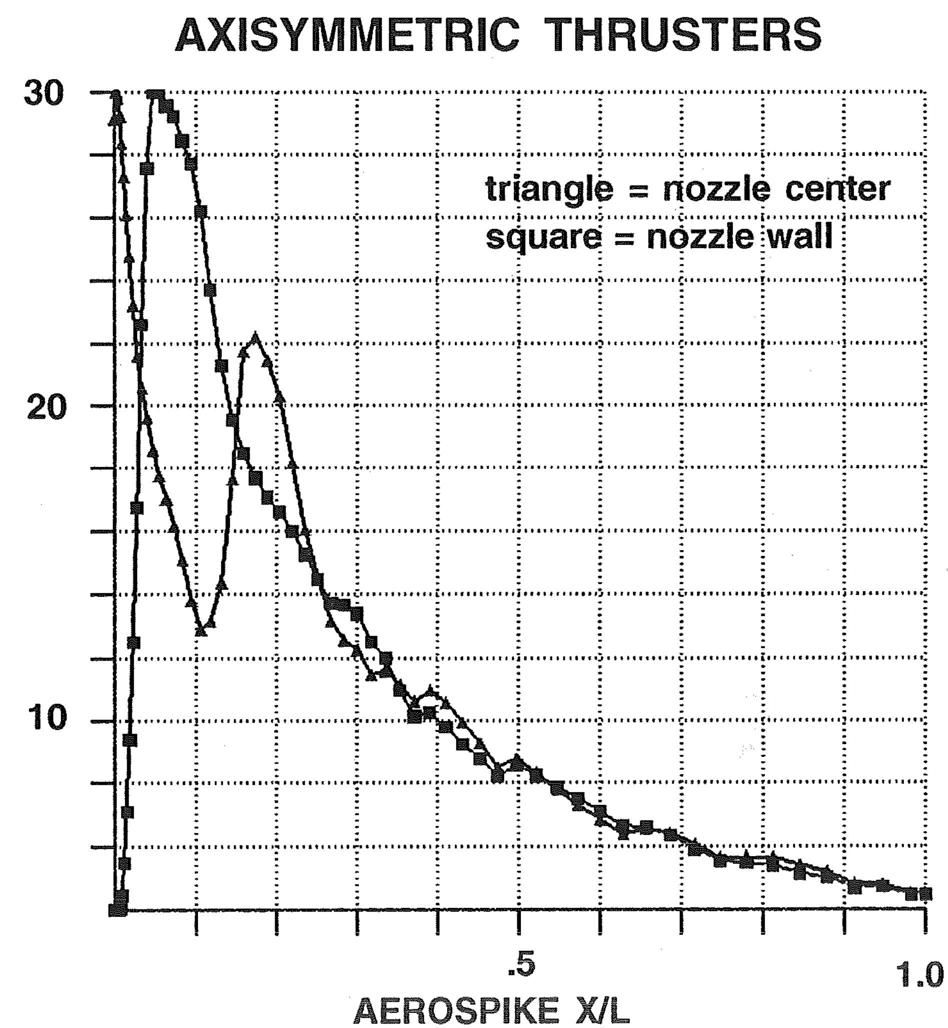

Rockwell Aerospace
Rocketdyne

CFD-95-009-009/D1/RJU

BASELINE COMPARISONS

INSTALLED BASELINE NOZZLE / AEROSPIKE PERFORMANCE

BASELINE SHAPE	NOZZLE THRUST*	FACE PdA*	AEROSPIKE THRUST*	AEROSPIKE FRICTION*	TOTAL THRUST*	Isp (SEC)
AXISYMMETRIC	12403	15	3748	129	16037	**430.2**
2-D PLANAR	12566	--	3554	125	15995	**429.0**
3-D SUPER ELLIPTIC	12493	< 1.0	3660	129	16024	**429.8**

* ALL VALUES LBS

- **CONCLUSIONS:**
  - PREDICTED VALUES OF INSTALLED PERFORMANCE ARE EFFECTIVELY EQUIVALENT
  - SIMILARITY OF PERFORMANCE ALLOWS FOR OTHER DESIGN ASPECTS (EG. THERMAL, STRUCTURAL) TO BE CONSIDERED IN NOZZLE SHAPE SELECTION

Rockwell Aerospace
Rocketdyne

CFD-95-009-016/D1/RJU

BASELINE COMPARISONS
TASK CONCLUSIONS

- CFD AND MOC PREDICT CONSISTENT RESULTS
- MOC CODES PROVIDE RAPID ANALYSIS CAPABILITY
- CFD CODE PROVIDE RANGE OF ANALYSIS OPTIONS
- INSTALLED BASELINE NOZZLE / AEROSPIKE PERFORMANCE PREDICTIONS FOR THREE NOZZLE SHAPES EFFECTIVELY THE SAME
- SIMILARITY OF PERFORMANCE ALLOWS FOR OTHER DESIGN ASPECTS (EG. THERMAL, STRUCTURAL) TO BE CONSIDERED IN NOZZLE SHAPE SELECTION

PROPELLANT CHEMISTRY FOR CFD APPLICATIONS

R.C. Farmer, P.G. Anderson, Gary C. Cheng

SECA, Inc.
Huntsville, AL

ABSTRACT

Current concepts for Reusable Launch Vehicle design have created renewed interest in the use of RP-1 fuels for high pressure and tri-propellant propulsion systems. Such designs require the use of analytical methodology which accurately accounts for the effects of real fluid properties, combustion of large hydrocarbon fuel molecules, and the possibility of soot formation. These effects are inadequately treated in current computational fluid dynamics (CFD) codes which are used for propulsion system analyses.

The objective of this investigation is to provide an accurate analytical description of hydrocarbon combustion thermodynamics and kinetics which is sufficiently computationally efficient to be practical design tool when used with CFD codes such as the FDNS code.

A rigorous description of real fluid properties for RP-1 and its combustion products will be derived from the literature and from experiments conducted in this investigation. Upon the establishment of such a description, the fluid description will be simplified by using the minimum of empiricism necessary to maintain accurate combustion analyses and including such empirical models into an appropriate CFD code. An additional benefit from this approach is that the real fluid properties analysis simplifies the introduction of the effects of droplet sprays into the combustion model.

Typical species compositions of RP-1 have been identified, surrogate fuels have been established for analyses, and combustion and sooting reaction kinetics models have been developed. Methods for predicting the necessary real fluid properties have been developed and essential experiments have have been designed. Verification studies are in progress, and preliminary results from these studies will be presented. The approach has been determined to be feasible, and upon its completion the required methodology for accurate performance and heat transfer CFD analyses for high pressure, tripropellant propulsion systems will be available.

1995 CFD Workshop
NASA/MSFC

PROPELLANT CHEMISTRY FOR CFD APPLICATIONS

R.C. Farmer, P.G. Anderson, Gary C. Cheng

SECA, Inc.
Huntsville, AL

RP-1 COMBUSTION CHEMISTRY

- RP-1 combustion model w/soot formation
- Verify model w/data from literature
- Verify model w/new test data
- Describe real fluid thermodynamic properties
- Add real fluid HC properties to CICM
- Real fluid single element model
    - Real fluid HC, H_2, and O_2
    - Real fluid tri-propellant
    - Additional turbulence models
- Account for radiation
- Assemble elements to make injector model

RP-1

RP-1 is a straight run kerosene fraction which is subjected to acid washing and sulfur dioxide extraction. The mean molecular weight is about 174, and the H/C ratio is about 1.9. This implies that RP-1 is a multicomponent hydrocarbon fuel without a specified species distribution.

Composition by Hydrocarbon Type	
Composition	Volume %
dinuclear aromatics	2.3
mononuclear aromatics	15.1
dicyclo-paraffins	11.6
monocycyclo-paraffins	33.8
branched-paraffins	15.1
normal paraffins	22.1
	100.0

or

Composition	Volume %
aromatics	17.4
cyclo-paraffins	45.4
paraffins	37.2
	100.0

Distillation Curve for RP-1

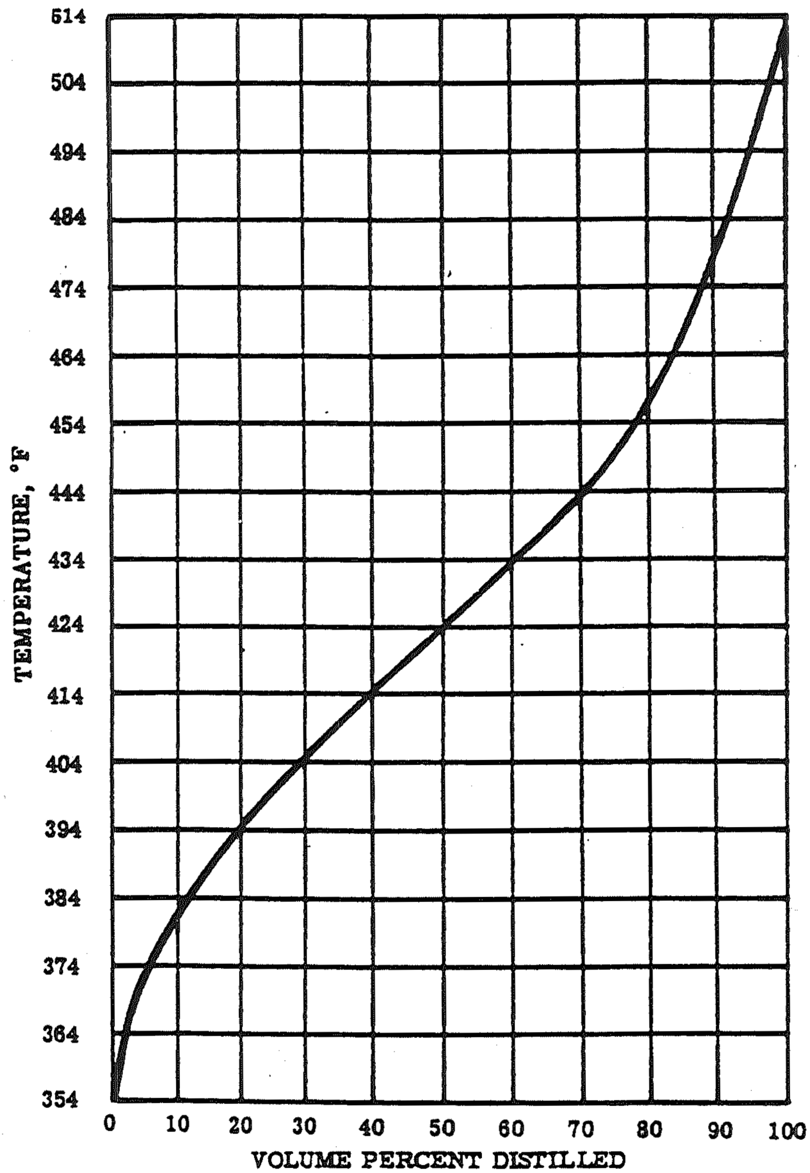

HYDROCARBONS ISOLATED FROM ONE REFERENCE PETROLEUM			
Molecular Formula	Name	Type	Normal Boiling Point
$C_{10}H_{14}$	1.3-Diethylbenzene	Benzene	181.10
$C_{10}H_{14}$	1-Methyl-3-propylbenzene	Benzene	181.80
$C_{10}H_{14}$	n-Bulylbenzene	Benzene	183.27
$C_{10}H_{18}$	Bicycloparaffin	Bicycloparaffin	183.4
$C_{10}H_{18}$	Bicycloparaffin	Bicycloparaffin	183.7
$C_{10}H_{14}$	1-Methyl-4-propylbenzene	Benzene	183.30
$C_{10}H_{14}$	1, 2-Diethylbenzene	Benzene	183.42
$C_{10}H_{14}$	1,3-Dimethyl-5-ethylbenzene	Benzene	183.58
$C_{10}H_{14}$	1, 4-Diethylbenzene	Benzene	183.78
$C_{10}H_{14}$	1, Methyl-2-propylbenzene	Benzene	184.80
$C_{10}H_{14}$	1, 4-Dimethyl-2-ethylbenzene	Benzene	186.83
$C_{10}H_{18}$	trans-Decahydro-naphthalene	Bicycloparaffin	187.25
$C_{10}H_{14}$	1, 3-Dimethyl-4-ethylbenzene	Benzene	188.20
$C_{10}H_{14}$	1, 2-Dimethyl-4-ethylbenzene	Benzene	189.48
$C_{10}H_{16}$	Tricyclo (3.3.1.1)- decane	Tricycloparaffin	190
$C_{10}H_{14}$	1, 3-Dimethyl-2-ethylbenzene	Benzene	190.01
$C_{10}H_{12}$	1-Methylindan	Aromatic-cycloparaffin	190.6
$C_{10}H_{12}$	2-Methylindan	Aromatic-cycloparaffin	191.4
$C_{10}H_{14}$	1, 2-Dimethyl-3 ethylbenzene	Benzene	193.91
$C_{10}H_{18}$	cis-Decahydro-naphthalene	Bicycloparaffin	195.69
$C_{11}H_{24}$	n-Undecane	Normal paraffin	195.89
$C_{10}H_{14}$	1,2,4,5-Tetramethyl-benzene	Benzene	196.80
$C_{10}H_{14}$	1,2,3,5-Tetramethyl-benzene	Benzene	198.00
$C_{11}H_{20}$	Bicycloparaffin	Bicycloparaffin	202.5
$C_{11}H_{16}$	1-Methyl-3-n-butylbenzene	Benzene	204.1
$C_{10}H_{14}$	1,2,3,4-Tetramethyl-benzene	Benzene	205.04
$C_{10}H_{12}$	4-Methylindan	Aromatic-cycloparaffin	205.5

HYDROCARBONS ISOLATED FROM ONE REFERENCE PETROLEUM (Continued)			
Molecular Formula	Name	Type	Normal Boiling Point
$C_{11}H_{16}$	1,3-Dimethyl-4-n propylbenzene	Benzene	206.6
$C_{10}H_{12}$	1,2,3,4-Tetra-hydronaphthalene	Aromatic-cycloparaffin	207.57
$C_{11}H_{16}$	1,2-Dimethyl-4-n-propylbenzene	Benzene	208.5
$C_{11}H_{16}$	Trimethylethylbenzene	Benzene	212.3
$C_{12}H_{26}$	n-Dodecane	Normal paraffin	216.28
$C_{10}H_{8}$	Naphthalene	Dinuclear aromatic	217.96
$C_{11}H_{14}$	2-Methyl-(1,2,3,4-tetra-hydronaphthalene)	Aromatic-cycloparaffin	220.7
$C_{11}H_{14}$	6-Methyl-(1,2,3,4-tetra-hydronaphthalene)	Aromatic-cycloparaffin	229.03
$C_{14}H_{30}$	2,6,10-Trimethylundecane	Branched paraffin	231
$C_{11}H_{14}$	5-Methyl-(1,2,3,4-tetra-hydronaphthalene)	Aromatic-cycloparaffin	234.35
$C_{13}H_{28}$	n-Tridecane	Normal paraffin	235.43
$C_{11}H_{10}$	2-Methylnaphthalene	Dinuclear aromatic	241.05
$C_{11}H_{10}$	1-Methylnaphthalene	Dinuclear aromatic	244.64
$C_{15}H_{32}$	2,6,10-Trimethyldodecane	Branched paraffin	249
$C_{14}H_{30}$	n-Tetradecane	Normal paraffin	253.52
$C_{12}H_{10}$	Biphenyl	Dinuclear aromatic	255.0
$C_{13}H_{12}$	2-Methylbiphenyl	Dinuclear aromatic	255.3
$C_{12}H_{12}$	2-Ethylnaphthalene	Dinuclear aromatic	257.9
$C_{12}H_{12}$	1-Ethylnaphthalene	Dinuclear aromatic	258.7
$C_{12}H_{12}$	2,6-Dimethylnaphthalene	Dinuclear aromatic	262
$C_{12}H_{12}$	2,7-Dimethylnaphthalene	Dinuclear aromatic	263
$C_{12}H_{12}$	1,7-Dimethylnaphthalene	Dinuclear aromatic	263
$C_{12}H_{12}$	1,6-Dimethylnaphthalene	Dinuclear aromatic	263
$C_{12}H_{12}$	1,3-Dimethylnaphthalene	Dinuclear aromatic	265
$C_{12}H_{12}$	1,5-Dimethylnaphthalene	Dinuclear aromatic	265
$C_{14}H_{14}$	2,5-Dimethylbiphenyl	Dinuclear aromatic	267
$C_{15}H_{16}$	Trimethylbiphenyl	Dinuclear aromatic	267
$C_{16}H_{18}$	Tetramethylbiphenyl	Dinuclear aromatic	267

RP-1 SURROGATE FUELS			
Formula	Species	Mol %	NBP(°C)
$C_{13}H_{12}$	methylbiphenyl	17.4	255
$C_{12}H_{24}$	n-heptylcyclopentane	45.4	224
$C_{12}H_{28}$	n-tridecane	37.2	235
		100.0	

$M_{wt} = 173.9$
$H/C = 1.922$

Note: Critical pressure for RP-1 is 340 psia, and critical temperature is 679°K.

RP-1 COMBUSTION PROPERTIES

HEAT OF COMBUSTION

HOC = -18640 (Btu/lbm) = -10.346 (kcal/gm)

HEAT OF VAPORIZATION

HOV = 106 (Btu/lbm)

HEAT OF FORMATION (HOF)

To determine a HOF for mixtures, an effective molecular formula must be specified and used to evaluate the HOF. Frequently, an arbitrary molecular weight of 100 gms is assumed for a basis for thermodynamic calculations.

H/C	HOF(kcal/100gm)	Source	Implied HOC (kcal/gm)
1.8624	-36.01	Lockheed	-10.287
1.90	-41.6	SAIC	-10.305
2.0	-44.36	Aerojet '78	-10.403
1.9063	-42.0	TMX - 1783	-10.305
1.9423	-33.068(v)	SP-273	-10.441(v)
1.9423	-38.946(l)	SP-273	-10.382(1)
1.922	-39.915	Surrogate Fuel	-10.346

SPECTROSCOPIC ANALYSIS OF H-1 GAS GENERATOR EXHAUST GASES			
Compound	Sample #1	Sample #3	Sample #4
CO	26.15*	36.82	37.93
CO_2	8.44	8.86	9.96
H_2O	2.66	1.14	0.85
H_2	1.97	2.22	2.34
CH_4	2.92	4.20	4.40
C_2H_2	4.16	5.62	4.27
C_2H_4	5.93	6.93	7.70
C_2H_6	0.72	...	...
Propyne	0.69	0.30	0.41
Propene	2.84	3.15	3.95
Diacetylene	0.12	0.08	0.21
1,3 Butadiene	1.30	1.32	1.52
2 Butene	1.57	0.80	1.16
- Butene	...	1.76	0.54
1.5 Hexadyne	1.98	1.58	1.73
3 Methyl Pentene -1	...	0.71	0.57
Cyclopentene	...	0.74	0.99
1,2,3 trimethylcyclopantane	...	1.14	0.97
Benzene	...	1.05	1.20
Ethyl Benzene	...	0.99	0.36
Carbon	...	5.22	2.06
RP-1	38.51	17.58	17.14

* Weight percentage composition of combustion products

Generalized Combustion Kinetics Model

I. PURE PYROLYSIS	$\begin{bmatrix}\text{ALIPHATICS}\\ \text{AROMATICS}\end{bmatrix} \rightarrow \begin{bmatrix}C_2H_2\\ CH_4\\ C_2H_4\\ H_2\end{bmatrix} \equiv \text{INTERMEDIATES}$	V. SOOT FORMATION	$\begin{bmatrix}\text{ALIPHATICS}\\ \text{AROMATICS}\\ \text{INTERMEDIATES}\end{bmatrix} \rightarrow \text{SOOT}$	
II. OXIDATIVE PYROLYSIS	$\begin{bmatrix}\text{ALIPHATICS}\\ \text{AROMATICS}\end{bmatrix} + \begin{bmatrix}OH\\ O_2\end{bmatrix} \rightarrow \begin{bmatrix}CH_4\\ C_2H_2\\ C_2H_4\end{bmatrix} + \begin{bmatrix}H_2\\ C_xH_yO_z\end{bmatrix}$	VI. SOOT GASIFICATION	$\text{SOOT} + \begin{bmatrix}O_2\\ CO\\ CO_2\\ H_2O\\ H_2\\ OH\end{bmatrix} \rightarrow \begin{bmatrix}CO\\ CO_2\\ CH_4\end{bmatrix}$	
III. PARTIAL OXIDATION	$\begin{bmatrix}\text{ALIPHATICS}\\ \text{AROMATICS}\\ CH_4\\ C_2H_2\\ C_2H_4\end{bmatrix} + \begin{bmatrix}O_2\\ OH\end{bmatrix} \rightarrow \begin{bmatrix}H_2\\ CO\\ C_xH_yO_z\\ CO_2\\ H_2O\end{bmatrix}$	VII. NO_x FORMATION	$\text{FUEL} + \begin{bmatrix}FBN\\ N_2\end{bmatrix} \rightarrow \begin{bmatrix}HCN\\ NH_i\end{bmatrix}$ $\begin{bmatrix}HCN\\ NH_i\end{bmatrix} + \begin{bmatrix}O_2\\ OH\end{bmatrix} \rightleftarrows \begin{bmatrix}NO\\ NO_2\end{bmatrix}$	BOUND NITROGEN AND/OR FUEL RICH NITROGEN CONVERSION
IV. ELEMENTARY STEPS TO COMPLETION	$\begin{bmatrix}CO\\ H_2\\ C_xH_yO_z\\ H_2O_2\end{bmatrix} + \begin{bmatrix}O\\ H\\ OH\\ CHO\\ HO_2\end{bmatrix} \rightleftarrows \begin{bmatrix}H_2O\\ CO_2\end{bmatrix}$		$\begin{bmatrix}N_2\\ O_2\\ N\end{bmatrix} + \begin{bmatrix}O\\ N\\ OH\end{bmatrix} \rightarrow NO + \begin{bmatrix}N\\ O\\ H\end{bmatrix}$	THERMAL FIXATION

Soot Model

Initial Polycyclic Aromatic Hydrocarbon (PAH) Formation

- Pyrolysis and combustion of fuel to form benzene and acetylene
- Implicit finite-rate chemistry

Planar PAH Growth

- HACA
    - Hydrogen abstraction, carbon addition (through reactions with acetylene)
- Oxidation
    - Implicit finite-rate chemistry using reactions from Frenklach, et al
- Properties for PAH compounds
    - Benson's group contribution method to obtain C_p for ideal gases
    - Benson data in tabular form for $300K < T < 1500K$
    - Used CEC data for selected species to generate group contributions as functions of temperature for $300K < T < 5000K$
    - Generated needed C_p data in CEC format
    - S^o_{298} corrected for symmetry and optical isomers using Benson's data.

Soot Model (Cont.)

Aerosol Dynamics Based on Frenklach and Harris's "Method II"

- Method of moments
- Nucleation
  - Collisions of planar PAH's to form 3-D particles
- Coagulation
  - Collisions of 3-D particles to form larger particles

Surface Growth on 3-D Particles

- Collisions with planar PAH's
- HACA
- Oxidation by reactions with O_2 and OH

Model provides soot formation and oxidation rates to be used to develop a quasiglobal reaction rate for soot production.

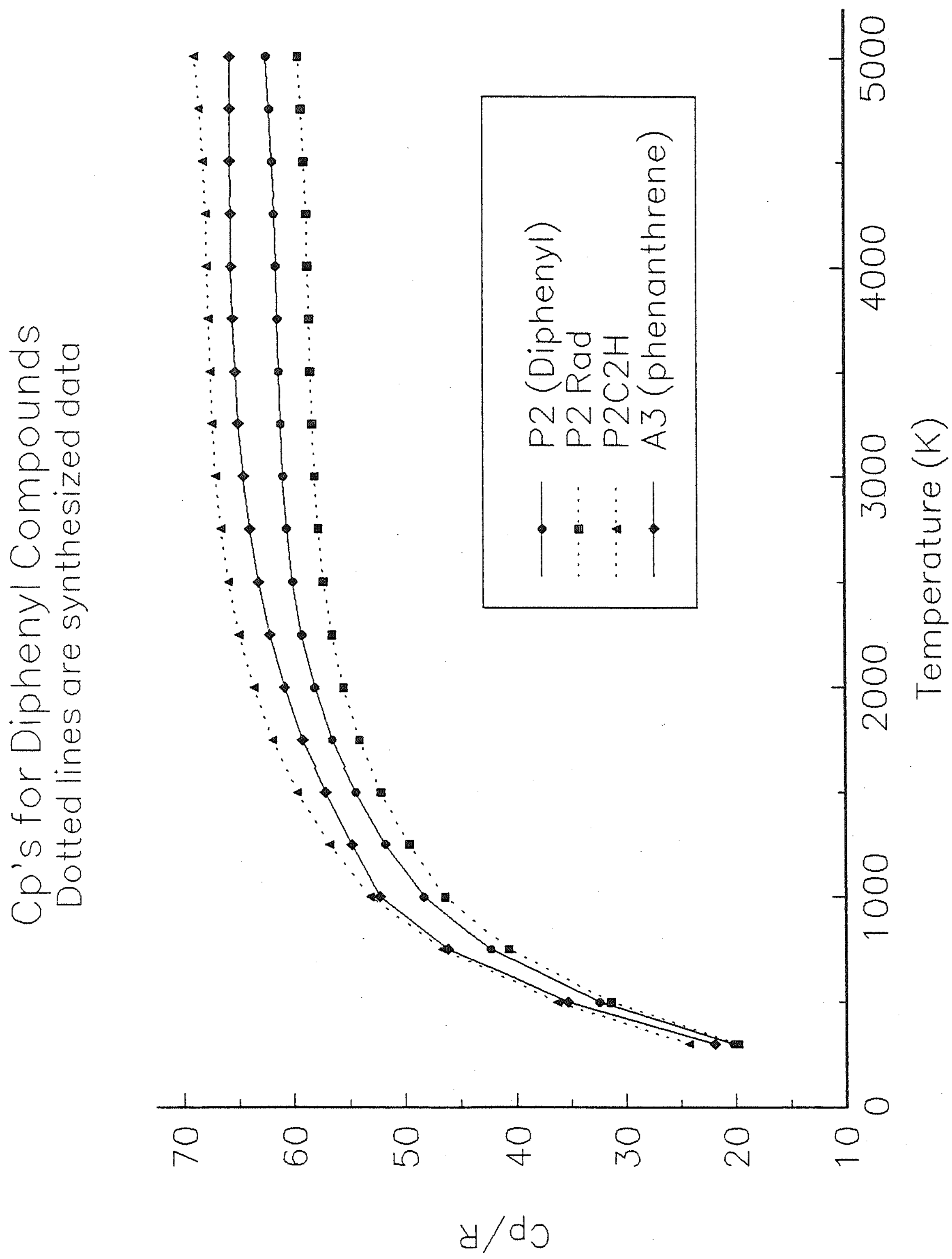

Cp's for Diphenyl Compounds
Dotted lines are synthesized data
P2 (Diphenyl)
P2 Rad
P2C2H
A3 (phenanthrene)
Cp/R
Temperature (K)
10
20
30
40
50
60
70
0
1000
2000
3000
4000
5000

Toluene and Iso-Octane Quasiglobal Kinetics Model

GLOBAL MECHANISM	A	B	E/R	POWER DEPENDENCIES
Toluene (aromatic)				
$C_7H_8 \rightarrow 3.5\ C_2H_2 + 0.5\ H_2$	1.7982 E10	0	3.5000 E4	$[C_7H_8]^{1.0}$
$C_7H_8 + 3.5\ O_2 \rightarrow 7\ CO + 4\ H_2$	4.4963 E9	1	2.6785 E4	$[C_7H_8]^{0.5}[O_2]^{1.0}$
$C_7H_8 + OH \rightarrow 3.25\ C_2H_2 + 0.5\ CO + 0.5\ H_2O + 0.75\ H_2$	1.4721 E17	0	1.4510 E4	$[C_7H_8]^{1.0}[OH]^{1.0}$
Iso-Octane (aliphatic)				
$C_8H_{18} \rightarrow 4\ C_2H_4 + H_2$	1.0473 E12	0	3.5229 E3	$[C_8H_{18}]^{1.0}$
$C_8H_{18} + 4\ O_2 \rightarrow 8\ CO + 9\ H_2$	1.2900 E9	1	2.5160 E4	$[C_8H_{18}]^{0.5}[O_2]^{1.0}$
$C_8H_{18} + OH \rightarrow 3.75\ C_2H_4 + 0.5\ CO + 0.5\ H_2O + 1.5\ H_2$	2.0000 E17	0	1.4919 E4	$[C_8H_{18}]^{1.0}[OH]^{1.0}$
Secondary Fuel				
$C_2H_2 + 6\ OH \rightarrow 4\ H_2O + 2\ CO$	4.7850 E15	0	1.3883 E4	$[C_2H_2]^{1.0}[OH]^{1.0}$
$C_2H_2 + 2\ OH \rightarrow 2\ CO + 2\ H_2$	2.8000 E16	0	0	$[C_2H_2]^{1.0}[OH]^{1.5}$
$C_2H_4 + 4\ OH \rightarrow 2\ CO + 2\ H_2O + 2\ H_2$	2.2020 E15	0	1.2079 E4	$[C_2H_4]^{1.0}[OH]^{1.0}$
$C_2H_4 + 2\ OH \rightarrow 2\ CO + 3\ H_2$	2.1129 E27	-3.0	6.3062 E3	$[C_2H_4]^{1.0}[OH]^{1.5}$
$C_2H_2 + O_2 = 2\ CHO$	4.0000 E12	0	1.4092 E4	$[C_2H_2]^{1.0}[O_2]^{1.0}$
$C_2H_4 + M = C_2H_2 + H_2 + M$	2.0893 E17	0	3.9810 E4	$[C_2H_4]^{1.0}[M]^{1.0}$
Soot Parameters				
C_7H_8 = HC→ soot	4.0465 E14	-2.0	1.6110 E4	$[HC]^{1.43}[O_2]^{-0.5}$
i = A	2.000 E1	0	1.5090 E4	As indicated by the equation for [soot]
B	4.4600 E-3	0	7.6490 E3	
T	1.5100 E5	0	4.8820 E4	
Z	2.1300 E1	0	-2.0630 E3	

SOOT PARAMETERS

$$soot + O_2 \rightarrow CO_2 \qquad 12\, P_{O_2}\, A_t \left[\frac{K_A X}{1 + K_Z P_{O_2}} + K_B (1 - X) \right]$$

$$X = \left[1 + K_T / \left(K_B\, P_{O_2} \right) \right]^{-1}$$

$$K_i = A_i \exp \{ -E_i / RT \}, \quad i = A, B, T, Z$$

where $A_t = 6\, [C_s / (\rho_s \bullet D_s)]$ (cm^2 surface/cm^3),
P_{O2} = partial pressure of O_2 (atm),

C_s = (g • soot/cm^3 of gas), ρ_s = (g • soot/cm^3 of soot),
D_s = diameter of soot (cm),

[soot] = mass of soot/volume of gas (g/cm^3).

Elementary Reactions

ELEMENTARY MECHANISM	A	B	E/R
<u>Wet CO Mechanism</u>			
$H_2 + O_2 = OH + OH$	1.7000 E13	0	2.4070 E4
$OH + H_2 = H_2O + H$	2.1900 E13	0	2.5900 E3
$OH + OH = O + H_2O$	6.0230 E12	0	5.5000 E2
$O + H_2 = H + OH$	1.8000 E10	1.0	4.4800 E3
$H + O_2 = O + OH$	1.2200 E17	-0.91	8.3690 E3
$M + O + H = OH + M$	1.0000 E16	0	0
$M + O + O = O_2 + M$	2.5500 E18	-1.0	5.9390 E4
$M + H + H = H_2 + M$	5.0000 E15	0	0
$M + H + OH = H_2O + M$	8.4000 E21	-2.0	0
$CO + OH = H + CO_2$	4.0000 E12	0	4.0300 E3
$CO + O_2 = CO_2 + O$	3.0000 E12	0	2.5000 E4
$CO + O + M = CO_2 + M$	6.0000 E13	0	0

RP-1 COMBUSTION VERIFICATION EXPERIMENTS

Criteria: Minimize Effect of Turbulent Mixing

- Single Drop Combustion - LSU
- Well Stirred Reactor - Exxon
- Rocket Test Motor - General Dynamics Corporation (GDC)

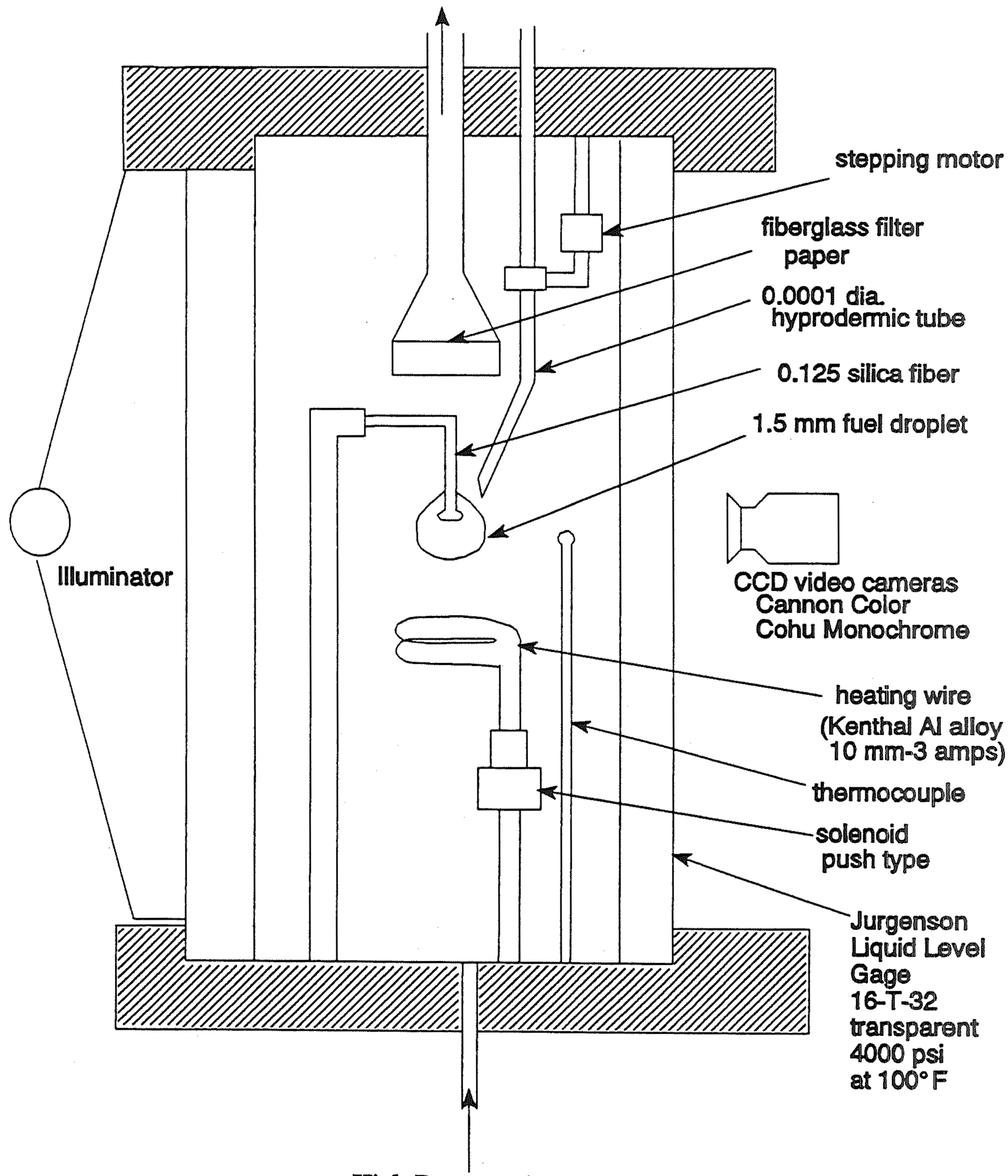

High Pressure Apparatus for the
Measurement of Single Droplet Combustion

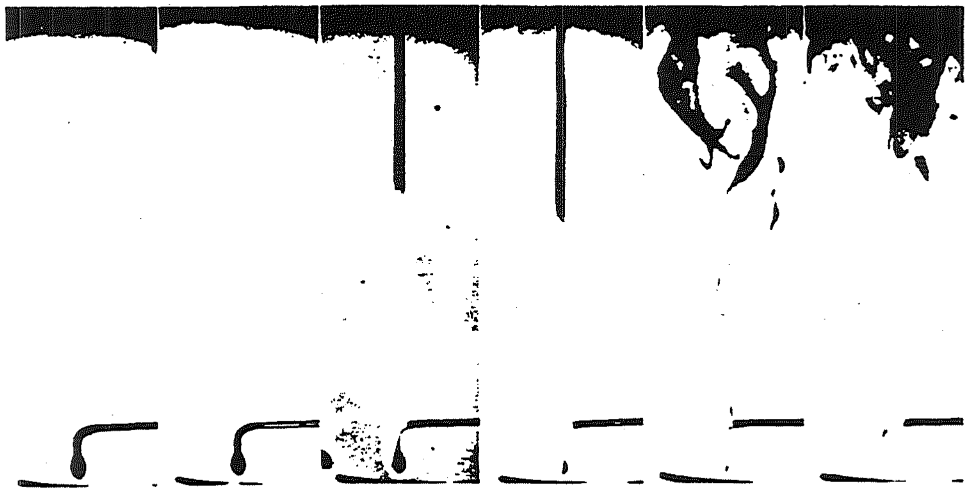

a. P=0.1MPa b. 0.2MPa c. 0.6MPa d. 1.1MPa e. 2.1MPa f. 3.0MPa

Photograph of Burning Droplets (n-heptane in air).

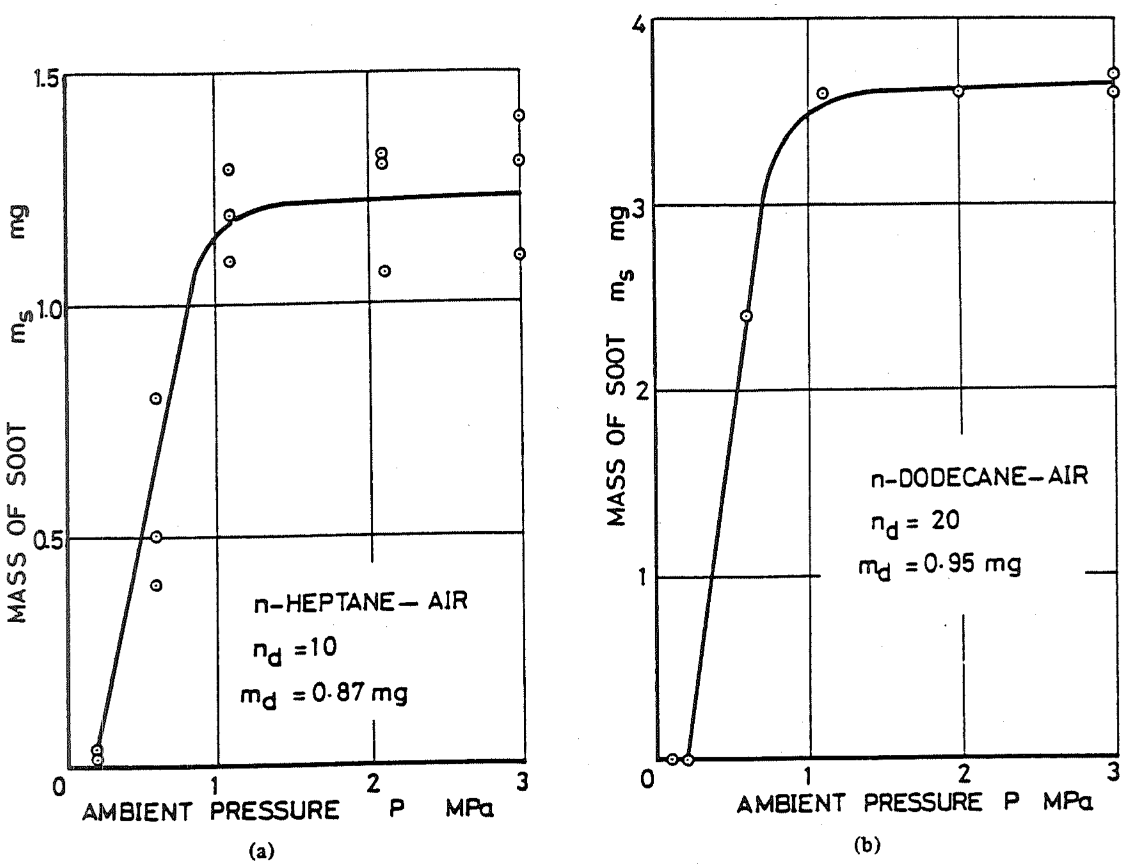

Effect of Pressure: (a) n-heptane; (b) n-dodecane.

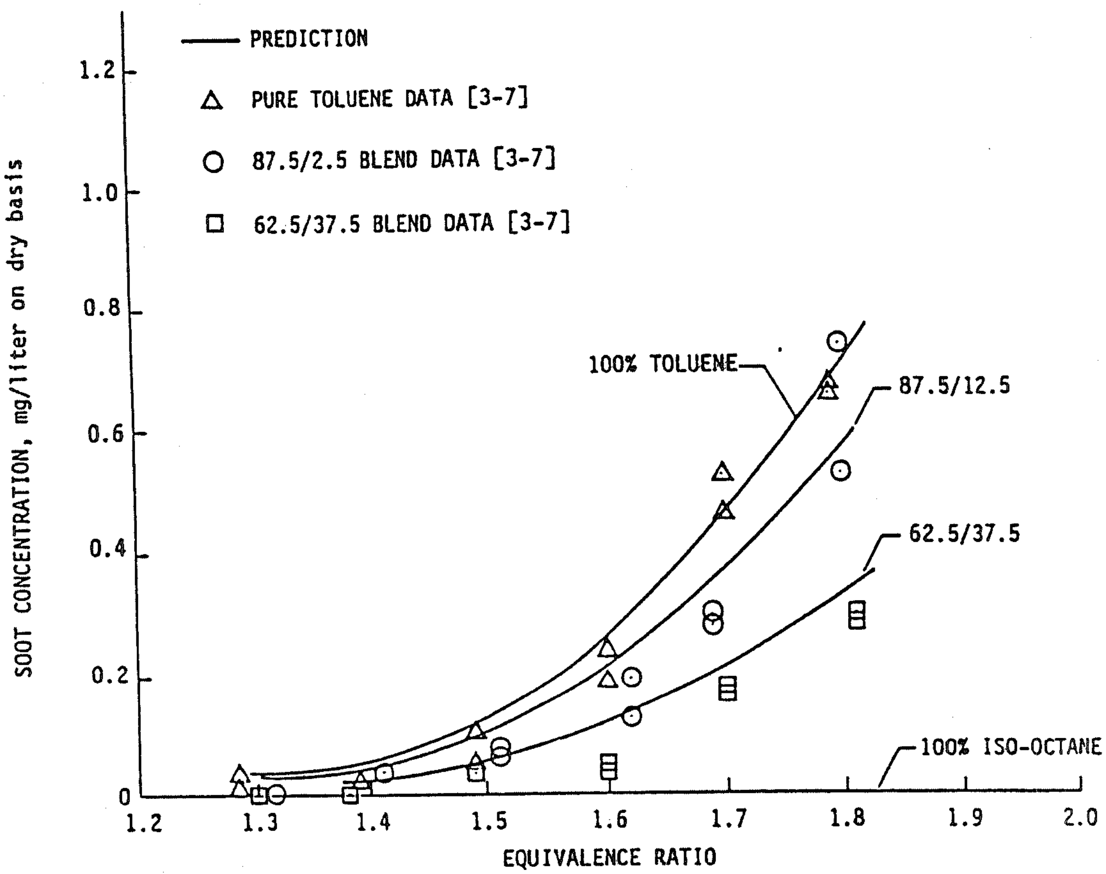

Comparison Of Quasiglobal Model Prediction Of Soot Emissions With Experimental Data For Toluene And Toluene/Iso-Octane Blends. Computation: Well-Stirred Reactor; Experiment: Jet-Stired Combustor.

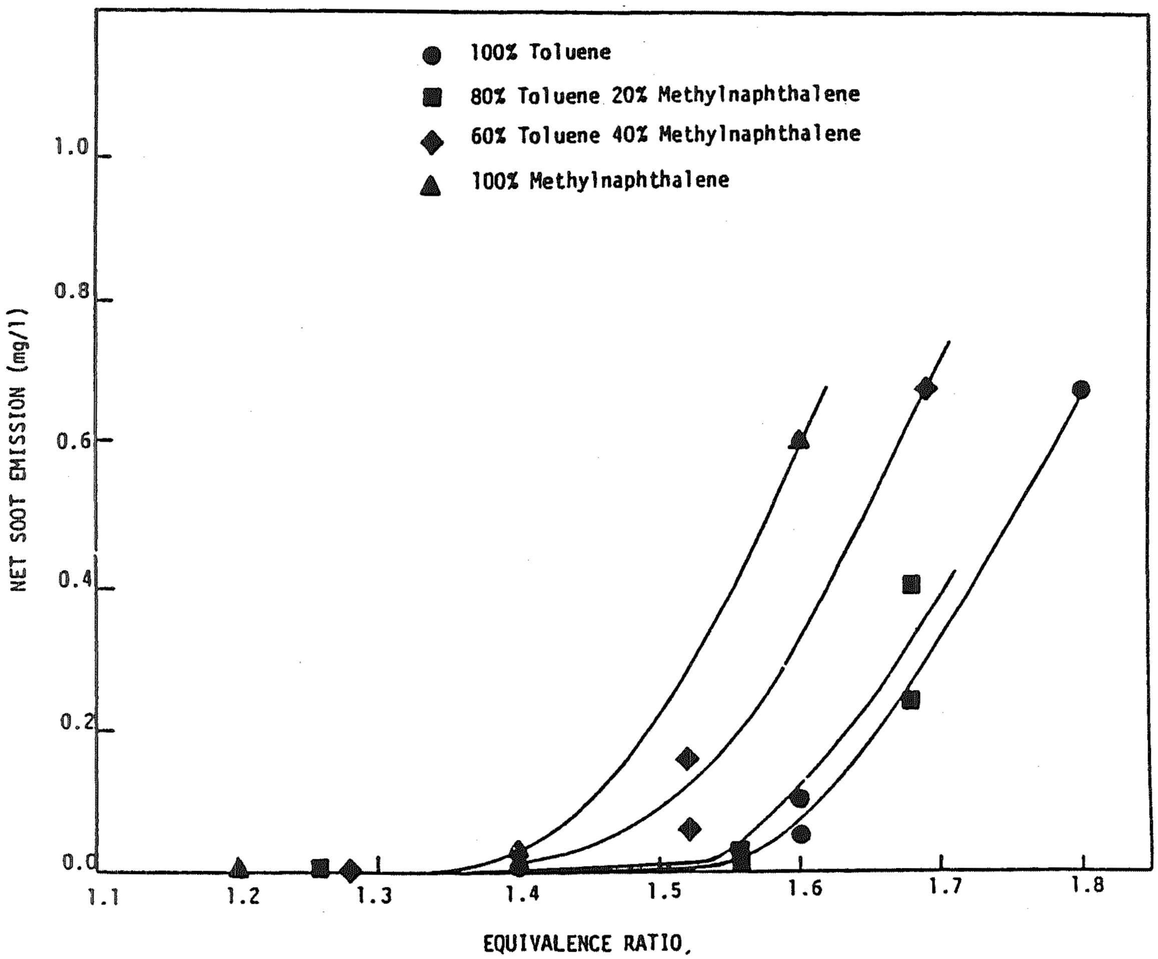

JSC Soot Emissions For Toluene/Methylnaphthalene Blends;
T = 1900 K; τ = 3 ms.

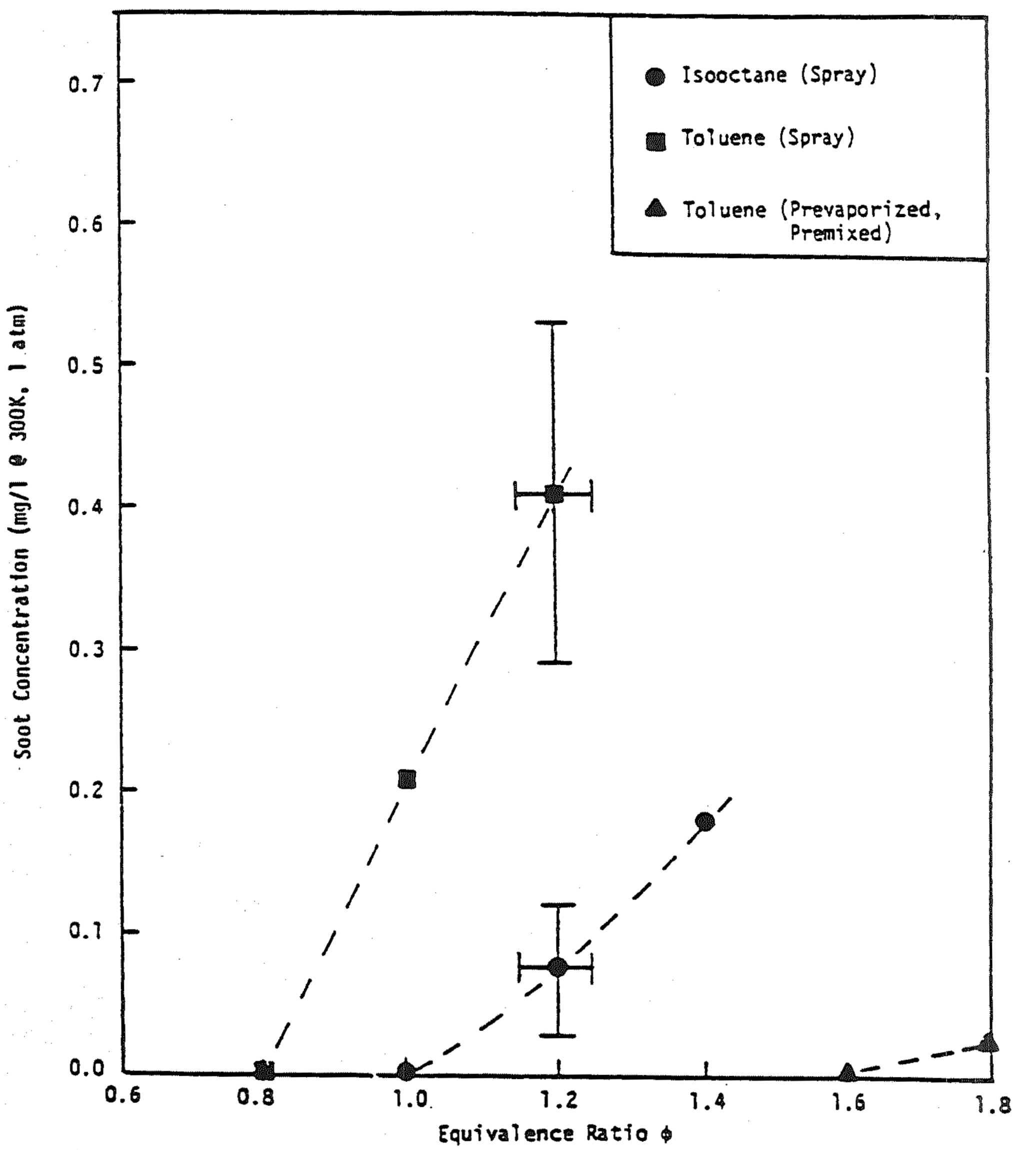

Dependence Of Soot Concentration On Equivalence Ratio; Ratio; Atomization Air = 15 g/min/nozzle; Indicated Temperature = 1900±35K.

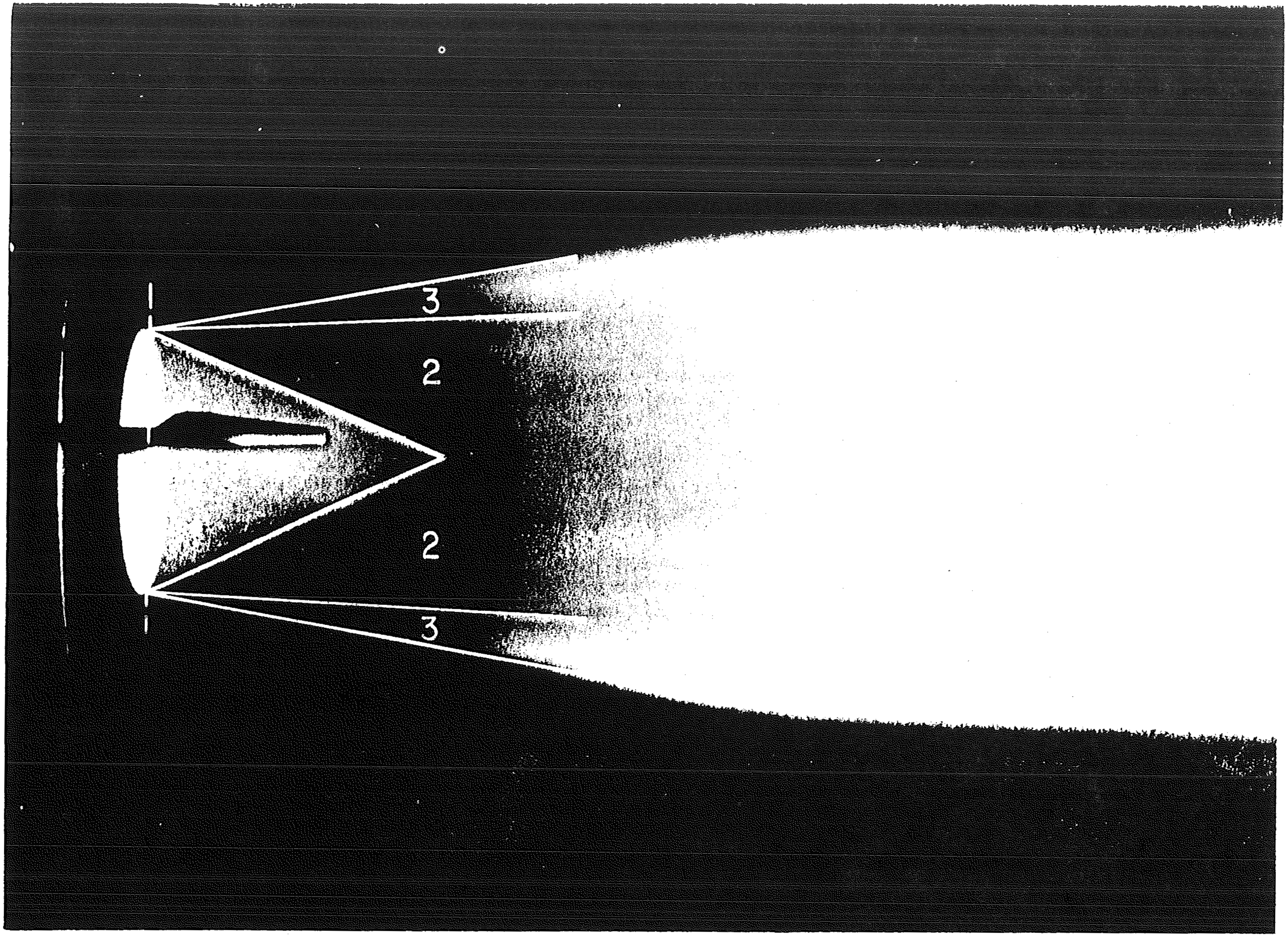

Photograph of the exit flow at an exit pressure of 2 atm. Region 1 is the undisturbed cone, region 2 is the Prandtl-Meyer expansion zone, and region 3 is the mixing zone. The spectrometer line of sight is indicated by a dotted line.

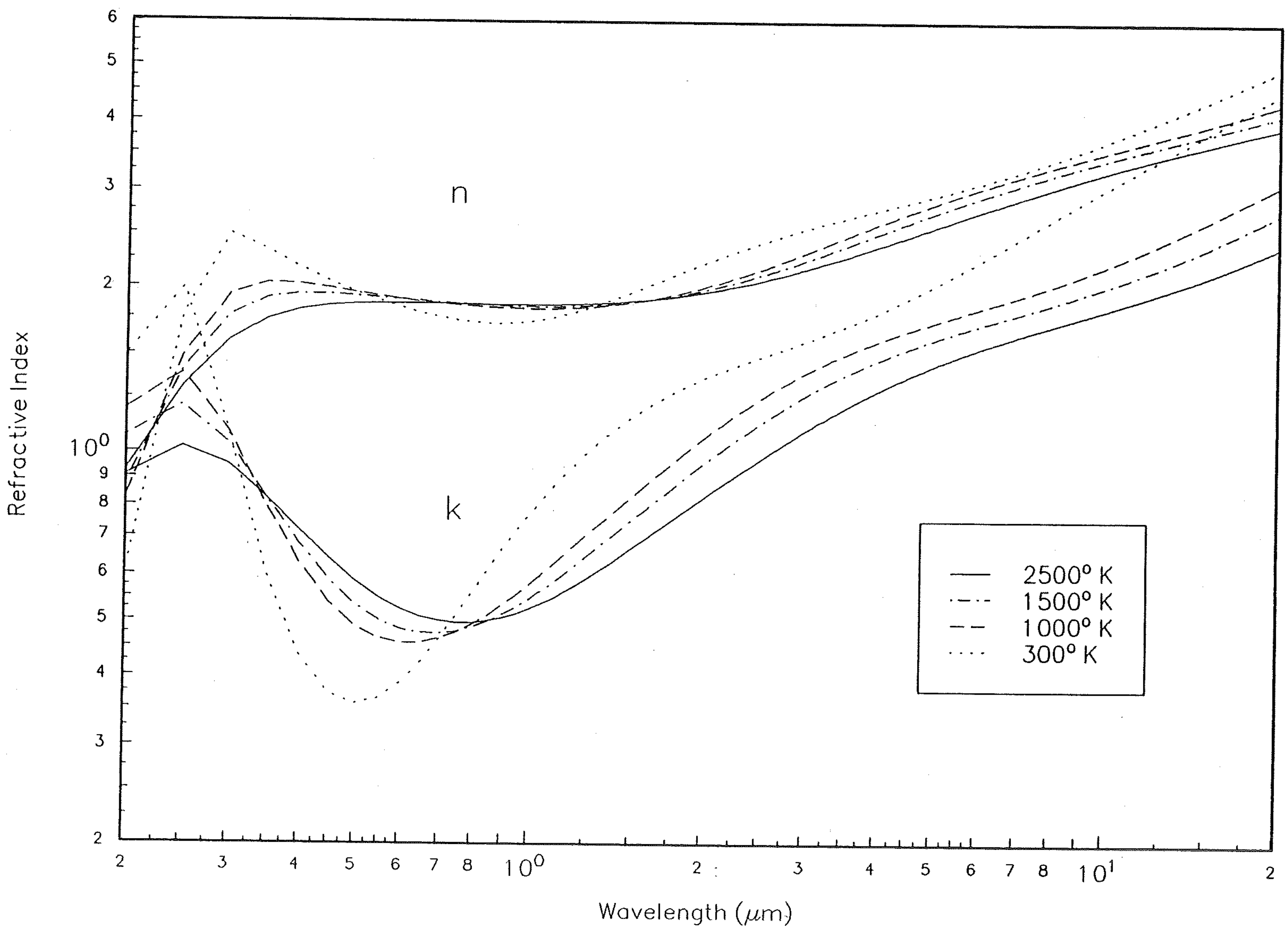

n
k
Refractive Index
Wavelength (μm)
2500° K
1500° K
1000° K
300° K

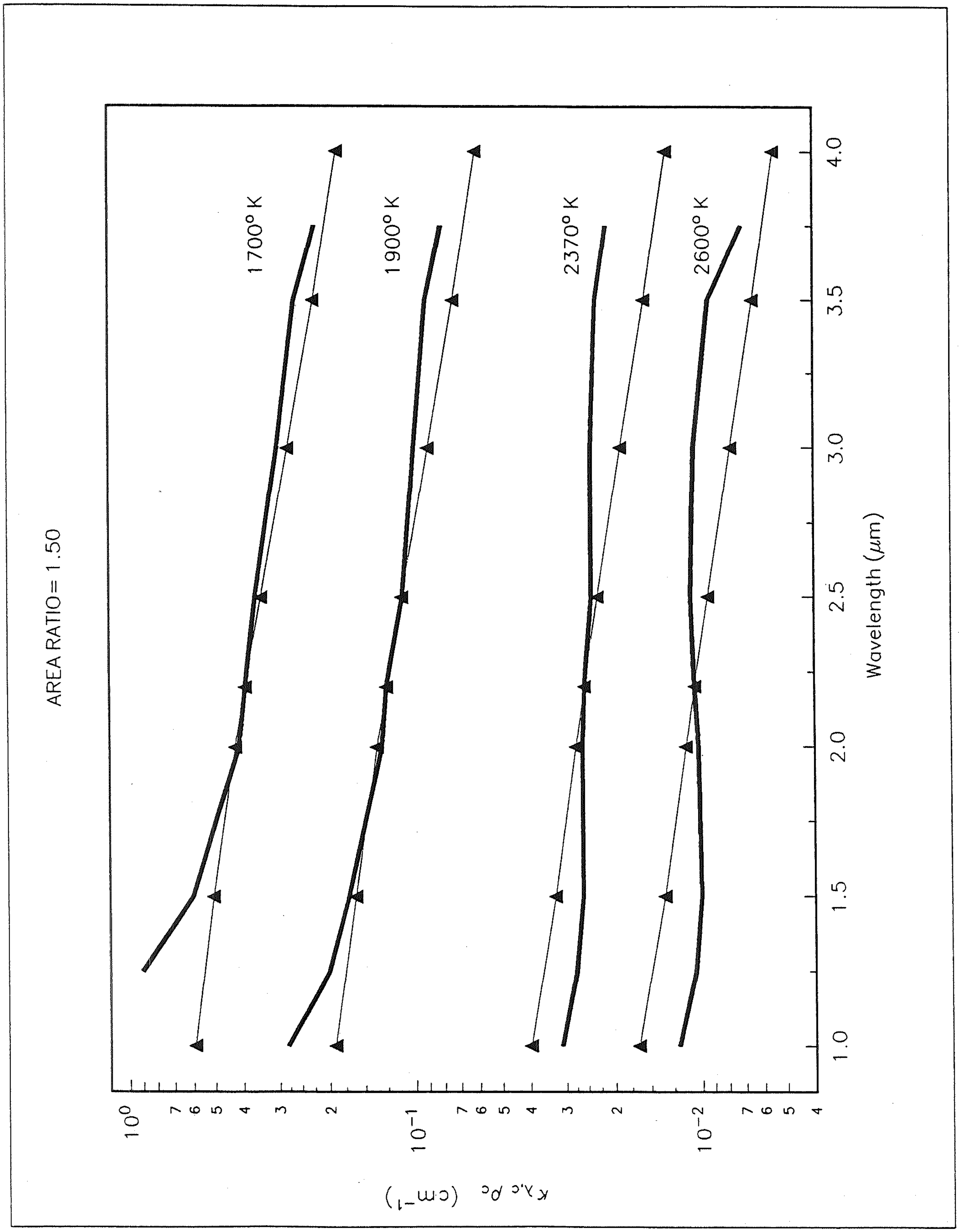
AREA RATIO= 1.50
1700° K
1900° K
2370° K
2600° K
Wavelength (μm)
1.0
1.5
2.0
2.5
3.0
3.5
4.0
$\kappa_{\lambda,c}\,\rho_c$ (cm^{-1})
10^0
10^{-1}
10^{-2}

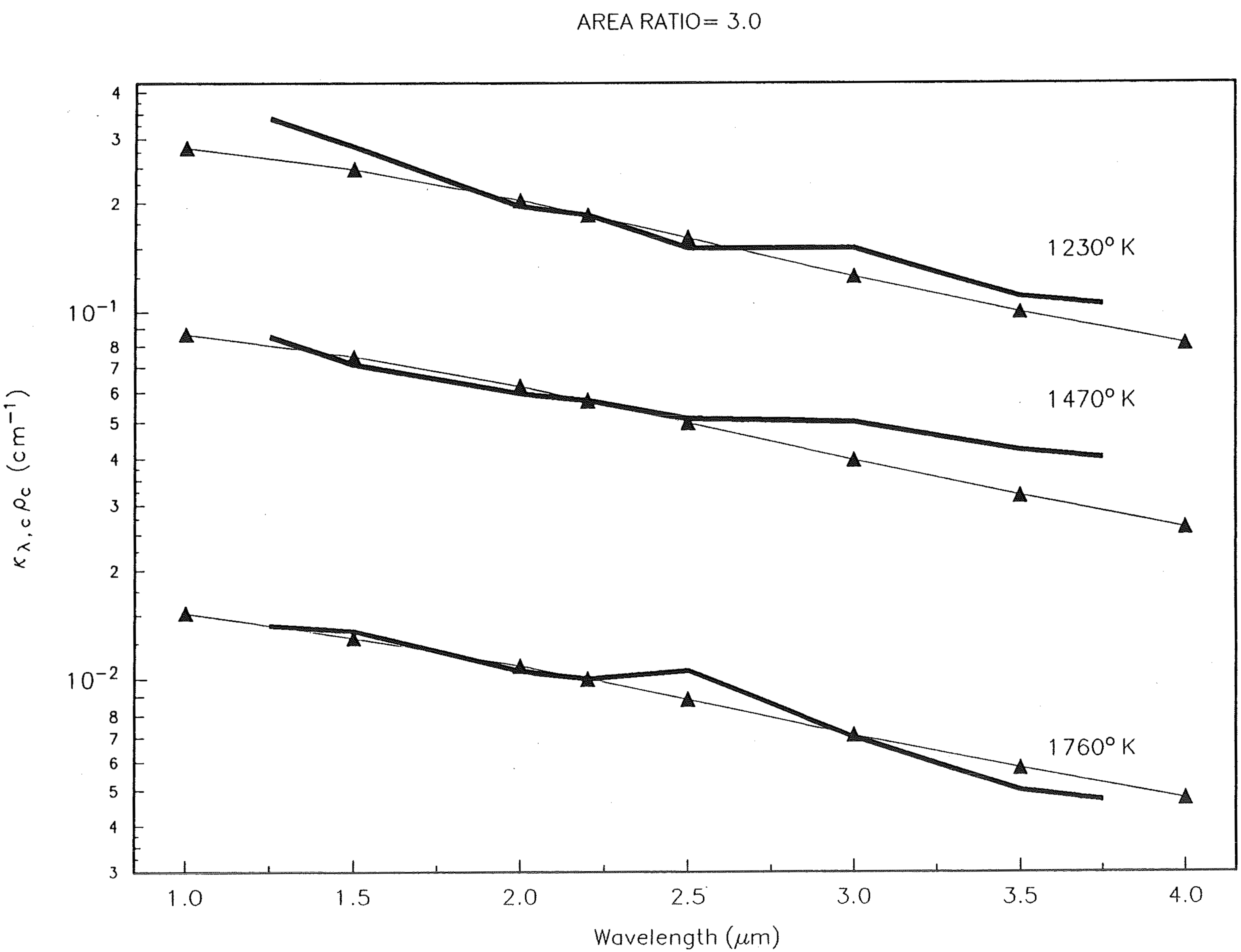
AREA RATIO= 3.0
1230° K
1470° K
1760° K
$\kappa_{\lambda,c}\,\rho_c$ (cm^{-1})
10^{-1}
10^{-2}
4
3
2
8
7
6
5
1.0
1.5
2.0
2.5
3.0
3.5
4.0
Wavelength (μm)

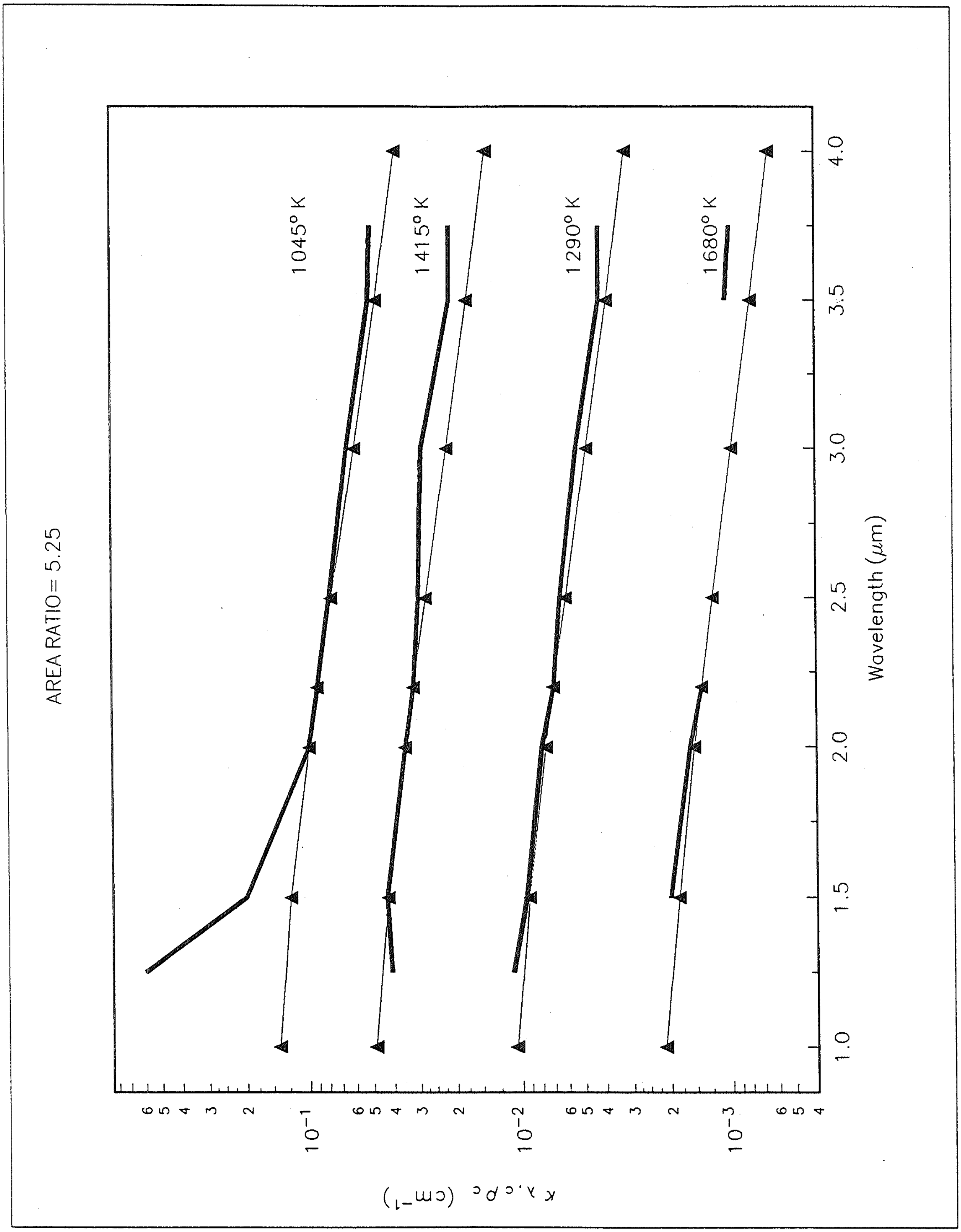
AREA RATIO= 5.25
1045° K
1415° K
1290° K
1680° K
Wavelength (μm)
κ λ,c ρc (cm⁻¹)

Soot Density from GDC Experiments				
$\kappa_\lambda \rho_c$ (cm^{-1})	T(°K)	O/F	ρ_c(gm/cc)	κ_λ(cm^2/gm)
0.1400E-02	1680.0000	1.8500	0.1087E-06	0.1288E+05
0.7000E-02	1415.0000	1.6000	0.5200E-06	0.1346E+05
0.3200E-01	1290.0000	1.5000	0.2343E-05	0.1366E+05
0.9000E-01	1045.0000	1.3300	0.6531E-05	0.1378E+05
0.1000E-01	1760.0000	1.6000	0.7886E-06	0.1268E+05
0.5700E-01	1470.0000	1.4500	0.4268E-05	0.1335E+05
0.1850E+00	1230.0000	1.2500	0.1348E-04	0.1373E+05
0.1050E-01	2600.0000	2.1000	0.9944E-06	0.1056E+05
0.2550E-01	2370.0000	1.8500	0.2295E-05	0.1111E+05
0.1250E+00	1900.0000	1.5000	0.1015E-04	0.1232E+05
0.3900E+00	1700.0000	1.4000	0.3040E-04	0.1283E+05

Rayleigh Theory for Small Particles

$$K_\lambda = \left(\frac{36\pi nk}{(n^2-k^2+2)^2 + 4n^2k^2}\right)\left(\frac{\rho_c}{\rho_o}\right)\left(\frac{1}{\lambda}\right)$$

$K_\lambda(cm^{-1}) = \kappa_\lambda \, \rho_c$ = linear absorption coefficient

$\kappa_\lambda(cm^2/gm)$ = mass absorption coefficient

ρ_c (gm/cc of volume) = soot density

ρ_o (gm/cc of soot) = bulk soot density

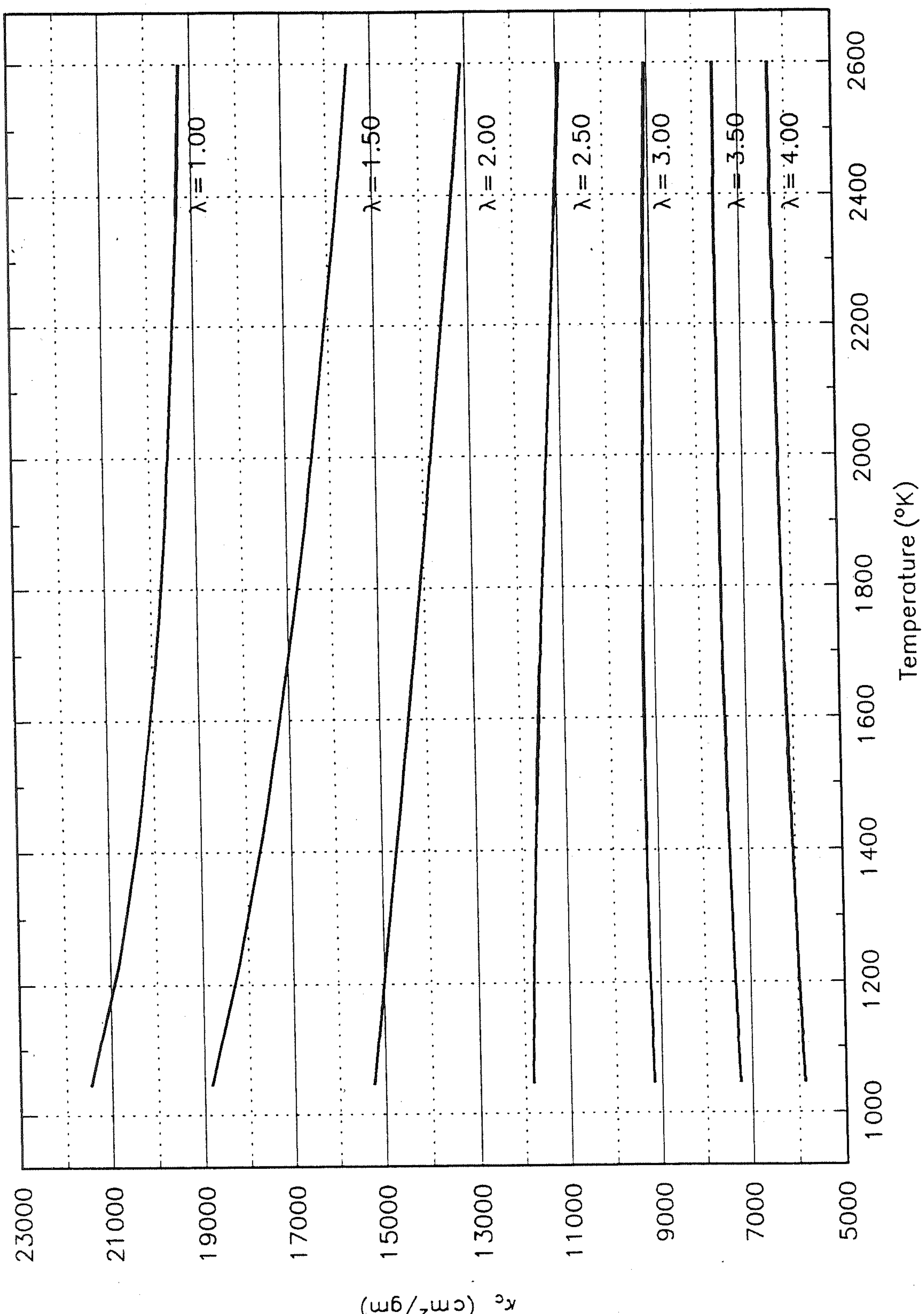
λ = 1.00
λ = 1.50
λ = 2.00
λ = 2.50
λ = 3.00
λ = 3.50
λ = 4.00
Temperature (°K)
κc (cm²/gm)
23000
21000
19000
17000
15000
13000
11000
9000
7000
5000
1000
1200
1400
1600
1800
2000
2200
2400
2600

CONCLUSIONS:

Real fluid RP-1 and H_2 combustion kinetics models will be incorporated into several element models and evaluated.

The element models will be assembled into an entire injector model and the motor performance evaluated.

Thermo-Kinetics Characterization of Kerosene/RP-1 Combustion for Tripropellant Engine Design Calculations

Ten-See Wang

Computational Fluid Dynamics Branch

NASA/Marshall Space Flight Center

13th Workshop for CFD Applications in Rocket Propulsion

and Launch Vehicle Technology

Session 10: Combustion/Nozzles/Tripropellant

April 26, 1995

NASA/Marshall Space Flight Center, MSFC, Alabama

Omit to
p 879

Acknowledgments

- The development of the thermo-kinetics models for kerosene/RP-1 combustion is performed under the Rocketdyne - Marshall Space Flight Center Cooperative Agreement.
- The multi-phase FDNS CFD code is being developed by Engineering Sciences, Inc. under the sponorship of SBIR Program.
- Several individuals have contributed to the discussion and collection of kerosene/RP-1 physical properties:

  - Dr. R.C. Farmer; SECA, Inc.

  - Dr. Y.-S. Chen; ESI

  - John Hutt, Hou Trinnh, Klaus Gross; NASA - MSFC

  - Dr. C.-P. Chen, UAH.

Objectives

- To develop a simple substitute fuel model representing kerosene/RP-1 and to develop its thermochemical properties according to the available database.
- To develop a simplified combustion kinetics model for the substitute fuel
- To test this thermo-kinetics model on 3 tri-axial, tri-propellant, single element injectors

Introduction

- Kerosene is derived from petroleum and RP-1 is a straignt run from kerosene fraction. Both are complex mixtures of many substances and the actual composition depends on the specifications.
- Elemental formulas have been formulated for thermo-equilibrium calculations, but they can not be used for CFD design applications.
- A molecular substitute fuel model has to be developed to approximate the general thermo-physical properties of kerosene/RP-1.
- While multi-component fuel model can be formulated if the information is available, for which it is not, a one-component model is most efficient for computational purpose.
- This fuel model can be refined to tailor specific fuel specifications if the information is available.

Physical-thermo-chemical properties of kerosene/RP-1.

	Kerosene	RP-1
Molecular Formula		
Molecular Weight	175[S6]	172-175[C4]
Elemental Formula		$CH_{1.95}$-$CH_{2.0}$[C4], $CH_{1.9423}$[S7], $CH_{1.953}$[S6]
Formula Weight		13.97-14.03[C4], 13.97[S7]
H_c, Btu/lb	-18500[M4], -18577[C3]	-18433[C4], -18640[S7]
$H_{f,298K}$, cal/mole		-5430[S7]/$CH_{1.9423}$
$C_{p,516k,1\ atm}$, cal/mole-K		101[C4]
Paraffins (n and iso) %		41[C4]
Naphthenes %		56[C4]
Aromatics %	5[M4]	5[N1], 3[C4]
Olefins %	1[M4]	0[C4]

Thermodynamic Consistency Test 1

- $C_nH_m + (n + 0.25m)\ O_2 = n\ CO_2 + 0.5m\ H_2O$

  $Hf(C_nH_m) = n\ Hf(CO_2) + 0.5m\ Hf(H_2O) - Hc$

Pioneering fuel models for kerosene/RP-1

Formula	$H_{f,298K}$	M	H/C	Composition	Reference
$C_{10}H_{19}$	-57.1	139	1.90	-	Harsha, et al., 1982
$C_{12}H_{26}$	-69.5	170	2.17	Paraffin	Lawver, 1982
$C_{12}H_{23}$	-57.1	167	1.91	-	Amsden, 1993
$C_{12.5}H_{28.8}$	-37.5	175	2.37	-	Chen, et al., 1993

One-Component Kerosene/RP-1 Substiture Fuel: $C_{12}H_{24}$
: Pentyl-Methylcyclohexane
:Pentyl-Methylcyclohexane/n-Dodecene

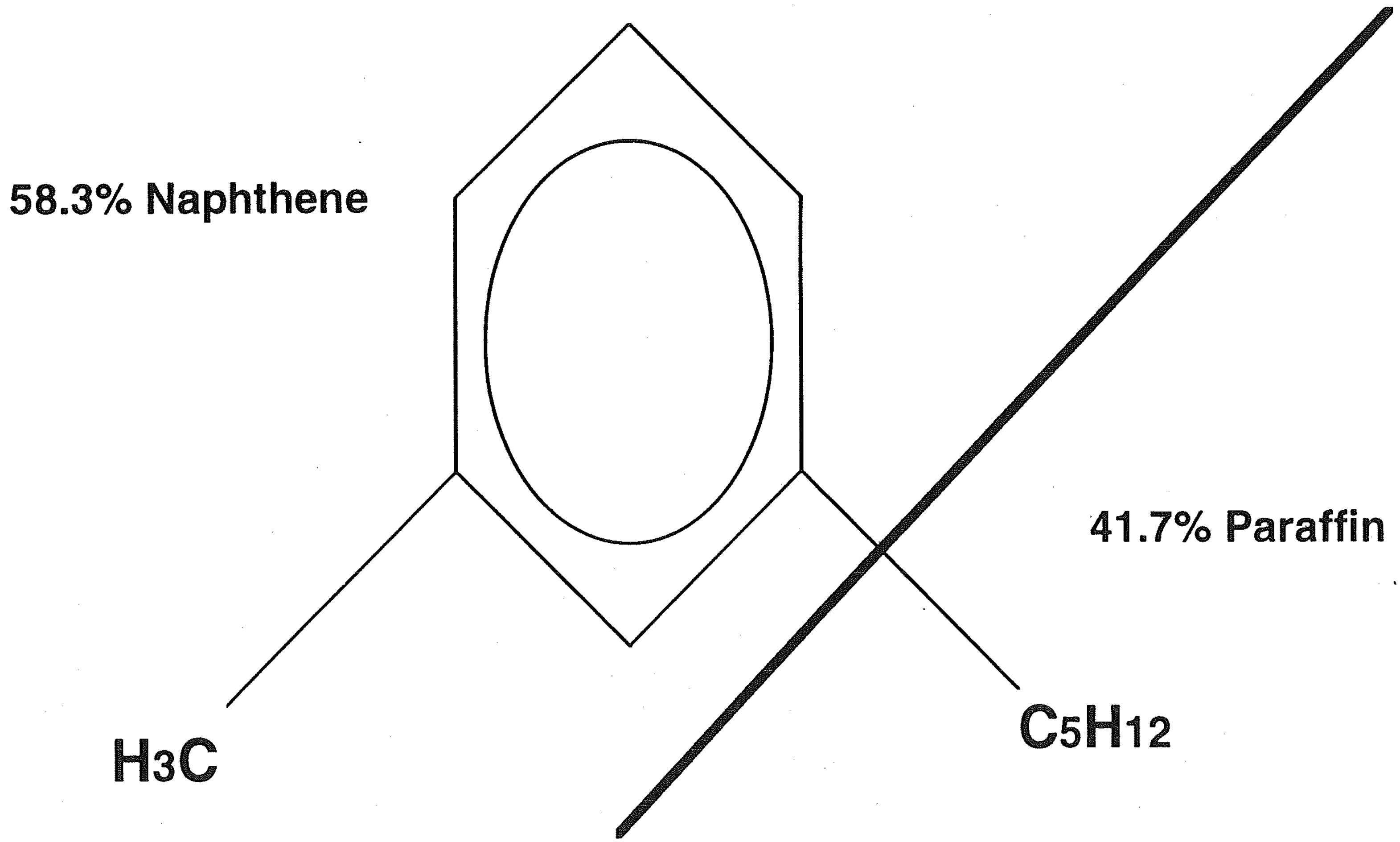

Comparison of thermo-chemical characterization of model fuel with reported data.

	Kerosene	RP-1	Kerosene/RP-1 substitute fuel model
Molecular Formula			$C_{12}H_{24}$
Molecular Weight	175[S6]	172-175[C4]	168
Elemental Formula		$CH_{1.95}$-$CH_{2.0}$[C4], $CH_{1.9423}$[S7],$CH_{1.953}$[S6]	$CH_{2.0}$
Formula Weight		13.97-14.03[C4],13.97[S7]	14.03
H_c, Btu/lb	-18500[M4], -18577[C3]	-18433[C4], -18640[S7]	-18500
$H_{f,298K}$, cal/mole		-5430[S7]/$CH_{1.9423}$	-92200/$C_{12}H_{24}$,-7683/$CH_{2.0}$
$C_{p,516k,1\ atm}$, cal/mole-K		101[C4]	103
Paraffins (n and iso) %		41[C4]	41.7
Naphthenes %		56[C4]	58.3
Aromatics %	5[M4]	5[N1],3[C4]	0
Olefins %	1[M4]	0[C4]	0

Thermodynamic Consistency Test 2

- The theoretical rocket performance of C_nH_m and its elemental form $CH_{m/n}$ should be identical

  - RD-170 operating conditions
  - equivalence ratio : 1.2939
  - SUPAR : 36.9
  - chamber pressure: 241.9 atm

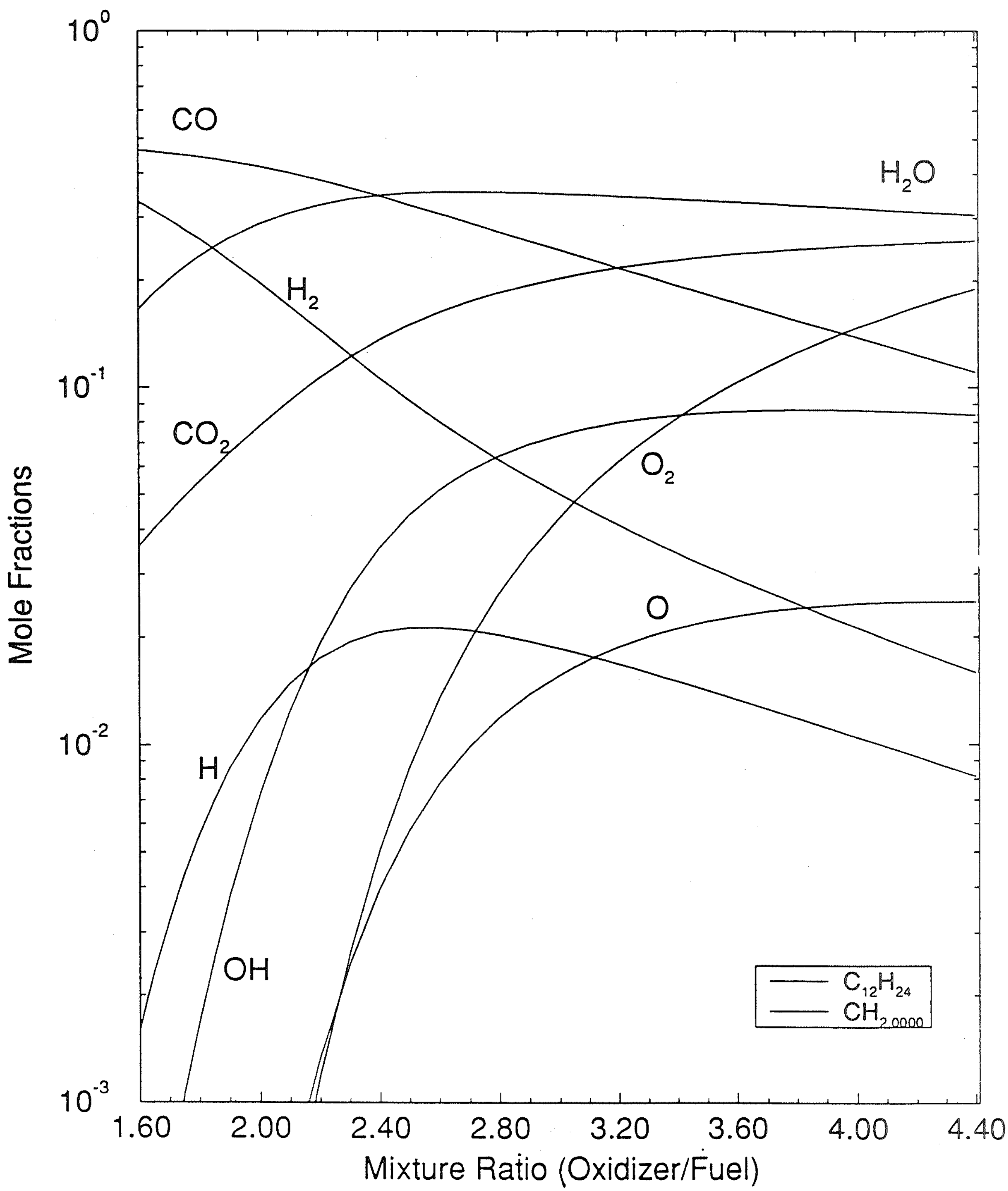

Fig. 1 Calculated chamber gas composition.

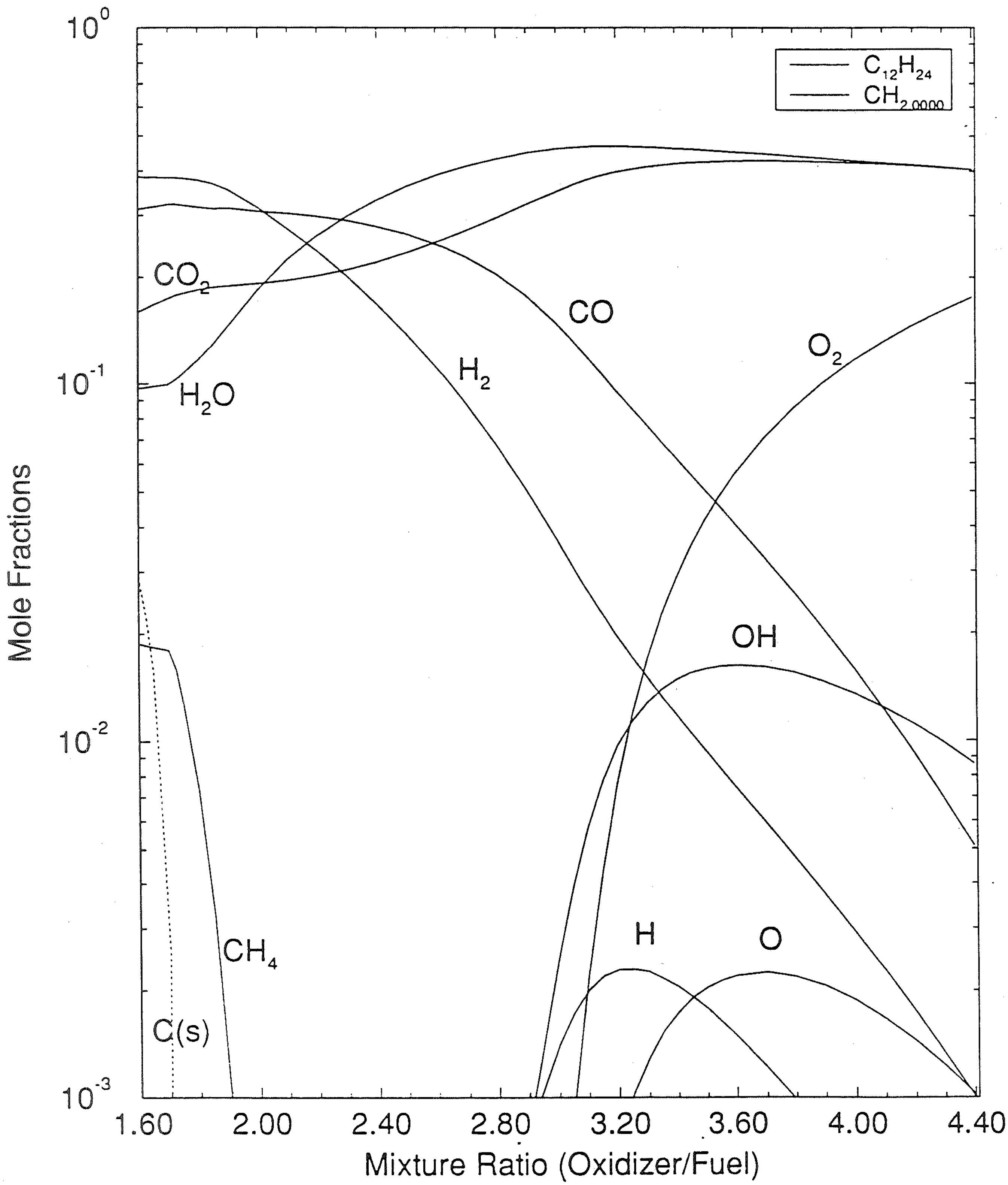

Fig. 2 Calculated nozzle exit gas composition.

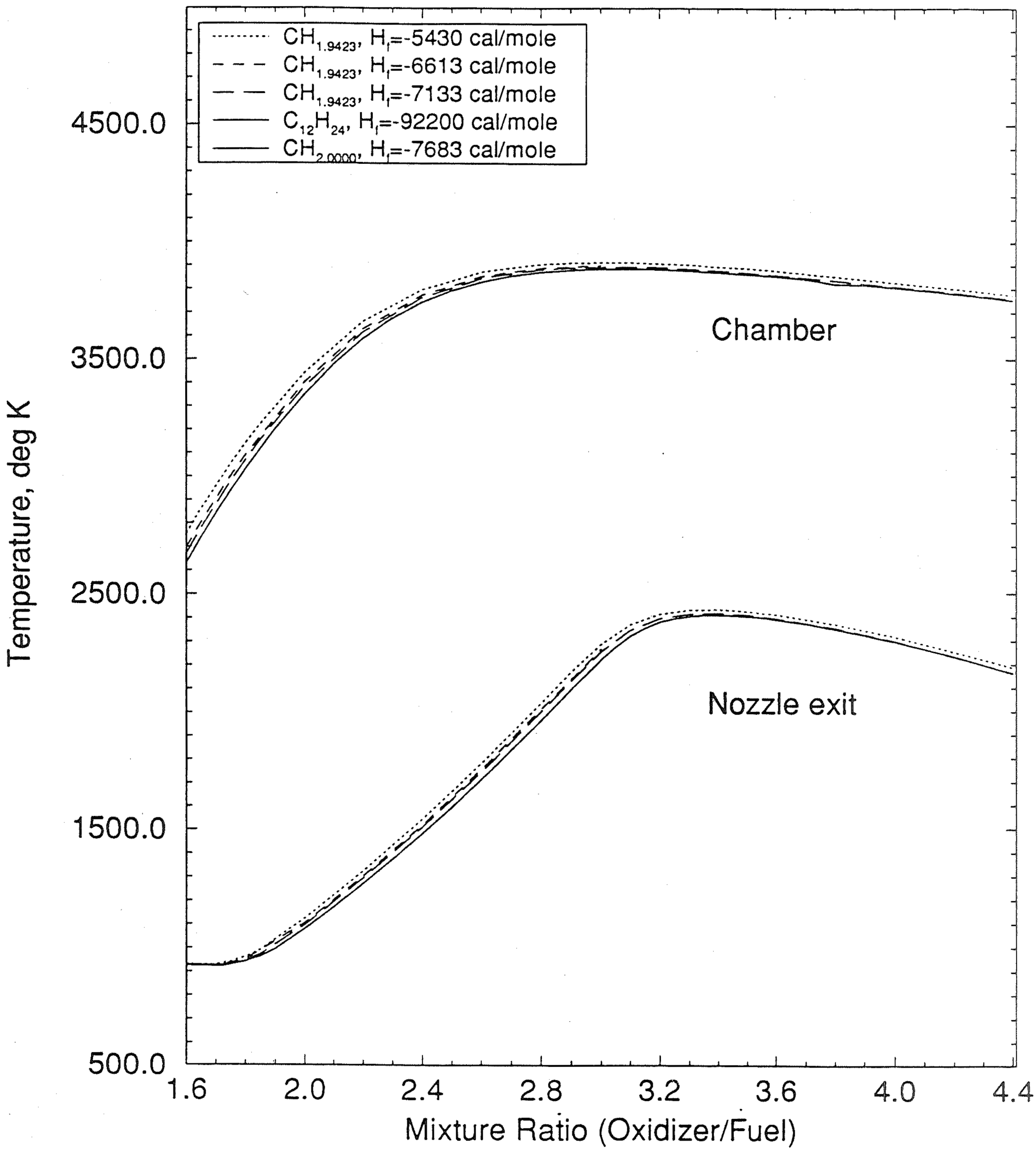
CH1.9423, Hf=-5430 cal/mole
CH1.9423, Hf=-6613 cal/mole
CH1.9423, Hf=-7133 cal/mole
C12H24, Hf=-92200 cal/mole
CH2.0000, Hf=-7683 cal/mole
Chamber
Nozzle exit
Temperature, deg K
4500.0
3500.0
2500.0
1500.0
500.0
1.6
2.0
2.4
2.8
3.2
3.6
4.0
4.4
Mixture Ratio (Oxidizer/Fuel)

Kerosene/RP-1 quasi-global combustion kinetics mechanism. $K_f = AT^B e^{-E/RT}$

Reaction	A	B	E/R	Form	Ref.
Paraffin Global Step					
$C_{12}H_{24} + 6O_2 \rightarrow 12CO + 12H_2$	3.888E4	1	1.220E4	$p^{0.3}[C_{12}H_{24}]^{0.5}[O_2]$	This Work
Naphthene Global Step					
$C_{12}H_{24} + 6O_2 \rightarrow 12CO + 12H_2$	2.132E7	1	1.965E4	$p^{0.3}[C_{12}H_{24}]^{0.5}[O_2]$	This Work
Wet CO Mechanism					
$H_2 + O_2 = OH + OH$	1.700E13	0	2.407E4	Stoichiometry	2
$OH + H_2 = H_2O + H$	2.190E13	0	2.590E3	Stoichiometry	2
$OH + OH = O + H_2O$	6.023E12	0	5.500E2	Stoichiometry	2
$O + H_2 = H + OH$	1.800E10	1.0	4.480E3	Stoichiometry	2
$H + O_2 = O + OH$	1.220E17	-0.91	8.369E3	Stoichiometry	2
$M + O + H = OH + M$	1.000E16	0	0	Stoichiometry	2
$M + O + O = O_2 + M$	2.550E18	-1.0	5.939E4	Stoichiometry	2
$M + H + H = H_2 + M$	5.000E15	0	0	Stoichiometry	2
$M + H + OH = H_2O + M$	8.400E21	-2.0	0	Stoichiometry	2
$CO + OH = H + CO_2$	4.000E12	0	4.030E3	Stoichiometry	2
$CO + O_2 = CO_2 + O$	3.000E12	0	2.500E4	Stoichiometry	2
$CO + O + M = CO_2 + M$	6.000E13	0	0	Stoichiometry	2

* M stands for third-body collision partner

Kerosene Substitute Fuel Model/Quasi-global Kerosene Kinetics/CFD Test on 3 Shear Triaxial Injectors

- GOX/GRP/GH2, LOX/GRP/GH2, and LOX/LRP/GH2 uni-element injectors
- Mixture ratio of RD-704 is used.
- The injector/combustor setup follows that of Penn-State shear coaxial/ optically accessible rocket chamber.

  - equivalence ratio : 1.2317
  - SUPAR : 2.6514
  - chamber pressure: 30.8 atm

Multiphase FDNS Numerical Methodology and Physical Models for Triaxial Tripropellant Injectors

- Multi-species VOF formulation for liquid jets and multi-species particle formulation for droplets
- Jet surface primary atomization - empirical mean particle size and empirical mass stripping rate (experimental data required for modeling)
- Droplet secondary breakup - Taylor Analogy Breakup
- Droplet vaporization - General Evaporization Model
- Lagrangian particle tracking with turbulence dispersion
- Finite-rate chemistry integration - Penalty Function Method
- Kinetics - Quasiglobal kerosene combustion kinetics (9 species and 14 reactions)
- Thermodynamics

  - real gas: kerosene and 8 other species

  - real liquid: LOX (NBS table)

    : kerosene (Lefebvre)

Summary

- A simple kerosene/RP-1 substitute fuel model and its thermochemical properties have been developed according to available database.
- This substitute fuel model and its thermodynamics have passed the thermodynamic consistency test.
- In addition, a simple kerosene/RP-1 quasiglobal combustion kinetics model has been developed based on the composition of the substitute fuel model.
- Preliminary CFD test of the thermo-kinetics model on 3 triaxial, tripropellant injectors have shown reasonable flame temperatures.

S9-20
51384
132106
10P

Application of Optimization Techniques to Design of Unconventional Rocket Nozzle Configurations

W. Follett, A. Ketchum, A. Darian, Y. Hsu
Rocketdyne Division, Rockwell International, Canoga Park, California

Abstract

Several current rocket engine concepts such as the bell-annular tripropellant engine, and the linear aerospike being proposed for the X-33, require unconventional three-dimensional rocket nozzles which must conform to rectangular or sector shaped envelopes to meet integration constraints. These types of nozzles exist outside the current experience database, therefore, application of efficient design methods for these propulsion concepts is critical to the success of launch vehicle programs.

The objective of this work is to optimize several different nozzle configurations, including 2-D and 3-D geometries. Methodology includes coupling CFD analysis to genetic algorithms and Taguchi methods, as well as implementation of a streamline tracing technique. Results of applications are shown for several geometry classes including: 3-D thruster nozzles with round or superelliptic throats and rectangular exits, 2-D and 3-D thrusters installed within a bell nozzle, and 3-D thrusters with round throats and sector shaped exits.

Due to the novel designs considered for this study, there is little experience base which can be used to guide the effort and limit the design space. With a nearly infinite parameter space to explore, simple parametric design studies cannot possibly search the entire design space within the time frame required to impact the design cycle. For this reason, robust and efficient optimization methods are required to explore and exploit the design space to achieve high performance engine designs. Five case studies which examine the applications of various techniques in the engineering environment are presented in this paper.

The first study uses two-dimensional CFD coupled to Taguchi methods to determine optimal design parameters for the D-1 test engine being built for the SSTO Advanced Propulsion Technology contract. The D-1 engine utilizes a ring of small thrusters within a larger bell nozzle. This study was used to determine the optimal value of four design variables to achieve the best overall performance during both low altitude (thrusters firing) and high altitude (thrusters not firing) operational modes. Two other case studies investigate the problem of using multidisciplinary techniques to optimize a 3-D thruster design with both genetic algorithms and Taguchi methods. The relative strengths and weaknesses of these two methods are apparent when using them to solve this problem using up to 21 design variables. This thruster is also designed using streamline tracing techniques for the fourth case study.

The final study uses Taguchi methods to determine the optimal 3-D thruster module design when installed in a bell nozzle. This requires full 3-D solutions of the thruster and bell nozzles to quantify module-to-module interaction effects.

Software which couples optimization techniques to CFD have tremendous potential as aerodynamic design tools. However, to function effectively in the engineering environment, the optimization algorithms must be robust and efficent. Several optimization techniques have been demonstrated for rocket nozzle design, and their performance on these real world applications has been assessed.

APPLICATION OF OPTIMIZATION TECHNIQUES TO DESIGN OF UNCONVENTIONAL ROCKET NOZZLE CONFIGURATIONS

W. Follett
A. Ketchum
A. Darian
Y. Hsu
Rocketdyne Division - Rockwell International

Computational Fluid Dynamics Branch
Fluid Dynamics Division
Structures and Dynamics Laboratory
Science and Engineering Directorate
Marshall Space Flight Center

13th Workshop for CFD
Applications in Rocket Propulsion
Huntsville, Alabama
April 25-28, 1995

Rockwell Aerospace
Rocketdyne

CFD Technology Center

CFD 95-016- 1/IBM/WWF/sdh

OPTIMIZATION OF UNCONVENTIONAL ROCKET NOZZLE CONFIGURATIONS

- **APPLICATIONS FOR NASA ADVANCED PROPULSION TECHNOLOGIES CONTRACT AND AIR FORCE MODULAR THRUST CELL CONTRACT**
- **GEOMETRY**
  - BELL-ANNULAR OR AEROSPIKE NOZZLES
  - 3-D THRUSTERS WITH RECTANGULAR OR SECTOR SHAPED EXITS
- **ANALYSIS METHODS**
  - 2-D AND 3-D CFD (EULER AND FNS)
  - 3-D MOC
- **OPTIMIZATION METHODS**
  - TAGUCHI, GENETIC ALGORITHMS, STREAMLINE TRACING

REPRESENTATIVE NOZZLE CONFIGURATIONS

AEROSPIKE

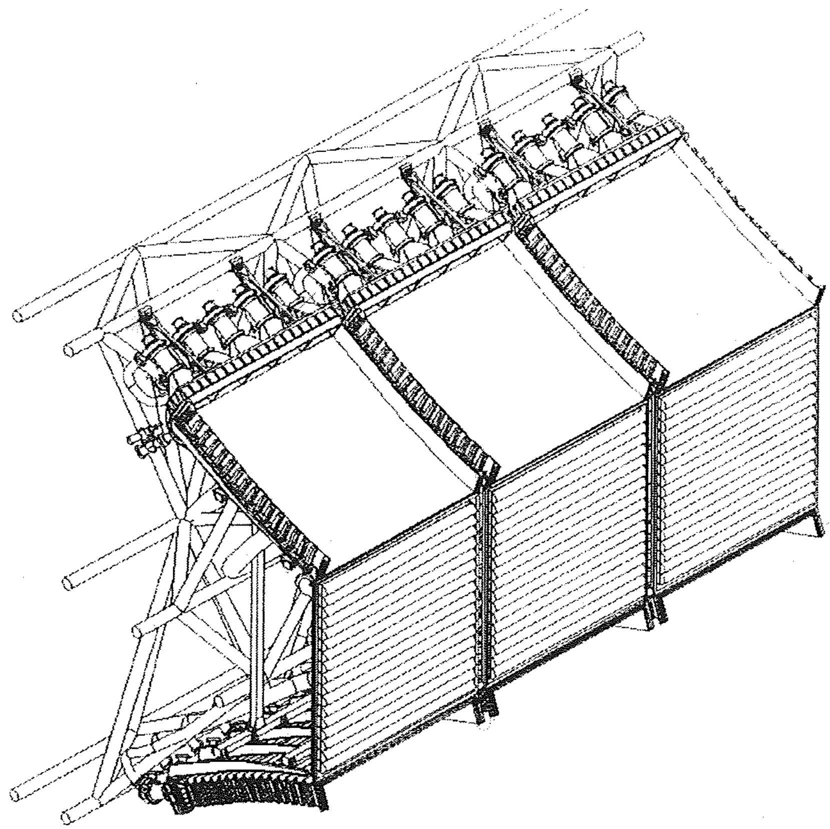

BELL-ANNULAR

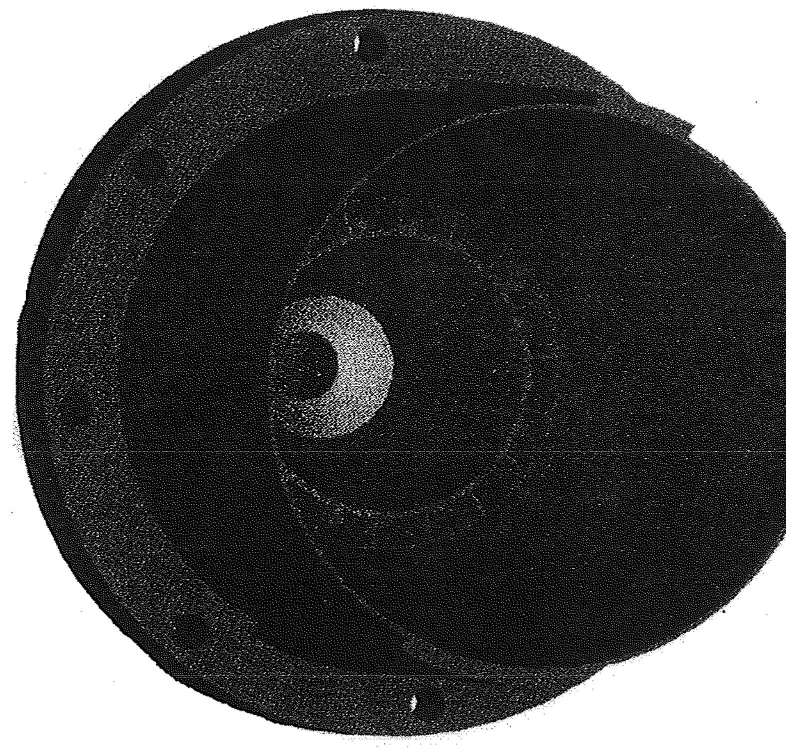

CFD 95-016- 3/IBM/WWF/sdh

2-D BELL-ANNULAR D-1 TEST ENGINE DESIGN STUDY

- **OBJECTIVE**
  - MAXIMIZE AVERAGE THRUST, ISP FOR THRUSTER ON AND THRUSTER OFF
- **OPTIMIZATION METHOD**
  - TAGUCHI L9 MATRIX
  - 4 DESIGN VARIABLES
  - 20 2-D CFD EVALUATIONS
- **IMPROVEMENT OVER BASELINE**
  - 1.2% IN THRUST & ISP

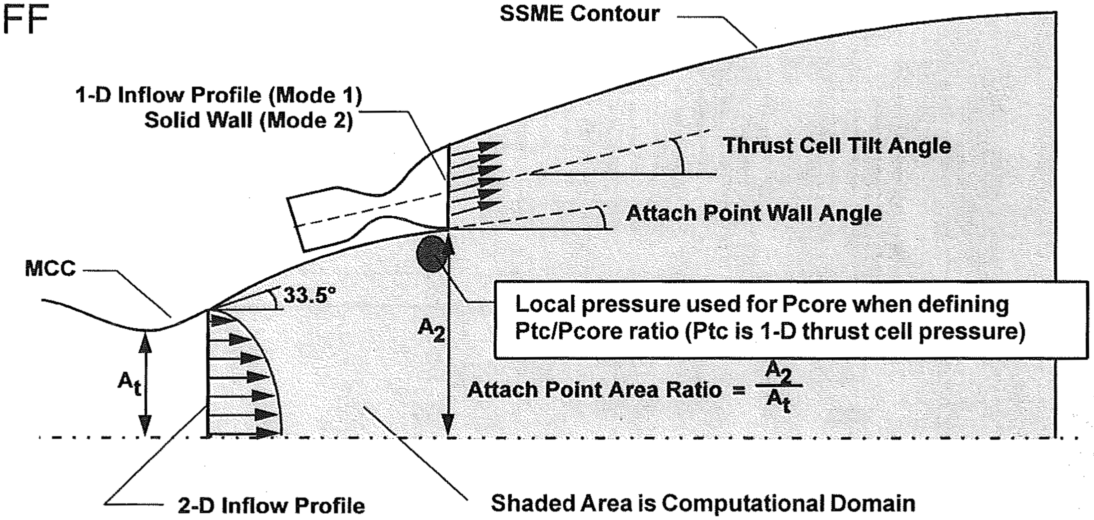

883

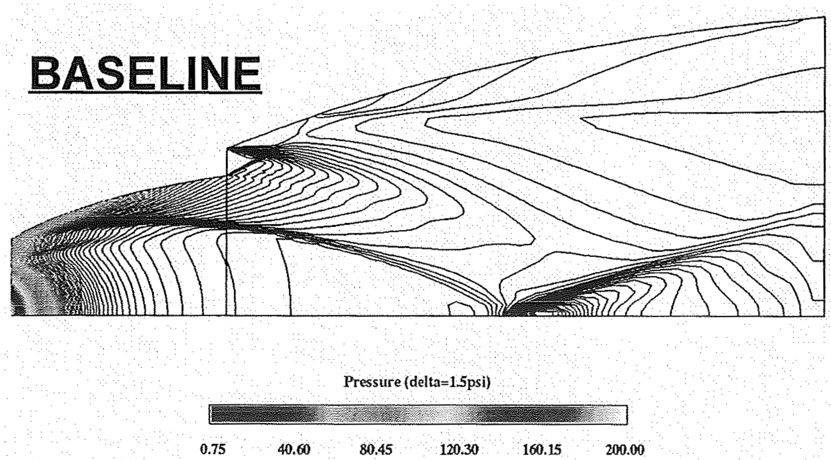

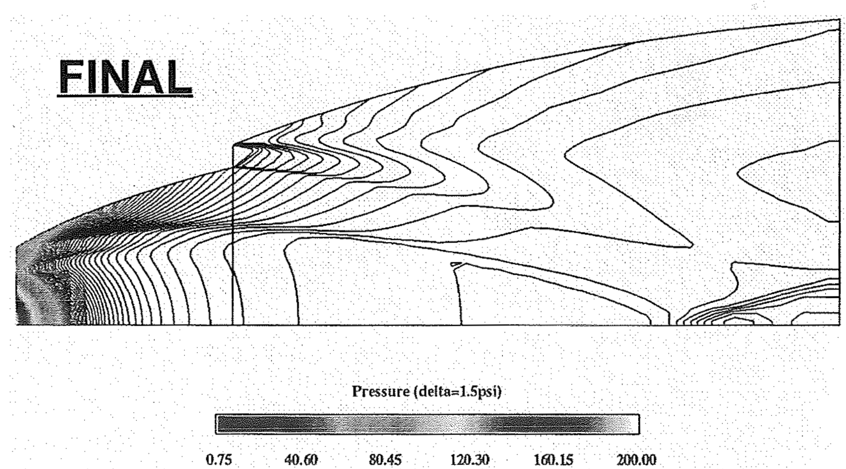

Rockwell Aerospace
Rocketdyne

CFD Technology Center

CFD 95-016- 4/IBM/WWF/sdh

3-D THRUST CELL OPTIMIZATION

- **OBJECTIVE**
  - MAXIMIZE: $\frac{\text{THRUST(THRUSTER ONLY)}}{\text{SYSTEM WEIGHT}}$
  - MINIMIZE PEAK HEAT LOAD
- **OPTIMIZATION METHODS**
  - TAGUCHI L32 & L64 MATRICES
  - GENETIC ALGORITHM
  - 15-21 DESIGN VARIABLES
- **3-D MOC EVALUATIONS**
  - 460 FOR TAGUCHI
  - 1000 FOR GENETIC
- **IMPROVEMENT OVER BASELINE**
  - 4.6% IN THRUST / WEIGHT

Thrust Cell Taguchi Optimum
Mach Number Contours

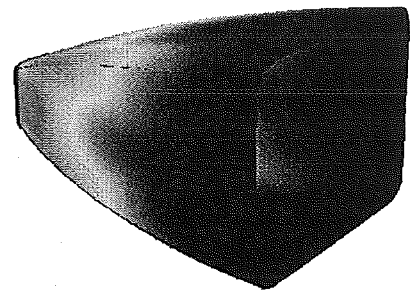

Mach Number Minimum = 1.0
Mach Number Maximum = 4.0

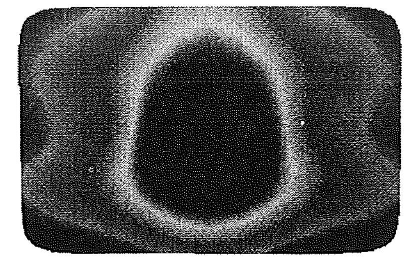

Mach Number Minimum = 3.0
Mach Number Maximum = 4.0

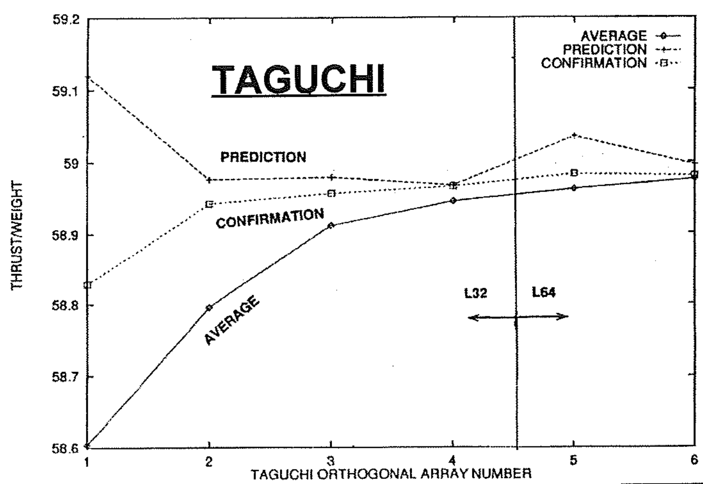

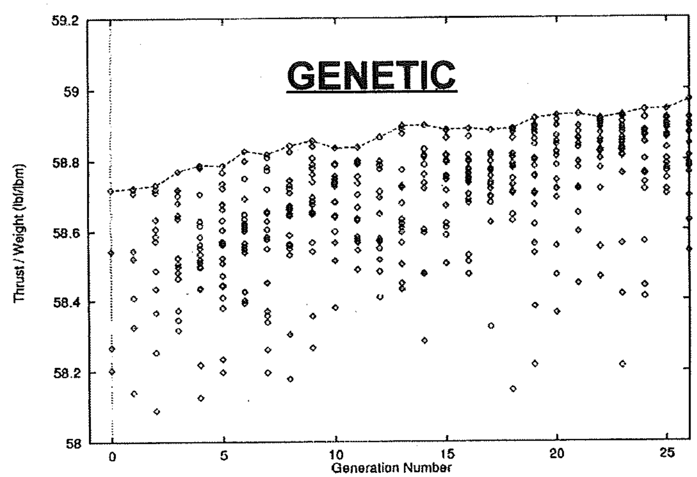

CONVERGENCE HISTORIES

Rockwell Aerospace
Rocketdyne

CFD Technology Center

CFD 95-016- 5/IBM/WWF/sdh

3-D THRUST CELL OPTIMIZATION

BASELINE
OPTIMIZED FOR AERO ONLY
T/W = 56.39

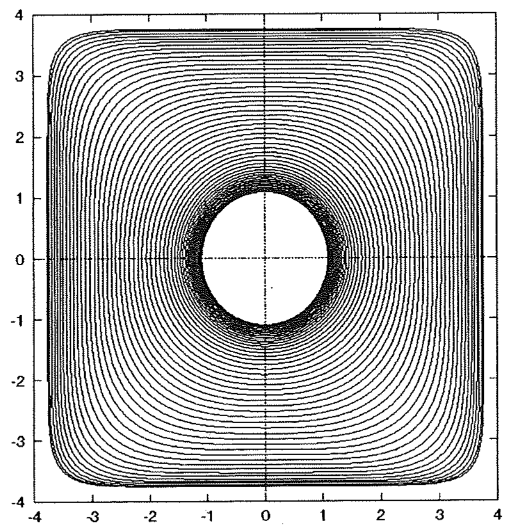

TAGUCHI OPTIMIZATION
T/W = 58.98

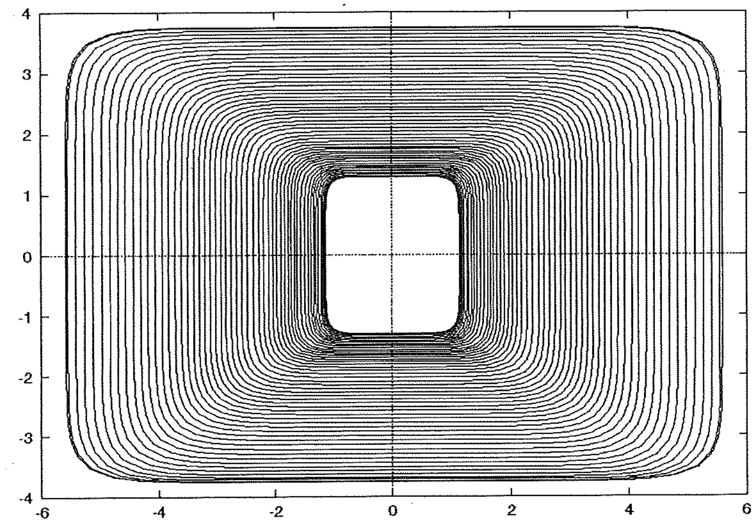

GENETIC ALGORITHM OPTIMIZATION
T/W = 58.97

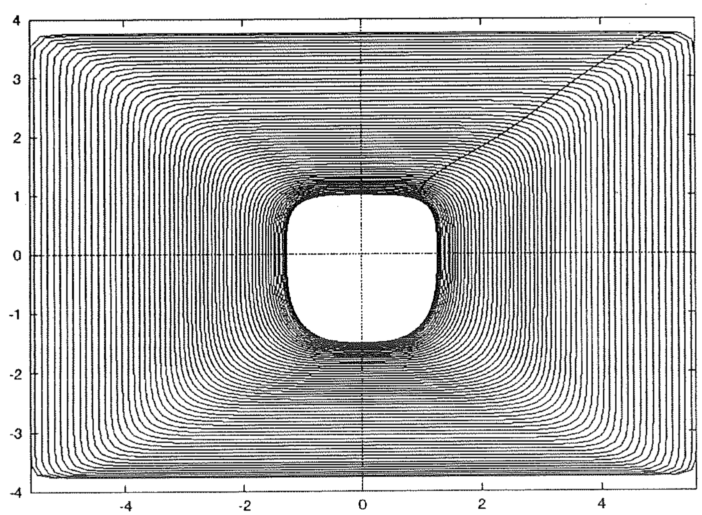

TAGUCHI OPTIMIZATION
RESTRICTED TO ROUND THROAT
T/W = 58.92

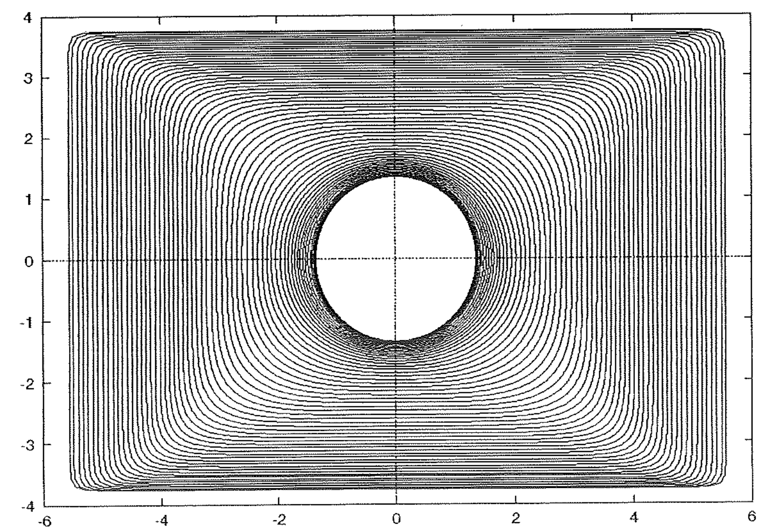

Rockwell Aerospace
Rocketdyne

CFD Technology Center

CFD 95-016- 6/IBM/WWF/sdh

3-D STREAMLINE TRACING METHOD

- **OBJECTIVE**
  - MAXIMIZE THRUST, ISP FOR STAND-ALONE THRUSTER
- **DESIGN METHOD**
  - STREAMLINE TRACING
  - RAO OPTIMUM NOZZLE-MODEL FLOWFIELD
  - THREE 2-D MOC EVALUATIONS
- **PERFORMANCE**
  - 0.15% LESS ISP THAN TAGUCHI & G.A. OPTIMUMS

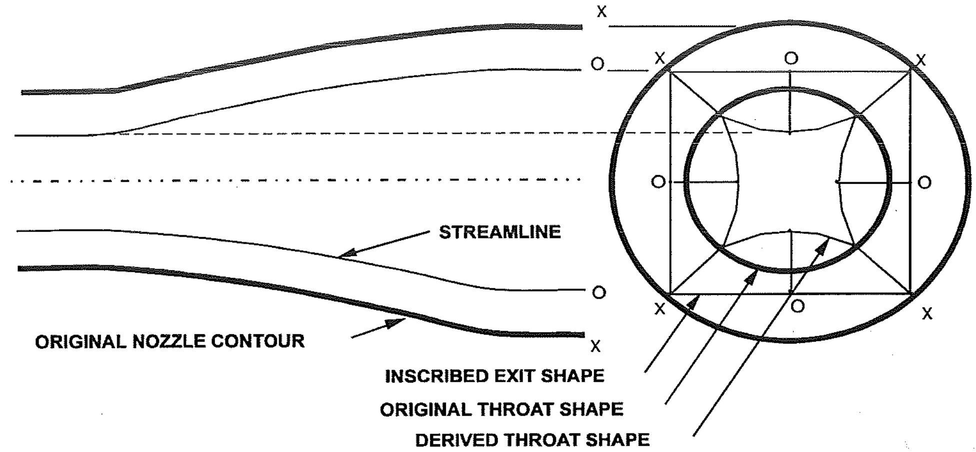

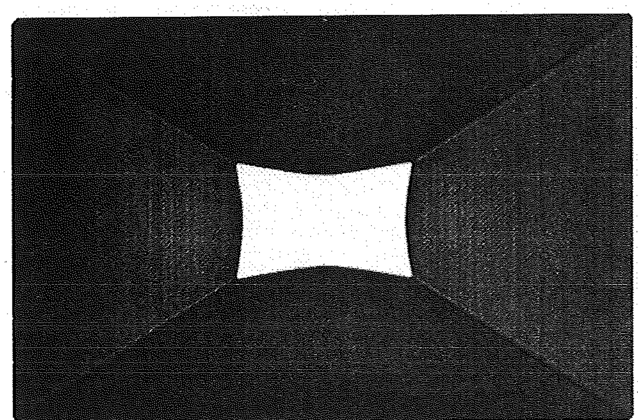

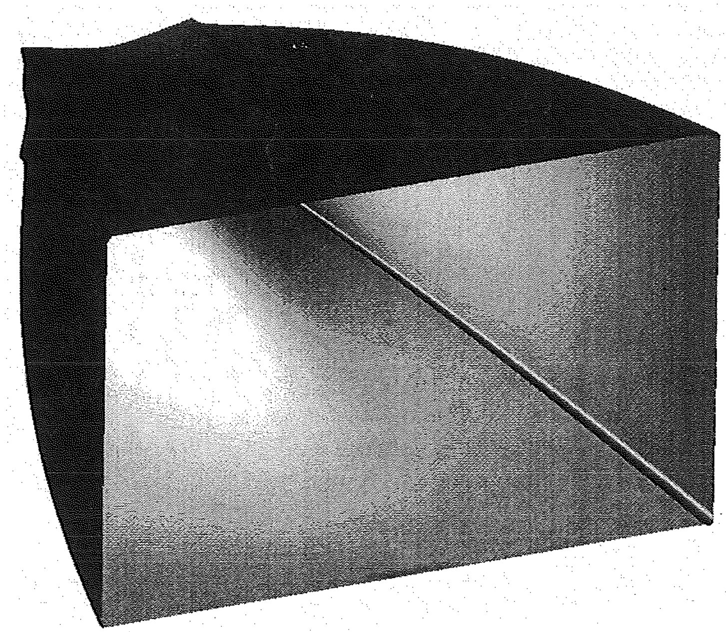

3-D BELL-ANNULAR D-1 INSTALLED THRUSTER DESIGN

- **OBJECTIVES**
  - MAXIMIZE THRUST, ISP
  - MINIMIZE PEAK HEAT LOAD

- **OPTIMIZATION METHOD**
  - TAGUCHI L9 MATRIX
  - 4 DESIGN VARIABLES
  - 10 3-D CFD EVALUATIONS

- **IMPROVEMENTS OVER BASELINE**
  - 0.1% IN THRUST
  - 23% REDUCTION IN PEAK HEAT FLUX

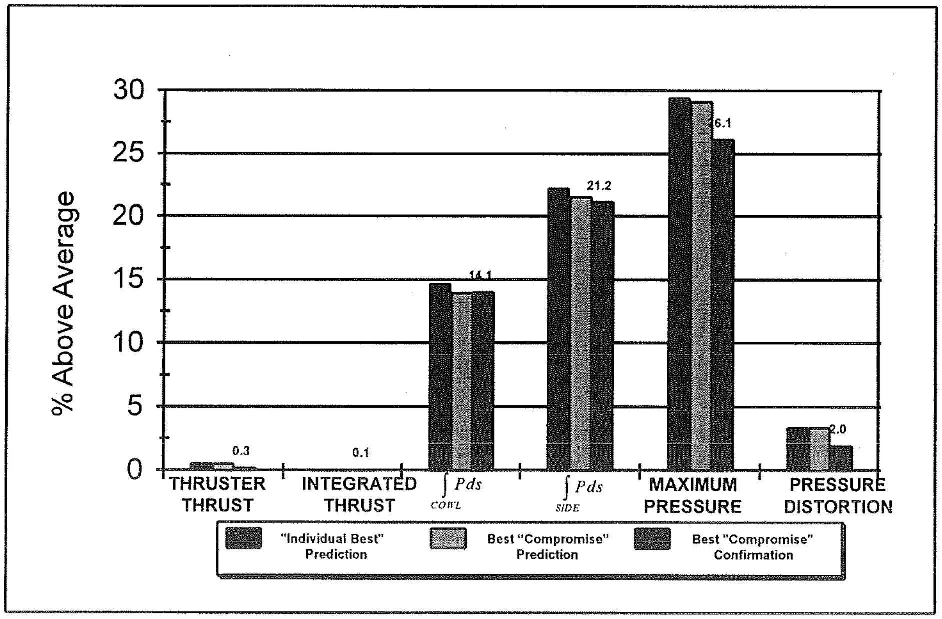

BASELINE

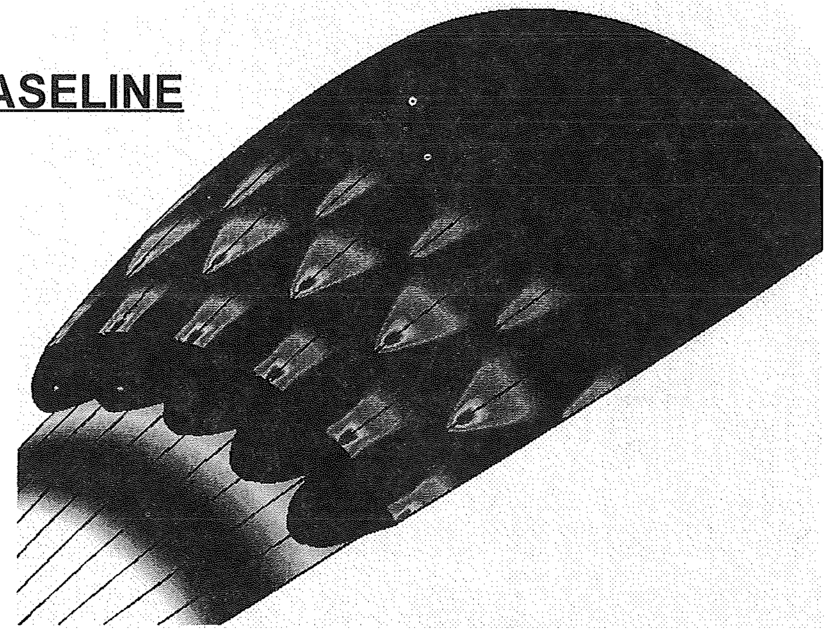

OPTIMUM

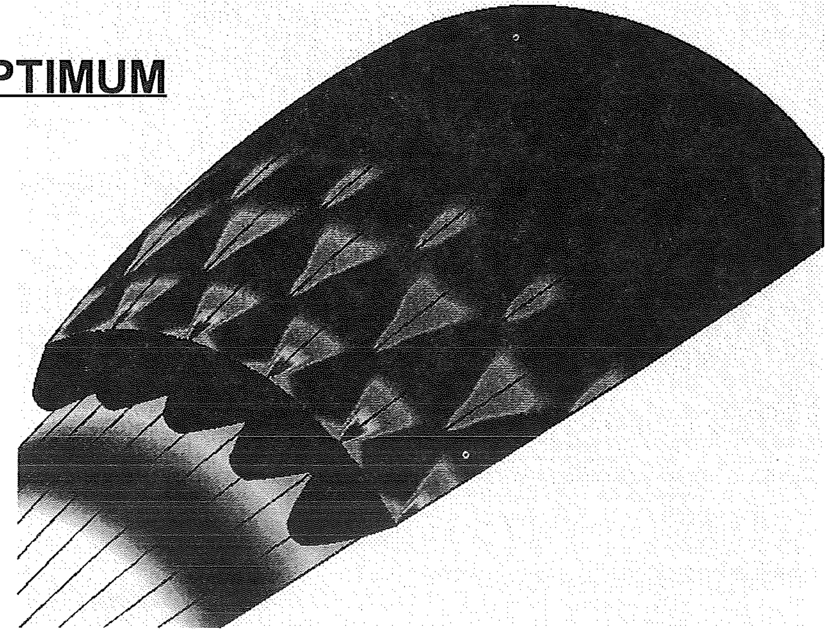

Rockwell Aerospace
Rocketdyne

CFD Technology Center

CFD 95-016- 8/IBM/WWF/sdh

OPTIMIZATION OF UNCONVENTIONAL ROCKET NOZZLE CONFIGURATIONS

CONCLUSIONS

- **OPTIMIZATIONS METHODS ARE COMBINED WITH 3-D CFD ANALYSIS TO CREATE A VERY POWERFUL AERODYNAMIC DESIGN TOOL**
  - ALLOWS DESIGN IF COMPLEX CONFIGURATIONS WHICH WERE PREVIOUSLY INFEASIBLE
  - PROVIDES HIGH FIDELITY ANALYSIS EARLY IN THE DESIGN CYCLE
- **MULTIDISCIPLINARY OPTIMIZATION IS CRITICAL FOR ROCKET NOZZLE DESIGNS**
  - ROBUST AERO PERFORMANCE ALLOWS DESIGN FLEXIBILITY
  - OTHER CONCERNS (THERMAL, WEIGHT, MANUFACTURING) MAY BE MORE IMPORTANT FOR DELIVERING OPTIMAL "SYSTEM" PERFORMANCE

Transonic Aerodynamic Characteristics of A Proposed Wing Body Reusable Launch Vehicle Concept

Anthony M. Springer
NASA Marshall Space Flight Center

A proposed wing body reusable launch vehicle was tested in the NASA Marshall Space Flight Center 14X14-inch trisonic wind tunnel during the winter of 1994. This test resulted in the vehicle's subsonic and transonic, Mach 0.3 to 1.96, longitudinal and lateral aerodynamic characteristics. The effects of control surface deflections on the basic vehicles aerodynamics including a body flap, elevons, ailerons, and tip fins are presented.

As an outcome of NASA's 1993 Access to Space study, a more in-depth follow on study was undertaken. Three candidate reusable launch vehicle configurations which would provide reusable single stage to orbit capability were selected. A wing body configuration was one of these candidate concepts, the other two concepts being a vertical lander and a lifting body. The wing body configuration was a direct outgrowth of the access to space option three reference single stage to orbit rocket vehicle. This vehicle matured during the subsequent reusable launch vehicle (RLV) study into the vehicle which was tested. Initially, the vehicles aerodynamic characteristics were determined using aerodynamic prediction codes. To obtain a better fidelity in the aerodynamic data, a series of scale models of the proposed wing body vehicle were tested at the NASA Marshall Space Flight Center (MSFC) and the NASA Langley Research Center (LaRC). The vehicle was tested at low subsonic and hypersonic conditions at LaRC and at subsonic, transonic, and supersonic conditions at MSFC. The results of the transonic testing in MSFC's 14-Inch Trisonic Wind Tunnel (TWT) facility are presented herein.

A .004 scale RLV wind tunnel model was tested during the winter of 1994 at the NASA Marshall Space Flight Center 14X14-inch trisonic wind tunnel (TWT). The subsonic and transonic, Mach 0.3 to Mach 2.0, aerodynamic characteristics of the WB001 reference wing-body vehicle were determined. This wind tunnel test provided aerodynamic data for the basic vehicle, wing and body contributions, and control surface increments. The data derived from this test were used to construct an aerodynamic database for flight mechanics and structural loads studies on the wing body vehicle.

The WB001 vehicle is generically a wing-body combination. The body consists of a drooped nose followed by a cylindrical core section 28.55 ft in diameter, full scale, with a total body length of 185.6 ft, full scale. The wing is a NACA-0010 airfoil at the root linearly varying to a NACA-0012 airfoil at the tip with a 54 degree leading edge sweep, 3.5 degrees of dihedral, and an aspect ratio of 1.91. Control surfaces for this configuration consist of ailerons, elevons and tip fins.

The vehicle is longitudinally stable and can be trimmed at both subsonic and transonic Mach numbers. This assumes a vehicle center of gravity at 68.6% body length or 127.32 feet aft of the nose. At subsonic Mach numbers, the vehicle is stable in trim for all control deflections. The vehicle for the subsonic Mach range can be trimmed at the desired angle-of-attack for entry, approximately 15 degrees. This trim angle is accomplished through various control surface deflections, see figure 84. The vehicle for the transonic Mach range, Mach 0.95 to 2.0, has stable trim points but not at the desired angle-of-attack, approximately 15 degrees angle-of-attack. It can be extrapolated from the current data trends that for a larger elevon deflection between 20 and 30 degrees, the vehicle will be neutrally stable at the desired trim point of 15 degrees.

The WB001 vehicle is laterally unstable for the subsonic and transonic Mach range. The tip fin deflections provide a trim angle range of approximately 1 to 2 degrees, therefore, larger tip fins and deflectable surfaces are desirable. Enlarging the tip fins by an approximate geometric factor of 3 to 4 should result in the vehicle being neutrally stable.

The Transonic Aerodynamic Characteristics Of A Proposed Wing Body Reusable Launch Vehicle Concept

Anthony M. Springer
NASA MSFC ED34
13th CFD Workshop
April 26, 1995

Introduction:

- Vehicle Configuration
- Wind Tunnel Description
- Test Summary
- Results and Conclusions
- Follow-Ons
- Data Availability

Vehicle Configuration:

- Generic Wing Body Configuration
- Length = 185.6 ft
- Drooped Nose
- Core Diameter = 28.55 ft
- Wing Span = 93 ft
- NACA-0010 to NACA-0012 Airfoil
- 54 Degree Leading Edge Sweep
- 3.5 Degree Dihedral
- Aspect Ratio = 1.91

Wind Tunnel Description:

- 14X14-Inch Trisonic Wind Tunnel
- 14X14-Inch Test Section
- Mach Range 0.3 to 5.0
- Intermittent Blow Down Type Tunnel

Test Summary:

- Static Stability Aerodynamic Characteristics
- Mach 0.3 to 1.96
- Basic WB001 Vehicle
- Elevon, Aileron, Body Flap Deflections (-10°)
- Tip Fin Deflections (10°, 20°)

WB001 Tip Fin Control Deflections Mach 1.10

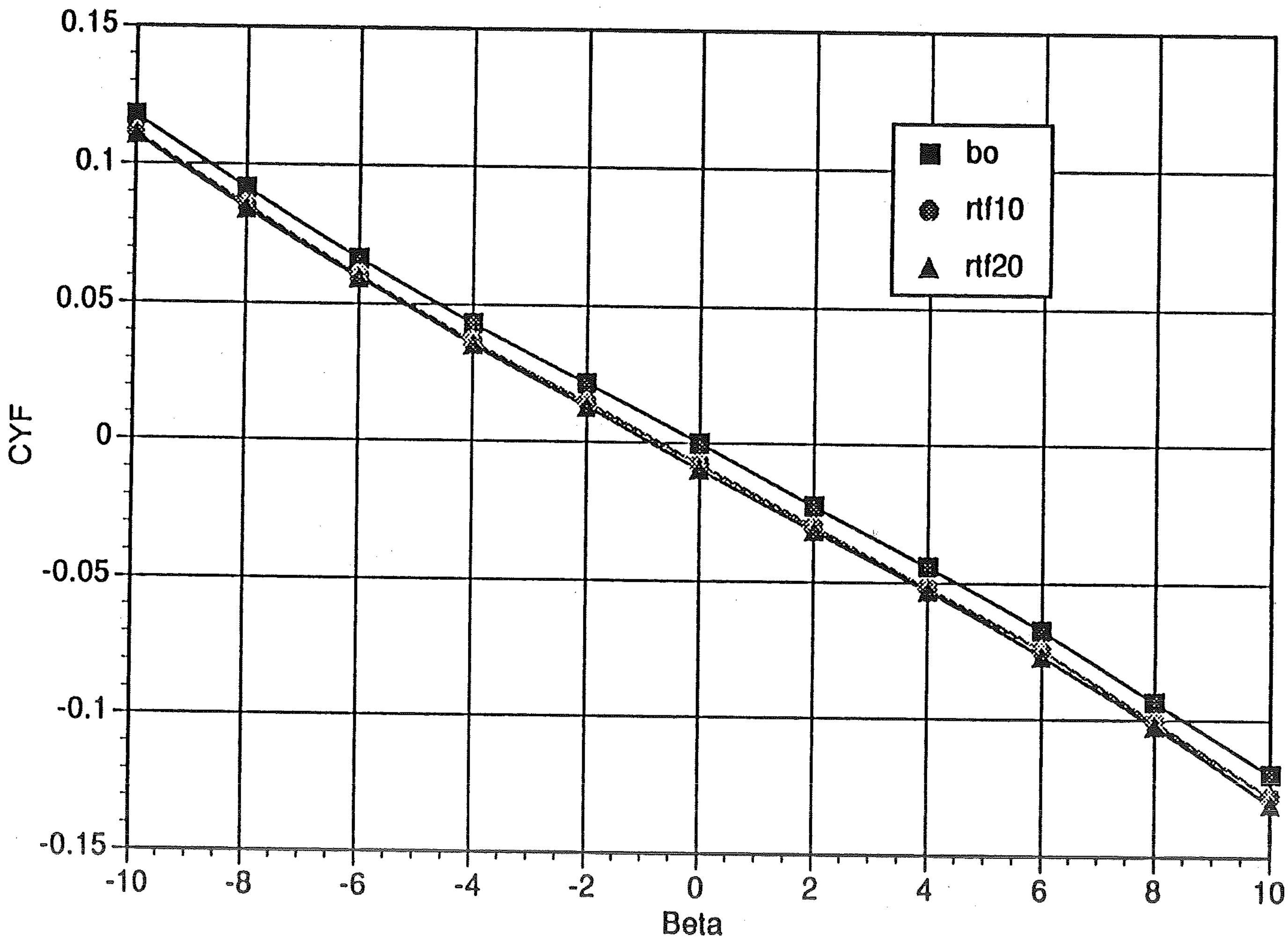

WB001 Tip Fin Control Deflections Mach 1.10

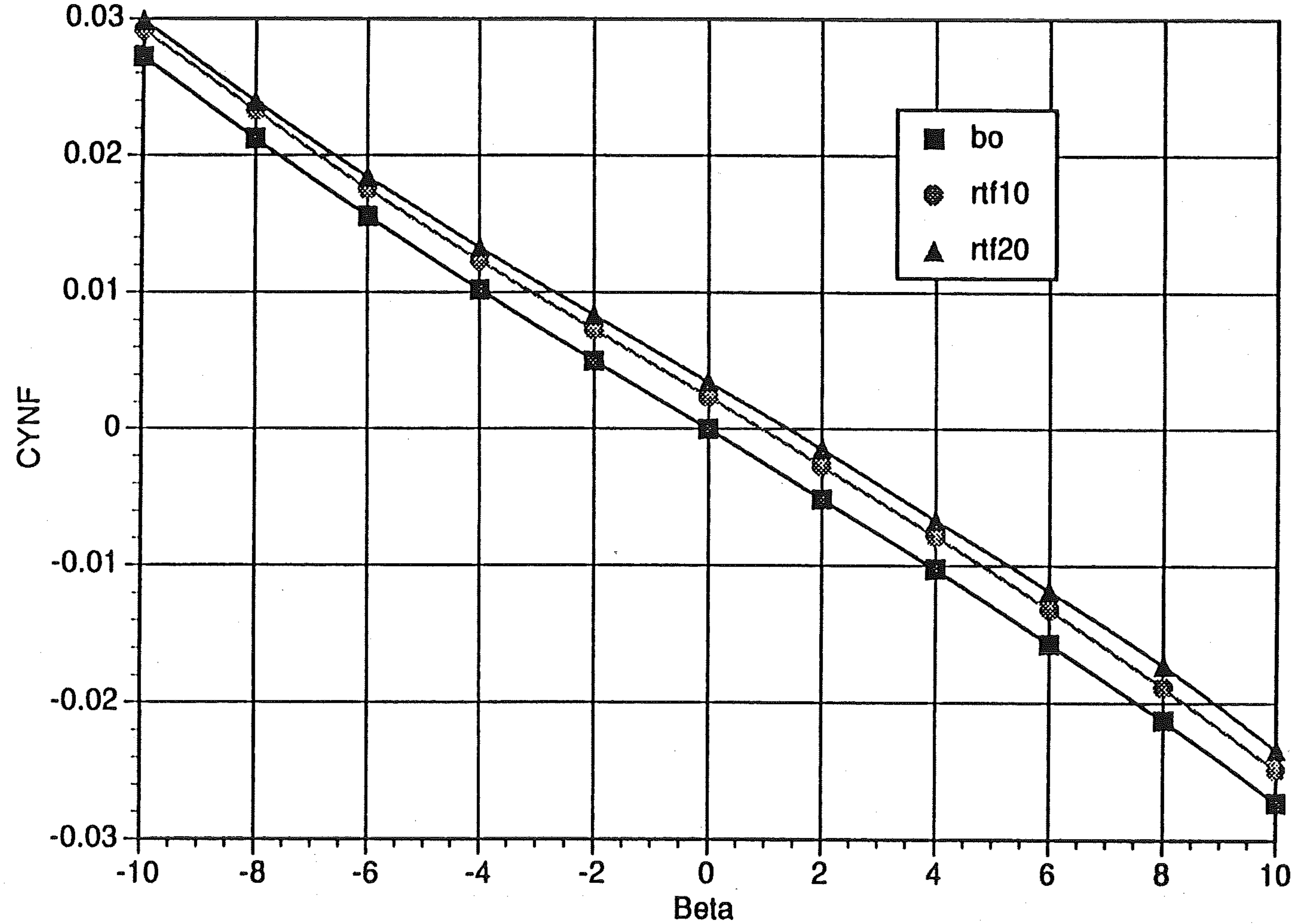

WB001 Tip Fin Control Deflections Mach 1.10

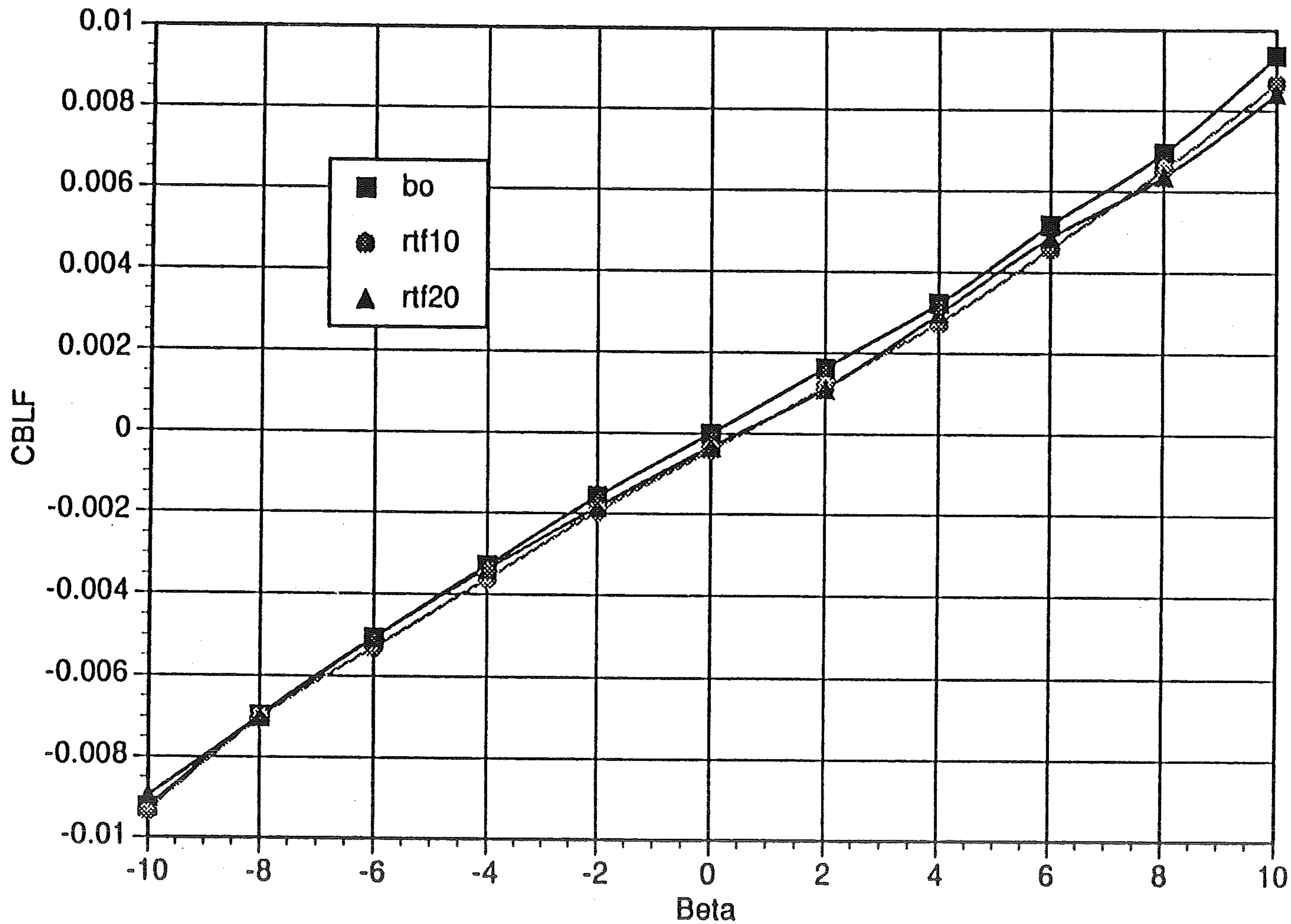

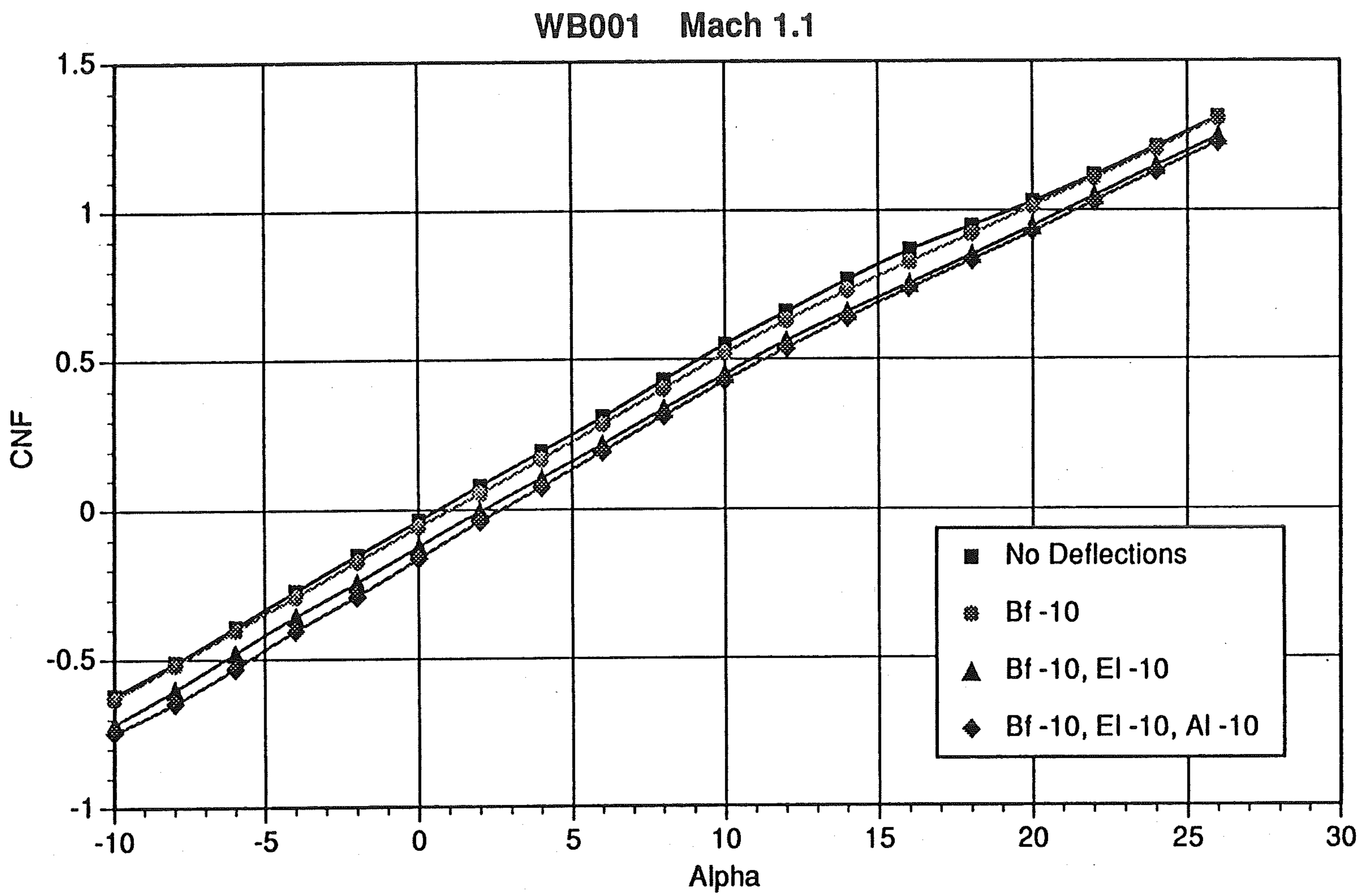
WB001 Mach 1.1
CNF
Alpha
1.5
1
0.5
0
-0.5
-1
-10
-5
0
5
10
15
20
25
30
No Deflections
Bf -10
Bf -10, El -10
Bf -10, El -10, Al -10

Wing Body Lift to Drag Ratio

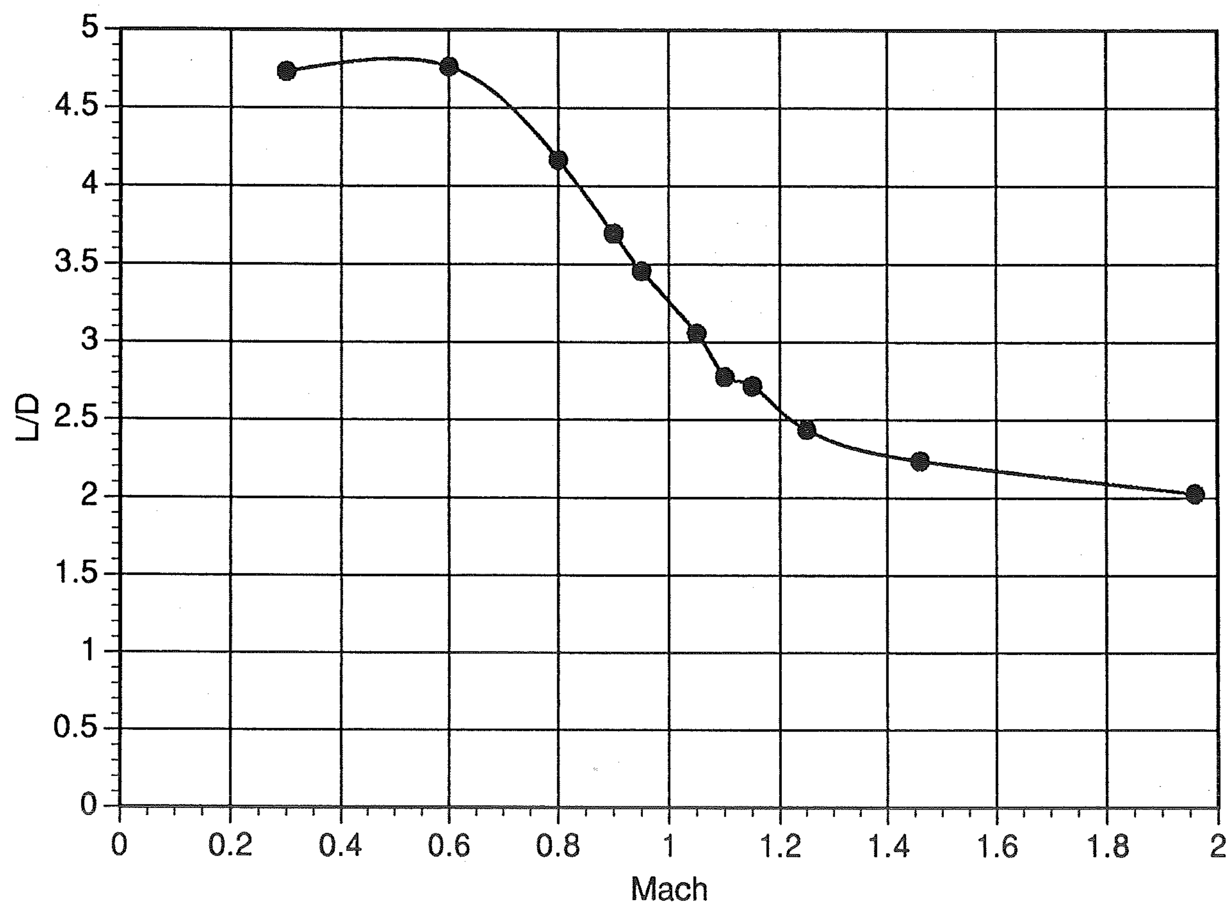

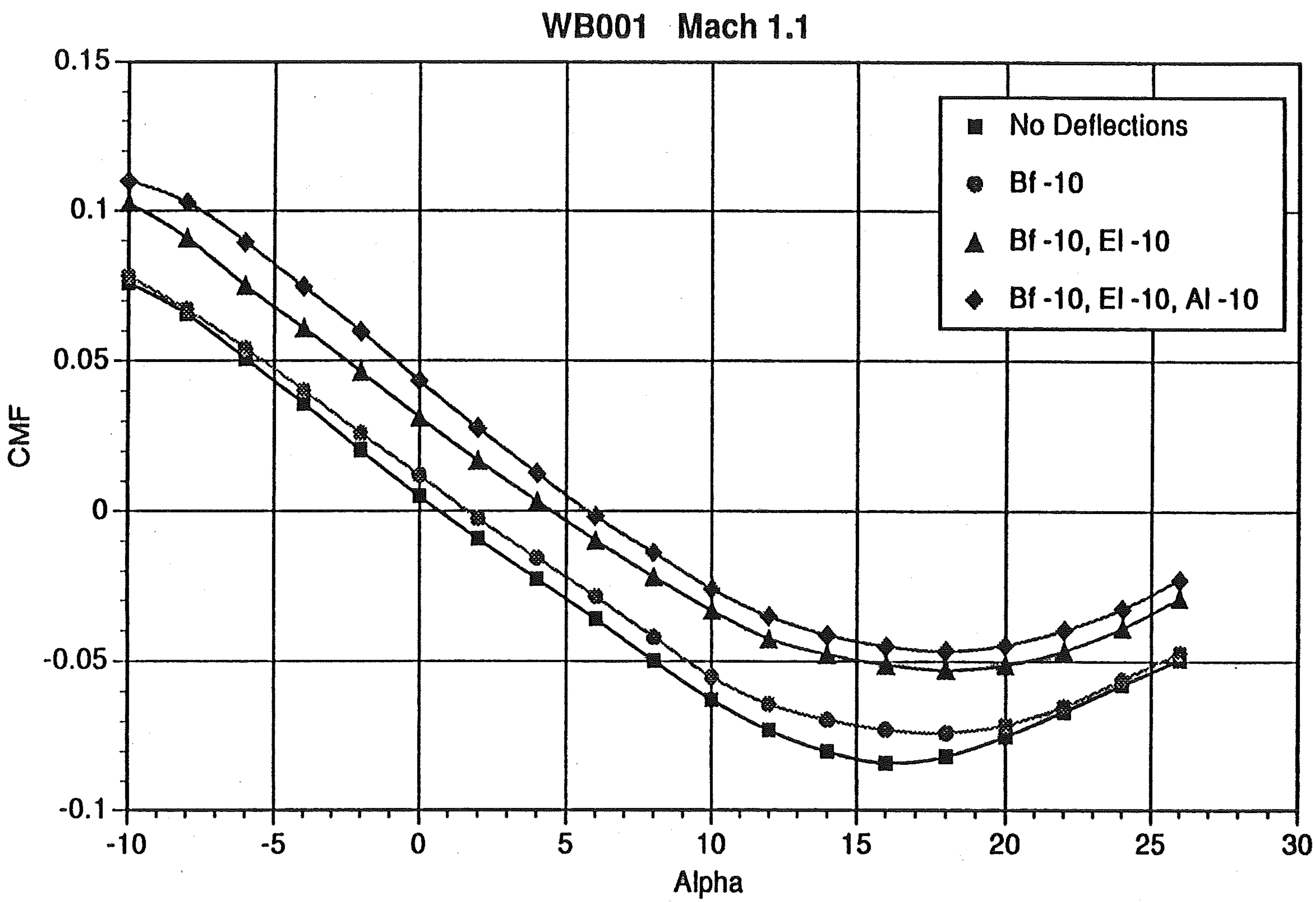
WB001 Mach 1.1
CMF
0.15
0.1
0.05
0
-0.05
-0.1
-10
-5
0
5
10
15
20
25
30
Alpha
No Deflections
Bf -10
Bf -10, El -10
Bf -10, El -10, Al -10

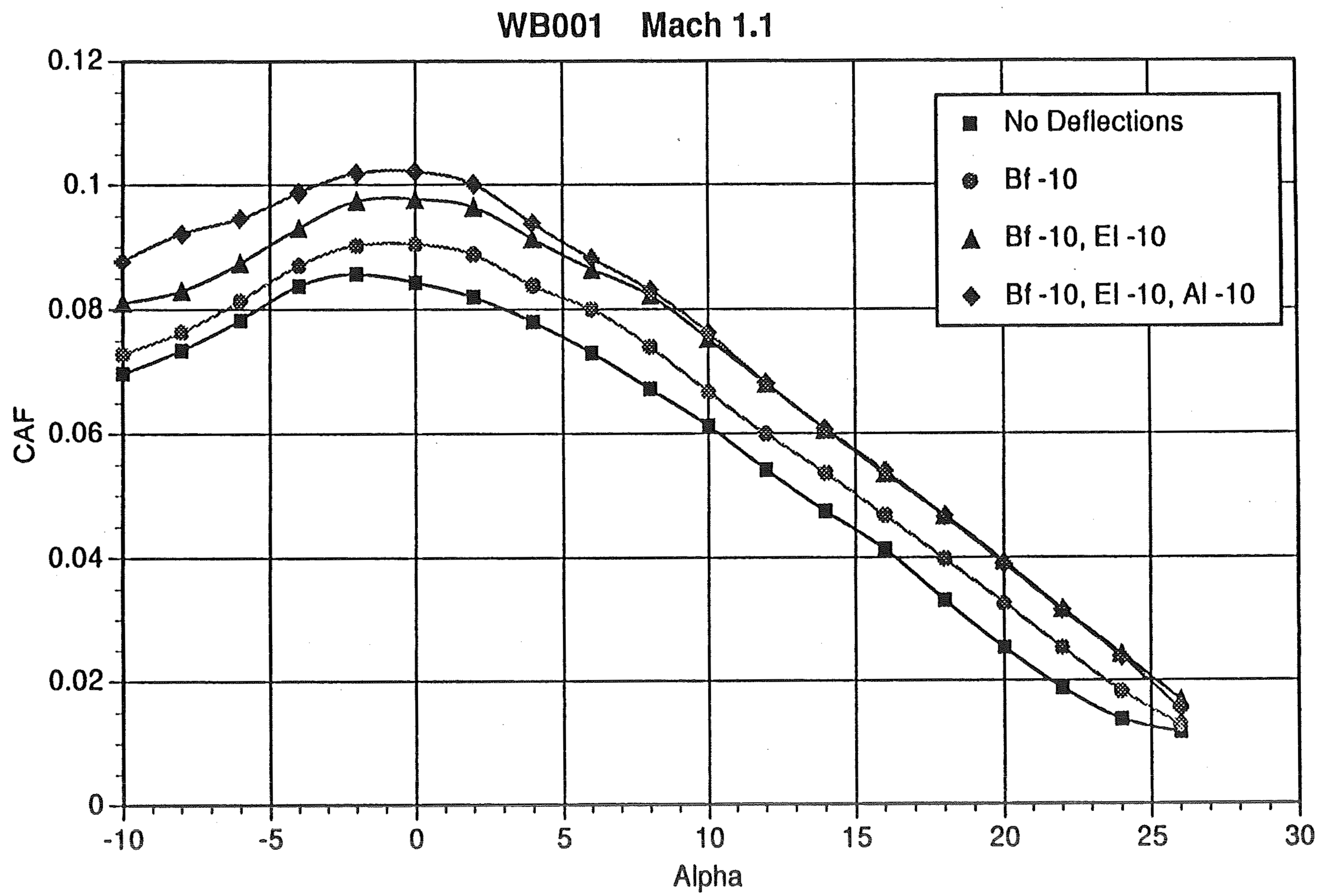
WB001 Mach 1.1
CAF
Alpha
0.12
0.1
0.08
0.06
0.04
0.02
0
-10
-5
0
5
10
15
20
25
30
No Deflections
Bf -10
Bf -10, El -10
Bf -10, El -10, Al -10

Wing Body Aerodynamic Center

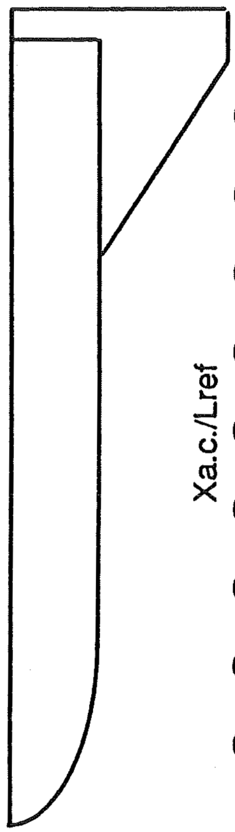

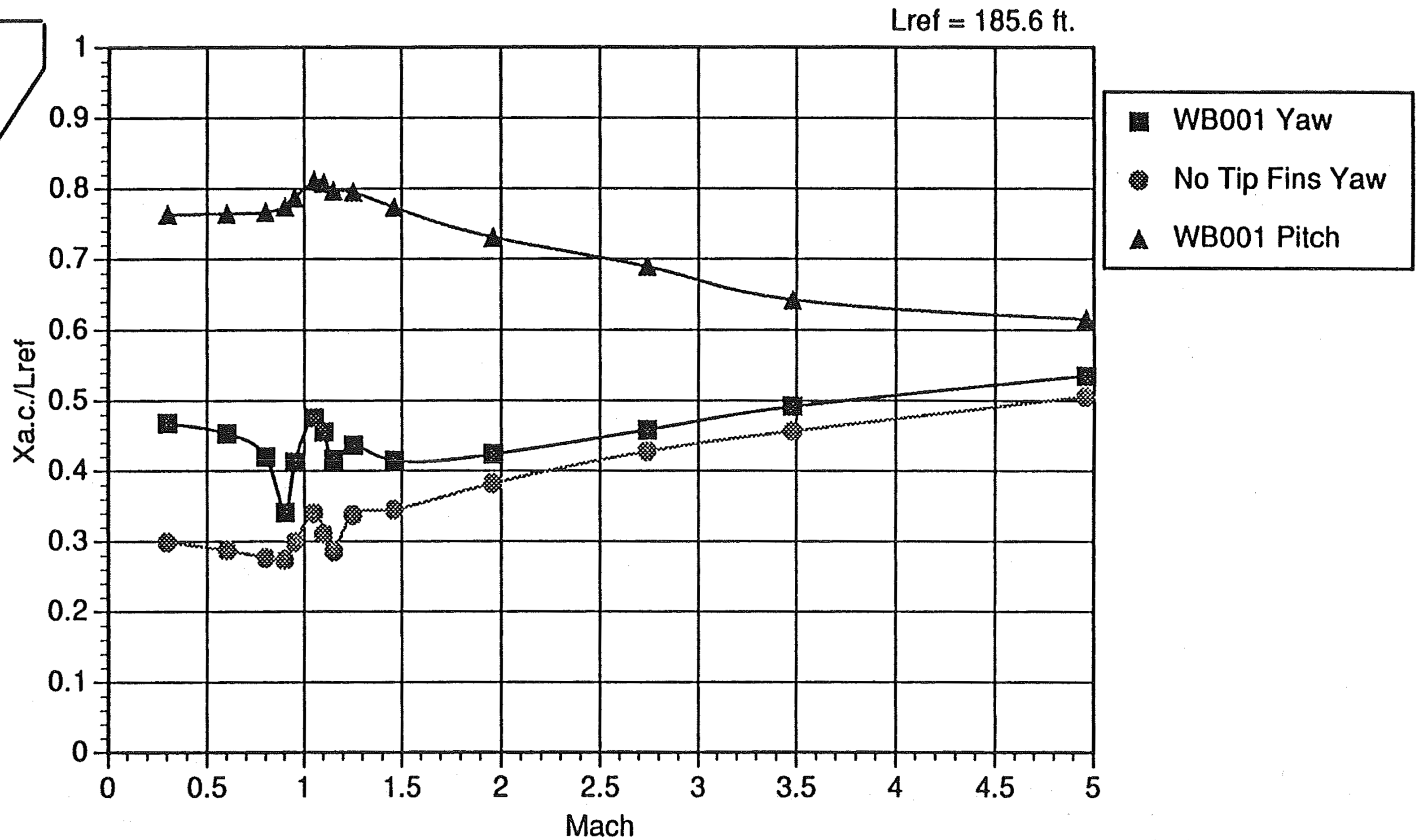

Note: Under 3% Change in Pitch
Xa.c. for No Tip Fin Configuration

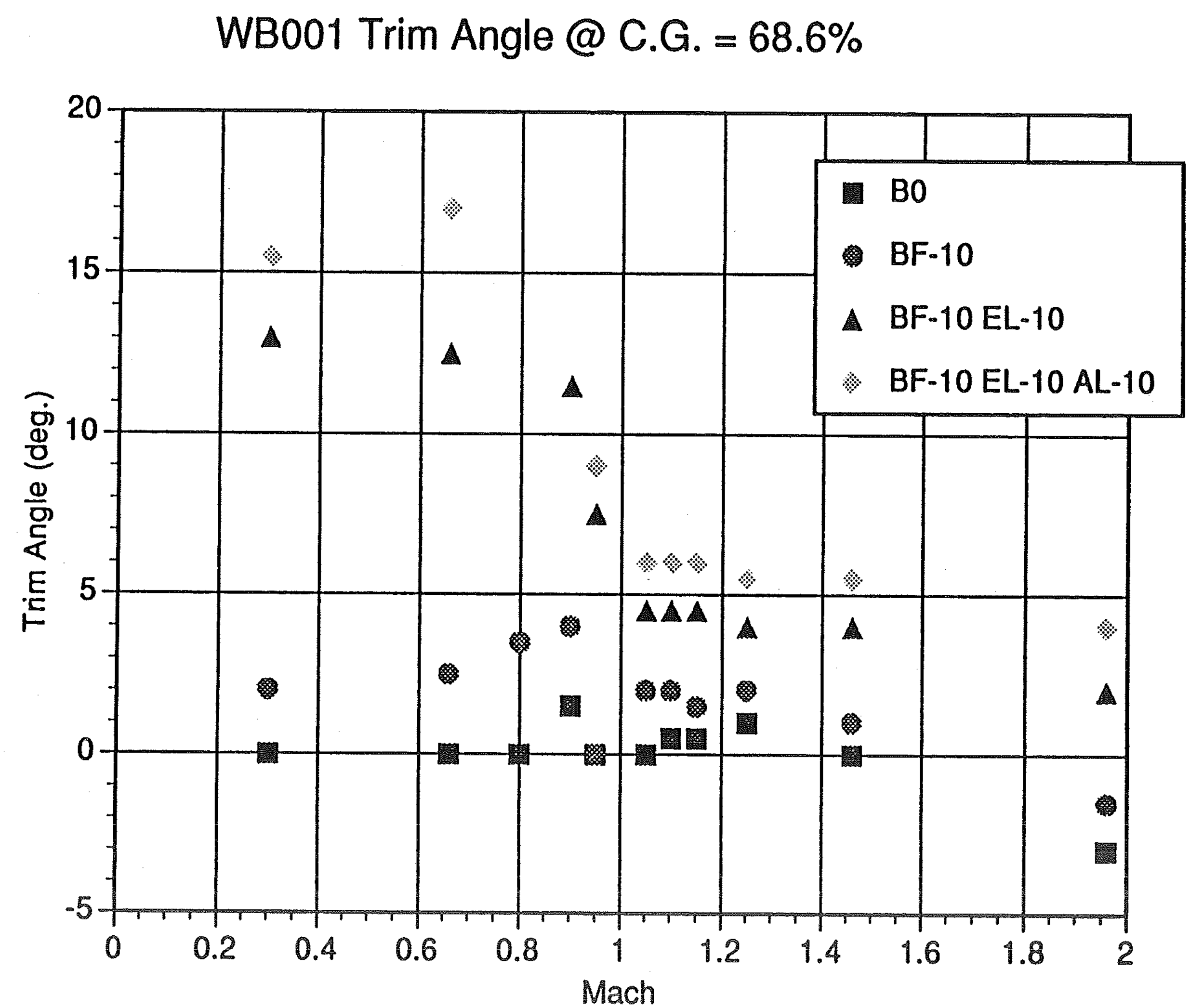
WB001 Trim Angle @ C.G. = 68.6%
Trim Angle (deg.)
Mach
B0
BF-10
BF-10 EL-10
BF-10 EL-10 AL-10
20
15
10
5
0
-5
0
0.2
0.4
0.6
0.8
1
1.2
1.4
1.6
1.8
2

Follow-Ons:

- Determine Supersonic Aerodynamic Char.
- Larger Elevon Deflections
- Vertical Tail
- Split V-Tail
- Larger Tip Fins (Factor of 3)

Data Availability

- Wing Body Transonic Aerodynamic Characteristics have been documented in NASA TM-XXXX
- This memo is available through NASA to interested parties
- The follow-on test will be documented in a forth coming NASA publication

511-02
51386
132108
28 p

Ascent Aerodynamic Pressure Distributions on WB001

B. Vu, J. Ruf, F. Canabal
CFD Branch

J. Brunty
System Load Branch

To support the reusable launch vehicle concept study, the aerodynamic data and surface pressure for WB001 were predicted using three CFD codes at several flow conditions during the ascent phase. The results have been compared between code to code and code to aerodynamic database as well as available experimental data. A set of particular solutions have been selected and recommended for use in preliminary conceptual designs. These CFD results have also been provided to the structure group for wing loading analyses.

Ascent Aerodynamics Analysis of WB001 Configuration

B.T. Vu
J.H. Ruf
F. Canabal
J. Brunty

OUTLINE

- Objectives
- Codes employed
- Cases considered
- Results and discussions
- Structural analyses
- Conclusions

OBJECTIVES

- Predict the flow field environment during ascent
- Compute the aerodynamic coefficients
- Provide three-dimensional surface pressure for structure analysis

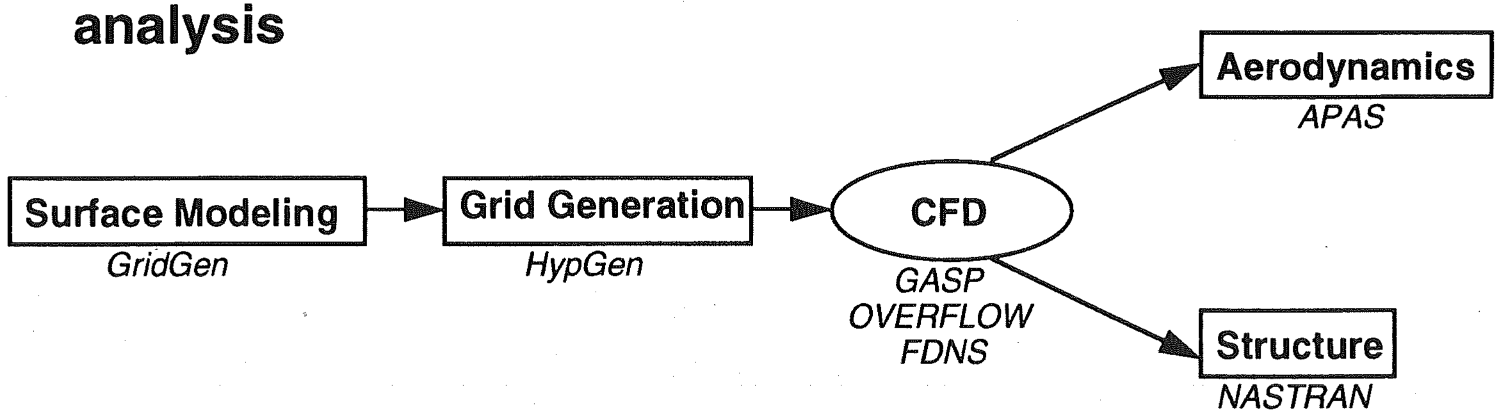

CODES EMPLOYED

- **OVERFLOW**
  - capable of solving overset grids
  - used at ARC and JSC for orbiter analyses
- **GASP**
  - finite-volume, density-based
  - used at LaRC and Wright Patterson for NASP vehicle design
- **FDNS**
  - finite-difference, pressure-based
  - used at MSFC for reacting flow analyses

CASES CONSIDERED

Transonic (M=1.1)	Supersonic (M=5.72)		
AOA 6°	AOA 0°	AOA 6°	AOA 8°
GASP inv./vis.		GASP vis.	
OVERFLOW inv/vis.	OVER FLOW vis.	OVER FLOW vis.	OVER FLOW vis.
FDNS vis.			

RESULTS & DISCUSSIONS

- Computational domain for both cases properly generated to capture physics associated flow conditions

- Surface pressure and symmetry Mach contours
  - good agreement for surface pressure
  - good agreement centerline Mach contours

- Pressure coefficients for vehicle nose
  - predicted stagnation Cp agrees with isentropic theory
  - **M = 1.1 Cp=1.36 (CFD / GASP)**
  - **M = 1.1 Cp=1.34 (Theory)**

Transonic Grid

(159x129x65)

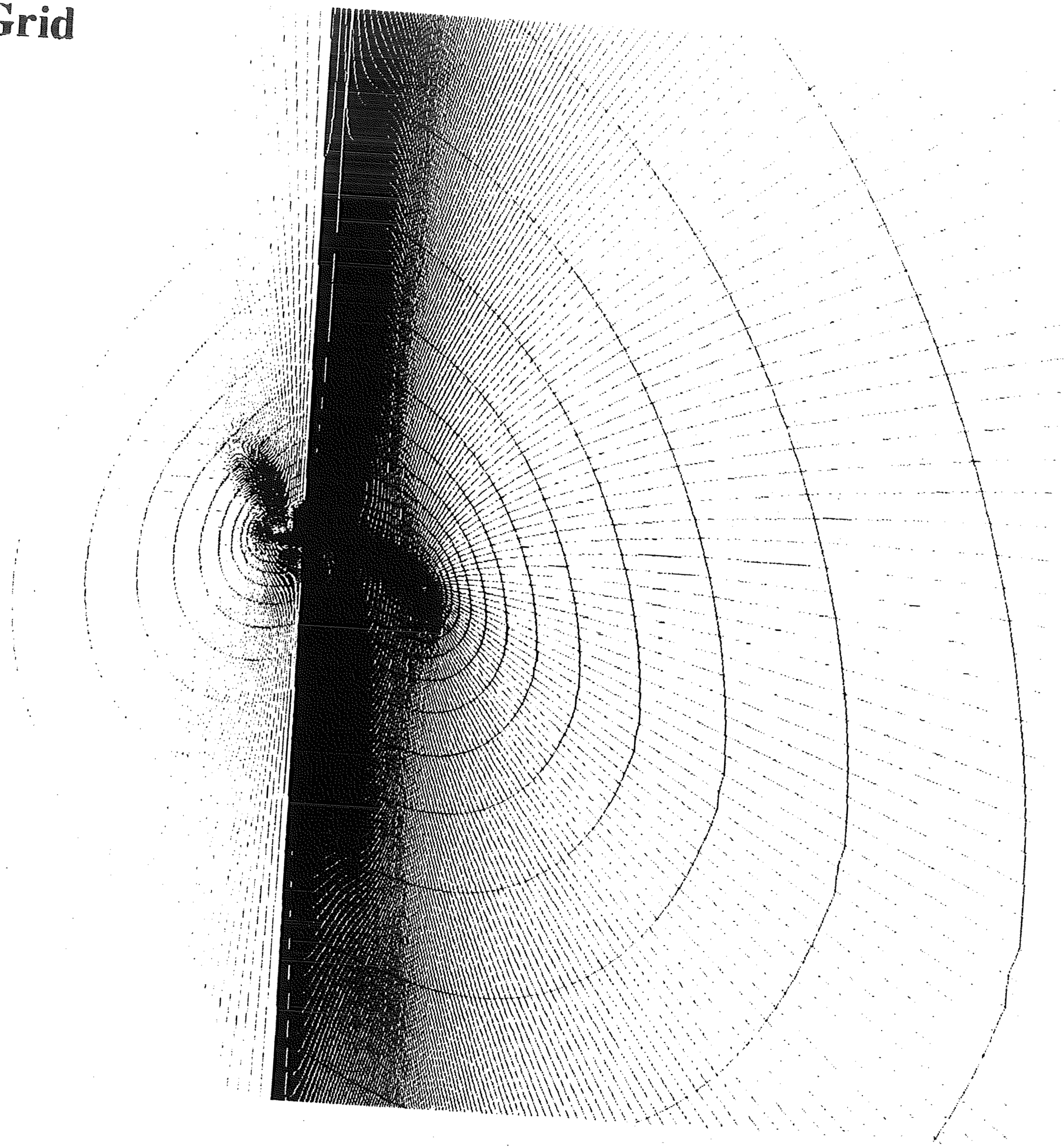

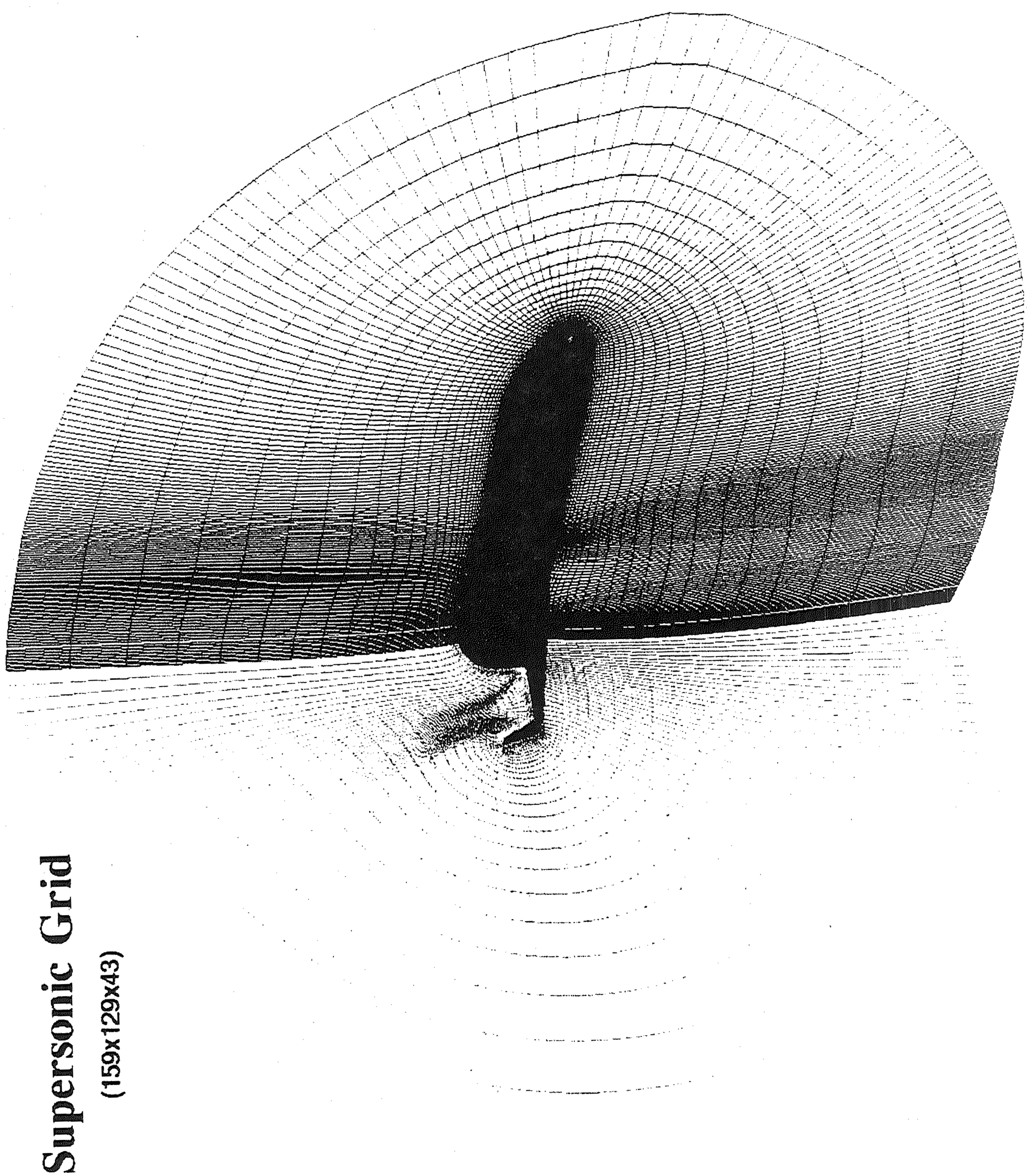

Supersonic Grid

(159x129x43)

COMPARISONS

- **Code-to-code comparison**
  - good agreement for surface pressure and centerline Mach contours

- **3 aerodynamic coefficients are compared between codes and with APAS database**
  - excellent agreement in high supersonic case
  - good agreement in transonic case

Surface Pressure and Centerline Mach Contours

M 1.1 & AOA 6deg. (FDNS soln)

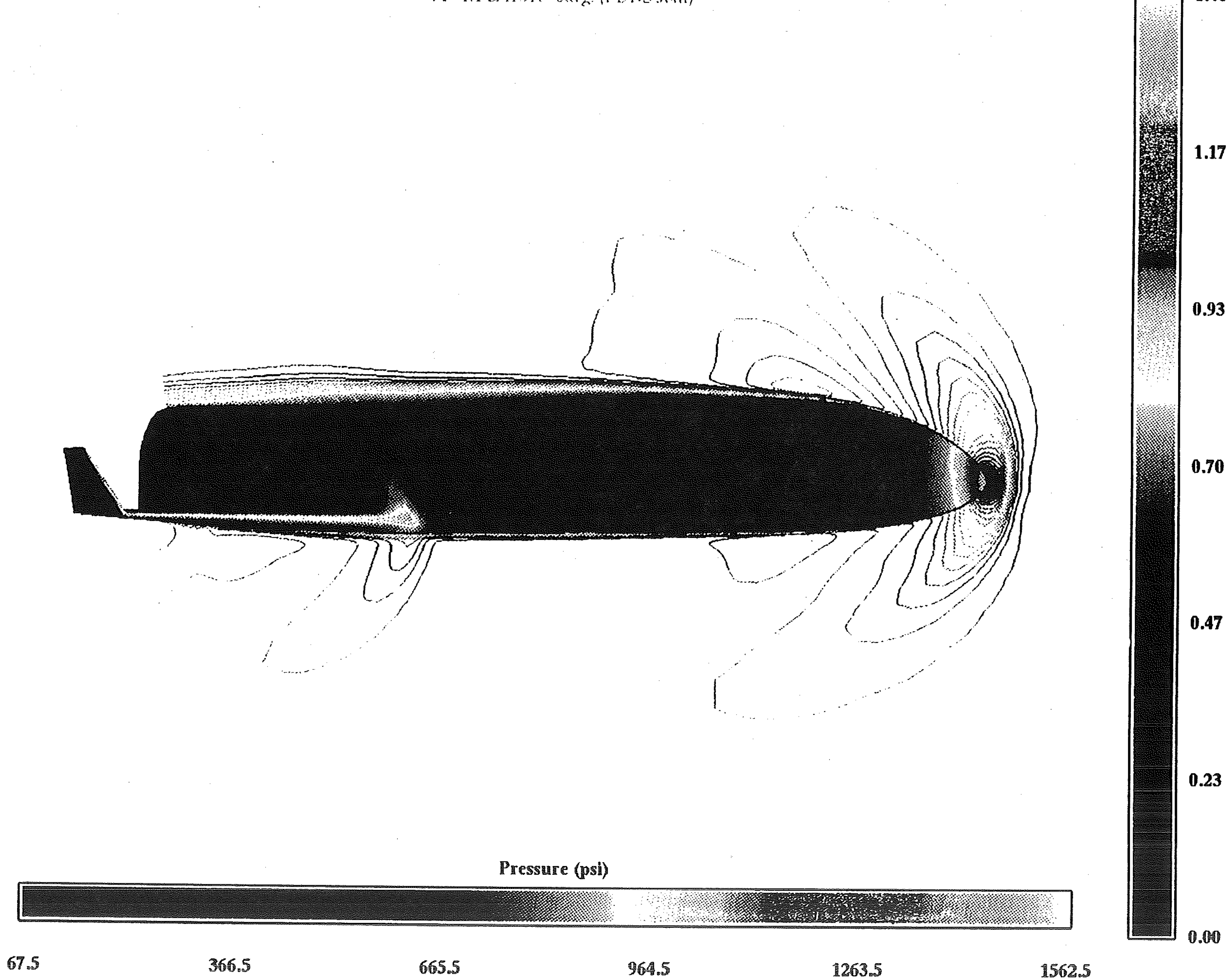

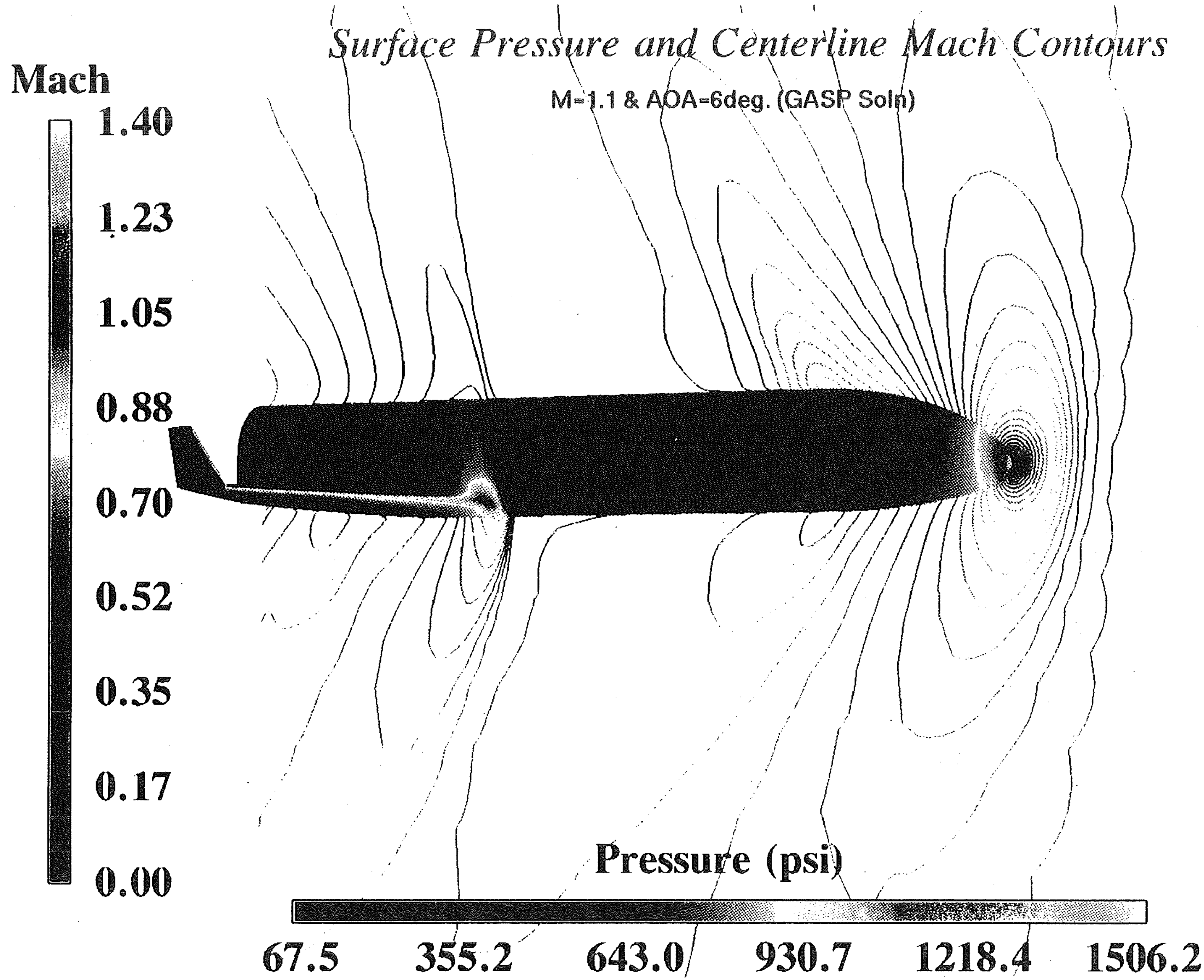
Surface Pressure and Centerline Mach Contours
M=1.1 & AOA=6deg. (GASP Soln)
Mach
1.40
1.23
1.05
0.88
0.70
0.52
0.35
0.17
0.00
Pressure (psi)
67.5
355.2
643.0
930.7
1218.4
1506.2

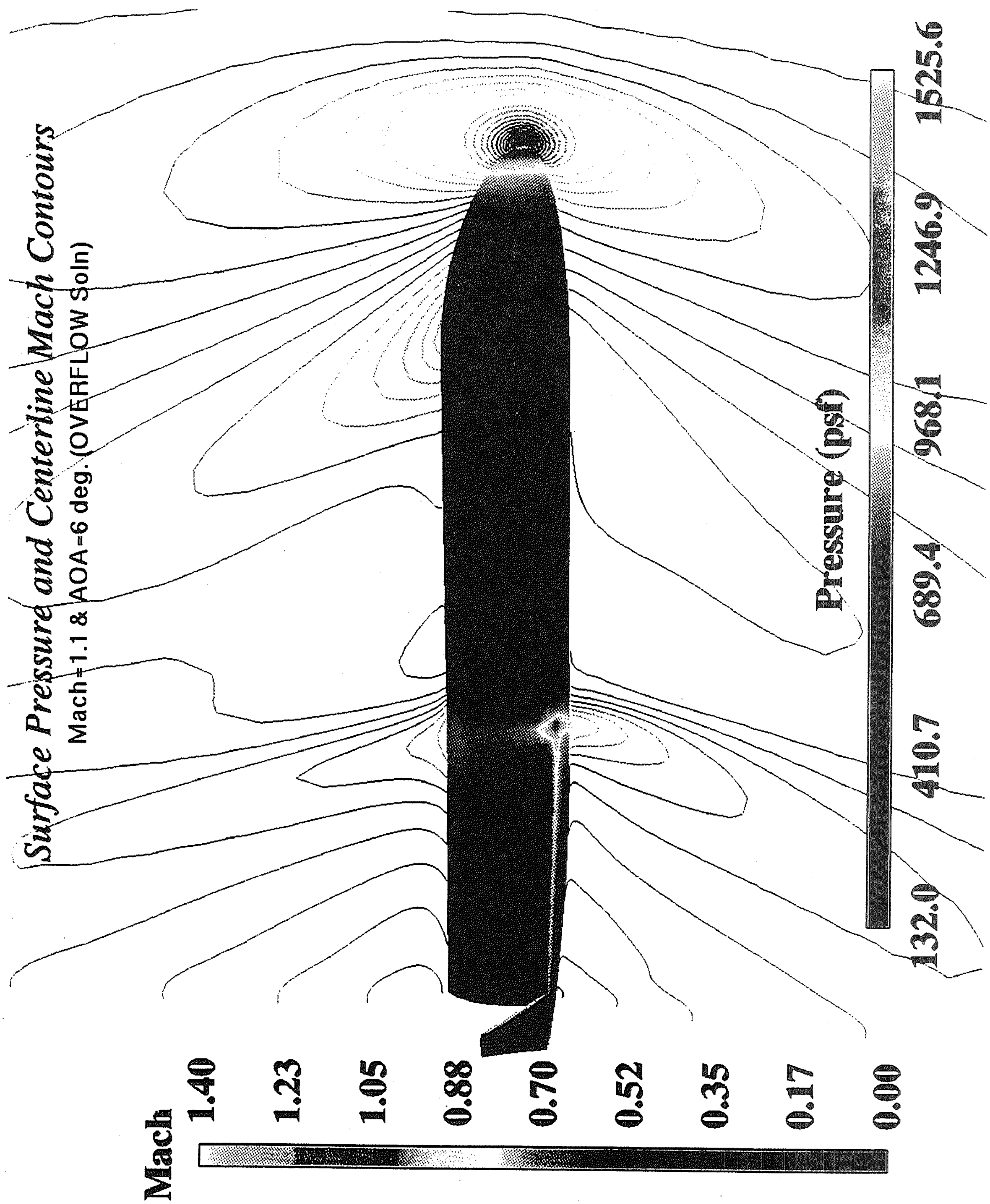
Surface Pressure and Centerline Mach Contours
Mach=1.1 & AOA=6 deg. (OVERFLOW Soln)
Pressure (psf)
132.0
410.7
689.4
968.1
1246.9
1525.6
Mach
1.40
1.23
1.05
0.88
0.70
0.52
0.35
0.17
0.00

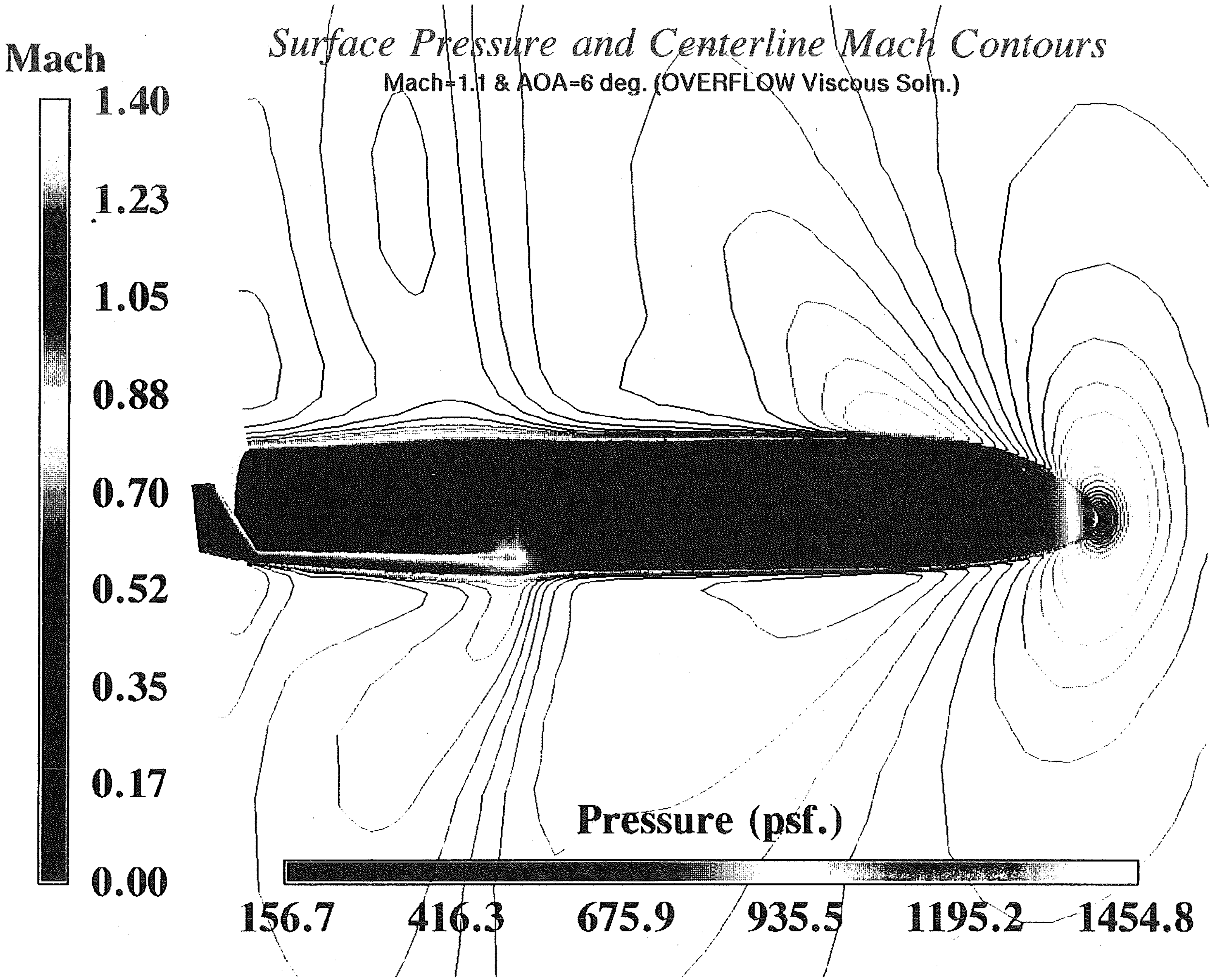
Surface Pressure and Centerline Mach Contours
Mach=1.1 & AOA=6 deg. (OVERFLOW Viscous Soln.)
Mach
1.40
1.23
1.05
0.88
0.70
0.52
0.35
0.17
0.00
Pressure (psf.)
156.7
416.3
675.9
935.5
1195.2
1454.8

Cp vs. X (Mach=1.1, AOA=6deg.)

Viscous Turbulent, FDNS solution

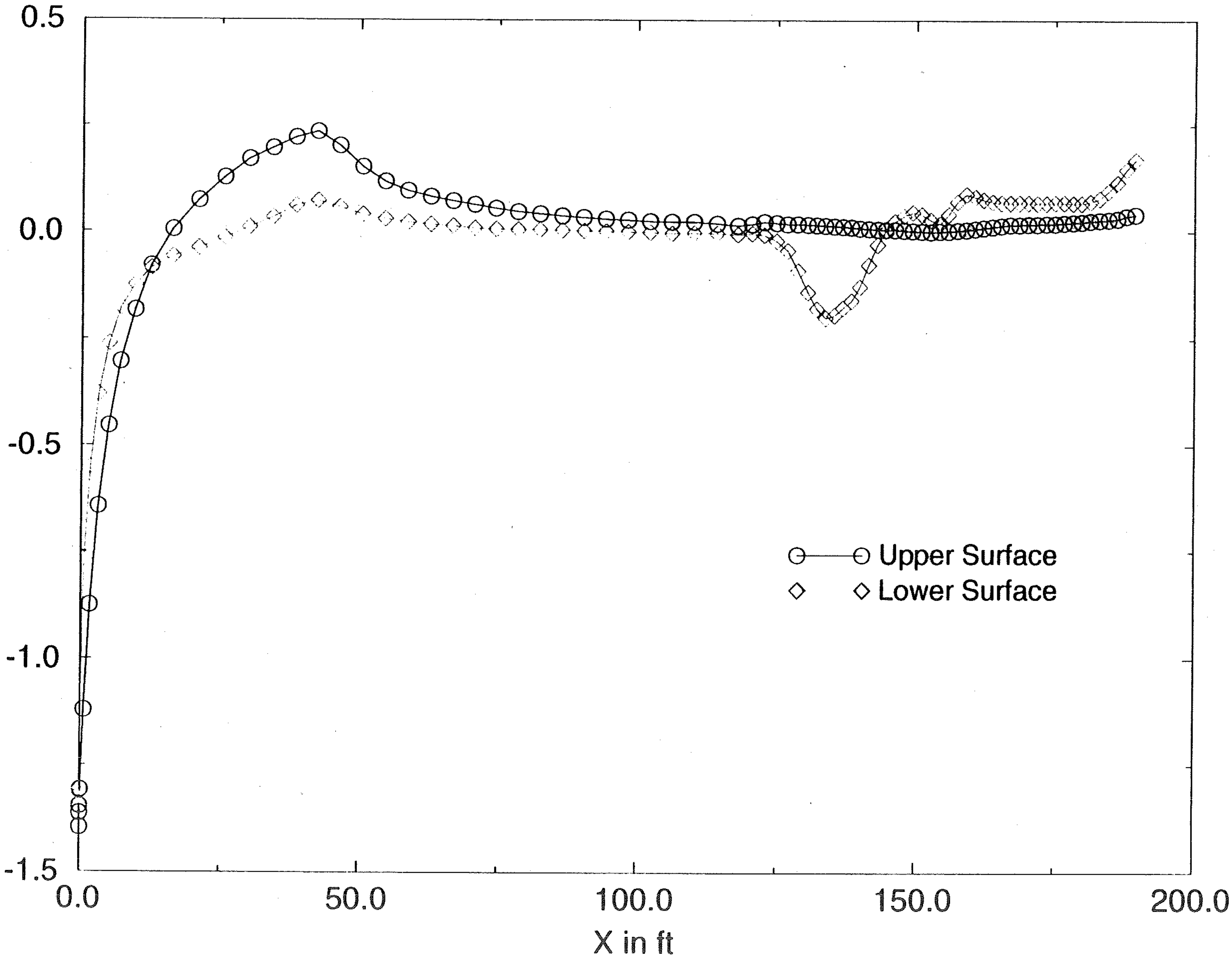

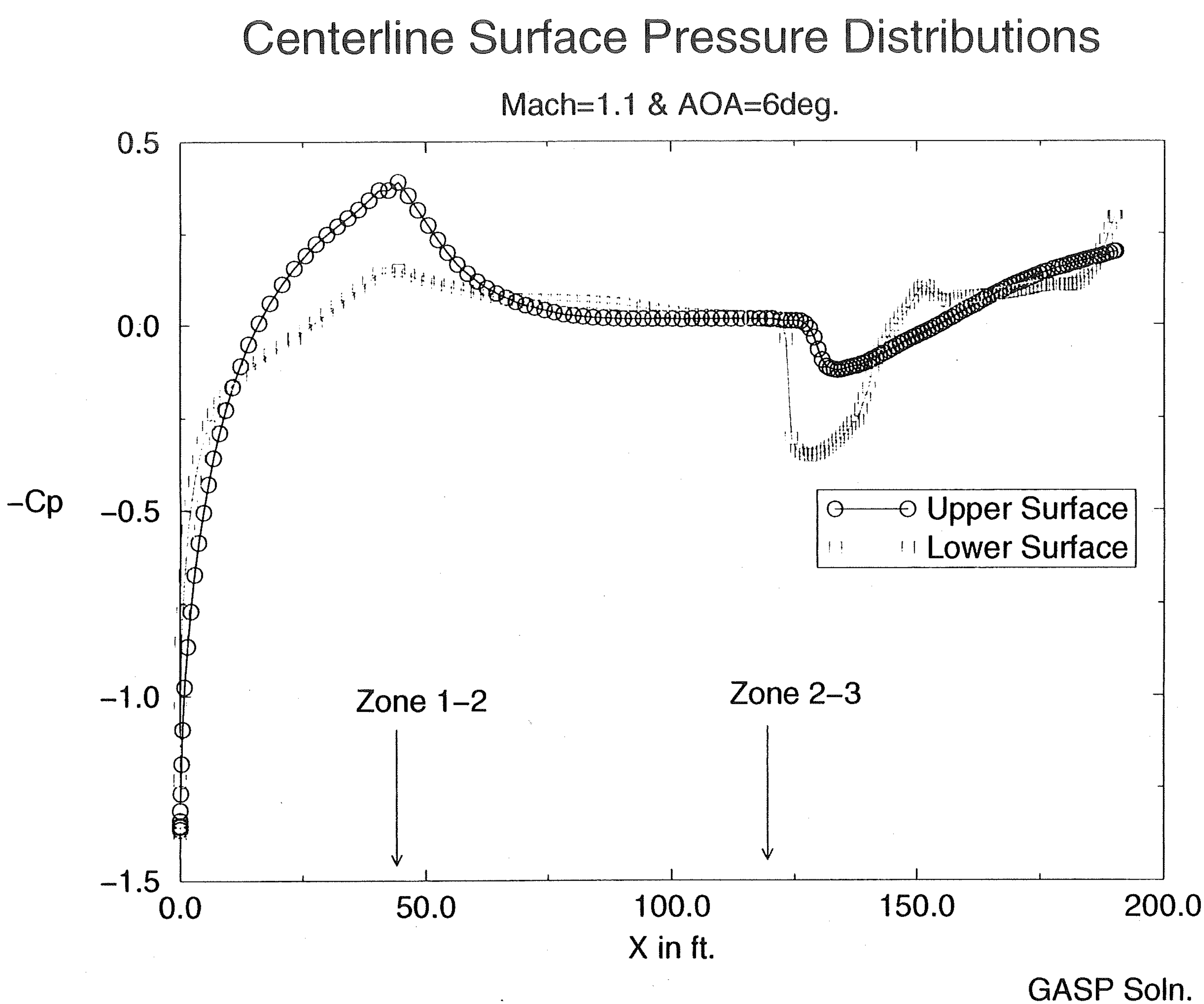
Centerline Surface Pressure Distributions
Mach=1.1 & AOA=6deg.
0.5
0.0
−0.5
−1.0
−1.5
−Cp
0.0
50.0
100.0
150.0
200.0
X in ft.
Upper Surface
Lower Surface
Zone 1−2
Zone 2−3
GASP Soln.

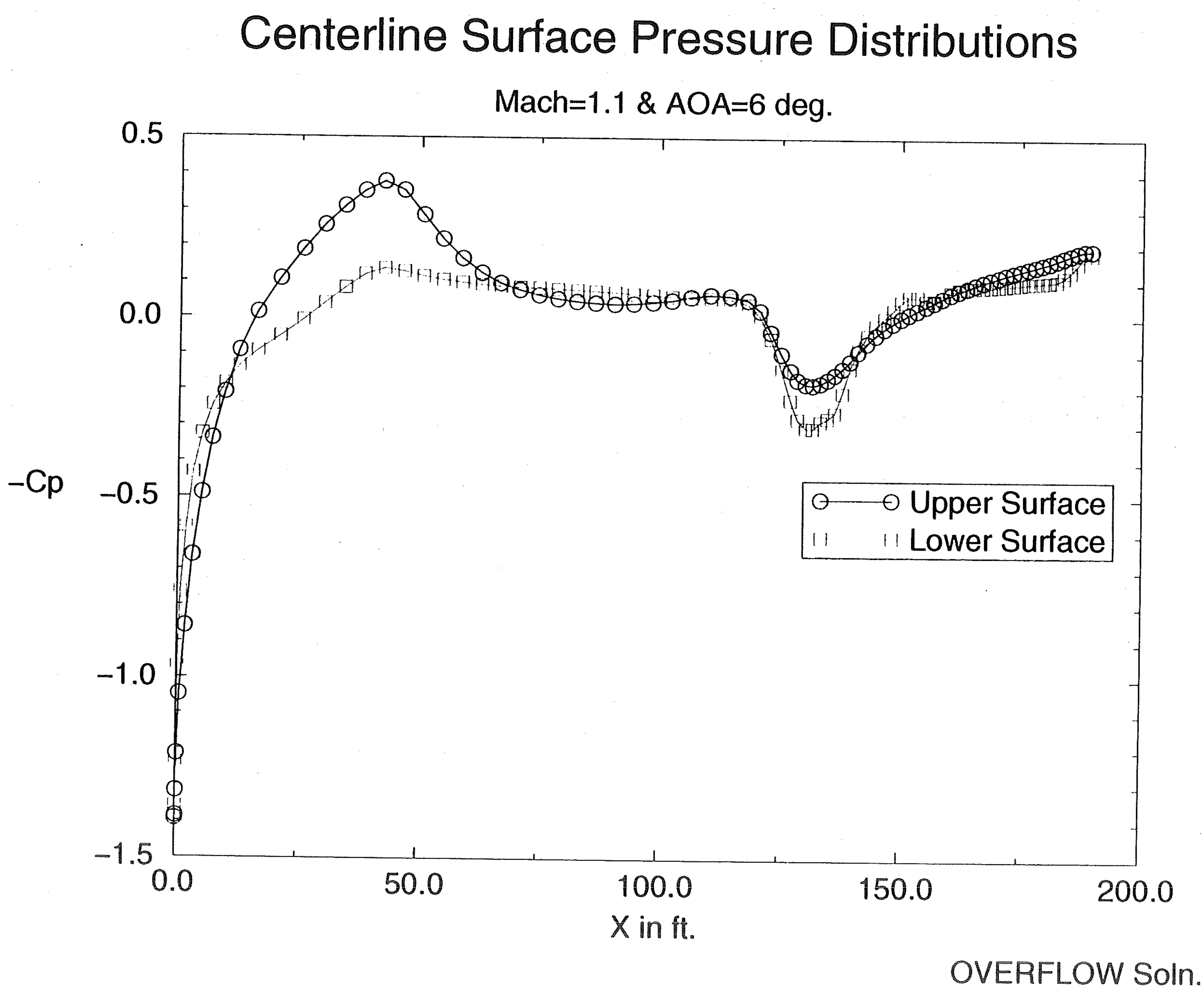
Centerline Surface Pressure Distributions
Mach=1.1 & AOA=6 deg.
−Cp
0.5
0.0
−0.5
−1.0
−1.5
0.0
50.0
100.0
150.0
200.0
X in ft.
Upper Surface
Lower Surface
OVERFLOW Soln.

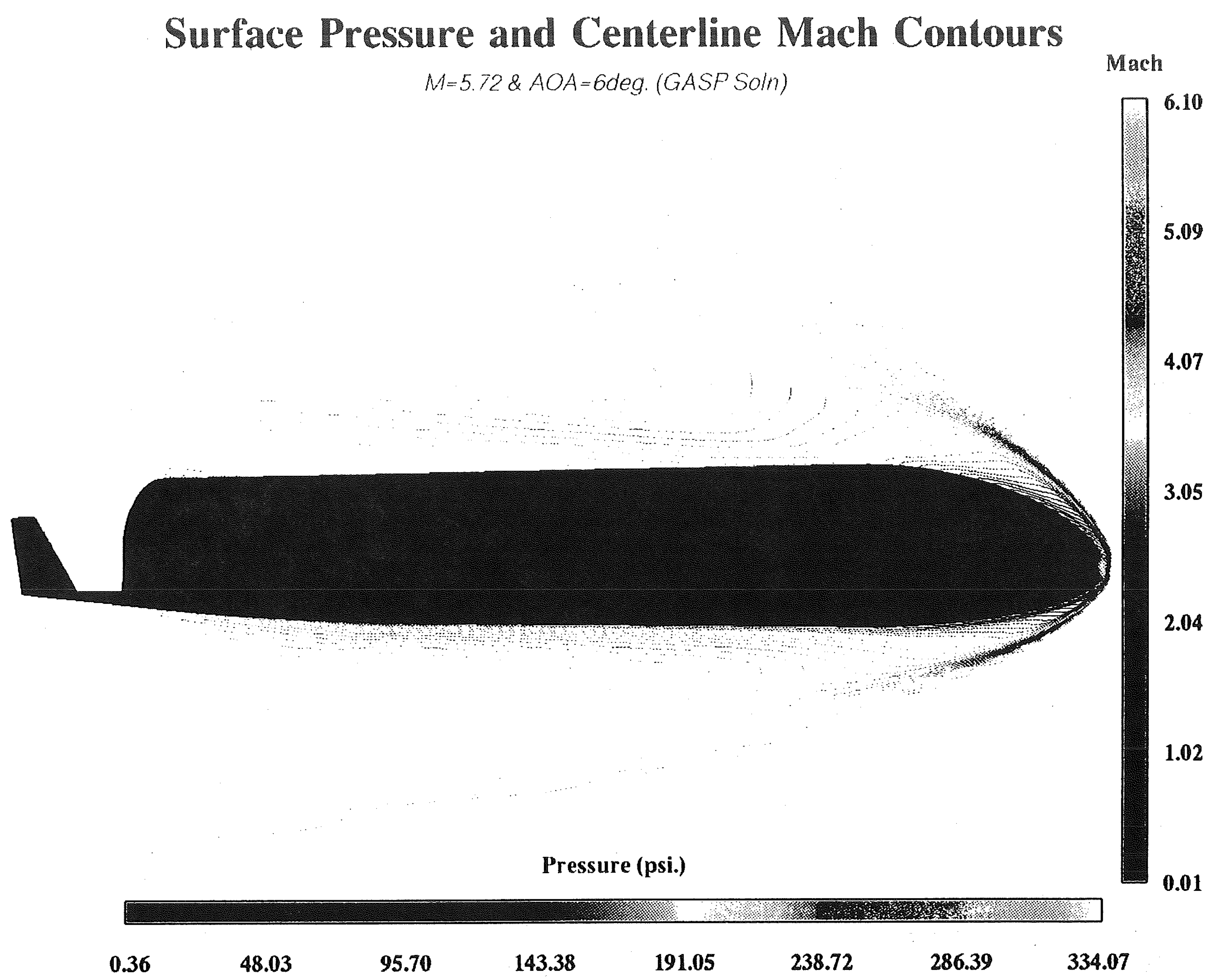
Surface Pressure and Centerline Mach Contours
M=5.72 & AOA=6deg. (GASP Soln)
Mach
6.10
5.09
4.07
3.05
2.04
1.02
0.01
Pressure (psi.)
0.36
48.03
95.70
143.38
191.05
238.72
286.39
334.07

Surface Pressure and Centerline Mach Contours

M=5.72 & AOA=6deg. (OVERFLOW Soln)

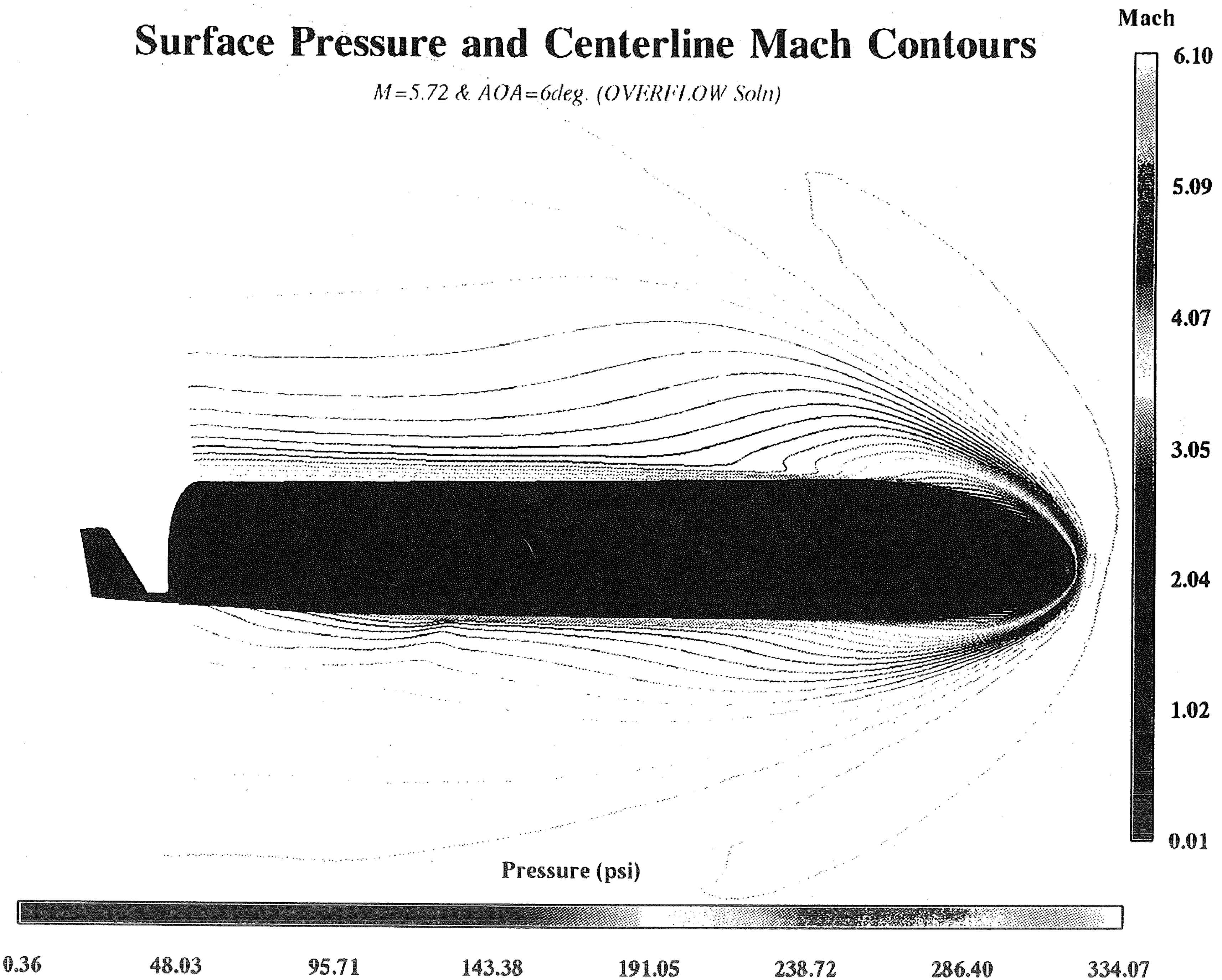

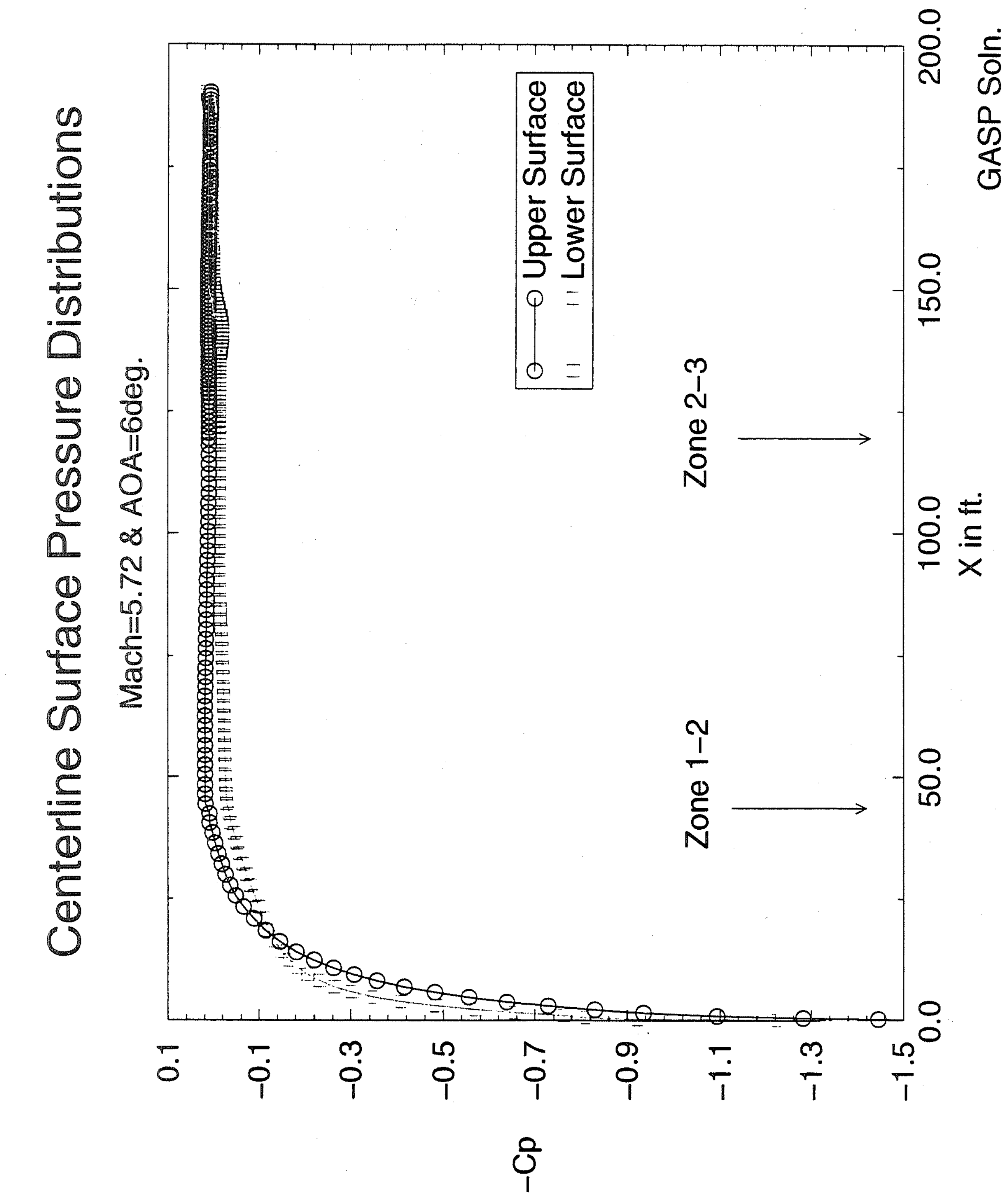

Centerline Surface Pressure Distributions
Mach=5.72 & AOA=6deg.
Upper Surface
Lower Surface
Zone 1–2
Zone 2–3
–Cp
0.1
–0.1
–0.3
–0.5
–0.7
–0.9
–1.1
–1.3
–1.5
0.0
50.0
100.0
150.0
200.0
X in ft.
GASP Soln.

Centerline Surface Pressure Distributions

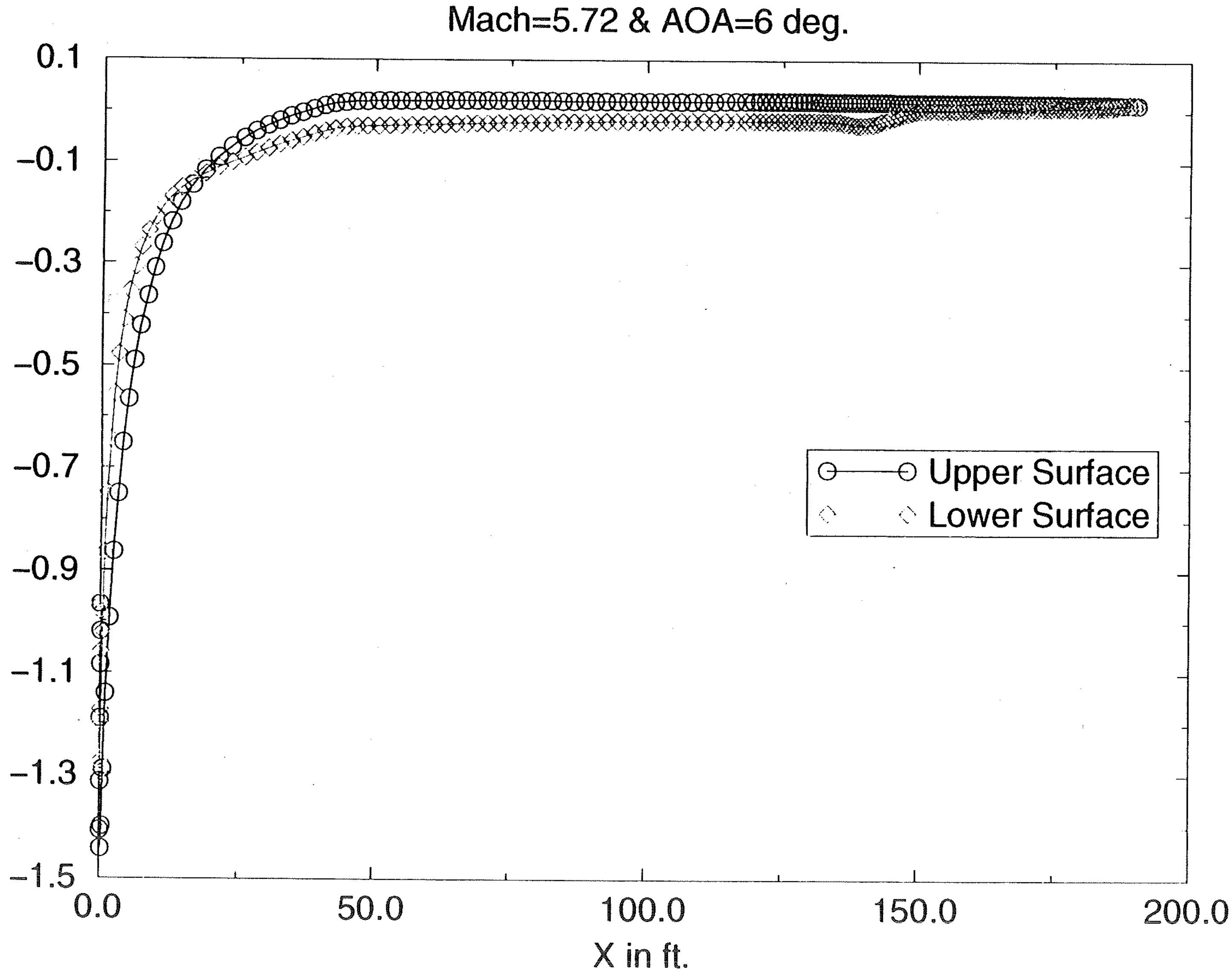

OVERFLOW Soln.

RLV Concept Study Review

- **Predicted aerodynamic coefficients**

	APAS	OVERFLOW	GASP (inv.)	GASP(vis.)
Transonic ***(M=1.10 & α=6 °)***				
C_N	0.34	0.31	0.32	0.31
C_A	0.12	0.23	0.20	0.22
C_M	-0.049	-0.035	-0.041	-0.04
Supersonic ***(M=5.72 & α=6 °)***				
C_N	0.07	0.0672	N/A	0.0651
C_A	0.07	0.0714	N/A	0.0735
C_M	-0.002	-0.0028	N/A	-0.0033

Surface Pressure

Ascent Aerodynamics Simulation

(Mach=0.51, Pitch=11 deg., Yaw=-8.6 deg.)

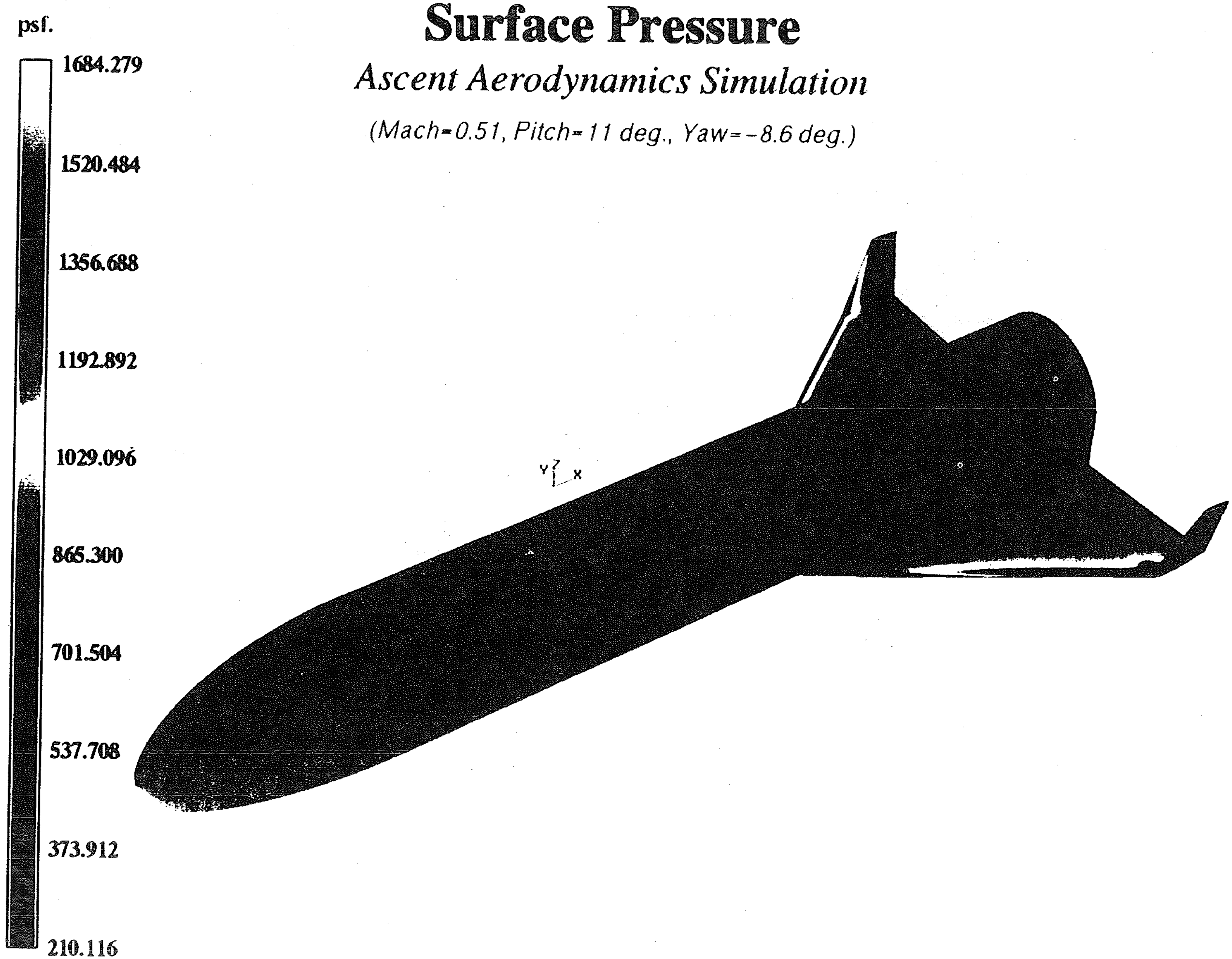

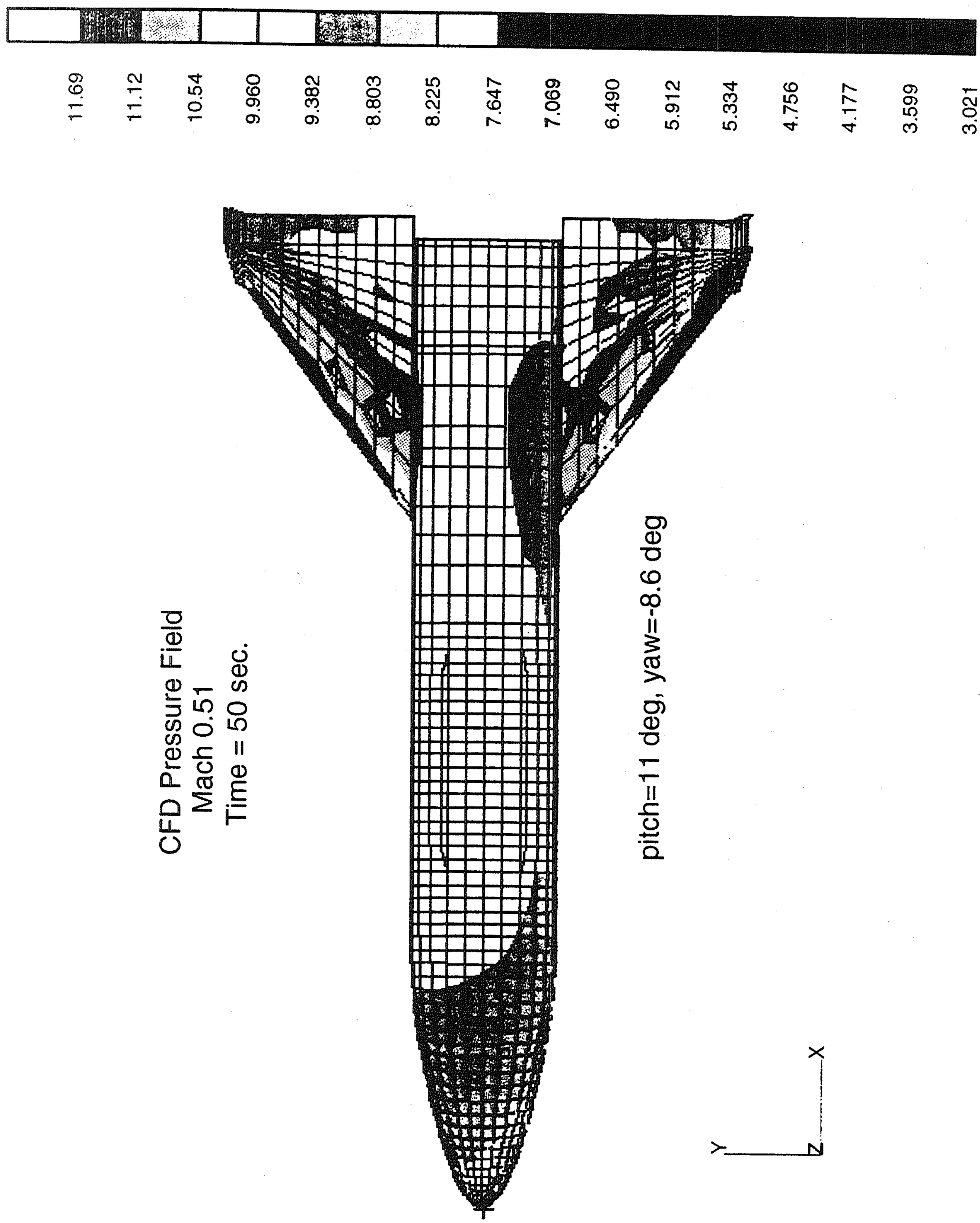

11.69
11.12
10.54
9.960
9.382
8.803
8.225
7.647
7.069
6.490
5.912
5.334
4.756
4.177
3.599
3.021
CFD Pressure Field
Mach 0.51
Time = 50 sec.
pitch=11 deg, yaw=-8.6 deg
Y
Z
X

Mach 0.51 T=50 sec. with Trim - Y Shear

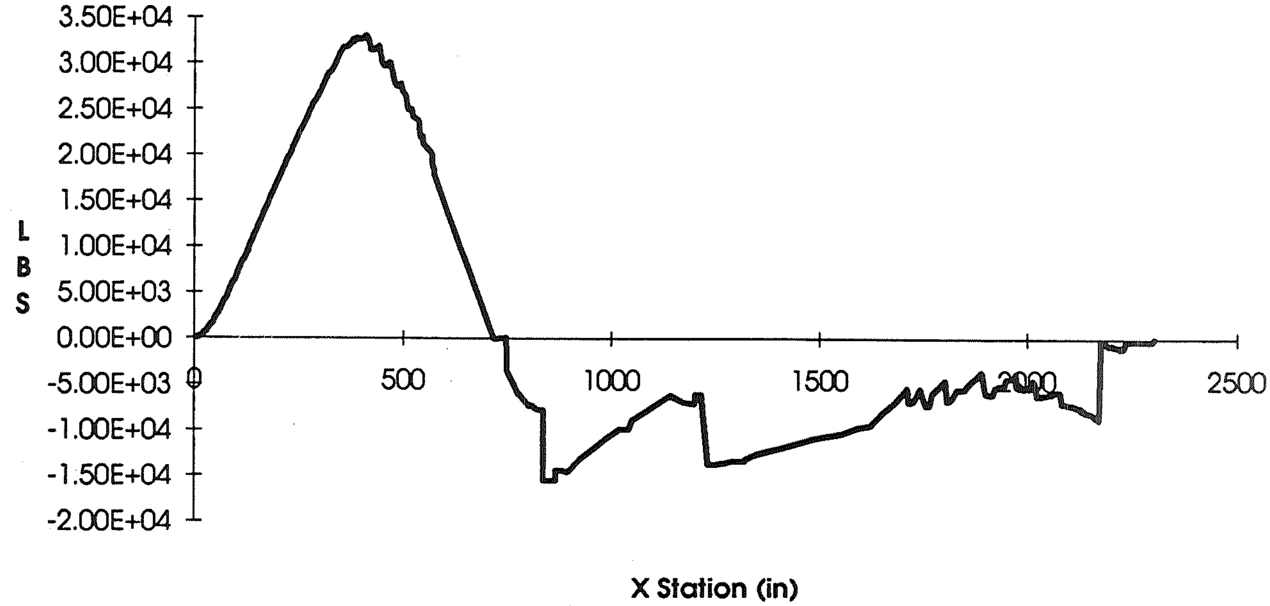

Mach 0.51 T=50 sec. with Trim - RZ Moment

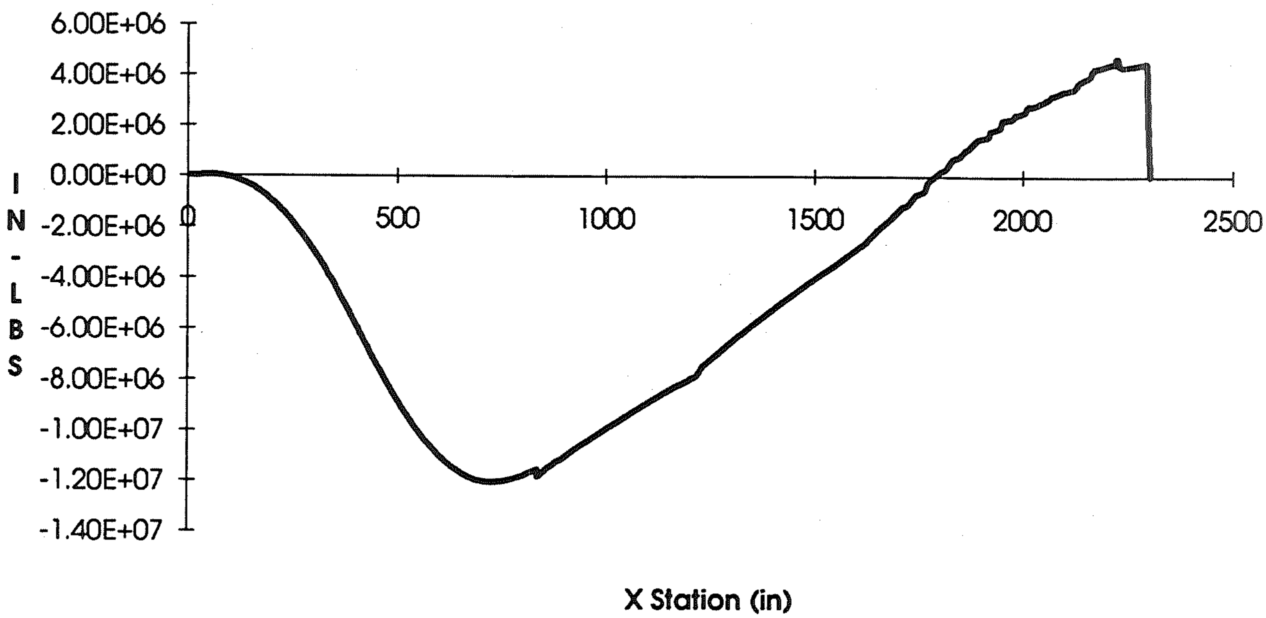

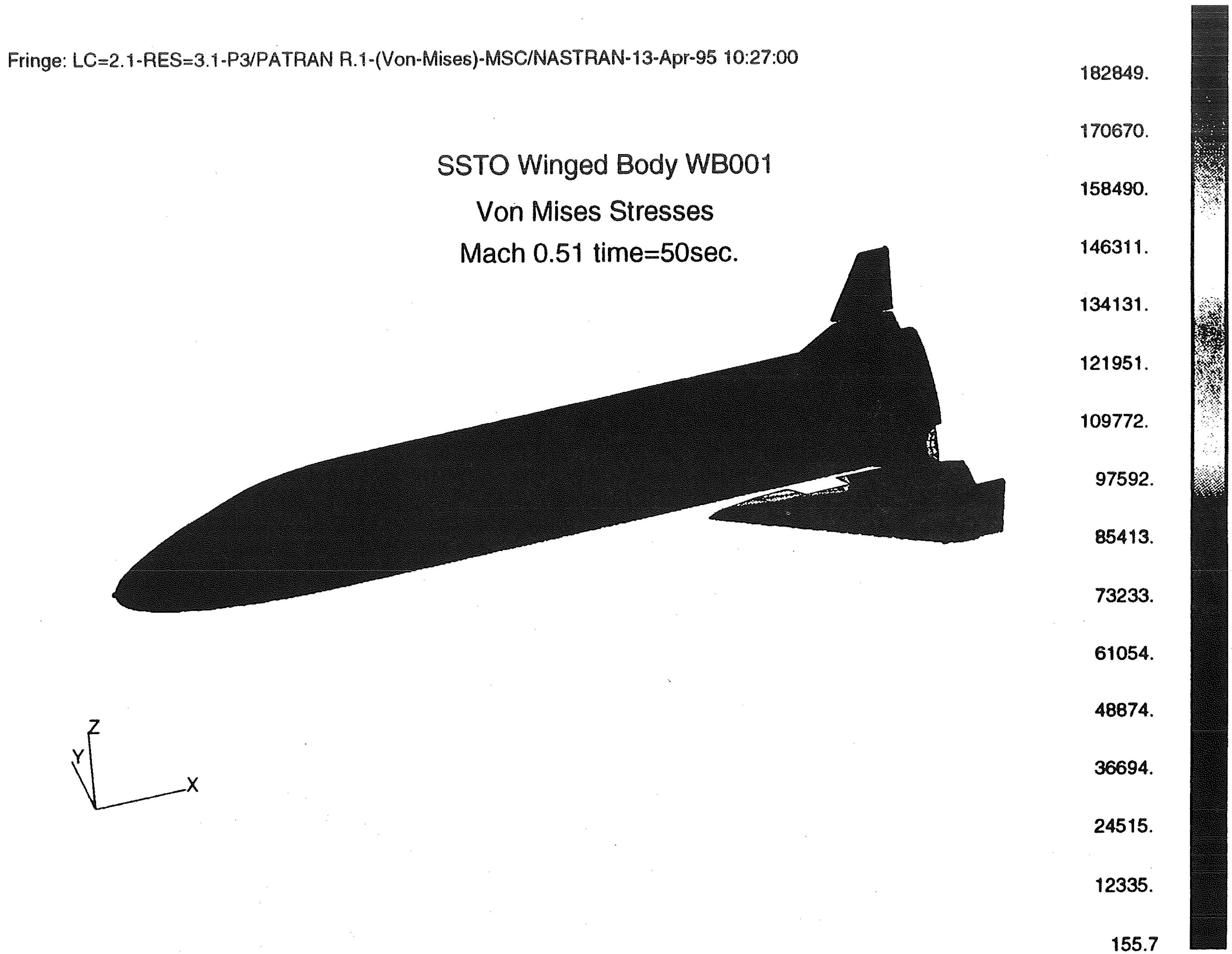
Fringe: LC=2.1-RES=3.1-P3/PATRAN R.1-(Von-Mises)-MSC/NASTRAN-13-Apr-95 10:27:00
SSTO Winged Body WB001
Von Mises Stresses
Mach 0.51 time=50sec.
182849.
170670.
158490.
146311.
134131.
121951.
109772.
97592.
85413.
73233.
61054.
48874.
36694.
24515.
12335.
155.7
Z
Y
X

CONCLUSIONS

- Predicted aerodynamic data and surface pressure for WB001 using 3 three codes at several flow conditions
- 3D finite element model and CFD pressure distribution provides the visual representation regarding structural deformations, load paths and stress patterns
- Base flow interactions (plume expansions, base recirculations, etc.) could affect the overall solutions; therefore must be considered in future work

5/2-02
51387
132109
28p

Assessment of Lifting Body Linear Aerospike Plume Effects on Vehicle Aerodynamics

Joseph H Ruf MSFC/ED32
Alonzo L. Frost MSFC/ED34
Bruce Vu MSFC/ED32
Francisco Canabal MSFC/ED32

The lifting body/linear aerospike is one of three configurations being studied for an SSTO vehicle. A preliminary aerodynamic database existed for then current lifting body configuration, however, this data base was developed without considering plume effects. A combined effort by the Computational Fluid Dynamics and Experimental Fluids Dynamics Branches was undertaken to determine first order effects of plume/external flow interactions on vehicle aerodynamics of this lifting body/linear aerospike configuration. Of interest were plume pumping/entrainment at low Mach numbers and plume induced separation of flow over the vehicle at higher altitudes. The CFD analysis included combinations of four Mach numbers, two angles of attack and four throttle settings. The majority of the CFD was two dimensional centerline analysis of the lifting body/aerospike. Incremental plume effects were derived by comparing the power-on, power-off, and throttled cases and were extrapolated to the preliminary aerodynamic database.

The plume had little effect on the vehicle aerodynamics for supersonic freestream velocities. At subsonic freestream velocities, the plume affected the vehicle aerodynamics through both jet pumping/entrainment and the jet flap effect.

National Aeronautics and
Space Administration

Computational Fluid Dynamics Branch
Fluid Dynamics Division
Structures and Dynamics Laboratory
George C. Marshall Space Flight Center

936

Assessment of Lifting Body Linear Aerospike Plume Effects on Vehicle Aerodynamics

Mr. Joseph H. Ruf
Mr. Bruce T. Vu
Mr. Francisco Canabal
Computational Fluid Dynamics Branch
Mr. Alonzo L. Frost
Experimental Fluid Dynamics Branch
Marshall Space Flight Center
April 27, 1995

Presented to:
Workshop for CFD Applications in Rocket Propulsion
Marshall Space Flight Center
MSFC, Alabama

Overview

- Introduction
- Objective and Approach
- 2D CFD Results
- Application of CFD
- Conclusions

Introduction

- **Lifting body with integrated linear aerospike is one of the three candidate configurations for X33/RLV.**
- **The then current lifting body configuration was the Lockheed K10.**
- **A preliminary aerodynamic database w/o plume effects and a preliminary flight trajectory existed.**
- **Because of vehicle configuration and close proximity of plume to vehicle, it was felt there were potential plume/external flow interactions.**
  - Subsonic/low altitude - plume entrainment/jet pumping
  - Supersonic/medium and high altitude - plume induced separated flow on vehicle (a la, Saturn, Shuttle)

CONFIGURATION K-10

Sref = 5,600 sq. ft.
Swet = 13,100 sq. ft.

Total Internal Volume = 67,000 cu. ft.
Main Hyd. Tank Volume = 47,500 cu. ft.
Fwd LOX Tank Volume = 5,200 cu. ft.
Aft LOX Tank Volume = 12,700 cu. ft.

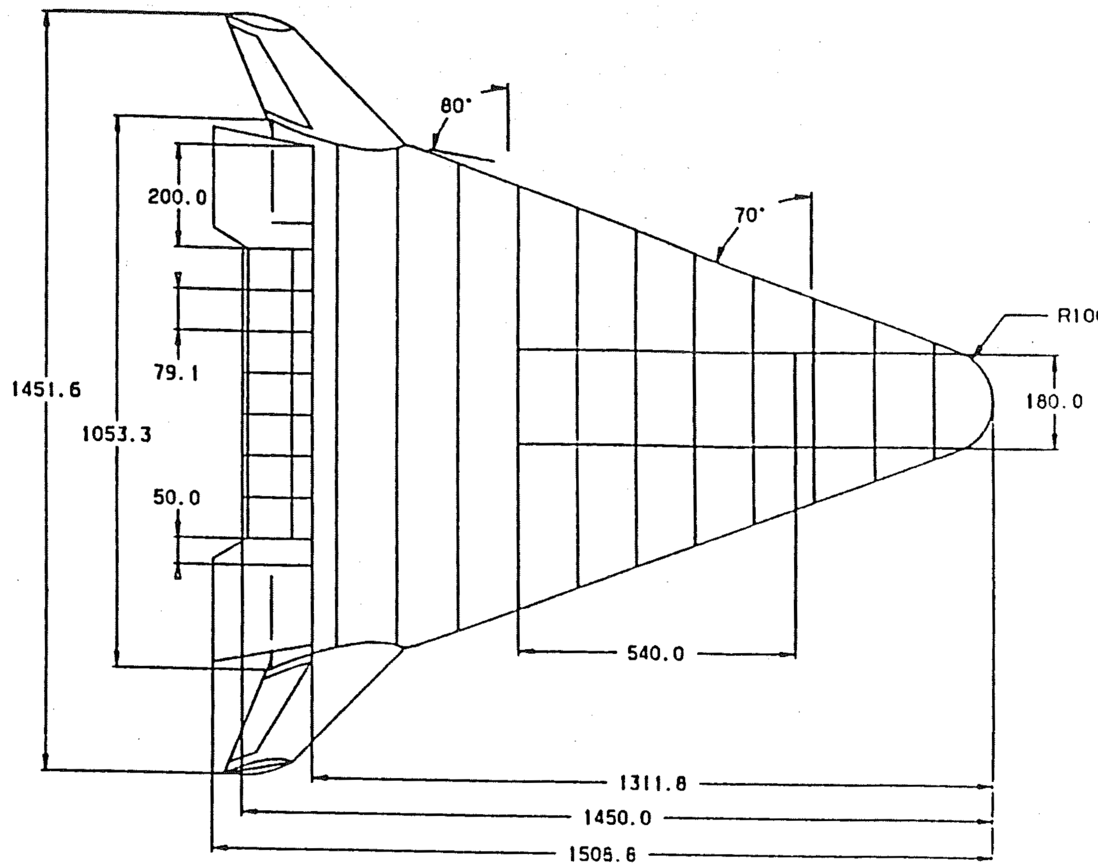

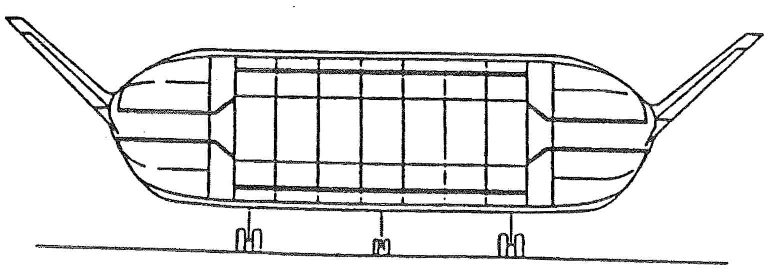

LOOKING FORWARD

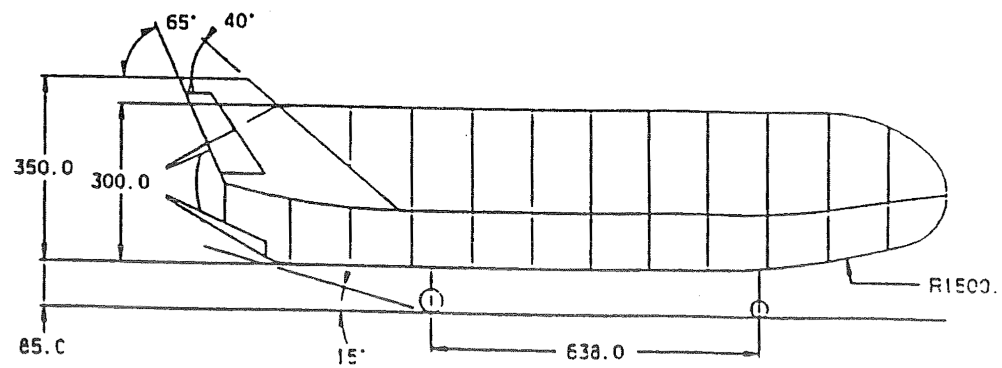

Objective

Determine first order effects of plume/external flow interactions on vehicle pitch plane aerodynamics to generate plume effect increments for the aerodynamic database.

Approach

- **Performed series of 2D CFD analyses of K10 centerline to determine vehicle aerodynamics at different flight conditions.**
  - Three Mach numbers: 0.6, 1.2, 3.0
  - Power-off, power-on, power-on-throttled
  - Two angles of attack: 0 and 6 degrees

- **Two Dimensional analysis was chosen for several reasons.**
  - Short deadline for decision on a flight test.
  - 3D geometry quite complex. Long turn around time for above parametrics with 3D CFD.
  - 2D would allow for many more cases to be perform in the parametric study.
  - 2D analysis would exaggerate plume/vehicle flow interaction - conservativism (axisymmetric calculations could also be run as lower bound on interactions).
  - The centerline pressure coefficients could be extrapolated to 3D vehicle.

Assessment of Lifting Body/Linear Aerospike Plume Effects on Vehicle Aerodynamics

	Two Dimensional							
Freestream Mach	0.6		1.2		3.0		5.0	
A.O.A.	α=0	α=6	α=0	α=6	α=0	α=6	α=0	α=6
Throttle Setting								
Power -off	x	x	x	x	x	x	x	
Power - on	x	x	x	x	x	x		
Power -on -throttled								
70%/130%	x	x						
130%/70%		x						

Approach, cont.

- **Grid(s)**
  - Vehicle centerline profile was extracted from 3D surface grid.
  - 2D grid generated with GENIE, refined with GEN2D. Two zone grid, one for forward part of vehicle, one for vehicle base/aerospike. 43000 points total.
  - Different grid wall spacing for each freestream Mach number for acceptable y+'s.

- **CFD**
  - GASP v2.3, Baldwin Lomax
  - Frozen flow, two species: air and a hot gas. Hot gas was average properties of exhaust products.
  - Convergence based on vehicle pressure coefficients reaching steady state.
  - CPU hours required varied from 0.5 to 15 hrs. Typical was about 8 hrs.

- **Derivation of plume effect increments**
  - Compared power-on, power-off and throttled cases to generate plume effect increments to preliminary data base.
  - Centerline 2D pressure deltas were applied to limited areas of total vehicle and extrapolated for the actual 3D geometry.
  - Incremental pressure distribution was integrated to determine total aerodynamic force and moment coefficients.

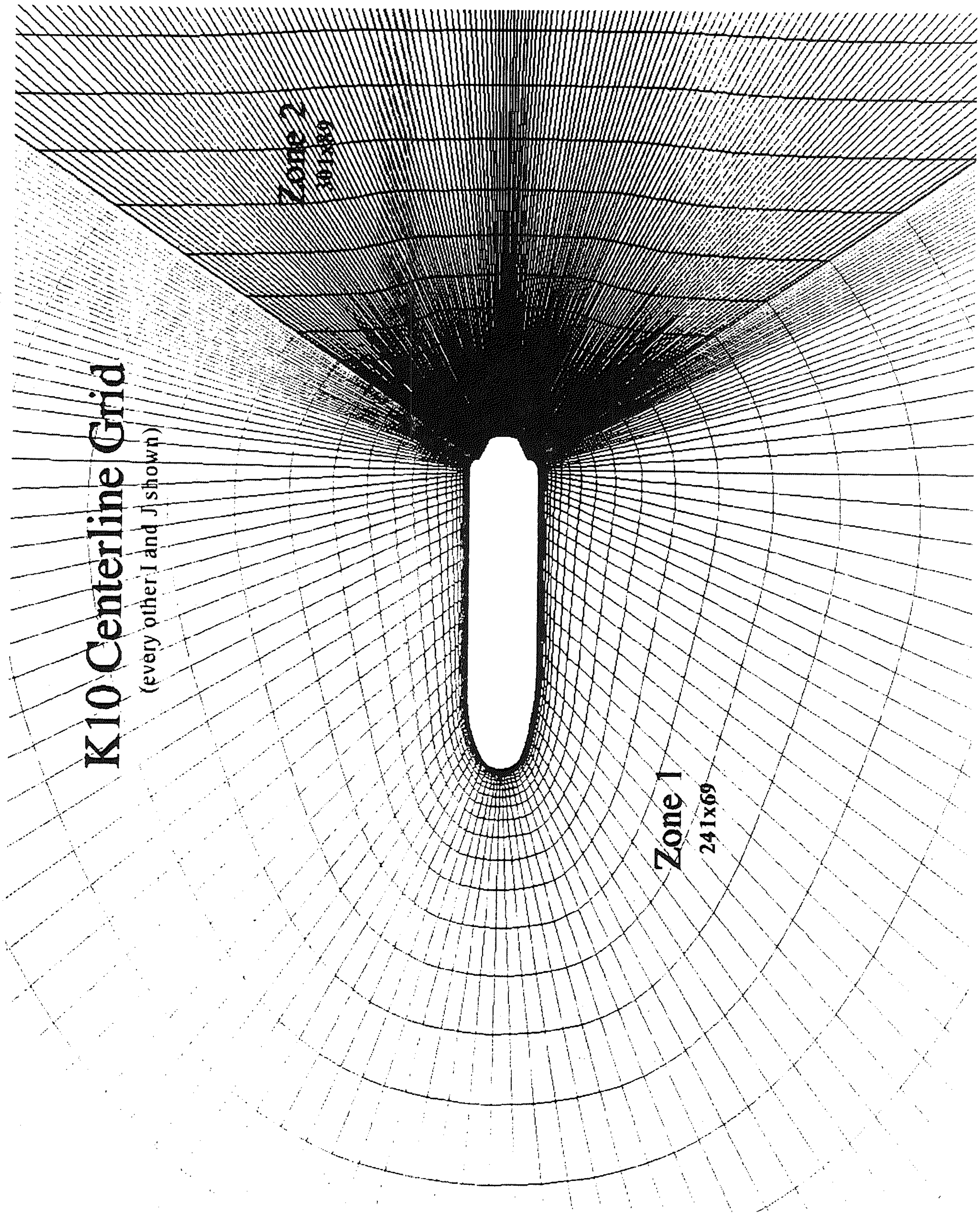
K10 Centerline Grid
(every other I and J shown)
Zone 2
Zone 1
241x69

CFD Results

- **Mach 5.0 ~ 124Kft**
  - no significant plume billowing present
  - no significant plume induced separation on the vehicle
- **Mach 3.0 ~ 76Kft**
  - no significant plume billowing
  - no significant plume induced separation on the vehicle
- **Mach 1.2 ~ 31Kft**
  - no significant plume effects
- **Mach 0.6 ~ 12Kft**
  - 0 degree α power-on vs. power-off
    - » minor effect seen
  - 6 degree α power-on vs. power-off
    - » significant plume effects through plume entrainment and jet flap effect

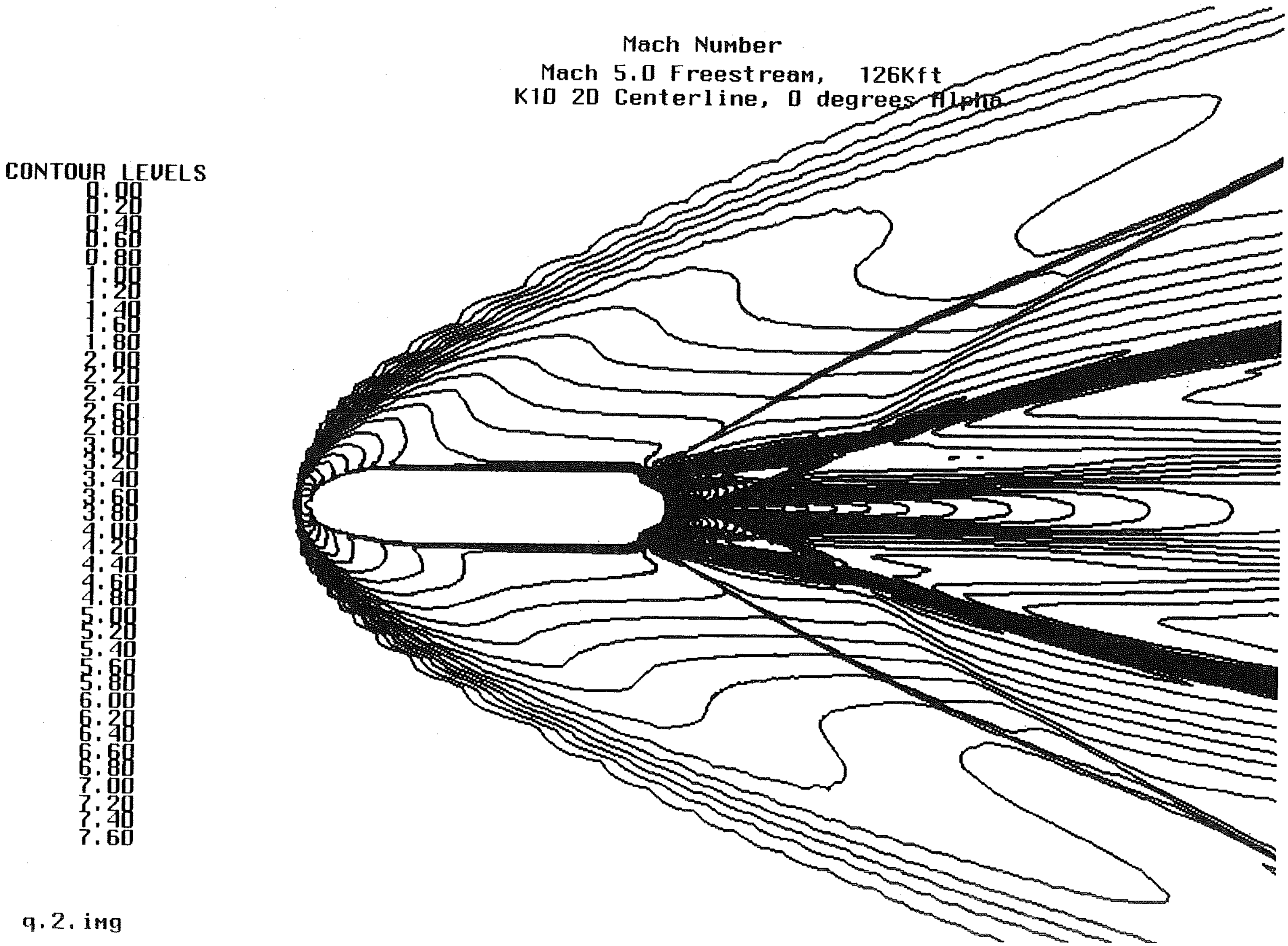
Mach Number
Mach 5.0 Freestream, 126Kft
K10 2D Centerline, 0 degrees Alpha
CONTOUR LEVELS
0.00
0.20
0.40
0.60
0.80
1.00
1.20
1.40
1.60
1.80
2.00
2.20
2.40
2.60
2.80
3.00
3.20
3.40
3.60
3.80
4.00
4.20
4.40
4.60
4.80
5.00
5.20
5.40
5.60
5.80
6.00
6.20
6.40
6.60
6.80
7.00
7.20
7.40
7.60
q.2.img

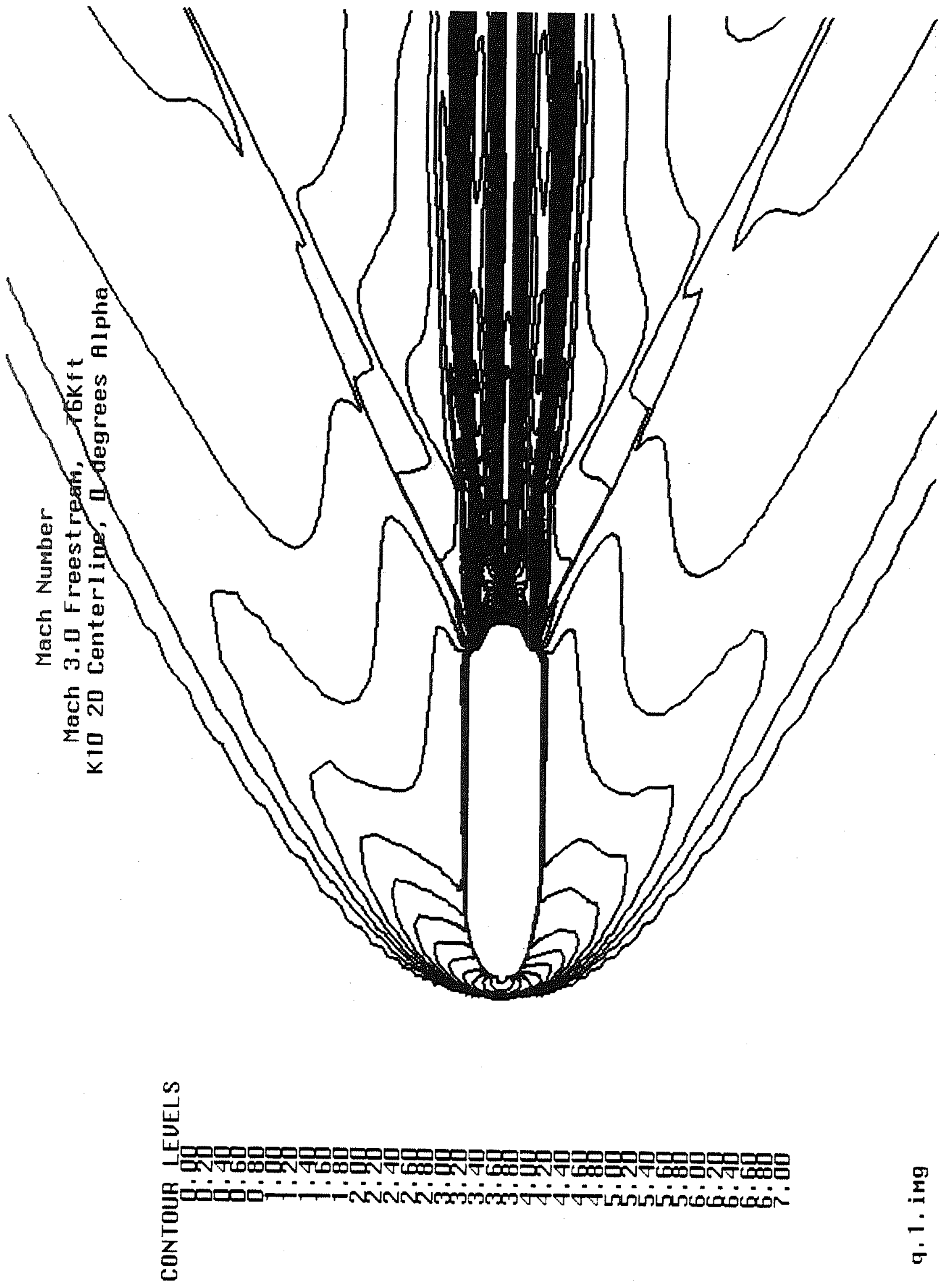
Mach Number
Mach 3.0 Freestream, 76Kft
K10 2D Centerline, 0 degrees Alpha
CONTOUR LEVELS
0.00
0.20
0.40
0.60
0.80
1.00
1.20
1.40
1.60
1.80
2.00
2.20
2.40
2.60
2.80
3.00
3.20
3.40
3.60
3.80
4.00
4.20
4.40
4.60
4.80
5.00
5.20
5.40
5.60
5.80
6.00
6.20
6.40
6.60
6.80
7.00
q.1.img

K10 2D Centerline Pressure Coefficients

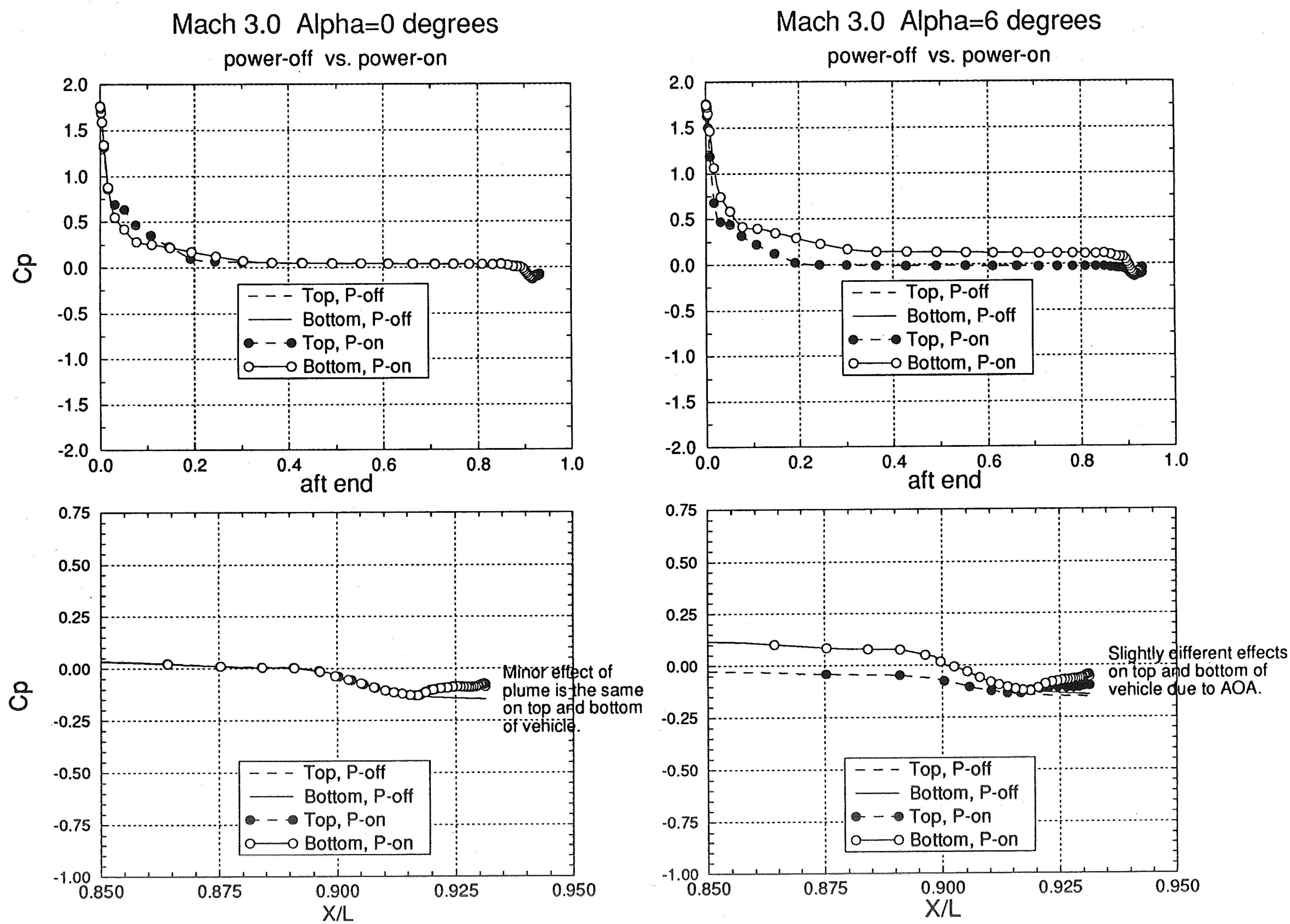

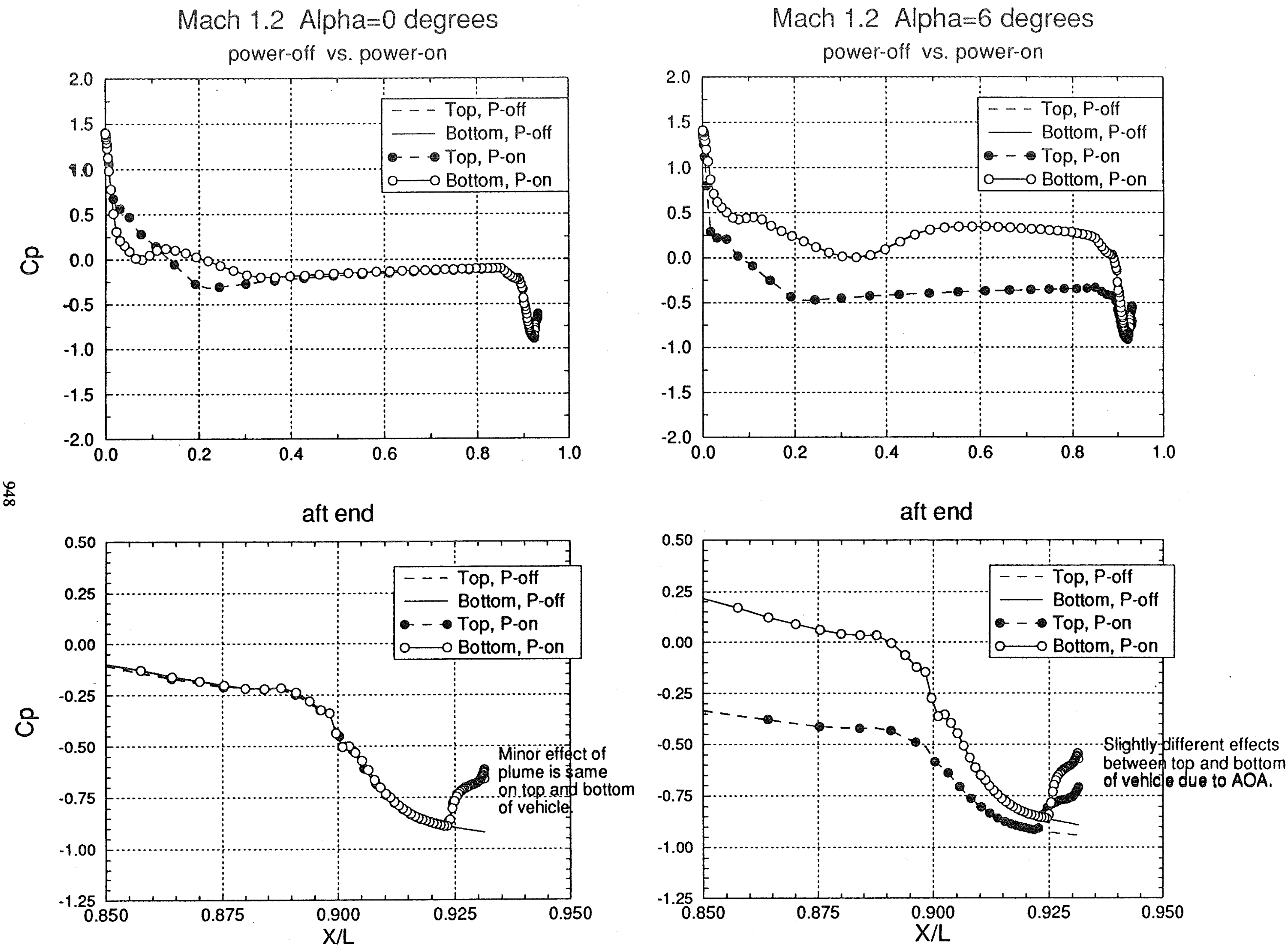
Mach 1.2 Alpha=0 degrees
power-off vs. power-on
Top, P-off
Bottom, P-off
Top, P-on
Bottom, P-on
Cp
aft end
Minor effect of plume is same on top and bottom of vehicle.
X/L
Mach 1.2 Alpha=6 degrees
power-off vs. power-on
aft end
Slightly different effects between top and bottom of vehicle due to AOA.

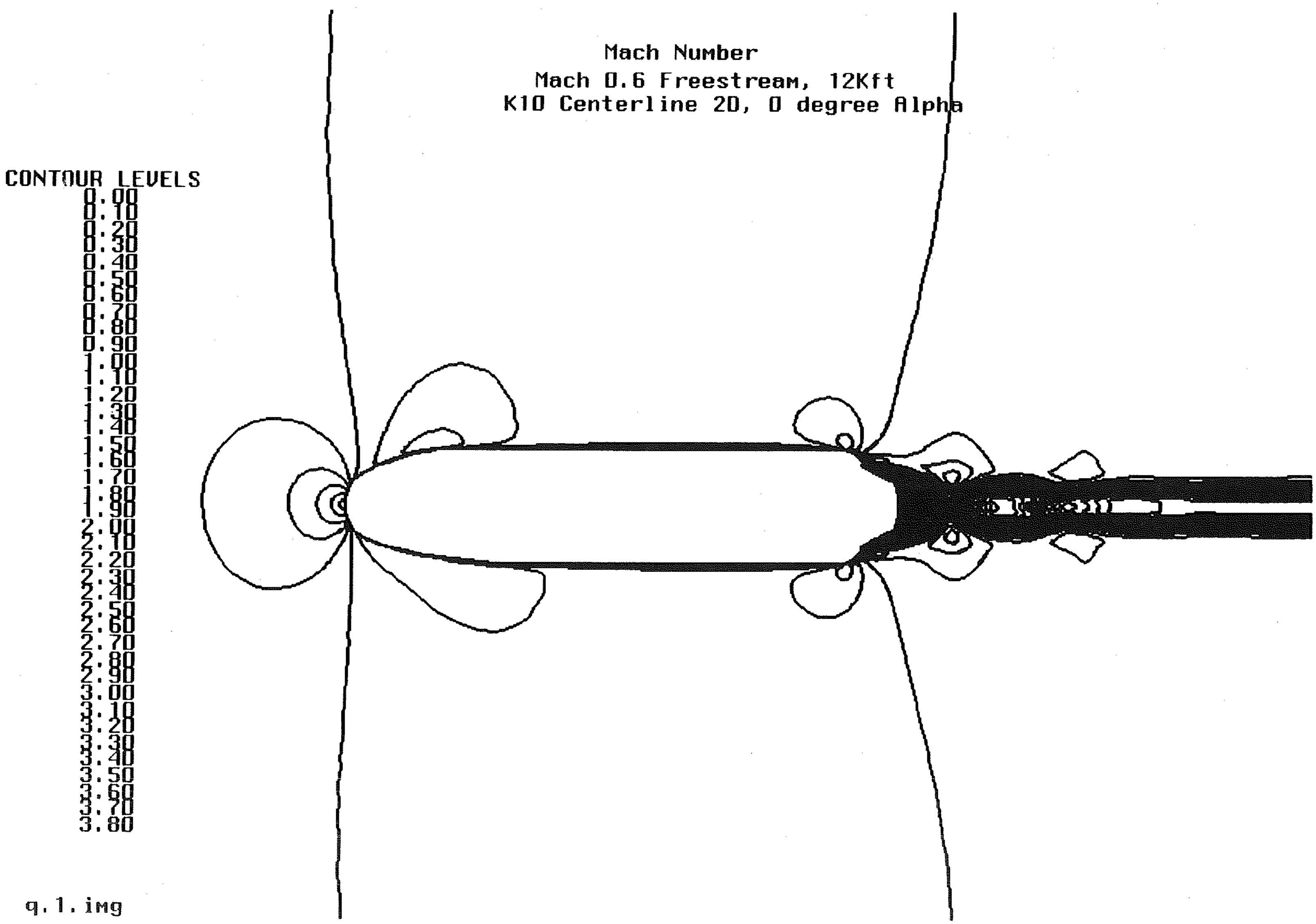
Mach Number
Mach 0.6 Freestream, 12Kft
K10 Centerline 2D, 0 degree Alpha
CONTOUR LEVELS
0.00
0.10
0.20
0.30
0.40
0.50
0.60
0.70
0.80
0.90
1.00
1.10
1.20
1.30
1.40
1.50
1.60
1.70
1.80
1.90
2.00
2.10
2.20
2.30
2.40
2.50
2.60
2.70
2.80
2.90
3.00
3.10
3.20
3.30
3.40
3.50
3.60
3.70
3.80
q.1.img

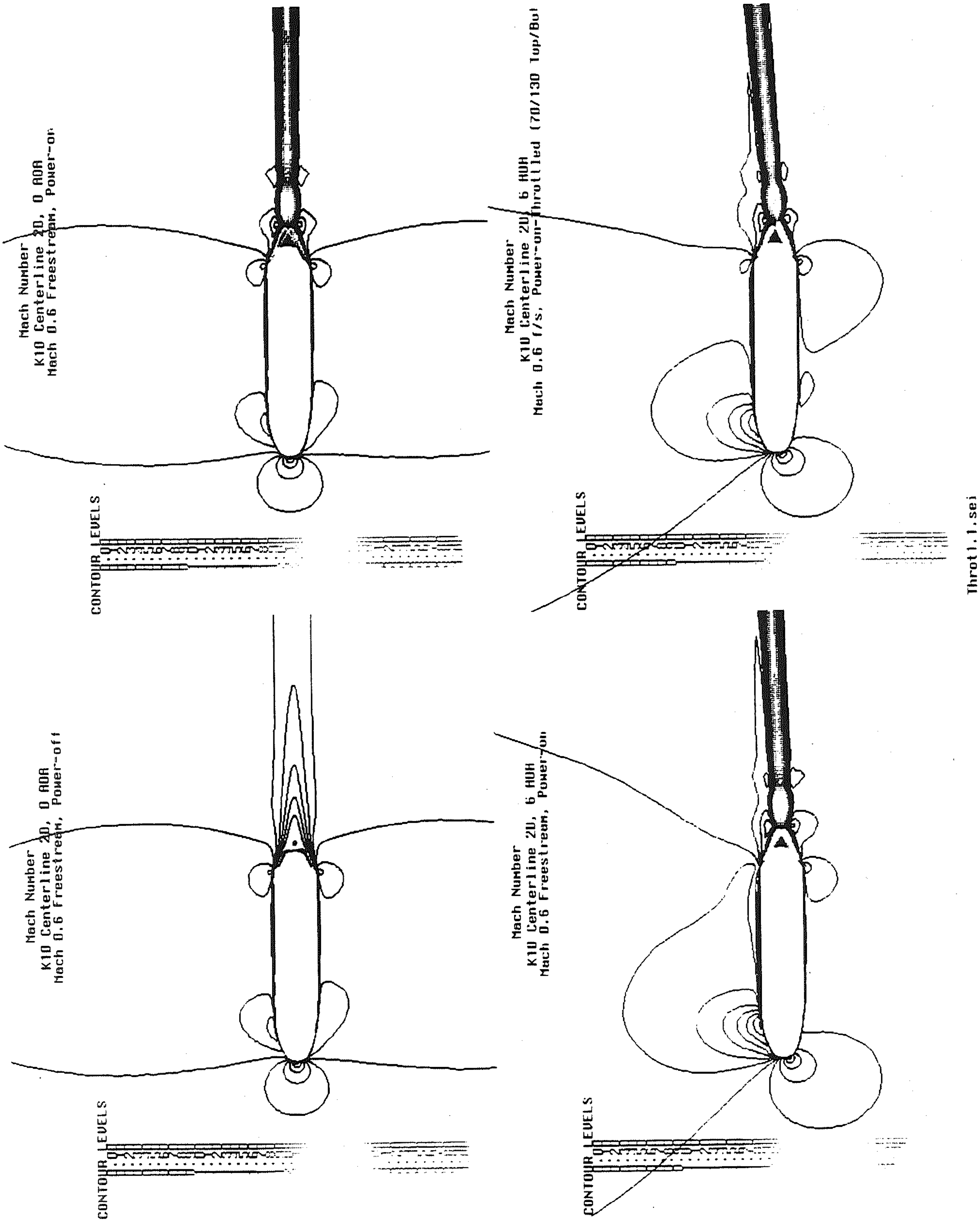
Mach Number
K10 Centerline 2D, 0 AOA
Mach 0.6 Freestream, Power-on
CONTOUR LEVELS
Mach Number
K10 Centerline 2D, 6 AOA
Mach 0.6 f/s, Power-on-Throttled (70/130 Top/Bot
CONTOUR LEVELS
Throttl.1.sei
Mach Number
K10 Centerline 2D, 0 AOA
Mach 0.6 Freestream, Power-off
CONTOUR LEVELS
Mach Number
K10 Centerline 2D, 6 AOA
Mach 0.6 Freestream, Power-on
CONTOUR LEVELS

K10 2D Centerline Pressure Coefficient

Mach 0.6 Alpha=0 degrees

power-off vs. power-on

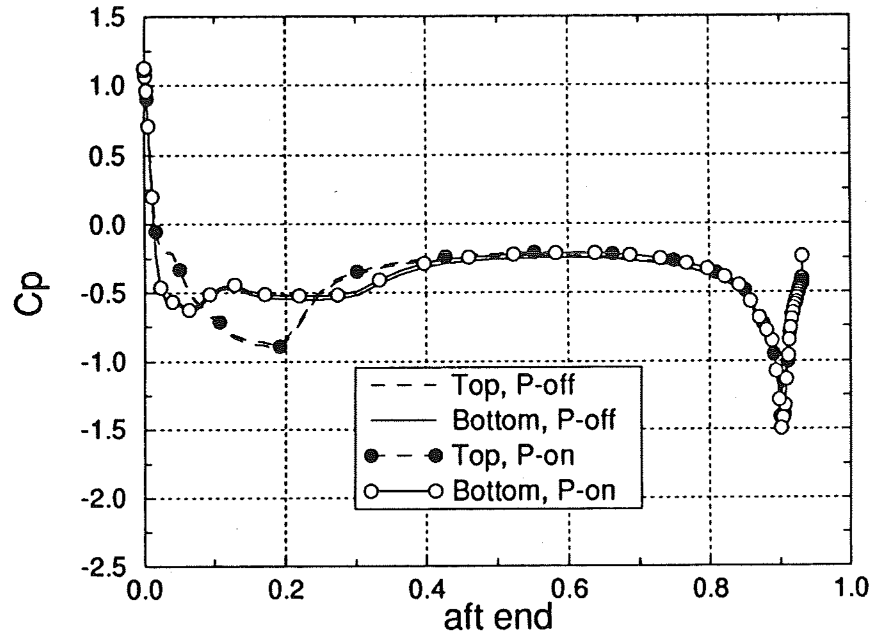

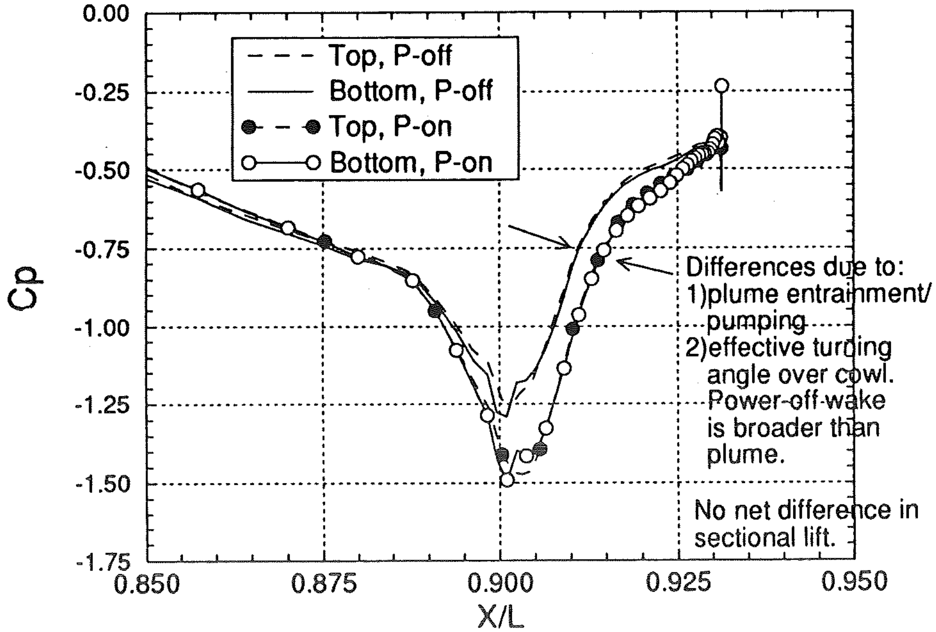

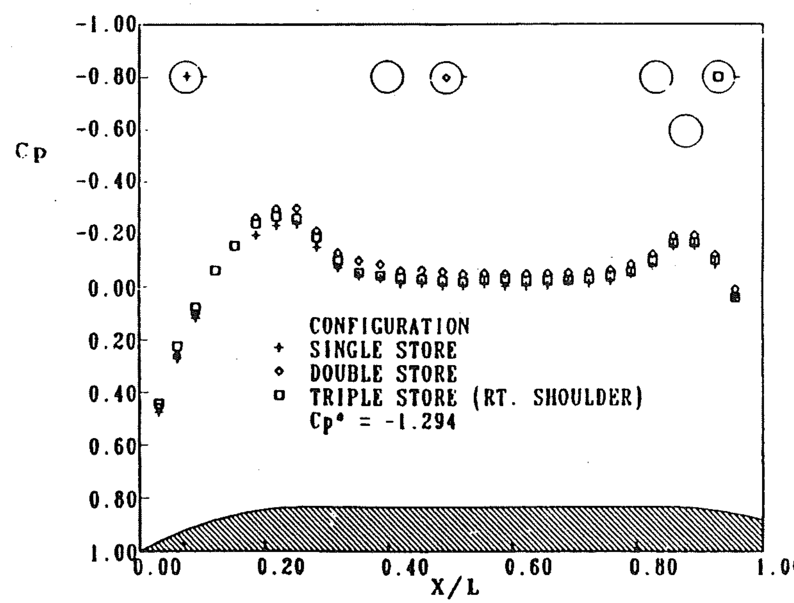

Mutual Interference Comparison,
M_∞ = 0.60, α = 0°, φ = 90°

Data from aircraft munition stores test, Cottrell, 1987.

K10 2D Centerline Pressure Coefficient

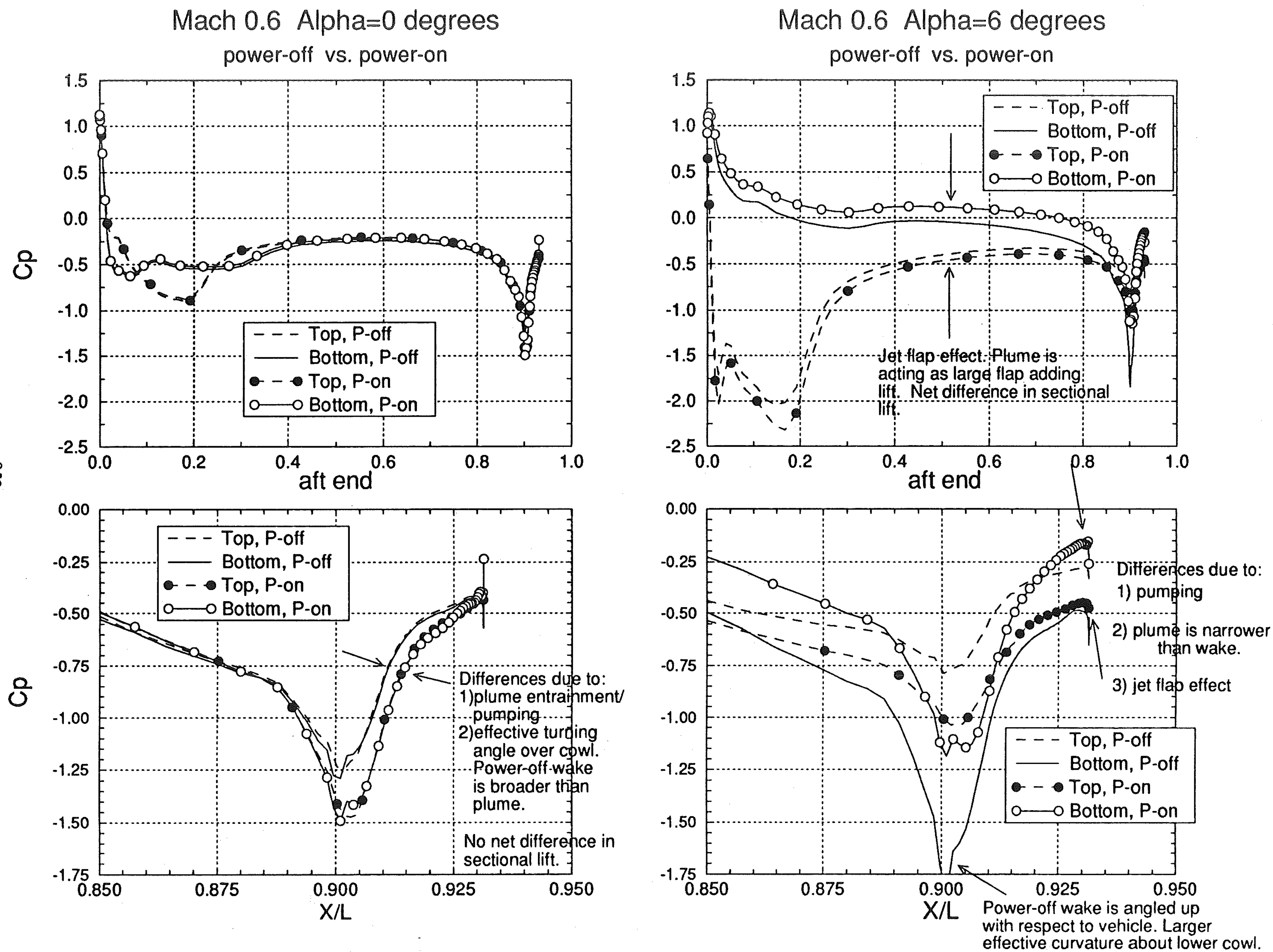

CFD Results, cont.

- **Mach 0.6 ~ 12Kft**
  - 0 degree α power-on vs. power-on-throttled
    - » Deflected plume effects lift consistently over length of vehicle through jet flap effect.
  - 6 degree α power-on vs. power-on-throttled
    - » Deflected plume effects lift differently on forward and aft part of vehicle through jet flap effect.

K10 2D Centerline Pressure Coefficients

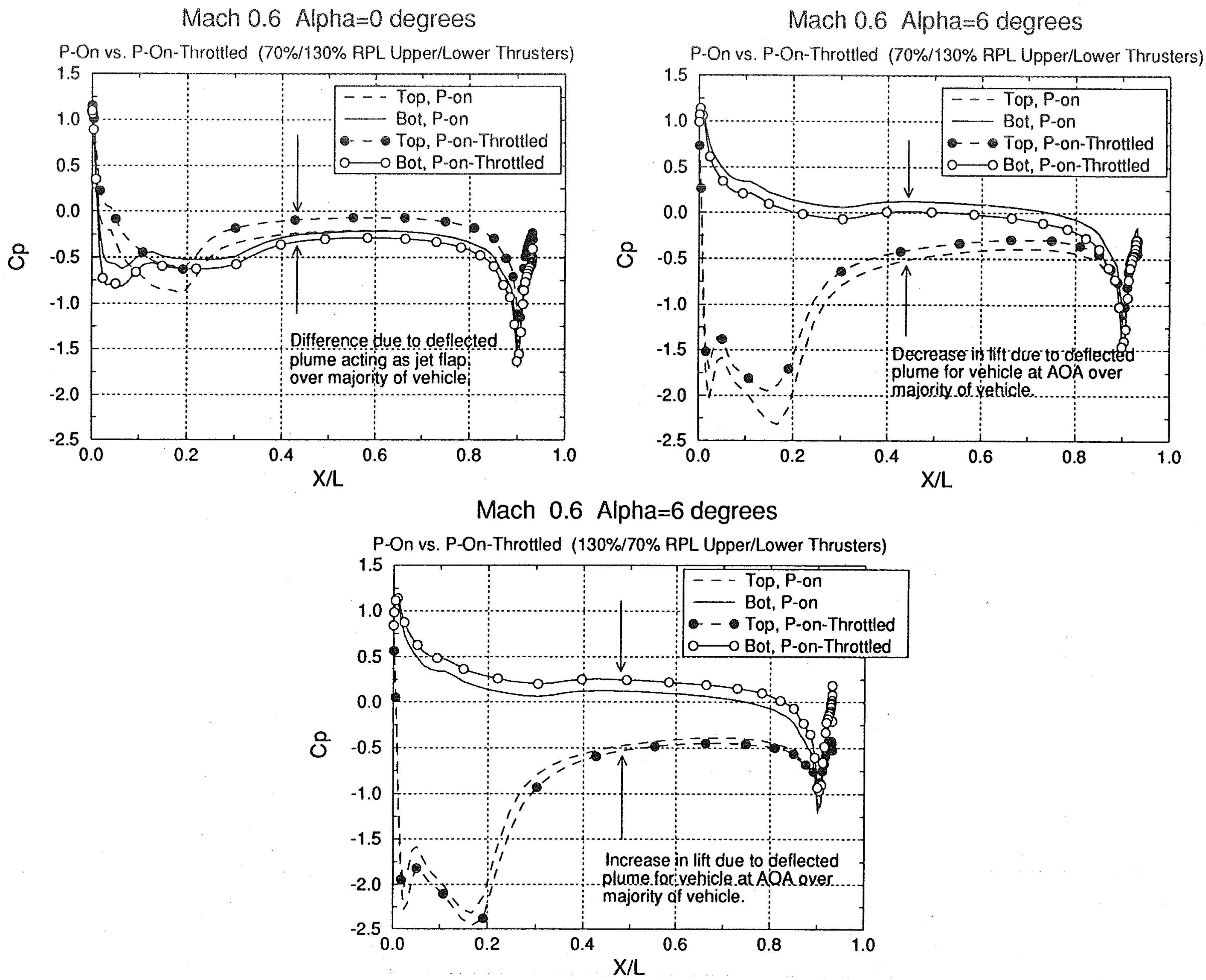

Mach 0.6 Alpha=0 degrees Aft End

P-On vs. P-On-Throttled (70%/130% RPL Upper/Lower Thrusters)

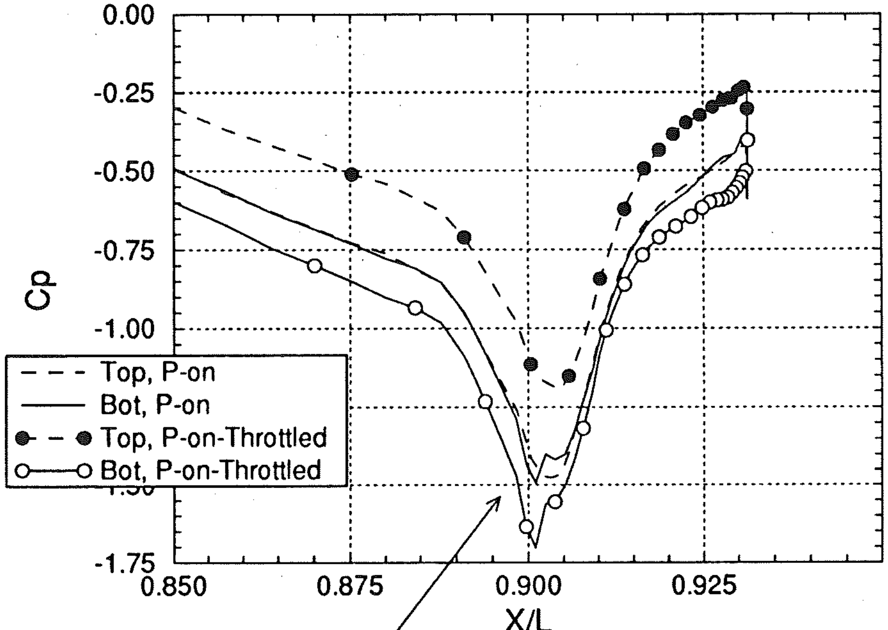

Mach 0.6 Alpha=6 degrees Aft End

P-On vs. P-On-Throttled (70%/130% RPL Upper/Lower Thrusters)

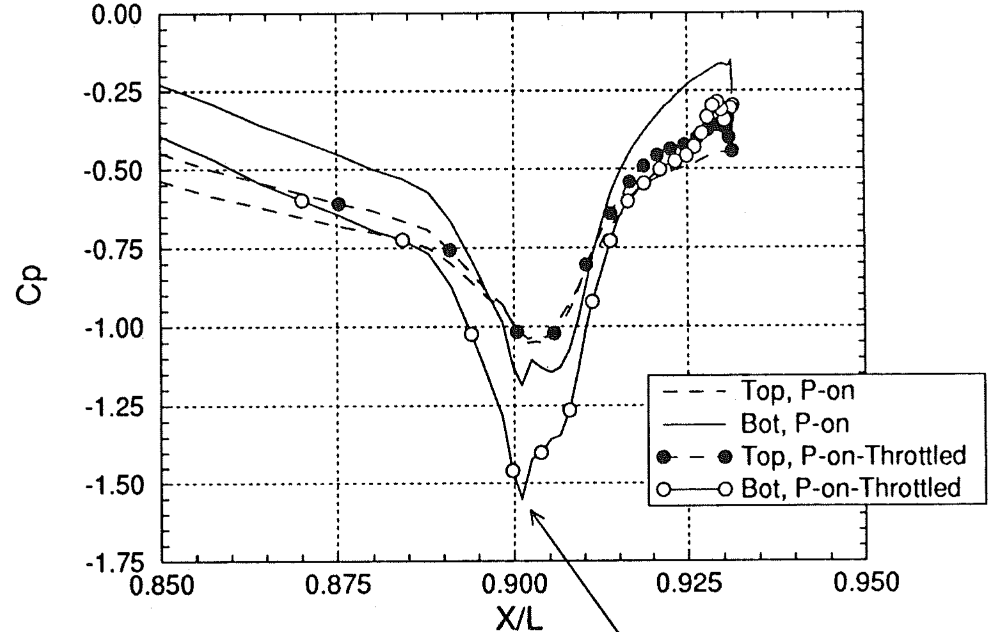

Mach 0.6 Alpha=6 degrees Aft End

P-On vs. P-On-Throttled (130%/70% RPL Upper/Lower Thrusters)

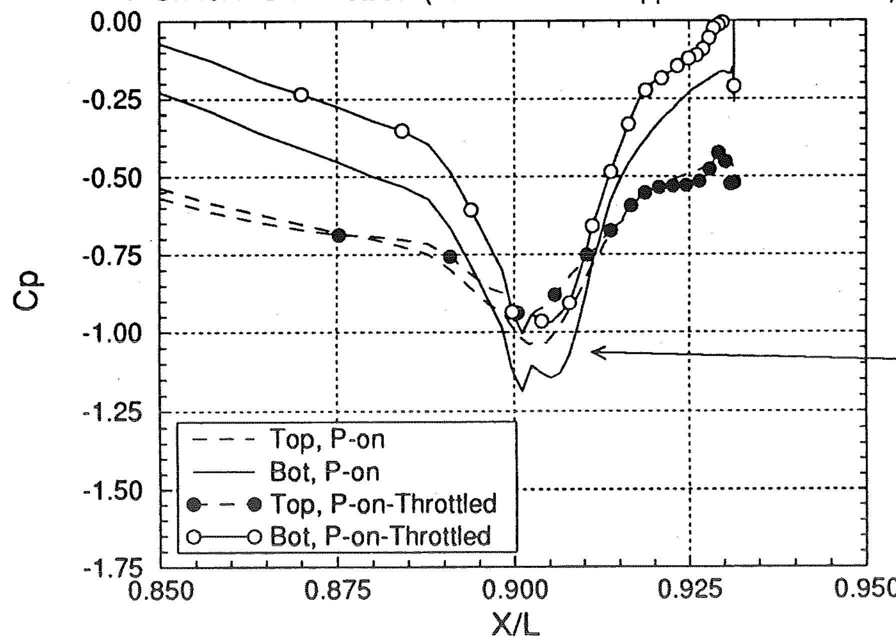

Plume deflection increases lift consistantly over entire vehicle.

Plume deflected up increases local negative lift on aft end.

Plume deflected down decreases local negative lift on aft end.

Application of CFD to Preliminary Database

- **Increments were only generated for subsonic portion of aero database**

- **Pressure deltas were applied to database by assuming full effect at aft end and linearly decreasing to no effect at forward end of vehicle**

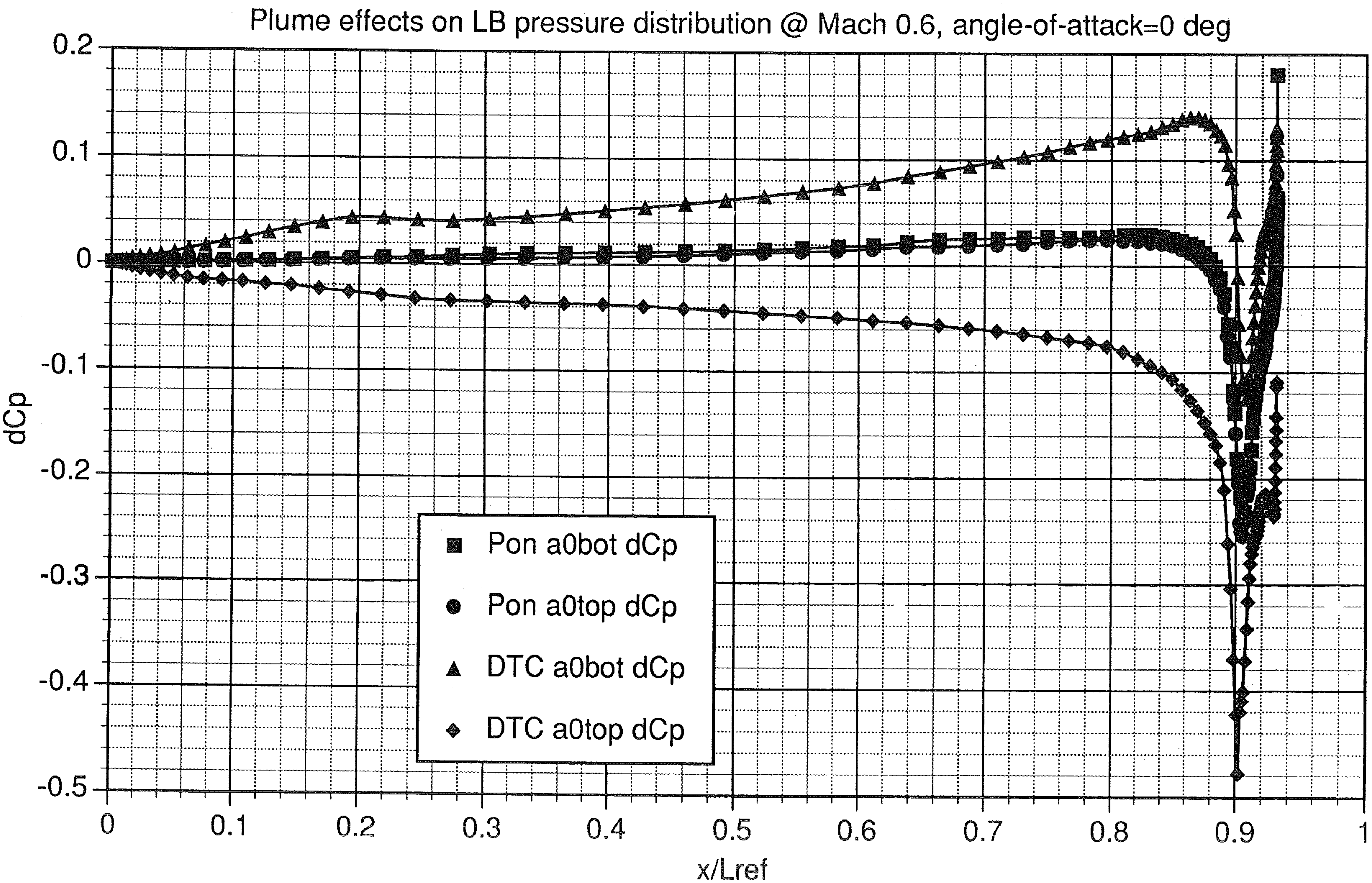

DTC - differential throttle control; upper/lower @ 130%/70%; Pon = 100%/100%
dCp = difference in pressure coefficient (power on - power off)

Plume effects on LB normal force coeff. @ alpha=0

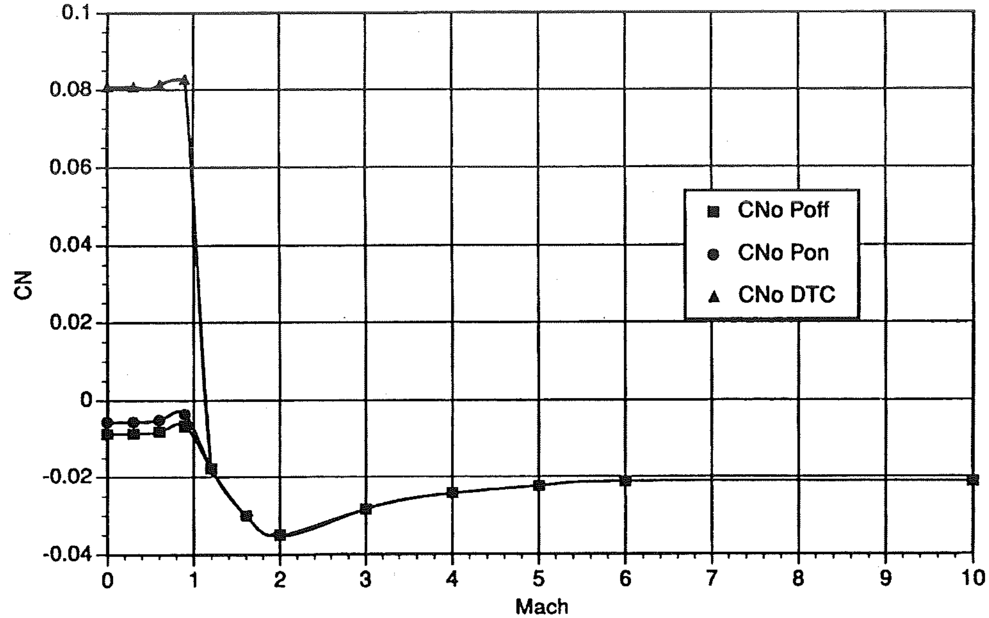

Plume effects on LB pitching moment coeff. @ alpha=0

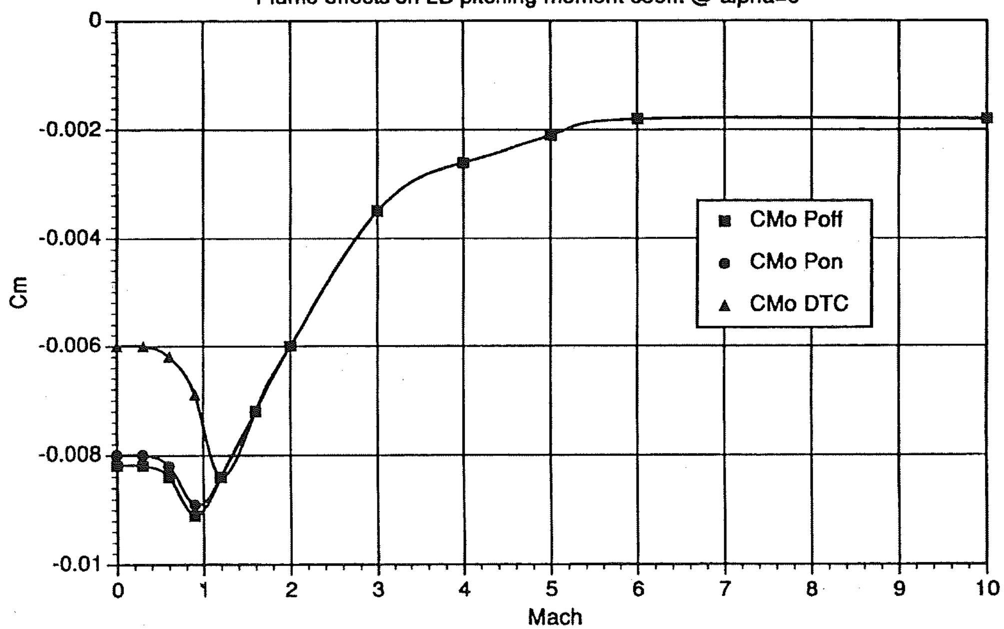

Sref=5600 sq ft; Lref=1450.0 in.; mom. ref. @ 72%.

Plume effects on LB pressure distribution @ Mach 0.6, angle-of-attack=6 deg

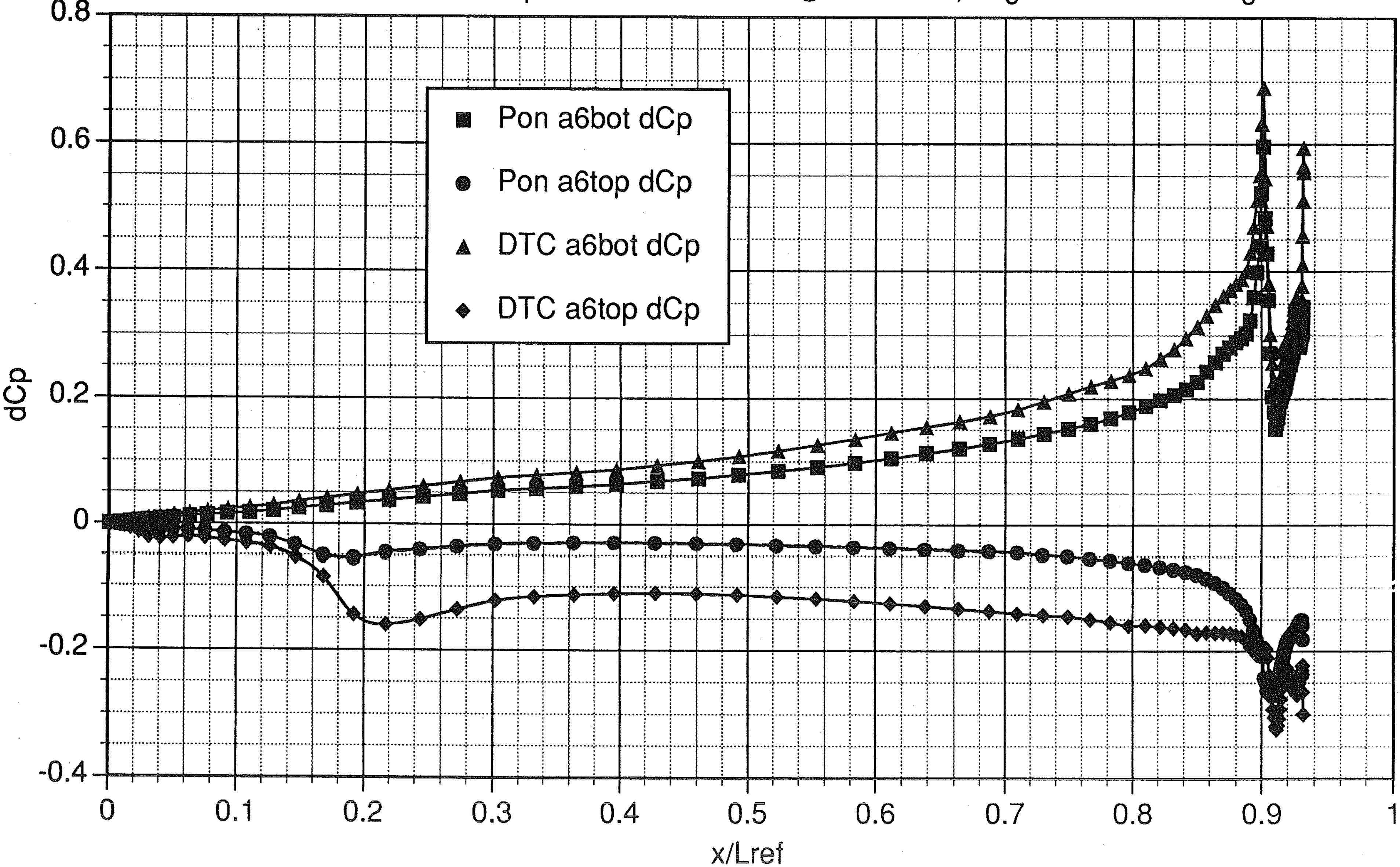

DTC - differential throttle control; upper/lower @ 130%/70%; Pon = 100%/100%
dCp = difference in pressure coefficient (power on - power off)

Plume effects on LB normal force coeff (M=0.6)

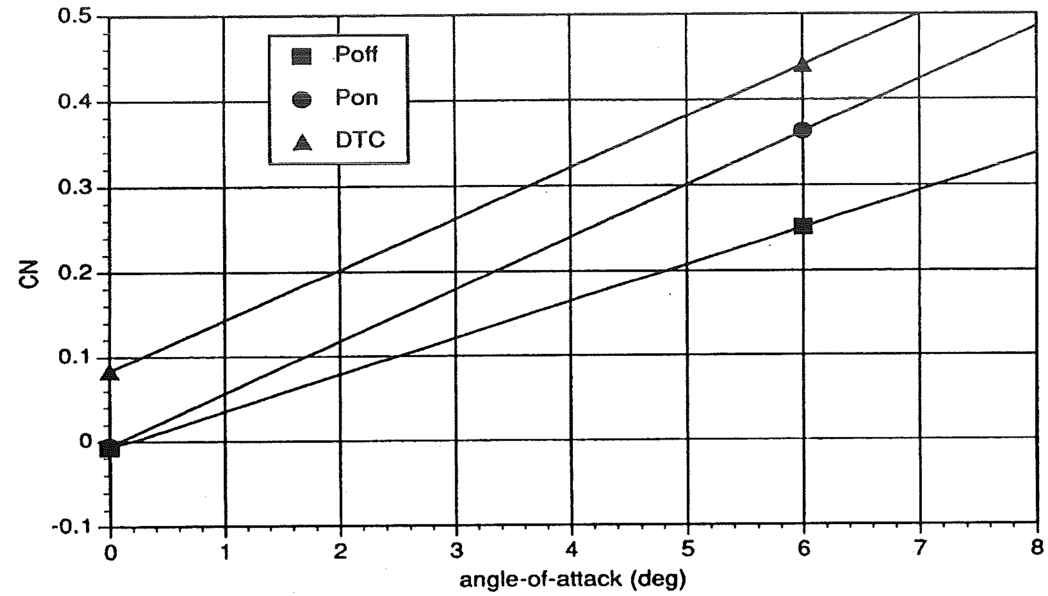

Plume effects on LB pitching moment coeff (M=0.6)

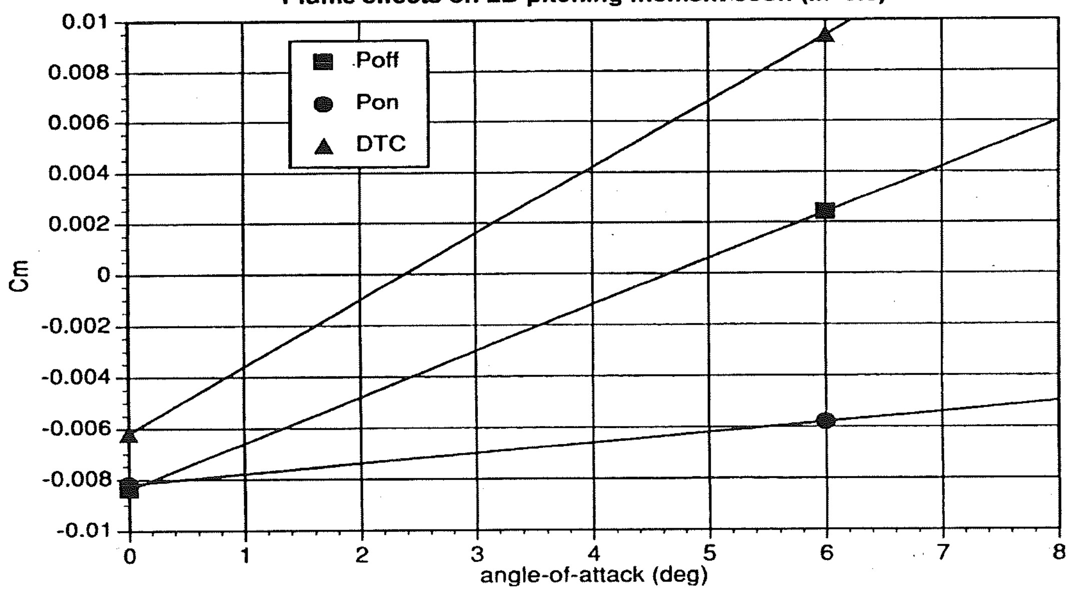

Sref=5600 sq ft; Lref=1450.0 in.; mom. ref. @ 72%.

Plume effects on LB aero normal force derivative (slope)

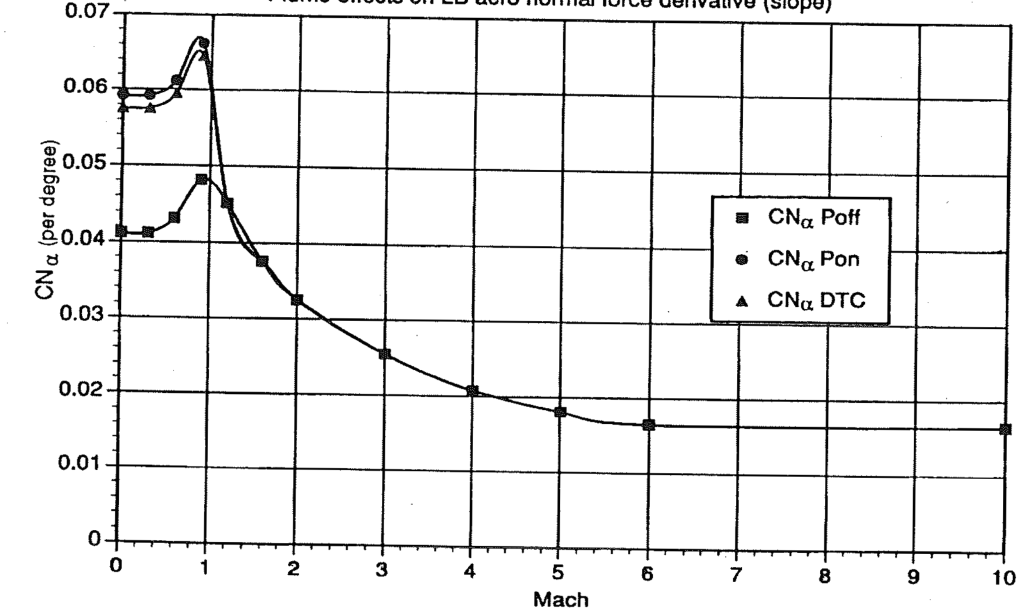

Plume effects on LB aero pitching moment derivative (slope)

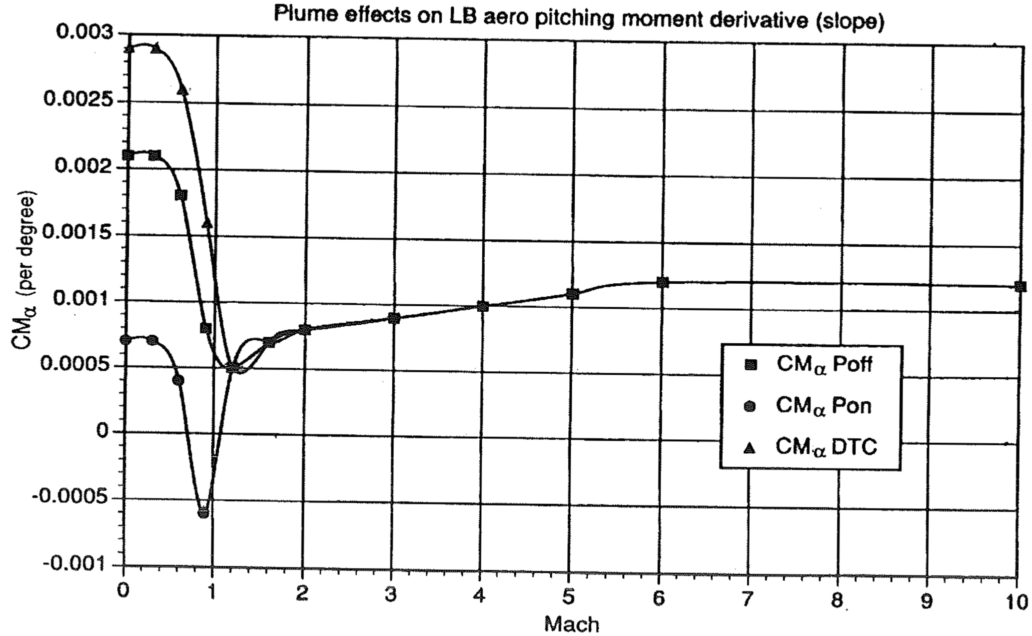

Sref=5600 sq ft; Lref=1450.0 in.; mom. ref. @ 72%.

Conclusions

- **No significant plume aerodynamic effects existed for supersonic flight regime. Plume induced separation of flow over vehicle was not a significant effect on aerodynamics of K10.**
- **No significant plume effects seen between power-on and power-off at 0 degree α for Mach numbers analyzed.**
- **Significant plume/external flow interactions existed for Mach 0.6 at angles of attack through jet flap effect, jet entrainment and change in effective cowl angle.**
  - Jet flap effect propagated well forward in 2D analysis.
  - Jet entrainment and increased/decreased effective cowl angle affected the aft end of K10.
- **3D calculations are under way. Initial results indicates less plume effect on the forward part of vehicle than in 2D analysis.**
- **A methodology has been developed to generate first order plume effect increments for a power-off aerodynamic database using 2D centerline CFD analysis.**

513-27
57388
132110
14p

TPS Sizing for Access-to-Space Vehicles

William Henline, David Olynick and Grant Palmer
NASA Ames Research Center, MS 230-2,
Moffett Field, CA 94035-1000
Y.-K. Chen
Eloret Institute, MS 234-1, Moffett Field, CA 94035-1000

Abstract

A study was carried out to identify, develop, and benchmark simulation techniques needed for optimum TPS material selection and sizing for reusable launch vehicles. Fully viscous, chemically reacting, Navier-Stokes flow solutions over the Langley wing-body single stage to orbit (SSTO) configuration were generated and coupled with an in-depth conduction code. Results from the study provide detailed thermal protection system (TPS) heat shield materials selection and thickness sizing for the wing-body SSTO. These results are the first ever achieved through the use of a complete, trajectory based hypersonic, Navier-Stokes solution database. TPS designs were obtained for both laminar and turbulent entry trajectories using the Access-to-Space baseline materials such as tailorable advanced blanket insulation (TABI). The TPS design effects (material selection and thicknesses) of coupling material characteristics to the aerothermal enviroment are illustrated. Finally, a sample validation case using the shuttle flight data base is included.

For the laminar trajectory, the TPS areal mass density is 1.2 lbm/ft^2, while the turbulent trajectory yields slightly less than 1.3 lbm/ft^2. An additional conclusion from this study is that the TABI blankets will have to be manufactured in thicknesses greater than 1.5-2.0 inches. Further, if typical turbulent flow conditions are found on these SSTO vehicles during re-entry, some of the baseline materials may experience significant over-temperatures.

TPS Sizing for Access to Space Vehicles

by

William Henline, David Olynick, Grant Palmer and Y.-K. Chen

NASA Ames Research Center

CFD Workshop April 27, 1995

Relationship Between Ames Complementary Analysis Tasks For All Candidate TPS

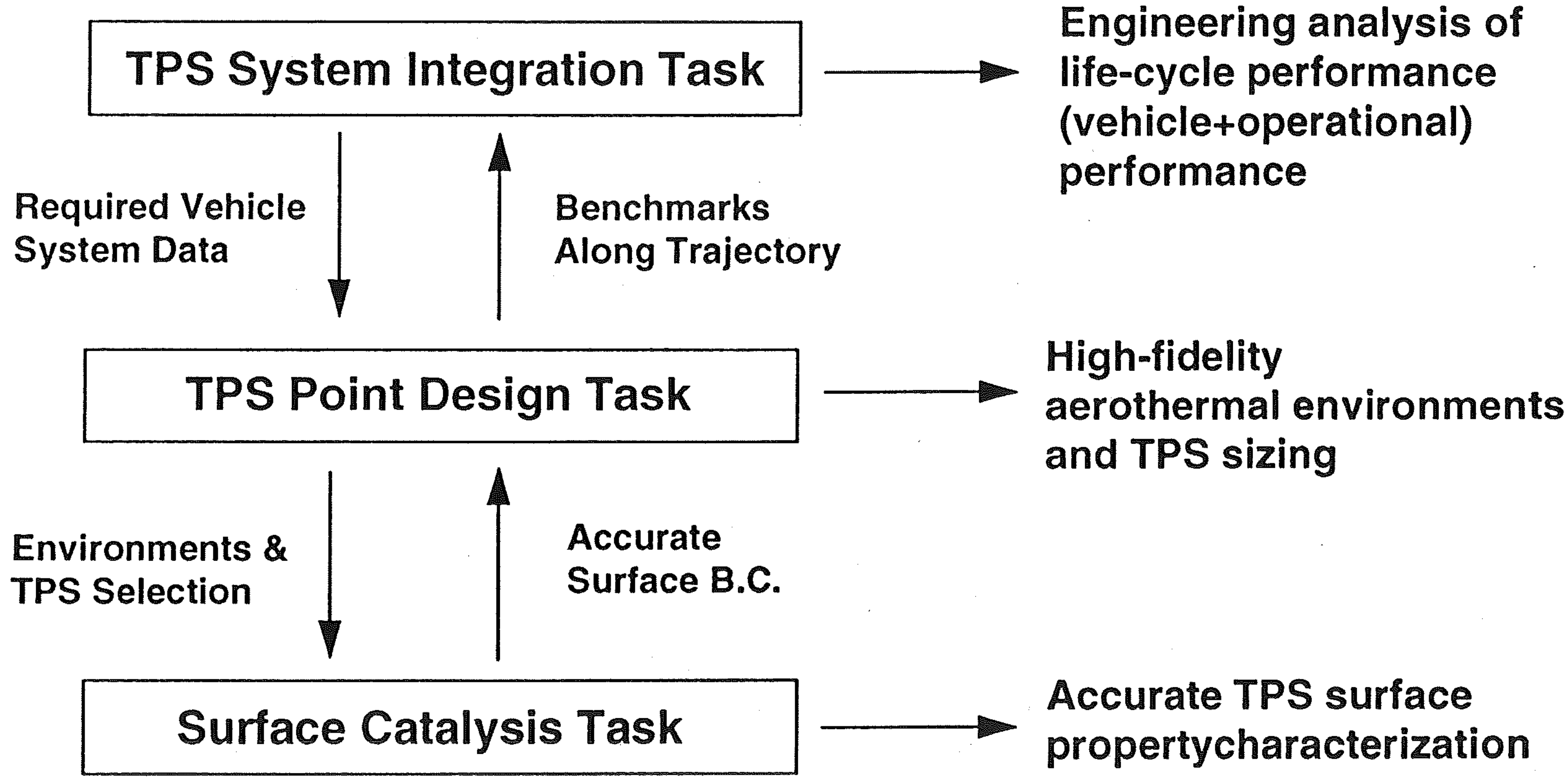

Tasks provide quantative methodology for assessing life-cycle performance (including operations) of all candidate TPS and thus OMB TPS criteria

TPS Sizing for Access to Space Vehicles

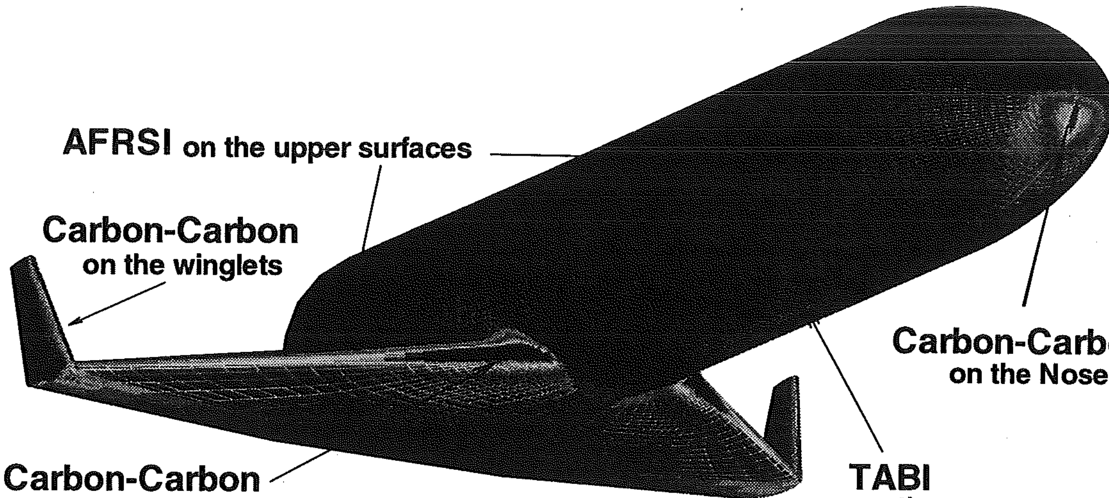

Winged Body Configuration

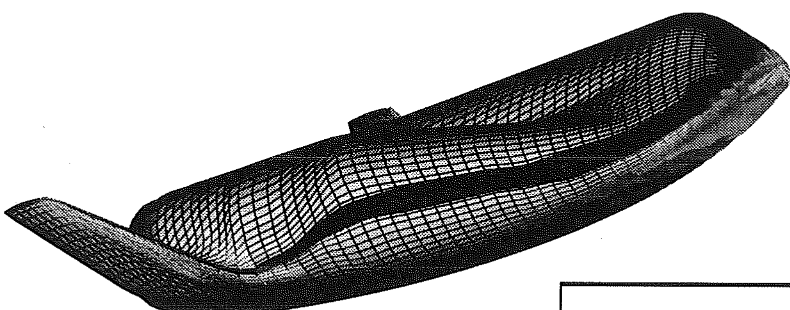

Lockheed Lifting Body

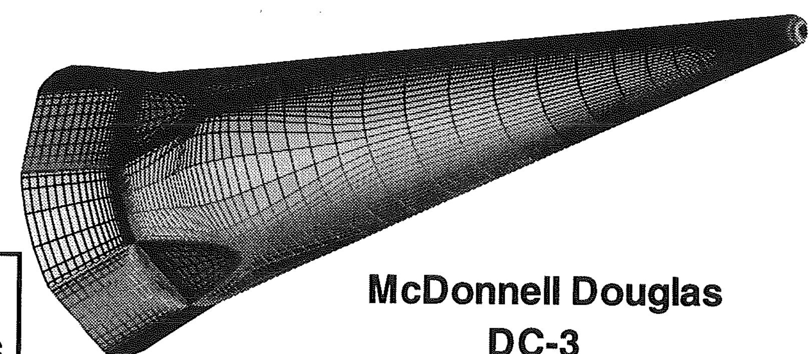

McDonnell Douglas DC-3

Use of New TPS Technology Reduces Life Cycle Cost by 20%

NASA Ames Research Center *Space Technology Division*

Fully Coupled Thermal Analysis for TPS Sizing

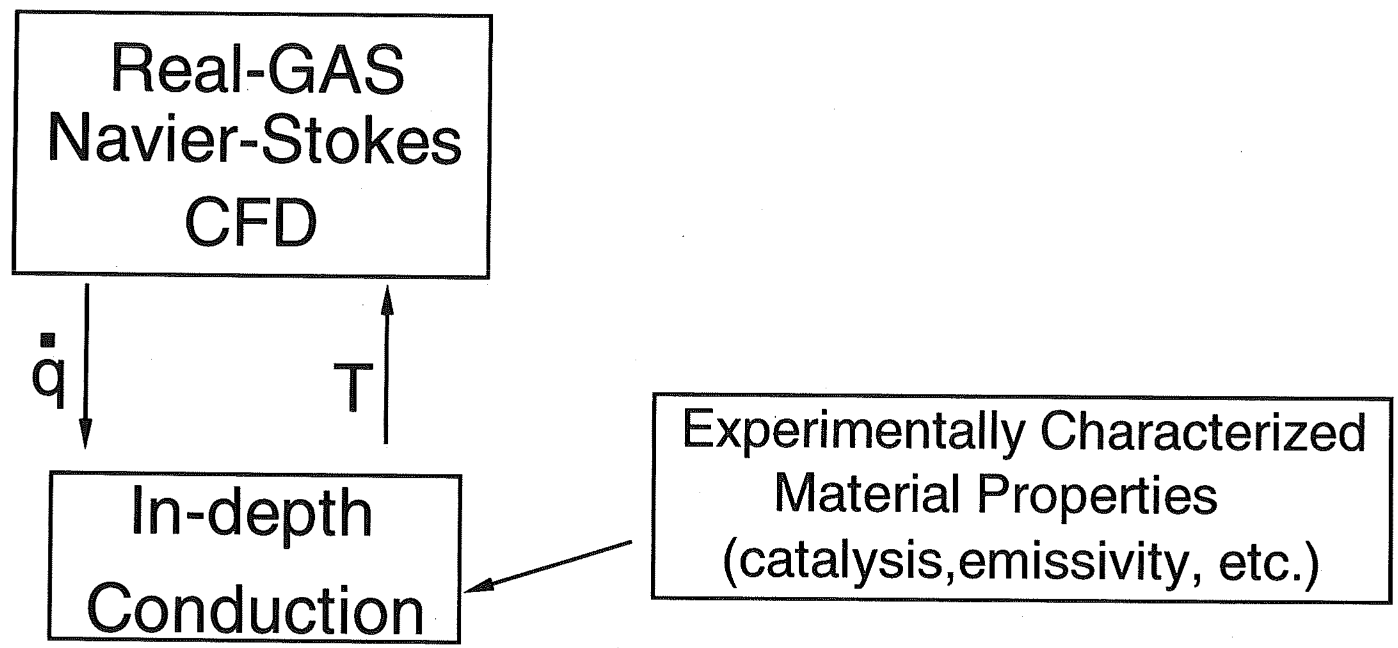

Trajectory (Altitude - Velocity) Plot for the LaRC SSTO Vehicle

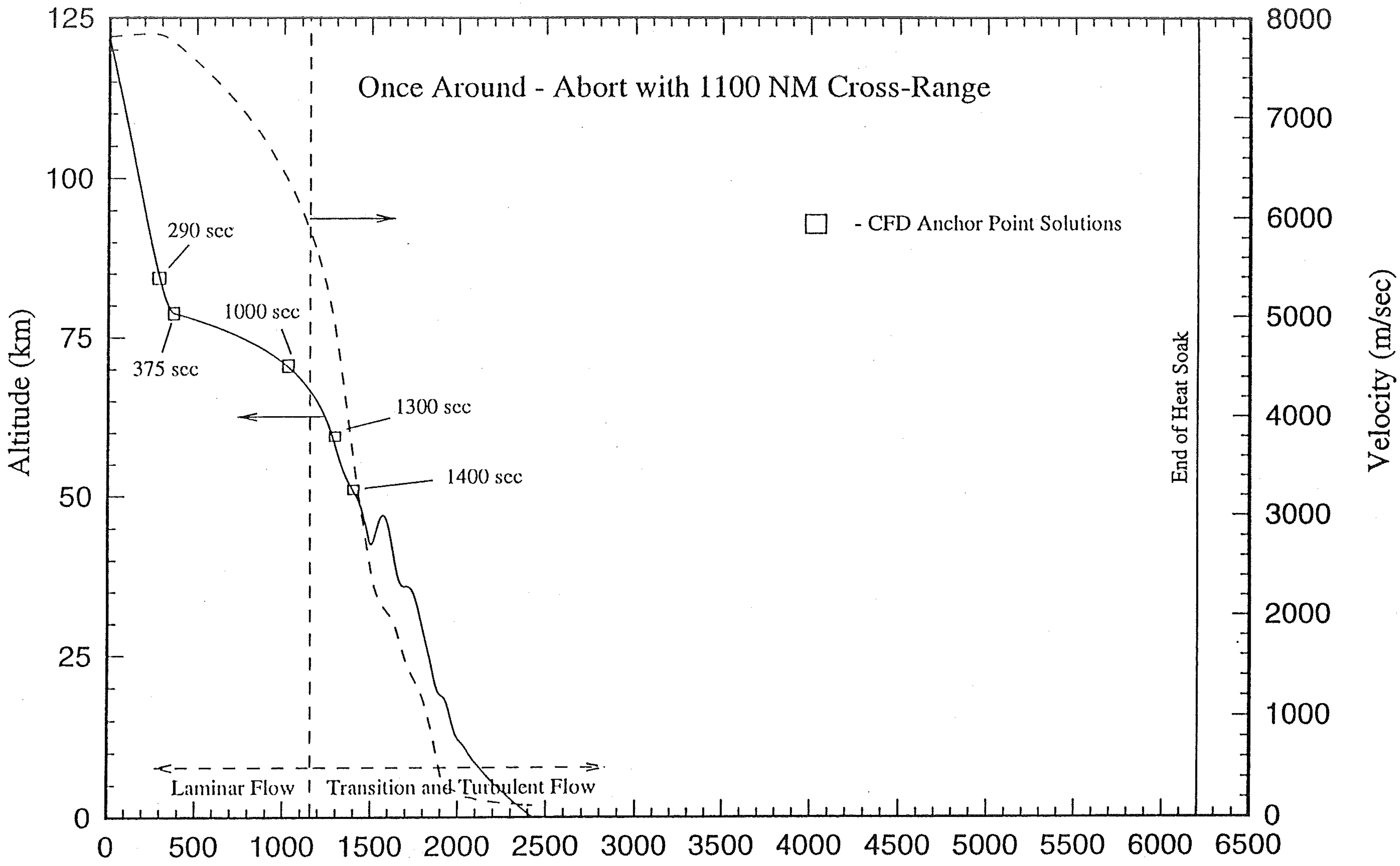

LaRC - Weilmeunster/Wurster 4/94

Stagnation Point Heating Plot for LaRC SSTO Trajectory

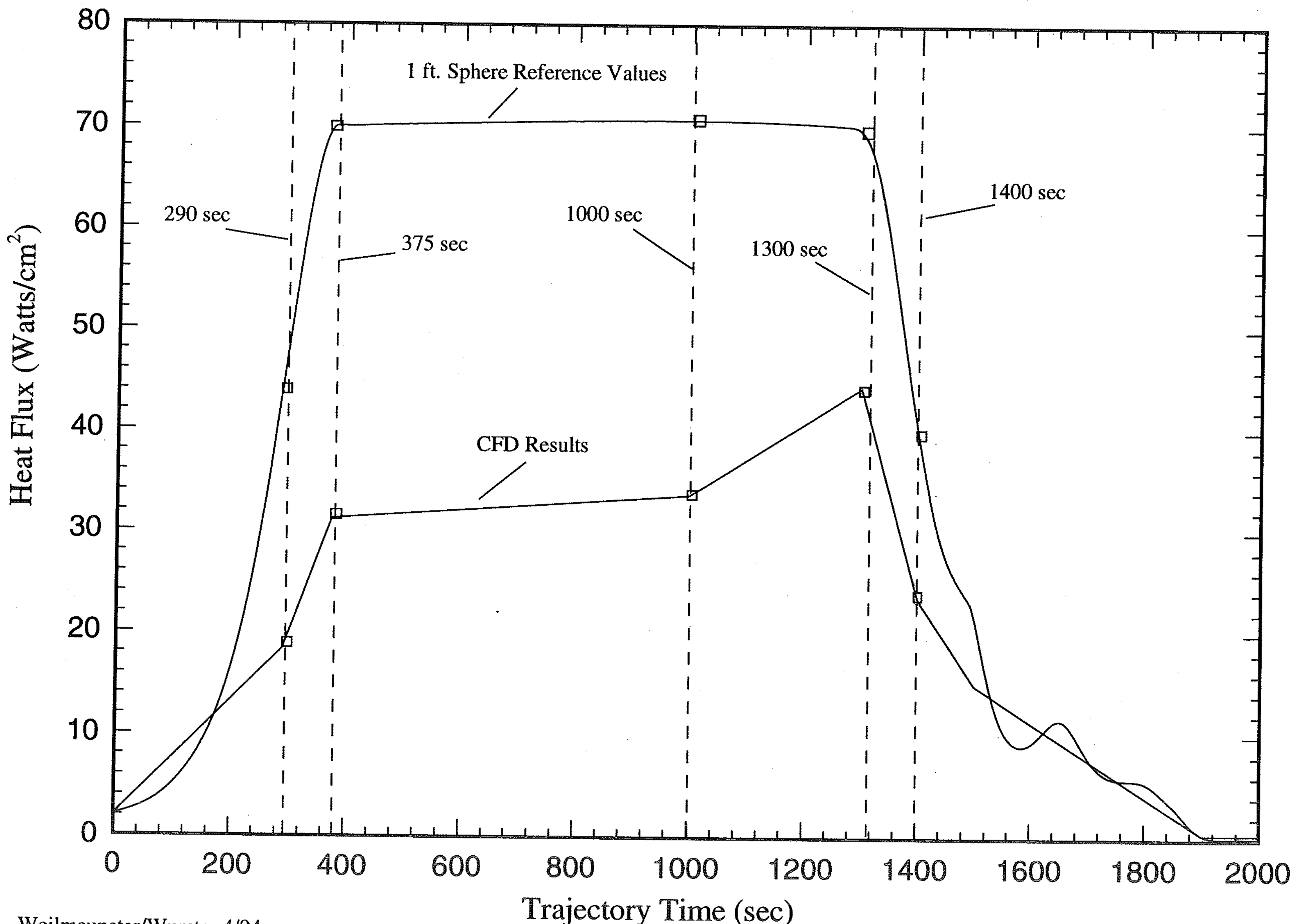

LaRC - Weilmeunster/Wurster 4/94

ARC/ST - W.D.Henline/G.E.Palmer/Y.-K.Chen/D.R.Olynick 4/4/95

Material Mapping From from CFD solution
at 1000 s
fully catalytic

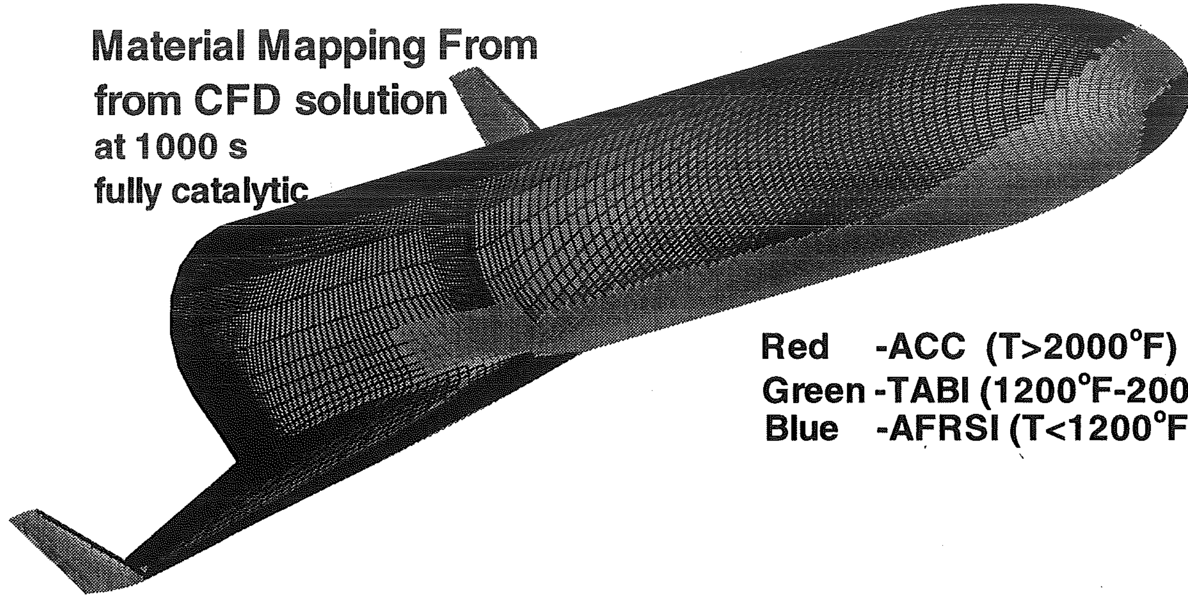

Red -ACC (T>2000°F)
Green -TABI (1200°F-2000°F)
Blue -AFRSI (T<1200°F)

Surface Temperature Contours using Material Dependent Surface Kinetics (Stewart/NRA) and Emissivity at Peak Heating (1300 s)

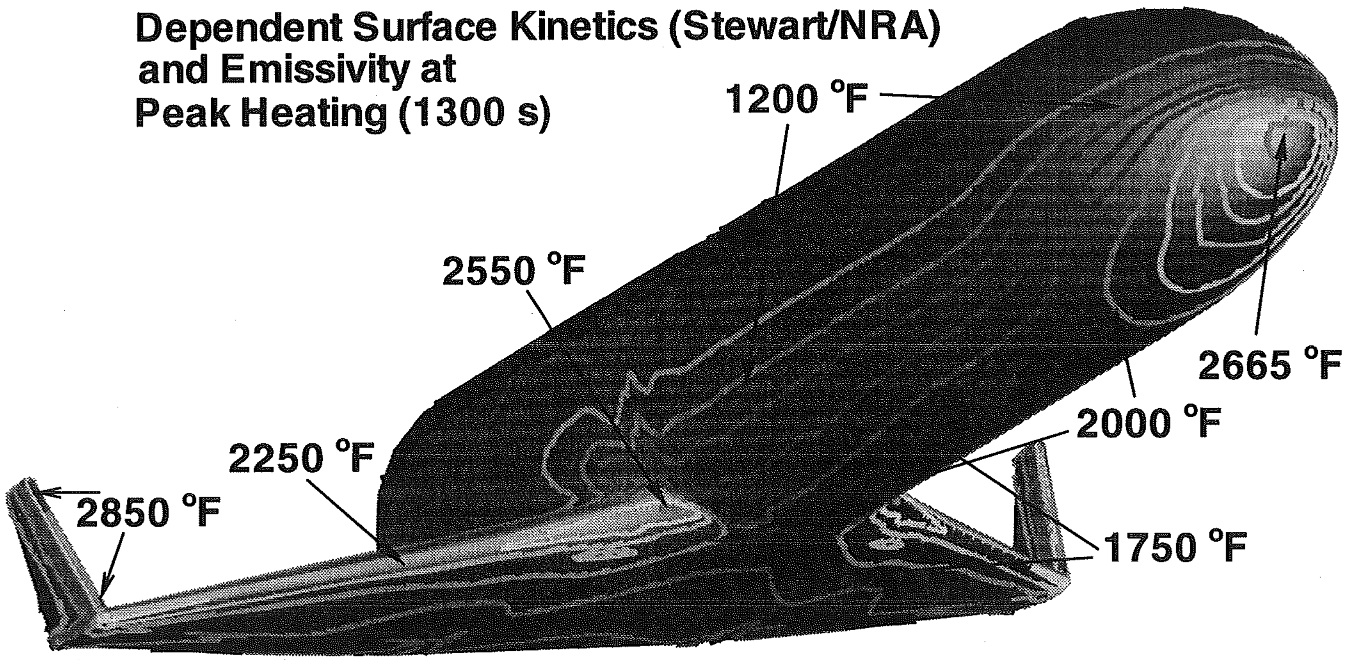

Winged Body Configuration 1300 s

Material Mapping

Orange-TABI (Temperature Limit Exceeded)

2000 °F<T<2300 °F

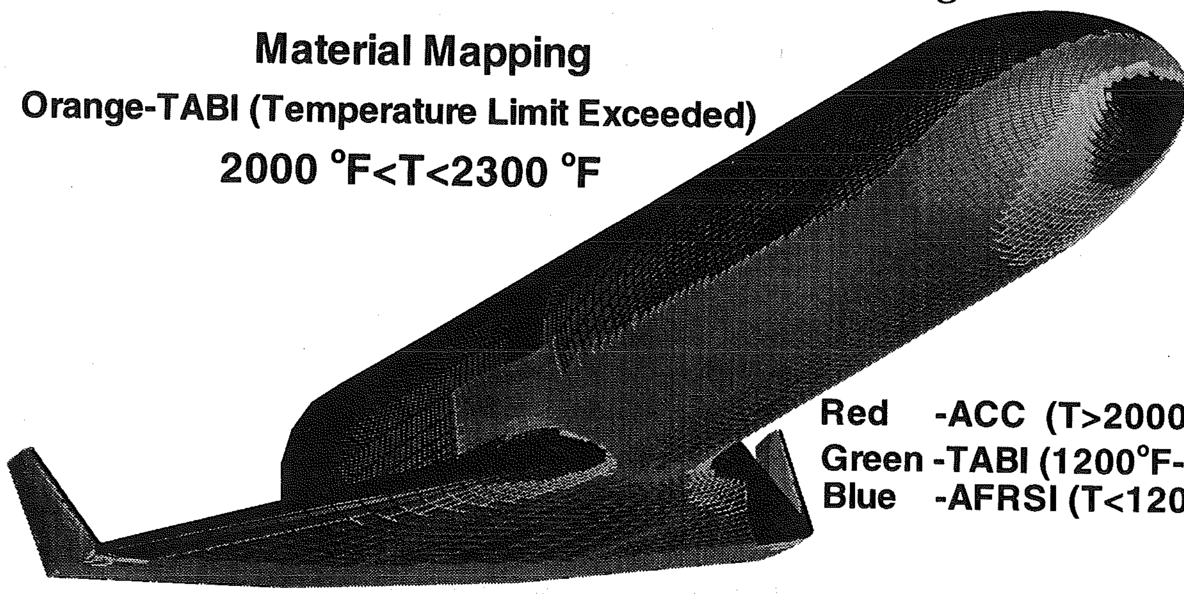

Red -ACC (T>2000°F)
Green -TABI (1200°F-2000°F)
Blue -AFRSI (T<1200°F)

Heat Transfer Contours (W/cm^2) using Material Dependent Surface Kinetics (Stewart/NRA) and Emissivity at Peak Heating

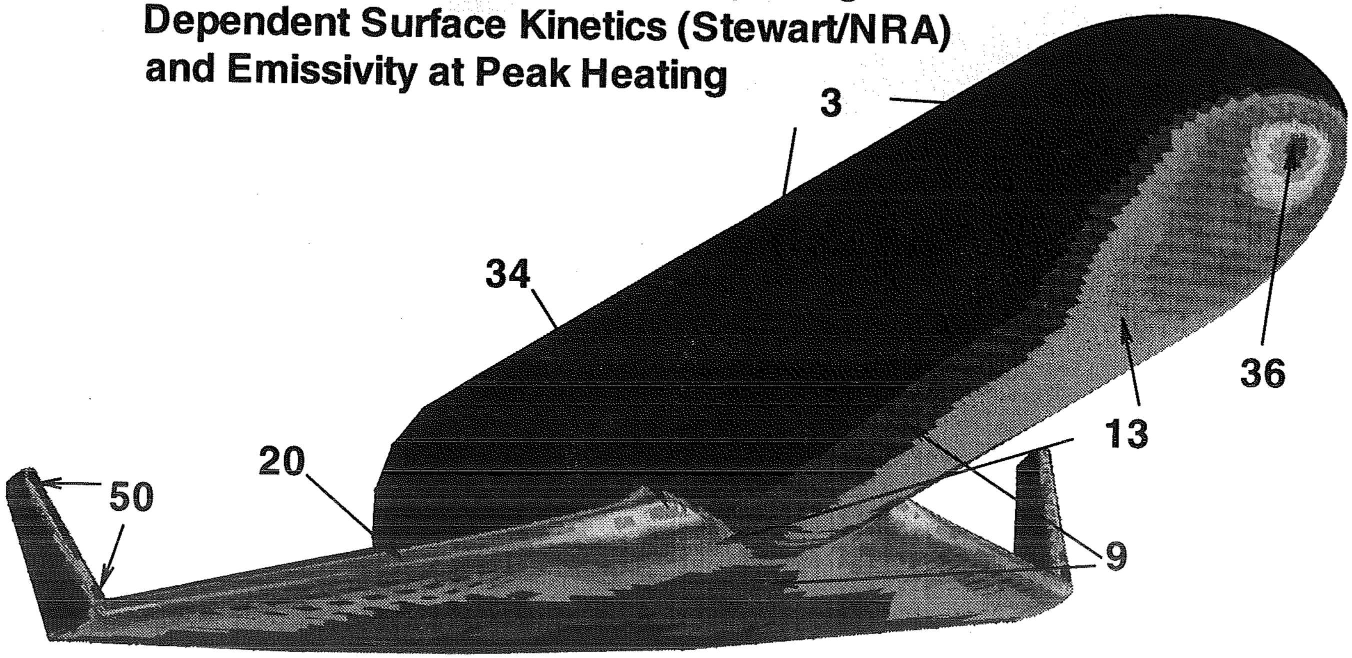

Winged Body Configuration 1300 S

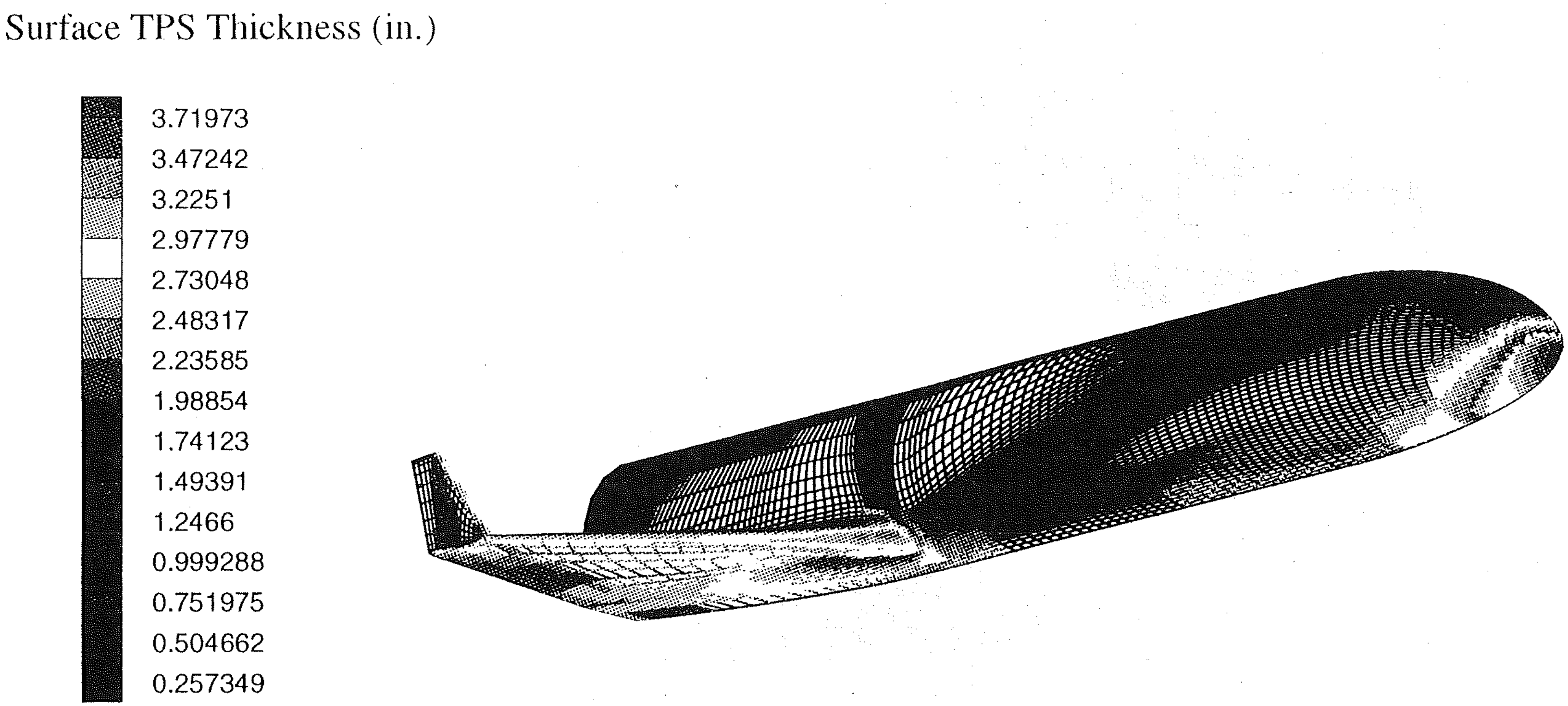

Top Layer TPS Thickness (in.) for the LaRC Winged Body SSTO Vehicle (Total Heating Time, 6200 sec)

(TURBULENT FLOW SOLUTION)

LaRC SSTO Vehicle Centerline TPS Thicknesses

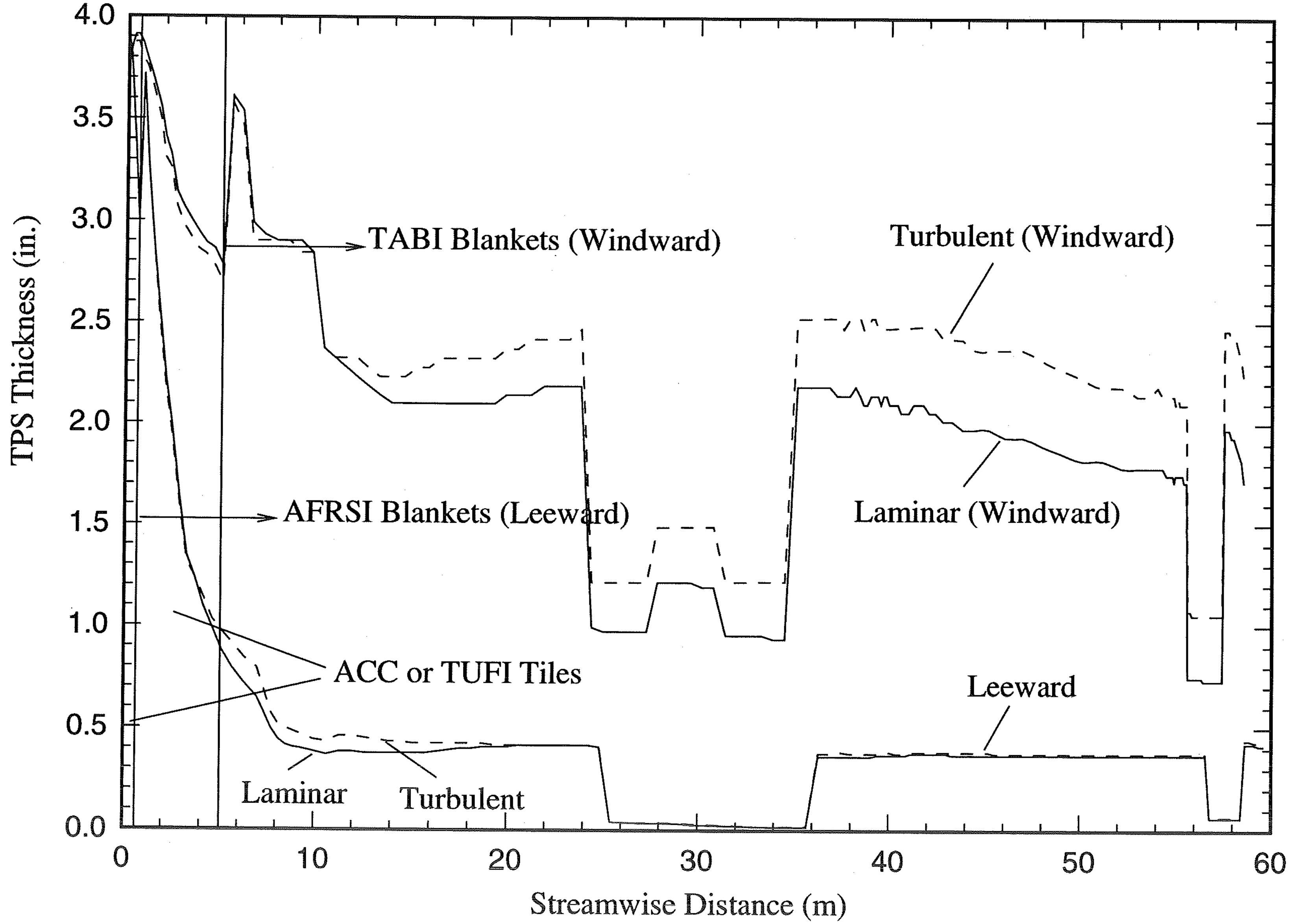

ARC/ST - W.D.Henline/F.S.Milos/Y.-K.Chen

Effect of TPS Material Properties on Surface Temperatures

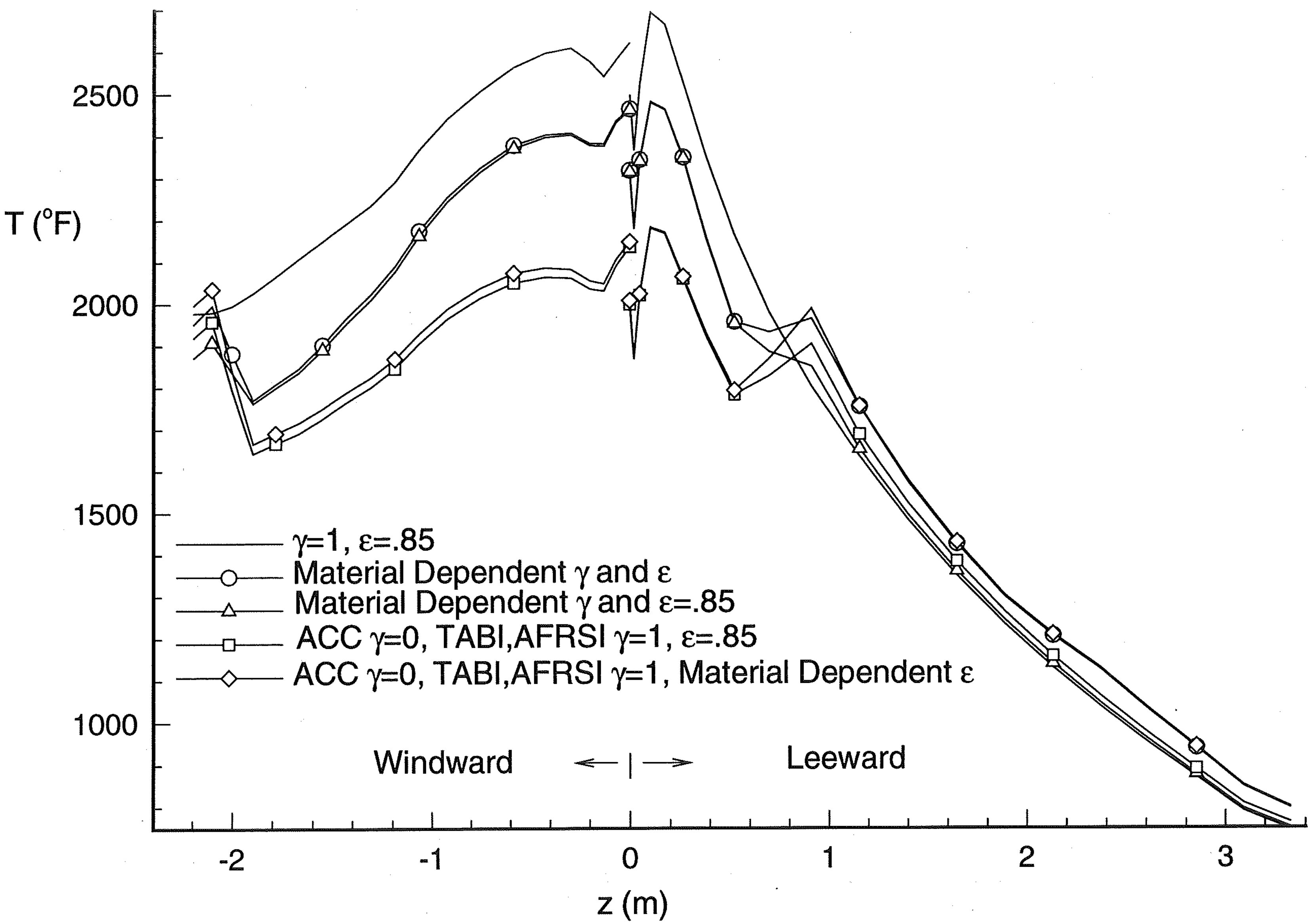

Shuttle Temperature Contours (STS-2)
M=24, 72.4 km, radiative equilibrium wall
RCG kinetics, ε=.85

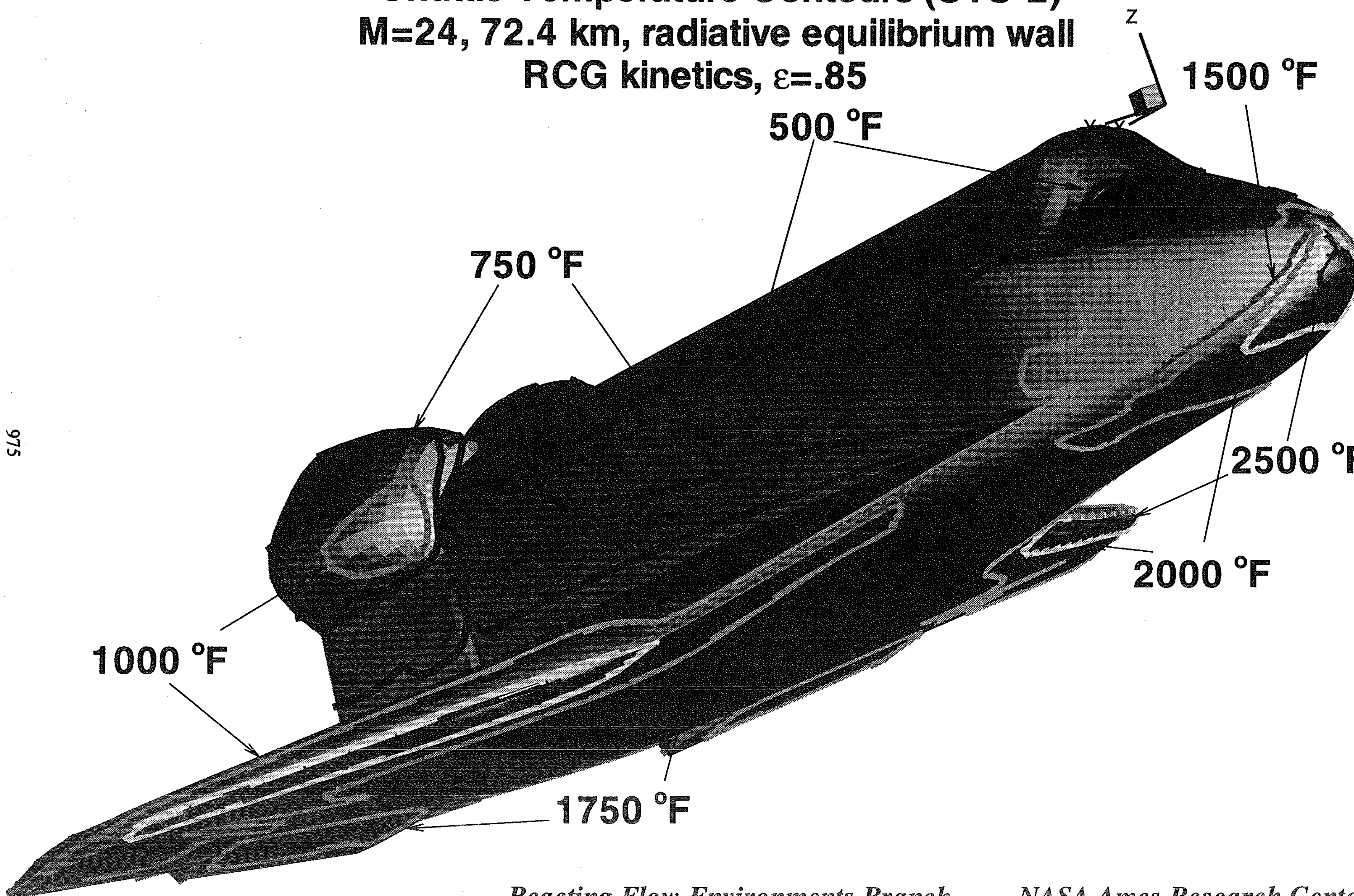

Reacting Flow Environments Branch *NASA Ames Research Center*

Heat Transfer Profile Along the Windward Centerline
STS-2, Mach 24.3, ε=.85, RCG kinetics
Radiative Equilibrium Wall

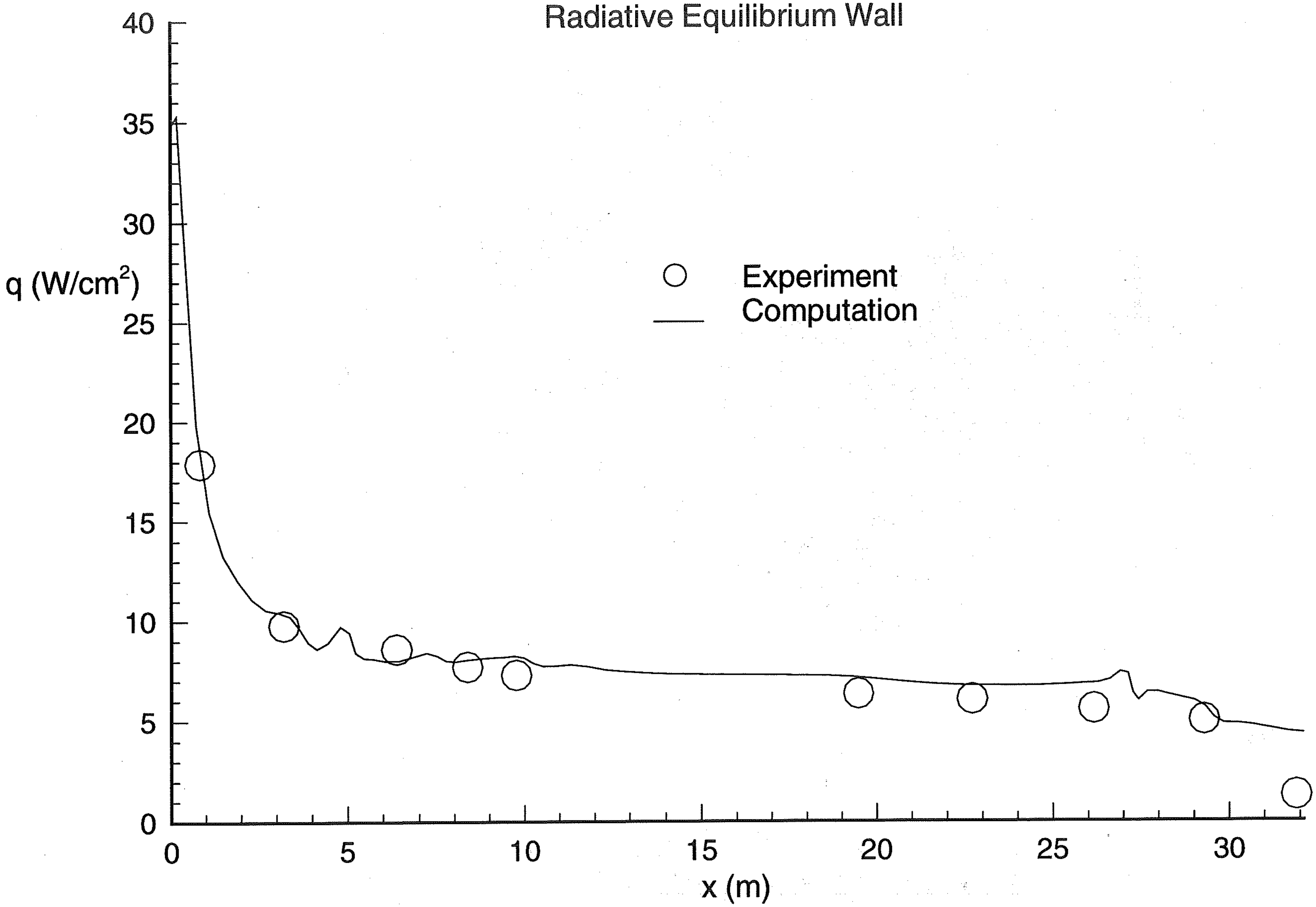

Reacting Flow Environments Branch

NASA Ames Research Center

MISSISSIPPI STATE UNIVERSITY / National Science Foundation

ENGINEERING RESEARCH CENTER FOR COMPUTATIONAL FIELD SIMULATION

COMPUTATIONAL ISSUES ASSOCIATED WITH TEMPORALLY DEFORMING GEOMETRIES SUCH AS THRUST VECTORING NOZZLES

Kishore Boyalakuntla, Bharat K. Soni, Hugh J. Thornburg and Robert Yu

NSF Engineering Research Center for Computational Field Simulation
Mississippi State University
Mississippi State, MS 39759

S4-20
57389
132111
30P

COMPUTATIONAL ISSUES ASSOCIATED WITH TEMPORALLY DEFORMING GEOMETRIES SUCH AS THRUST VECTORING NOZZLES

Kishore Boyalakuntla, Bharat K. Soni, Hugh J. Thornburg and Robert Yu
NSF Engineering Research Center for Computational Field Simulation
Mississippi State University
Mississippi State, MS 39762

ABSTRACT

During the past decade Computational Simulation of fluid flow around complex configurations has progressed significantly and many notable successes have been reported, however unsteady time–dependent solutions are not easily obtainable. The present effort involues unsteady time dependent simulation of temporally deforming geometries. Grid generation for a complex configuration can be a time consuming process and temporally varying geometries necessitate the regeneration of such a grid for every time step. Traditional grid generation techniques have been tried and demonstrated to be inadequate to such simulations. NURBS based techniques provide a compact and accurate representation of the geometry. This definition can be coupled with a distribution mesh for a user defined spacing. The present method greatly reduces cpu requirements for time dependent remeshing, facilitating the simulation of more complex unsteady problems. A Thrust Vectoring Nozzle has been chosen to demonstrate the capability as it is of current interest in aerospace industry for better manoeverability of fighter aircraft in close combat and in post stall regimes. This current effort is the first step towards multidisciplinary design optimization which involues coupling the aerodynamic heat transfer and structural anlysis techniques. Applications include simulation of temporally deforming bodies and areoelastic problems.

A NURBS based volume grid generation technique is used for remeshing at each timestep. Remeshing is easily accomplished by varying the control points and time dependent motion is contained in the motion of the control points. Timestep controls the movement of control points. Great flexibility in geometric definition is achieved. The grid generation code is succesfully coupled with UBIFLOW and INS3d which are compressible and incompressible flow solvers respectively.

Various geometries such as converging diverging nozzle, duct and thrust vectoring nozzle have been simulated ~~and will be presented~~.

OBJECTIVE:

The objective of this work is to devolop a capability for CFD simulation of temporally deforming geometries such as thrust vec toring nozzles.

1. Efficient grid generation system.

2. Flow solver that can handle moving geometries.

MOTIVATION:

1. **Biomedical flows (heart valve, blood flow in arteries or veins).**

2. **Flapping of wing, helicopter rotor.**

3. **Thrust vectoring.**

4. **Wear and deformation on bodies, molding.**

5. **Coupling with finite elment for structural analysis for design optimisation.**

DESIRED FEATURES:

1. Good control over mesh point spacing.
2. Grid quality.
3. Grid generation must be user independent.
4. Geometric fidelity.
5. Consume moderate CPU time.
6. Handle severe deflections.
7. Flowsolver that can handle moving boundaries.

OVERVIEW OF STUDY :

1. Approach.
2. Grid generation.
3. Why NURBS?
4. Flow solver.
5. Why thrust vectoring ?
6. Ongoing research
7. Results.

PRETTY PICTURES IN BETWEEN

and ????????

APPROACH:

1. Grid Generation is descretised representation of volume in interest.

2. Temporally deforming bodies require remeshing every time–step.

3. TFI and Elliptic Grid Generation techniques have been found to be inadequate.

4. NURBS based volume grid generation techniques are well suited for temporally varying geometries.

NURBS based volume grid generation (YU Method):

1. SIGNIFICANT FEATURE IS THAT IT ONLY REQUIRES THE CONTROL POINTS, WEIGHTS AND DISTRIBUTION MESH.

2. REDUCES CPU REQUIREMENT.

3. REMESHING IS EASILY DONE.

4. CONTROL POINTS AND THE ORDER DEFINE THE GEOMETRY.

5. USER DEFINED SPACING IS ACCOMPLISHED THROUGH USE OF DISTRIBUTION MESH.

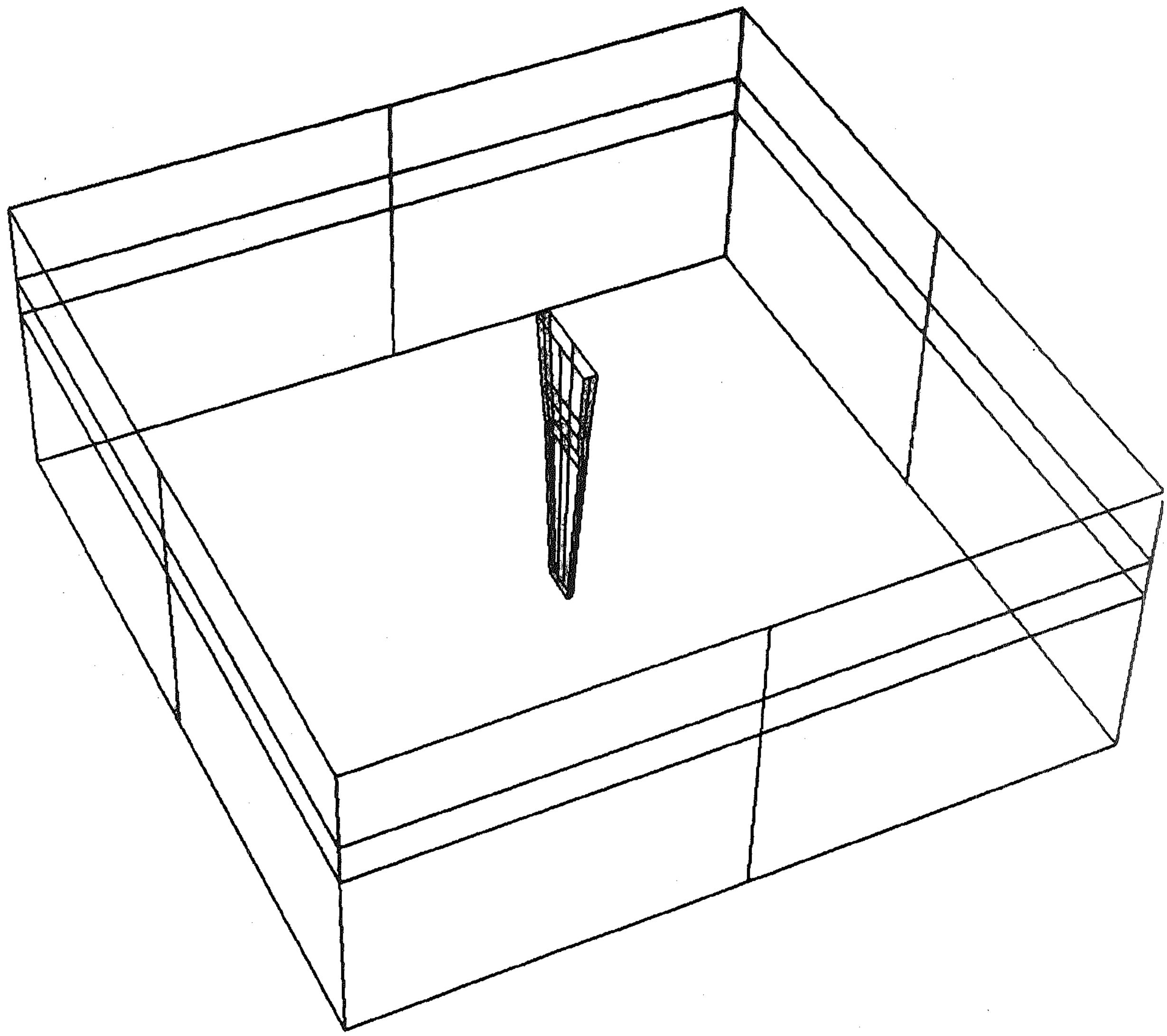

CONTROL POINTS FOR AIRCRAFT WING (4 x 2 x 9)

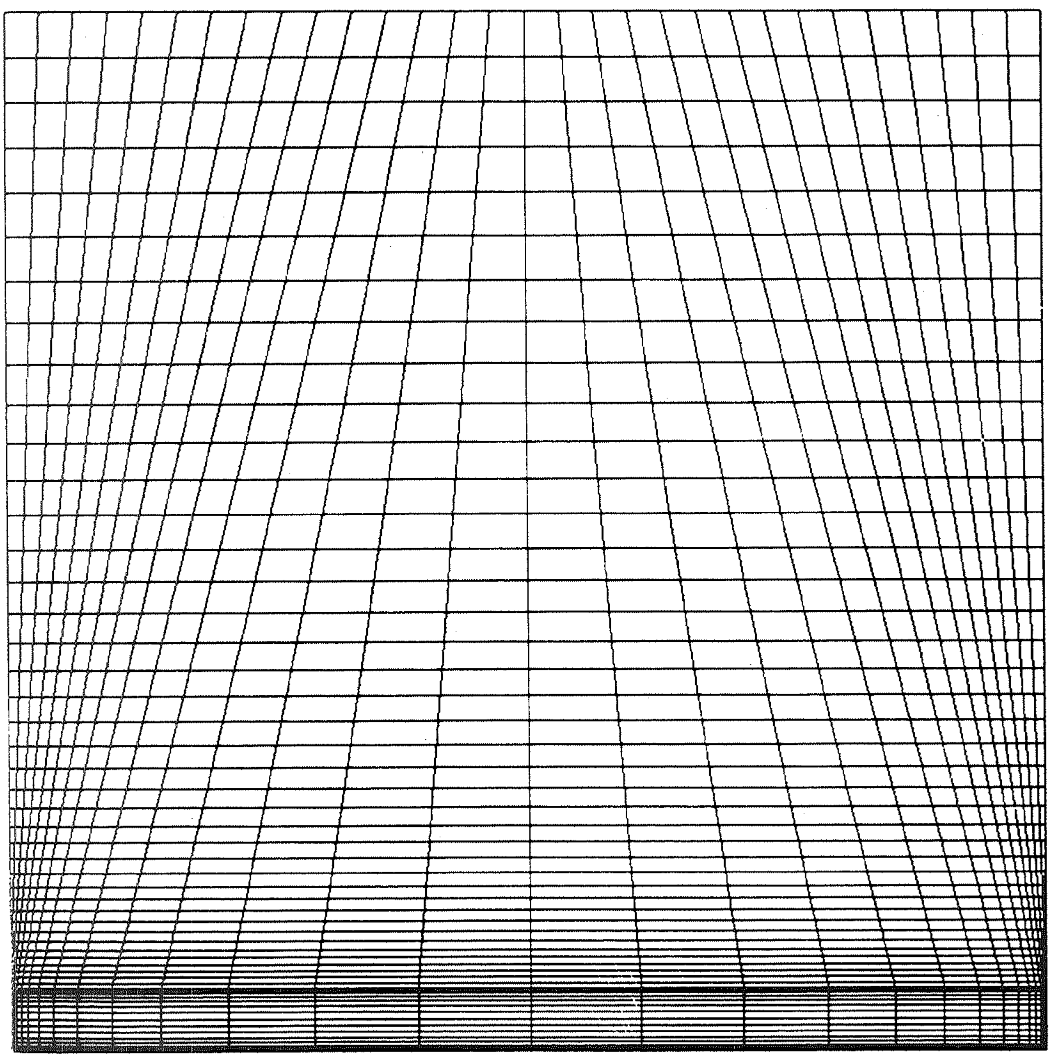

Distribution Mesh

Wing generated with control points and distribution mesh

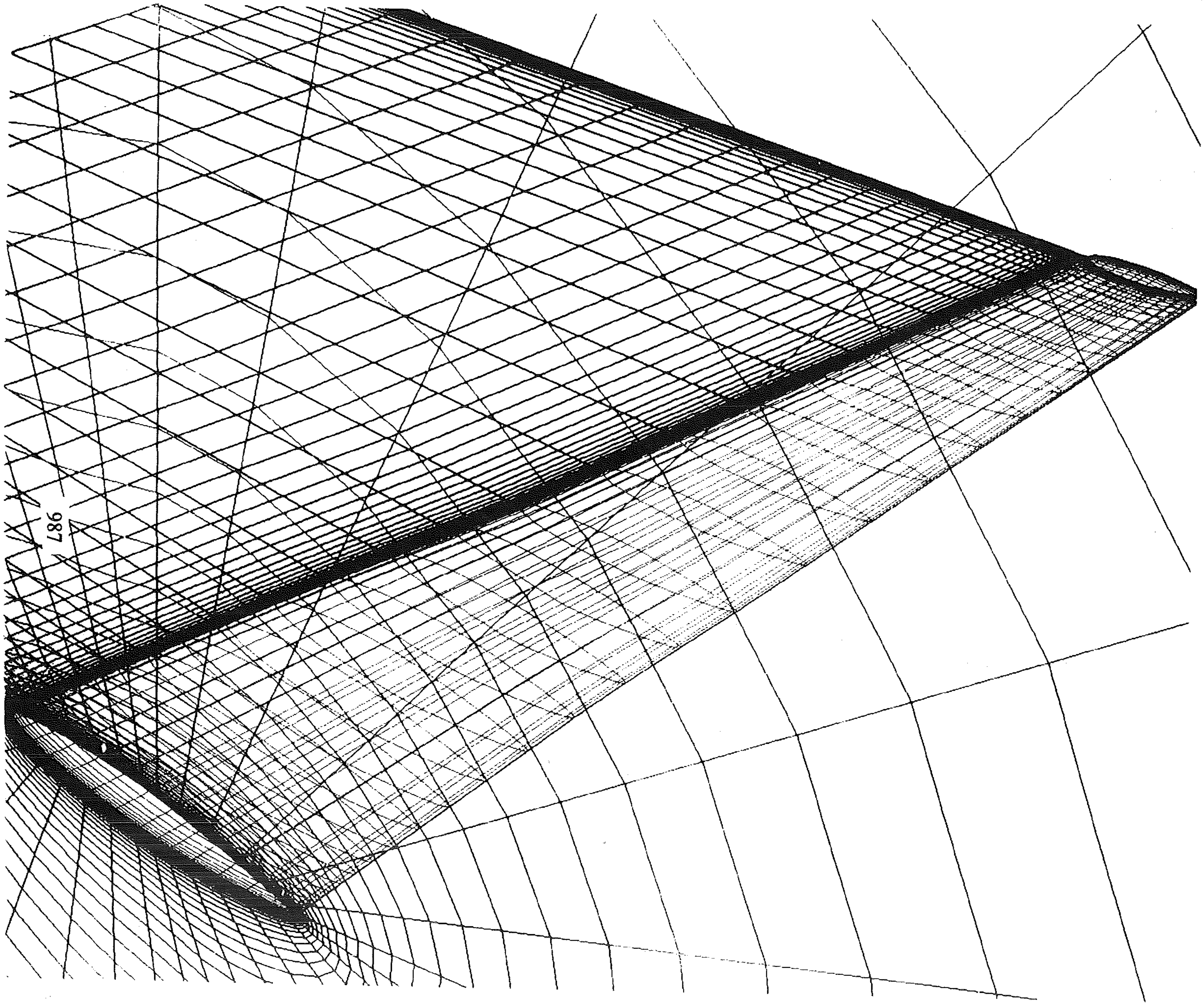

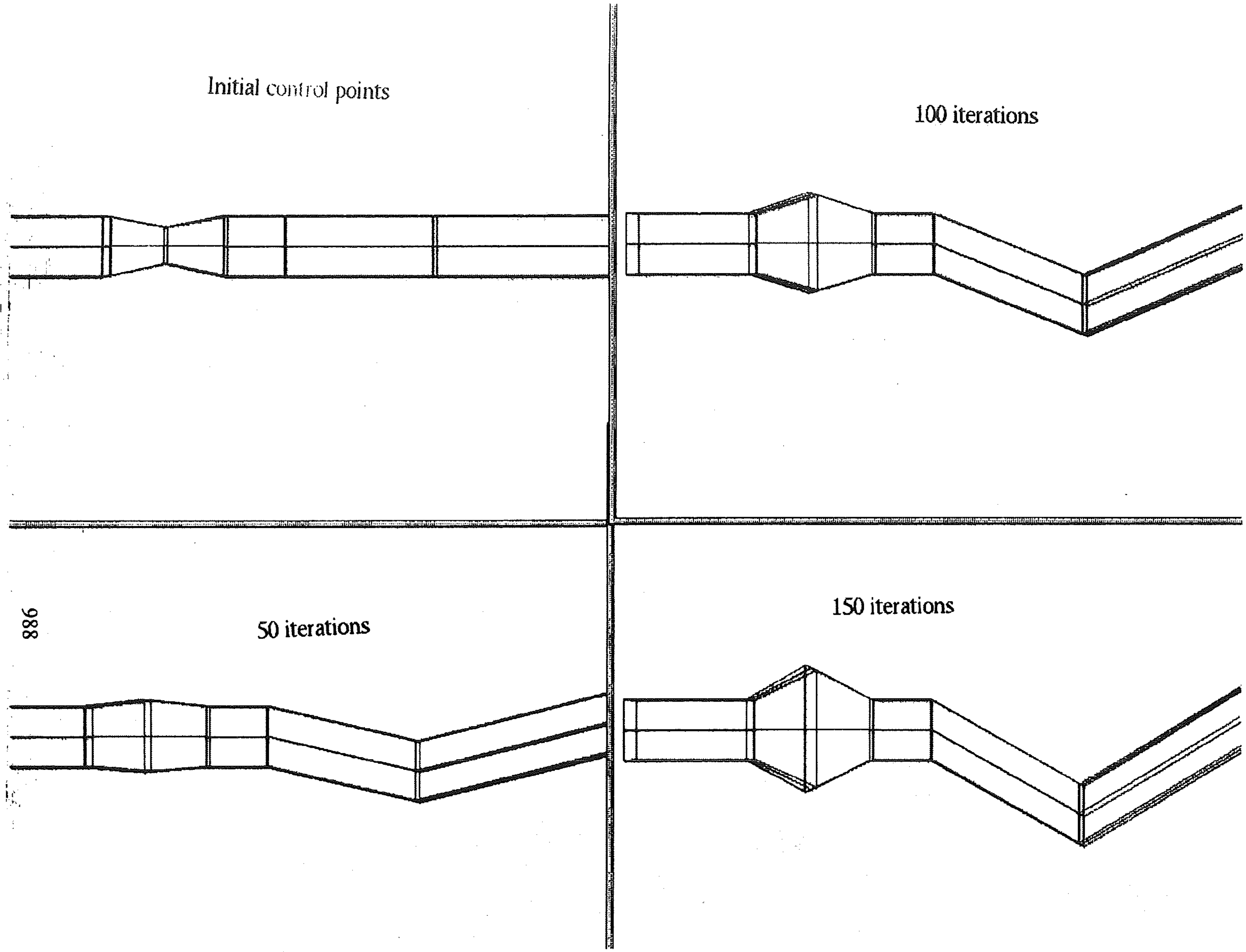
Initial control points
100 iterations
50 iterations
150 iterations

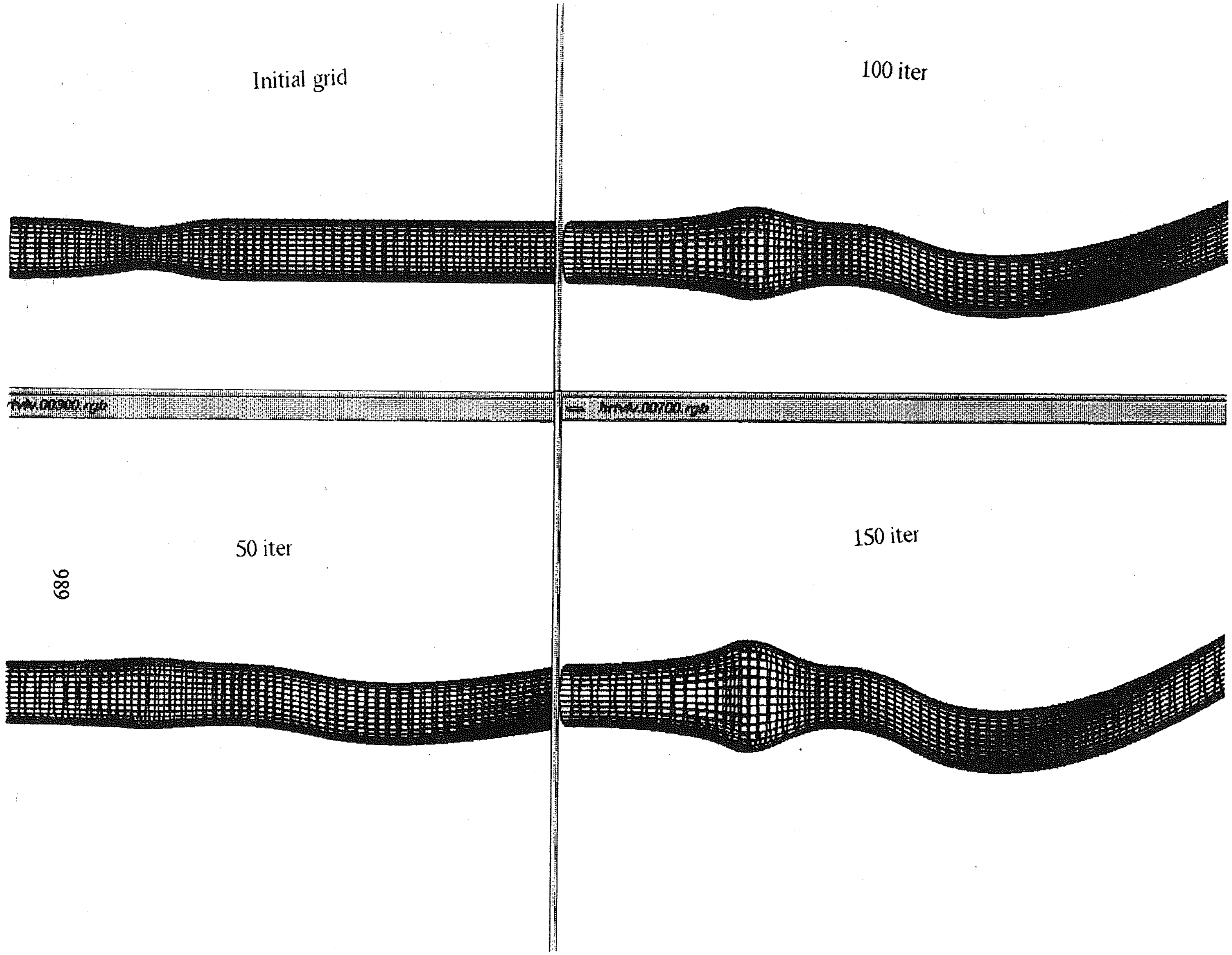
Initial grid
100 iter
50 iter
150 iter

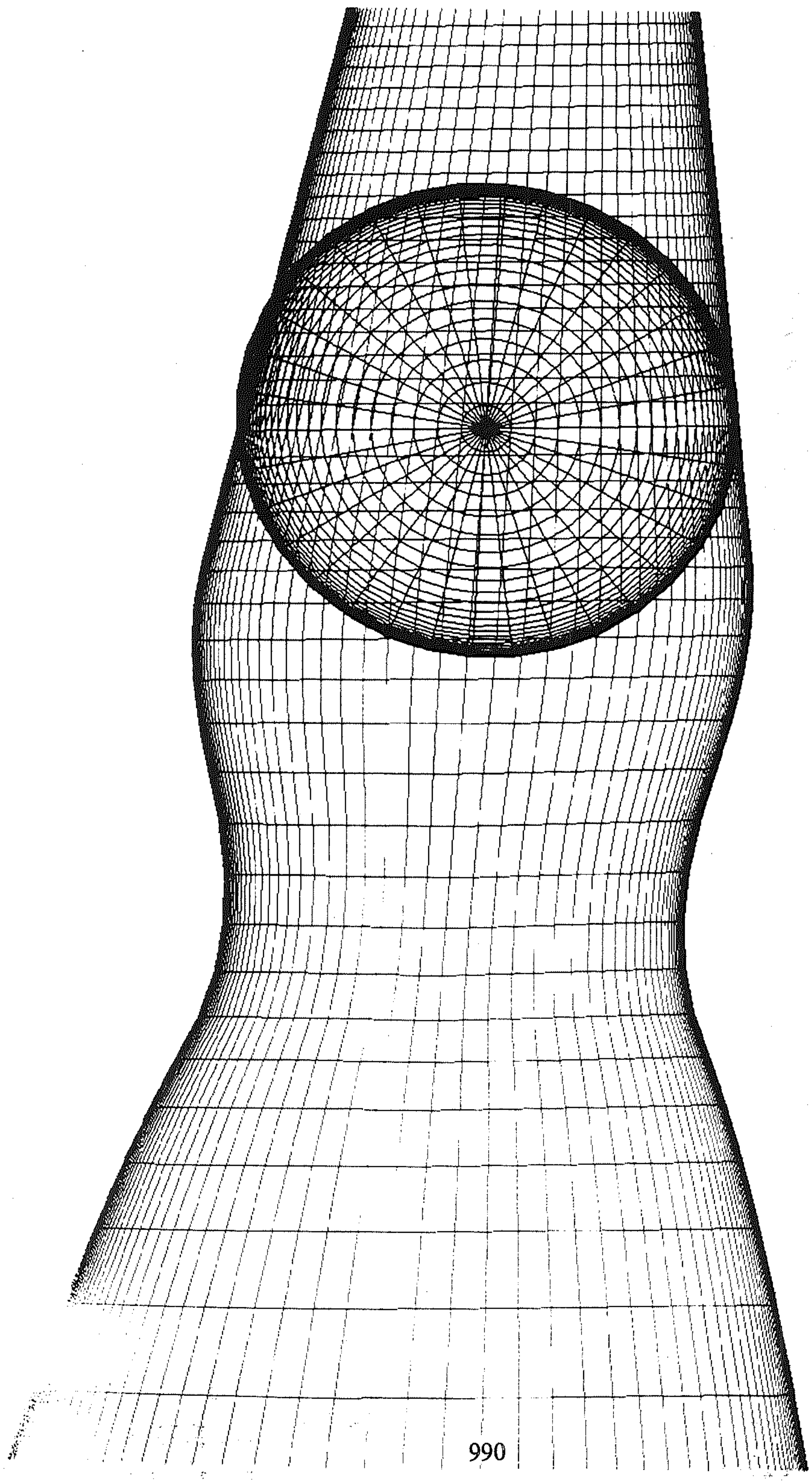

6. TIME DEPENDENT MOTION IS ACCOMPLISHED BY MOVING THE CONTROL POINTS OR BY INTERPOLATION .

7. THE AMOUNT OF MOVEMENT IS CONTROLLED BY THE TIME STEP.

8. FLEXIBILITY IN GEOMETRIC DEFINITION

9. ADAPTATION CAN BE EASILY ACHIEVED BY ADAPTING THE DISTRIBUTION MESH.

Wing with 45 degrees bend and twist of 8 degrees

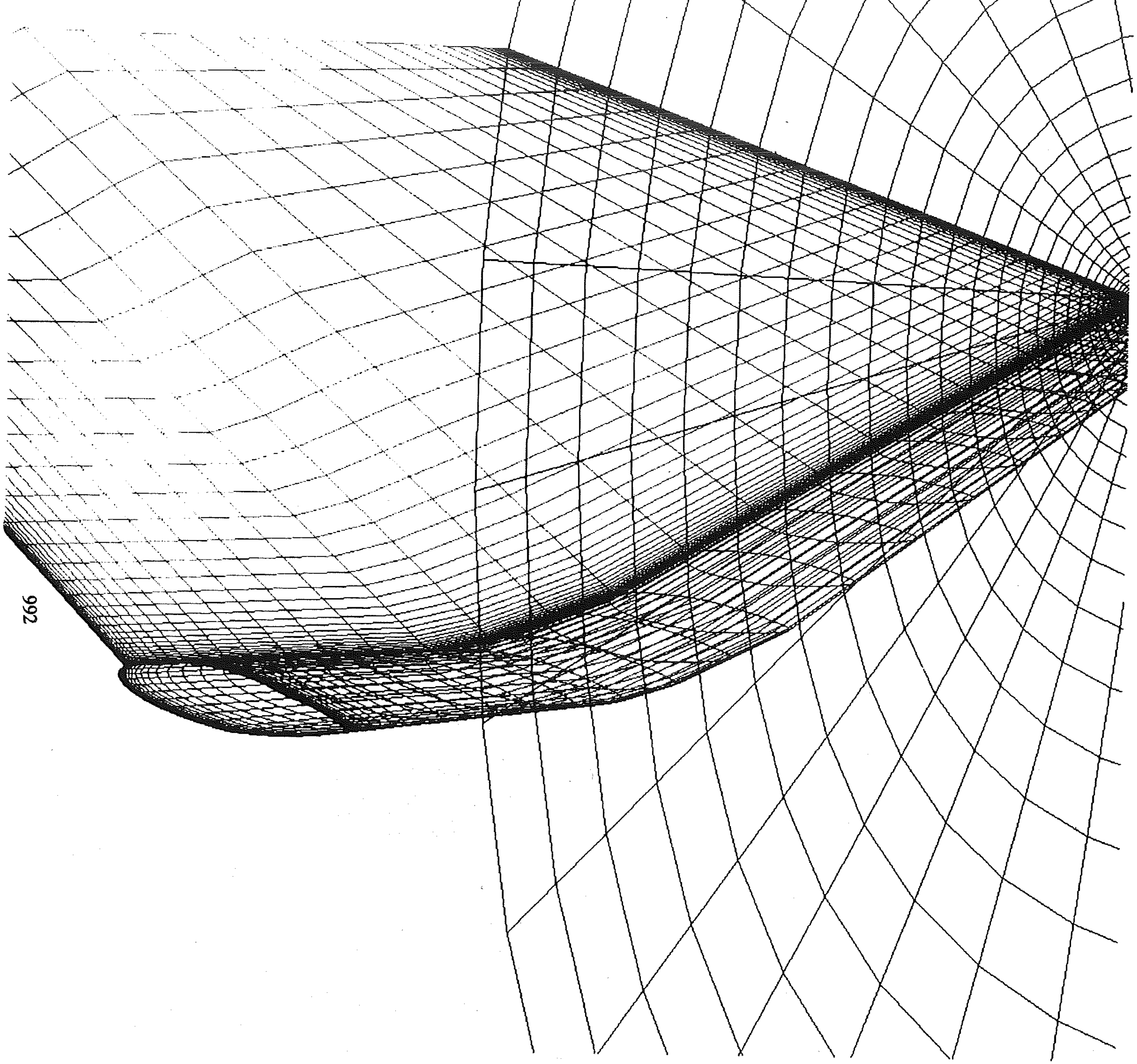

FLOW SOLVER:

- Grid generation code is coupled with

UBIFLOW
INS3D

- Time metrics are calculated as

$$dxdt(i,j,k) = (x(i,j,k) - x0(i,j,k))/dt$$

$$dydt(i,j,k) = (y(i,j,k) - y0(i,j,k))/dt$$

$$dzdt(i,j,k) = (z(i,j,k) - z0(i,j,k))/dt$$

UBIFLOW calculates the time metrics

Time metrics have to be calculted in grid code in INS3D

- UBIFLOW (Whitfield and Arabshasi) :

- Multiblock compressible Navier–Stokes solver

- Cell centered finite volume scheme.

- Flux difference splitting on the RHS and upwind difference using flux splitting on LHS.

- Accounts for the block boundary movement.

- INS3D is a incompressible Navier–Stokes solver and both can solve unsteady and time varying flow.

THRUST VECTORING:

1. Reasonably complex problem.

2. Increase performance.

3. Shrink high drag, radar reflecting horizontal and vertical tail.

4. Better maneuvarability in high angle of attack and and low speed.

5. Reduce landing and take–off distances.

6. Greater payload capability for air – to ground mission aircraft.

7. Reduce over the deck wind speed requirements for aircraft operating on aircraft carriers.

Grid at time steps of 0, 273, 363, 423(1/2 cycle)

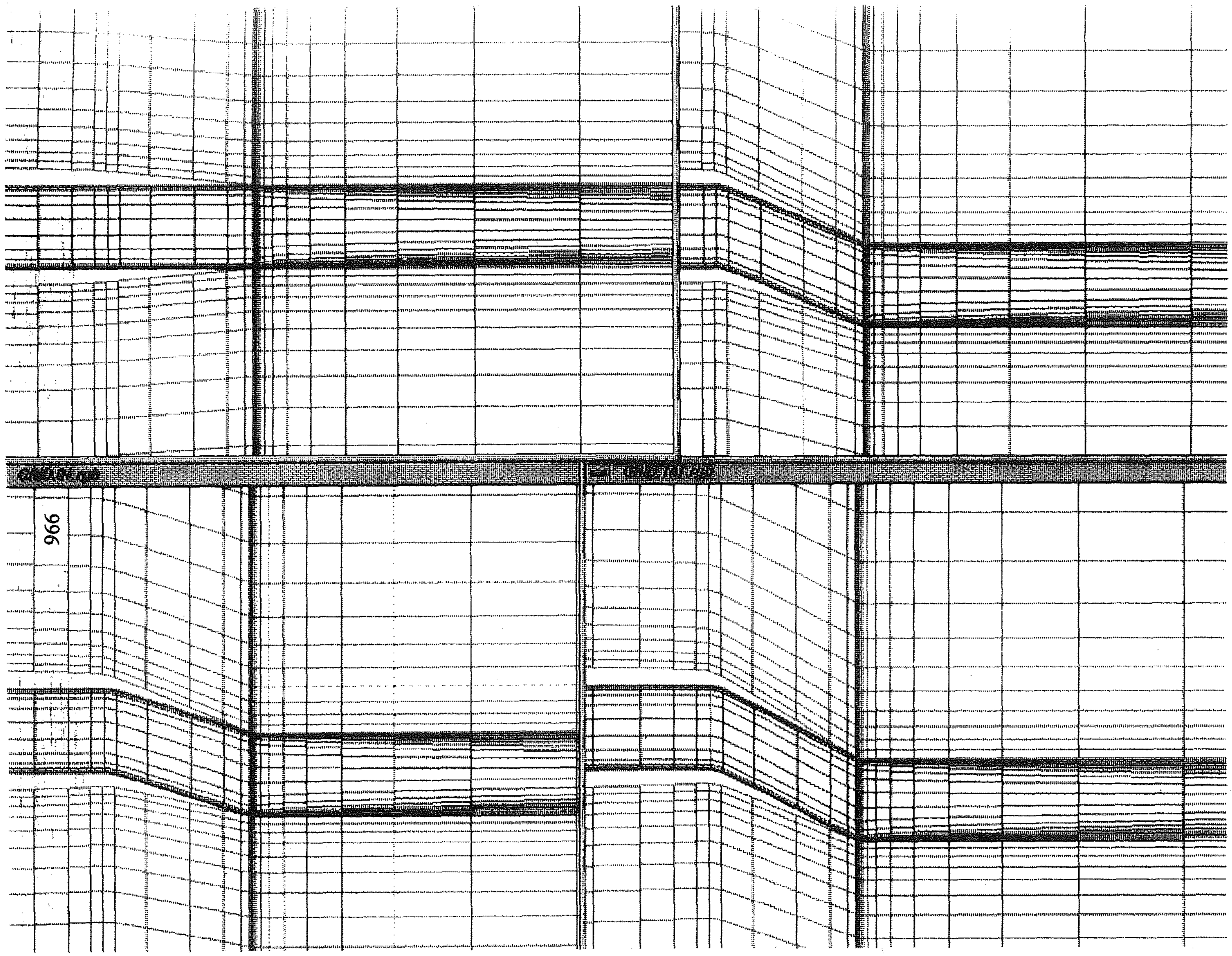

Pressure Distribution for timesteps of 0, 273,363,423

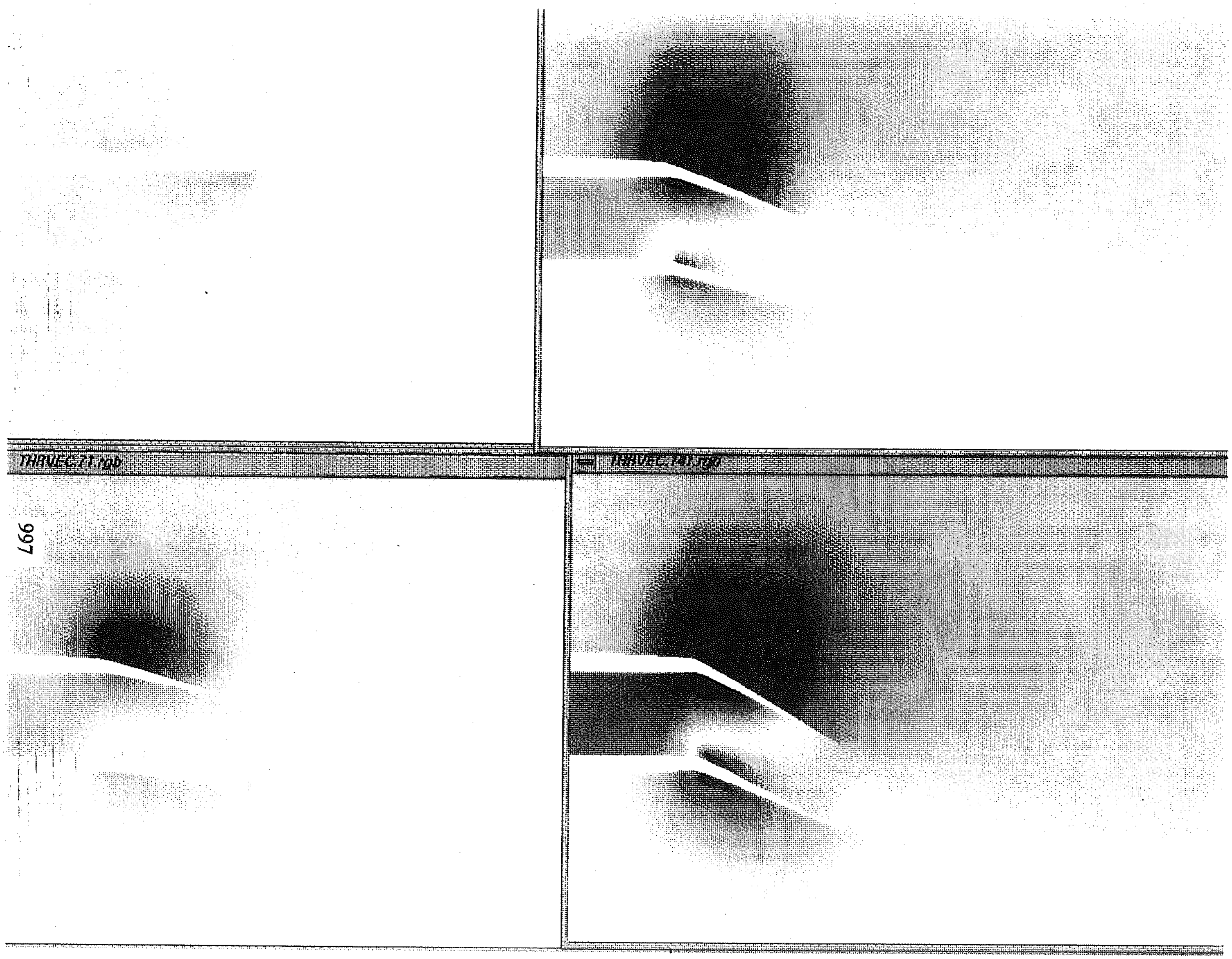

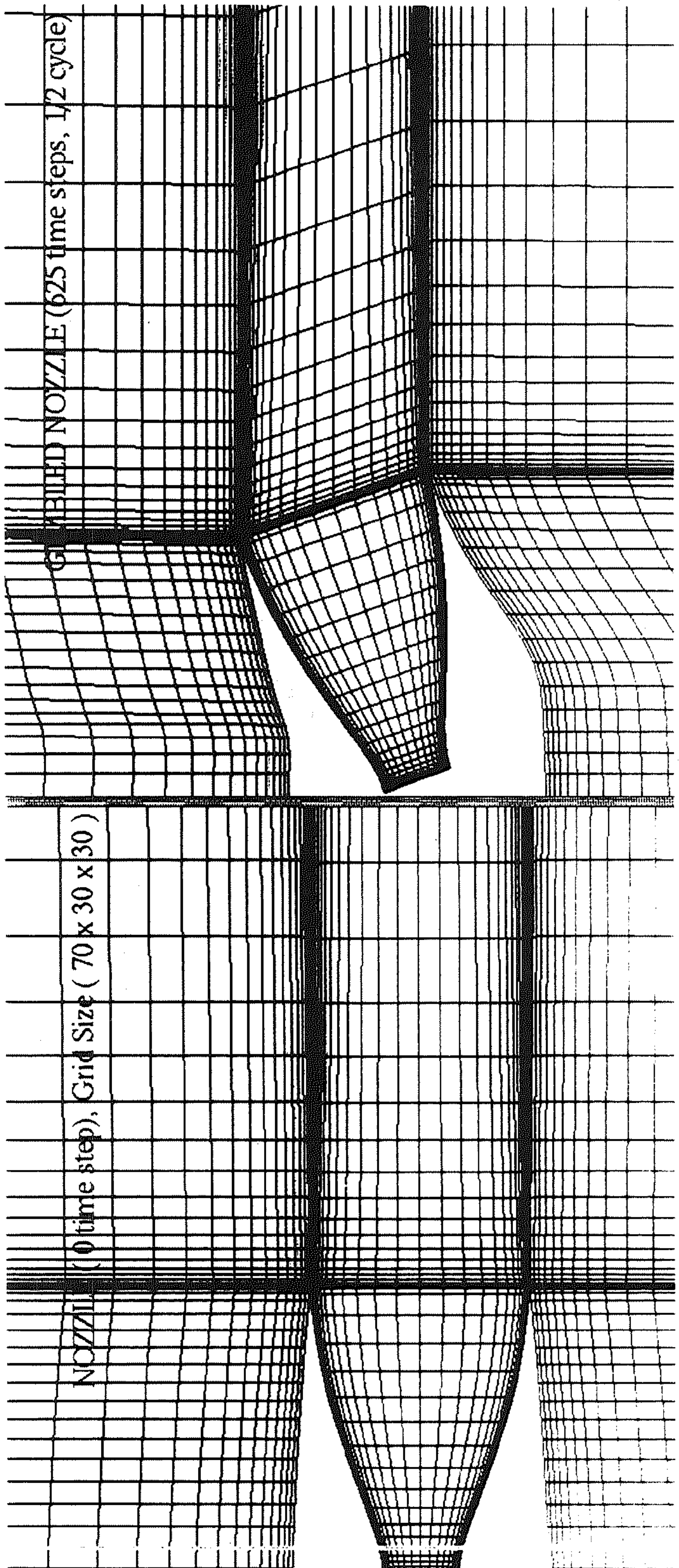
NOZZLE (625 time steps, 1/2 cycle)
NOZZLE (0 time step), Grid Size (70 x 30 x 30)

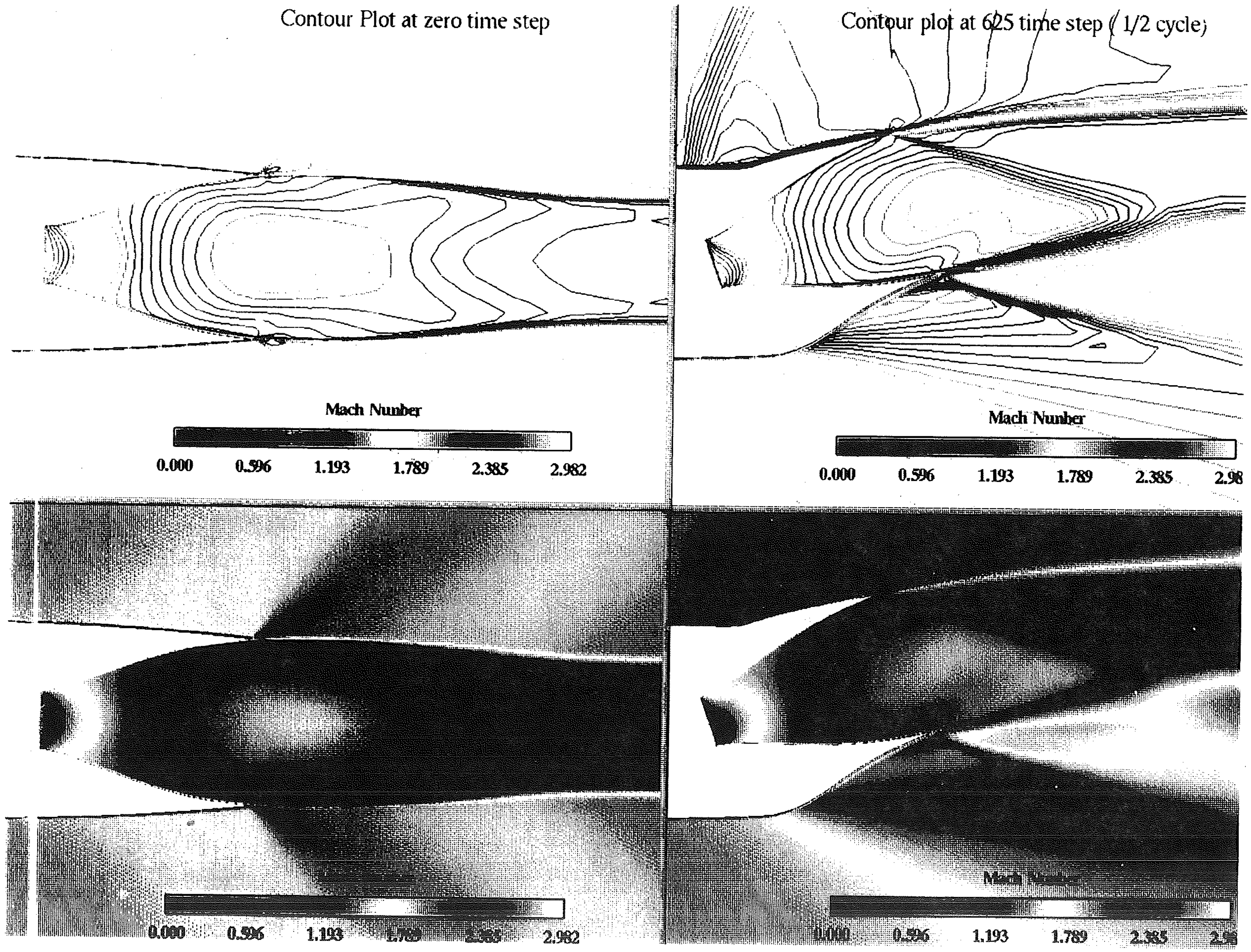
Contour Plot at zero time step
Mach Number
0.000
0.596
1.193
1.789
2.385
2.982
Contour plot at 625 time step (1/2 cycle)
Mach Number
0.000
0.596
1.193
1.789
2.385
2.98

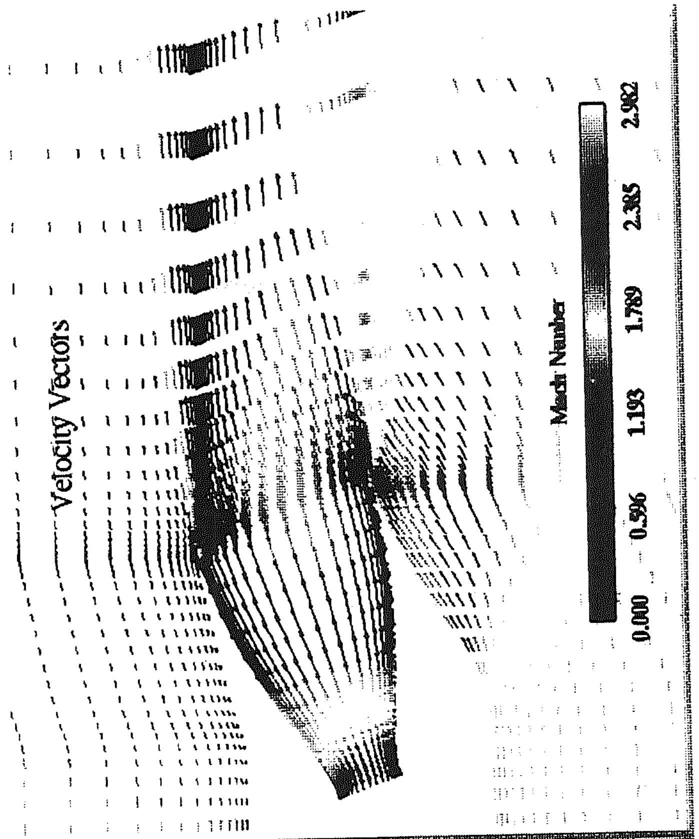
Velocity Vectors
Mach Number
0.000
0.596
1.193
1.789
2.385
2.982

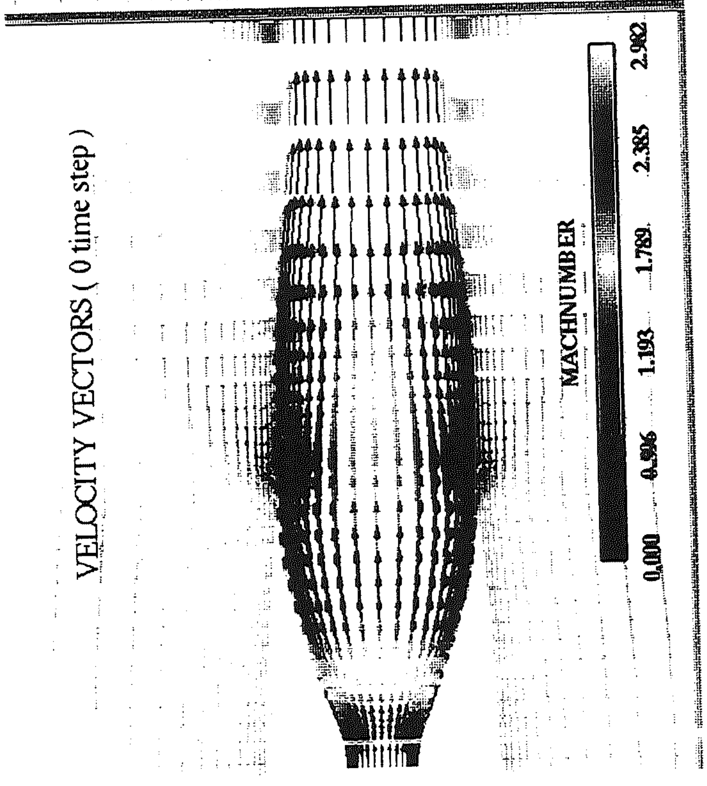
VELOCITY VECTORS (0 time step)
MACHNUMBER
0.000
0.596
1.193
1.789
2.385
2.982

Circular to Rectangular Transition Duct

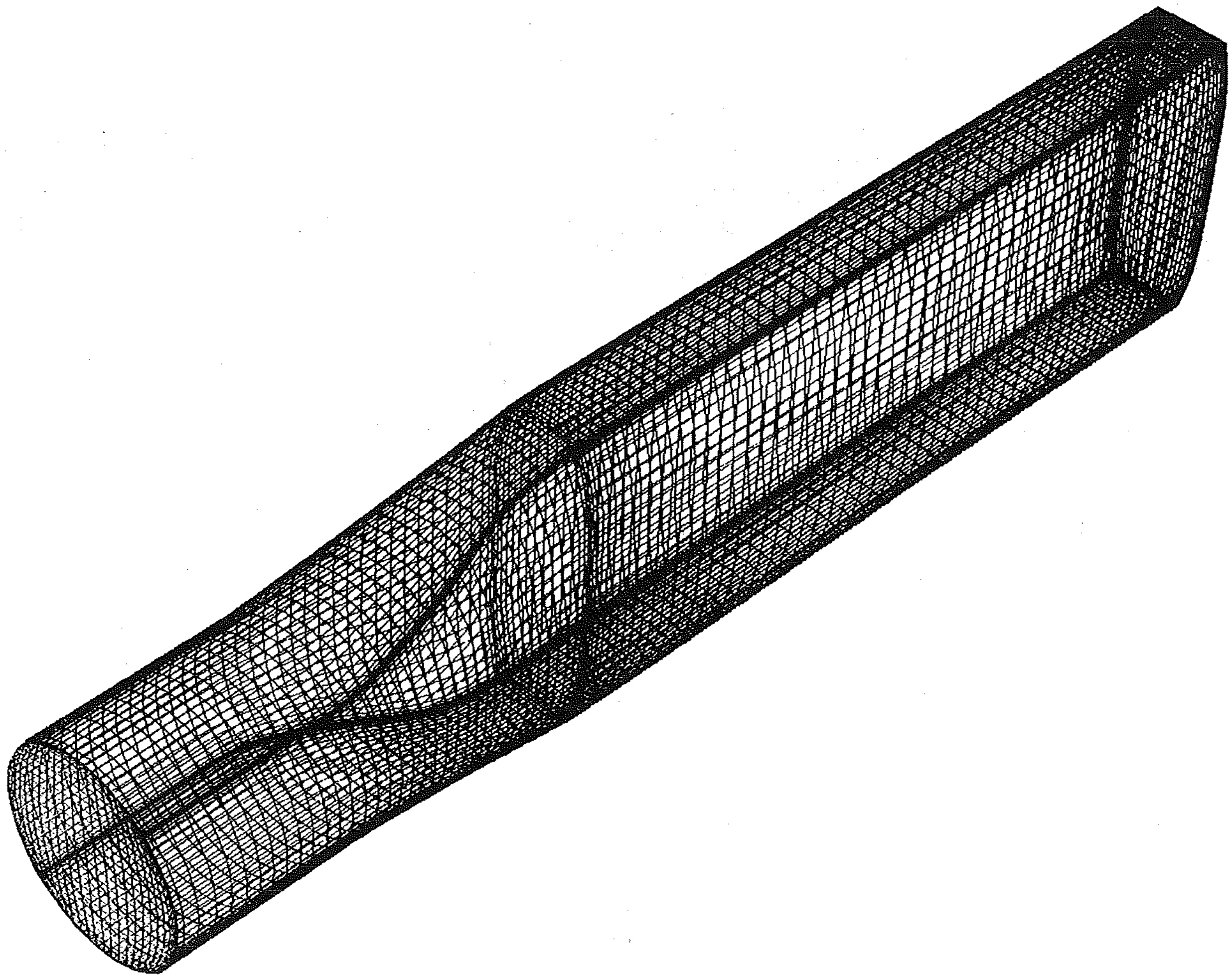

ƎCULAR TO RECTANGULAR TRANSITION DUCT (0 timestep)

grid size (100 x 50 x 50) k = 25 plane

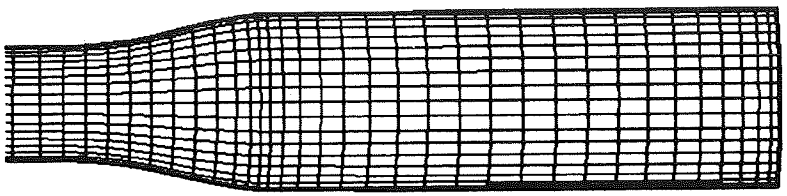

Thrust Vectoring (70 timestep)

grid size (100 x 50 x 50) k = 25 plane

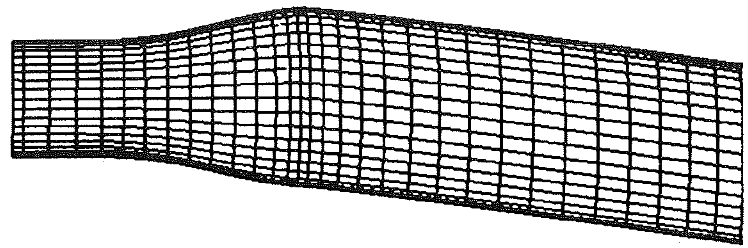

Thrust Vectoring (30 timestep)

grid size (100 x 50 x 50) k = 25 plane

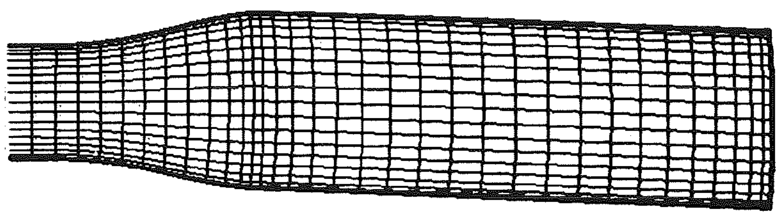

Thrust Vectoring (150 timestep)

grid size (100 x 50 x 50) k = 25 plane

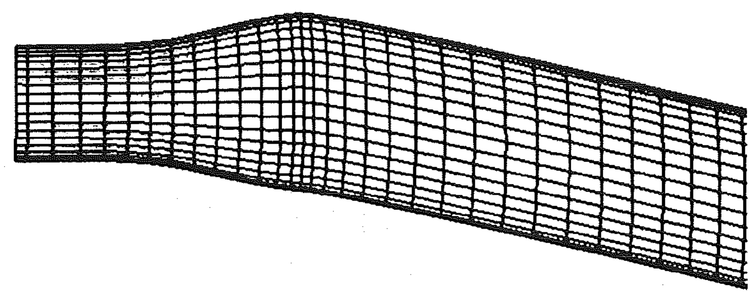

1003

Circular to rectanguler transition duct
0 timestep

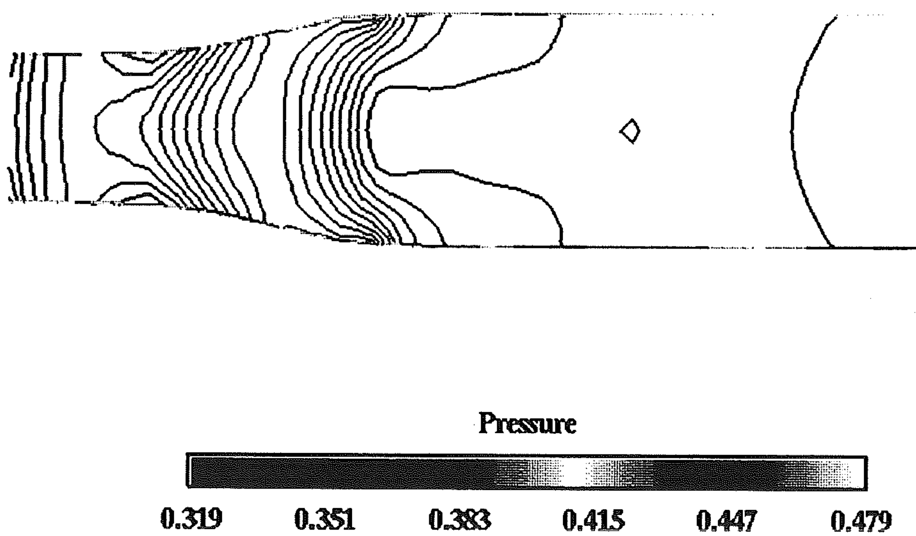

THRUST VECTORING (150 timesteps)

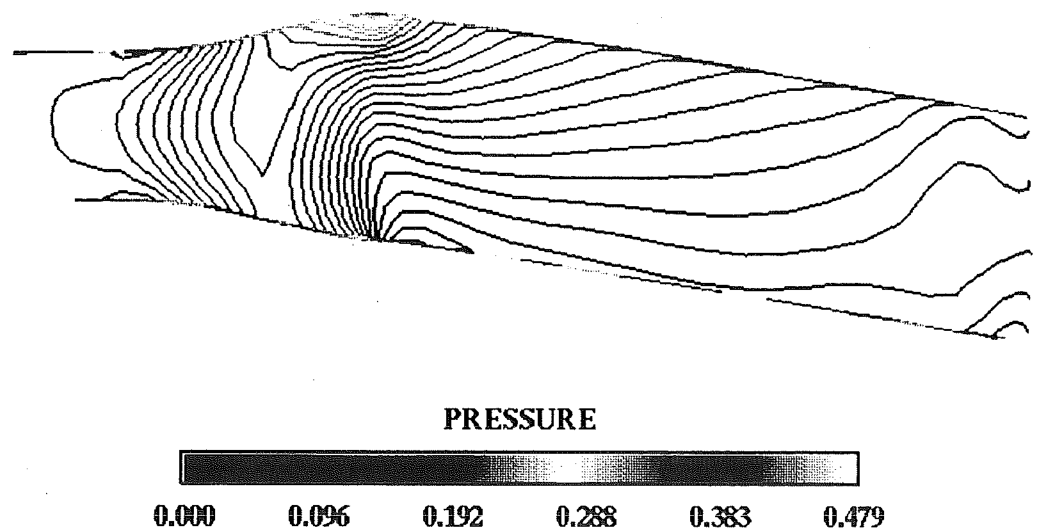

ONGOING REASERCH:

Adaption on the distribution mesh and link it with the moving grid code

RESULTS:

1. CPU of 2.1 secs / iteration for a grid size of 60*40*35 on a onyx 150 MHz processer

2. Memory of the moving grid code is 1.8 Megs

3. Linked with flowsolver it does not consume any memory.

4. Flow solver consumes 75 secs of CPU per / iteration.

5. Adaption is easy to perform as it is on the distribution mesh.

6. Linked succesfully to UBIFLOW and INS3D.

7. Converging –diverging , 2–D and axisymmetric thrust vectoring nozzle have been succesfully simulated.

HYBRID GRID TECHNIQUES FOR PROPULSION APPLICATIONS

Roy P. Koomullil, Bharat K. Soni, and Hugh J. Thornburg
NSF Engineering Research Center for
Computational Field Simulation
Mississippi State University
Mississippi State, MS 39762

ABSTRACT

During the past decade computational simulation of fluid flow for propulsion applications has progressed significantly, and many notable successes have been reported in the literature. However, the generation of a high quality mesh for such problems has often been reported as a pacing item. Hence, much effort has been expended to speed this portion of the simulation process. Several approaches have evolved for grid generation. Two of the most common are structured multi–block, and unstructured based procedures. Structured grids tend to be computationally efficient, and high aspect ratio cells necessary for efficiently resolving viscous layers. Structured multi–block grids may or may not exhibit grid line continuity across the block interface. This relaxation of the continuity constraint at the interface is intended to ease the grid generation process, which is still time consuming. Flow solvers supporting non–contiguous interfaces require specialized interpolation procedures which may not ensure conservation at the interface. Unstructured or generalized indexing data structures offer greater flexibility, but require explicit connectivity information and are not easy to generate for three-dimensional configurations. In addition unstructured mesh based schemes tend to be less efficient and it is difficult to resolve viscous layers. Recently, hybrid or generalized element solution and grid generation techniques have been developed with the objective of combing the attractive features of both structured and unstructured techniques. In the present work recently developed procedures for hybrid grid generation and flow simulation are critically evaluated, and compared to existing structured and unstructured procedures in terms of accuracy and computational requirements.

In the present grid generation procedure multi–body configurations are decomposed into a number of simple geometric entities. A structured grid generator is first employed to construct a high quality grid around the body with appropriate packing. One grid must be designated as a main grid and enclose the solid surfaces of all other component grids. Upon completion these structured grids are converted to the hybrid grid data structure format. Based upon an input normal distance from the surface, holes are cut in the main grid for each component grid. Overlapping and hole cells are deleted from the hybrid grid data structure. Delaunay triangulation is then used to construct cells to fill the void between the cut main grid and the truncated component grid. Upon completion of this procedure the hybrid grid is written in a format useable by the flow solver.

The non–dimensionalized Euler equations in integral form provide the mathematical formulation for this scheme. The discretized flow domain is represented by a set of non overlapping polygons and the cell averaged variables are stored at each cell center. Each individual cell is treated as its own control volume. The numerical flux at the cell edge is calculated using Roe's approximate Riemann solver. An assumed linear distribution in each cell is employed to reconstruct the edge values, which results in a second order discretization. The flux limiting procedure of Barth is used to suppress spurious oscillations near discontinuities. An implicit pseudo–time integration procedure using the Generalized Minimum RESidual (GMRES) method for solving the sparse matrix system is employed. The results has been varified with the standard benchmark results.

Hybrid Grid Techniques For Propulsion Applications

Roy P Koomullil, Dr. Bharat K. Soni and Dr. Hugh J. Thornburg

Sponsors : Teledyne Brown Engineering and AFOSR

National Science Foundation Engineering Research Center For Computational Field Simulation Mississippi State University.

ENGINEERING RESEARCH CENTER FOR COMPUTATIONAL FIELD SIMULATION

COMPLEX GEOMETRY / COMPLEX PHYSICS

OUTLINE

- MOTIVATION
- GRID GENERATION APPROACH
- DATA STRUCTURE
- FLOW SOLVER
- RESULTS
- CONCLUSIONS

MOTIVATION

UNSTRUCTURED GRIDS

- GREATER FLEXIBILITY IN HANDLING COMPLEX CONFIGURATIONS
- EASE OF GRID ADAPTION
- DIFFICULT TO MAKE HIGHLY STRETCHED VISCOUS GRIDS
- DIFFICULT TO RESOLVE CONVECTIVE AND VISCOUS FLUXES FOR HIGH REYNOLDS NUMBERS
- TURBULENCE MODELLING IS DIFFICULT

HYBRID GRIDS

- COMBINING ADVANTAGES OF STRUCTURED AND UNSTRUCTURED GRIDS
- GRID GENERATION TIME CAN BE REDUCED

HYBRID GRID

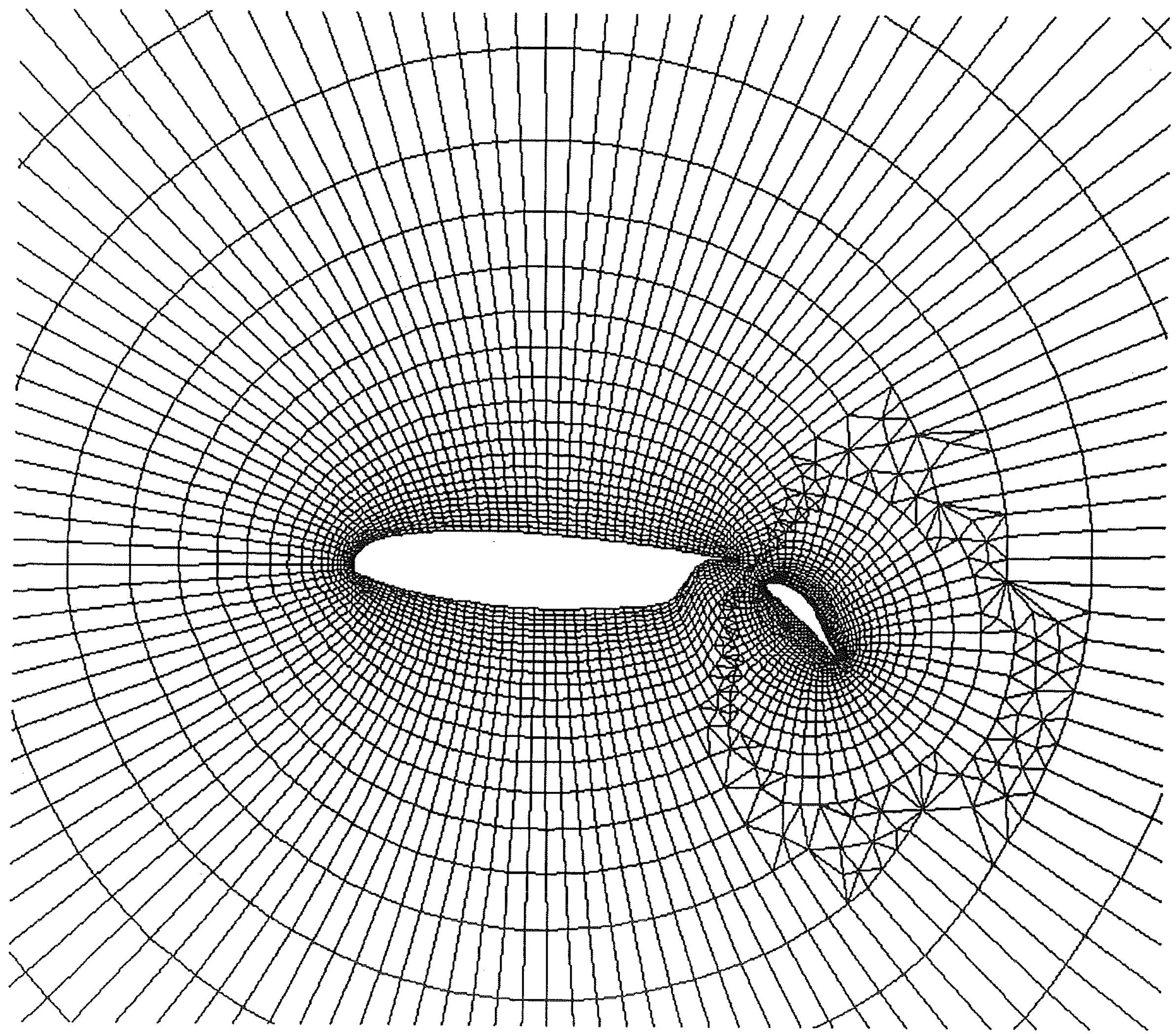

APPROACH

GRID GENERATION

- DECOMPOSE COMPLEX BODIES INTO SIMPLE ENTITIES
- GENERATE STRUCTURED GRIDS FOR THESE GEOMETRIC ENTITIES USING STANDARD PACKAGES
- CUT HOLES IN THE MAIN GRID WHERE THE COMPONENTS OVERLAPS
- CONNECT COMPONENT GRIDS USING UNSTRUCTURED GRIDS BY DELAUNAY TRIANGULATION OR OTHER METHODS
- AVOIDED INTERPOLATIONS OF CONSERVED VARIABLES BETWEEN THE COMPONENT AND MAIN GRIDS AS IN CAMERA GRIDS

DATA STRUCTURE

- EDGE BASED DATA STRUCTURE

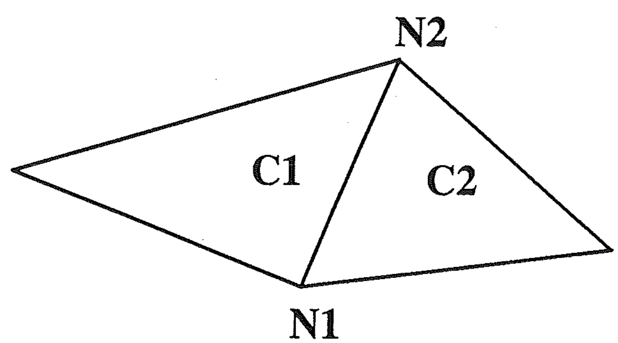

- EDGE(K,1) = FIRST NODE (N1)
- EDGE(K,2) = SECOND NODE (N2)
- EDGE(K,3) = CELL ON LEFT (C1)
- EDGE(K,4) = CELL ON RIGHT (C2) or BOUNDARY CONDITION

- ADVANTAGE : ANY ARBITRARY POLYGONS CAN BE HANDLED

CELL AREA

$$Area = \oint_{\partial\Omega} x \, dy = \sum_{edges} x_e \, dy$$

```
Loop over the edge
    N1  = EDGE ( I, 1 )
    N2  = EDGE ( I , 2 )
    C1  = EDGE ( I , 3 )
    C2  = EDGE ( I , 4 )
    dy  = Y ( N2 ) - Y ( N1 )
    XE  = ( X( N2 ) + X ( N1 ) ) * 0.5
    AREA(C1) = AREA(C1) + XE * dy
    AREA(C2) = AREA(C2) - XE * dy
endloop
```

GOVERNING EQUATIONS

$$\frac{\partial}{\partial t} \oint_{\Omega} Q \, dA + \oint_{\partial\Omega} \underline{F}(Q) \, . \, \underline{n} \, ds = 0$$

Where

$$\underline{F} = f\, i + g\, j \qquad \underline{n} = n_x\, i + n_y\, j$$

$$Q = \begin{bmatrix} \varrho \\ \varrho u \\ \varrho v \\ E \end{bmatrix} \qquad f = \begin{bmatrix} \varrho u \\ \varrho u^2 + p \\ \varrho uv \\ u(E+p) \end{bmatrix} \qquad g = \begin{bmatrix} \varrho v \\ \varrho uv \\ \varrho v^2 \\ v(E+p) \end{bmatrix}$$

$$p = (\gamma - 1)\left[E - \varrho\left[\frac{u^2 + v^2}{2}\right]\right]$$

Non Dimensionalization w.r.t freestream conditions

FINITE VOLUME DISCRETIZATION

$$A_i \frac{\partial Q_i}{\partial t} = - \oint_{\partial\Omega} \underline{F}(Q_i) \cdot \underline{n} \, ds = - \sum_{j=1}^{k} \underline{F}_{i,j} \cdot \underline{n}_j \, ds_j$$

Where **k** **Number of sides of the polygon**
i **Cell number**
j **Edge number**

SUMMATION OF FLUXES

Loop Over the edges

CALCULATE F_{ij}

FLUX (C1) = FLUX(C1) + F_{ij}

FLUX (C2) = FLUX(C2) - F_{ij}

Endloop

APPROXIMATE RIEMANN SOLVER (ROE)

$$F_{i,j} = \frac{1}{2}\left[\, F(Q_R) + F(Q_L) - |\,\overline{A}\,|\,(Q_R - Q_L) \right]$$

where

$$|\,\overline{A}\,|\,(Q_R - Q_L) = |\,\Delta F_{1,2}\,| + |\,\Delta F_3\,| + |\,\Delta F_4\,|$$

Corresponding to 3 different eigen values

$\lambda_{1,2} = u$ and $\lambda_{3,4} = u \pm c$

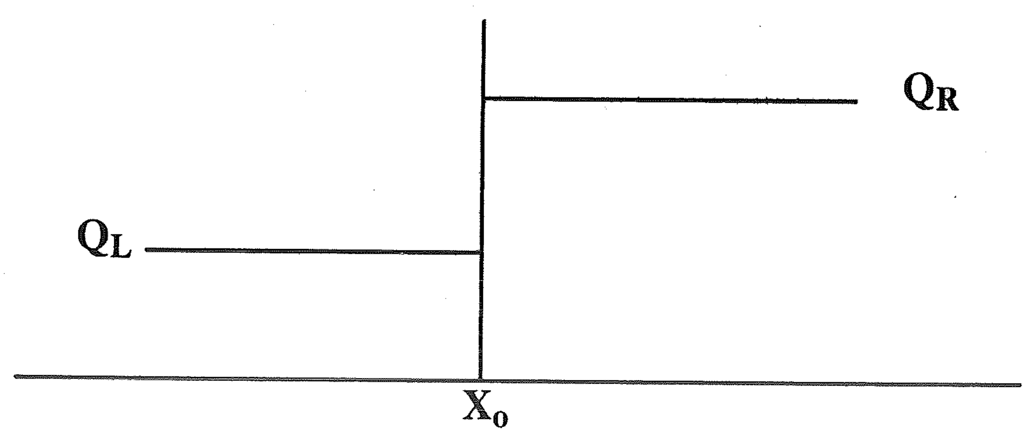

EXPLICIT SCHEME
(RUNGE–KUTTA TIME INTEGRATION)

$$Q^{(0)} = Q^{(N)}$$

$$Q^{(1)} = Q^{(0)} + \alpha_1 \frac{\Delta t}{A} R(Q^{(0)})$$

$$Q^{(2)} = Q^{(0)} + \alpha_2 \frac{\Delta t}{A} R(Q^{(1)})$$

$$Q^{(3)} = Q^{(0)} + \alpha_3 \frac{\Delta t}{A} R(Q^{(2)})$$

$$Q^{(3)} = Q^{(0)} + \alpha_4 \frac{\Delta t}{A} R(Q^{(3)})$$

$$Q^{(N+1)} = Q^{(4)}$$

$$\alpha_1 = 0.0833 \qquad \alpha_2 = 0.2069 \qquad \alpha_3 = 0.4265 \qquad \alpha_4 = 1.0$$

Where $R = - \sum_{edges} \underline{F}_{ij} \cdot \underline{n}\, ds$

IMPLICIT SCHEME

$$F_{ij}^{n+1} = \frac{1}{2}\left(F(\,Q_R^{n+1}\,) + F(\,Q_L^{n+1}\,) - |\,\overline{A}\,|\,.\,(\,Q_R^{n+1} - Q_L^{n+1}\,)\right)$$

LINEARIZATION

$$F_{ij}^{n+1} = F_{ij}^{n} + \left[\frac{\partial F_{ij}}{\partial Q_R}\right]^n \Delta Q_R + \left[\frac{\partial F_{ij}}{\partial Q_L}\right]^n \Delta Q_L$$

APPROXIMATE ANALYTIC JACOBIANS

NUMERICAL JACOBIANS

APPROXIMATE ANALYTIC JACOBIANS

$$F_{ij}^{n+1} = \frac{1}{2}\left(F(\, Q_R^{n+1}\,) + F(\, Q_L^{n+1}\,) - |\,\overline{A}\,| \,.\, (\, Q_R^{n+1} - Q_L^{n+1}\,)\right)$$

$$D_i\, \Delta Q_i + \sum_{j=1}^{k} \left(\, U_{n(j)}\, \Delta Q_{n(j)} \right) = R^n$$

Where $D_i = \frac{V_i}{\Delta t}\, I + \frac{1}{2} \sum_{j=1}^{k} \left(H_i + |\,\overline{H}\,|_{\frac{i+n(j)}{2}} \right)$

$$U_{n(j)} = \frac{1}{2} \left(H_{n(j)} - |\,\overline{H}\,|_{\frac{i+n(j)}{2}} \right)$$

$$A\, N_x + B\, N_y = H\,, \qquad |\,\overline{A}\,|\, N_x + |\,\overline{B}\,|\, N_y = |\,\overline{H}\,|$$

$$A = \frac{\partial f}{\partial Q}\,, \quad \& \quad B = \frac{\partial g}{\partial Q}$$

NUMERICAL FLUX JACOBIAN

$$A_{ij}(Q) = \frac{F_i (Q + h e_j) - F_i (Q)}{h}$$

Where e_j, j^{th} unit vector

$h = (\text{ machine zero })^{1/2}$

$$j^{th} \text{ Column of } F'(Q) = \frac{F (Q + h e_j) - F (Q)}{h}$$

SPARSE MATRIX STRUCTURE

GRID

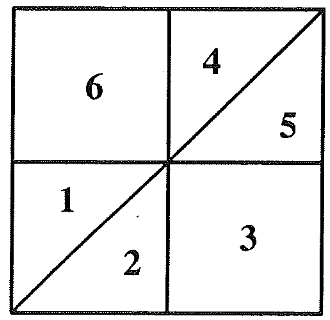

MATRIX STRUCTURE

	1	2	3	4	5	6
1	x	x				x
2	x	x	x			
3		x	x		x	
4				x	x	x
5			x	x	x	
6	x			x		x

HIGHER ORDER SCHEME

$$Q(x, y) = Q(x_i, y_i) + \nabla Q(x_i, y_i) \cdot \Delta \underline{r}$$

Where

$$\Delta \underline{r} = (x - x_i)\, \underline{i} + (y - y_i)\, \underline{j}$$

Using Green's Theorem

$$\nabla (Q) = \frac{1}{V_i} \oint_{\partial\Omega} Q\, \underline{n}\, ds$$

$$Q_{n_i} = \frac{\sum_{j=1}^{nk} \frac{Q_{c_j}}{r_j}}{\sum_{j=1}^{nk} \frac{1}{r_j}}$$

LIMITER (Barth)

$$Q(x, y) = Q(x_{i,} y_i) + \phi_i \nabla Q(x_i, y_i) \cdot \Delta \underline{r}$$

$$Q_i^{min} = \min (Q_{ci}, Q_{adj})$$

$$Q_i^{max} = \max (Q_{ci}, Q_{adj})$$

$$\text{then} \quad Q_i^{min} \leqslant Q(x,y) \leqslant Q_i^{max}$$

$$\phi_{ij} = \begin{cases} \min\left[1, \dfrac{Q_i^{max} - Q_{ij}}{Q_i - Q_{ij}}\right] & \text{if } Q_i - Q_{ij} > 0 \\ \min\left[1, \dfrac{Q_i^{min} - Q_{ij}}{Q_i - Q_{ij}}\right] & \text{if } Q_i - Q_{ij} < 0 \\ 1 & \text{if } Q_i - Q_{ij} = 0 \end{cases}$$

$$\text{and} \quad \phi_i = \min(\phi_{ij's})$$

VARIFICATION OF THE RESULTS

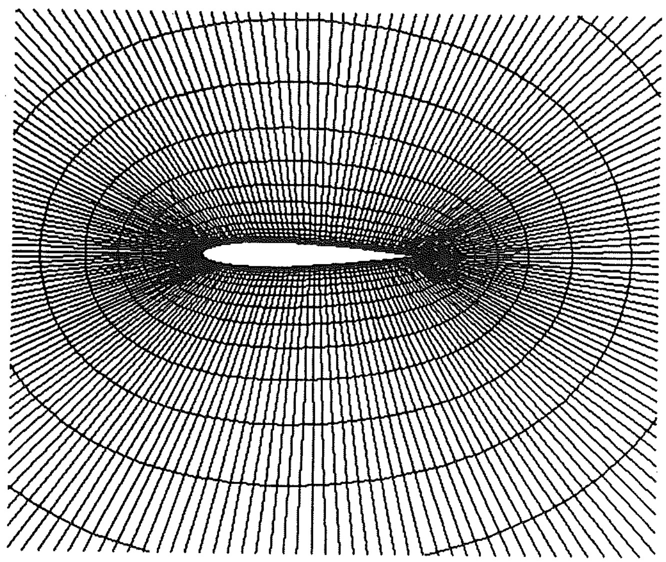

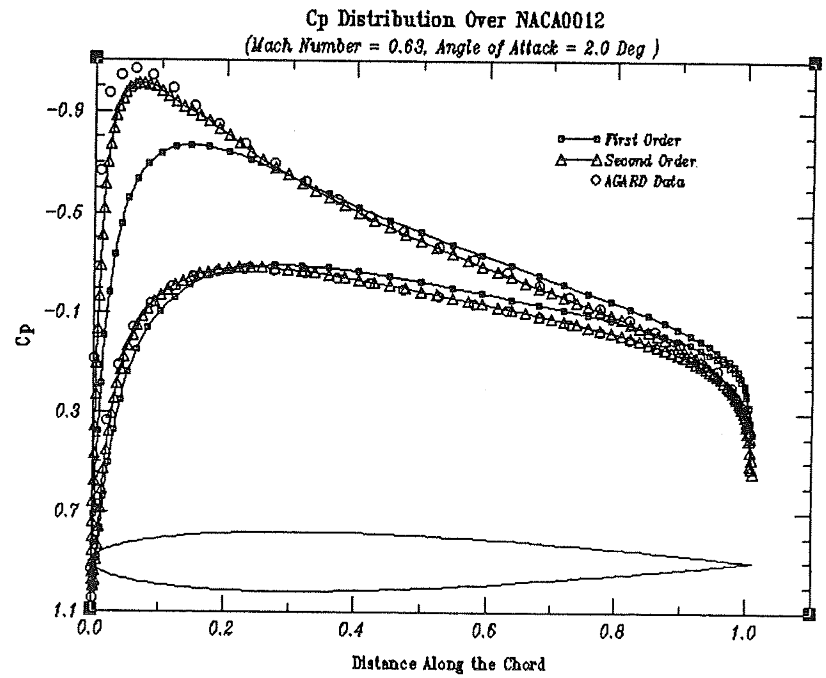

Comparison with NPARC Solution

Pressure Contours (Mach No = 2.5)

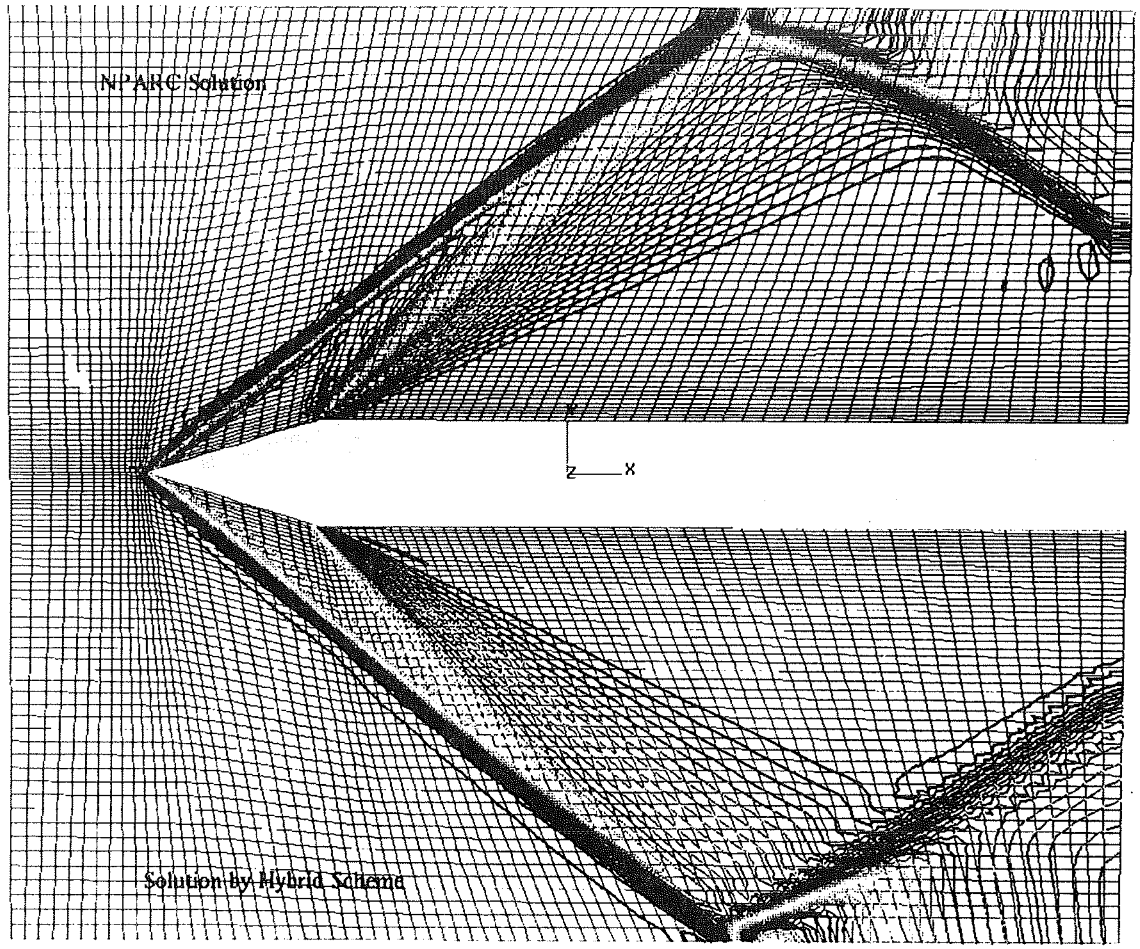

COMPARISON OF CONVERGENCE

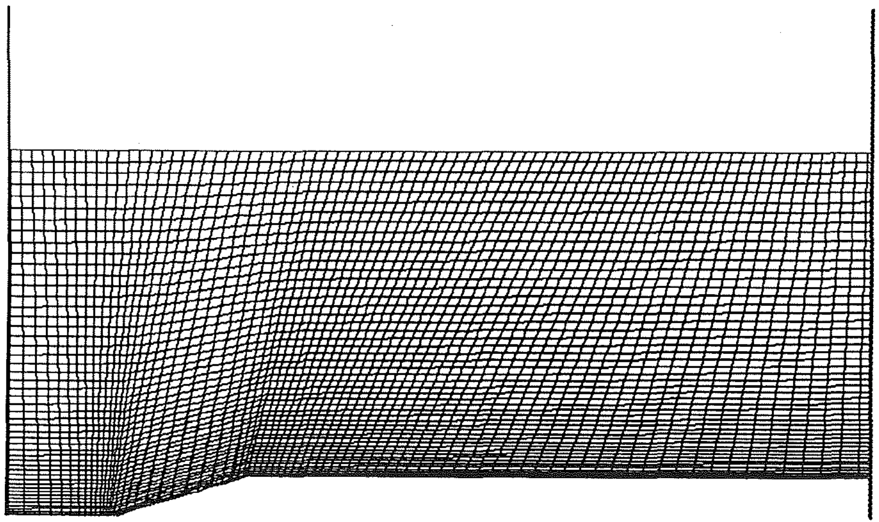

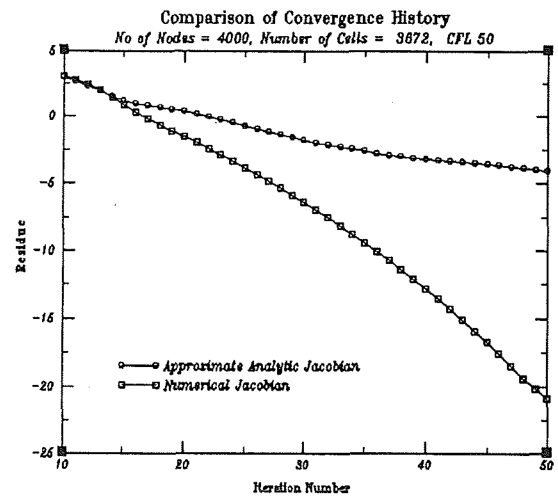

SCRAMJET INLET GEOMETRY

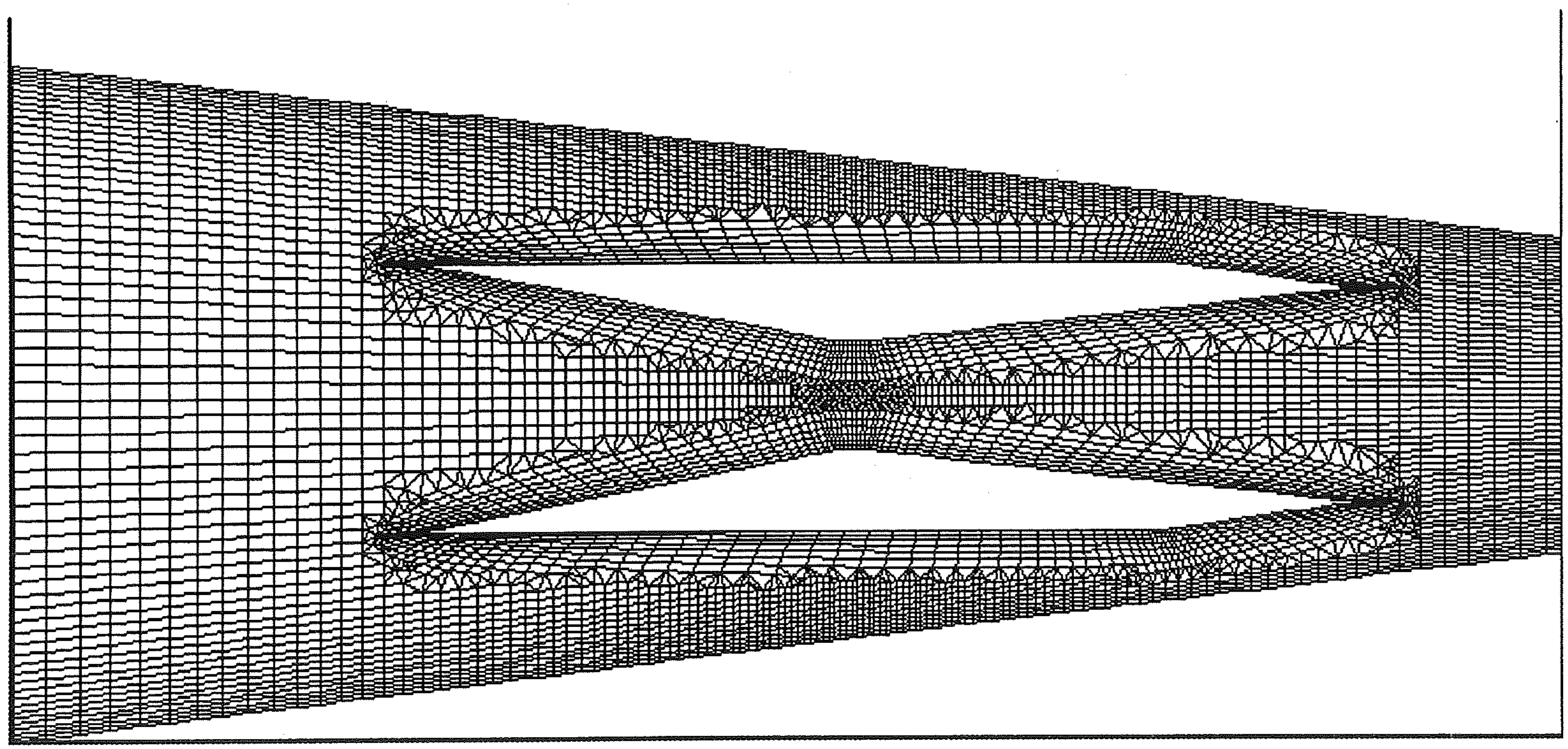

Scramjet Inlet Like Geometry (NPARC)

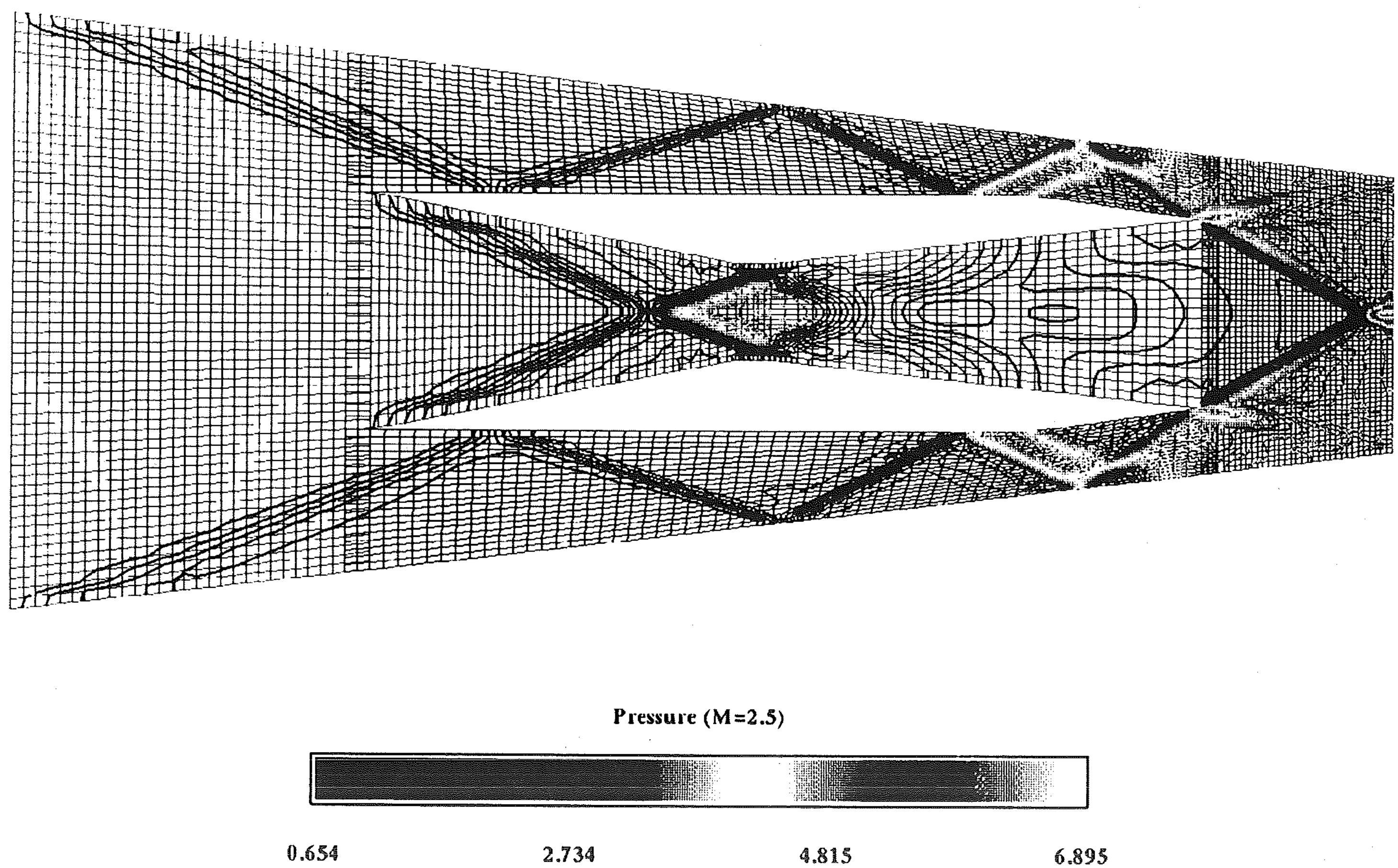

Pressure Distribution in Scramjet Inlet Like Geometry

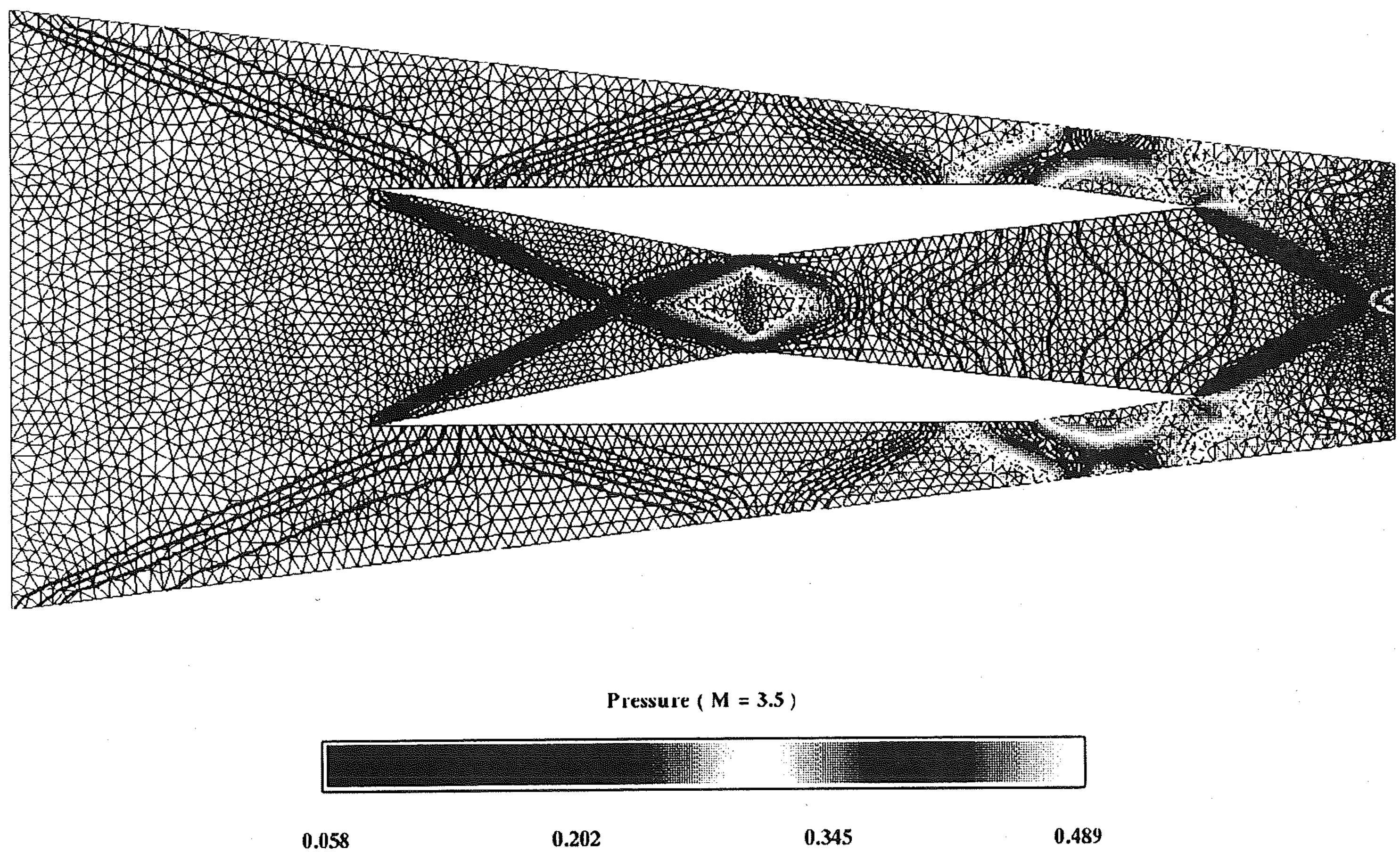

Scramjet Inlet Like Geometry (HYBRID)

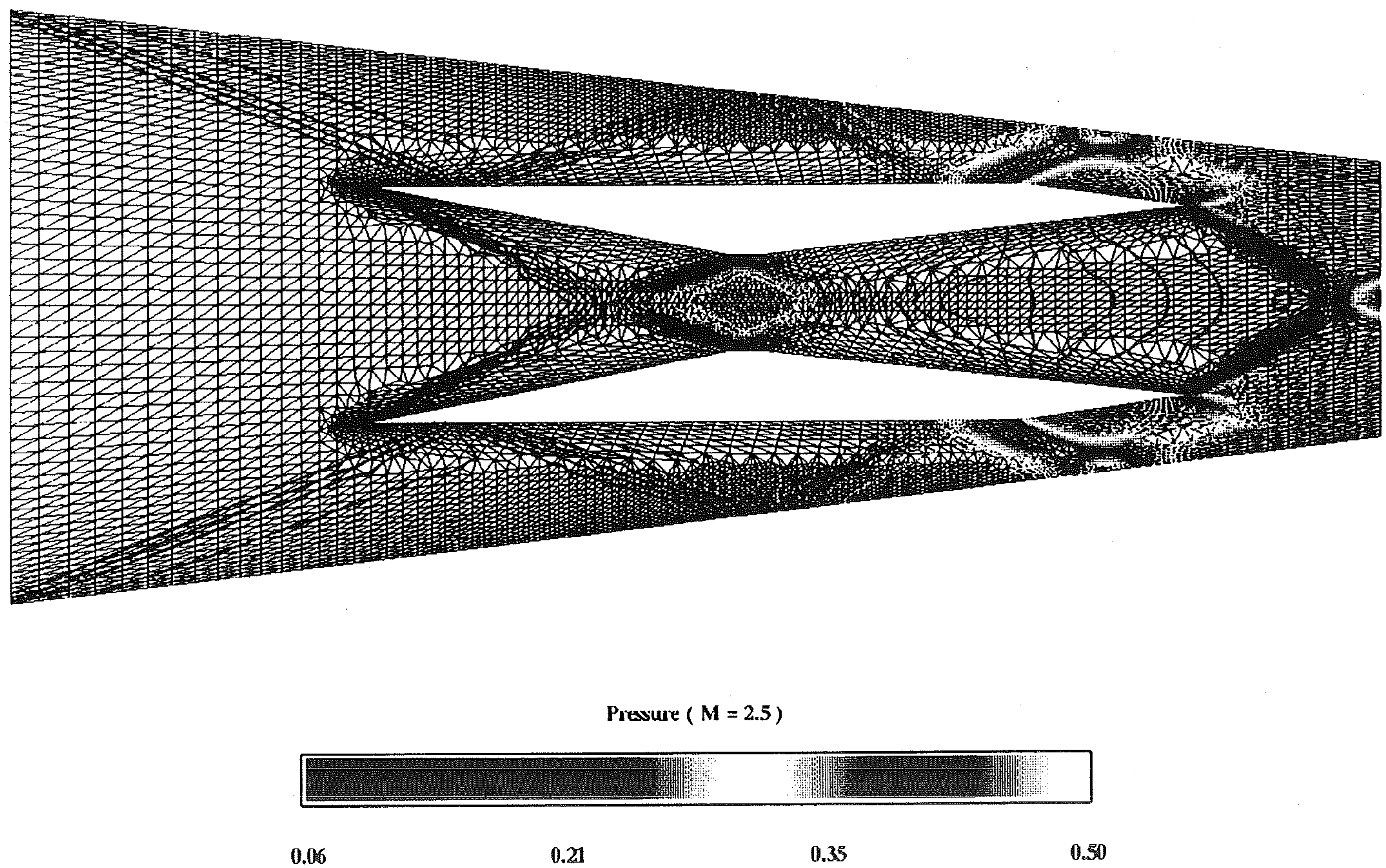

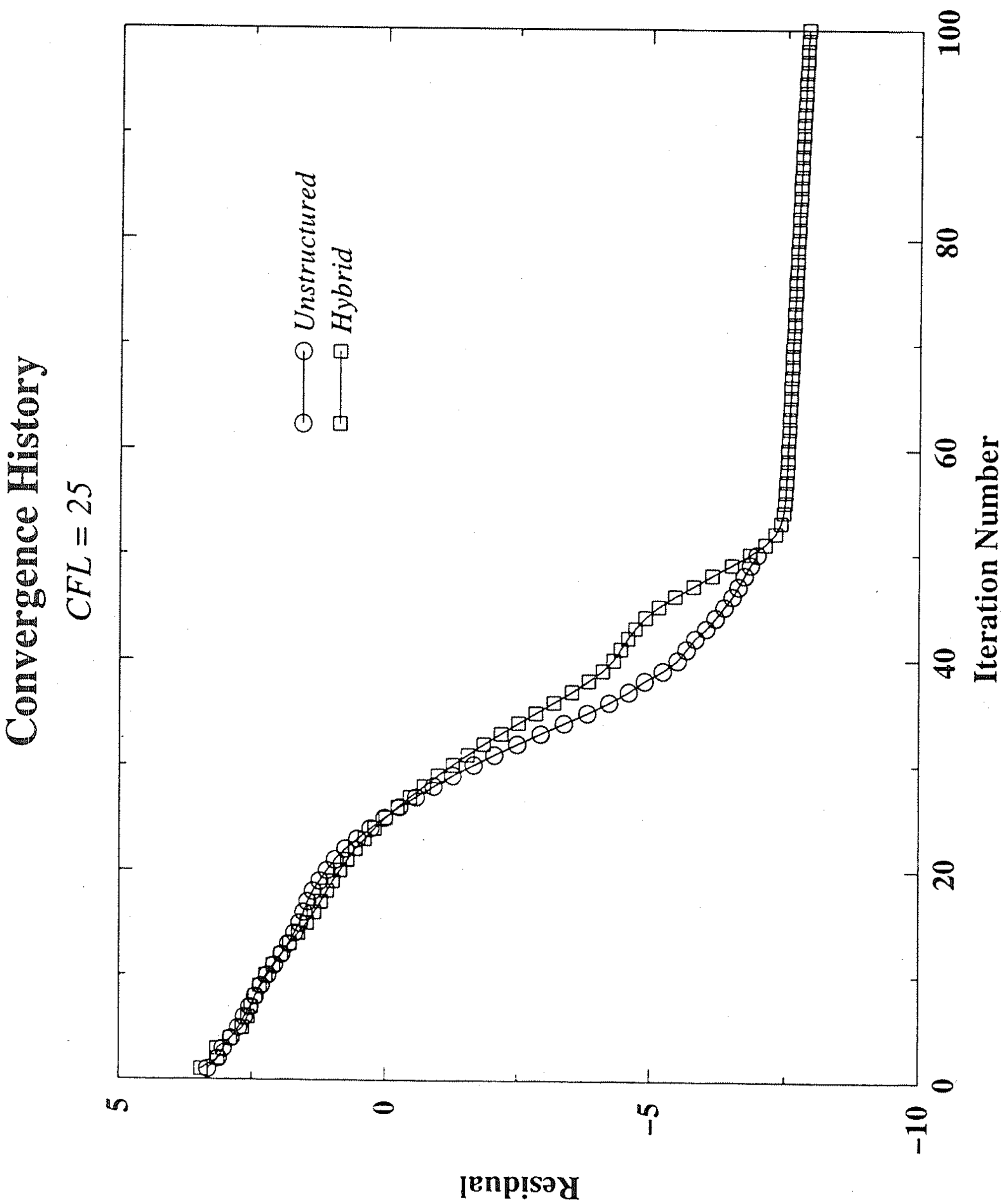
Convergence History
CFL = 25
Unstructured
Hybrid
Residual
Iteration Number
5
0
−5
−10
0
20
40
60
80
100

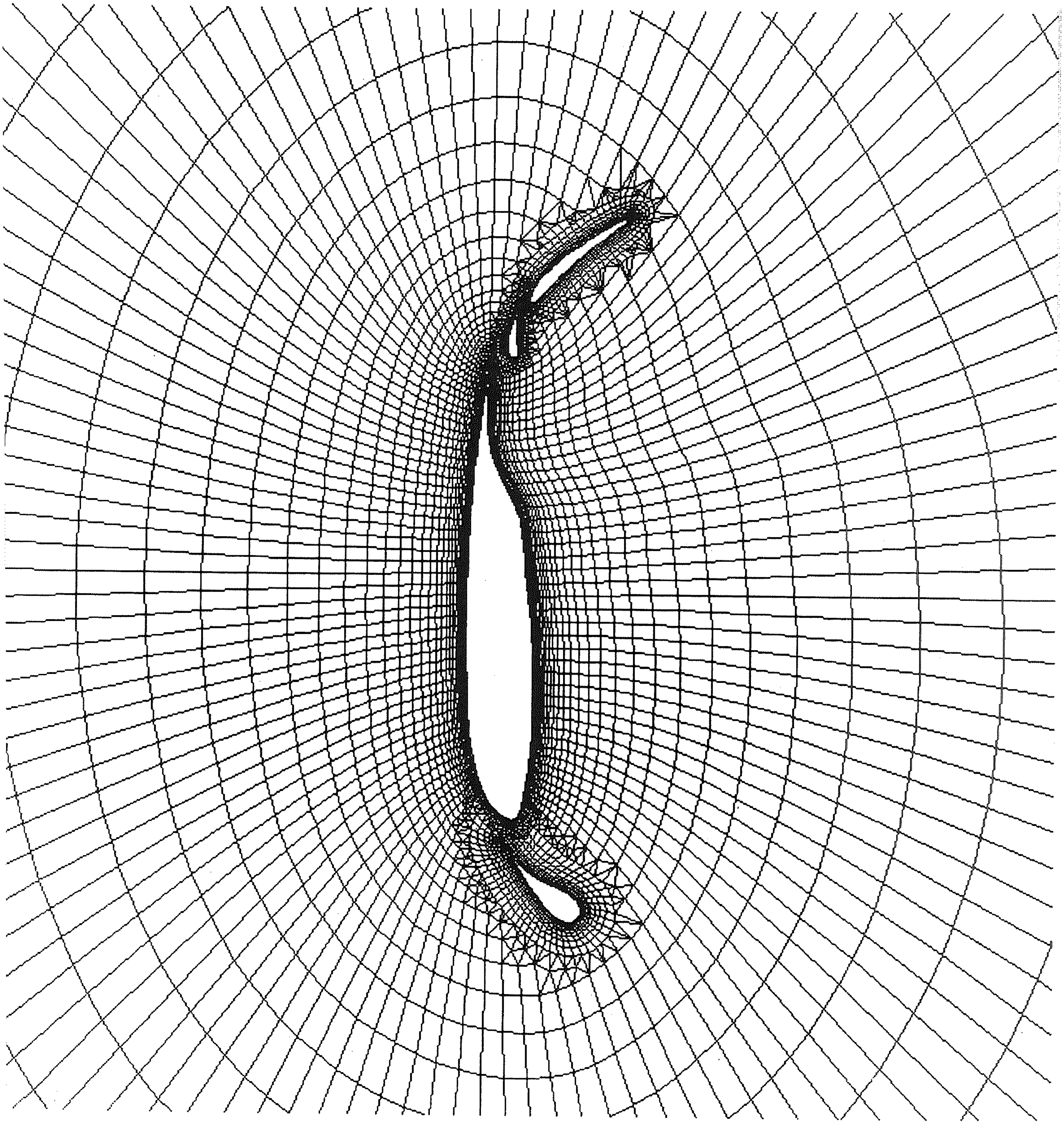

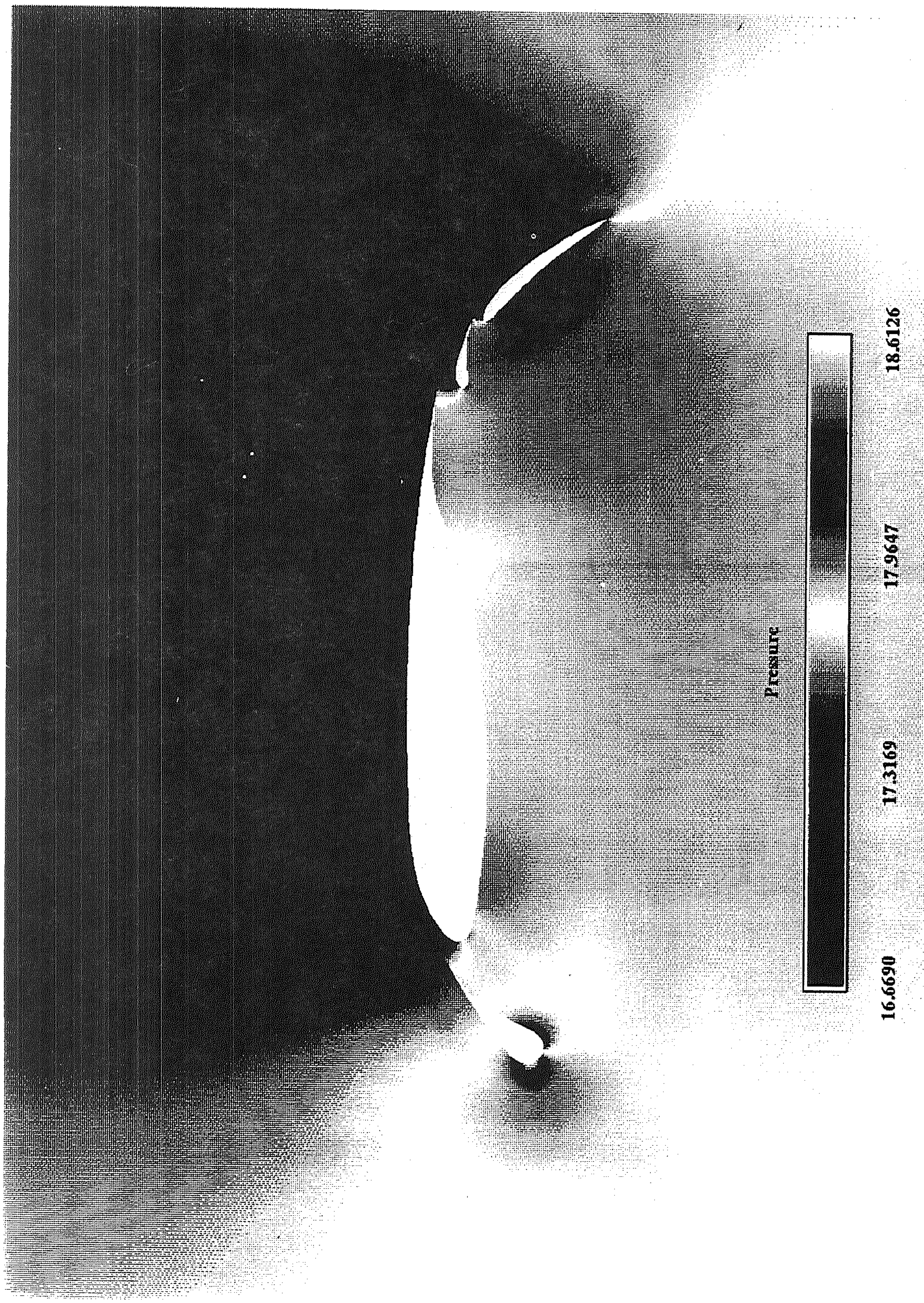

Mach Number 0.201, Alpha = 0.0, CFL = 1.5

CONCLUSION

- DEVELOPED AND VARIFIED 2-D HYBRID FLOW SIMULATION SYSTEM.
- NUMRICAL FLUX JACOBIANS GIVES BETTER CONVERGENCE
- TREATED STRUCTURED AND UNSTRUCTURED GRIDS IN HYBRID SYSTEM AS A SINGLE BLOCK

FUTURE WORK

- DEVELOP A 3–D NAVIER–STOKES FLOW SIMULATION SYSTEM USING HYBRID GRIDS
- TEST THE SYSTEM FOR INTERNAL AND EXTERNAL FLOW PROBLEMS

A Structured Grid Based Solution–adaptive Technique for Complex Separated Flows

by

Hugh Thornburg, Bharat K. Soni, Boyalakuntla Kishore, and Robert Yu
NSF Engineering Research Center for
Computational Field Simulation
Mississippi State University
Mississippi State, MS 39762

ABSTRACT

The objective of this work has been to enhance the predictive capability of widely used CFD codes through the use of solution adaptive gridding. Most problems of engineering interest involve multi–block grids and widely disparate length scales. Hence, it is desirable that the adaptive grid feature detection algorithm be developed to recognize flow structures of different type as well as differing intensity, and adequately address scaling and normalization across blocks. In order to study the accuracy and efficiency improvements due to the grid adaptation, it is necessary to quantify grid size and distribution requirements as well as computational times of non–adapted solutions. Flowfields about launch vehicles of practical interest often involve supersonic freestream conditions at angle of attack exhibiting large scale separated vortical flow, vortex–vortex and vortex–surface interactions, separated shear layers and multiple shocks of different intensity. In this work a weight function and an associated mesh redistribution procedure is presented which detects and resolves these features without user intervention. Particular emphasis has been placed upon accurate resolution of expansion regions and boundary layers.

Flow past a wedge at Mach = 2.0 is used to illustrate the enhanced detection capabilities of this newly developed weight function. Figure 1 presents weight functions evaluated using the previous procedure, lower half plane, as well as the current procedure, upper half plane.

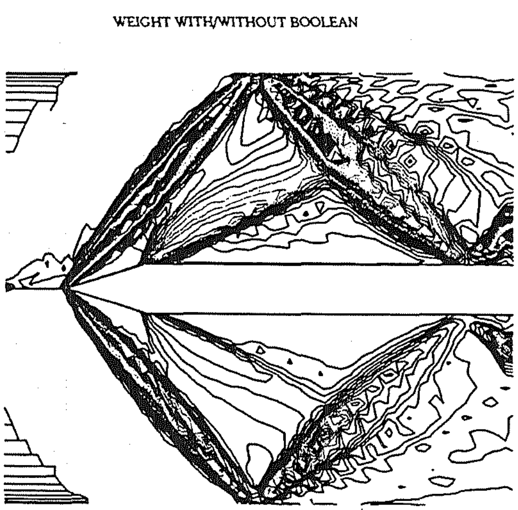

Figure 1. Comparison of Weight Functions.

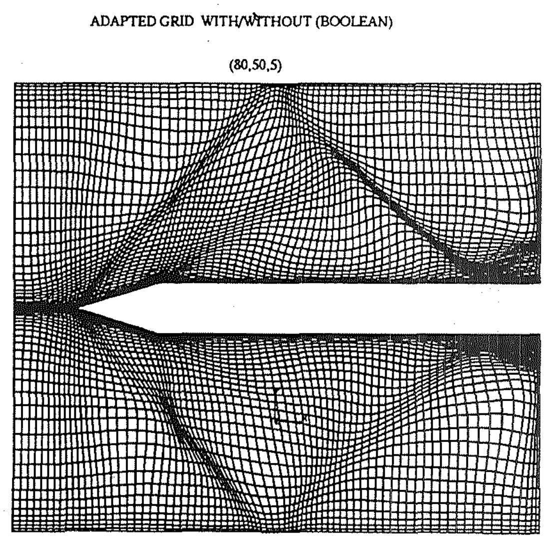

Figure 2. Comparison of Adapted Grids.

It can be observed that both weight functions clearly detected the primary shock. It can also be seen that the expansion fan, boundary layer, and the reflected shocks are much more clearly represented in the current weight function. Adapted grids using both weight function formulations are presented in Fig. 2. The high gradient regions of the expansion region are only reflected in the adapted grid using the new weight function. The reflected shock is also much sharper. Figure 3 compares the solution obtained using the current adaption procedure with that obtained using the original grid. The enhanced resolution is clearly evident.

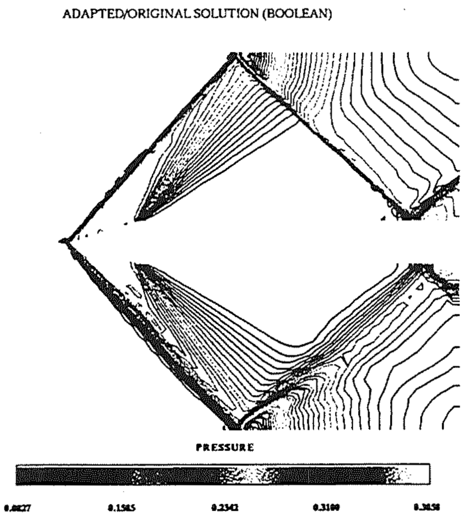

Figure 3. Comparison of Solutions Using Adapted Grid.

Supersonic flow at Mach=1.45 and 14 degree angle of attack has been simulated around a tangent–ogive cylinder. The grid and associated flow solution constructed after two adaption cycles using hybrid differencing of the grid equations and the current weight functions is presented is presented in Figure 4.

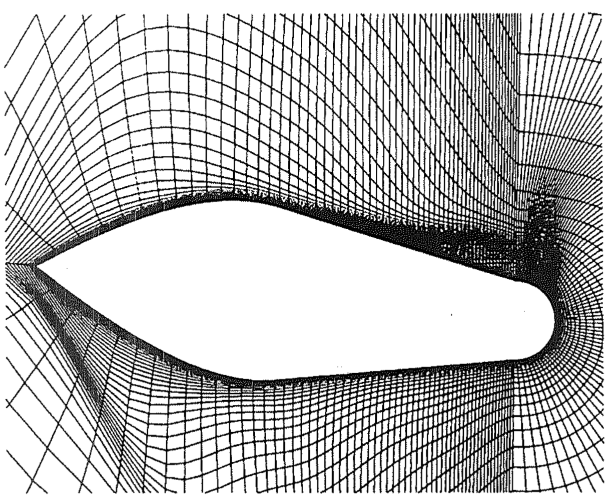

Figure 4. Adapted grid after two cycles.

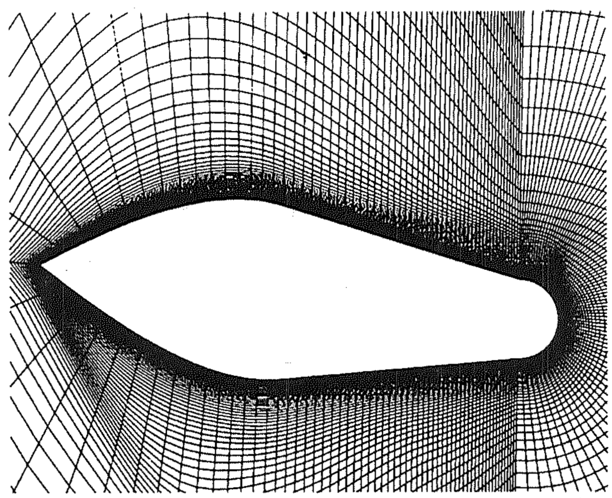

Figure 5. Adapted grid after two cycles.

Figure 5 presents the grid constructed using the previous weight function and the same flow conditions and number of adaptation cycles. Figures 5 and 6 present streamwise cuts of the two grids shown in Figs 4 and 5 at X/D = 5.5 and 7.5 respectively

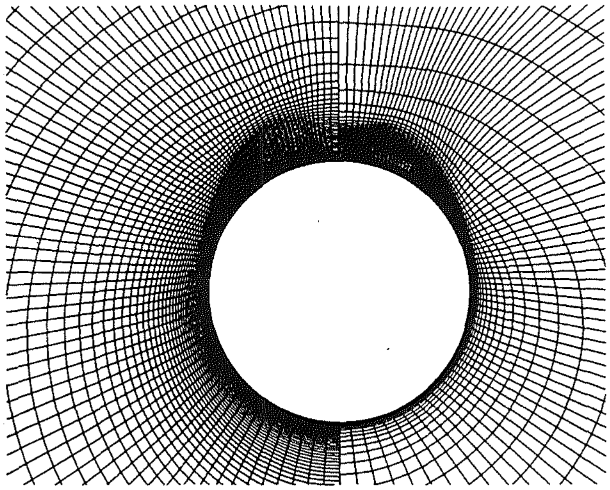

Figure 6. X/D = 5.5

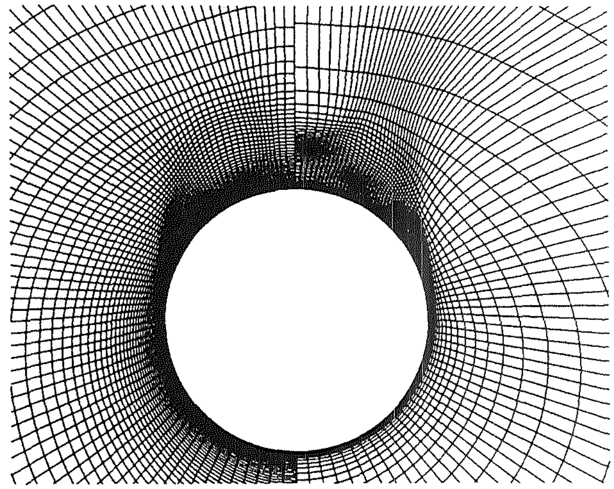

Figure 7. X/D = 8.5.

Figure 8 present the flow solution obtained using the NPARC [NASA 1993] flow solver, the KE turbulence model option and two adaptation cycles. Figure 9 presents the associated weight function.

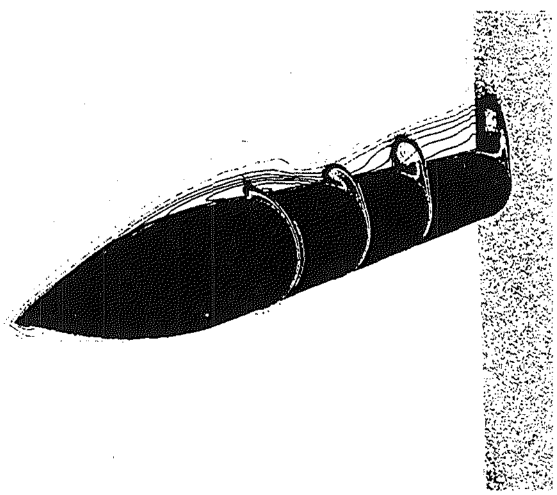

Figure 8 Normalized Stagnation Pressure.

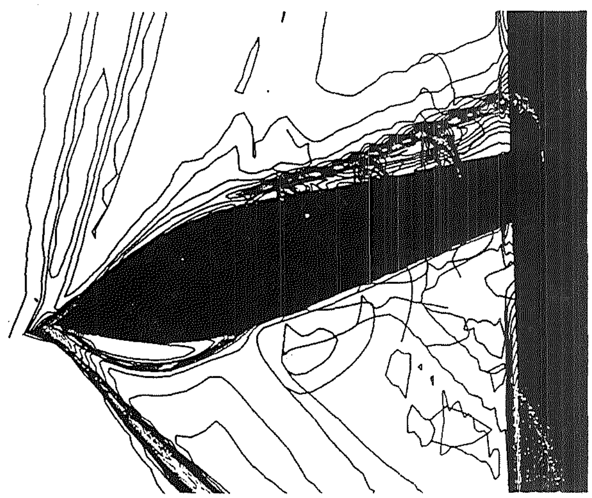

Figure 9. Weight Function.

Examples will presented to demonstrate the capability for solution–adaptive regridding of multi-block launch vehicle simulations.

References

1. Thompson, J.F., Warsi, Z.U.A. and Mastin, C.W., Numerical Grid Generation: Foundations and Applications, North–Holland, Amsterdam. 1985.
2. Eiseman, P.R., "Alternating Direction Adaptive Grid Generation," AIAA Paper 83–1937, 1983.
3. Soni, B.K., "Structured Grid Generation in Computational Fluid Dynamics," Vichnevetsky, R., Knight, D., and Richter, G. (eds.), Advances in Computer Methods for Partial Differential Equations VII, Rutgers University, pp 689–695, June 1992.

4. Buning, P.G. and Steger, J.L., "Graphics and Flow Visualization in Computational Fluid Dynamics," AIAA Paper 85–1507–CP, Proceedings of the AIAA 7th Computational Fluid Dynamics Conference, 1985.
5. NASA LeRC and USAF AEDC, "NPARC 1.0 User Notes," June 1993.
6. Ghia, K.N., Ghia, U., Shin, C.T. and Reddy, D.R., "Multigrid Simulation of Asymptotic Curved–Duct Flows Using a Semi–Implicit Numerical Technique," Computers in Flow Prediction and Fluid Dynamics Experiments, ASME Publication, New York 1981.
7. Soni, B.K. and Yang, J.C., "General Purpose Adaptive Grid Generation System," AIAA–92–0664, 30th Aerospace Sciences Meeting, Reno, NV, Jan. 6–9, 1992.
8. Thornburg, H.J. and Soni, B.K., "Weight Functions inGrid Adaption," Proceedings of the 4th International Conference in Numerical Grid Generation in Computational Fluid Dynamics and Related Fields held at Swansea, Wales 6–8th April 1994.
9. Soni, B.K., Thompson, J.F., Stokes, M.L. and Shih, M.H., "GENIE++, EAGLEView and TIGER: General and Special Purpose Interactive Grid Systems," AIAA–92–0071, 30th Aerospace Sciences Meeting, Reno, NV, Jan. 6–9, 1992.
10. NASA LaRC, "User Document for CFL3D/CFL3DE (Version 1.0)", 1993.
11. Thompson, J.F., "A Survey of Dynamically–Adaptive Grids in Numerical Solution of Partial Differential Equations," Applied Numerical Mathematics, vol. 1, pp 3–27, 1985.

MISSISSIPPI STATE UNIVERSITY / National Science Foundation

A Structured Grid Based Solution–Adaptive Technique for Complex Separated Flows [1]

Hugh J. Thornburg, Bharat K. Soni, Kishore Boyalakuntla, and Robert Yu

Workshop for CFD Applications in Rocket Propulsion and Launch Vehicle Technology
April 25–27, 1995
Huntsville, Alabama

[1] *This research was supported, in part, by the Army Research Laboratory.*

ENGINEERING RESEARCH CENTER FOR COMPUTATIONAL FIELD SIMULATION
COMPLEX GEOMETRY / COMPLEX PHYSICS

OBJECTIVES

Improved resolution of complex flows through the use of solution adaptive gridding

1. Develop a weight function suitable for use with a solution adaptive grid redistribution procedure for complex flows, including viscous dominated separation.
2. Minimum user inputs.
3. Appropriate feature detection for a wide range of flow features (Vorticies, Shear layers, Shocks).
4. Robust redistribution procedure for use with weight function.

GOVERNING EQUATIONS FOR GRID MOVEMENT

1. Inverted form:

$$\sum_{i=1}^{3}\sum_{j=1}^{3} g^{ij}\,\vec{r}_{\xi^i\xi^j} + \sum_{k=1}^{3} g^{kk}\,P_k\,\vec{r}_{\xi^k} = 0$$

Where:

$\bar{r}_{ij}$: Position vector,
g^{ij} : Contravariant metric tensor,
ξ^i : Curvilinear coordinate, and
P_k : Control Function.

2. Control of distribution and characteristics of grid system can be achieved by varying control Functions P_k.

$$P_i = (P_{\substack{\text{initial}\\\text{geometry}}})_i + c_i \, (P_{wt}) \qquad (i = 1,2,3)$$

where $(P_{\substack{\text{initial}\\\text{geometry}}})$: control function based on initial grid geometry

P_{wt} : control function based on gradient of flow parameter

c_i : constant weight factors

$$P_i^{(n)} = P_i^{(n-1)} + c_i \, (P_{wt})^{(n-1)} \qquad (i = 1,2,3)$$

where

$$P_i^{(1)} = (P_{\substack{\text{initial}\\\text{geometry}}})_i^{(0)} + c_i \, (P_{wt})^{(0)} \qquad (i = 1,2,3)$$

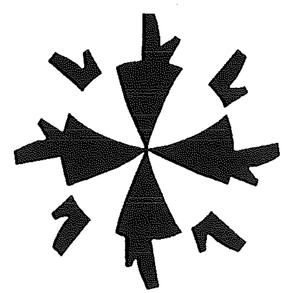

EVALUATION OF FORCING FUNCTIONS

1. Smoothnes.
2. Near orthogonality.
3. Equidistribution of 'error' or weight function.
4. One–dimensional equidistribution law

   $W X_\xi$ = constant, where W is a weight factor.
5. Poisson equation form, (Anderson, Thompson), obtained by differentiating equidistribution law.

   $W X_{\xi\xi} + W_\xi X_\xi = 0,$

   $X_{\xi\xi} + P X_\xi = 0,$

   i.e. $P = W_\xi / W$
6. For Multiple dimensions:

   $P_k = W_\xi{}^k / W, \; k = 1,2,3$

CHARACTERISTICS OF WEIGHT FUNCTIONS

1. Weight functions approximately equidistributed over solution domain.
2. Determine grid spacing and characteristics.
3. Approximation to local truncation error.
   - Use lower order derivatives to approximate high order truncation error terms.
   - Detect structures of disparate strength.
   - Minimum variation of coefficients.

EVALUATION OF WEIGHT FUNCTIONS

1. Density or pressure is not sufficient for viscous flows.
2. Boolean sums used to eliminate 'multiplying' effect.
3. Relative derivatives are necessary to detect features of varying intensity.
4. Regions of zero flow variables require special treatment.
5. Nearly uniform flowfields require minimum normalization value.

WEIGHT FUNCTIONS

$$W = \frac{W^1}{max(W^1, W^2, W^3)} \oplus \frac{W^2}{max(W^1, W^2, W^3)} \oplus \frac{W^3}{max(W^1, W^2, W^3)}$$

Where, $k=1,2,3,$ *and*

$$W^k = 1 + \frac{\frac{|\varrho_{\xi^k}|}{|\varrho|+\varepsilon}}{\left(\frac{|\varrho_{\xi^k}|}{|\varrho|+\varepsilon}\right)_{max}} \oplus \frac{\frac{|(\varrho u)_{\xi^k}|}{|(\varrho u)|+\varepsilon}}{\left(\frac{|(\varrho u)_{\xi^k}|}{|(\varrho u)|+\varepsilon}\right)_{max}} \oplus \frac{\frac{|(\varrho v)_{\xi^k}|}{|(\varrho v)|+\varepsilon}}{\left(\frac{|(\varrho v)_{\xi^k}|}{|(\varrho v)|+\varepsilon}\right)_{max}} \oplus \frac{\frac{|(\varrho w)_{\xi^k}|}{|(\varrho w)|+\varepsilon}}{\left(\frac{|(\varrho w)_{\xi^k}|}{|(\varrho w)|+\varepsilon}\right)_{max}}$$

$$\oplus \frac{\frac{|\varrho_{\xi^k\xi^k}|}{|\varrho|+\varepsilon}}{\left(\frac{|\varrho_{\xi^k\xi^k}|}{|\varrho|+\varepsilon}\right)_{max}} \oplus \frac{\frac{|(\varrho u)_{\xi^k\xi^k}|}{|(\varrho u)|+\varepsilon}}{\left(\frac{|(\varrho u)_{\xi^k\xi^k}|}{|(\varrho u)|+\varepsilon}\right)_{max}} \oplus \frac{\frac{|(\varrho v)_{\xi^k\xi^k}|}{|(\varrho v)|+\varepsilon}}{\left(\frac{|(\varrho v)_{\xi^k\xi^k}|}{|(\varrho v)|+\varepsilon}\right)_{max}} \oplus \frac{\frac{|(\varrho w)_{\xi^k\xi^k}|}{|(\varrho w)|+\varepsilon}}{\left(\frac{|(\varrho w)_{\xi^k\xi^k}|}{|(\varrho w)|+\varepsilon}\right)_{max}}$$

The symbol $\oplus$ represents the Boolean sum. Note that the directional weight functions are scaled using a common maximum in order to maintain the relative strength.

OVERALL SOLUTION PROCEDURE

1. Obtain initial flow solution.
2. Adapt grid.
3. Interpolate solution onto adapted grid.
4. Restart flow solution.
5. Repeat steps 2–4 until satisfactory result.

ADAPTIVE GRID PROCEDURE

1. Read PLOT3D grid and solution files.
2. Evaluate weight function,
   (no input pararmeters).
3. Evaluate and smooth P_k.
4. Integrate grid.
5. Interpolate P_k onto current adapted grid.
6. Repeat steps 4 and 5 until convergence.
7. Ouput adapted grid.

SOLUTION OF GRID EQUATIONS

1. Solution difficulties transferred form flow equations to grid equations.
2. Accuracy not as important for postulated law.
3. Adaptive Central/Upwind differencing scheme, based upon forcing function gradients.
4. Integrated in time using CSIP.
5. Non–linear terms are quasi–linearized.
6. Explicit boundary point movement.
7. Precise geometry definition is critical.

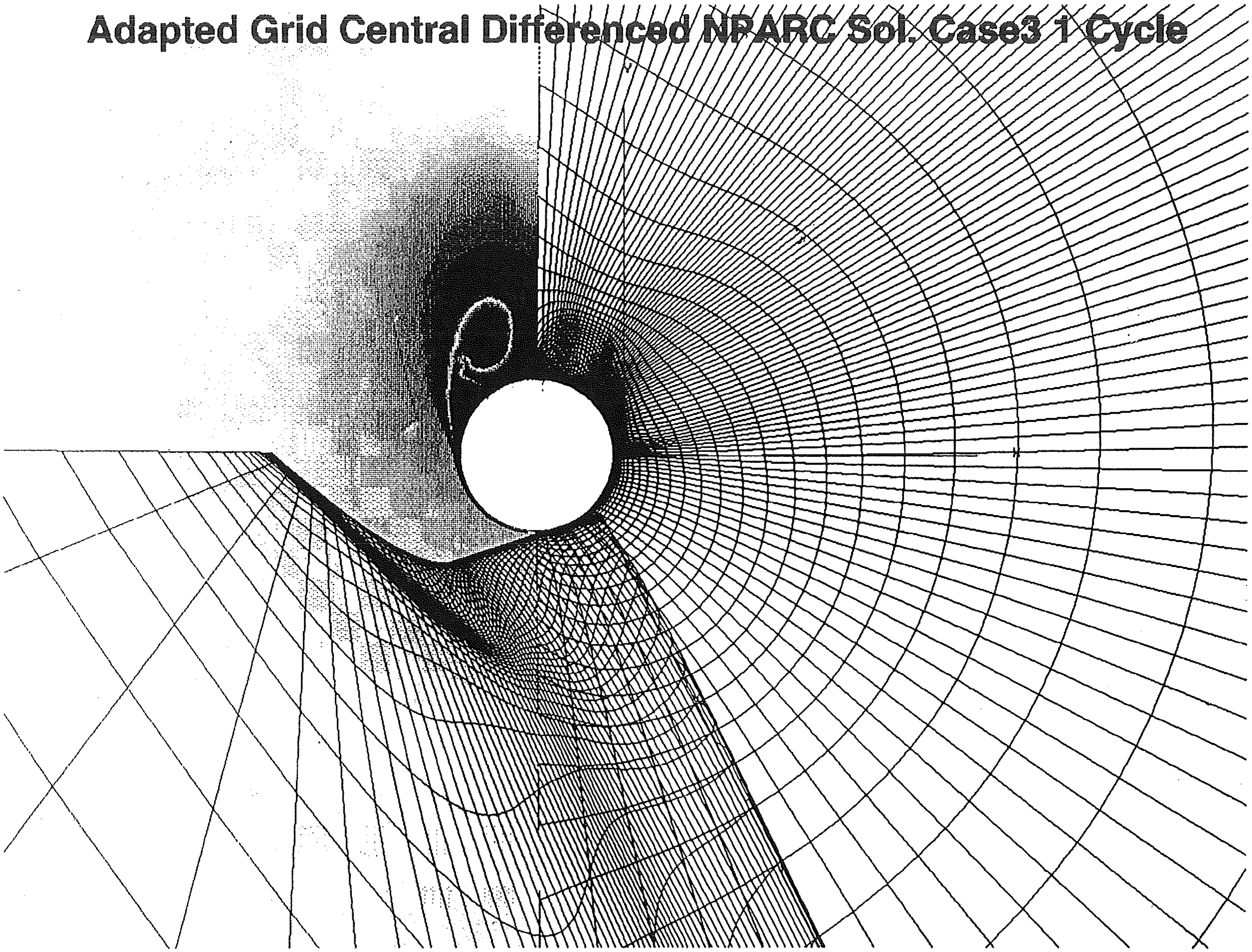
Adapted Grid Central Differenced NPARC Sol. Case3 1 Cycle

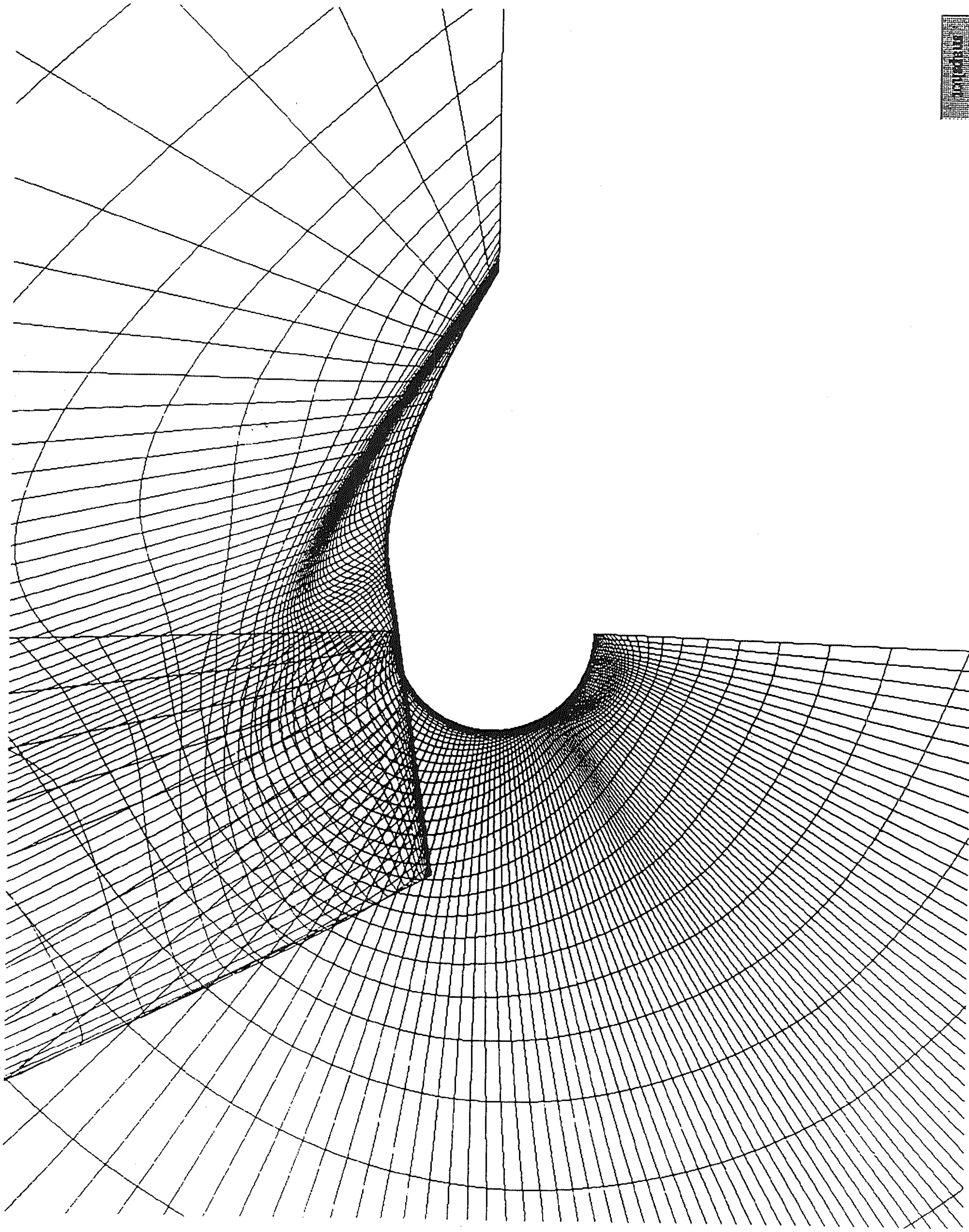

BOUNDARY POINT MOVEMENT

1. Very important.
   - Orthogonality.
   - Skewness.
2. Non Uniform Rational B–Spline (NURBS) representaion of arbitrary surface(Yu).
3. Boundary surface redistribution based on specified region of surface.
   - Explicit.
   - Local iteration for desired distribution.
   - Can be used to keep sharp corners, and to transfer information between blocks.

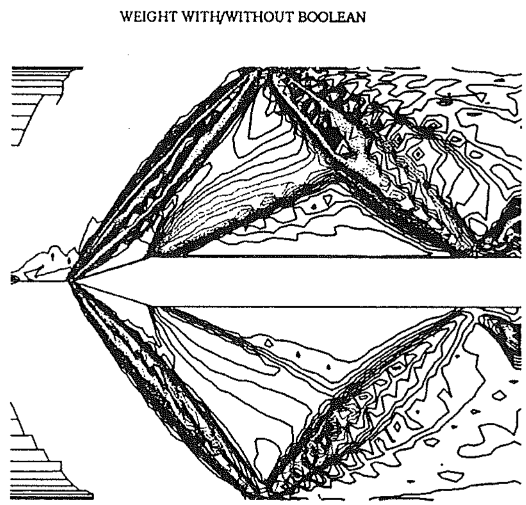

Figure 1. Comparison of Weight Functions.

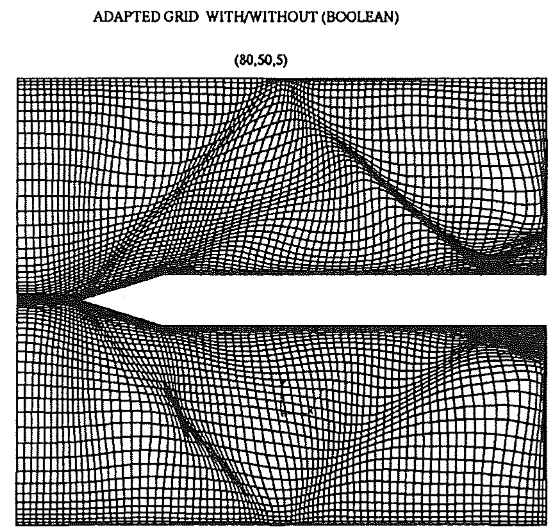

Figure 2. Comparison of Adapted Grids.

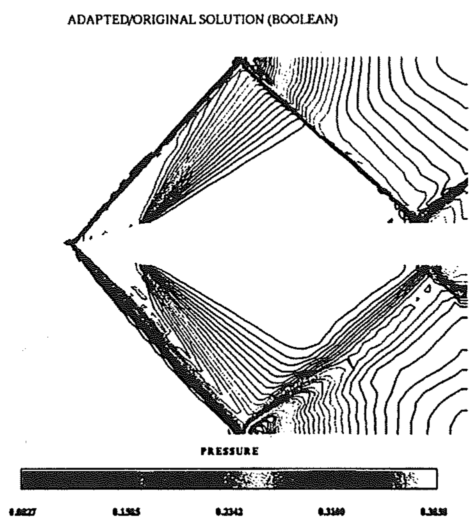

Figure 3. Comparison of Solutions Using Adapted Grid.

Case 1 NPARC Sol Grid 7 KE Model

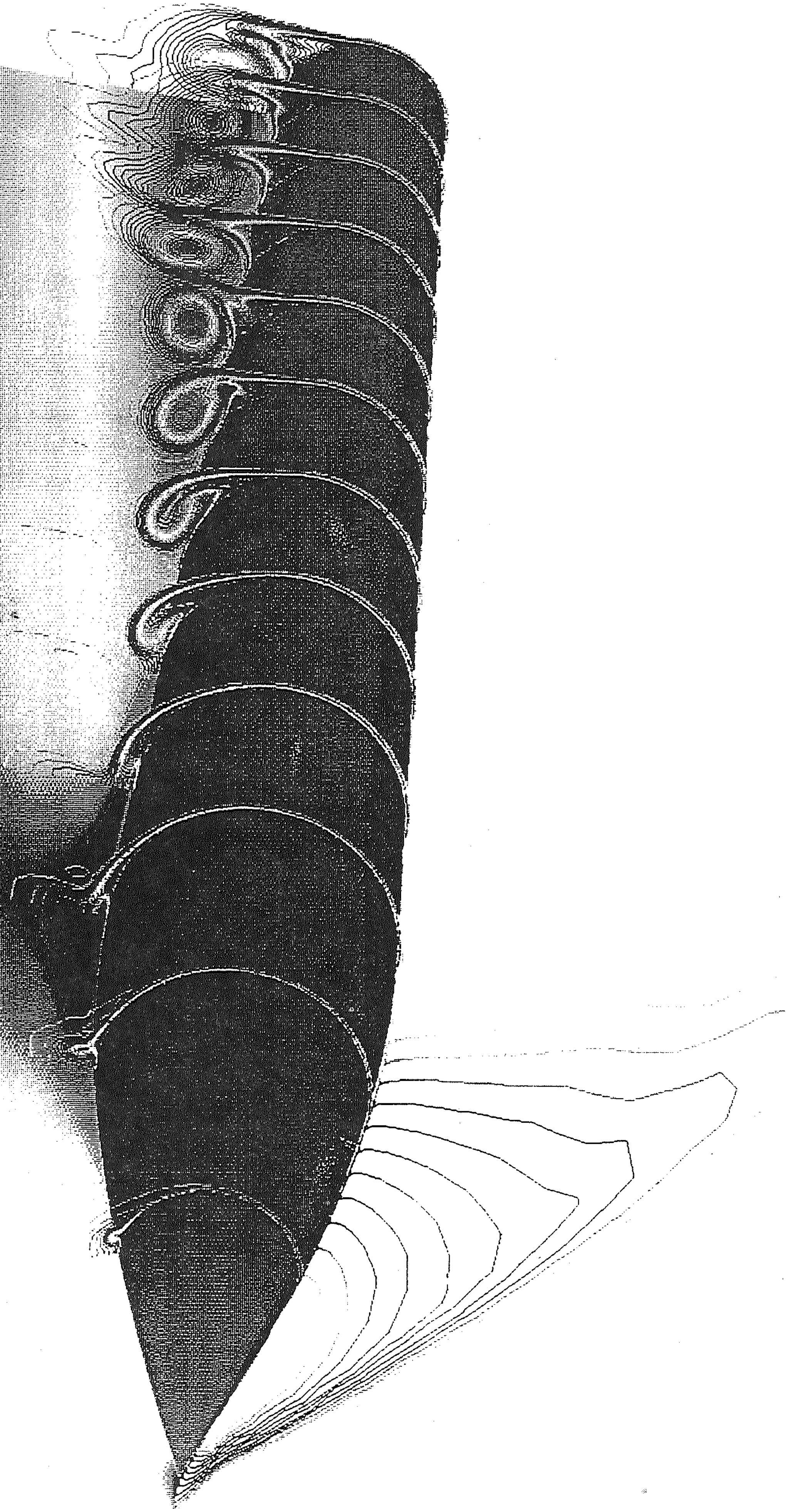

Case 1 NPARC Grid 7 a2 KE Model

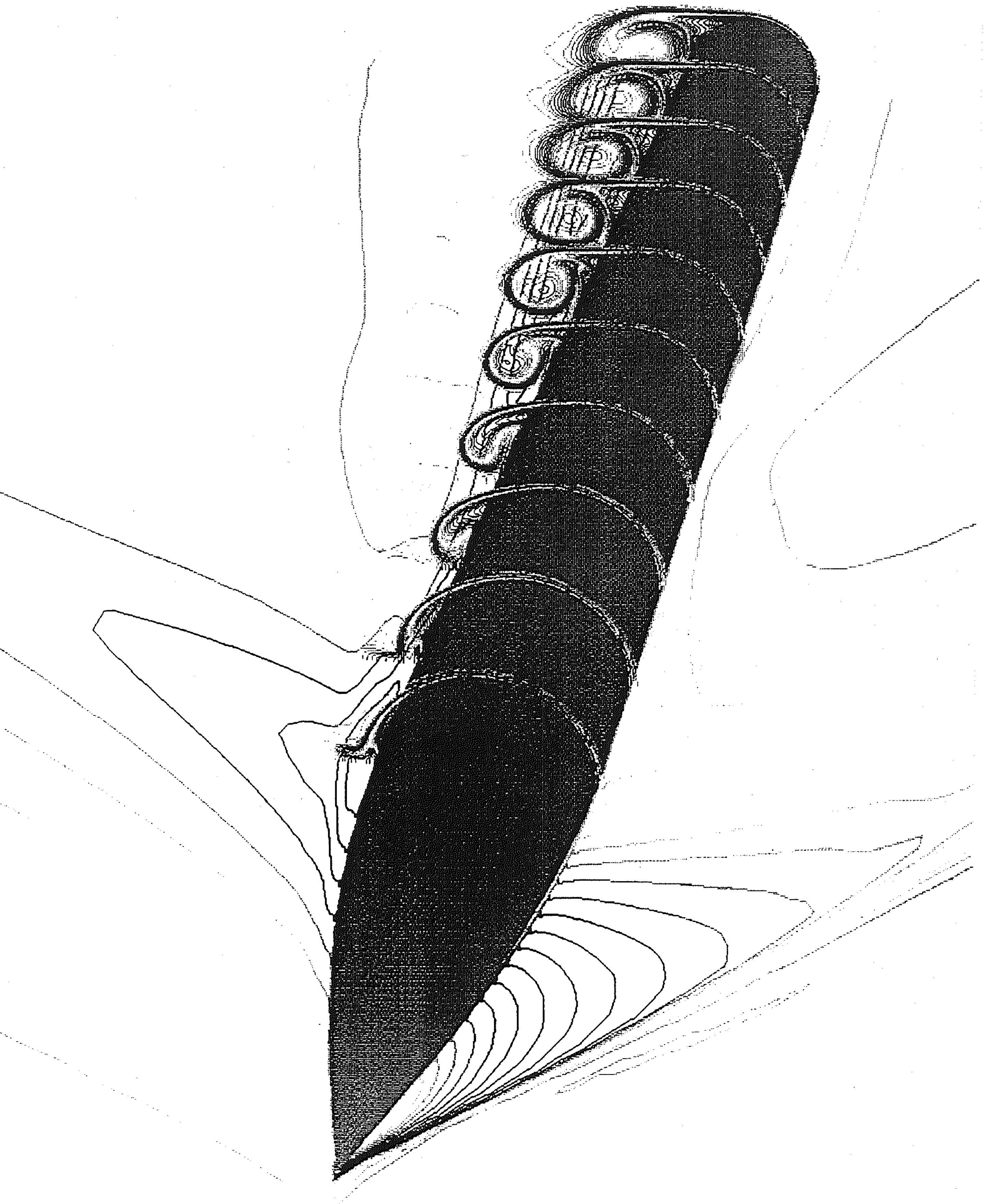

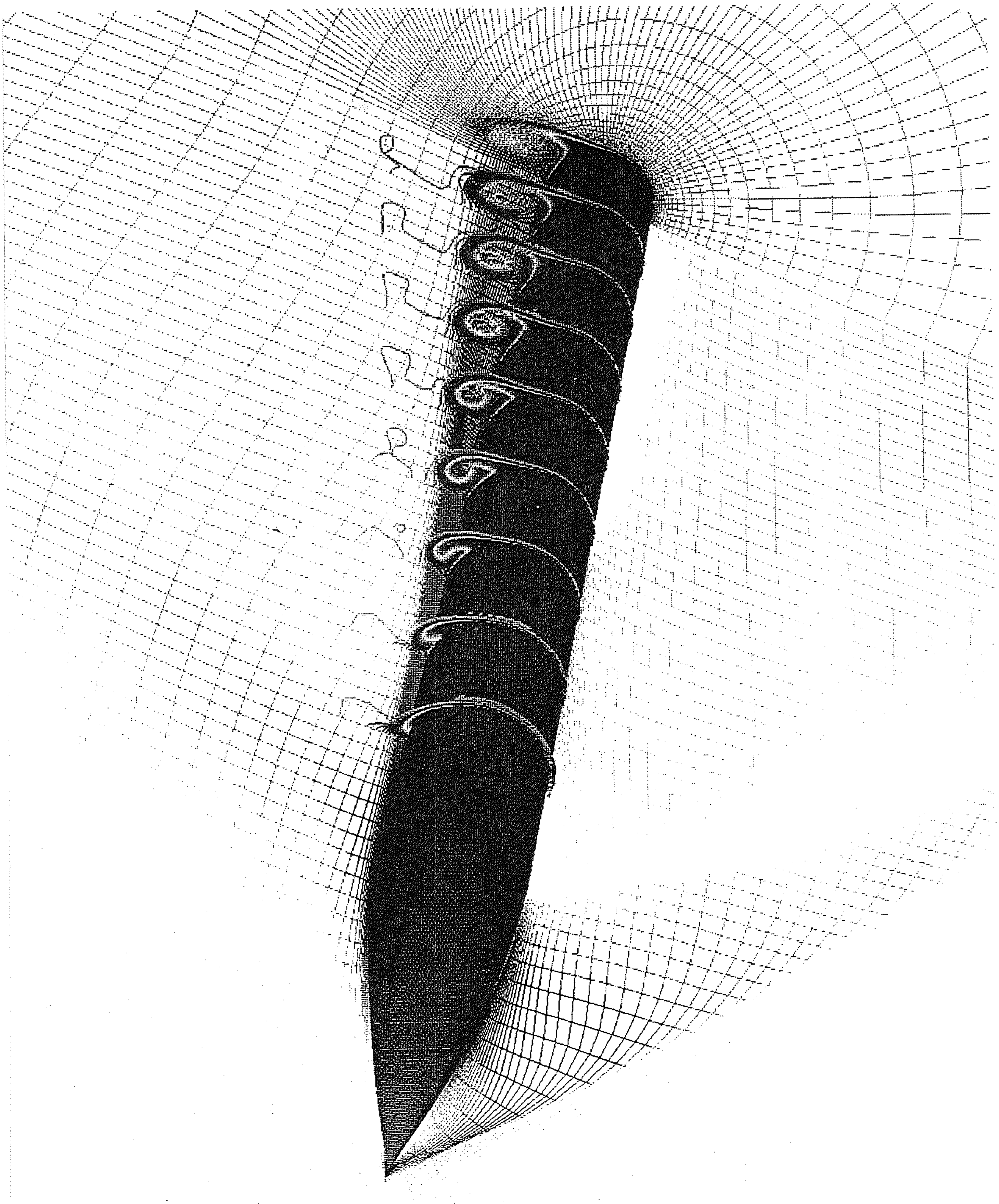

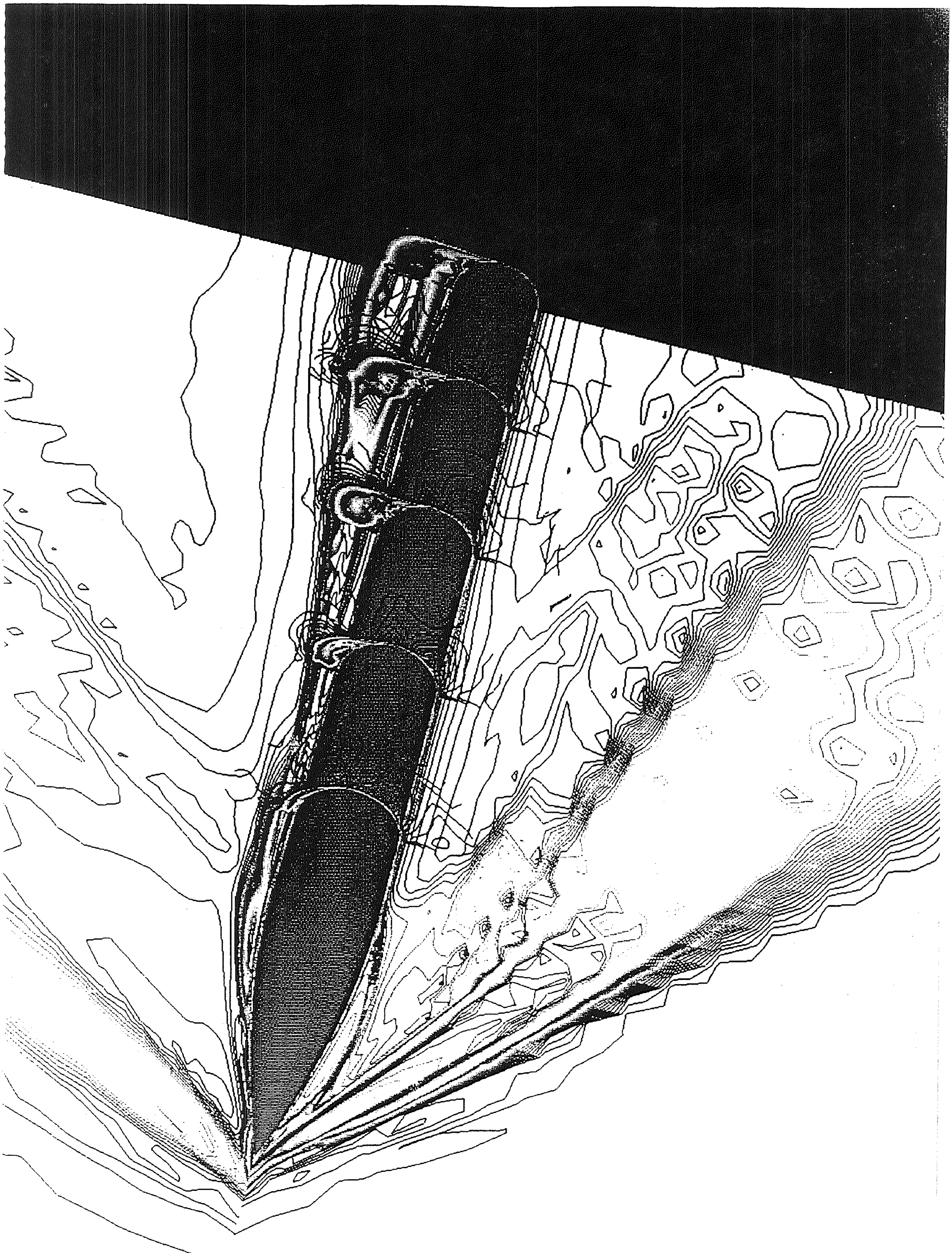

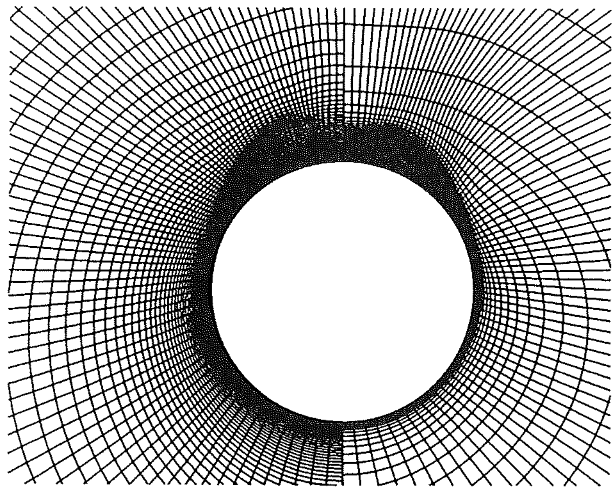

Figure 6. X/D = 5.5

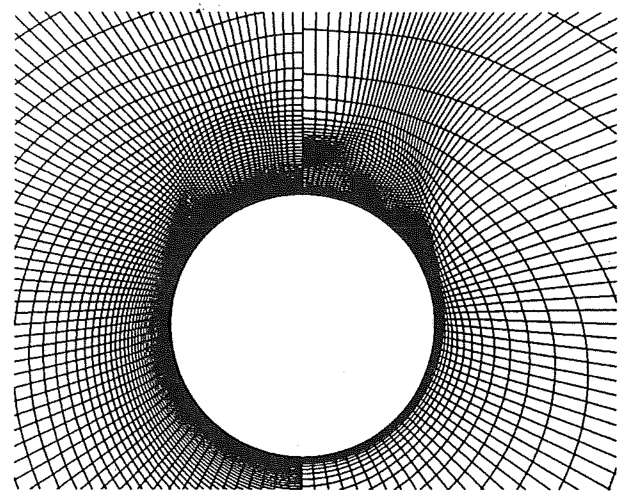

Figure 7. X/D = 8.5.

Gimble Nozzle, Left UBIFLOW Density, Right Weight Function

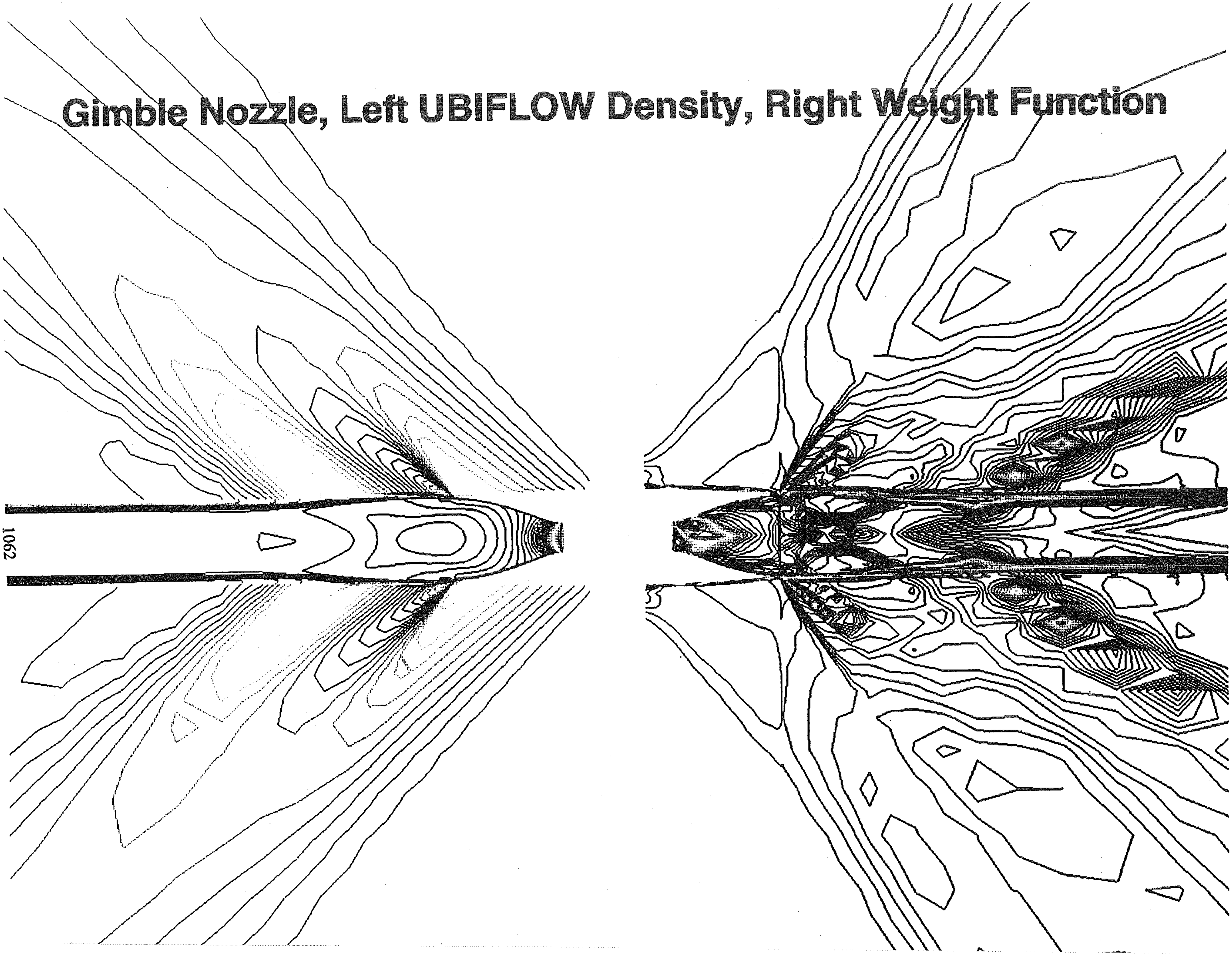

Gimble Nozzle, Left UBIFLOW Density, Right Marked Cells

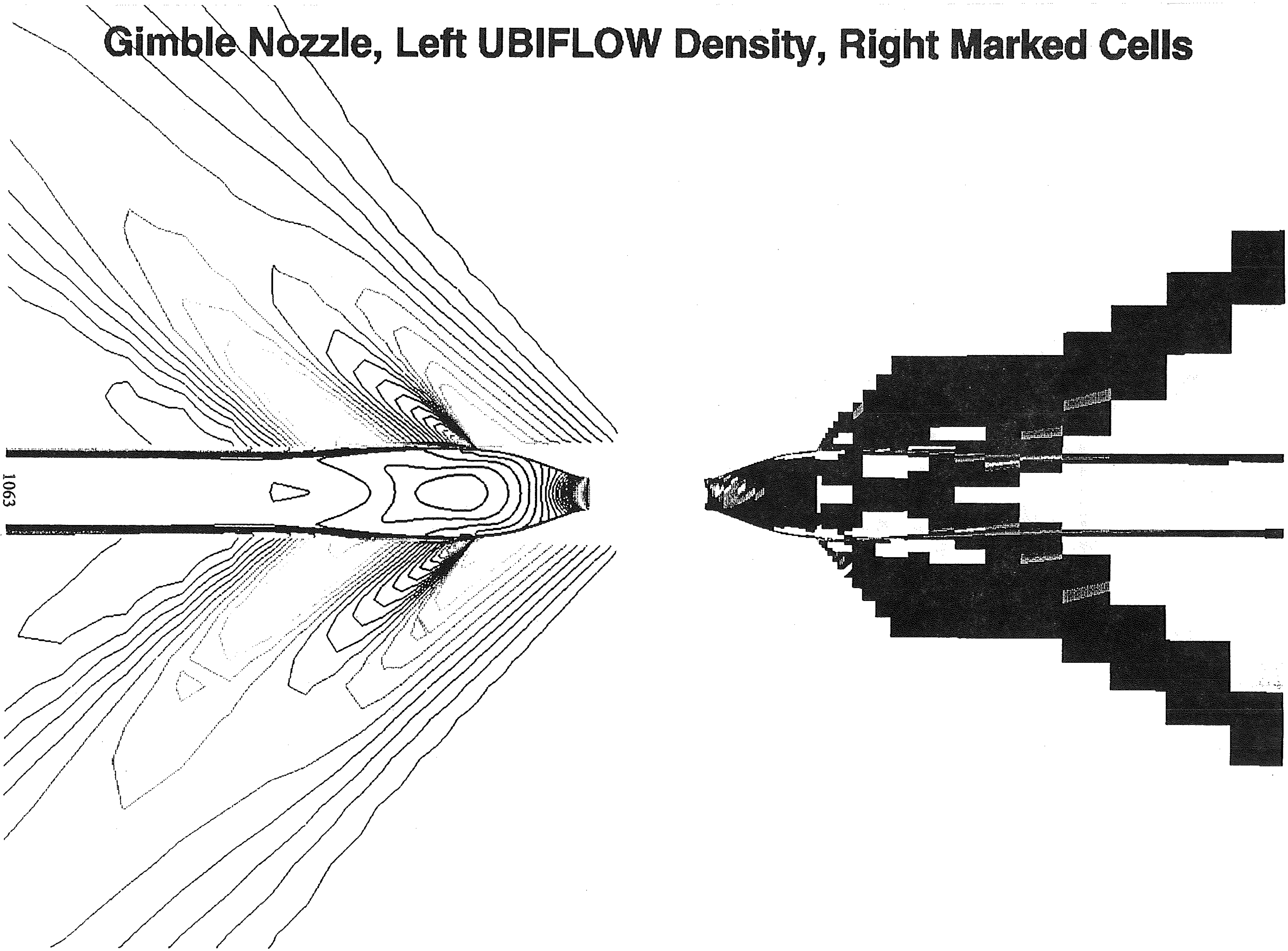

Gimble Nozzle, Left UBIFLOW Density, Right Weight Function

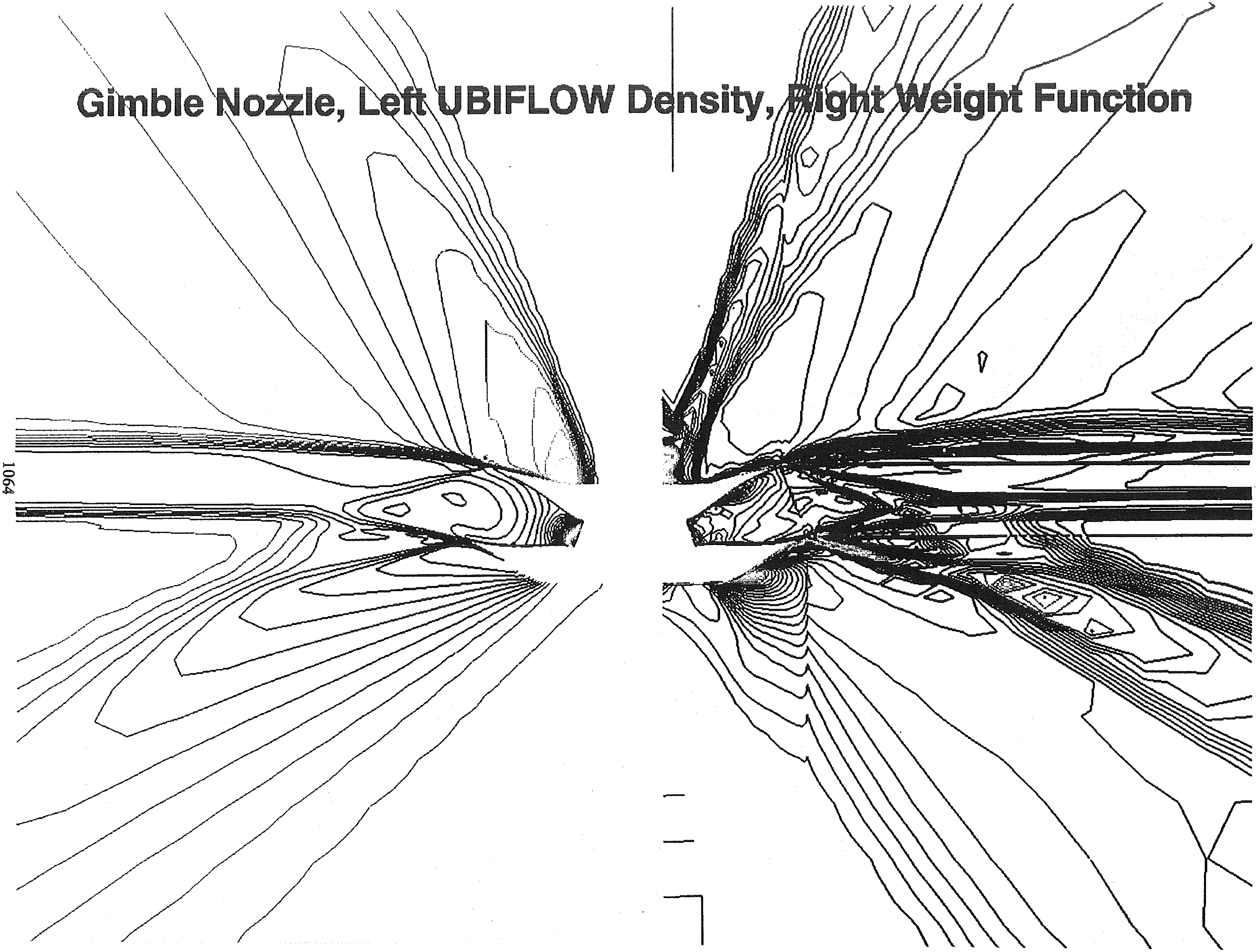

Gimble Nozzle, Left UBIFLOW Density, Right Marked Cells

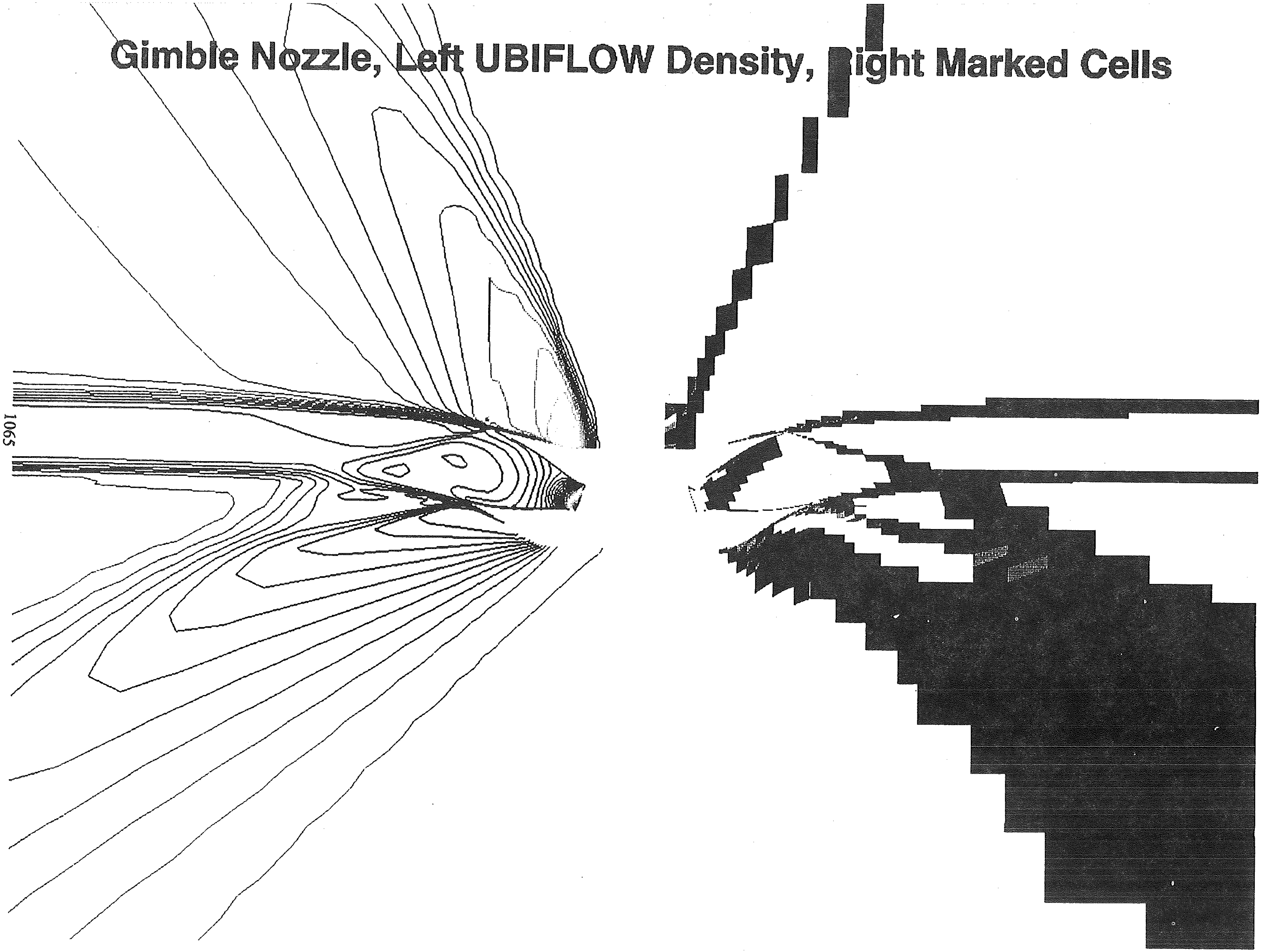

SUMMARY

1. Developed Weight function which requires no user input.
2. Implemented adaptive upwind/central difference scheme.
3. Demonstrated enhanced grid resolution.
   - Thinner shocks.
   - Stronger circular vorticies.
   - Lower values of artificial dissipation may be used.
   - Larger time steps may be used.
   - Improved convergence behaviour.
   - More closely resembles experimental data.

ONGOING WORK

1. Multiblock problems.
   - Global scaling across blocks.
   - Block interface or block point movement.
2. Local refinement (Solver of Koomullil)
3. Coupling with flow solver.
4. Coding efficiency.
5. Reacting flow.
   - Include temperature in weight function.
6. Unsteady flow problems.
   - P_k, viewed as velocities in temporally parabolized grid equations.

ADAPTED DISTRIBUTION MESH

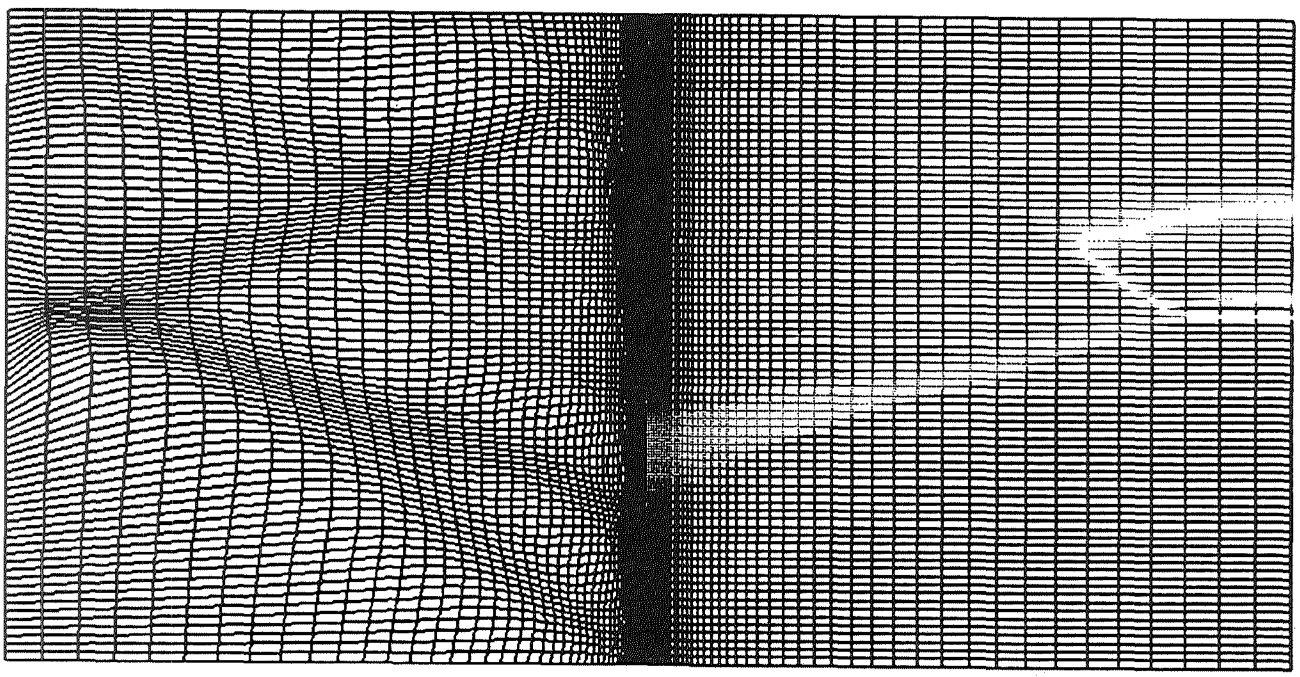

ADAPTED GRID

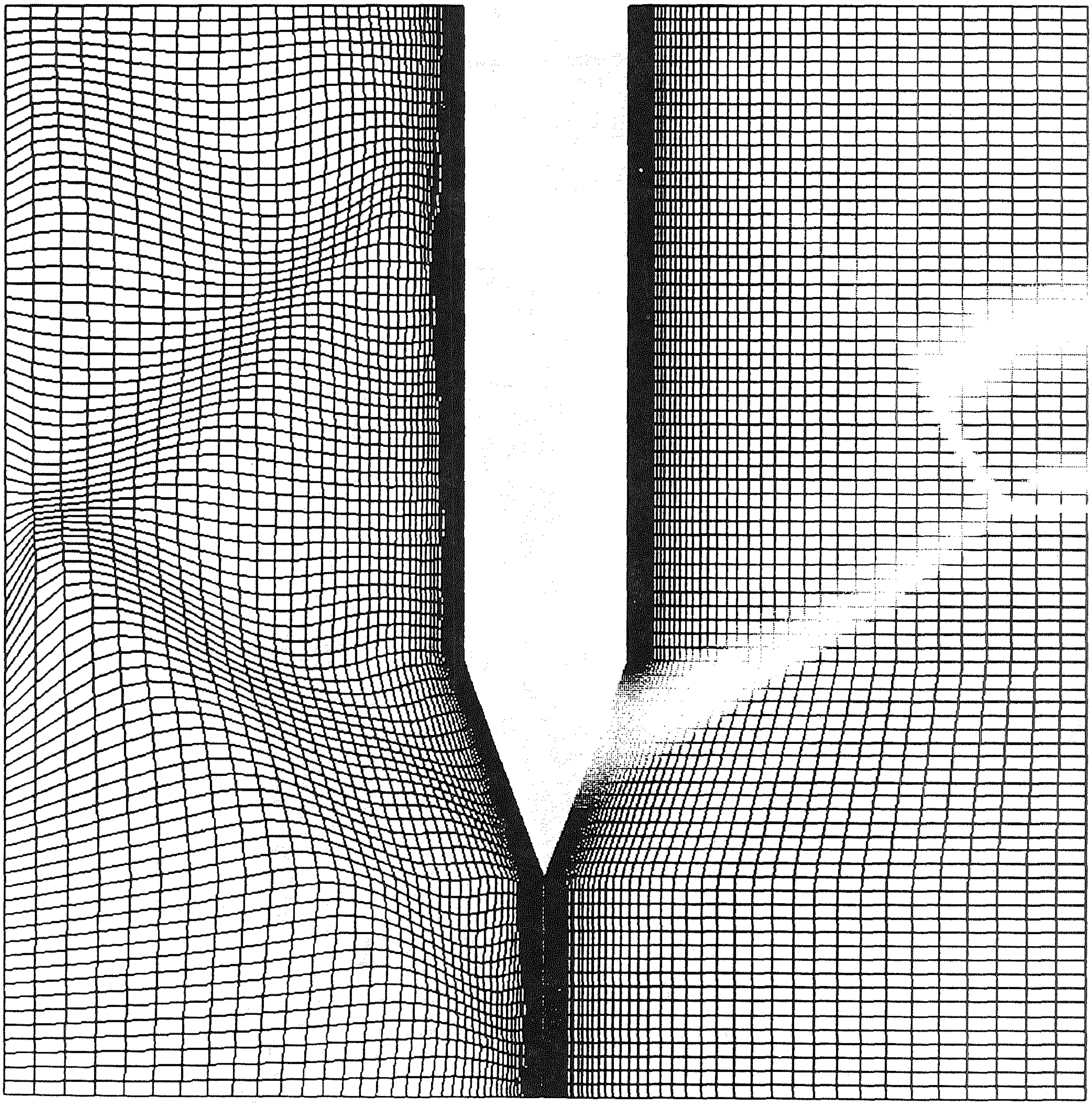

Scramjet Inlet NPARC Solution (lower), Weight Func (upper)

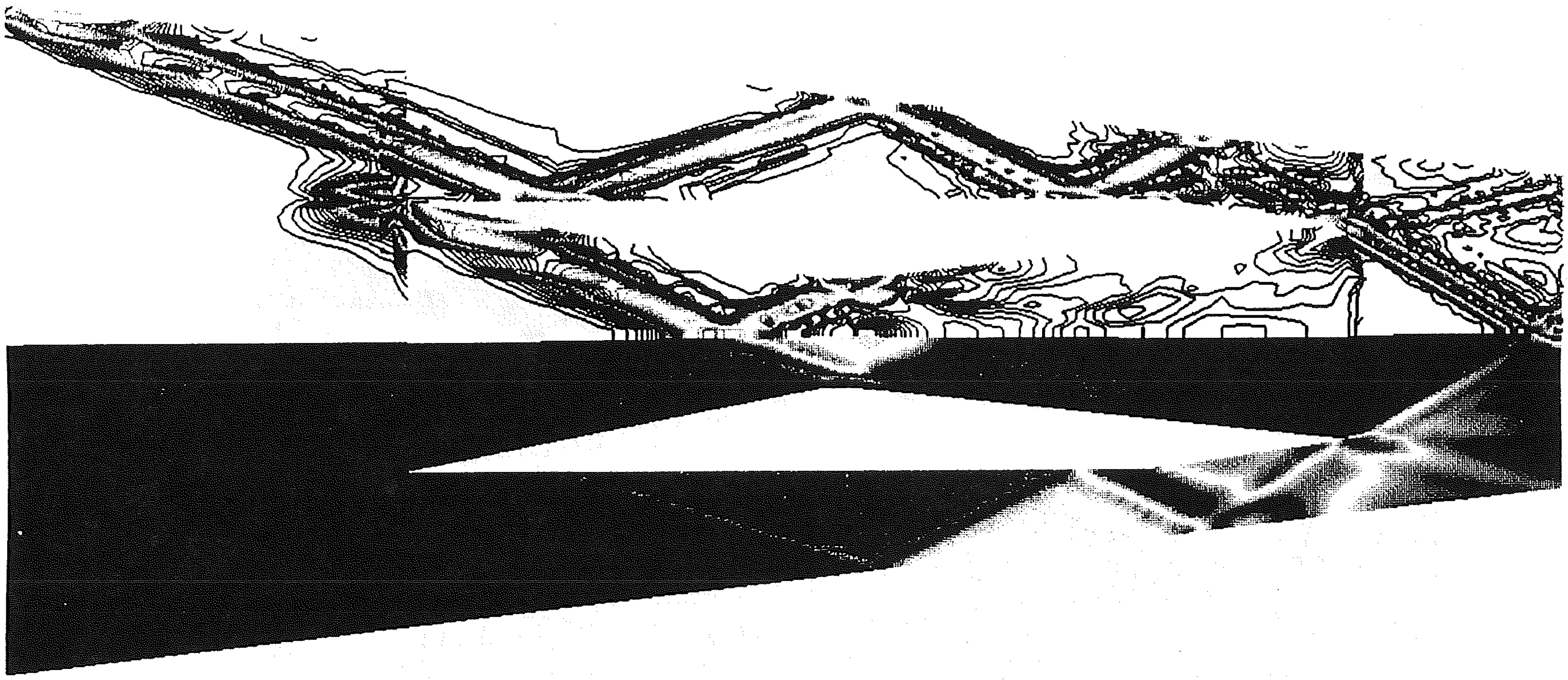

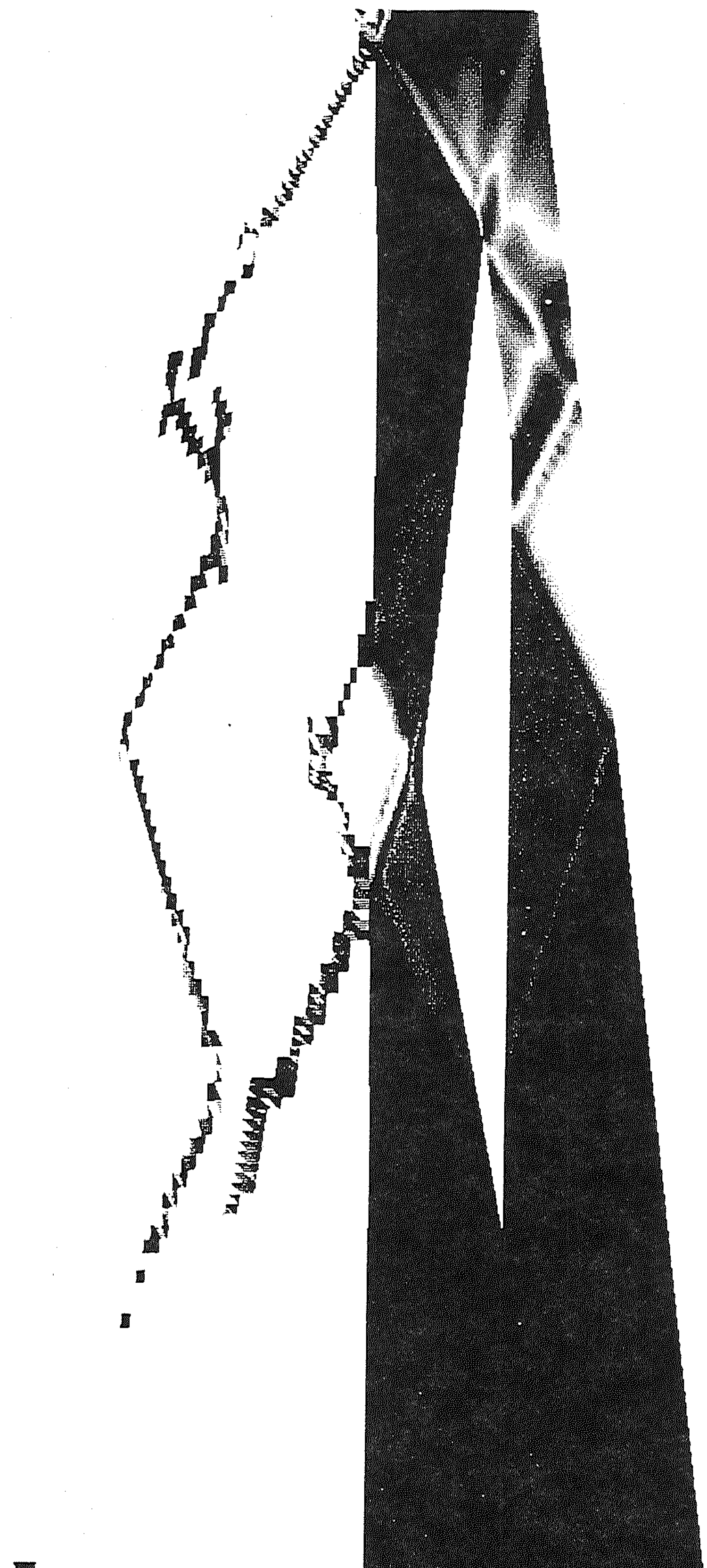

GENIE++ - A Multi-Block Structured Grid System

by

Tonya Williams, Naren Nadenthiran, Hugh Thornburg, and Bharat K. Soni
NSF Engineering Research Center for
Computational Field Simulation
Mississippi State University
Mississippi State, MS 39762

ABSTRACT

The computer code GENIE++ (Soni *et al.* 1992) is a continuously evolving grid system containing a multitude of proven geometry/grid techniques. The generation process in GENIE++ is based on an earlier version. The process uses several techniques either separately or in combination to quickly and economically generate sculptured geometry descriptions and grids for arbitrary geometries. The computational mesh is formed by using an appropriate algebraic method. Grid clustering is accomplished with either exponential or hyperbolic tangent routines which allow the user to specify a desired point distribution. Grid smoothing can be accomplished by using an elliptic solver with proper forcing functions. B-spline and Non-Uniform Rational B-splines (NURBS) algorithms are used for surface definition and redistribution. The built-in sculptured geometry definition with desired distribution of points, automatic Bezier curve/surface generation for interior boundaries/surfaces, and surface re-distribution is based on NURBS. Weighted Lagrange/Hermite transfinite interpolation methods, interactive geometry/grid manipulation modules, and on-line graphical visualization of the generation process are salient features of this system, which result in a significant time savings for a given geometry/grid application.

The development of the system, as well as computational examples of practical interest will be presented to demonstrate the success of these methodologies. Complete documentation is available using Mosaic. Versions are available for PC's, X window, and SGI systems. It is planned to place this code in the public domain by August 1995.

MISSISSIPPI STATE UNIVERSITY/National Science Foundation

GENIE^{++}: A Structured Multi-Block Grid System

Bharat K. Soni
Hugh Thornburg
Tonya Williams
Nadesan Narenthiran

ENGINEERING RESEARCH CENTER FOR
COMPUTATIONAL FIELD SIMULATION
COMPLEX GEOMETRY / COMPLEX PHYSICS

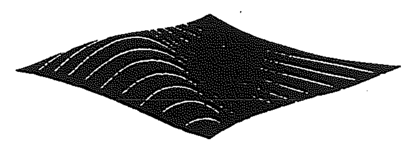

MOTIVATION

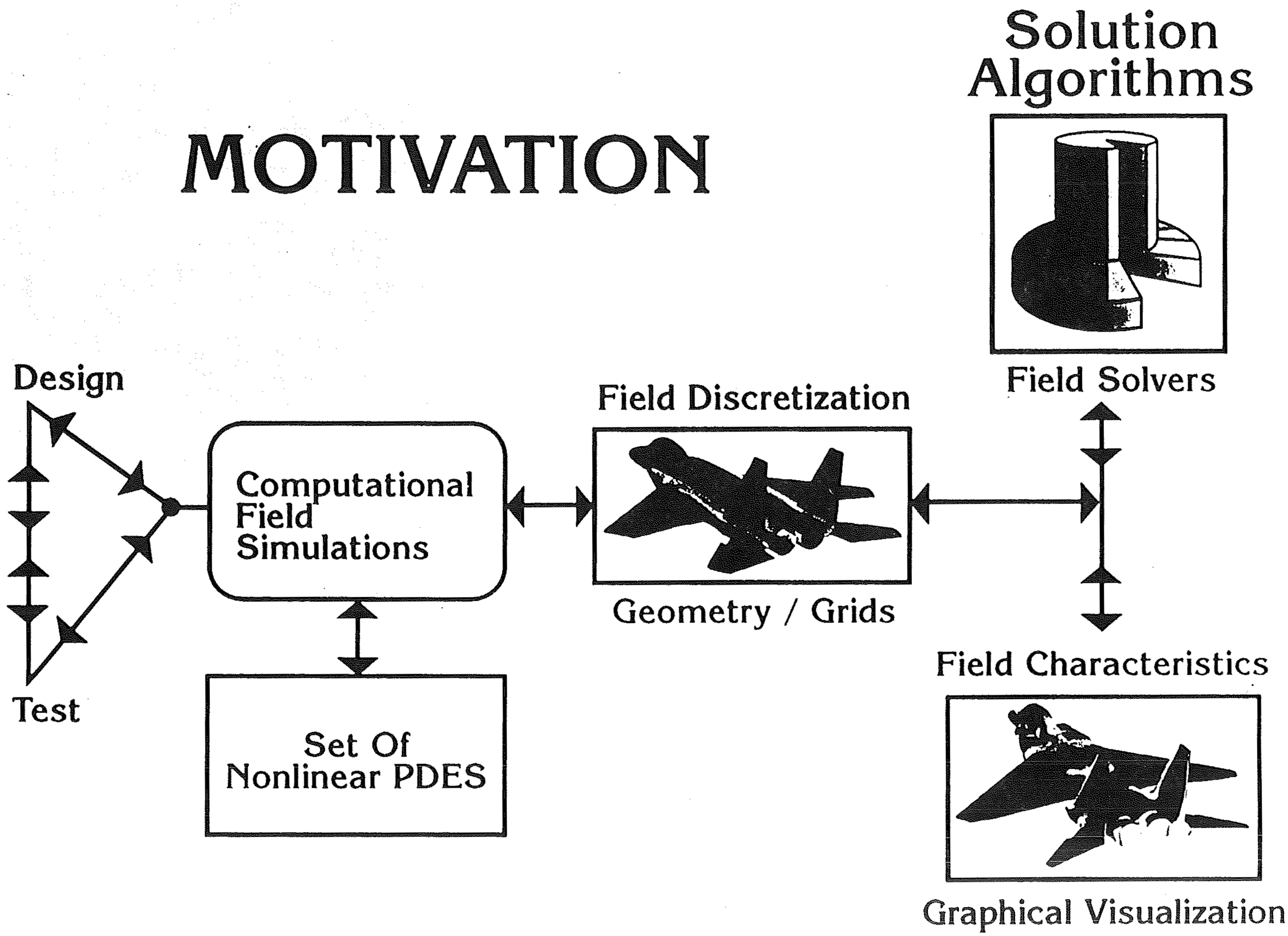
Solution
Algorithms
Design
Test
Computational
Field
Simulations
Field Discretization
Geometry / Grids
Field Solvers
Field Characteristics
Graphical Visualization
Set Of
Nonlinear PDES

Grid Strategies

Structured

- Algebraic
- PDES
- Other

Unstructured

- Advancing Front
- Delaunay
- PDES
- Other

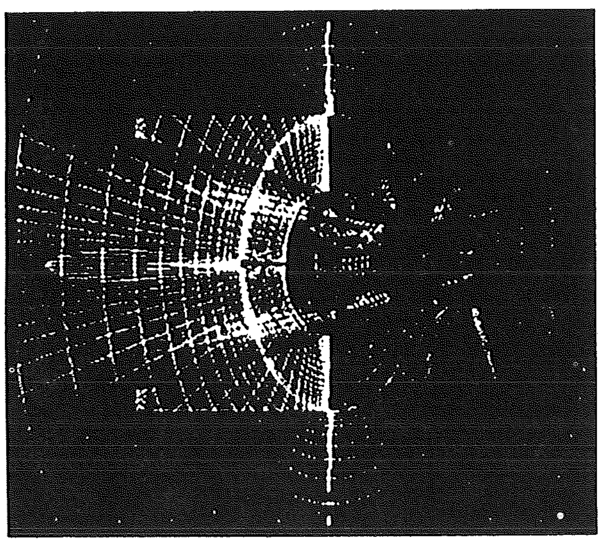

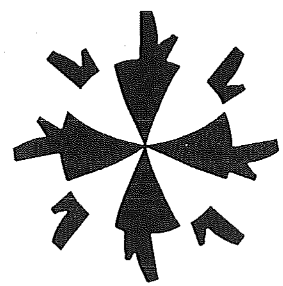

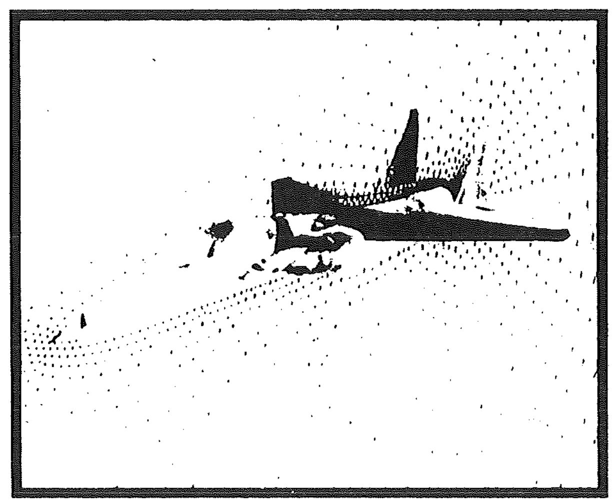

GRID INFLUENCE

- Accuracy
- Truncation Errors
- Stability
- Treatment of BCS
- Economy ($)

- All Positive or All Negative Volumes
- Orthogonality (Not Too Skewed)
- Smooth
- Aspect Ratio

GENERATION STEPS

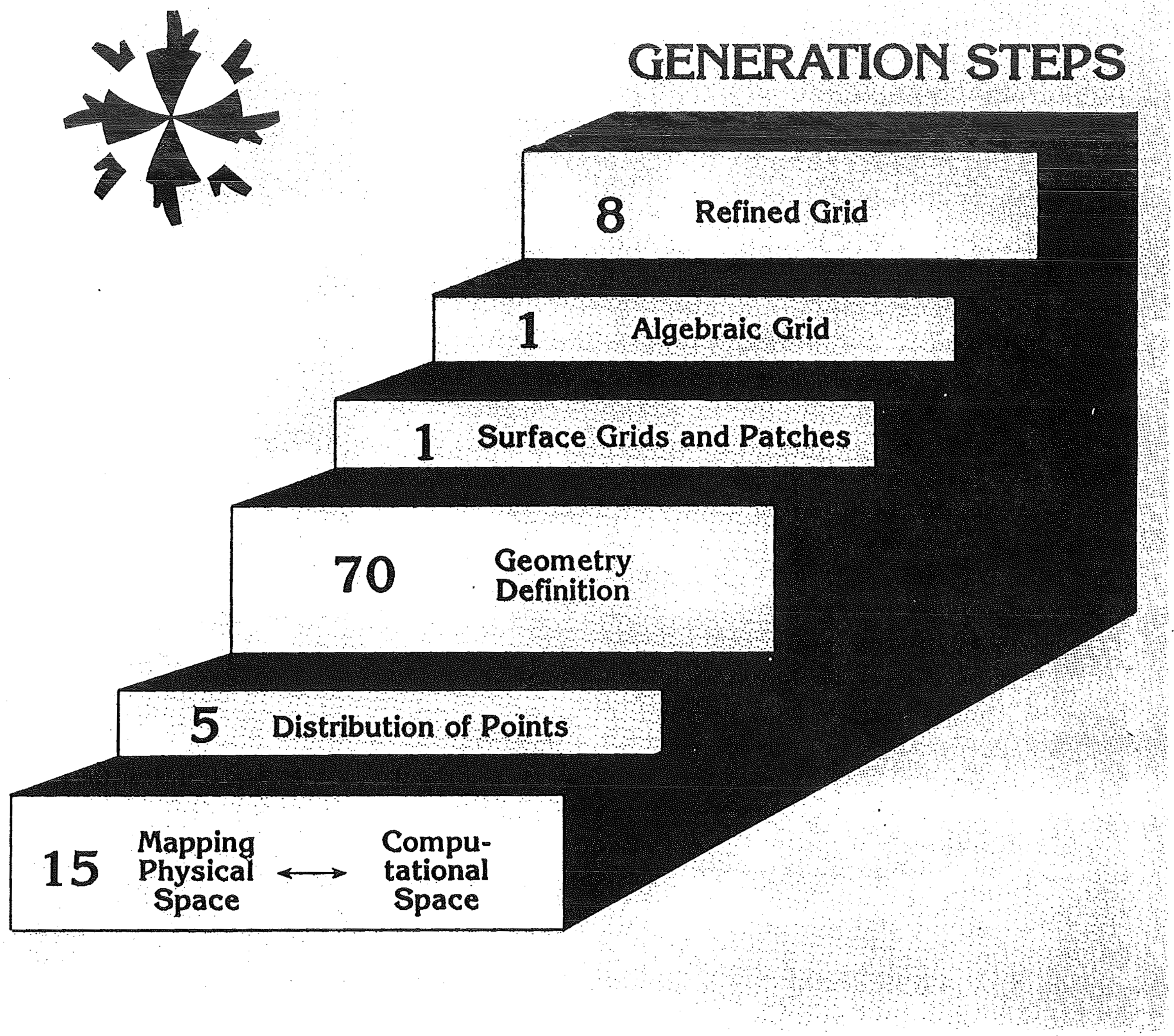

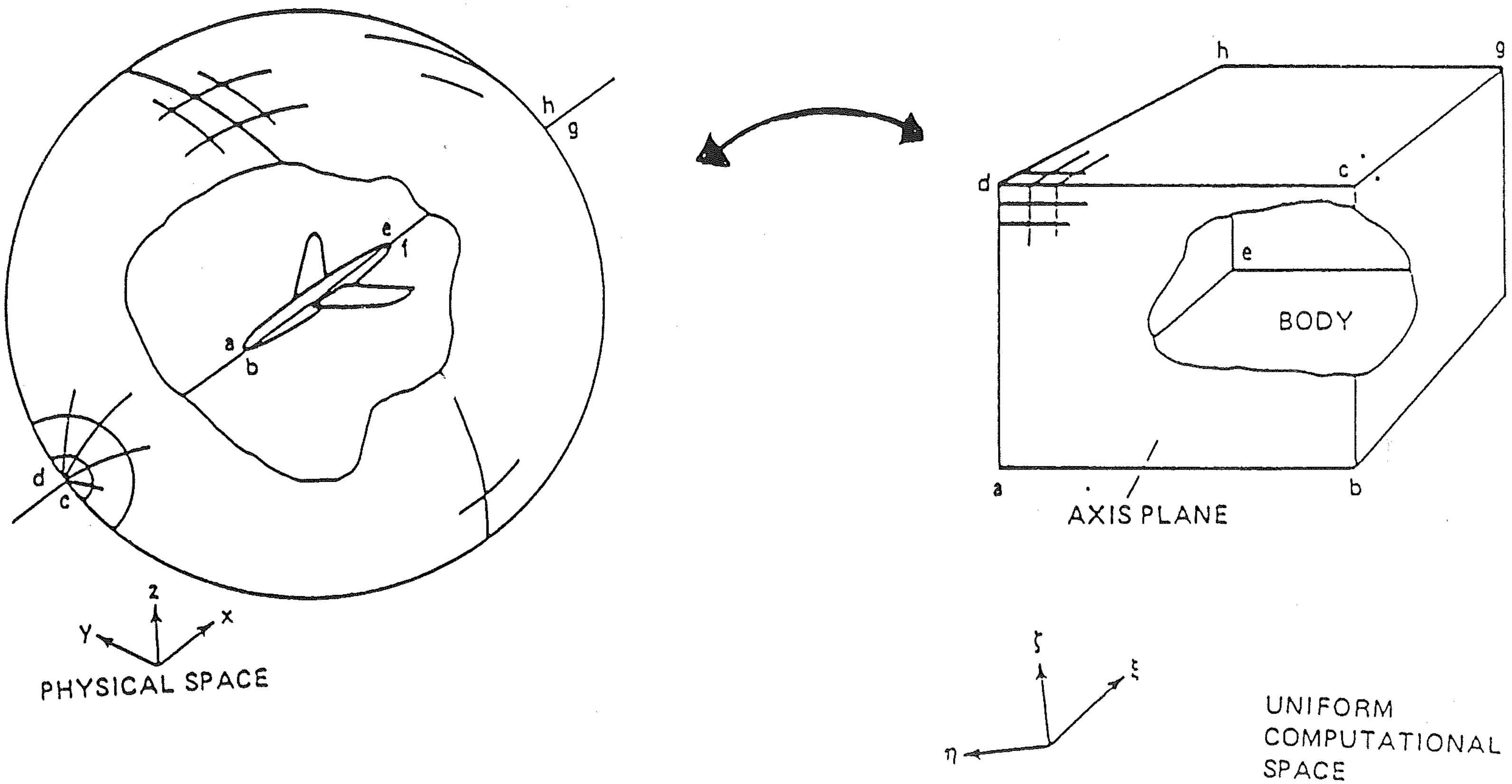

h
g
e
f
a
b
d
c
z
Y
x
PHYSICAL SPACE
h
g
d
c
e
BODY
f
a
b
AXIS PLANE
ζ
ξ
η
UNIFORM
COMPUTATIONAL
SPACE

STRETCHING FUNCTIONS

- Exponential $\longrightarrow f(x) = \dfrac{e^{\alpha x} - 1}{e^{\alpha} - 1}$

- Hyperbolic Tangent $\longrightarrow f(x) = 1 + \dfrac{\tanh(\alpha(x-1))}{\tanh\alpha}$

- Hyperbolic Sine $\longrightarrow f(x) = 1 - \dfrac{\sinh(\alpha(1-x))}{\sinh\alpha}$

STRETCHING OPTIONS

Exponential

Hyperbolic Tangent

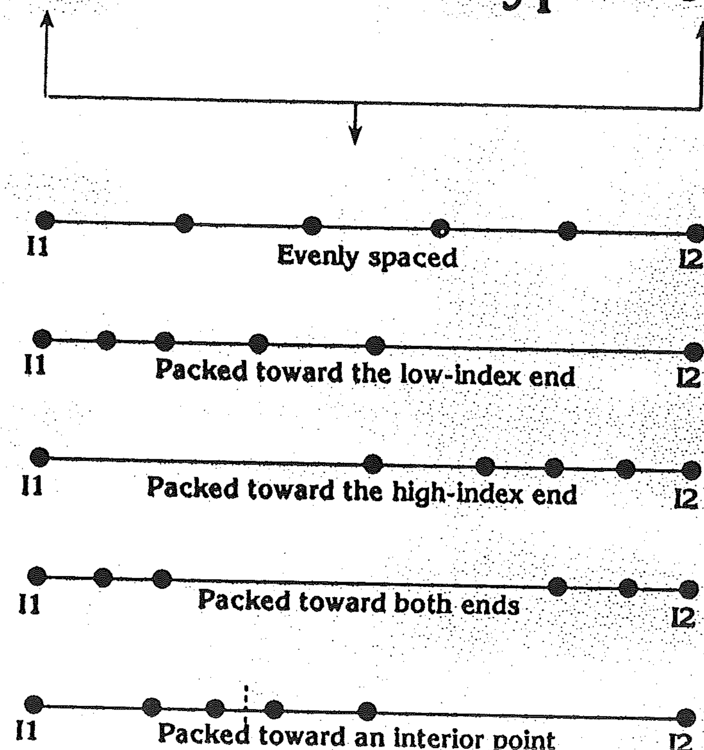

Options for Distributing Points

A BOUNDARY CURVE, SURFACE, OR VOLUME

G(I1 → I2, → J1 → J2, K1 → K2)

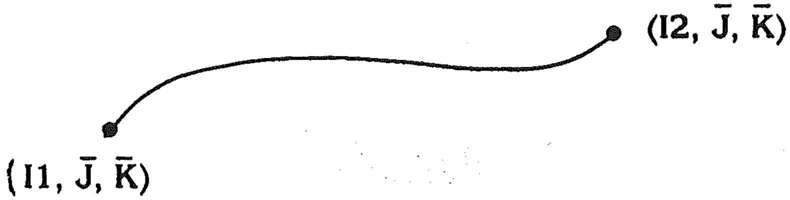

Curve [G(I1 → I2, J̄ → J̄, K̄ → K̄)]

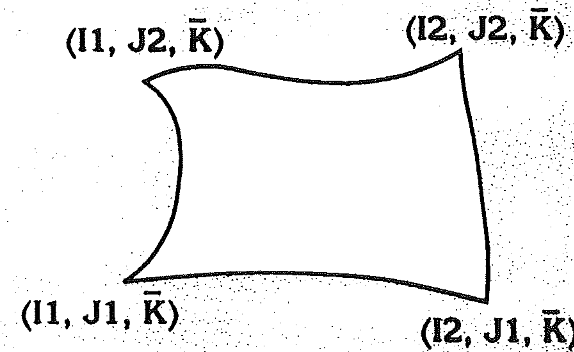

A Surface [G(I1 → I2, J1 → J2, K̄ → K̄)]

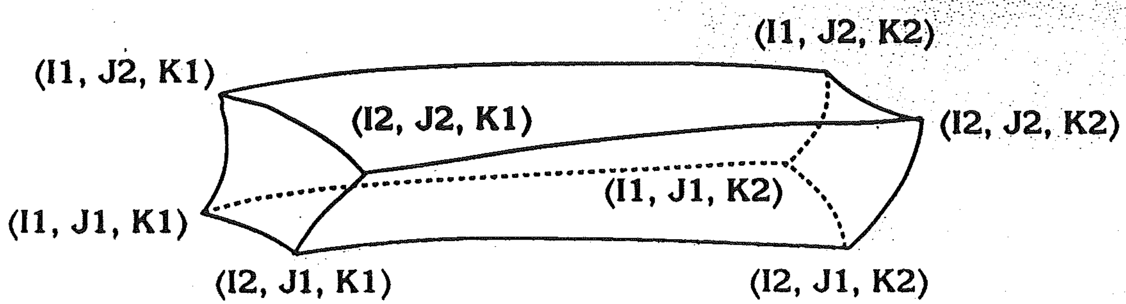

A Volume [G(I1 → I2, J1 → J2, K1 → K2)]

GENIE

Grid Generation Process / Geometry Definition

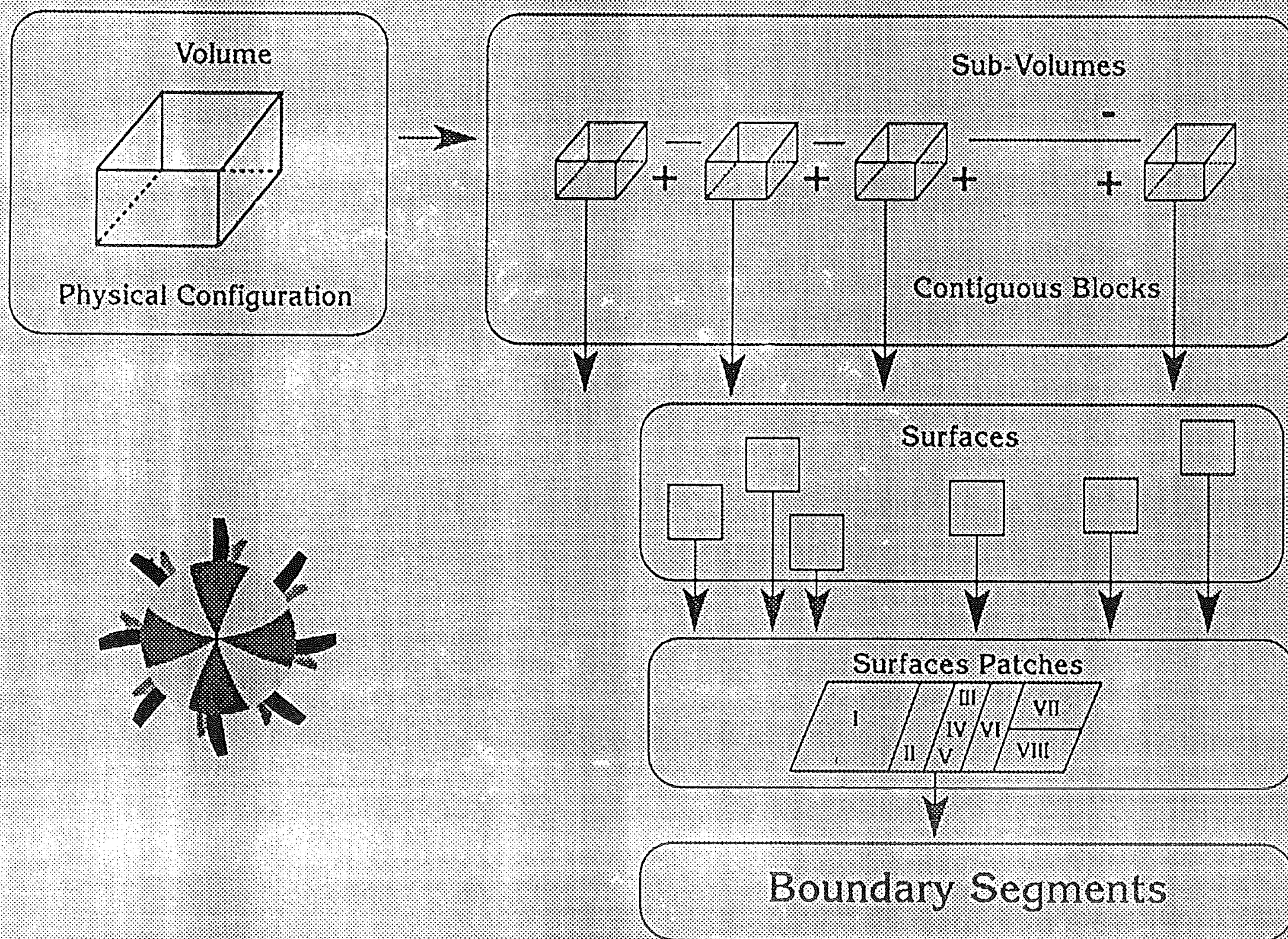

GEOMETRY GENERATION

- Semi-Interactive Construction
- Analytic:

  Points, Line, Circle, Ellipse, Super-Ellipse, Polynomial, Plane, Ruled Surface, Ellipsoid, Hyperboloid, Paraboloid, NASA Airfoils, . . .
- Sculptured:

  Spline-Akima, B-Spline, Rational B-Spline, Polynomial-Hermite, LaGrange, Bezier, Coon's Patch, NURBS, . . .

GEOMETRY MANIPULATION

- Body of Revolution
- Ruling, Marching, TFI, Coon's Patch
- Transformations: Translation, Rotation, Scaling, Mirror Image
- Cut. Paste, Patch, Blend, . . .
- Intersections and Projections

ALGEBRAIC

- Fast
- Precise Spacing Control
- Interactive User Interface
- Possible Overlapping
- Requires High Degree of Understanding
- Generalization!
- Propagation of Slope Discontinuites

PDES

- Inherent Smoothness
- Resistant To Grid Line Overlapping
- No Propagation of Slope Discontinuities
- Competitive Enhancement of Smoothness, Orthoganality and Concentration
- Readily Adaptable for Generalization
- Distribution Loss

APPROACH

Objective: Accomplish othogonality – smoothness without any distribution loss.

- Work hard with Algebraic
  - Precise Spacing Control (Grid Spacings, Areas, Volume)
  - Inexpensive and Fast
  - Interior Bezier Curve/Surface Specification for Sub-blocks
  - Weighted Transfinite Lagrange and Hermite Interpolation
  - Precise Spacing Control (Grid Spacings, Areas, Volume)
- Use elliptic for a quick fix
  - Smart Forcing Functions
  - 3-5 Iterations (maximum)

WEIGHTED TRANSFINITE INTERPOLATION

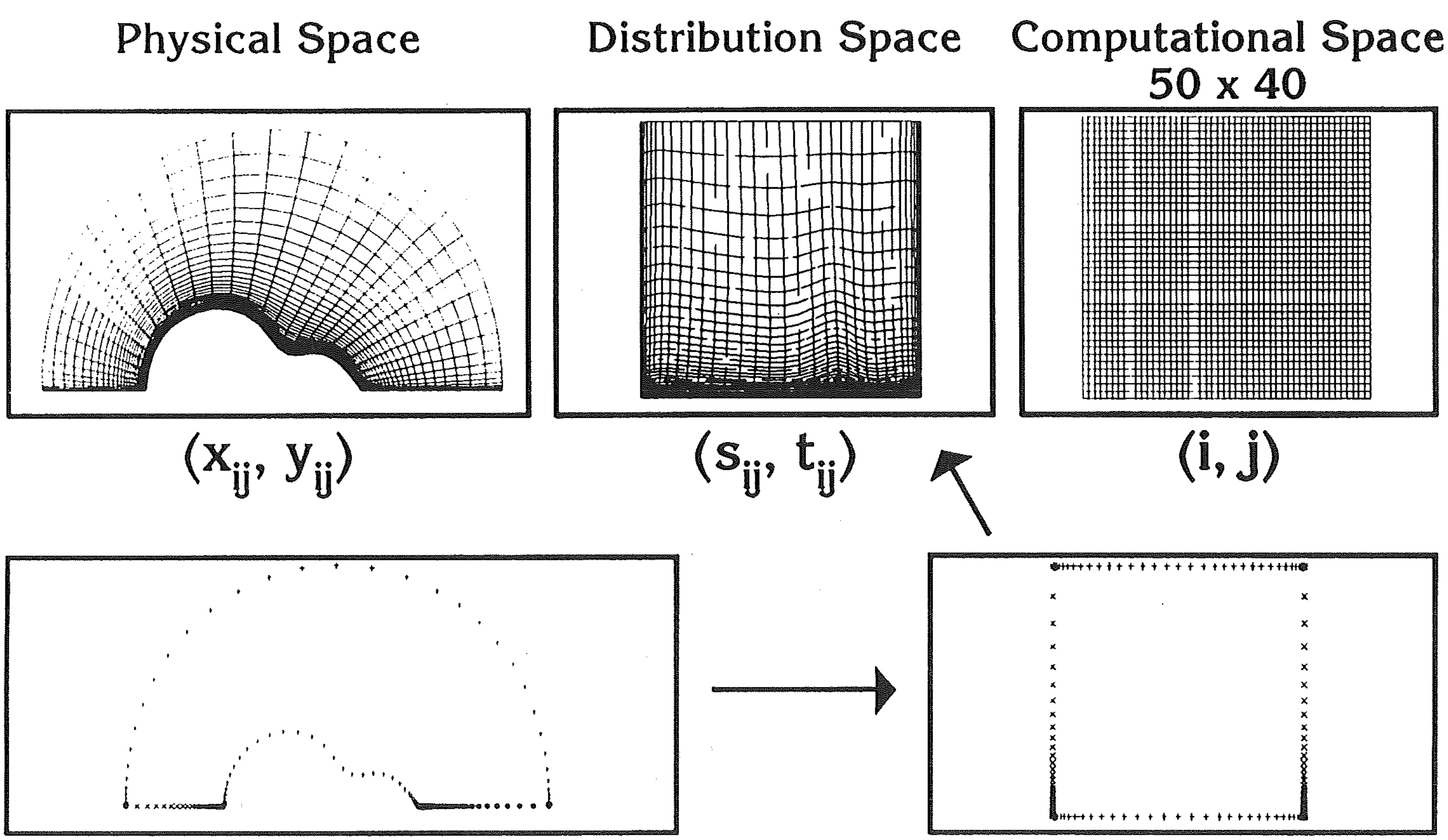

GENERAL ELLIPTIC GENERATION SYSTEM

$$\sum_{i-1}^{3} \sum_{j-1}^{3} g^{ij} \, r_{\xi^i \xi^{\bar{j}}} + \sum_{k=1}^{3} \phi_k r_{\xi^k} = 0$$

$$g^{il} = \frac{1}{g} \left(g_{jm} g_{km} - g_{jn} g_{kn} \right)$$ ***i = 1, 2, 3; j = 1, 2, 3; (i, j, k) and (l, m, n) cyclic***

EVALUATION OF FORCING FUNCTIONS

$$\sum_{i-1}^{3} \sum_{j-1}^{3} g^{ij} (g_{iq})_{\xi^j} + \sum_{k=1}^{3} \phi_k g_{kq} - \sum_{i-1}^{3} \sum_{j-1}^{3} g^{ij} \left(\frac{(g_{ij})_{\xi^k} - (g_{jq})_{\xi^i}}{2} \right) = 0$$

$$q = 1, 2, 3$$

$$g_{ij} = \underline{r}_{\xi^i} \cdot \underline{r}_{\xi^j} = \left\| r_{\xi^i} \right\| \cdot \left\| r_{\xi^j} \right\| \cdot \cos\Theta$$

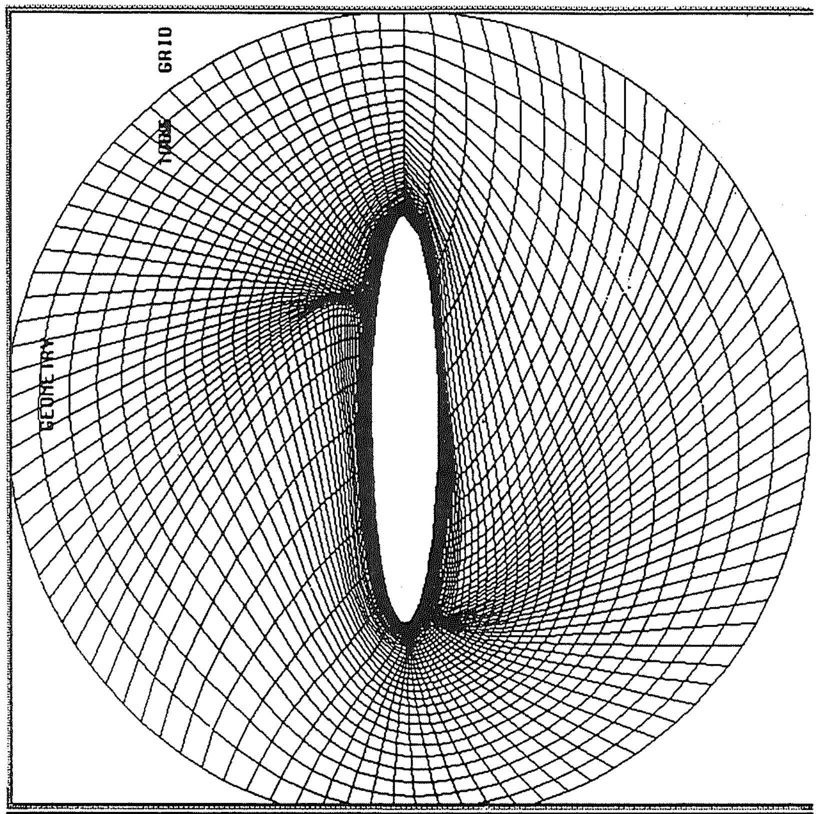
GEOMETRY
GRID

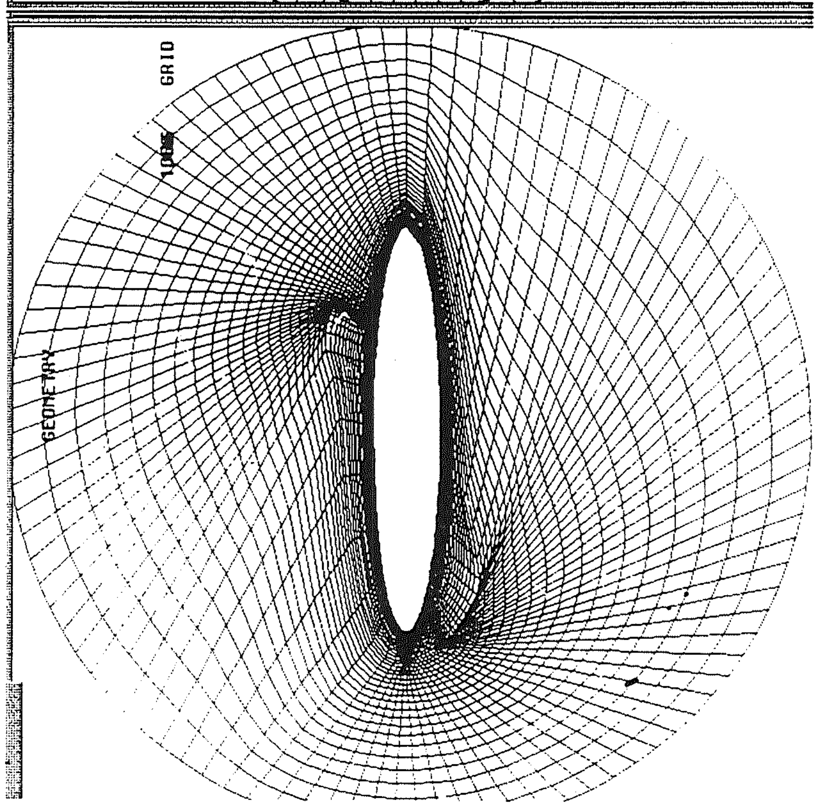
GEOMETRY
GRID

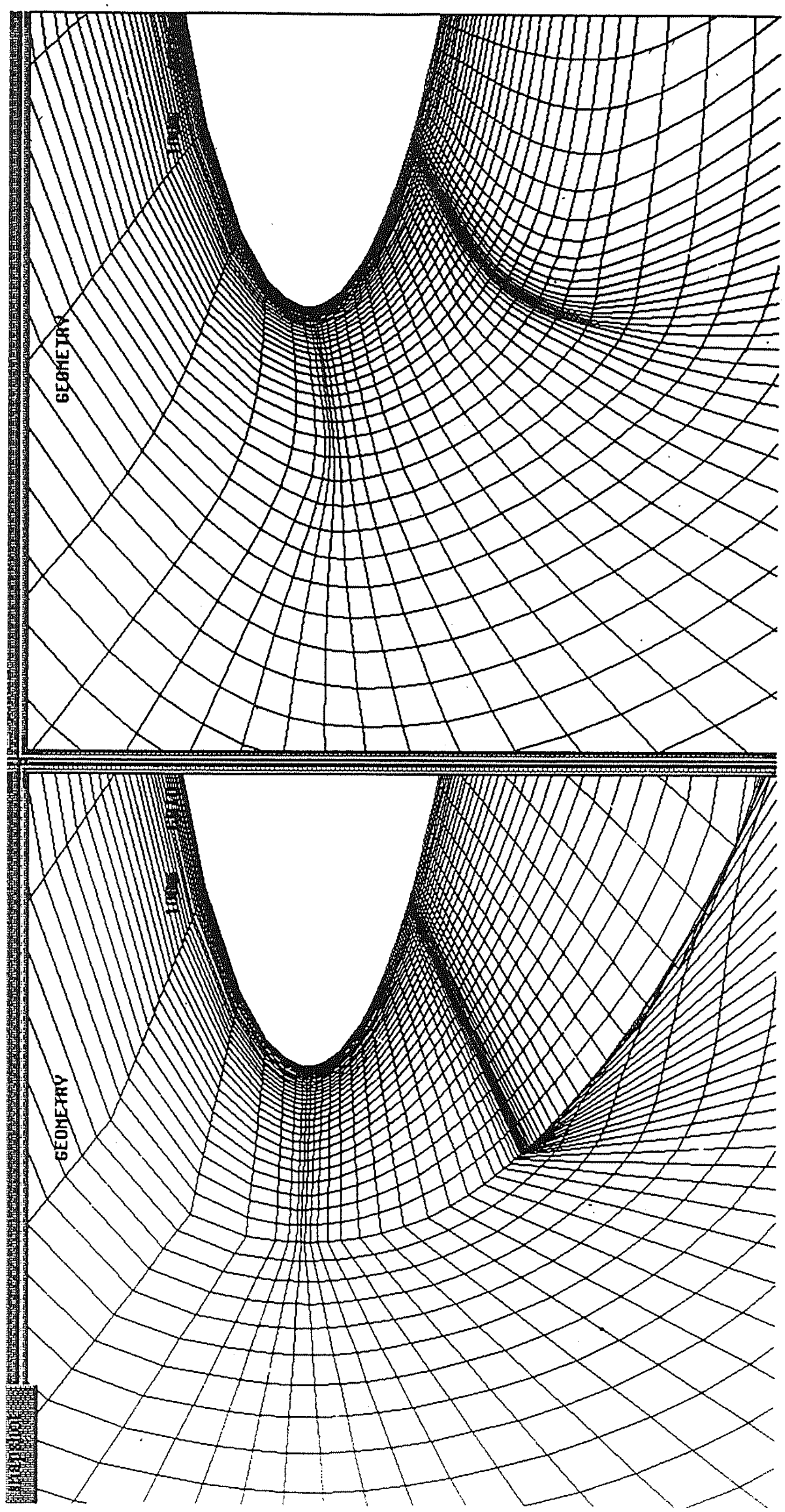
GEOMETRY
GEOMETRY

GENIE Family of Grid Generation Codes

GENIE++ User's Manual

Version 1.0

Dr. Bharat [illegible] Soni

Mississippi State University / National Science Foundation
Engineering Research Center for Computational Field Simulation

GENIE++
Characteristics

GENIE^{++}

Geometry Mode	Computational Mode
• Sculptured Curves and Surfaces	• One Block at a Time With One Extra Block in On-Line Memory

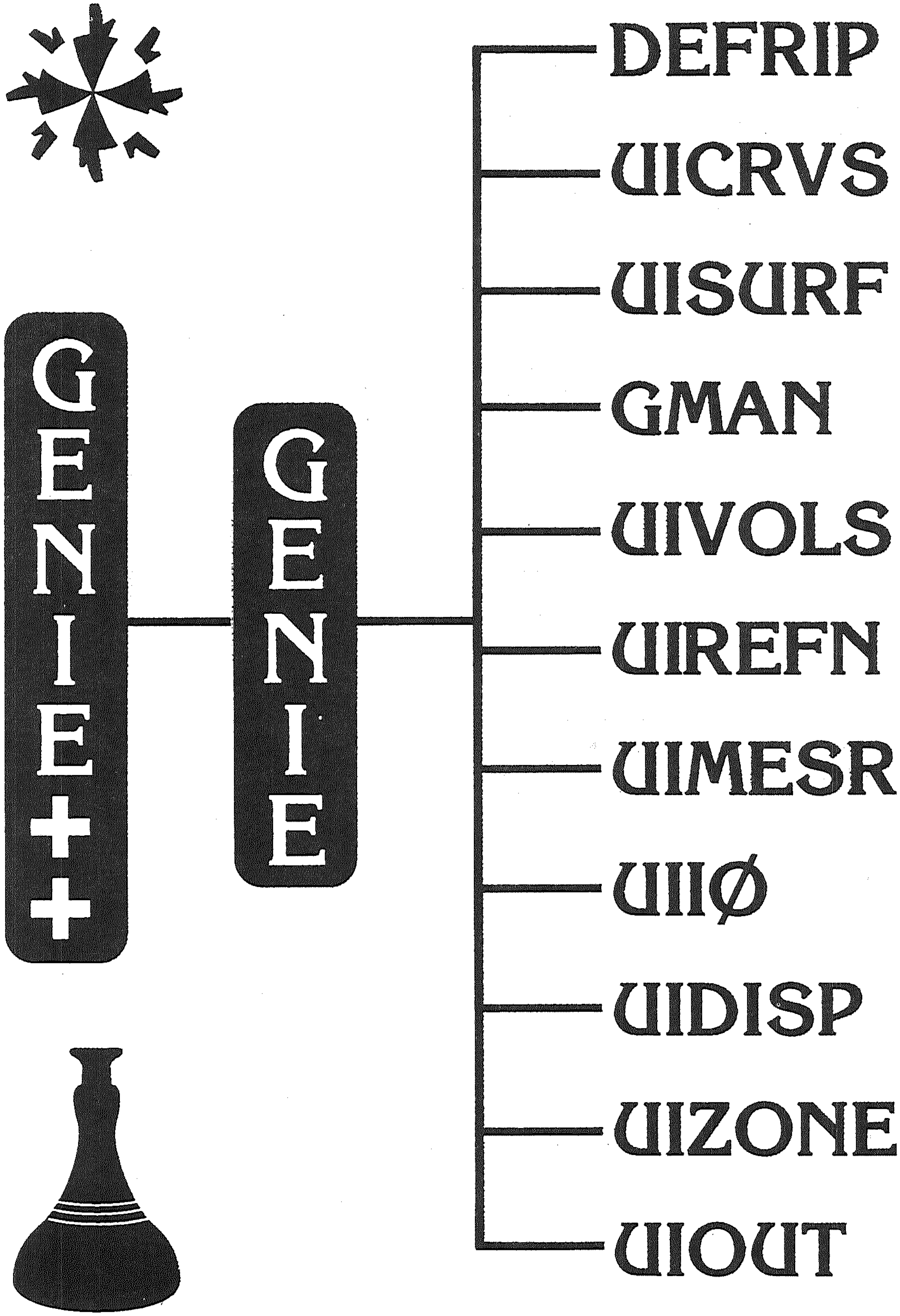
GENIE++
GENIE
DEFRIP
UICRVS
UISURF
GMAN
UIVOLS
UIREFN
UIMESR
UIIØ
UIDISP
UIZONE
UIOUT

INITIALIZATION OPTIONS

1 TOGGLE REAL TIME PLOTTING
2 TOGGLE PROMPTING
3 GIVE TITLE TO GRID
4 CHANGE CURRENT GRID BLOCK SIZE
5 CHANGE MAXIMUM GRID SIZES
6 CHANGE CURRENT BLOCK NUMBER
7 CHANGE MAXIMUM NUMBER OF BLOCKS
8 TOGGLE GRID GENERATION MODE
9 INITIALIZE DATABASE
10 INITIALIZE ZONAL INFORMATION
11 VIEW NON-BLOCK GRID
12 VIEW ONE BLOCK
13 VIEW ALL BLOCKS
14 EXIT INITIALIZATION
15 QUIT GRID GENERATION

INPUT OPTION NUMBER

Genie++ Main Menu

This chapter is about using GENIE++ to generate grids. Descriptions of the facilities [illegible] and instructions on using them are included. If you have not used GENIE++ before, [illegible] on GENIE++ basics before going any further.

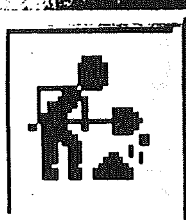

Grid Generation Activity Options

Choosing option [illegible] brings you to the grid generation module [illegible] following Activity Options [illegible]

Activity Option Menu
1. Curve or Boundary Generation
2. Surface or Surface Grid Generation
3. Volume Grid Generation
4. Multi-Block Treatment
5. Grid Measures and Characteristics
6. Display Geometry or Grid
7. Output Files and Formats
8. Input/Output [illegible]
9. Batch [illegible] Information
10. Change Parameters
11. Utilities

BOUNDARY SEGMENT DEFINED BY

1 A CURVE PROJECTED ONTO A PARALLEL PLANE
2 OTHER CURVE PROJECTION OPTIONS
3 A STRAIGHT LINE
4 A 3D BEZIER / HERMITE CUBIC CURVE
5 SCULPTURED CURVE DEFINITION
6 CURVE MANIPULATION OPTIONS

INPUT OPTION NUMBER

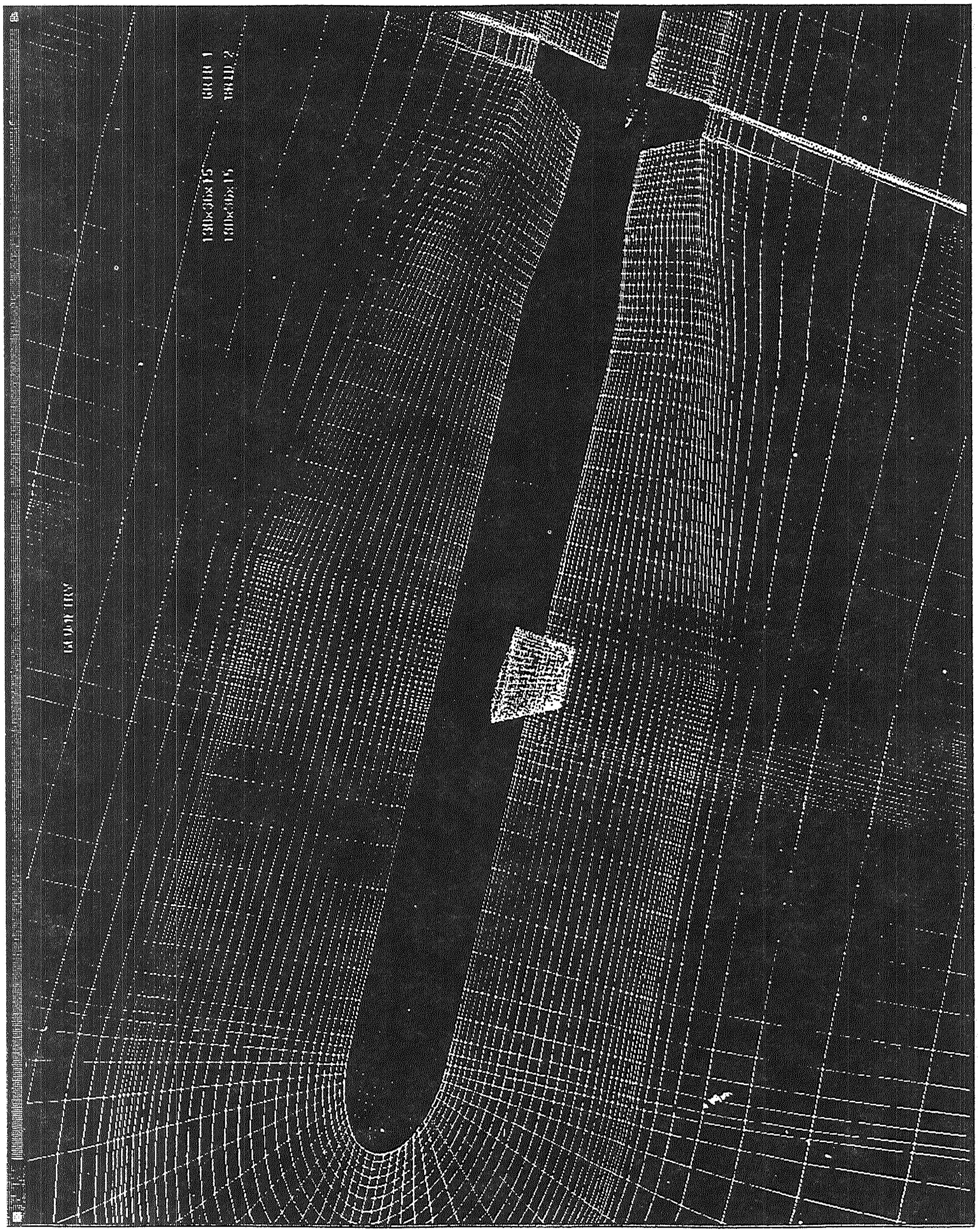

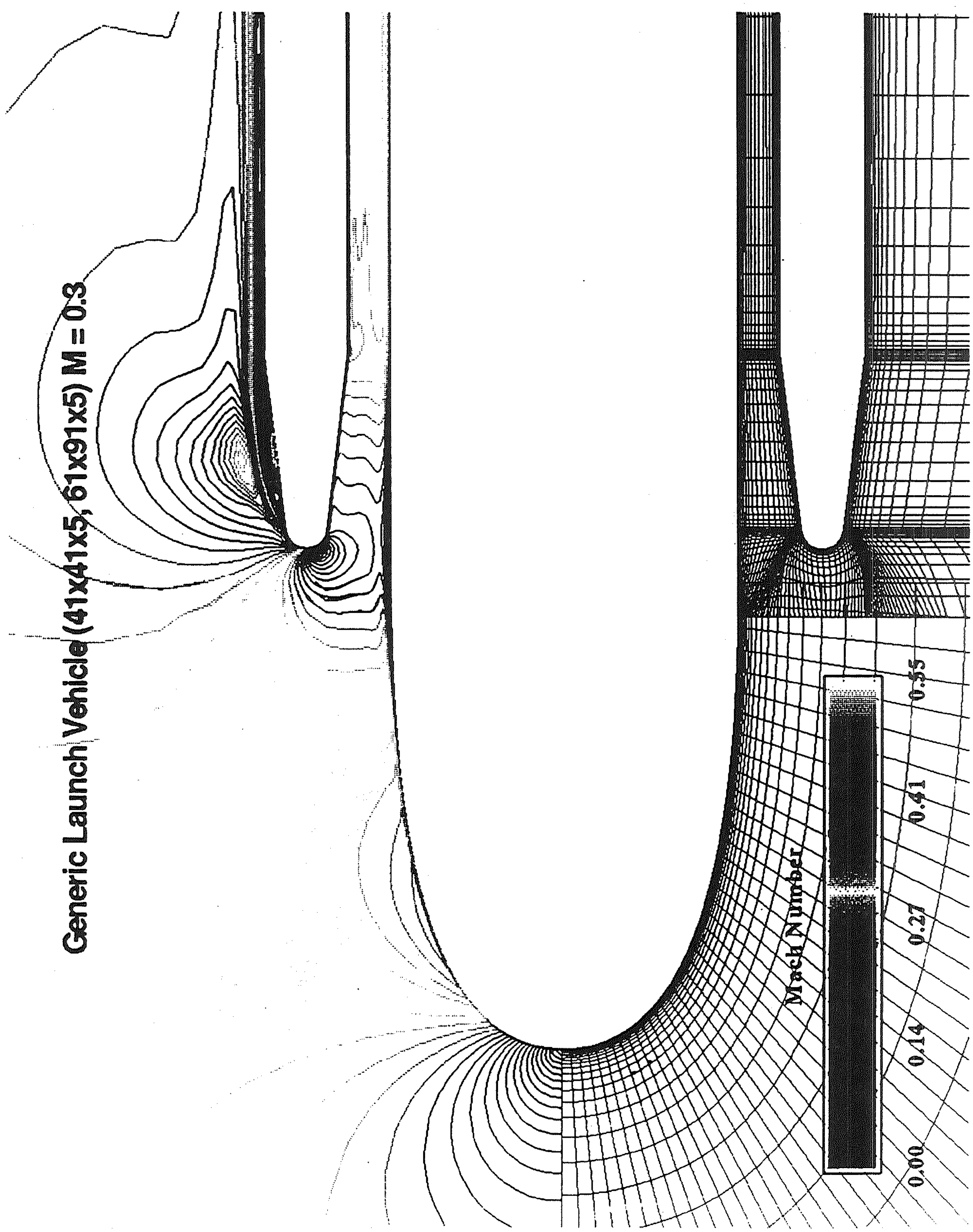

Generic Launch Vehicle (41x41x5, 61x91x5) M = 0.3
Mach Number
0.00
0.14
0.27
0.41
0.55

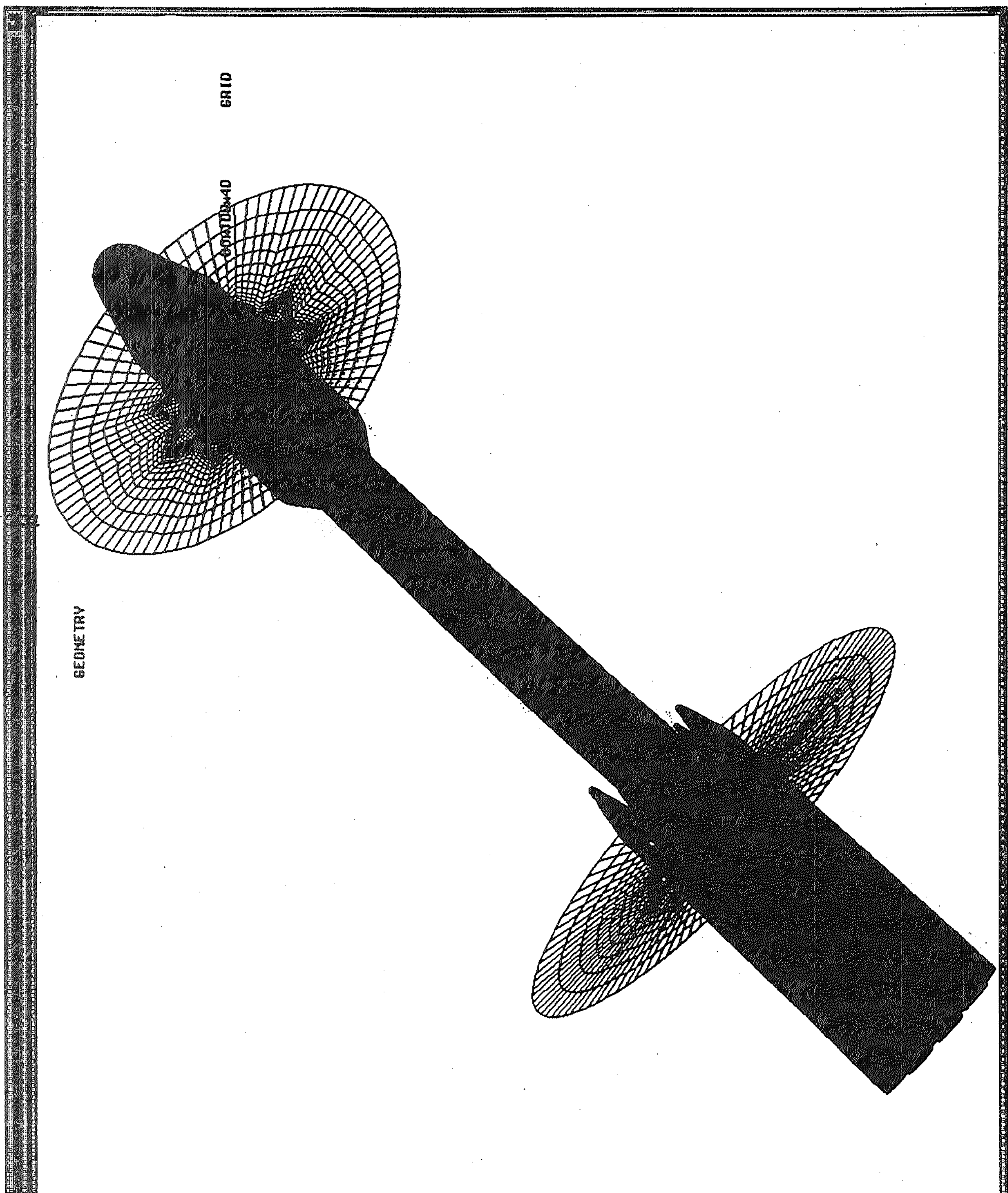
GEOMETRY
GRID

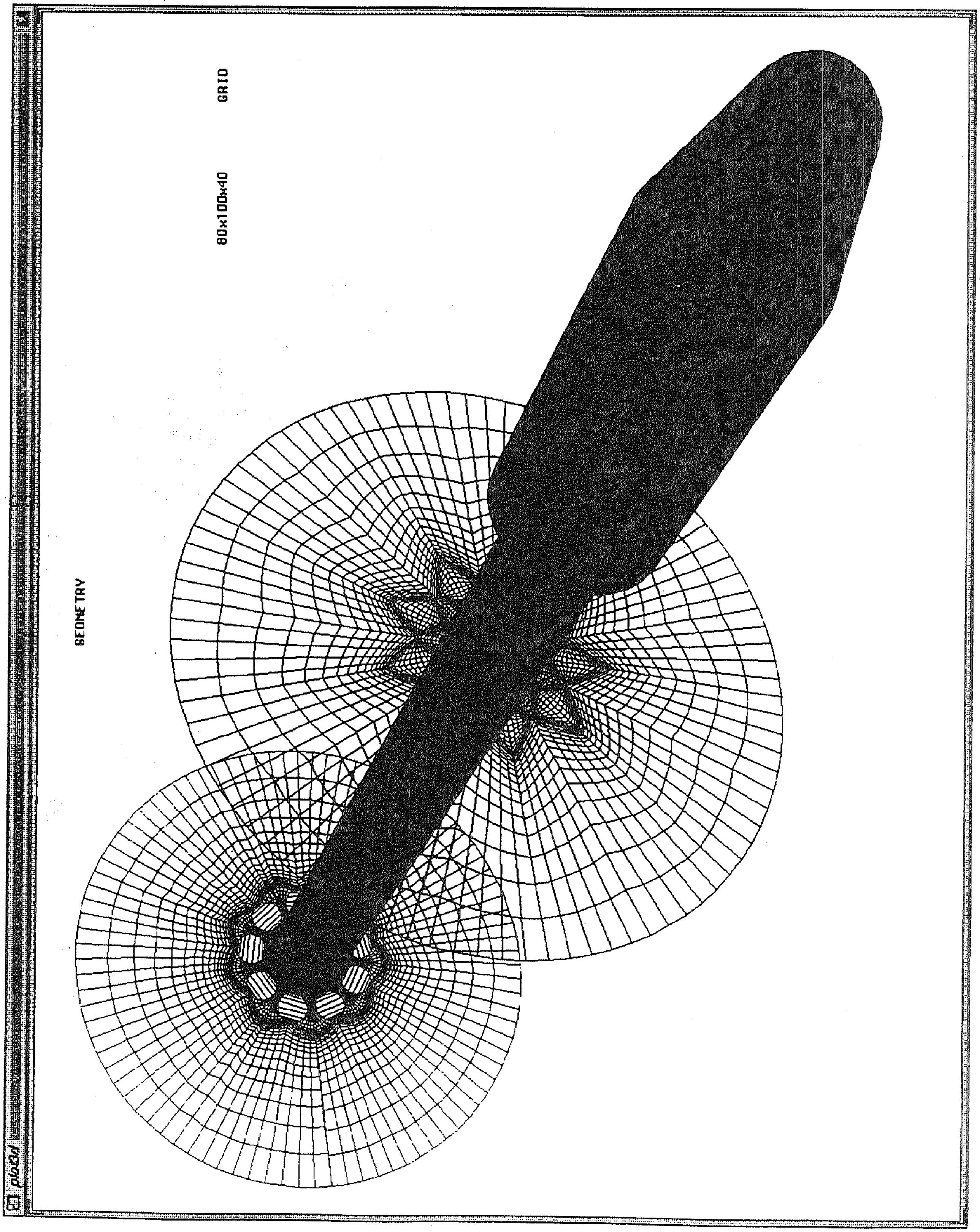
plot3d
GEOMETRY
80x100x40
GRID

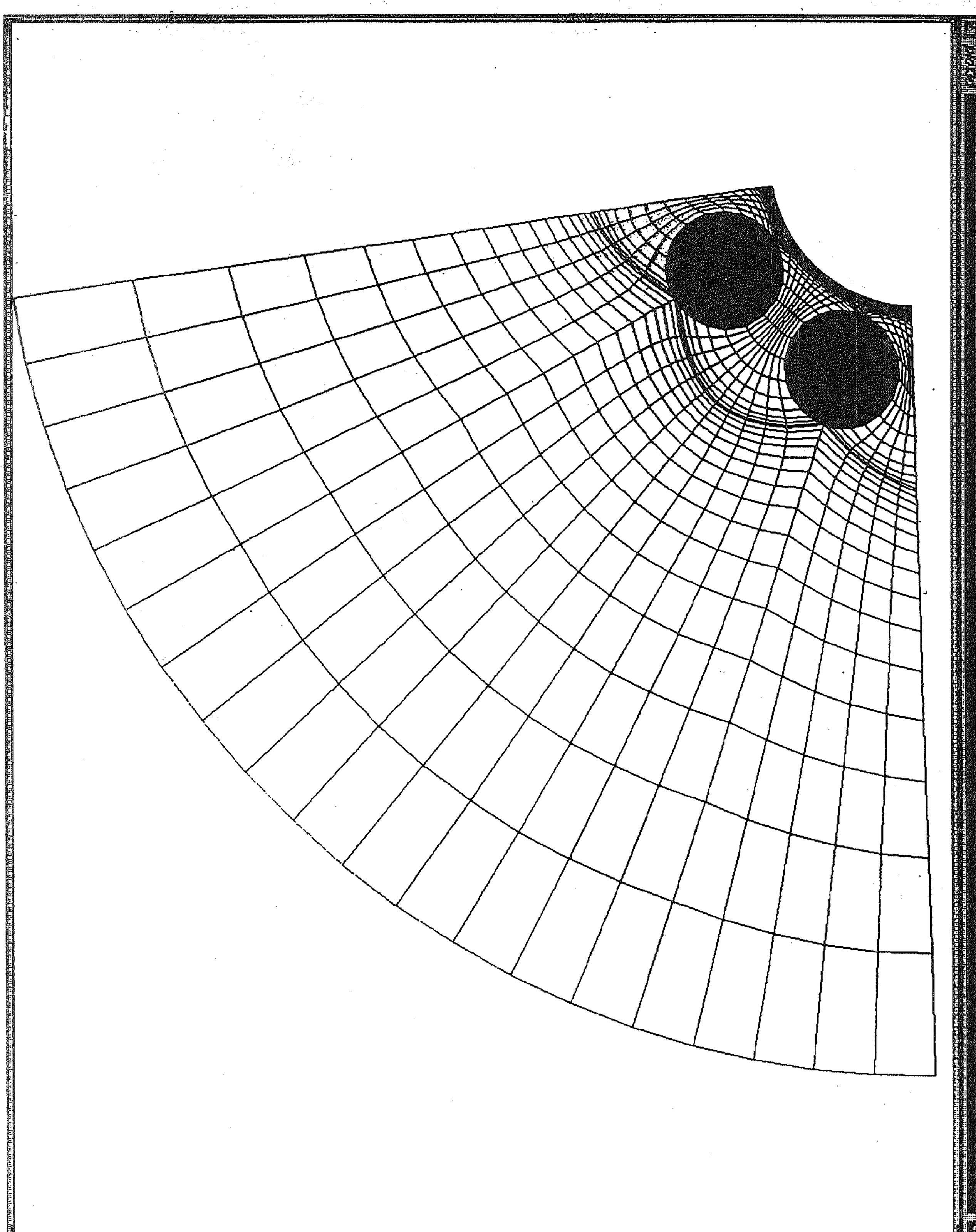

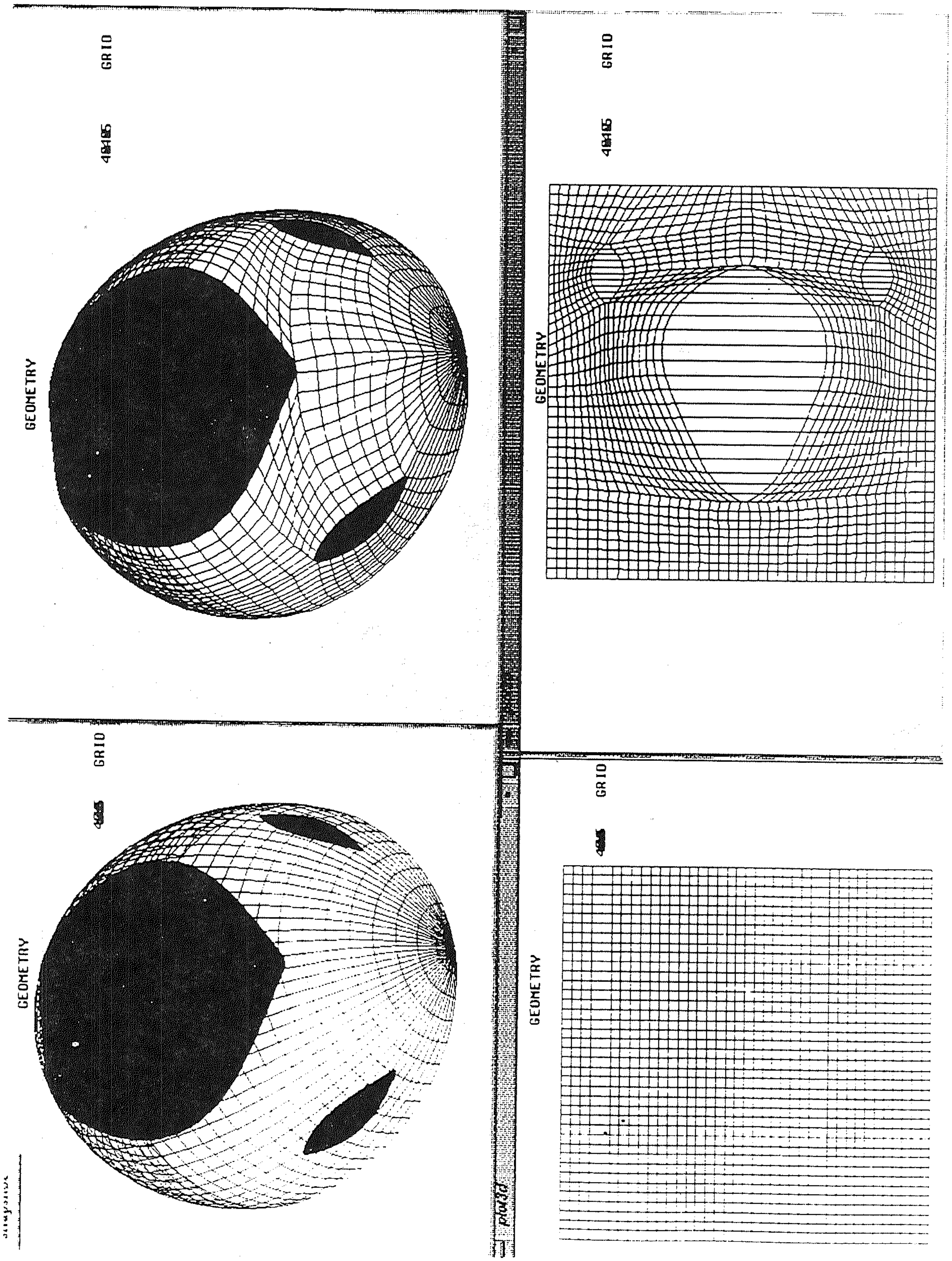
GEOMETRY
GRID
GEOMETRY
GRID
GEOMETRY
GRID
GEOMETRY
GRID

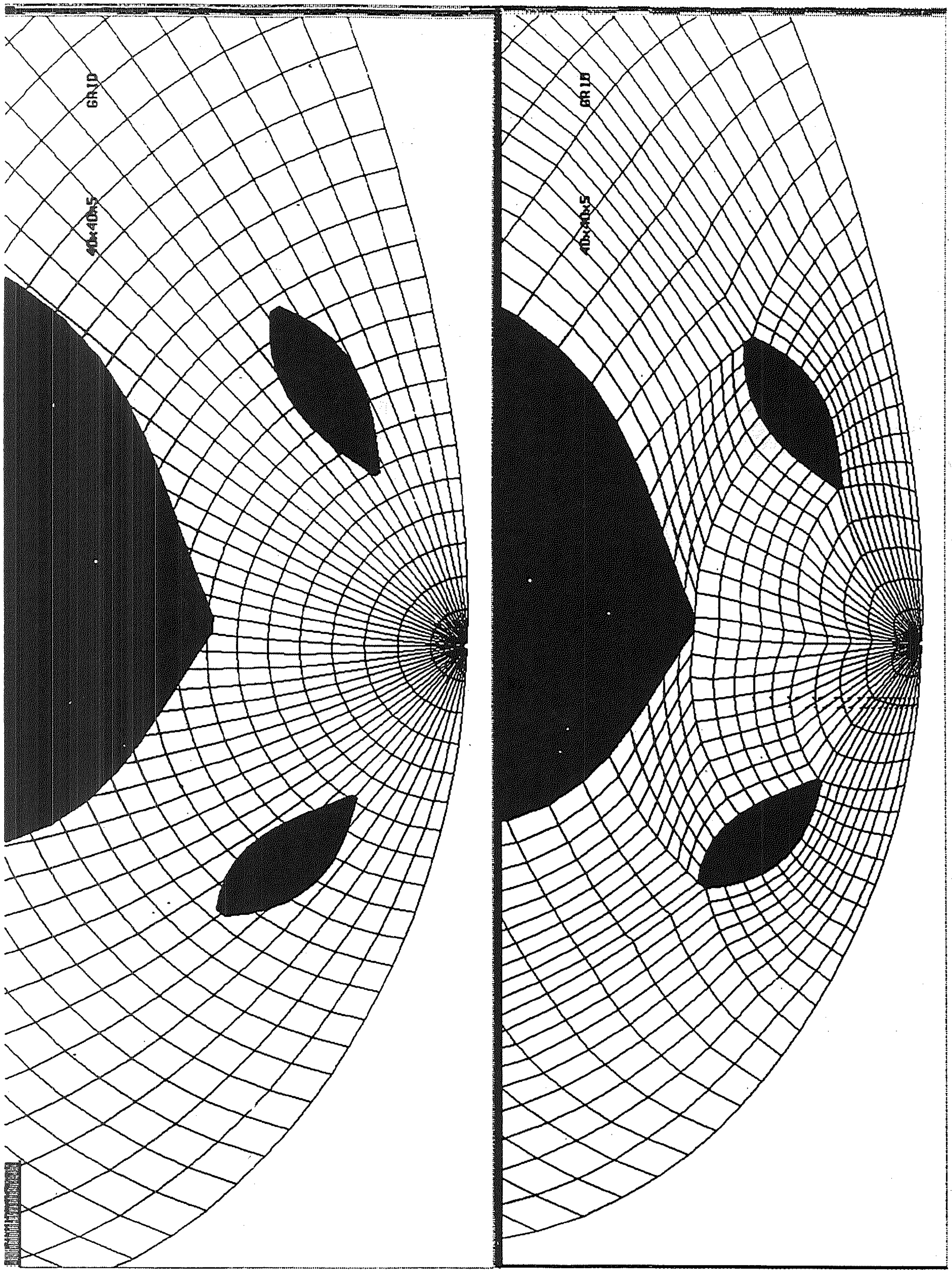
40x40x5
GRID
40x40x5
GRID

MISSISSIPPI STATE UNIVERSITY / National Science Foundation

RESEARCH CENTER
COMPUTATIONAL FIELD SIMULATION

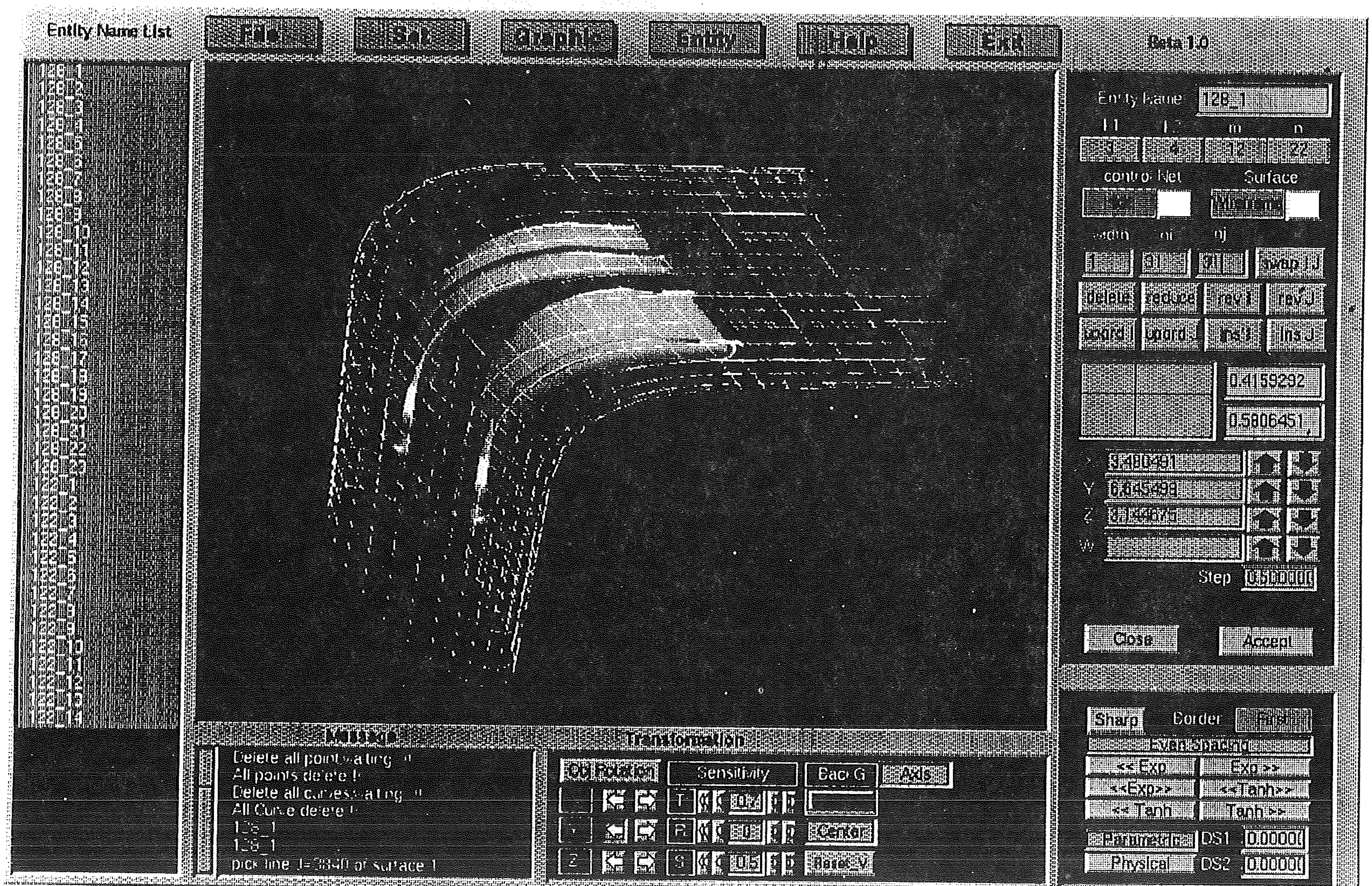

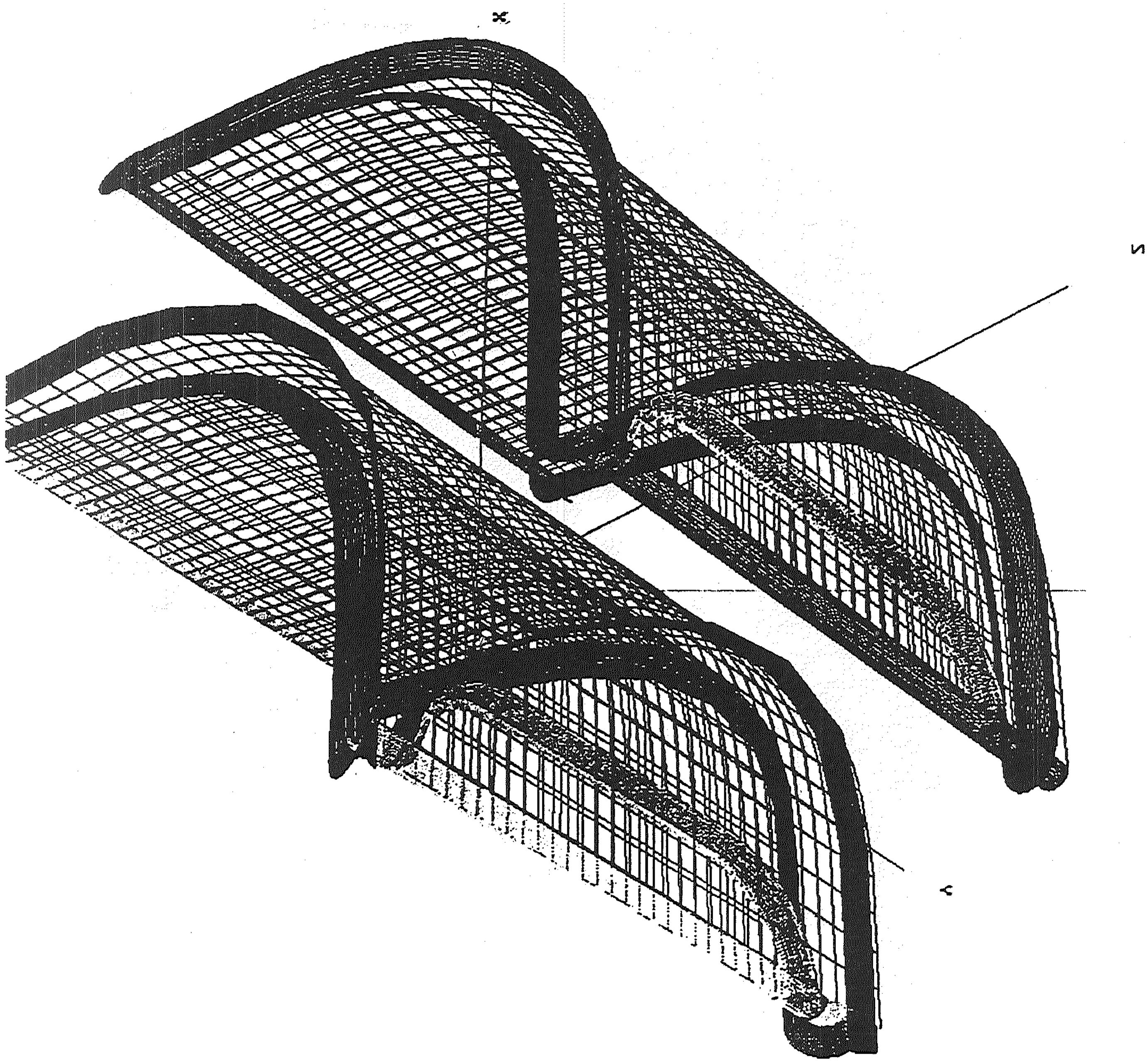

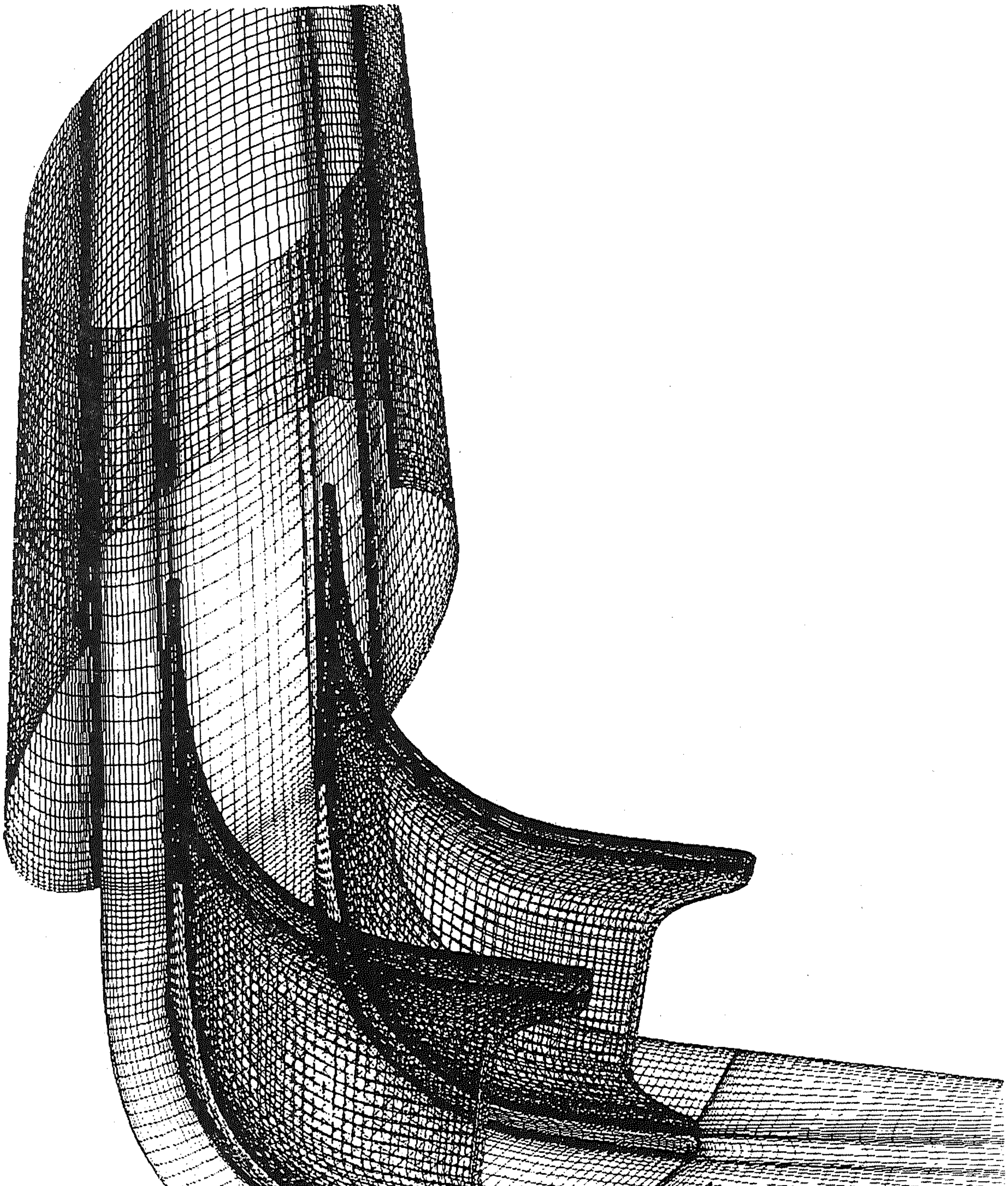

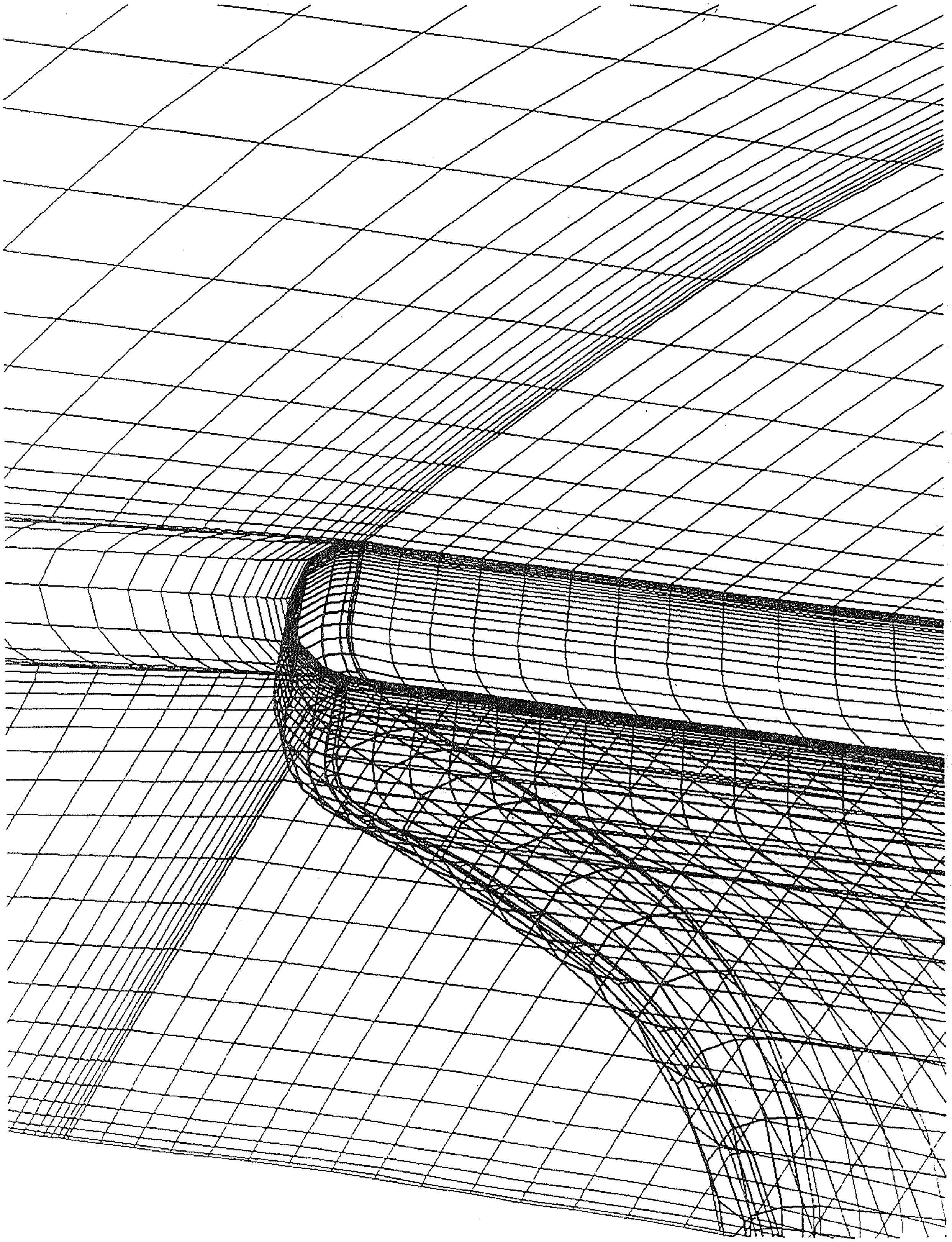

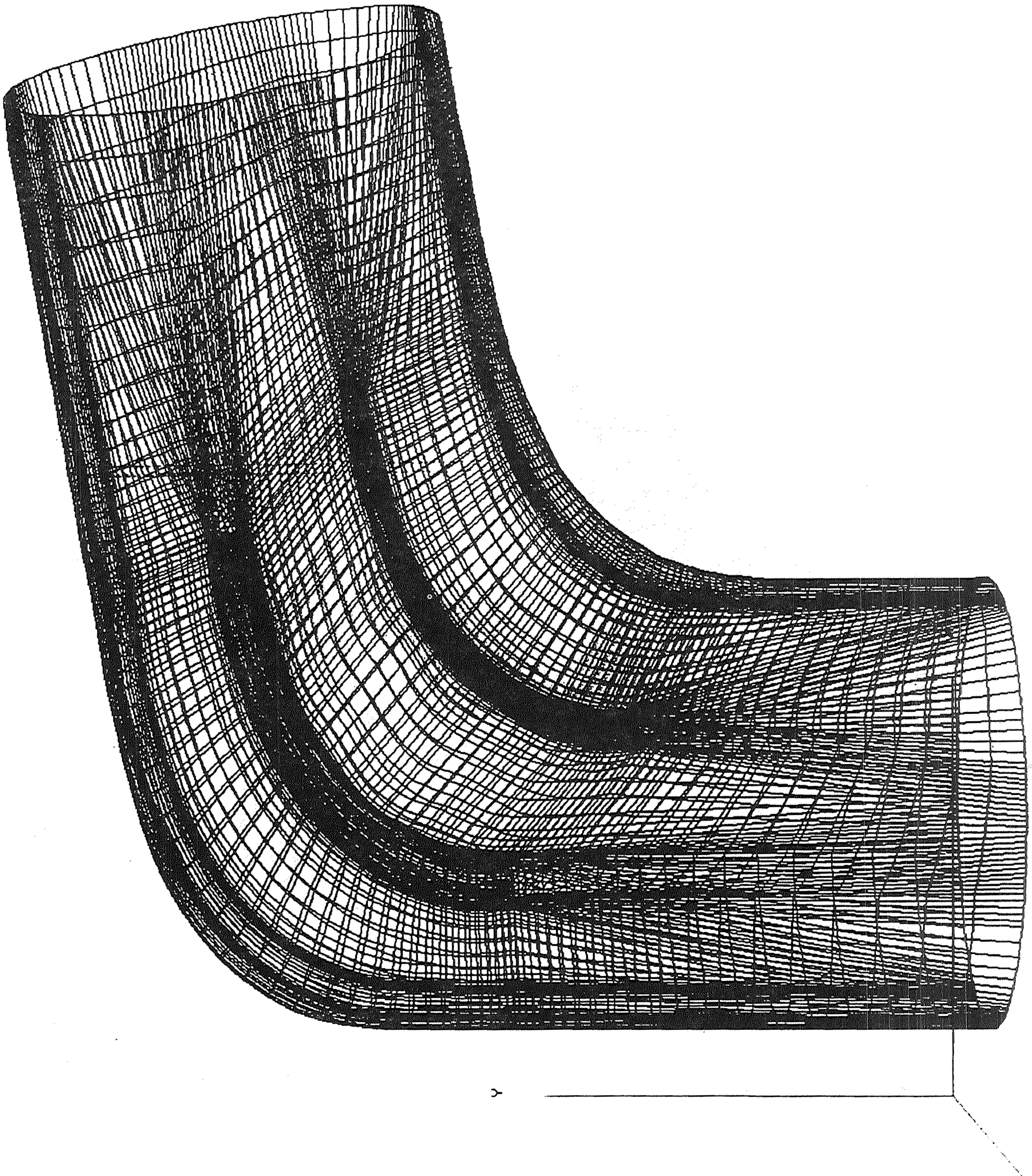

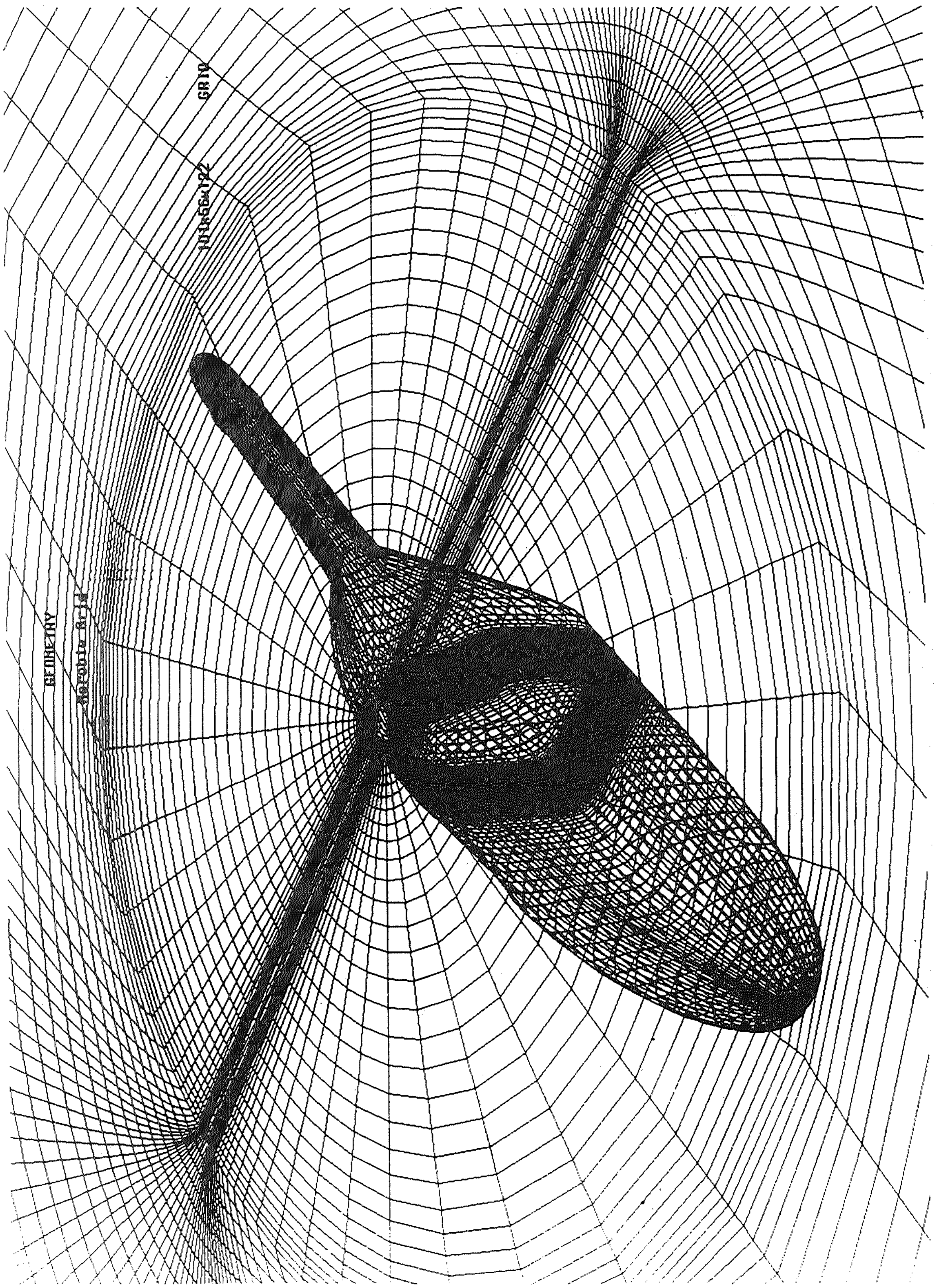
GEOMETRY
101x56x122
GRID

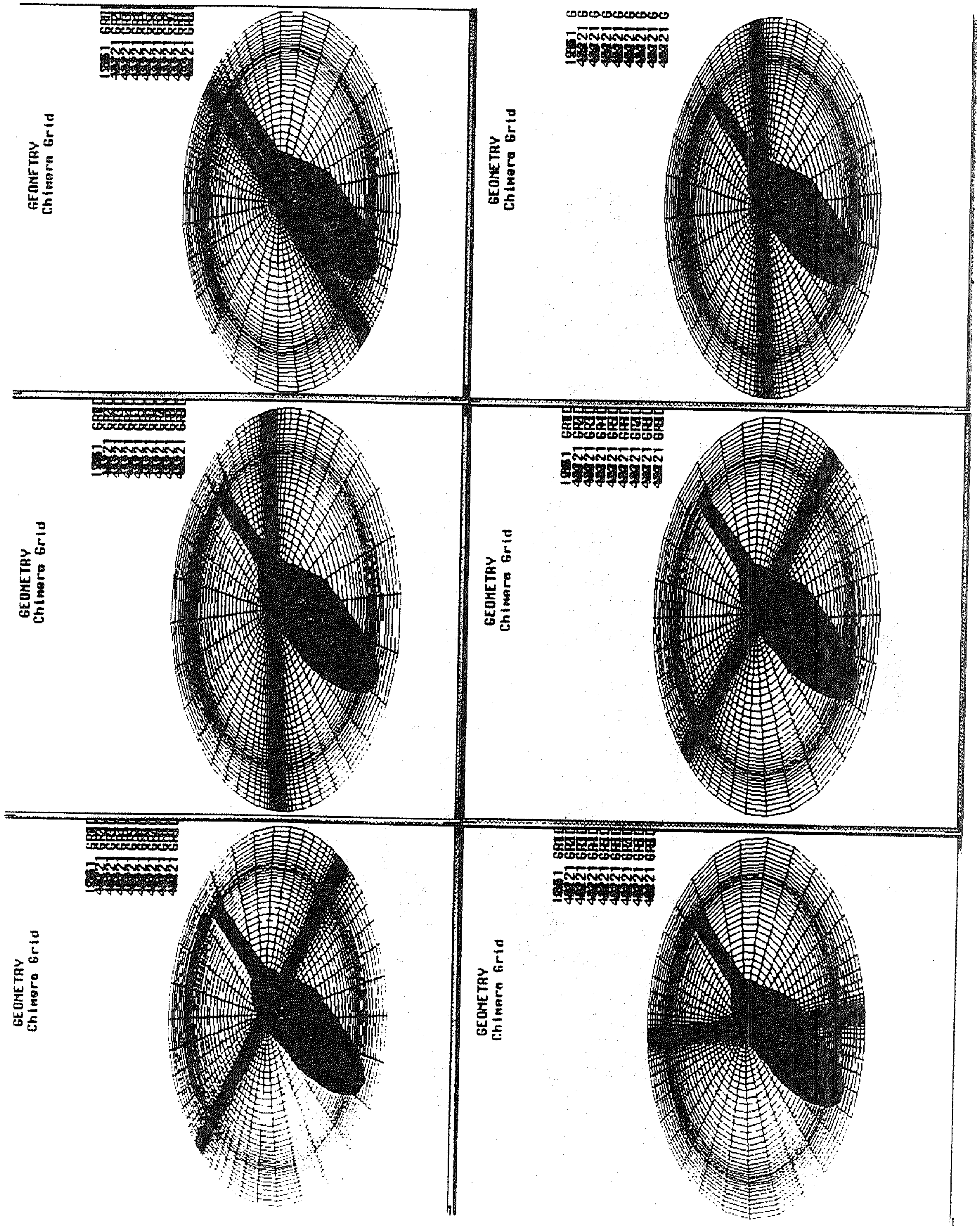
GEOMETRY
Chimera Grid
GEOMETRY
Chimera Grid
GEOMETRY
Chimera Grid
GEOMETRY
Chimera Grid
GEOMETRY
Chimera Grid
GEOMETRY
Chimera Grid

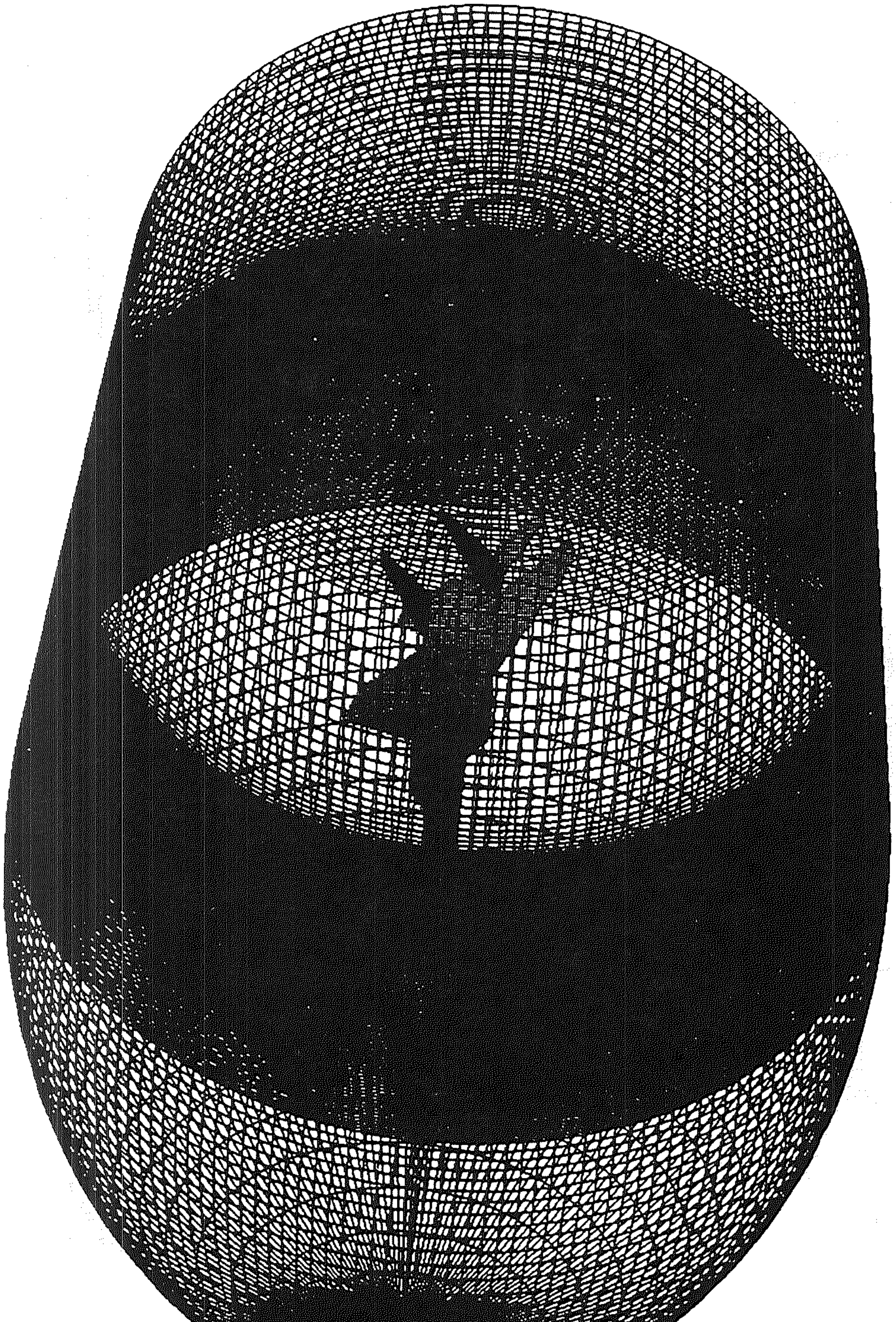

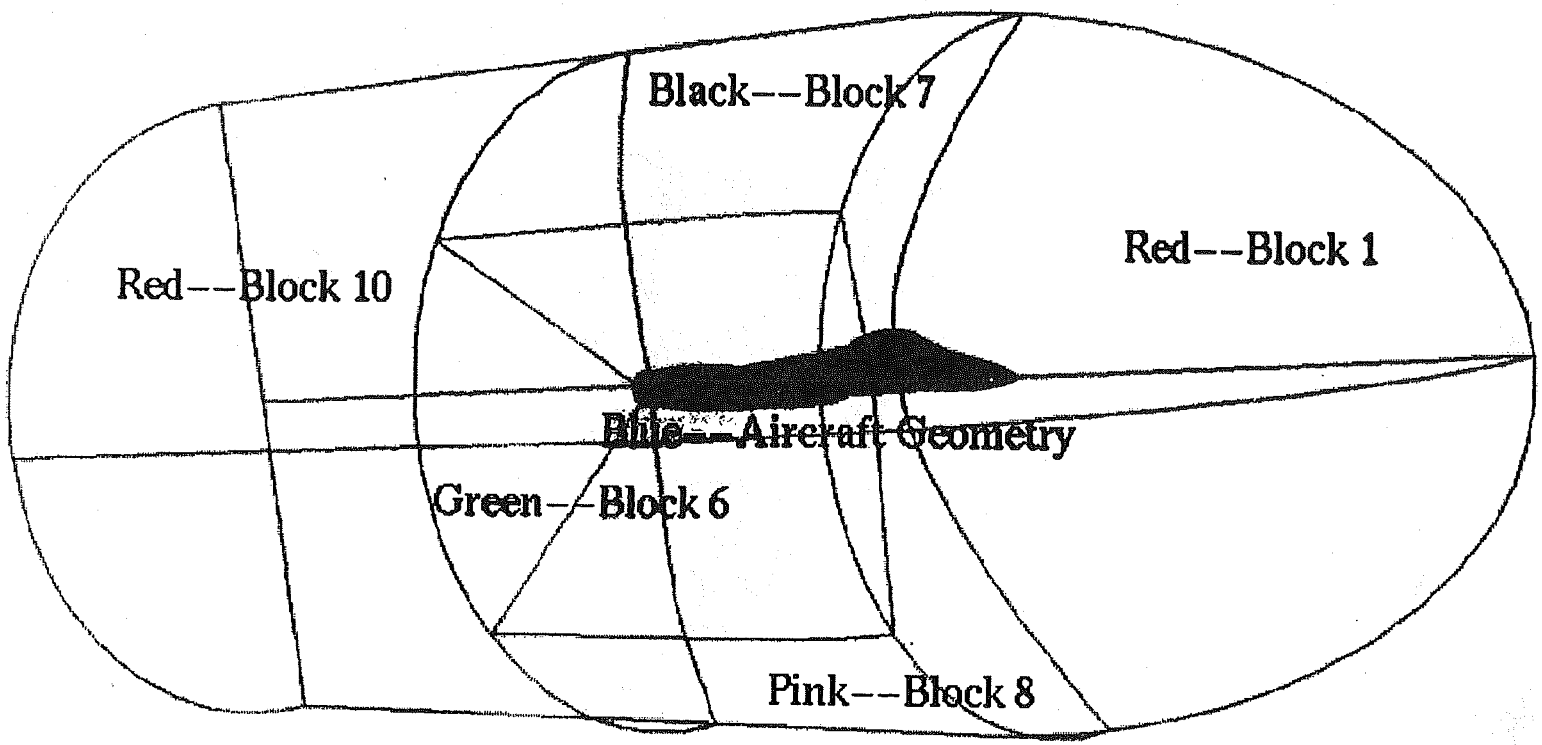

F15e Blocking Strategy

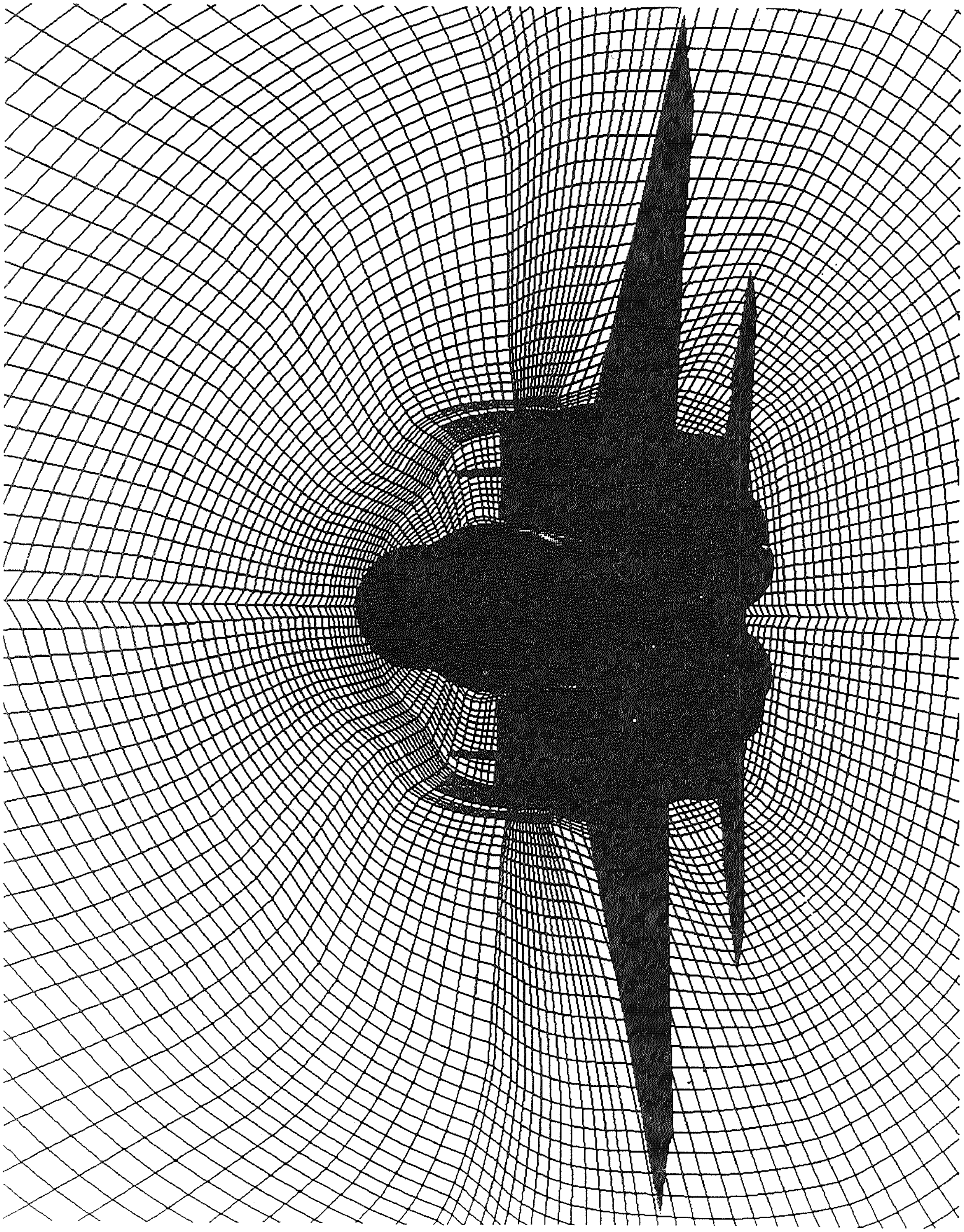

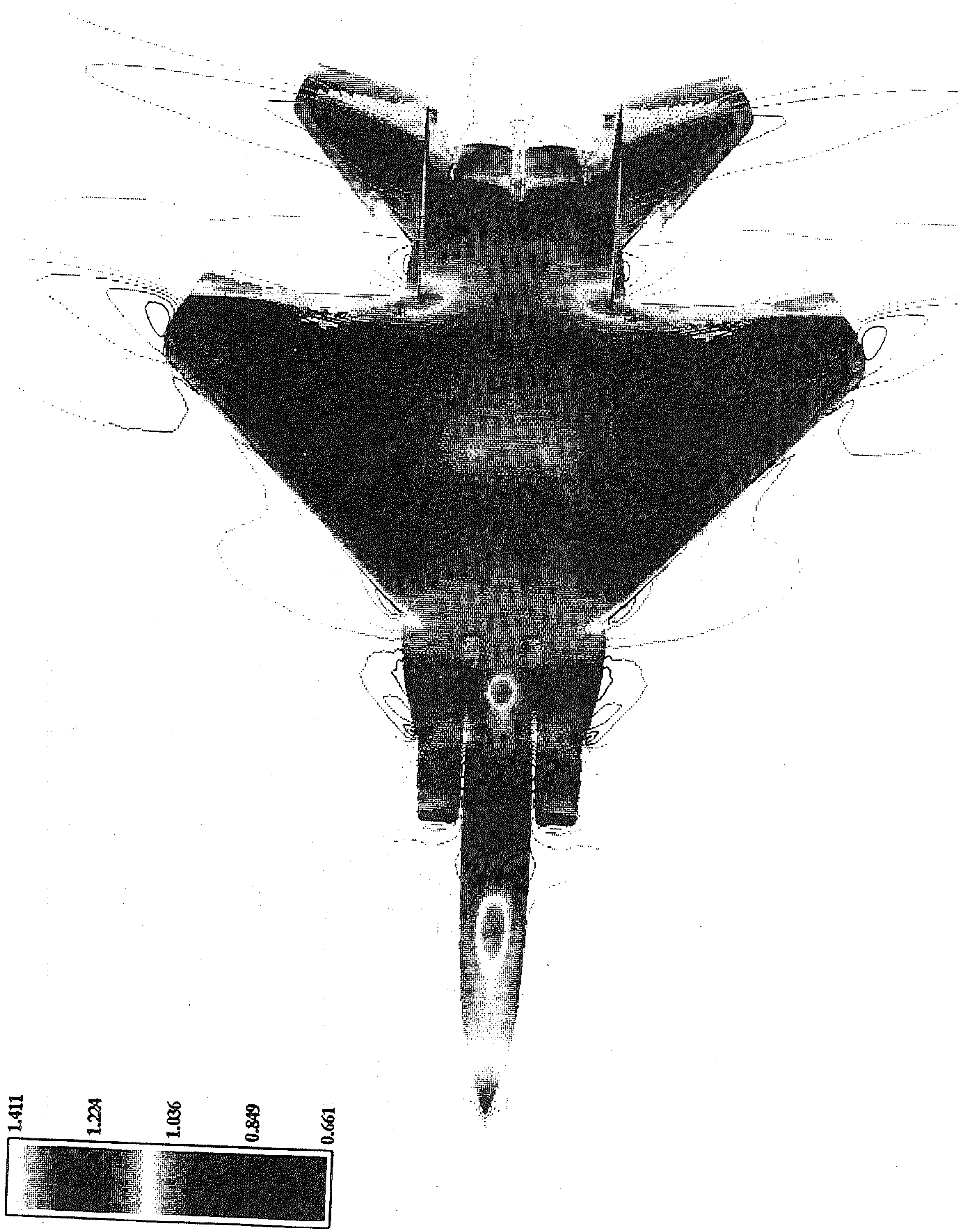
1.411
1.224
1.036
0.849
0.661

GENIE^{++}

- Semi-Interactive - Simple Minded
- Portable, Modular
- Journal File Execution Control
- Batch-Interactive Execution
- CadType Geometry Construction
- SOA Grid Generation Algorithms
- Quality Control & Extenstive Error Checking
- Online Graphical Visualization of Overall Process
- User Friendly & Researcher Friendly
- SGI, X-Window, PC Versions
- bsoni@erc.msstate.edu

Surface and Volume grid generation in parametric form

by

Tzuyi Yu, Bharat K. Soni

NSF/ERC For Computational Field Simulation

Mississippi State University, MS39762

Ted Benjamin, Robert Williams

Marshall Space Flight Center, AL 35812

ABSTRACT

The algorithms for surface modeling and volume grid generation using parametric NURBS geometric representation are presented. The enhanced re–parameterization algorithm which can yield a desired physical distribution on the curve, surface and volume is also presented. This approach bridges the gap between CAD surface / volume definition and surface / volume grid generation.

INTRODUCTION

Surface grid generation is the most labor intensive part of the overall complex three dimensional grid generation process. Also, a significant amount of effort is required in changing the resolutions (grid sizes) and / or the distribution of the grid while maintaining geometry fidelity. In the last few years, various researchers have concentrated on utilizing the Computer Aided Geometry Design (CAGD) techniques to expedite the overall surface generation process. In this presentation, a parametric formula which has been used in CAD system is extended with re–parameterization approach to numerical grid generation for modeling the surface as well as the volume grid.

There are many parametric approaches for representing sculptured geometry, such as rational or non–rational Bezier, cubic splines, rational or non–rational B–spines, ... ,etc. Among these representation, the Non–Uniform Rational B–Splines (NURBS) has been widely accepted among these researchers. NURBS has been widely utilized to represent and design geometry in the CAD/CAM and the graphics community due to its powerful features, such as the local control property, variation diminishing, convex hull and affine invariance [Ref 1,2]. Also the geometry tool kits, such as curve/surface interpolation, data reduction, degree elevation, knot insertion and splitting, are well–developed [Ref 1,2,]. These properties have made NURBS representation very popular in recent developments in CAD/CAM. However, the distribution requirements in CFD application are much complicated than those in CAD system. Hence, the NURBS must be cooperated with re–parameterization algorithm so that it can be more useful in grid generation. Computational examples associated with practical configurations are shown in Figure 1 and 2. The re–parameterization approach described in many research [Ref 2,3] is implemented by iteration process, which needs a lot of computation time. The more efficient and robust approach presented here needs only one interpolation process.

The development of the software based on NURBS representation package: CAGI (Computer Aided Grid Interface) was initiated by authors under the sponsorship of NASA Marshall Space Flight Center. The purpose of this presentation is to present the progress realized in enhancing the NURBS based curve / surface grid generation techniques into a 3D volume grid generation technique. To this end, various options for generating 3D volume geometry–grid are discussed. A reparameterization scheme has been developed to achieve desired distribution in physical space. Computational examples for modeling practical configurations have been exercised using the volume options and the reparameterization scheme.

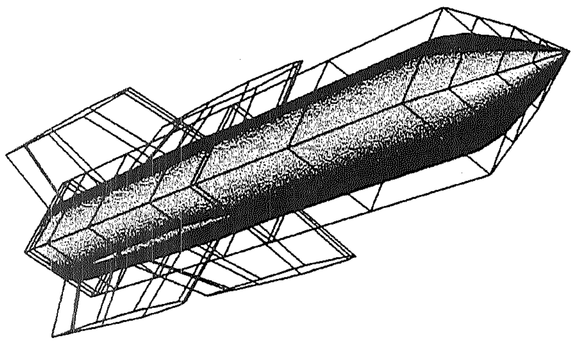

Figure 1: Propulsional example.
3D NURBS control patches model
the missile (with fins) geometry.

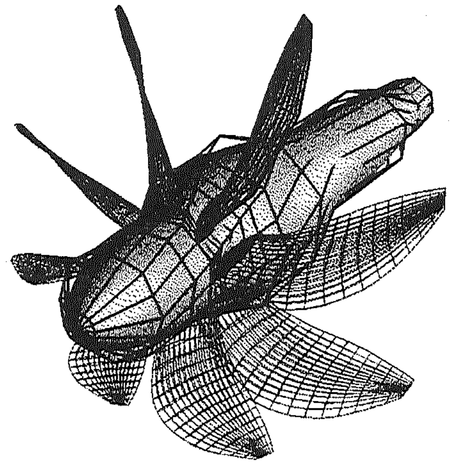

Figure 2:
3D NURBS control patches model
the single rotation propfan.

References

[1] Piegl, L., – '*On NURBS: A survey' IEEE Computer Graphics & Applications,* Vol 11, No 1, pp 57 – 71, January, 1991.

[2] FARIN, G. "NURB curves and surfaces: from projective geometry to practical use," First Edition, A K Peters, Ltd., 1995.

[3] Yu, T.Y. and Soni, B.K.,"Geometry Transformer and NURBS in grid Generation," 4th International Conference on Numerical Grid Generation in CFD and Related Fields, Swansea, UK., April 6–8, 1994.

[4] Yu, T.Y., Soni, B.K., and Shih M. H. "CAGI: Computer Aided Grid Interface," AIAA–95–0243, 33nd Aerospace Sciences Meeting & Exhibit., Reno, Nevada January 09~12,1995.

Title: Surface and Volume grid generation in parametric form

Authors: Tzu–Yi Yu, Bharat K. Soni

Missisippi State University /Engineering Research Center
2 Research Blvd., Starkville, MS 39759, USA

Ted Benjamin, Robert Williams

NASA/Marshall Space Flight Center

Sponsor: NASA/Marshall Space Flight Center

Geometry generated in parametric space:

Advantages:

1> Natural for grid generation algorithm.

2> Easy manipulation. ← Designer's Dream.

3> Less storage & standard data structure.

4> Way of future.

Disadvantage:

0> Distribution differs in parametric space
and physical space.

NURBS: Non–Uniform Rational BSpline is selected.

1> Stable and robust geometric properties.

Degree raising, spliting/join algorithm, convex hull, shape preserving, local support, ... etc.

2> IGES (Initial Graphics Exchange Specification) ,NASA IGES, NINO.

3> Way of Future :

Solid Geometry Modeling.

STEP.

CAGI: A NURBS database package.

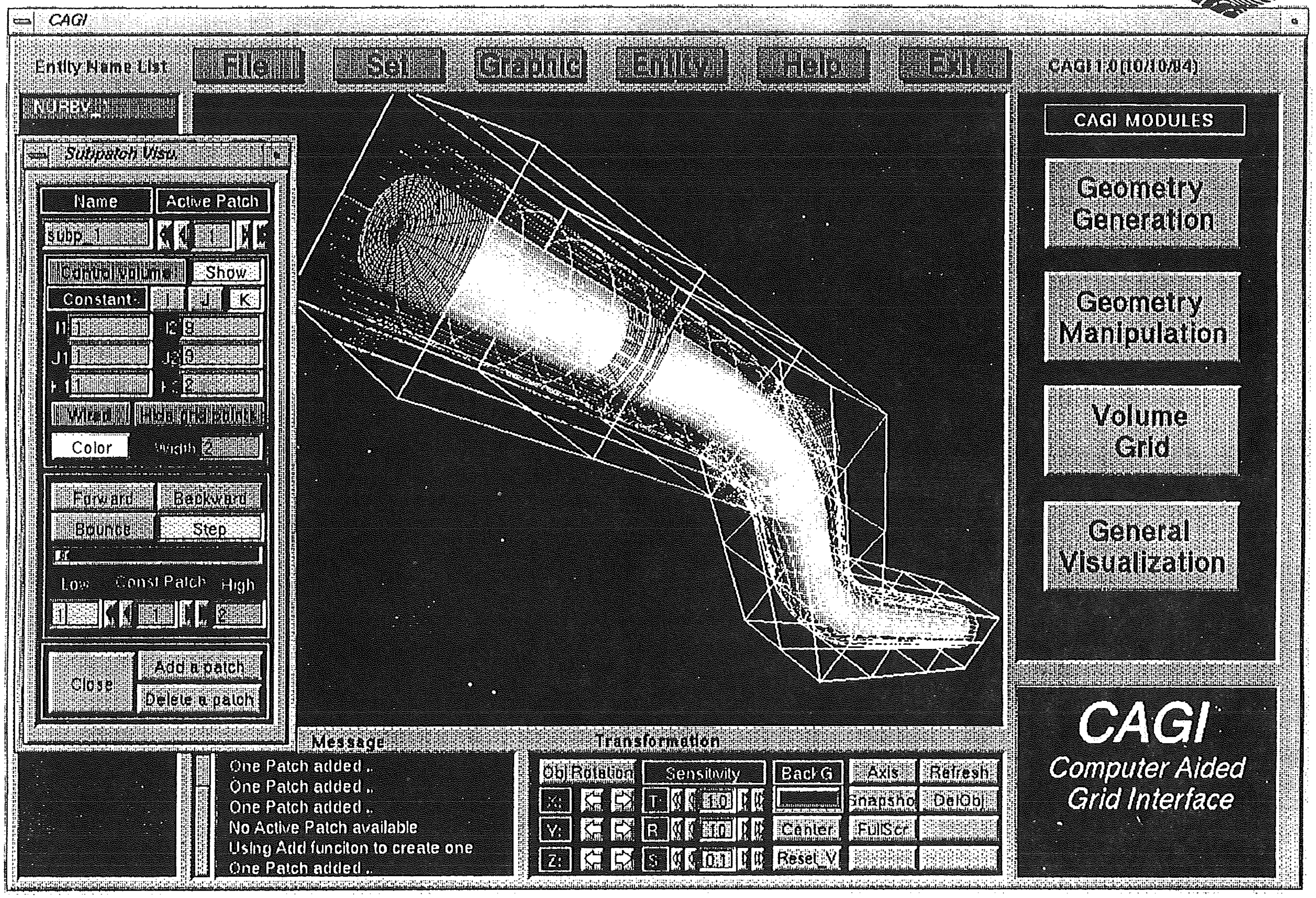
CAGI
Entity Name List
File
Set
Graphic
Entity
Help
Exit
CAGI 1.0 (10/10/94)
Subpatch Visu
Name
Active Patch
Show
Constant
Color
Forward
Backward
Bounce
Step
Low
Const Patch
High
Close
Add a patch
Delete a patch
Message
One Patch added ..
One Patch added ..
One Patch added ..
No Active Patch available
Using Add funciton to create one
One Patch added ..
Transformation
Obj Rotation
Sensitivity
BackG
Axis
Refresh
Snapsho
DelObj
Center
FullScr
Reset_V
CAGI MODULES
Geometry Generation
Geometry Manipulation
Volume Grid
General Visualization
CAGI
Computer Aided Grid Interface

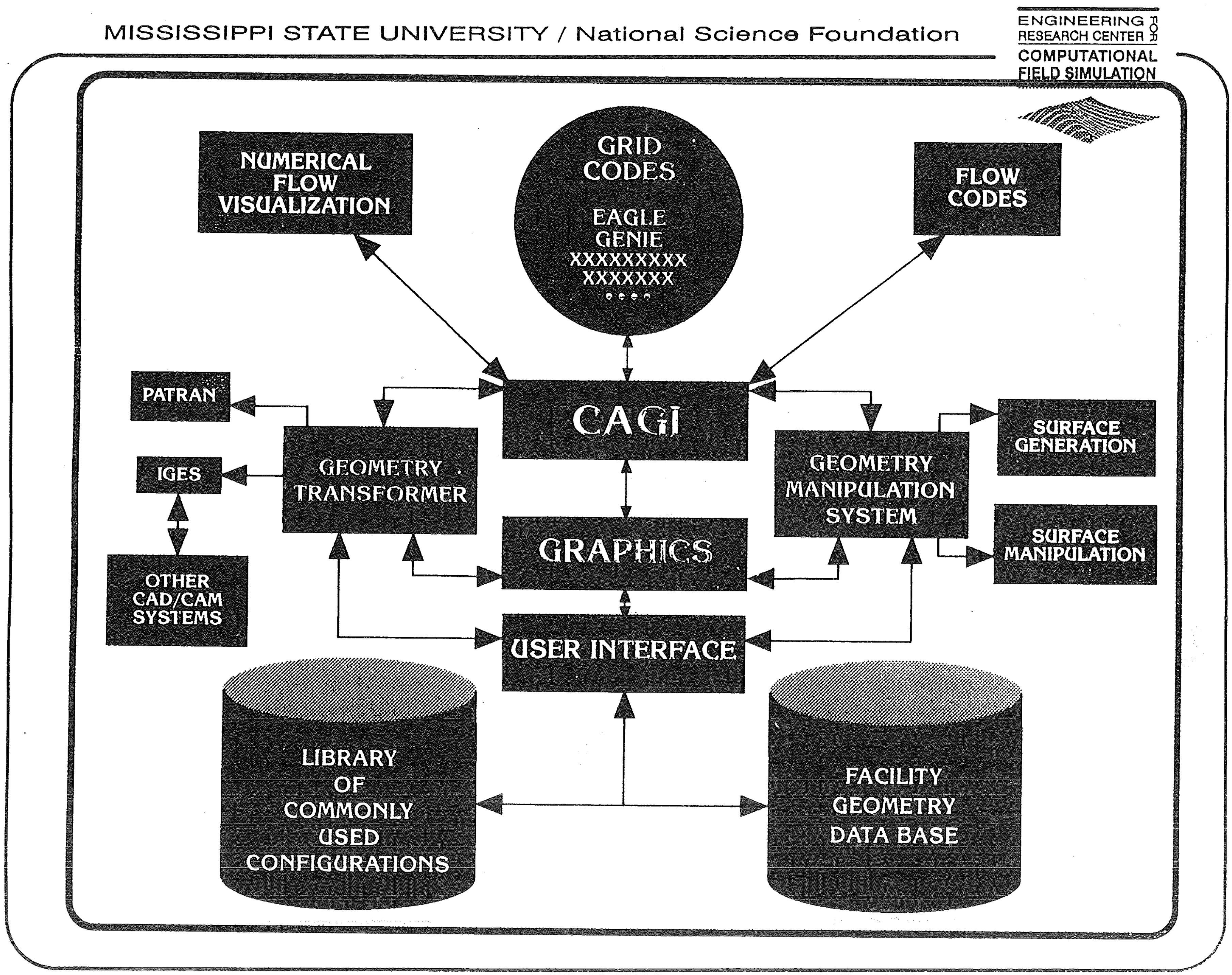
MISSISSIPPI STATE UNIVERSITY / National Science Foundation
ENGINEERING RESEARCH CENTER FOR COMPUTATIONAL FIELD SIMULATION
NUMERICAL FLOW VISUALIZATION
GRID CODES
EAGLE
GENIE
XXXXXXXXX
XXXXXXX
FLOW CODES
PATRAN
IGES
OTHER CAD/CAM SYSTEMS
GEOMETRY TRANSFORMER
CAGI
GRAPHICS
USER INTERFACE
GEOMETRY MANIPULATION SYSTEM
SURFACE GENERATION
SURFACE MANIPULATION
LIBRARY OF COMMONLY USED CONFIGURATIONS
FACILITY GEOMETRY DATA BASE

MISSISSIPPI STATE UNIVERSITY / National Science Foundation

ENGINEERING RESEARCH CENTER FOR COMPUTATIONAL FIELD SIMULATION

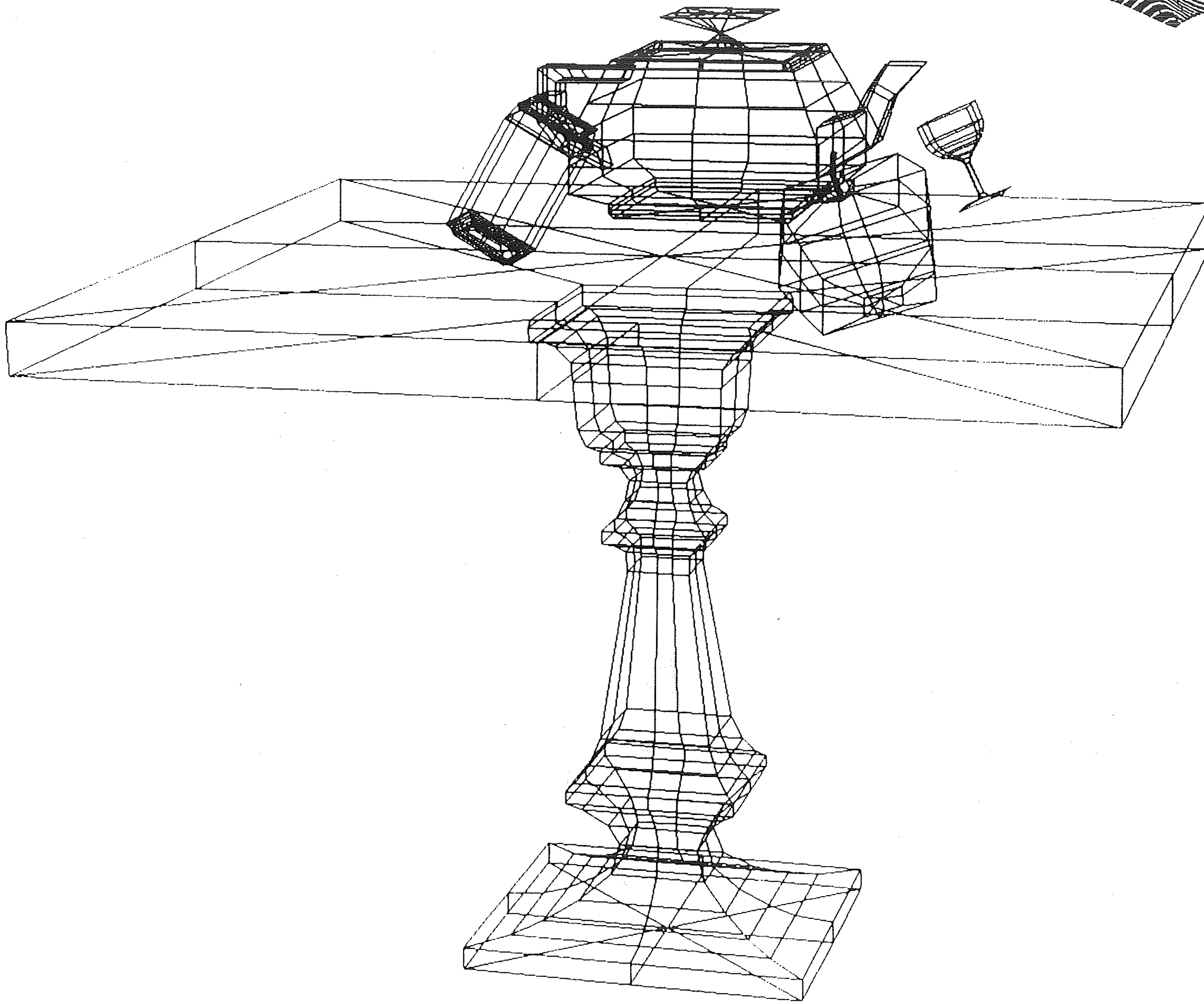

MISSISSIPPI STATE UNIVERSITY / National Science Foundation

ENGINEERING RESEARCH CENTER FOR COMPUTATIONAL FIELD SIMULATION

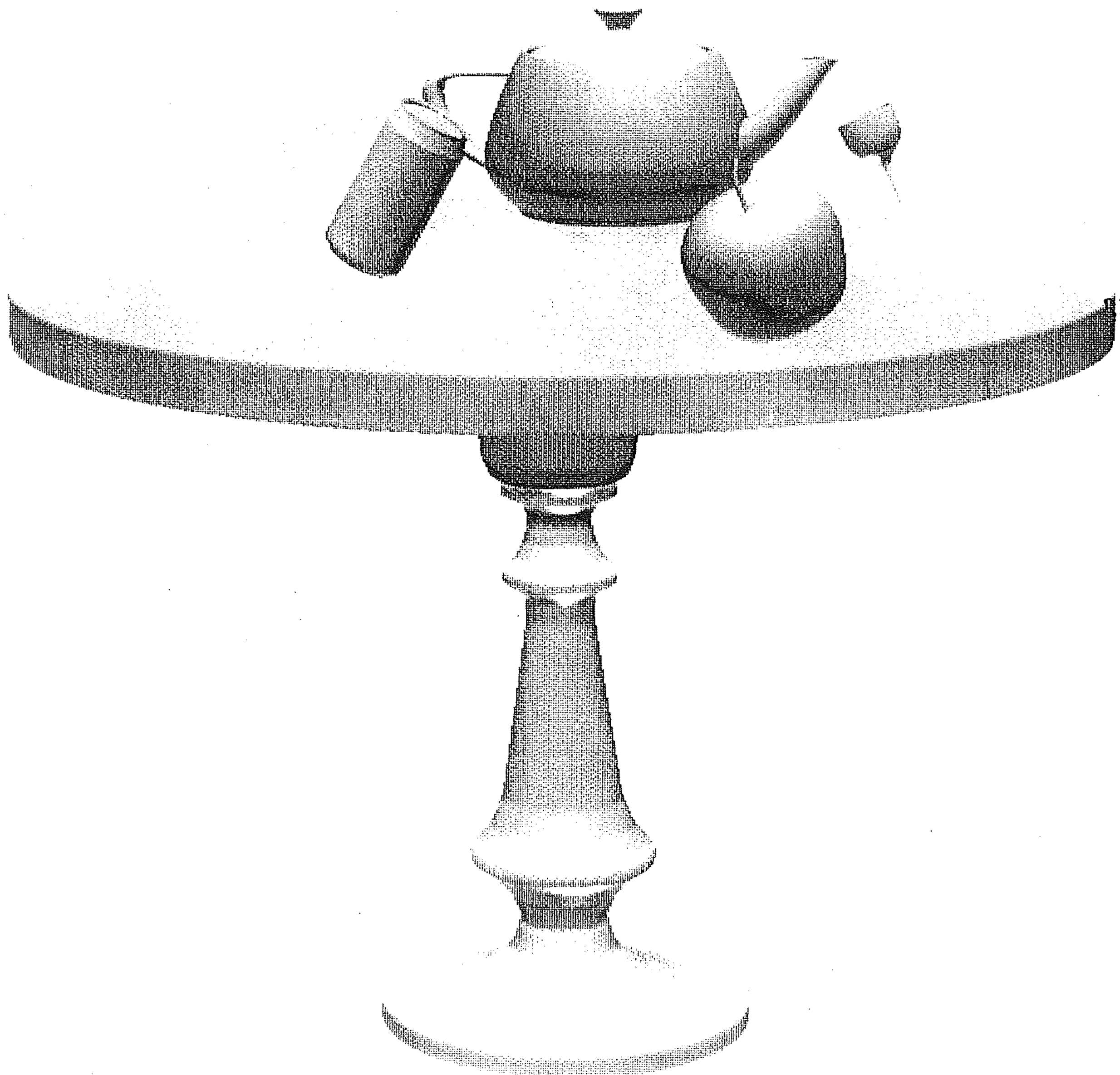

MISSISSIPPI STATE UNIVERSITY / National Science Foundation

ENGINEERING RESEARCH CENTER FOR COMPUTATIONAL FIELD SIMULATION

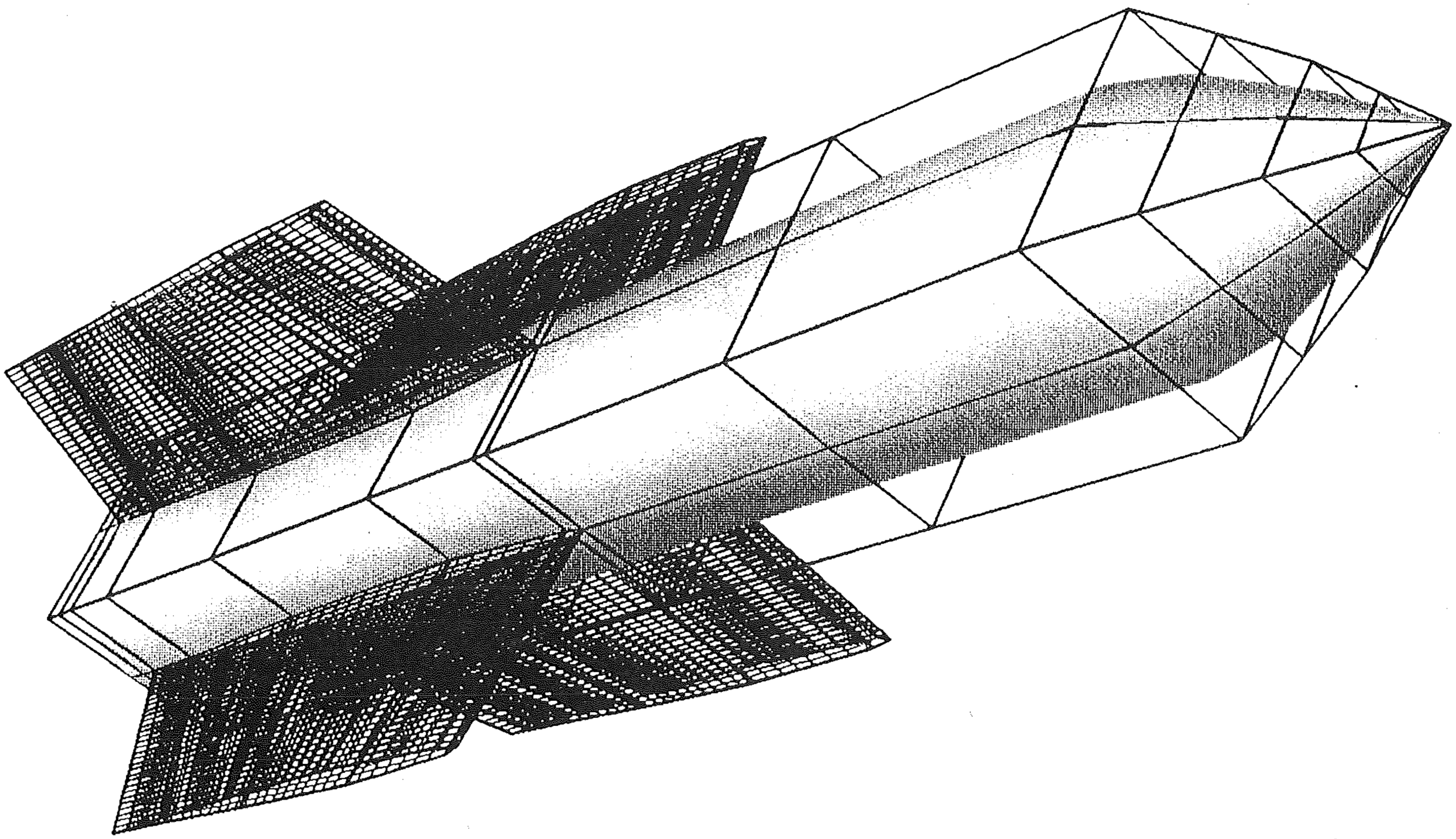

MISSISSIPPI STATE UNIVERSITY / National Science Foundation

ENGINEERING RESEARCH CENTER FOR COMPUTATIONAL FIELD SIMULATION

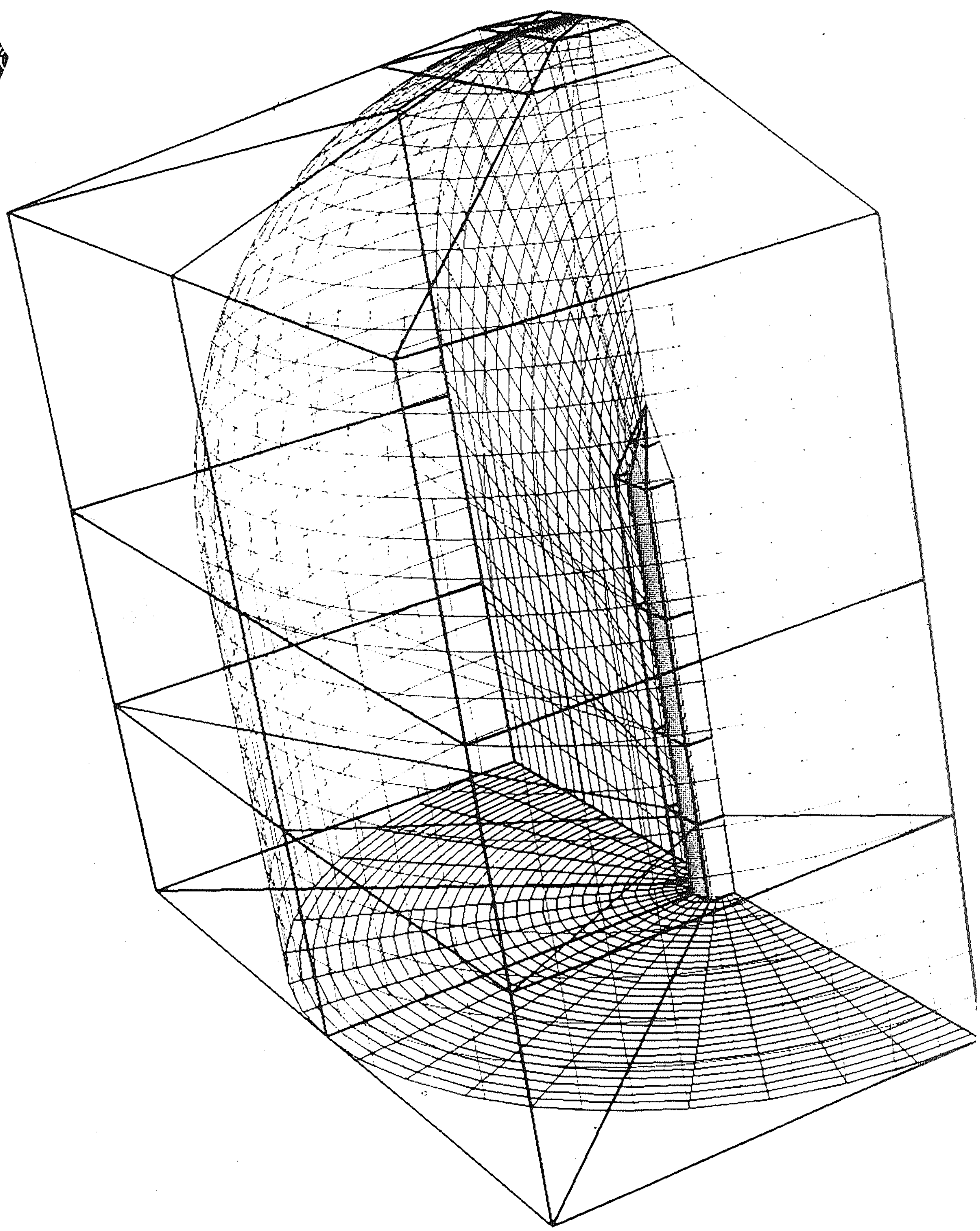

NURBS CONTROL NET WITH MOCKED ENGINE

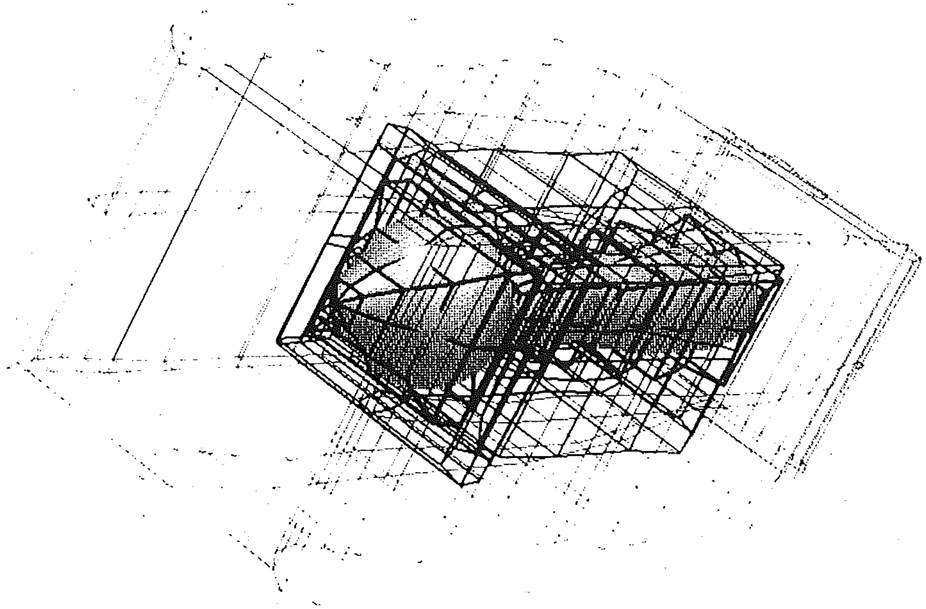

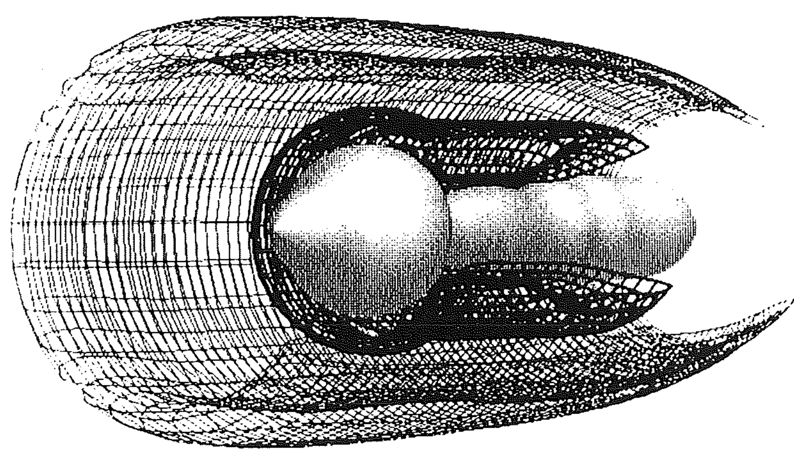

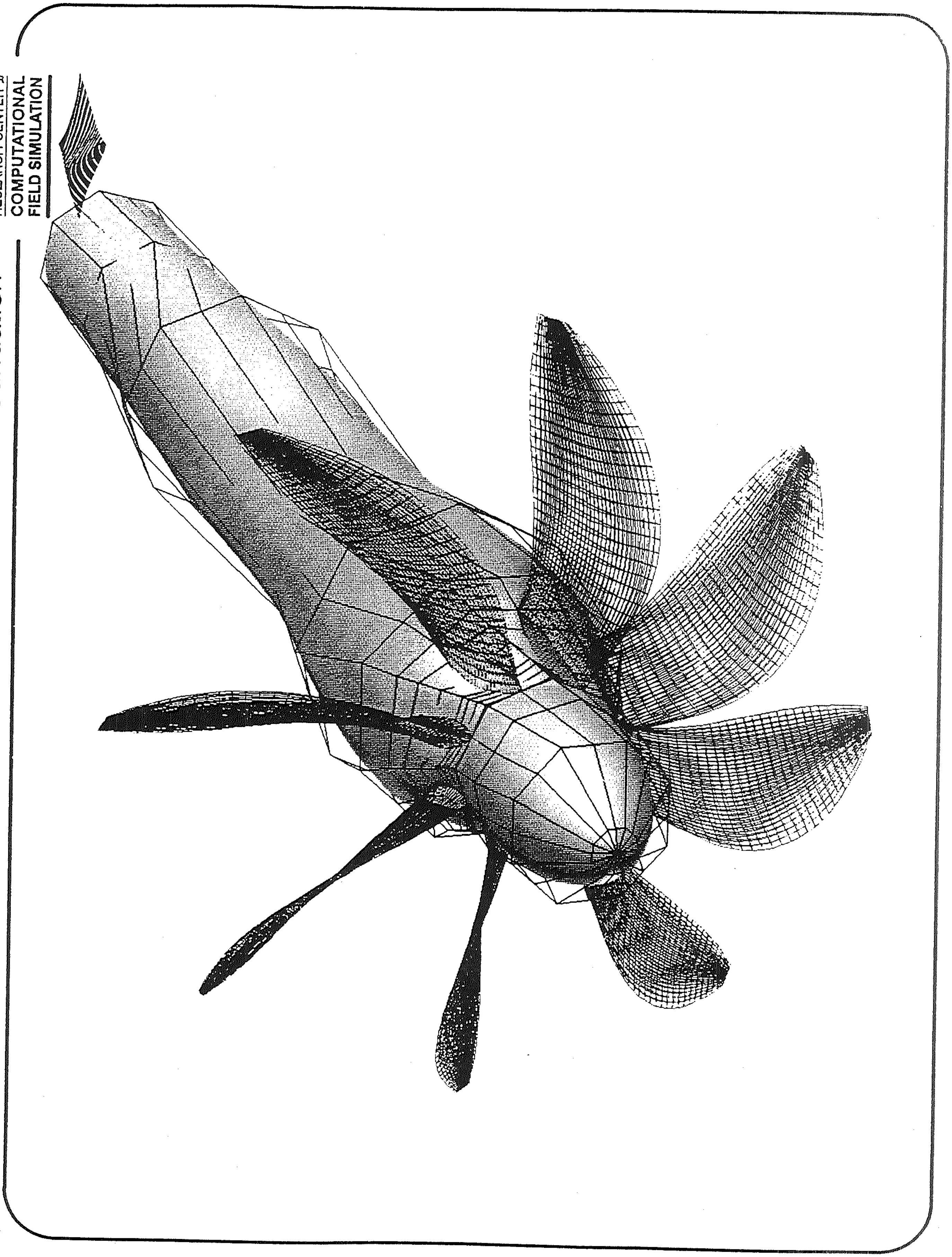
MISSISSIPPI STATE UNIVERSITY / National Science Foundation
ENGINEERING RESEARCH CENTER FOR COMPUTATIONAL FIELD SIMULATION

MISSISSIPPI STATE UNIVERSITY / National Science Foundation

ENGINEERING RESEARCH CENTER FOR COMPUTATIONAL FIELD SIMULATION

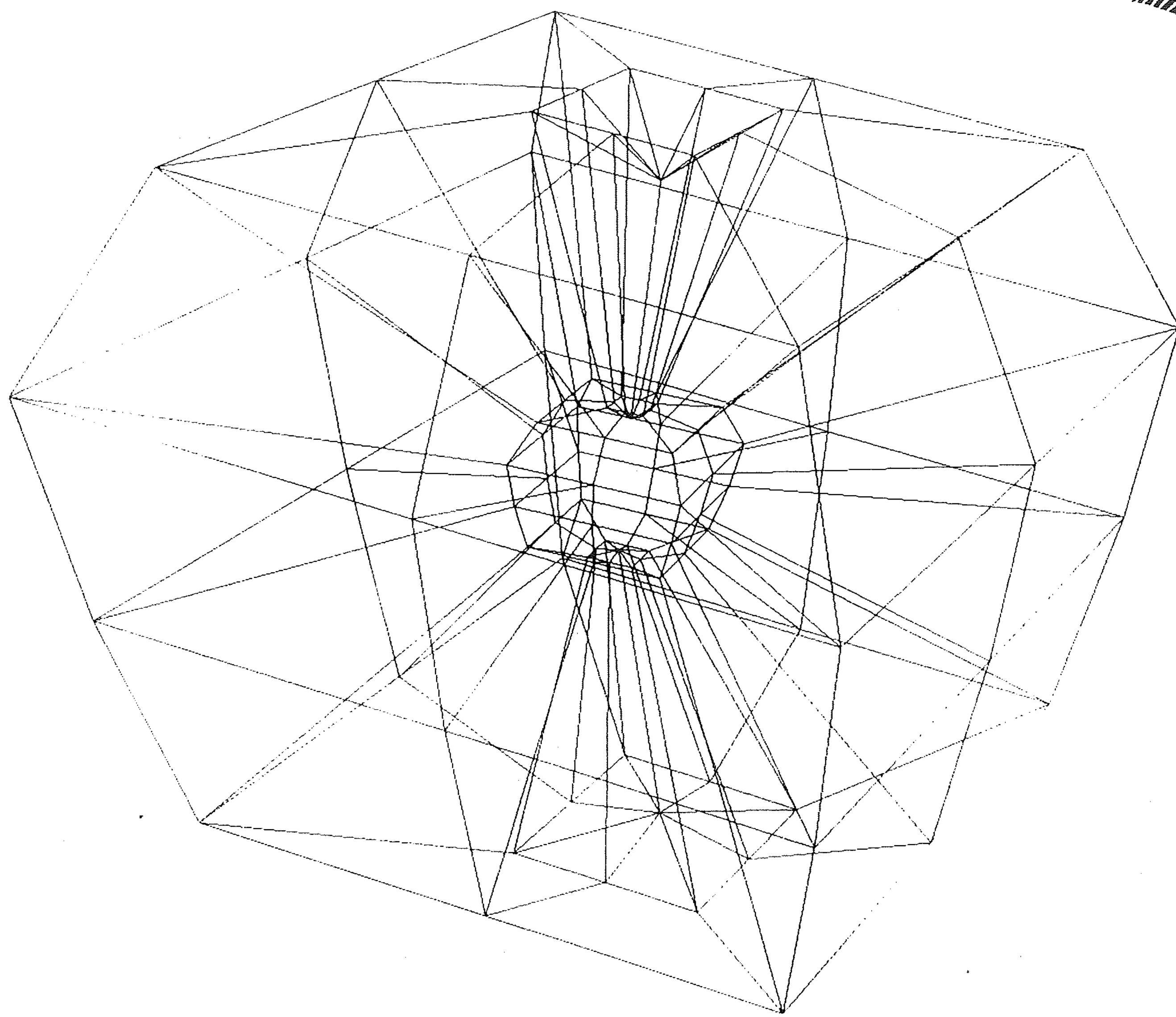

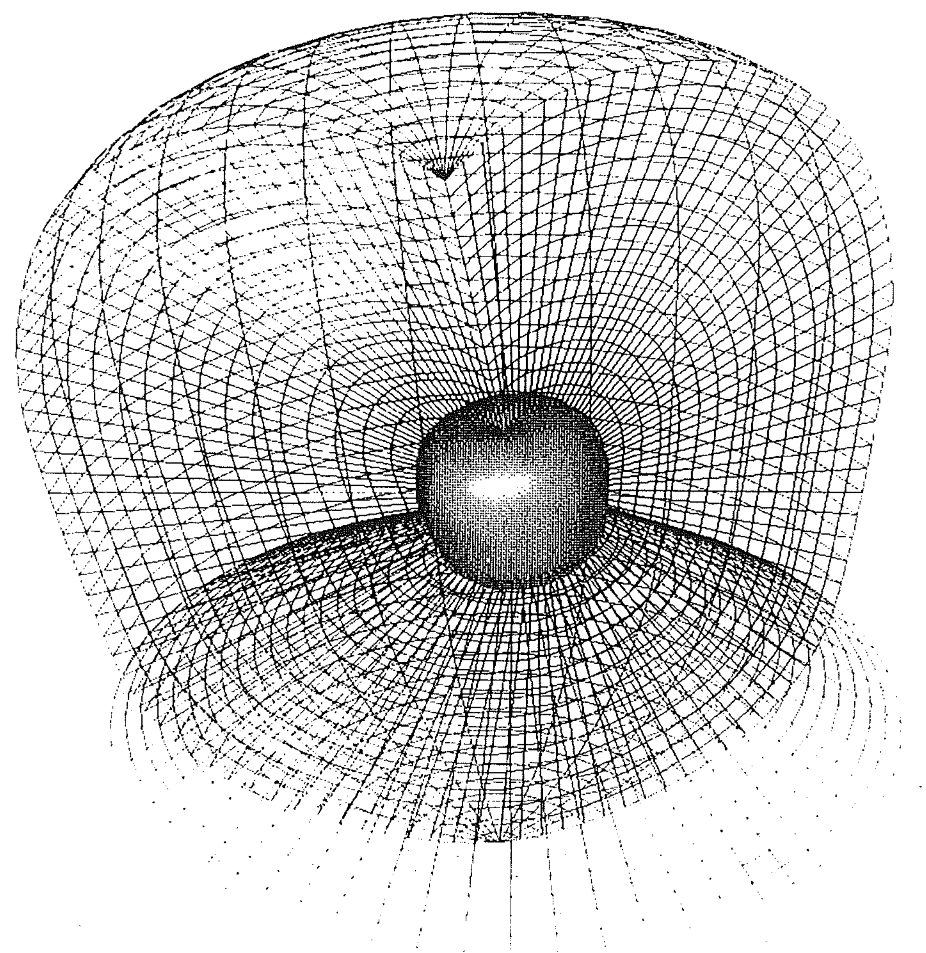

NURBS control volume for a nozzle with square-ellipse-circle sections
(O Type Control Volume)

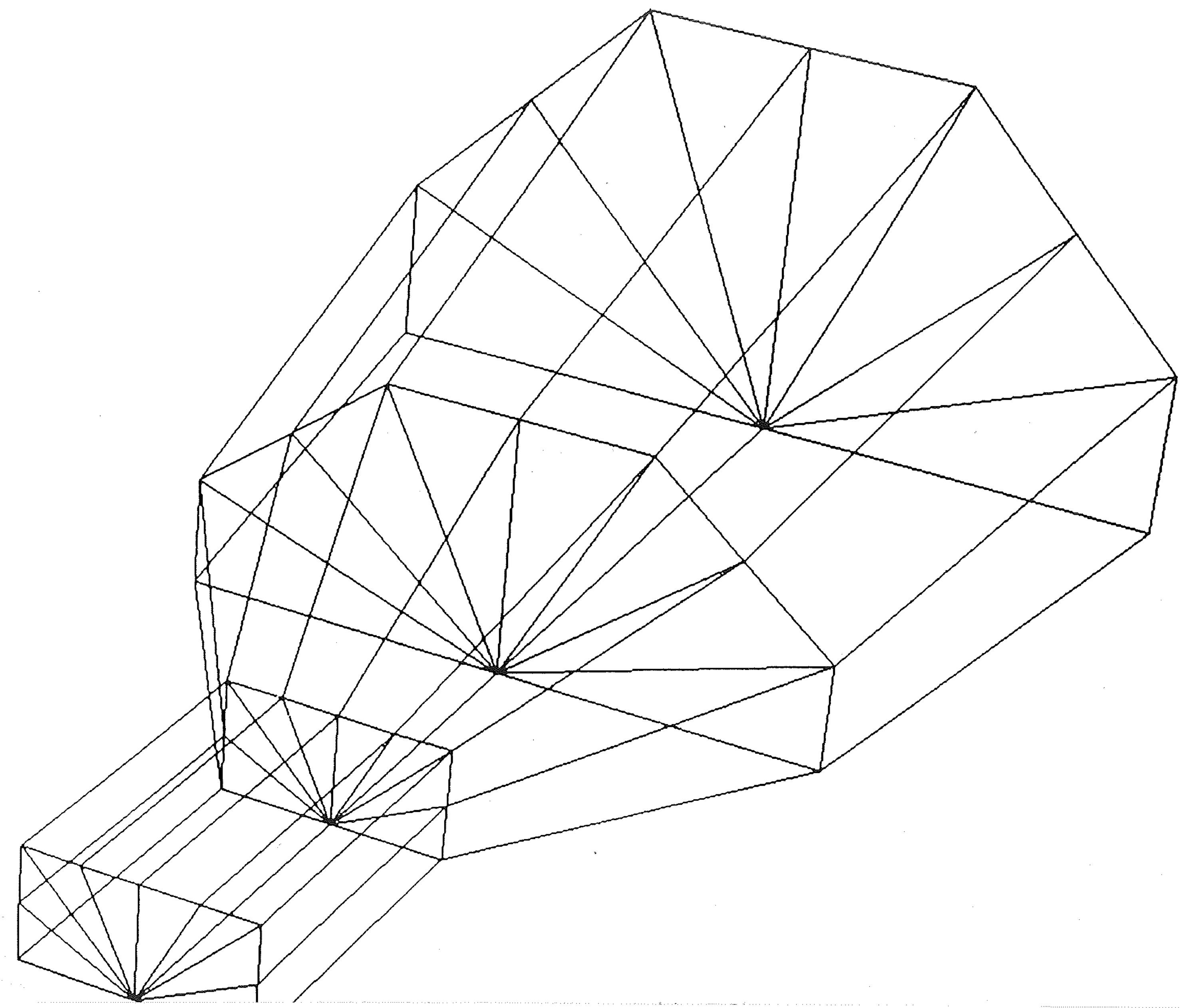

Nozzle with square–ellipse–circle section

(O Type Volume Grid)

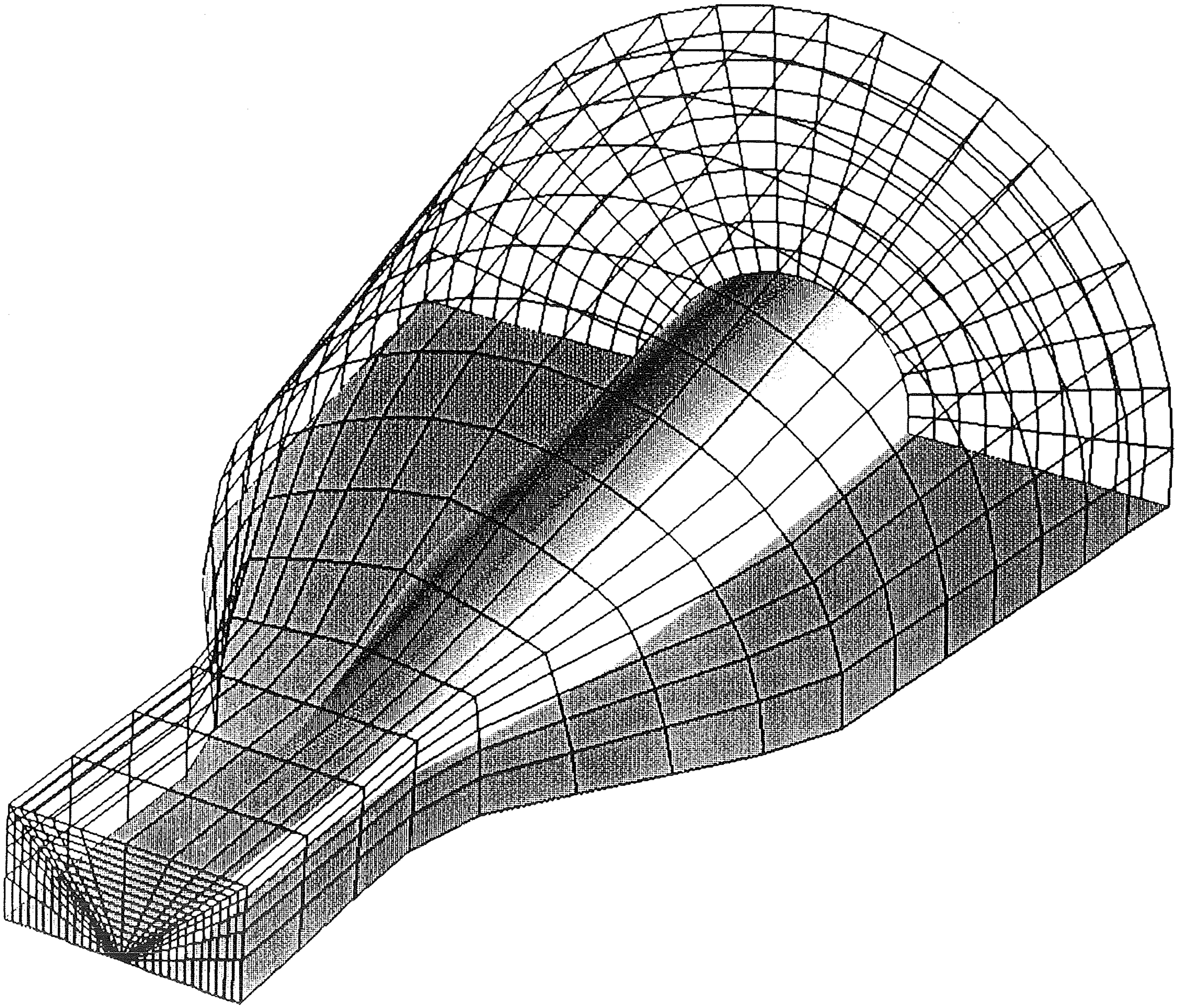

NURBS control volume for a nozzle with square-elliptic-circular sections
(H Type Control Volume)

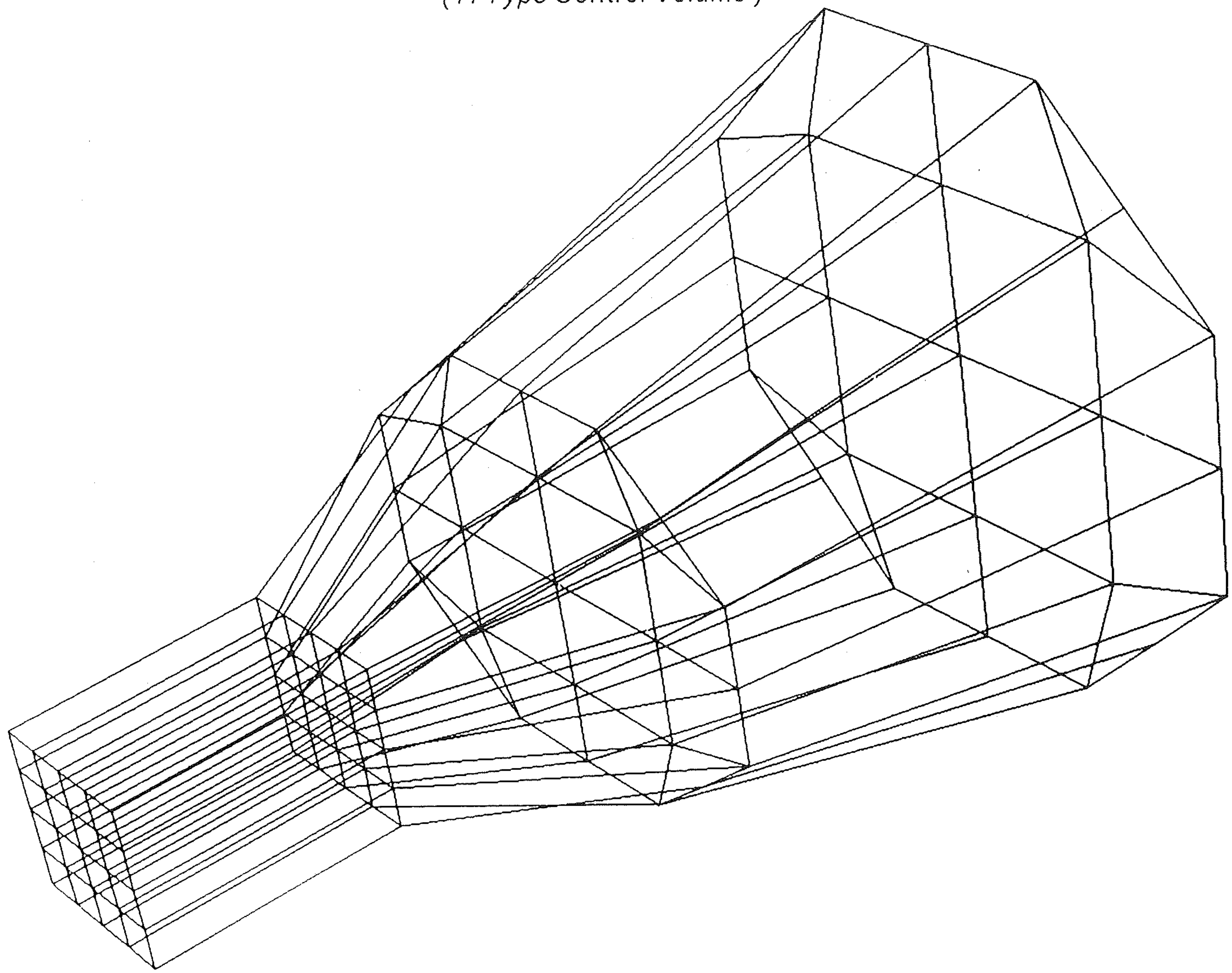

MISSISSIPPI STATE UNIVERSITY / National Science Foundation

ENGINEERING RESEARCH CENTER FOR
COMPUTATIONAL FIELD SIMULATION

A Nozzle with square-ellipse-circular sections
(H Type Volume Grid)

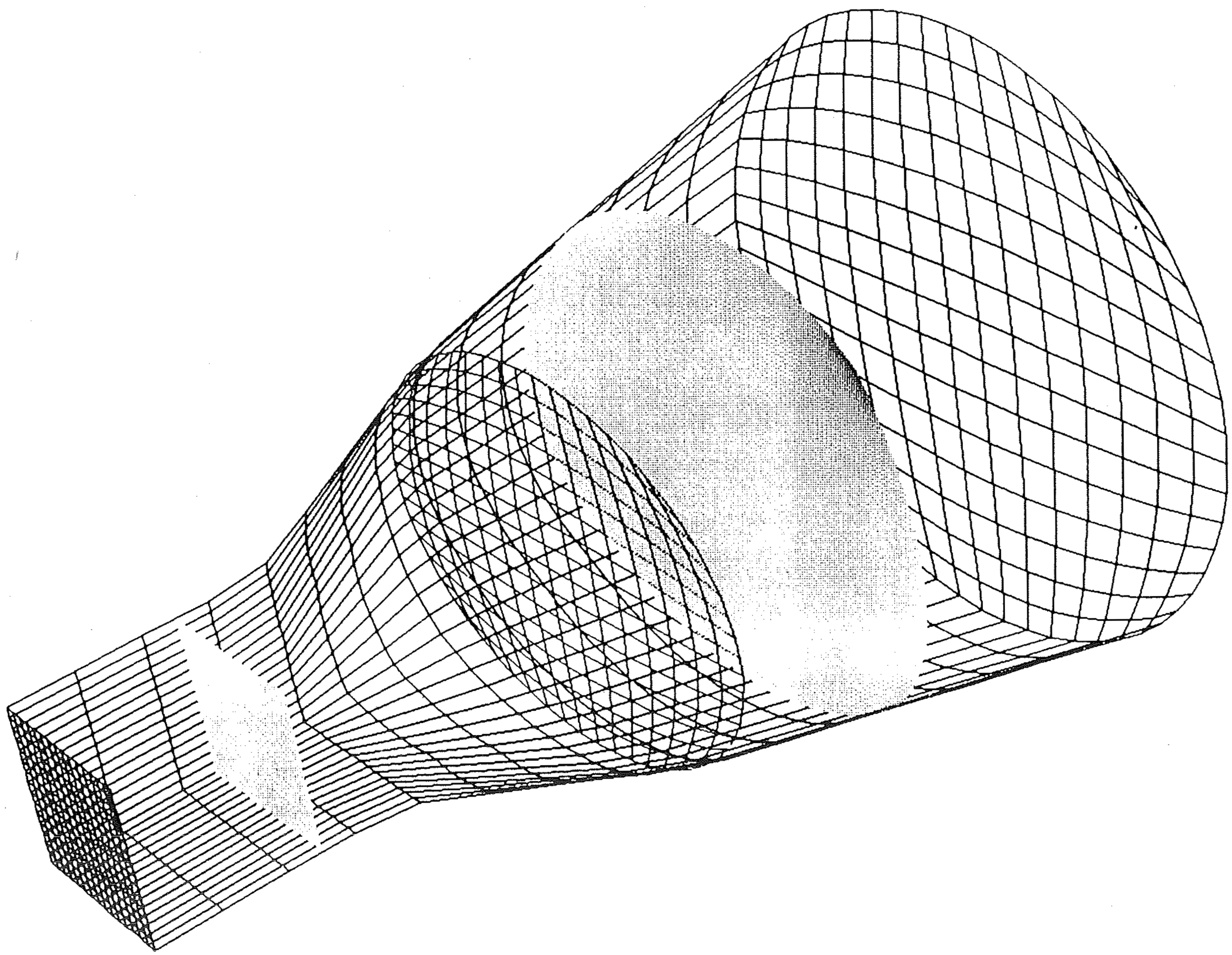

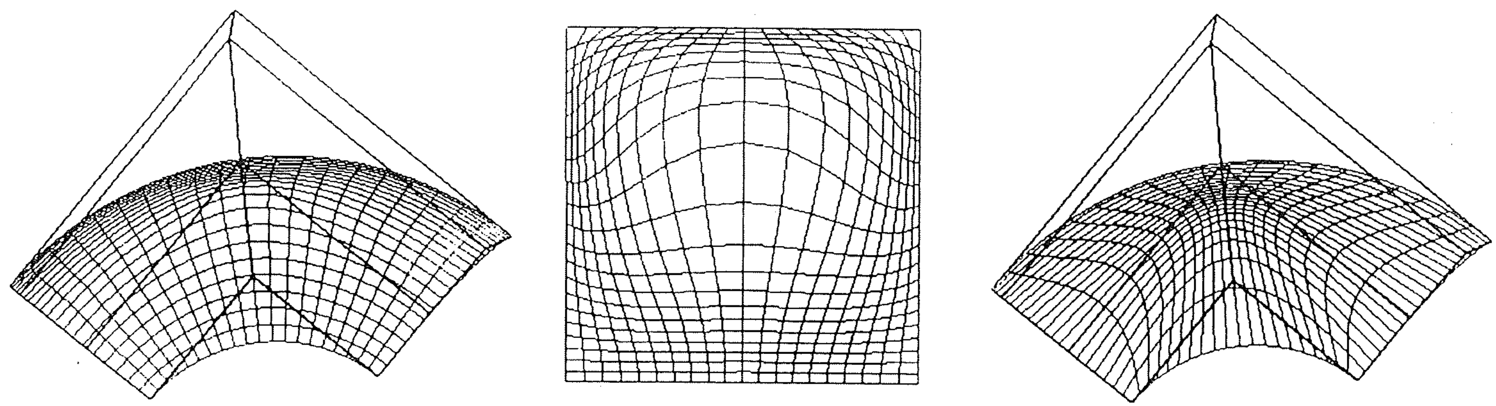

Original Geometry (from CAD/CAM System)

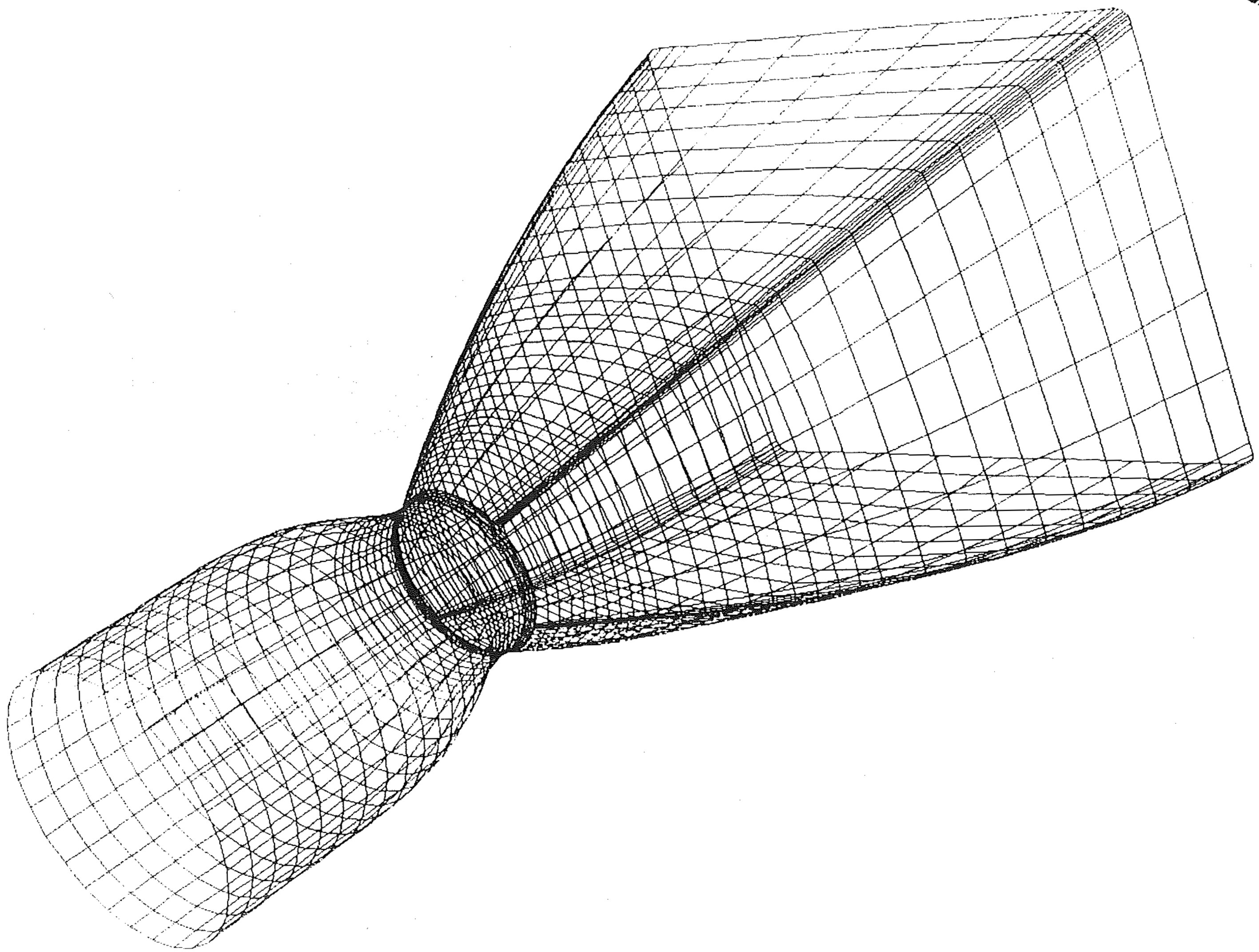

Original NURBS control net from CAD/CAM

NURBS surfaces are defined with C^{-1}

NURBS orders	Size of NURBS control net
9 by 12	17 X 47
6 by 6	17 X 65
6 by 6	17 X 65

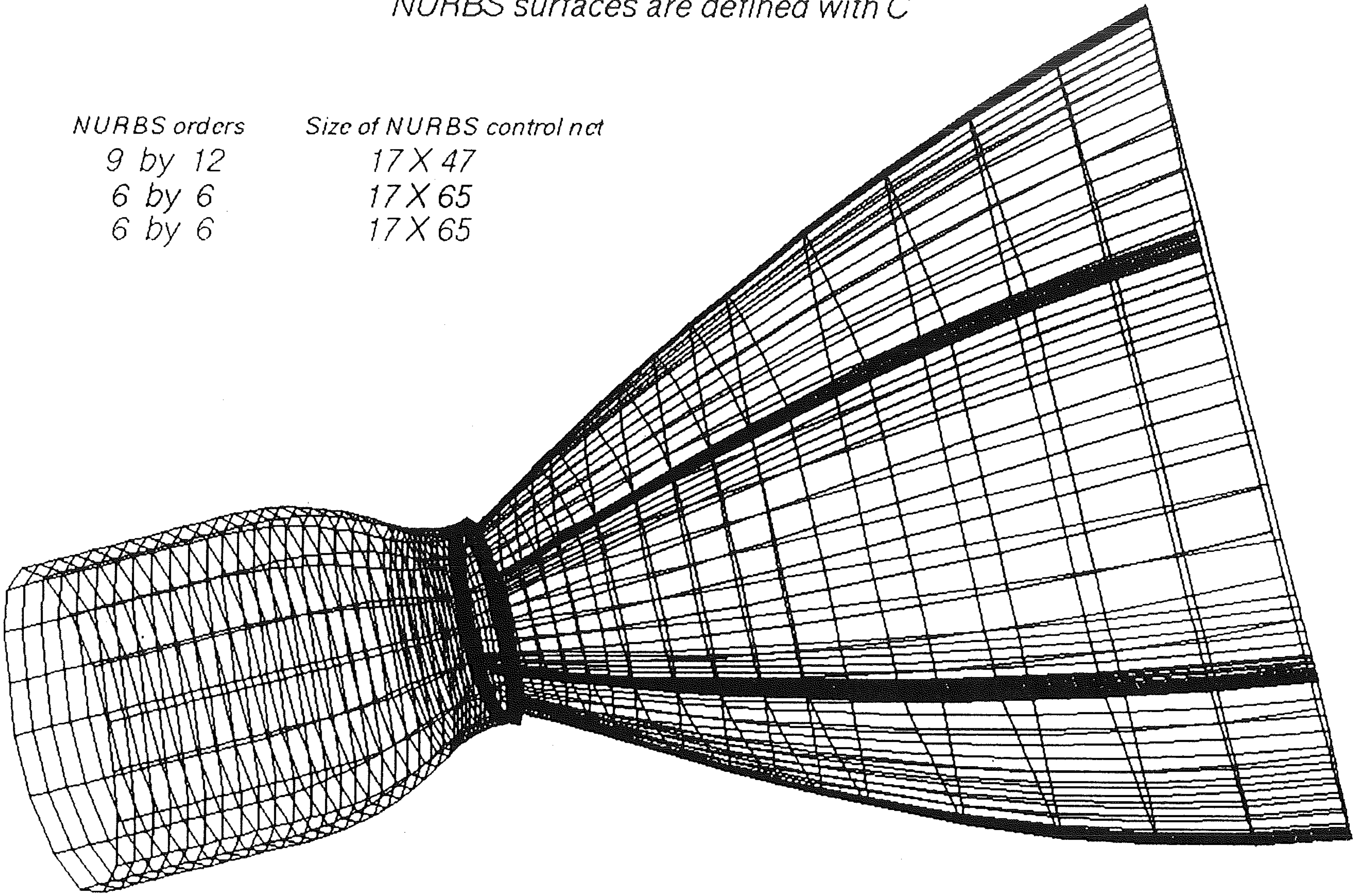

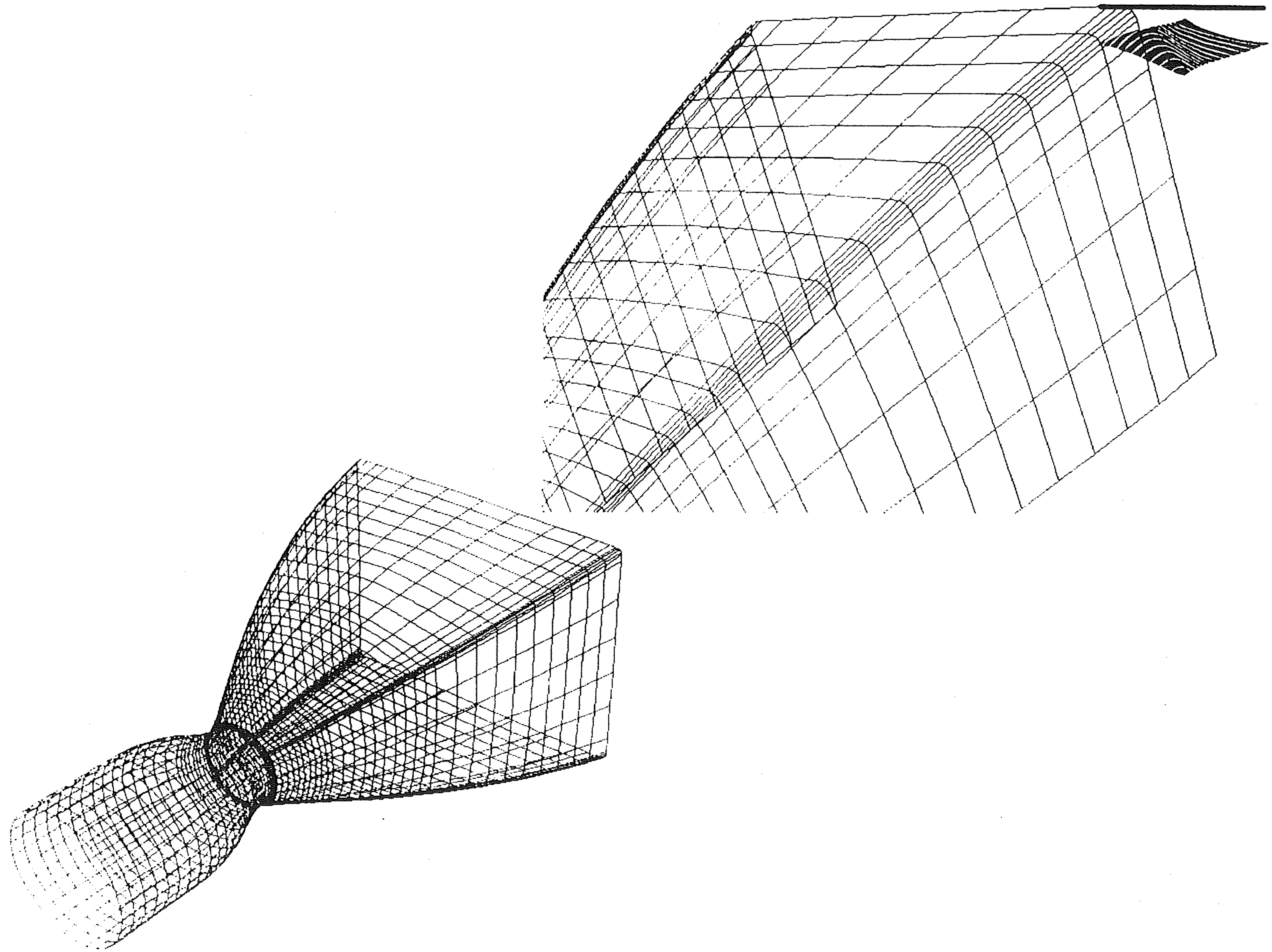

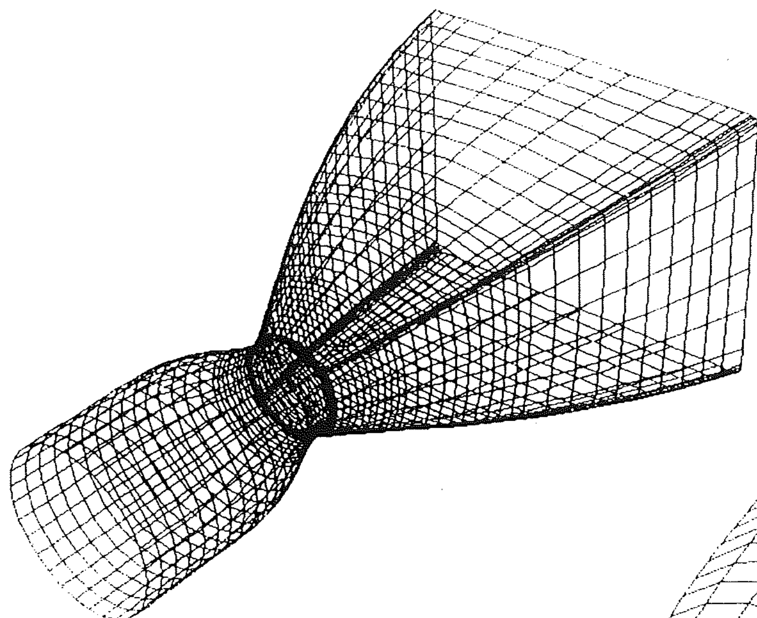

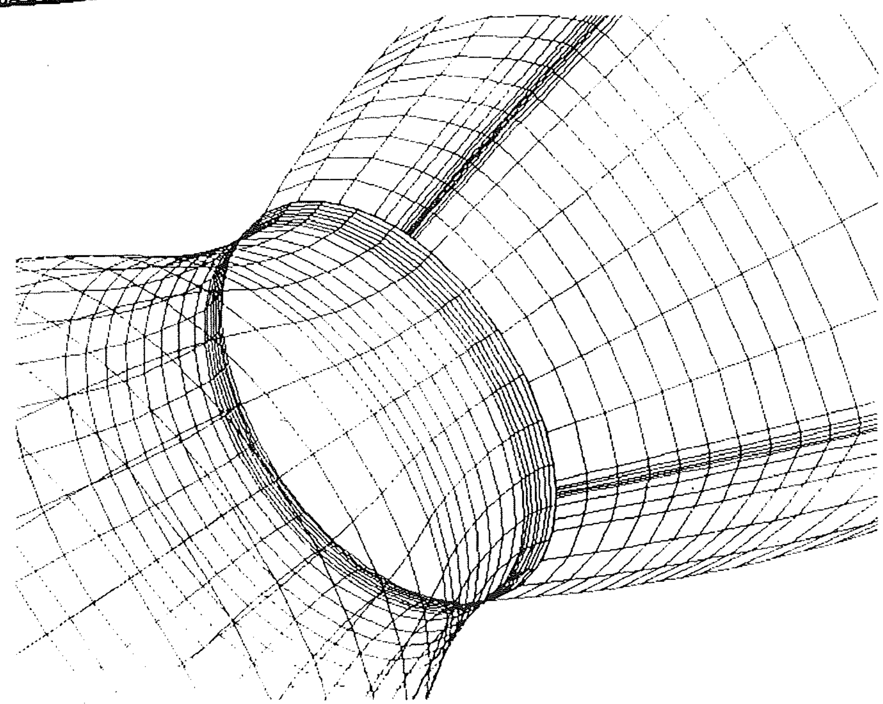

Manipulating CAD geometry and generating the volume grid
(O Type Grid)

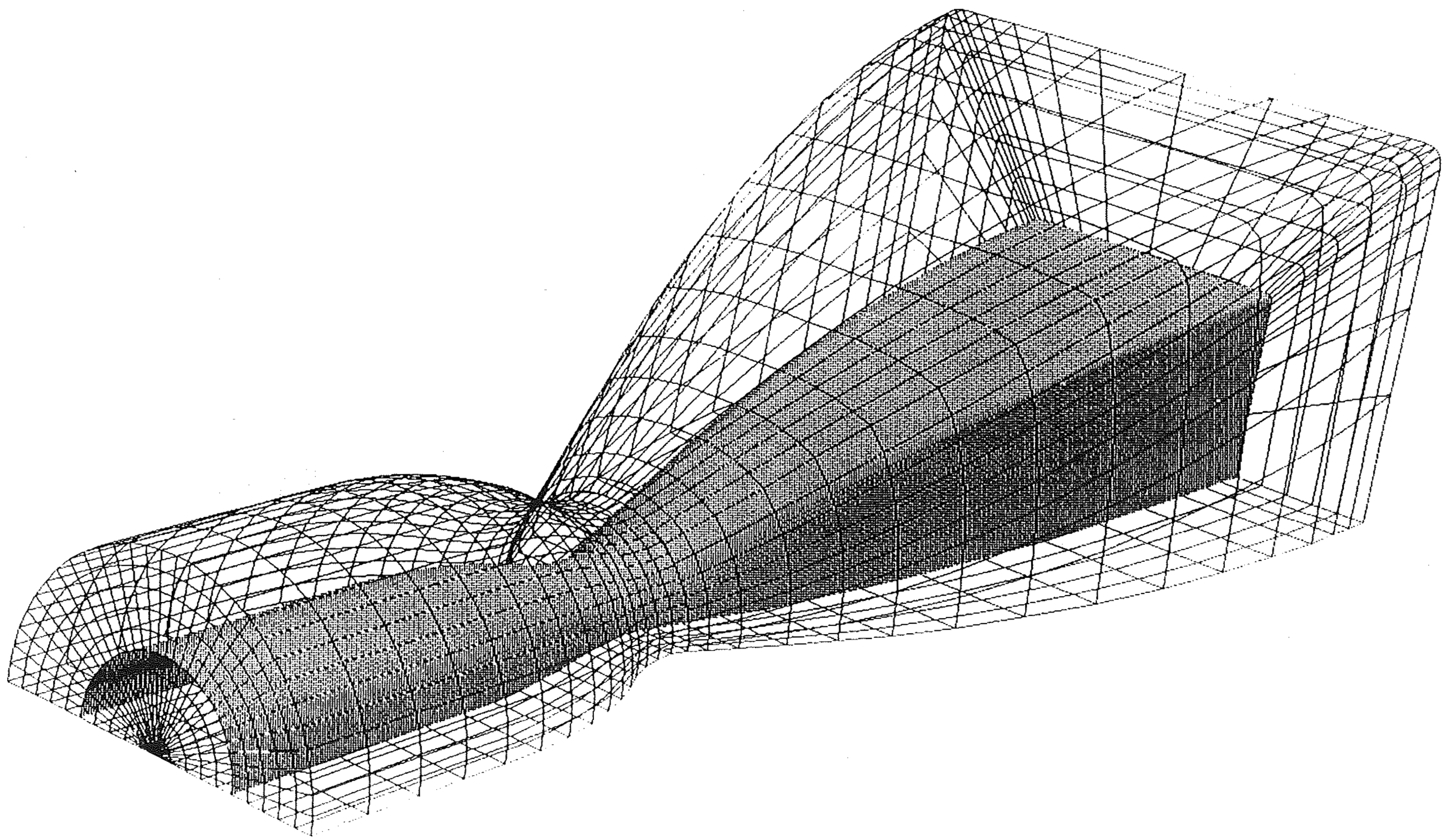

Manipulating CAD geometry and generating the volume grid
(O Type Grid)

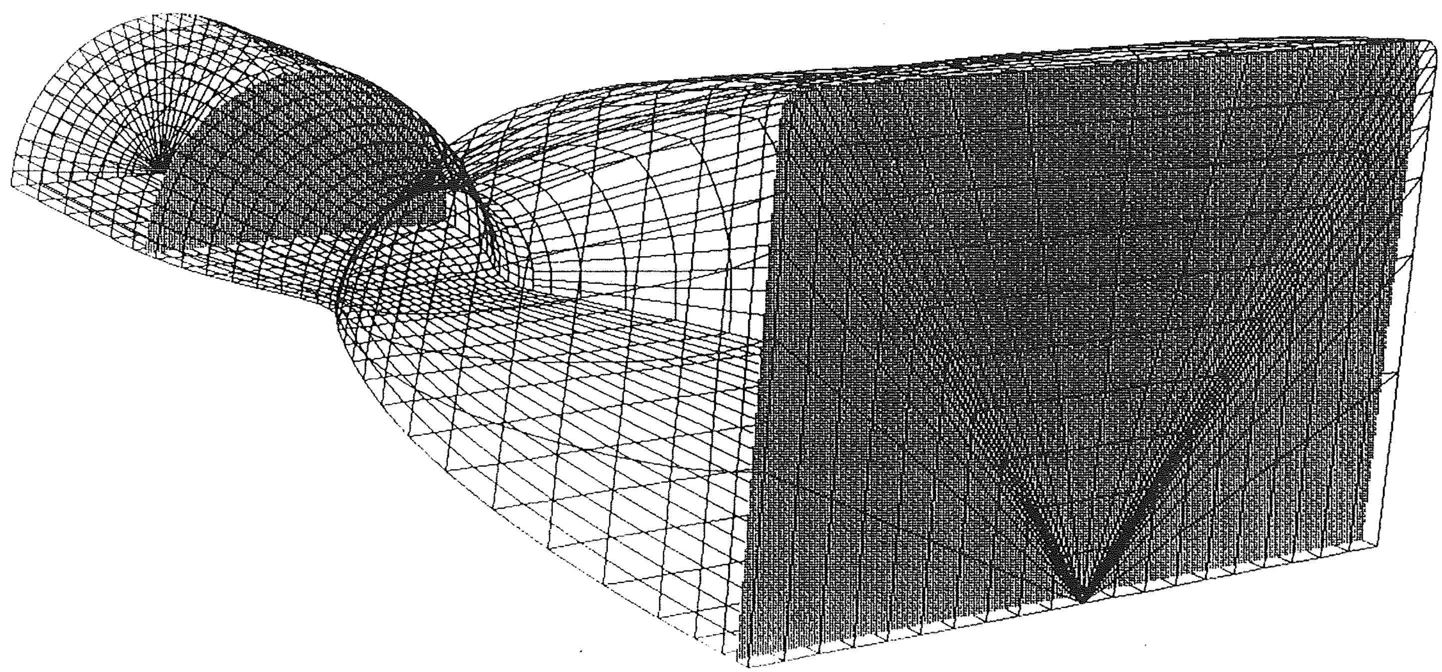

Manipulating CAD geometry and generating the volume grid

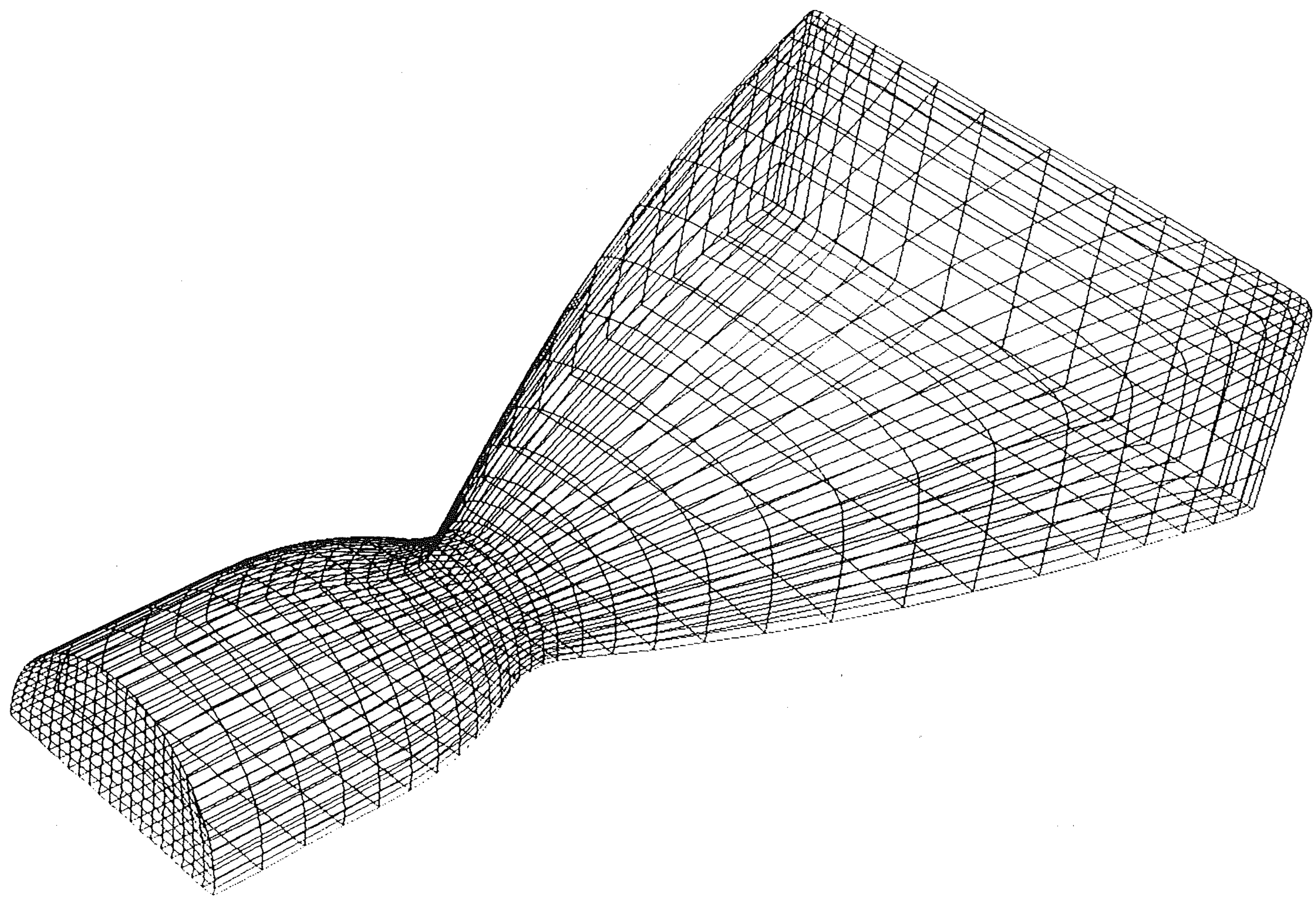

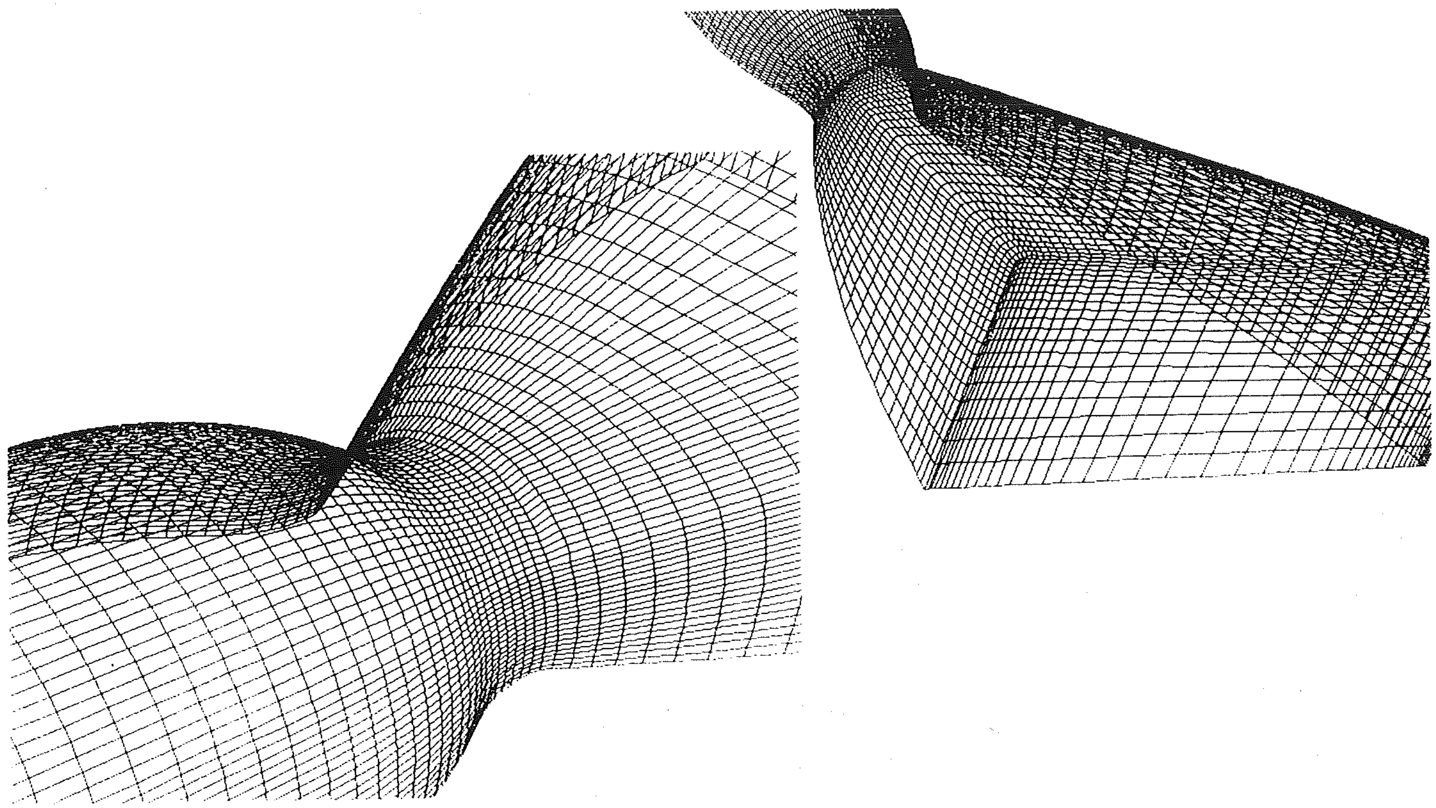

MISSISSIPPI STATE UNIVERSITY / National Science Foundation

ENGINEERING RESEARCH CENTER FOR COMPUTATIONAL FIELD SIMULATION

Converge/Diverge nozzle with circular-rectangular section

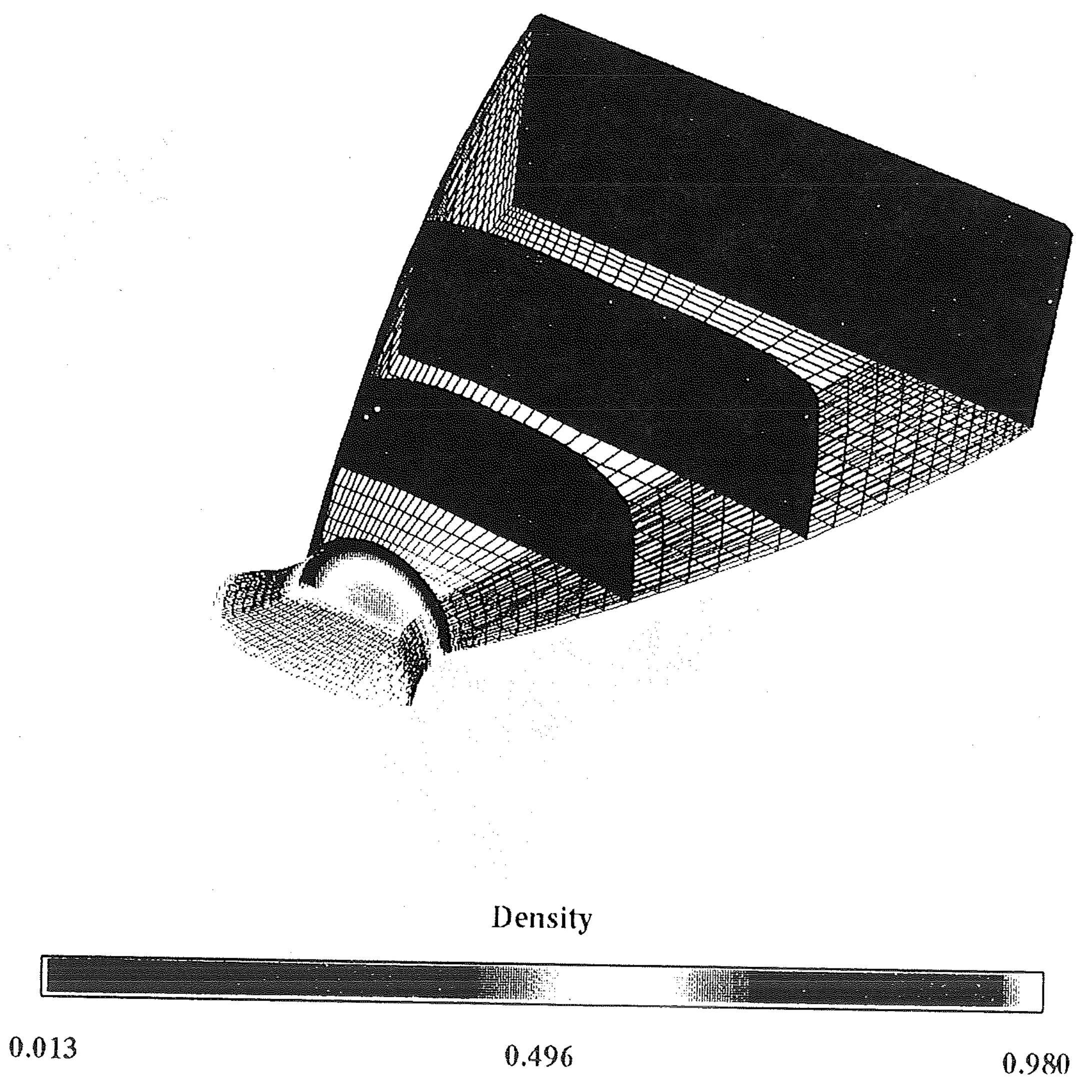

MISSISSIPPI STATE UNIVERSITY / National Science Foundation

ENGINEERING RESEARCH CENTER FOR COMPUTATIONAL FIELD SIMULATION

Converge/Diverge nozzle with circular-rectangular section

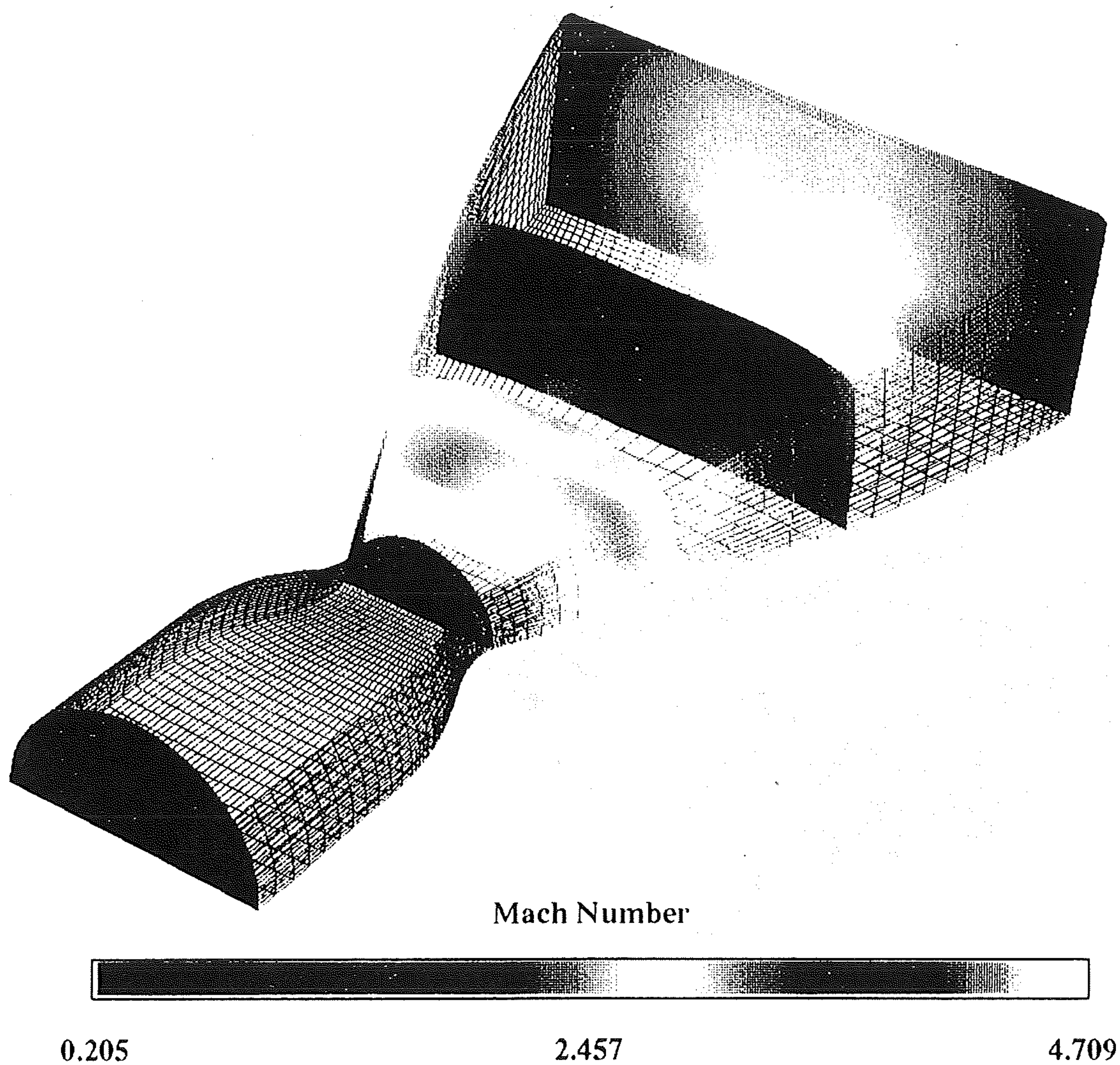

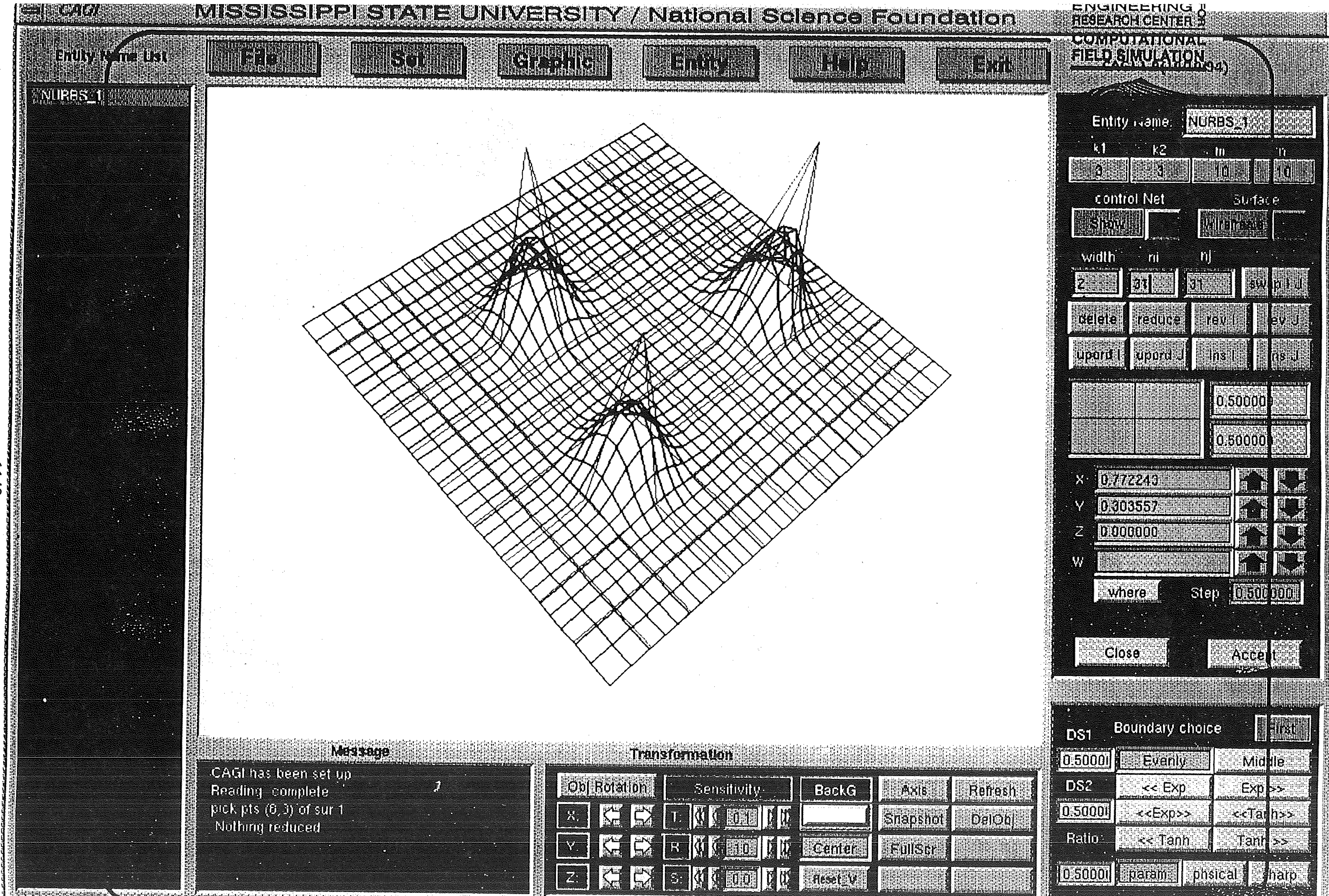
CAGI
MISSISSIPPI STATE UNIVERSITY / National Science Foundation
RESEARCH CENTER
COMPUTATIONAL
FIELD SIMULATION
Entity Name List
File
Set
Graphic
Entity
Help
Exit
NURBS_1
Entity Name
NURBS_1
k1
k2
m
n
3
3
10
10
control Net
Surface
Show
width
ni
nj
2
31
31
delete
reduce
rev I
upord I
upord J
ins I
0.50000
0.50000
X
Y
Z
W
0.772243
0.303557
0.000000
where
Step
Close
DS1
Boundary choice
0.5000
Evenly
DS2
<< Exp
0.5000
<<Exp>>
Ratio
<< Tanh
0.5000
param
phsical
Message
CAGI has been set up
Reading complete
pick pts (6,3) of sur 1
Nothing reduced
Transformation
Obj Rotation
Sensitivity
BackG
Axis
Refresh
Snapshot
DelObj
Center
FullScr
Reset V
X
Y
Z
T
R
S
0.1
1.0
0.0

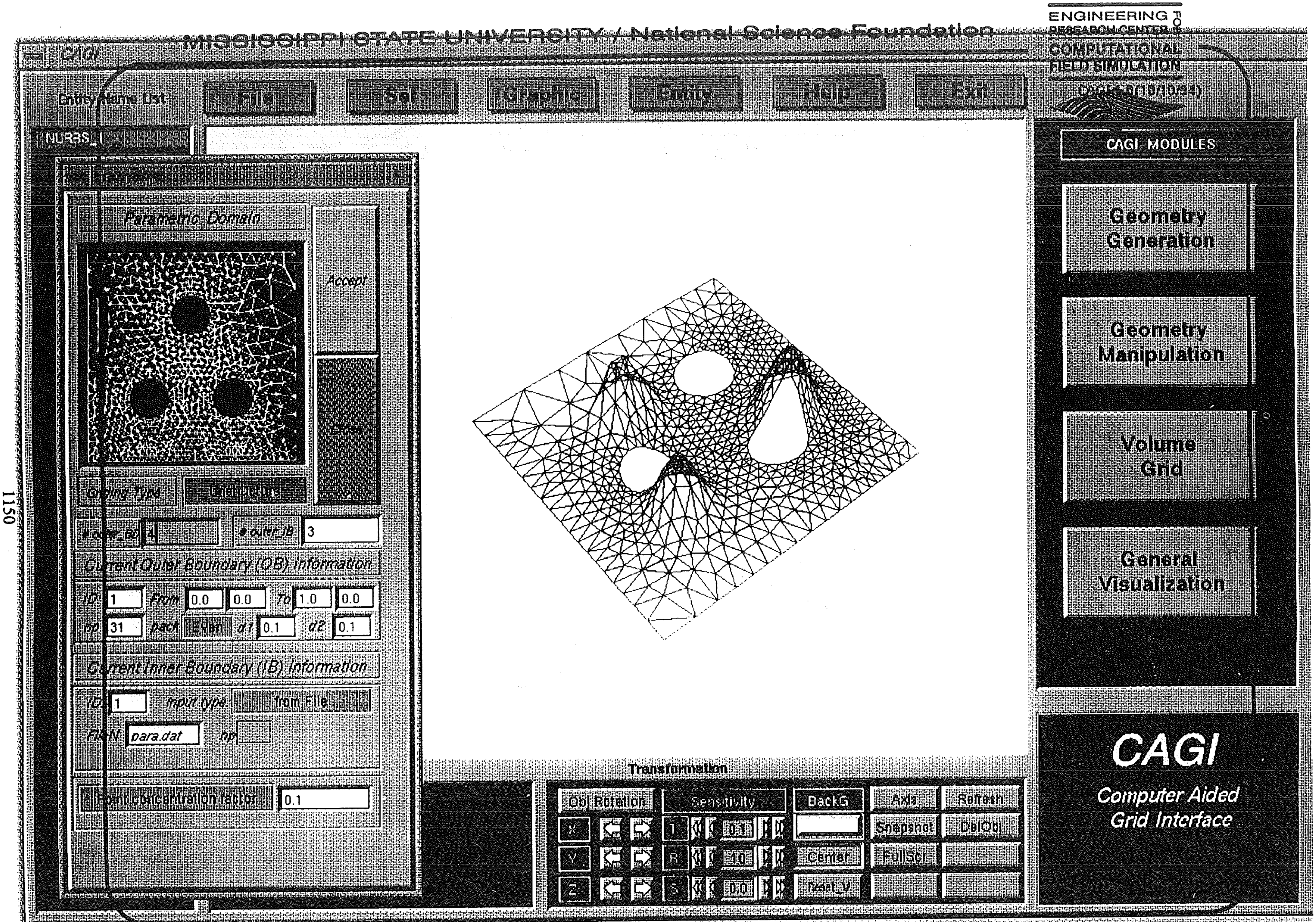
MISSISSIPPI STATE UNIVERSITY / National Science Foundation
ENGINEERING RESEARCH CENTER FOR COMPUTATIONAL FIELD SIMULATION
CAGI
Entity Name List
NURBS
File
Set
Graphic
Entity
Help
Exit
Parametric Domain
Accept
Gridding Type
Distribution
outer_IB
3
Current Outer Boundary (OB) Information
ID
1
From
0.0
0.0
To
1.0
0.0
np
31
pack
Even
d1
0.1
d2
0.1
Current Inner Boundary (IB) Information
ID
1
input type
from File
FileN
para.dat
np
Point concentration factor
0.1
Transformation
Obj Rotation
Sensitivity
BackG
Axis
Refresh
Snapshot
DelObj
Center
FullScr
Reset_V
X
Y
Z
T
R
S
0.1
1.0
0.0
CAGI MODULES
Geometry Generation
Geometry Manipulation
Volume Grid
General Visualization
CAGI
Computer Aided Grid Interface

On Going Activities:

- Surface/Volume grid characteristic improvement.
  (Distribution control, Orthogonality, smoothness ...)
- General algorithm allowing trim surface for structured grid.
- Enhance geometric generation/manipulation functions.
- Reparametration algorithm for unstructured grid.
- Unstructured/Hybrid grid generation.

S19-34
51394
132116 16p

Overview of CFD Analyses Supporting the Reusable Solid Rocket Motor (RSRM) Program at MSFC

E. Stewart, P. McConnaughey, J. Lin, E. Reske, and D. Doran, NASA/MSFC, R. H. Whitesides, ERC, Inc., Huntsville, AL, and Y.-S. Chen ESI, Huntsville, AL

During the past year, various CFD analyses were performed at MSFC to support the RSRM program. The successful completion of these analyses was realized through the cooperation of ESI, ERC, and The Computational Fluid Dynamics Branch (ED32) at MSFC and involved application of the CFD codes FDNS and CELMINT. The topics addressed by the analyses were; 1. the design and prediction of slag accumulation within the five inch test motor, 2. prediction of slag pool behavior and its response to lateral accelerations, 3. the clogging of potential insulation debonds within the nozzle by slag accumulation, 4. the behavior of jets within small voids inside nozzle joint gaps, 5. the effect of increased inhibitor stiffness on motor acoustics, and 6. the effect of a nozzle defect on particle impingement enhanced erosion. Topics 1, 2, and 5 will be discussed in some detail by other speakers at the conference and are only mentioned here for the sake of completeness. Thus, the emphasis of this presentation will be to further discuss the work involved in topics 3, 4, and 6.

Eric Stewart

Overview of

CFD Analyses Supporting

the Reusable Solid Rocket Motor

(RSRM) Program at MSFC

Presented at 13th Workshop for CFD
Applications in Rocket Propulsion
and Launch Vehicle Technology,
MSFC, AL, April 27-30, 1995

E. Stewart, P. McConnaughey, E. Reske,
J. Lin, and D. Doran, NASA/MSFC,
R. H. Whitesides, ERC, Inc., Huntsville,
AL, and Y.-S. Chen ESI, Huntsville, AL

Overview

- Overview of RSRM CFD analyses at MSFC
- Insulation Debond Analysis
- Potential RTV Flaw Analysis
- Nose Inlet Assembly Wetline Investigation
- Future efforts

RSRM CFD Analyses at MSFC

Overview of RSRM CFD Analyses at MSFC

- **Slag (Al_2O_3) behavior and accumulation**
  - 5 inch spin motor design and analysis
  - Accumulation within RSRM at 67 seconds
  - Response of slag pool to lateral accelerations using VOF methodology
- **Increase in Nitrile Butadiene Rubber (NBR) stiffness**
  - Aerodynamic torque on nozzle
  - Potential effect on internal acoustics/pressure oscillations
    - Change in inhibitor deflections
    - Vortex shedding by the inhibitors
- **Code validation for the 8-percent ASRM cold flow model**
- **Insulation debond analysis**
- **Potential RTV flaw analysis**
- **Nose inlet assembly wetline Investigation**

RSRM CFD Analyses at MSFC

Computational Fluid Dynamics Branch
Fluid Dynamics Division
Structures and Dynamics Laboratory
George C. Marshall Space Flight Center

Insulation Debond Analysis

Issues
- Prediction of flow/clogging through potential insulation defect flow paths during motor operation

Approach
- Use two-phase flow and condensation models to predict propensity for pore clogging during motor operation
  - prescribed thermal boundary conditions

Results
- Small (0.01") pores probably clog quickly (.05 sec) under severe thermal gradients
- Lower probability of clogging during start pressurization transient

Impact
- Joint gap clogging prediction methodology is available to support potential anomalies

National Aeronautics and
Space Administration

RSRM CFD Analyses at MSFC

Computational Fluid Dynamics Branch
Fluid Dynamics Division
Structures and Dynamics Laboratory
George C. Marshall Space Flight Center

- **Results (Problem 1, debond vent to ambient)**

gap width	time to clog
0.010″	0.05 sec.
0.005″	0.02 sec.
0.002″	0.006 sec.

- **Results (Problem 2, start-up transient through debond)**
  - clogging of debond predicted in 0.61 sec. after initiation of particle flow
  - lower mass flow rate (4X less) due to cavity fill results in fewer particles to condense on pore wall

RSRM CFD Analyses at MSFC

National Aeronautics and Space Administration

Computational Fluid Dynamics Branch
Fluid Dynamics Division
Structures and Dynamics Laboratory
George C. Marshall Space Flight Center

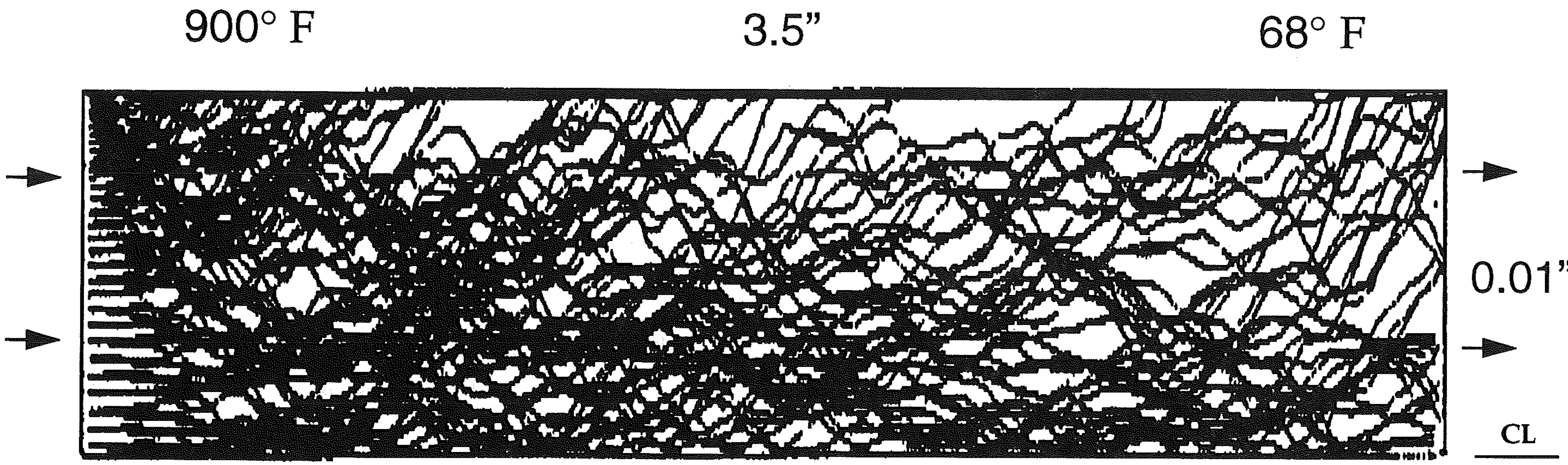

Joint Gap Clogging Prediction

1159

RSRM CFD Analyses at MSFC

Potential RTV Flaw Analysis

Issues
- Hot gas jet impingement environments on O-rings within RSRM nozzle due to potential RTV flaws
- Predict jet spreading within irregularly shaped cavities

Approach
- Predict 3-D Jet Spreading for potential joint gap/cavity flows for input into thermal models

Results
- Hot gas jet spreading within joint cavities is smaller than that used in previous non-CFD analyses

Impact
- Jet spread width used in thermal models should be 0.7″ (rather than 1.25″)
- Jet spreading predictions are available to support potential anomalies

National Aeronautics and
Space Administration

RSRM CFD Analyses at MSFC

Computational Fluid Dynamics Branch
Fluid Dynamics Division
Structures and Dynamics Laboratory
George C. Marshall Space Flight Center

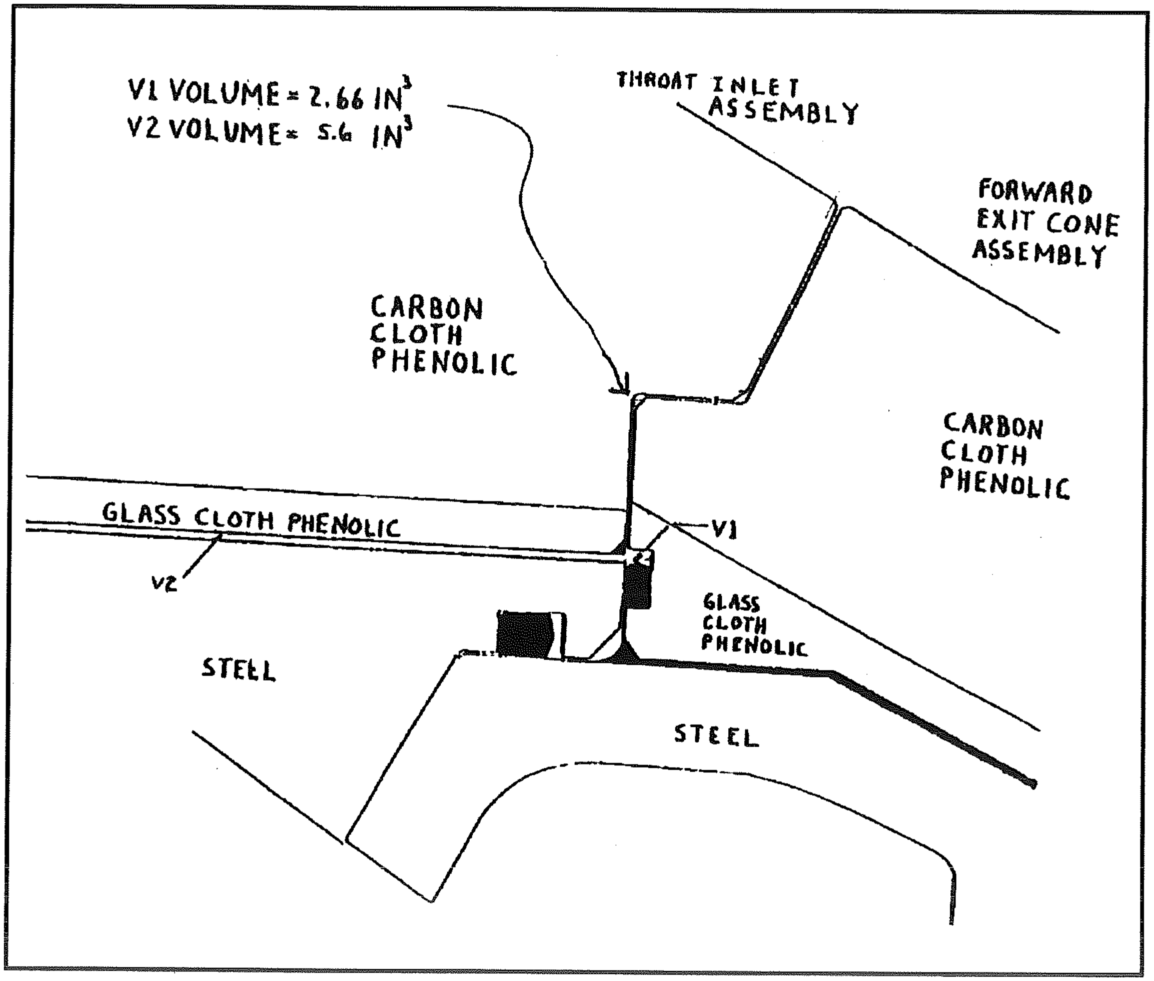

Geometry of Internal Nozzle, Joint #4

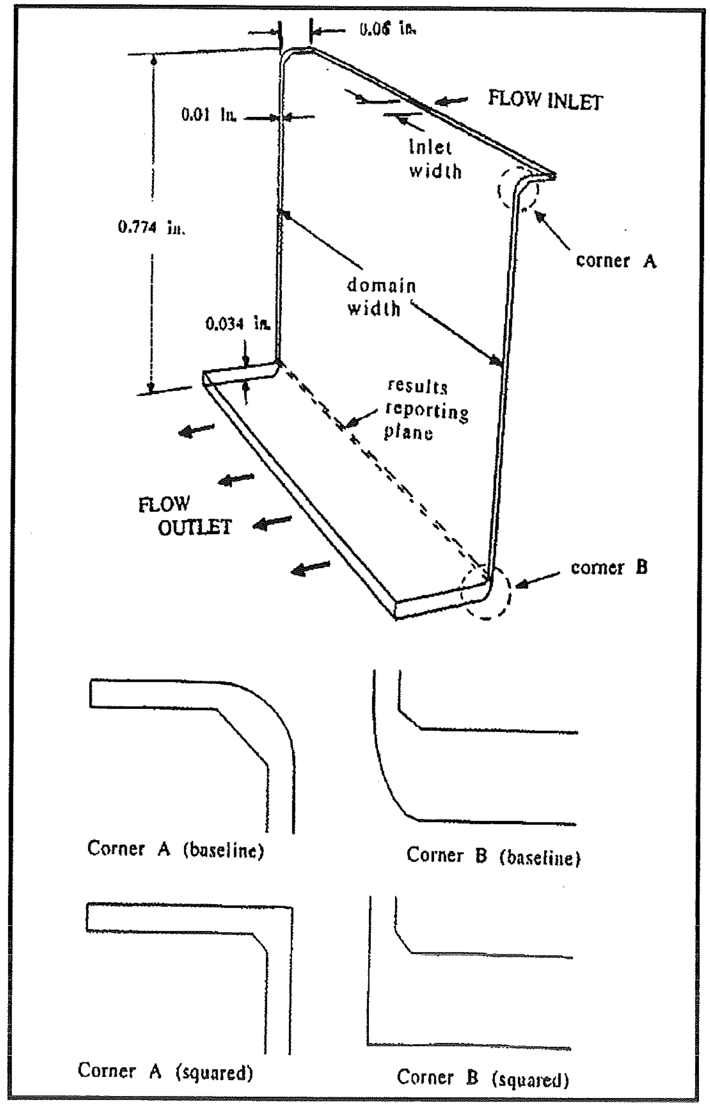

Computational Geometry

RSRM CFD Analyses at MSFC

- **Analysis matrix and results**

case	flowrate (lbm/s)	domain width (in)	corners	inlet width (in)	jet spread width (in)
1	0.0001	8.0	rounded	0.1	1.5
2	0.0002	8.0	rounded	0.1	1.1
3	0.0005	8.0	rounded	0.1	0.6
4	0.001	8.0	rounded	0.1	0.5
5	0.00155	8.0	rounded	0.1	0.5
6	0.00155	16.0	rounded	0.1	0.5
7	0.00155	8.0	square	0.1	0.75
8	0.00155	8.0	rounded	0.2	0.75

National Aeronautics and
Space Administration

RSRM CFD Analyses at MSFC

Computational Fluid Dynamics Brar
Fluid Dynamics Division
Structures and Dynamics Laboratory
George C. Marshall Space Flight Cer

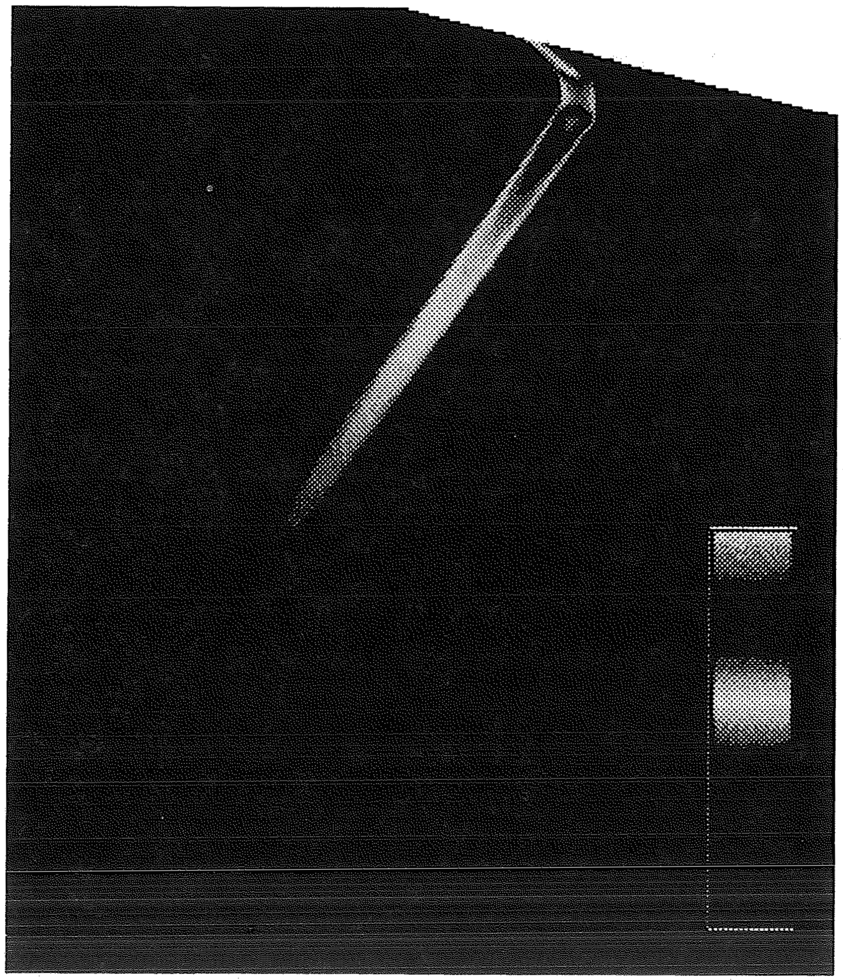

Velocity Magnitudes

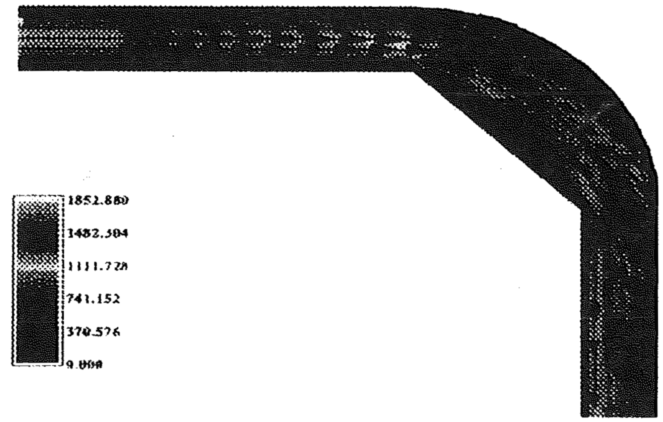

Center Line Velocity Profile Through Corner A

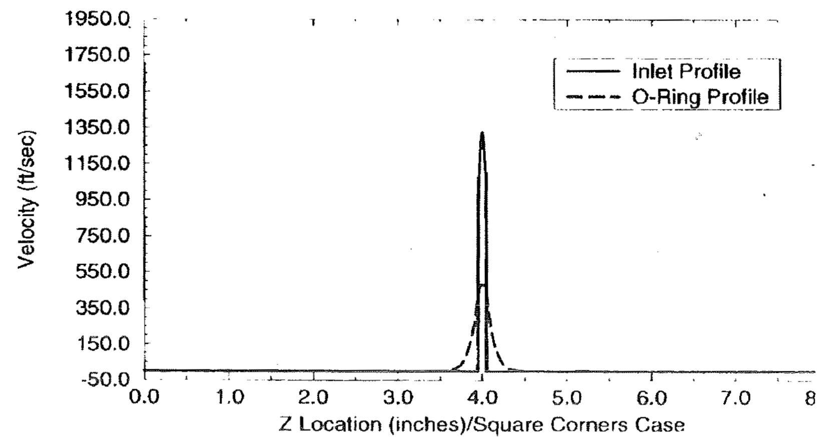

Average Velocity Magnitudes

Nose Inlet Assembly Wetline Investigation

Issues
- Enhancement of nozzle erosion due to presence of defect
- Effect of defect on slag particle impingement

Approach
- Assume wedge shaped nozzle defect
- Use two-phase flow results to assess flow environment near defect
- Use current data/experience base to assess potential flow deviations

Results
- Size of defect relative to local boundary layer is not sufficient to significantly alter flow external to boundary layer
- Main source of particle impingement is external to boundary layer
- Erosion enhancement due to particle impingement is not significantly altered by presence of defect

Impact
- Recommend nozzle in question for flight

National Aeronautics and
Space Administration

RSRM CFD Analyses at MSFC

Computational Fluid Dynamics Branch
Fluid Dynamics Division
Structures and Dynamics Laboratory
George C. Marshall Space Flight Center

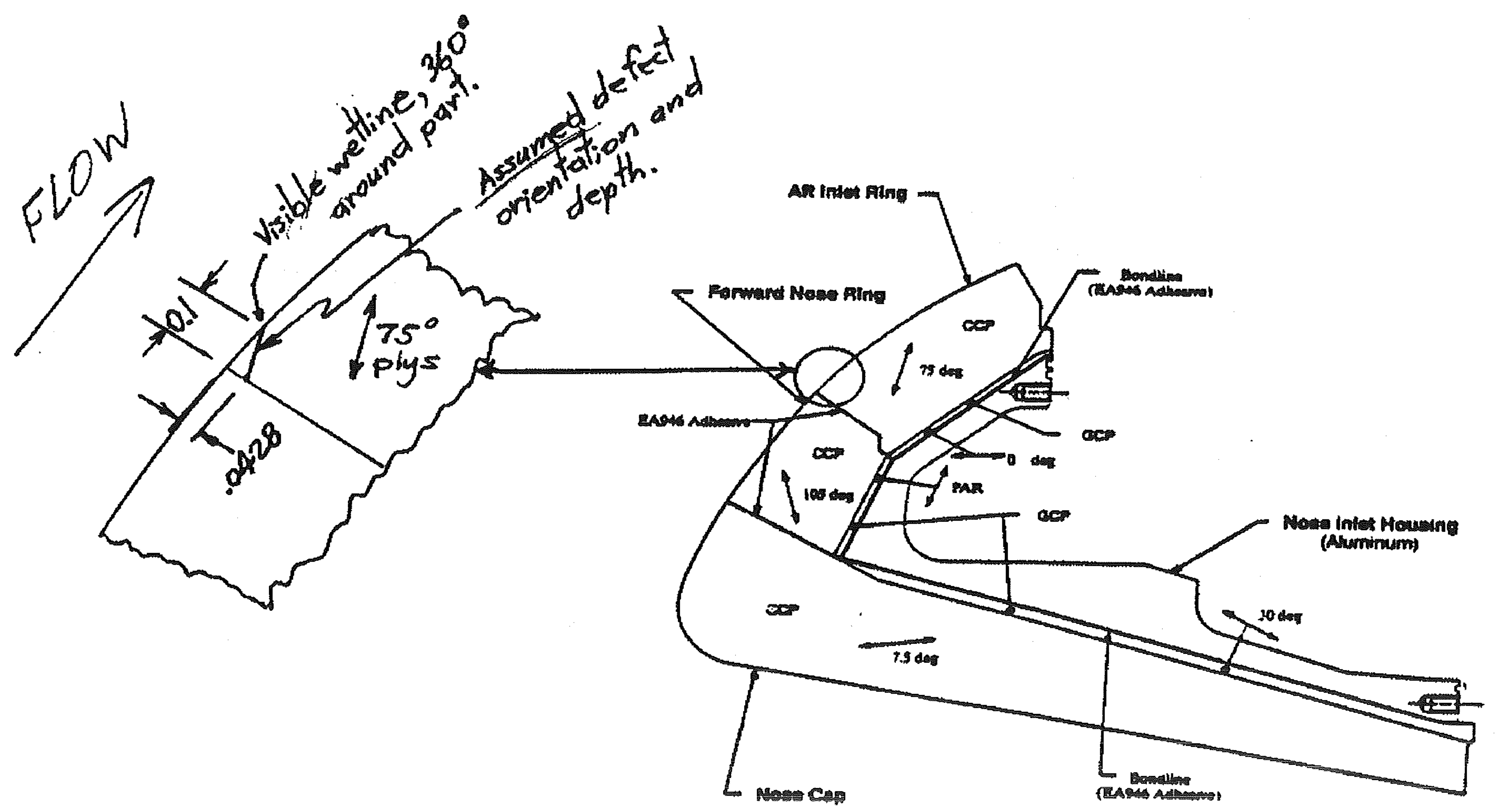

Geometry of Nozzle Nose Region

National Aeronautics and
Space Administration

RSRM CFD Analyses at MSFC

Computational Fluid Dynamics Branch
Fluid Dynamics Division
Structures and Dynamics Laboratory
George C. Marshall Space Flight Center

RSRM 67 Sec. Burn Time, 150 Micron Particle Trajectories

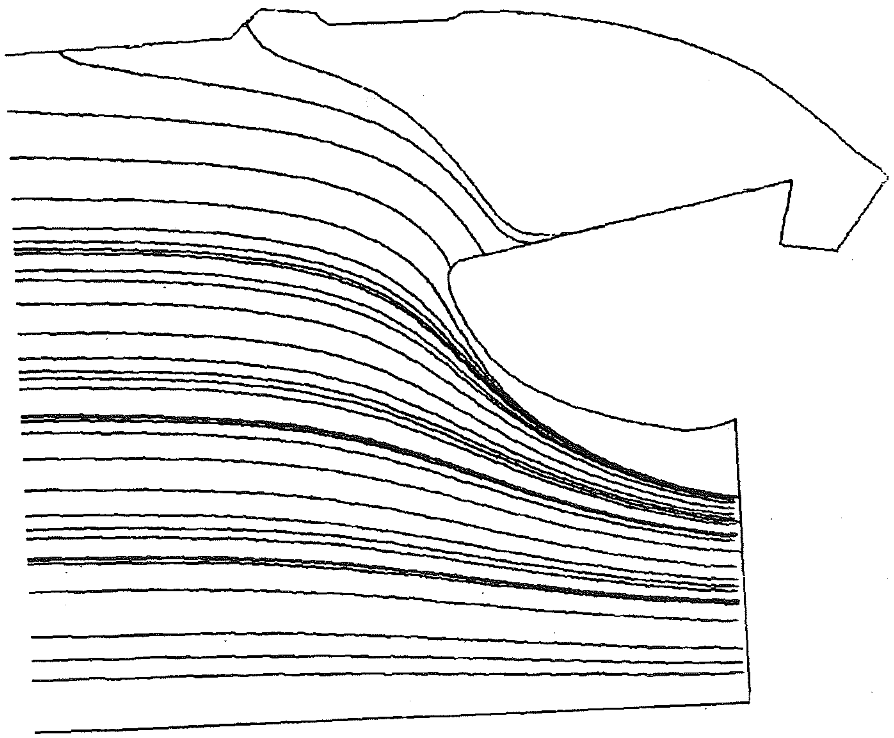

ED32 Results

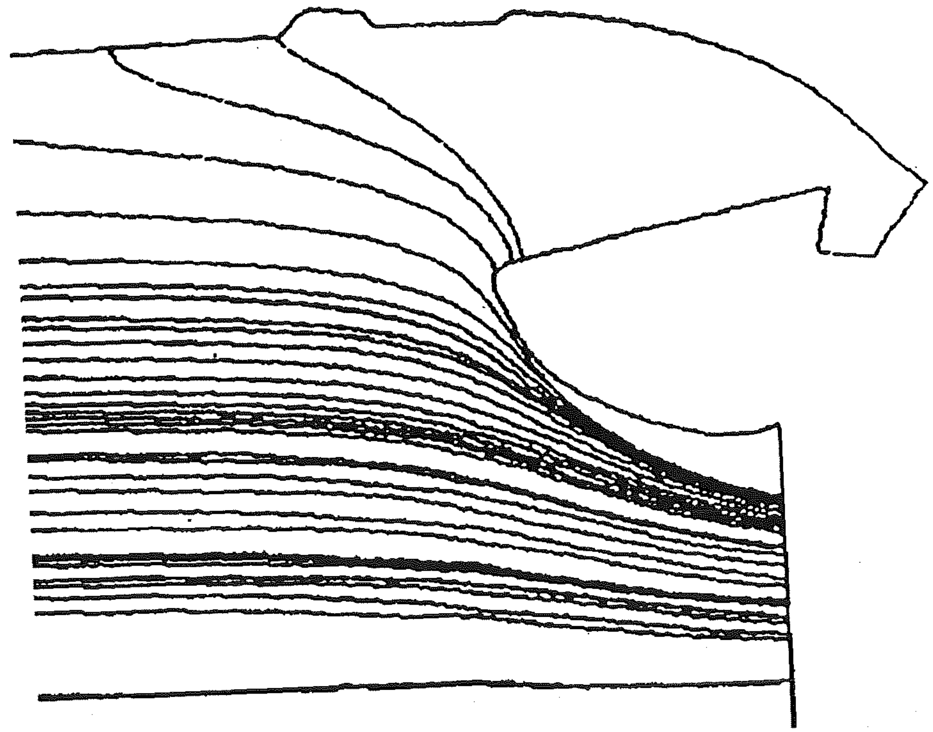

ERC Results

RSRM CFD Analyses at MSFC

Computational Fluid Dynamics Branch
Fluid Dynamics Division
Structures and Dynamics Laboratory
George C. Marshall Space Flight Center

Future Effort

- Continue code validation
- Continue to enhance modeling capabilities
  - two-phase flow
  - combustion
  - turbulence
  - slag accumulation
  - unsteady flow
- Improve readiness to address potential anomalies
  - Perform similar analyses at additional burn times

S20-34
57395
132117
20P

RSRM Chamber Pressure Oscillations: Transit Time Models and Unsteady CFD

Tom Nesman and Eric Stewart
Fluid Dynamics Division
National Aeronautics and Space Administration, MSFC
Marshall Space Flight Center, AL 35812

Abstract

Space Shuttle solid rocket motor (SRM) low frequency internal pressure oscillations have been observed since early testing. The same type of oscillations are also present in the redesigned solid rocket motor (RSRM). The oscillations, which occur during RSRM burn, are predominantly at the first three motor cavity longitudinal acoustic mode frequencies. Broadband flow and combustion noise provide the energy to excite these modes at low levels throughout motor burn, however, at certain times during burn the fluctuating pressure amplitude increases significantly. The increased fluctuations at these times suggests an additional excitation mechanism.

The RSRM has inhibitors on the propellant forward facing surface of each motor segment. The inhibitors are in a slot at the segment field joints to prevent burning at that surface. The aft facing segment surface at a field joint slot burns and forms a cavity of time varying size. Initially the inhibitor is recessed in the field joint cavity. As propellant burns away the inhibitor begins to protrude into the bore flow. Two mechanisms (transit time models) that are considered potential pressure oscillation excitations are cavity edge-tones, and inhibitor hole-tones. Estimates of frequency variation with time of longitudinal acoustic modes, cavity edge-tones, and hole-tones compare favorably with frequencies measured during motor hot firing. It is believed that the highest oscillation amplitudes occur when vortex shedding frequencies coincide with motor longitudinal acoustic modes.

A time accurate CFD analysis was made to replicate the observations from motor firings and to observe the transit time mechanisms in detail. FDNS is the flow solver used to detail the time varying aspects of the flow. The fluid is approximated as a single-phase ideal gas. The CFD model was an axisymmetric representation of the RSRM at 80 seconds into burn. Deformation of the inhibitors by the internal flow was determined through an iterative structural and CFD analysis. The analysis domain ended just upstream of the nozzle throat. This is an acoustic boundary condition that caused the motor to behave as an closed-open organ pipe. This differs from the RSRM which behaves like a closed-closed organ pipe.

The unsteady CFD solution shows RSRM chamber pressure oscillations predominantly at the longitudinal acoustic mode frequencies of a closed-open organ pipe. Vortex shedding in the joint cavities and at the inhibitors contribute disturbances to the flow at the second longitudinal acoustic mode frequency. Further studies are planned using an analysis domain that extends downstream of the nozzle throat.

RSRM - Chamber Pressure Oscillations: Transit Time Models and Unsteady CFD

Workshop for CFD Applications in Rocket Propulsion and Launch Vehicle Technology

Tom Nesman and Eric Stewart
Fluid Dynamics Division - NASA - MSFC

Introduction

- Space Shuttle SRM Pc oscillations issues have surfaced at various times in past
  - Pre- STS-1 loads analysis
  - Post STS-1 loads evaluation
  - STD to HPM change
  - FWC testing (ASRM)
  - HPM to RSRM change
  - Inhibitor stiffening evaluation (present study)
- SRM Pc oscillation evaluation based primarily on test and flight data
- Mechanisms evaluated empirically
- Unsteady CFD activities initiated in early 1990's (funded thru 1993)
- Unsteady RSRM CFD activities revived for inhibitor stiffening evaluation

Background

- Space Shuttle solid rocket motor low frequency internal pressure oscillations observed since early testing
- Same type oscillations present in redesigned solid rocket motor (RSRM)
- Predominantly at first three motor internal longitudinal acoustic mode frequencies
- Broadband flow and combustion noise provide energy to excite these modes at low levels throughout motor burn
- At certain times during burn fluctuating pressure amplitude increases significantly
- Increased fluctuations at these times suggests an additional excitation mechanism

Typical RSRM Pc Isoplot

Head-end Chamber Pressure (Pc) Measurement

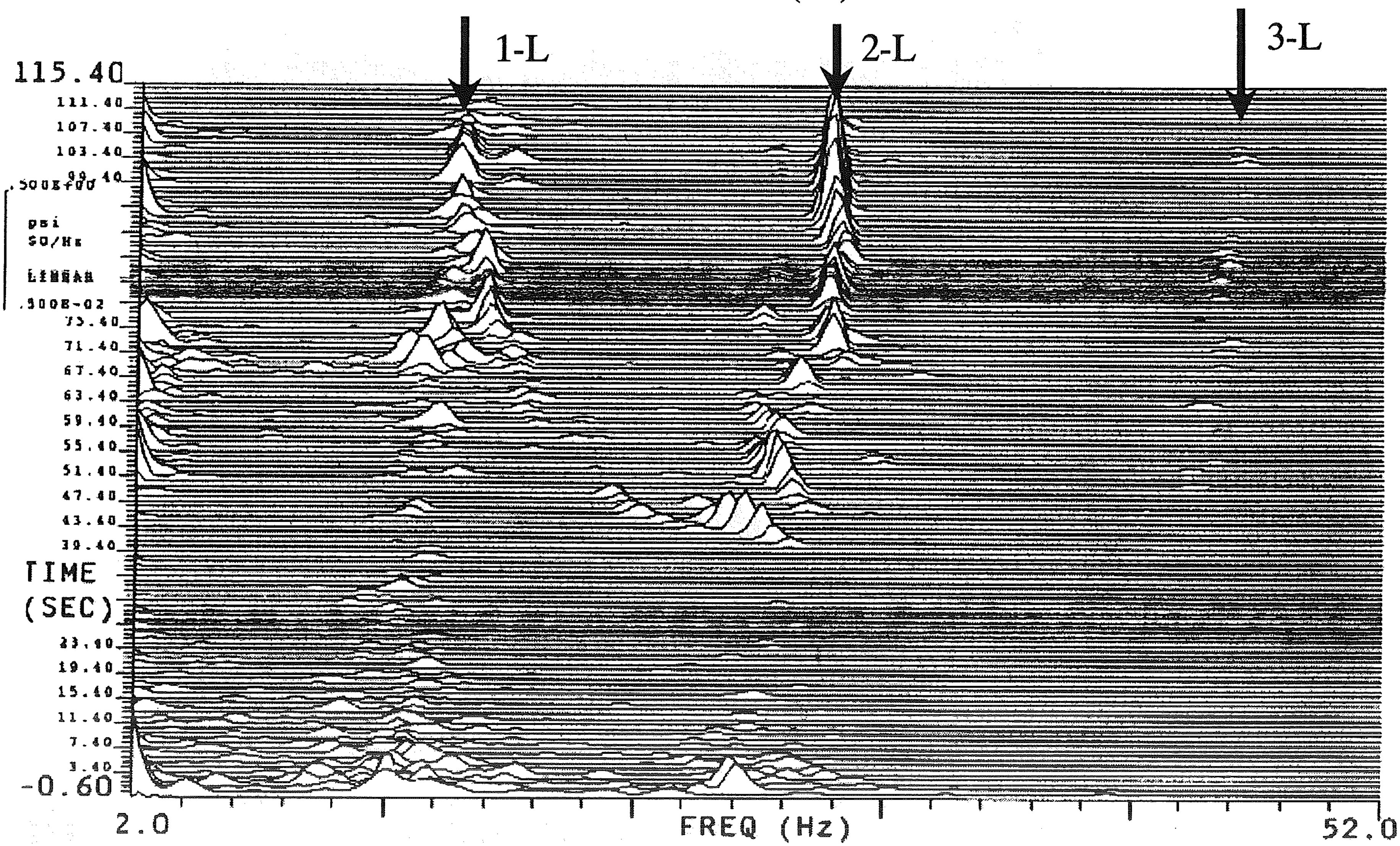

Typical RSRM Pc Timehistory
(Bandpass Filtered Data)

This is actually an HPM

Head-end Chamber Pressure (Pc) Measurement

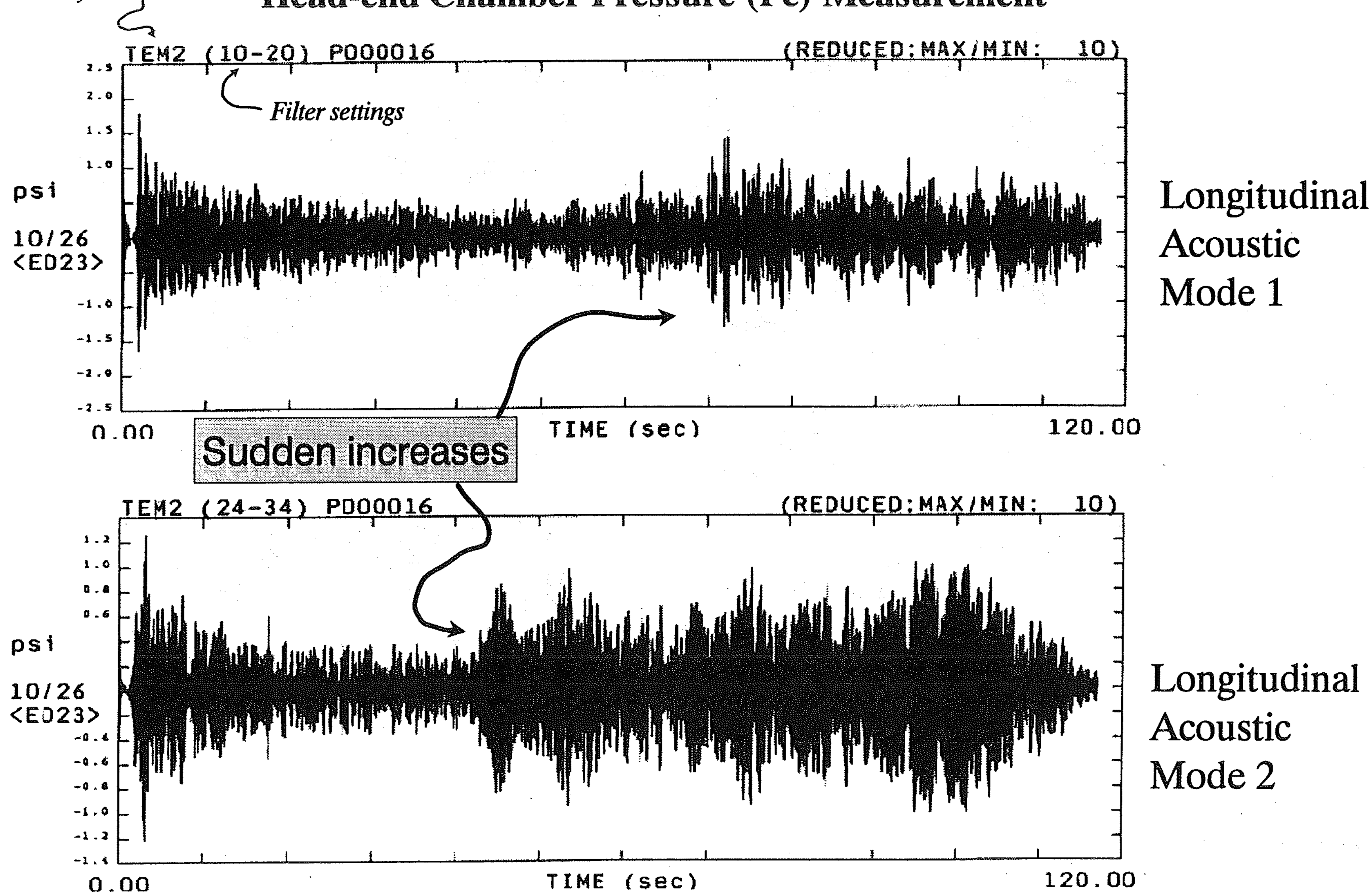

General Characteristics

- RSRM inhibitors on propellant forward facing surface of each motor segment
- Inhibitors in slot at segment field joints to prevent burning at forward facing surface
- Aft facing segment surface at field joint slot burns to form cavity of time varying size
- Initially inhibitor recessed in field joint cavity
- As propellant burns away inhibitor protrudes into bore flow
- Two mechanisms considered potential pressure oscillation exciters
    - Feedback transit-time models
    - 1. Cavity edge-tones
    - 2. Inhibitor hole-tones
- Estimates of frequency variation with time of longitudinal acoustic modes, cavity edge-tones, and hole-tones compare favorably with frequencies measured during motor hot firing
- Highest oscillation amplitudes occur when vortex shedding frequencies coincide with motor longitudinal acoustic modes

Excitation Mechanisms

George C. Marshall Space Flight Center
Fluid Dynamics Division

Cavity Edge-Tone Mechanism

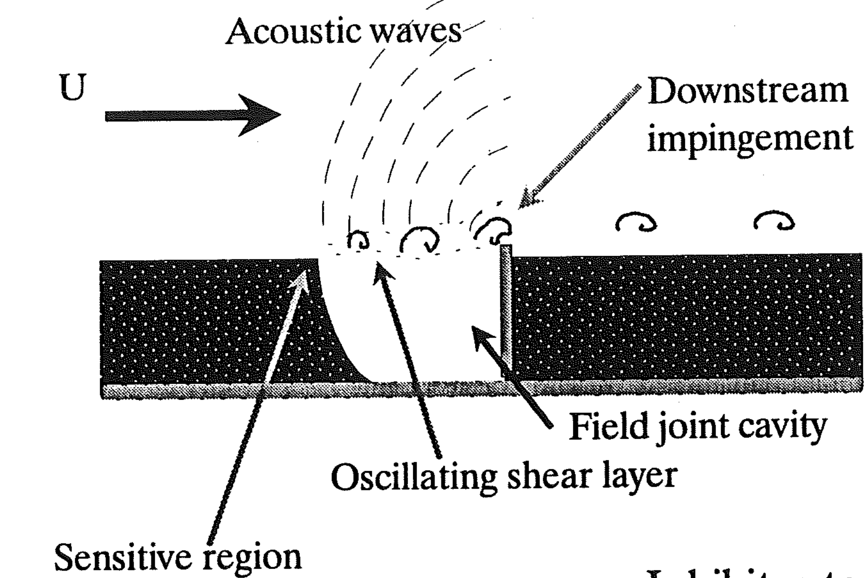

Feedback Transit Time Models

Empirical estimates - time for disturbance to travel downstream plus time for feedback to sensitive region

Analytical estimates - sum of phase of downstream traveling wave and phase of upstream traveling acoustic wave

Inhibitor to Inhibitor Hole-tone Mechanism

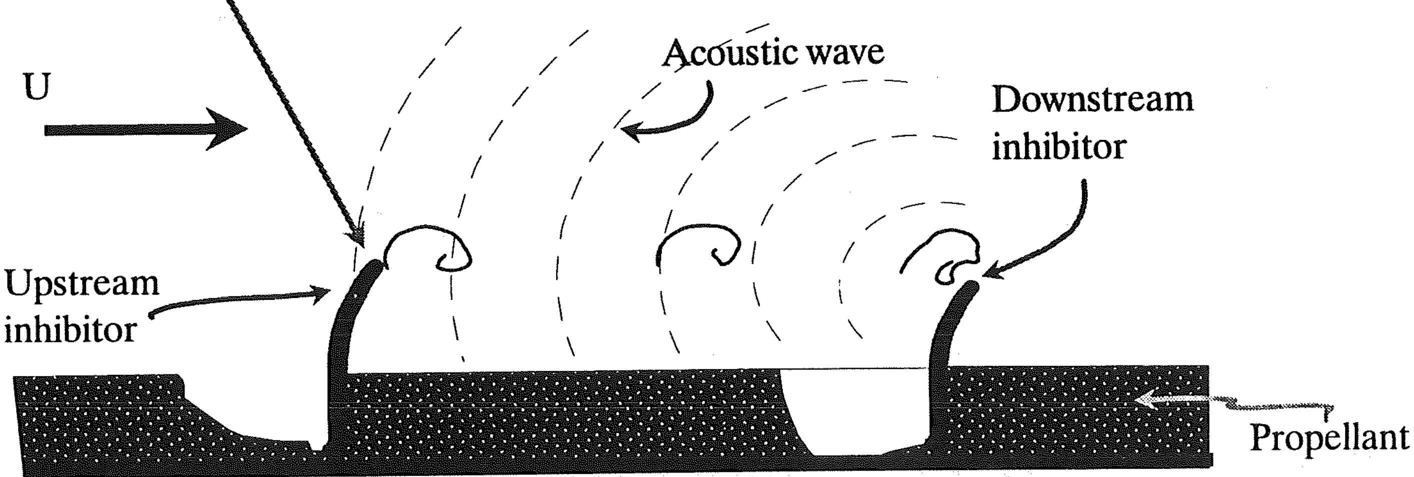

Measured Fluctuating Pressure, p'

RSRM Static Firing Head End Chamber Pressure

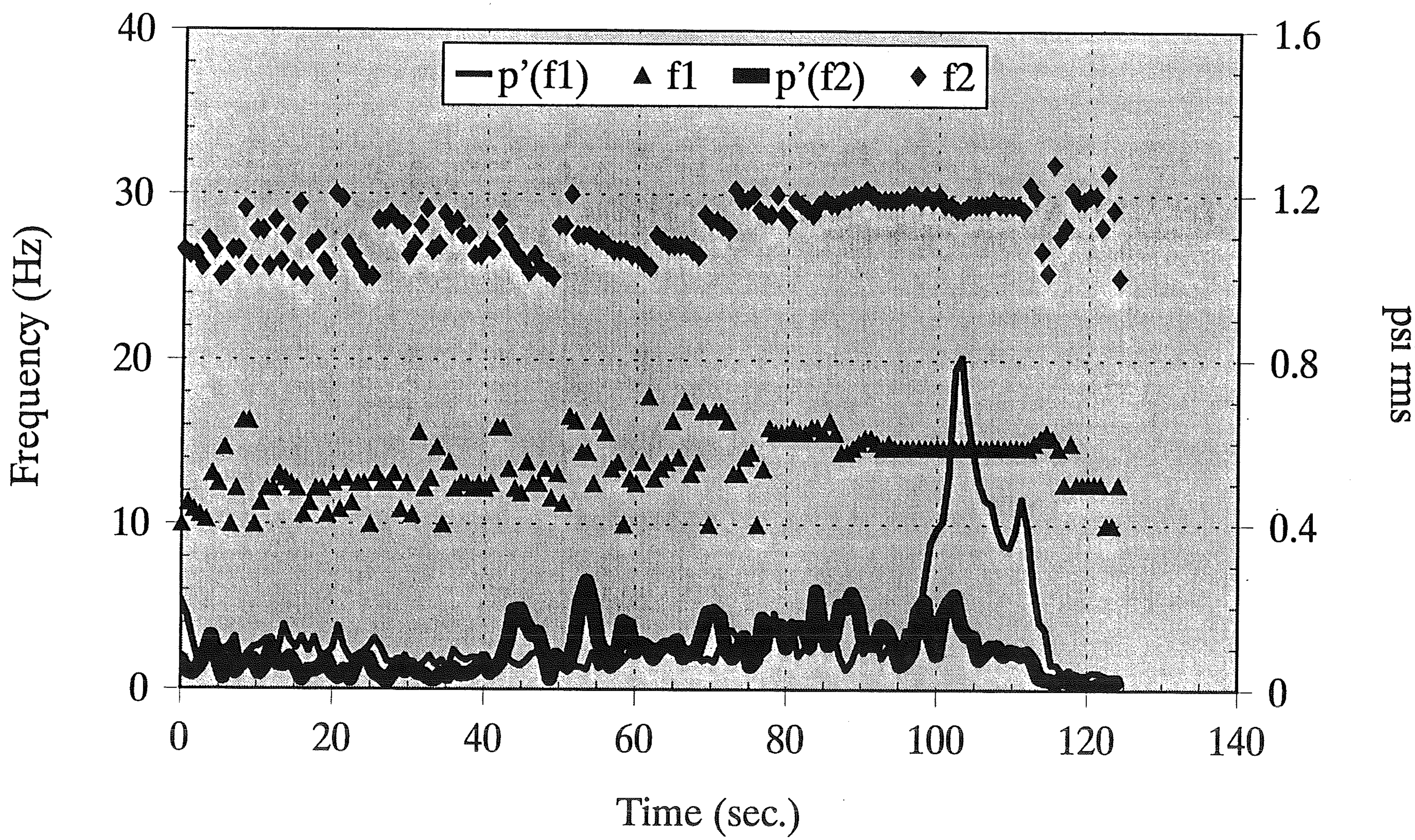

Measured p' Comparison

Predicted Hole Tone Frequencies

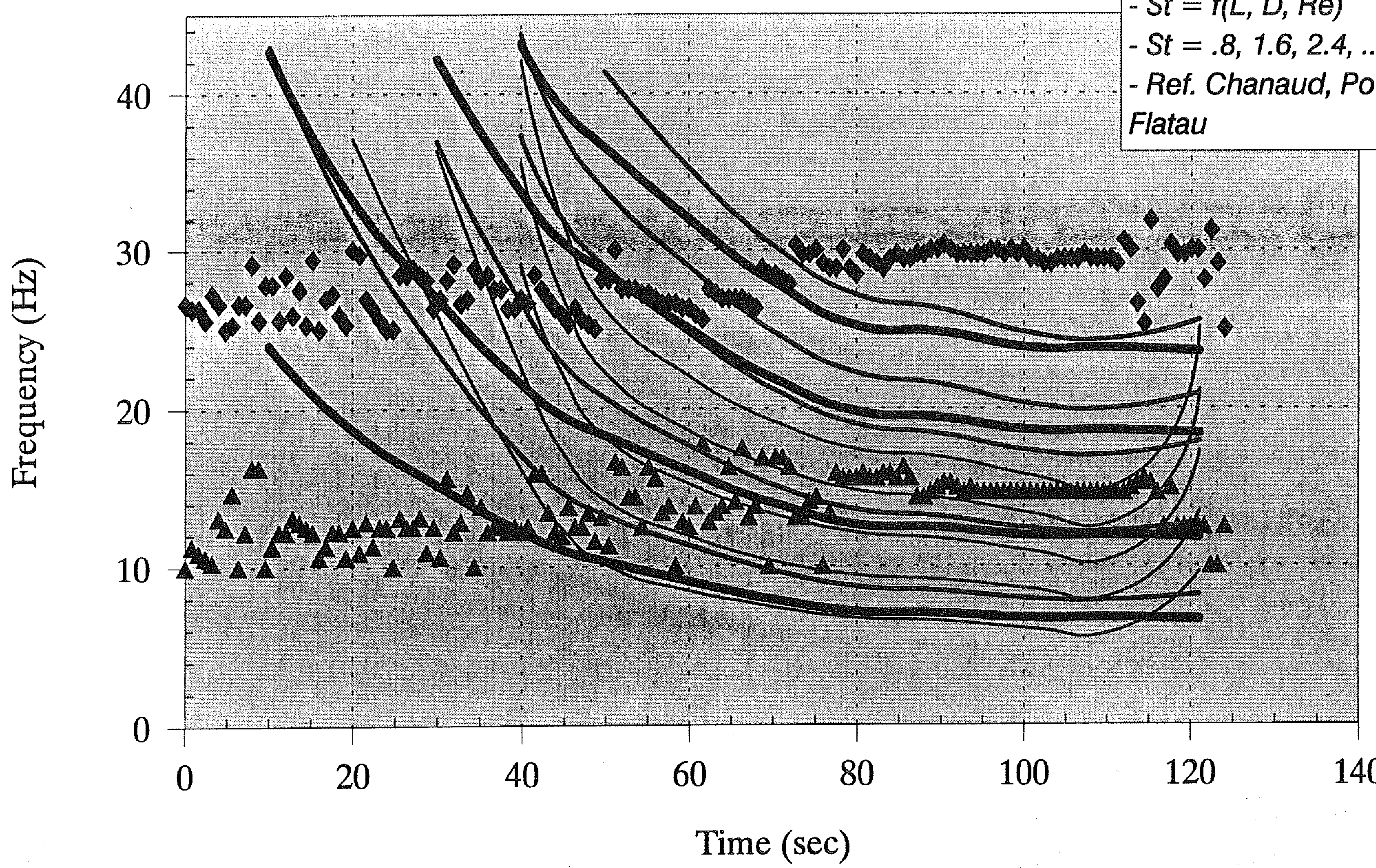

Hole Tones:
- *St = f(L, D, Re)*
- *St = .8, 1.6, 2.4, ...*
- *Ref. Chanaud, Powell, Flatau*

Measured p' Comparison

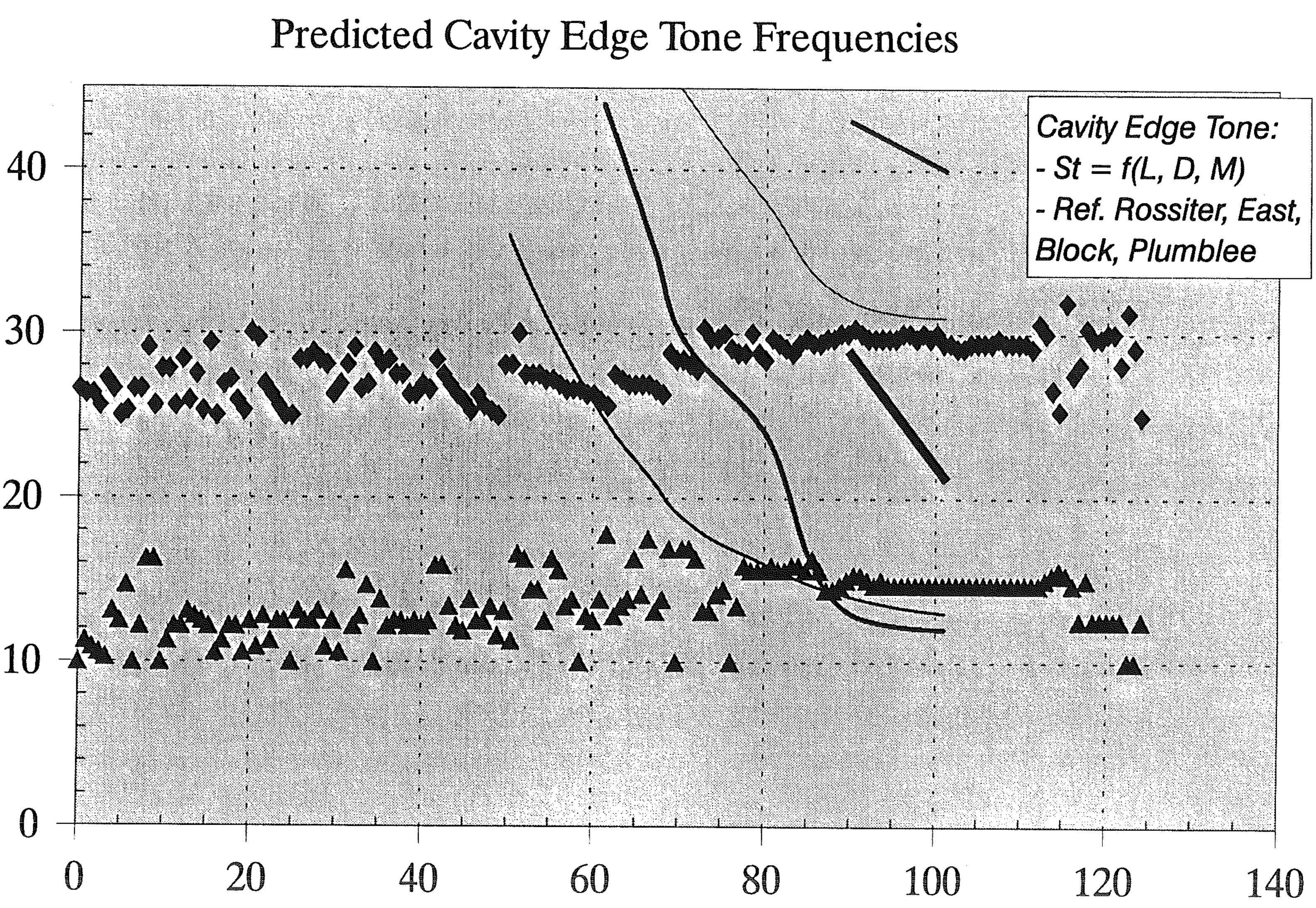

Background

- Numerical simulation of "edge-tone" phenomenon (NASA CR 4581)
    - Performed by Rockwell-Huntsville in 1992 using USA flow solver
    - Solved Navier-Stokes equation for low speed flows
    - Dipole nature of edge-tone
- Numerical simulation of RSRM (NAS8-38550)
    - Performed by Rockwell-Huntsville in 1993 using USA flow solver
    - S+80 sec and S+105 sec burn time geometry and flow
    - Objective: evaluate the effect of inhibitors on Pc oscillations
    - Head-end p' dominated by 1L, 2L, and 3L organ pipe modes
    - Inhibitors generate oscillations , however, head-end p' lower with inhibitor than without inhibitor (not tuned ?)

Present Study

- Time accurate CFD analysis made to replicate observations from motor firings and observe transit time mechanism details
- CFD model is axisymmetric representation of RSRM at 80 seconds into burn
- Objective: determine effect of stiffer inhibitors on Pc oscillations
- Deformation of inhibitors by internal flow determined through iterative structural and CFD analysis
- FDNS is flow solver used to detail time varying aspects of flow
- Fluid approximated as single-phase ideal gas
- Analysis domain ends upstream of nozzle throat

RSRM Unsteady CFD

Aft segment pressure contours

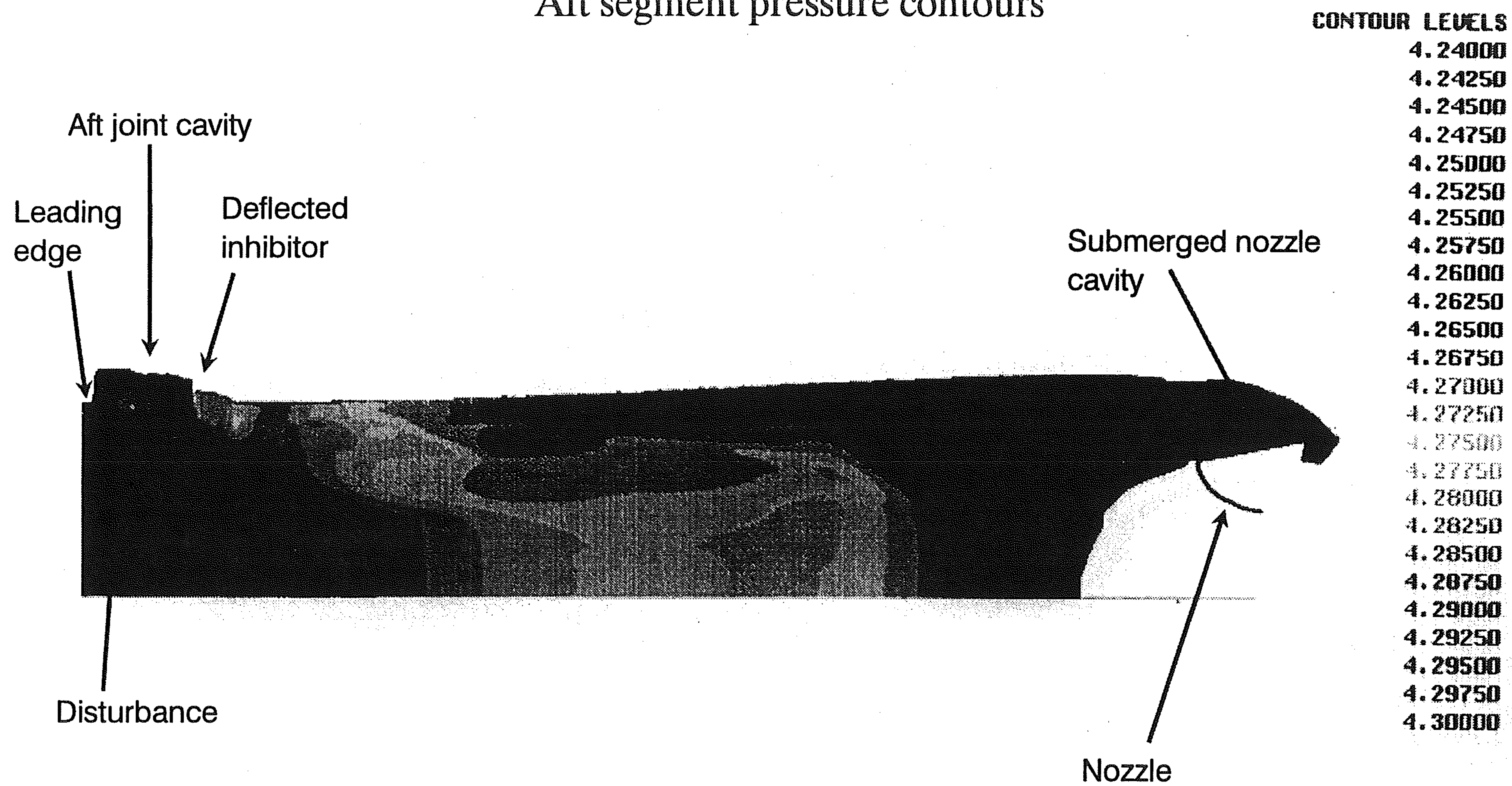

RSRM Unsteady CFD

Aft segment pressure contour sequence

t=0 sec

t=.01 sec

t=.02 sec

t=.03 sec

t=.04 sec

t=.05 sec

t=.06 sec

t=.07 sec

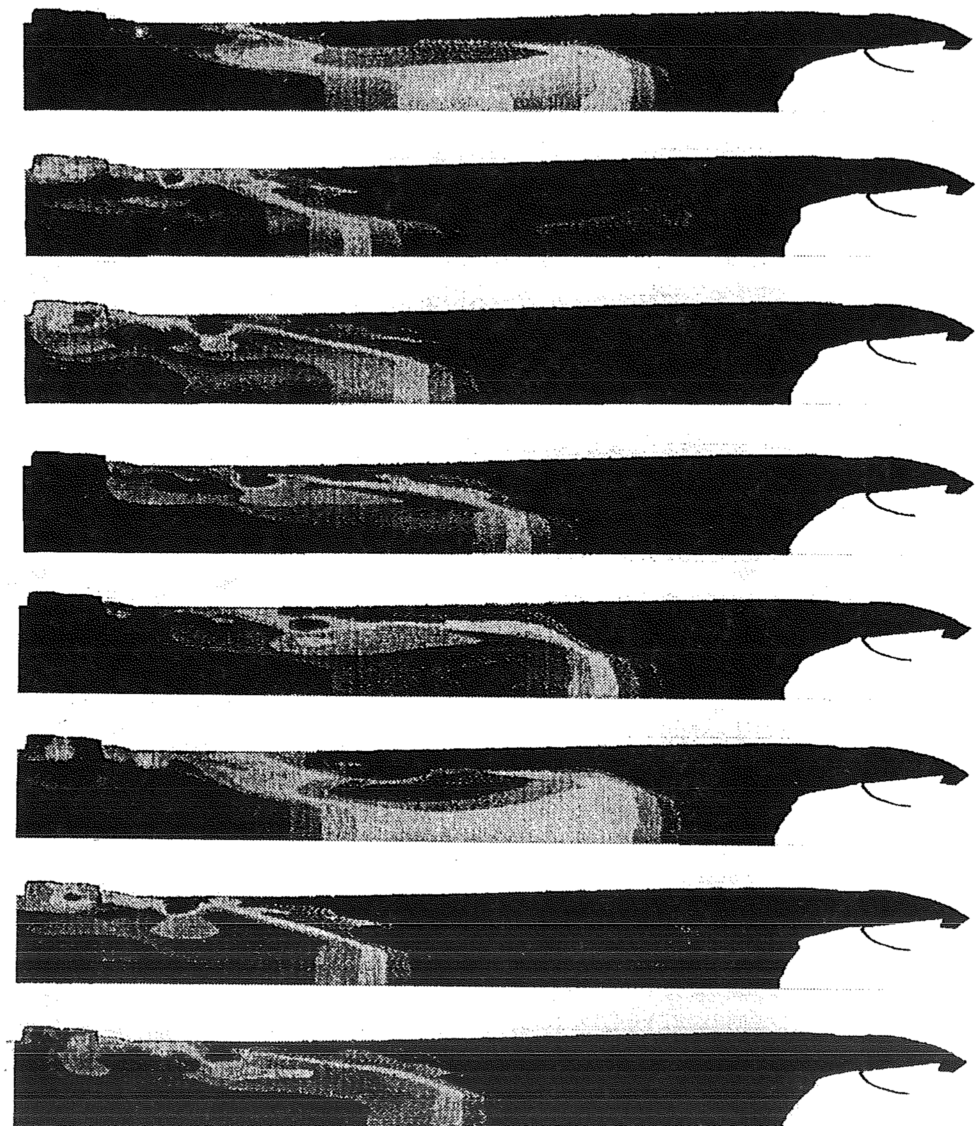

RSRM Unsteady CFD

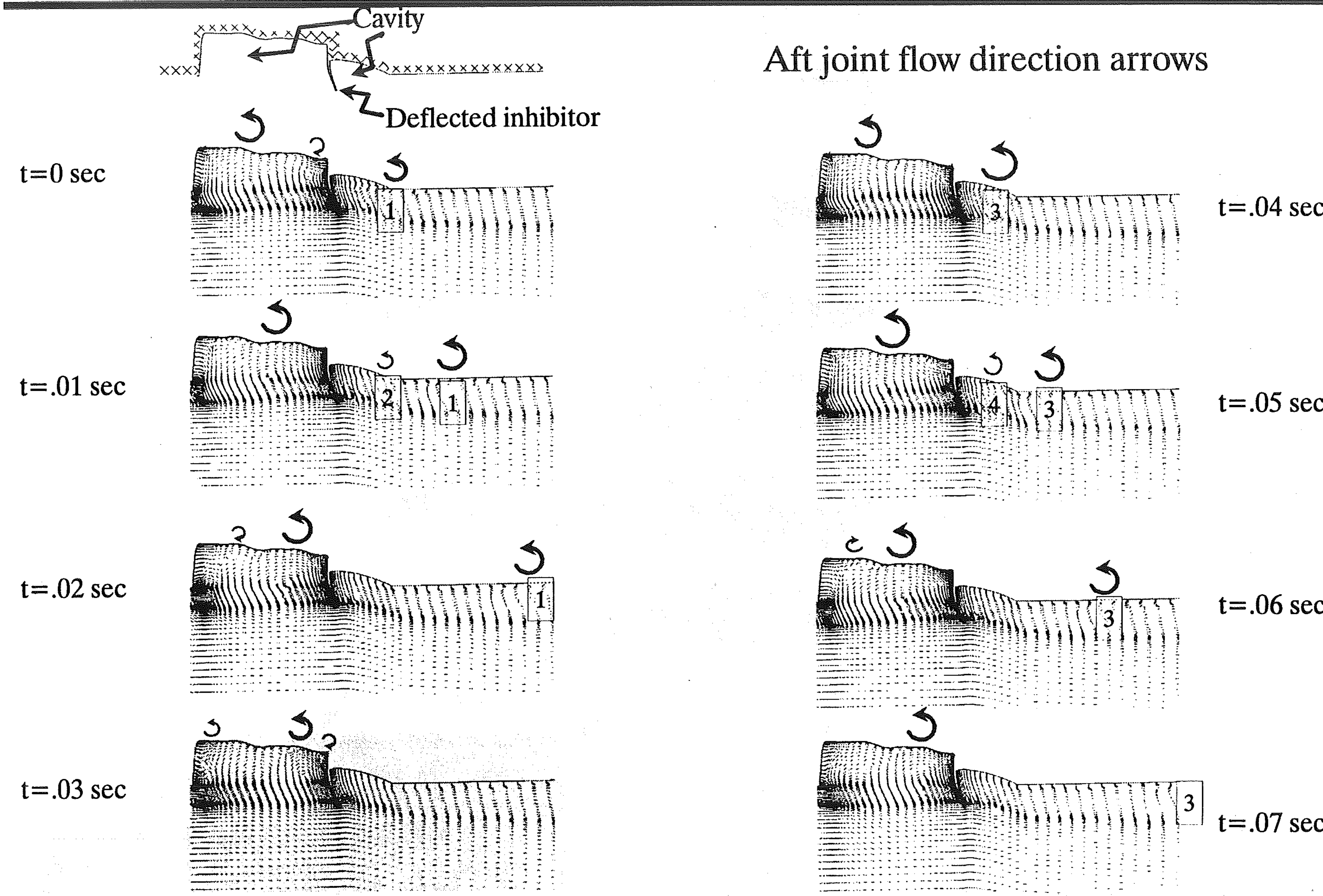

RSRM Unsteady CFD Timeplot

George C. Marshall Space Flight Center
Fluid Dynamics Division

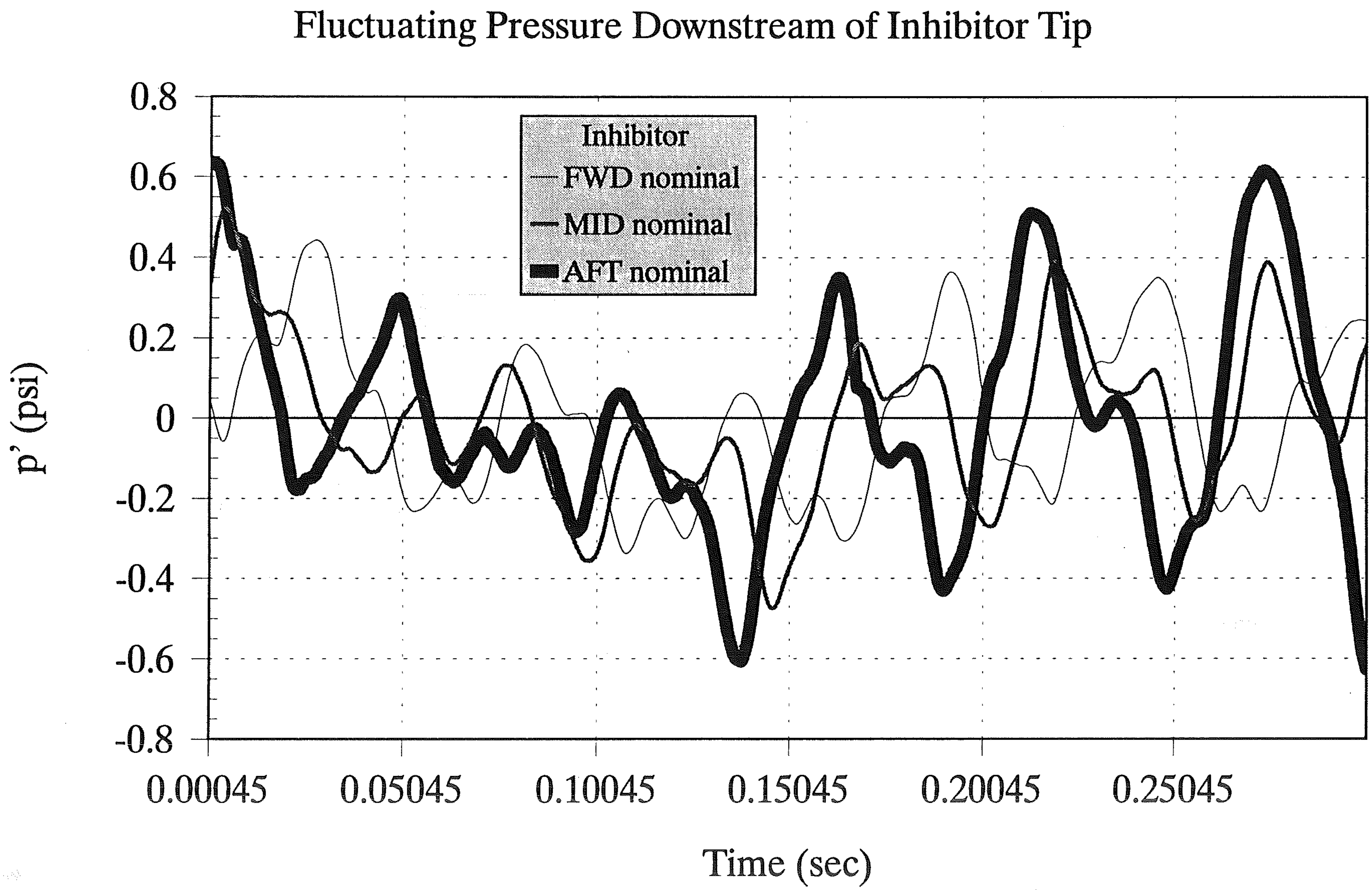

RSRM Unsteady CFD
Power Spectral Density

George C. Marshall Space Flight Center
Fluid Dynamics Division

Fluctuating Pressure Downstream of Inhibitor Tip

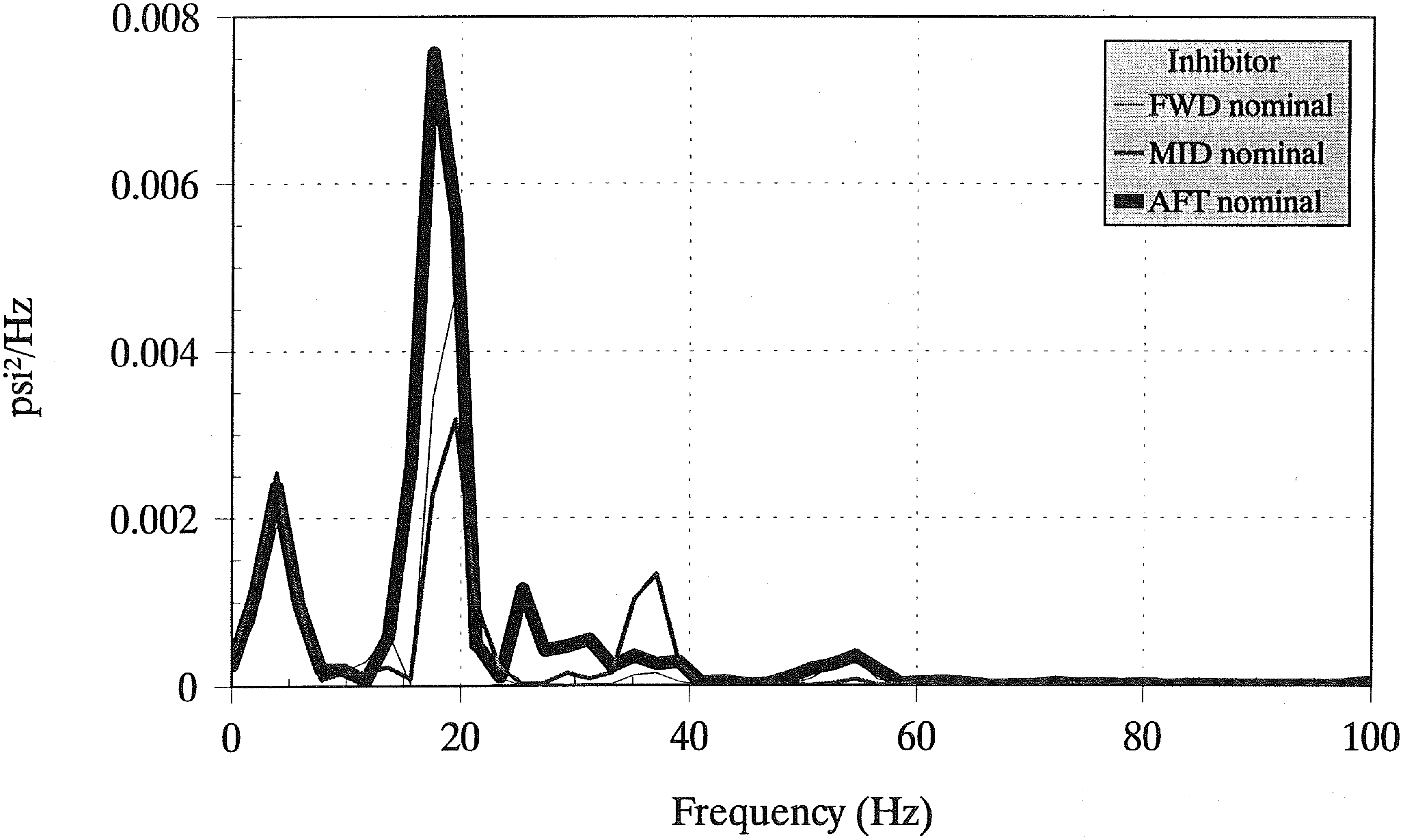

Summary of Present Unsteady CFD Results

- RSRM Pc oscillations dominated by organ pipe modes
- These acoustic modes excite or are excited by shedding of vortices within motor
- Vortex shedding in joint cavities and at inhibitors
- Vortex shedding at second open-closed organ pipe frequency
- Essential questions remain unanswered
    - Do vortices gain energy from feedback mechanism?
    - What is the feedback mechanism?
- Further studies planned with this model
    - Extend analysis domain downstream of nozzle throat
    - Evaluate using pressure gradient magnitude

S21-34
57396
132118
38p

A Coupled CFD/FEM Structural Analysis to Determine Deformed Shapes of the RSRM Inhibitors

Richard A. Dill and R. Harold Whitesides
ERC, Incorporated, Hunstville, AL 35816

Abstract

ACRYLONITRILE BUTADIENE RUBBER

Recent trends towards an increase in the stiffness of the NBR insulation material used in the construction of RSRM propellant inhibitors prompted questions about possible effects on RSRM performance. The specific objectives of the CFD task included: 1) the definition of pressure loads to calculate the deformed shape of stiffer inhibitors, 2) the calculation of higher port velocities over the inhibitors to determine shifts in the vortex shedding or edge tone frequencies and 3) the quantification of higher slag impingement and collection rates on the inhibitors and in the submerged nose nozzle cavity.

A coupled CFD/Finite element structural analysis was required to calculate the deformed inhibitor geometry. Since the NBR inhibitor material erodes at a different rate than the motor propellant burns, an inhibitor stub which protrudes above the propellant into the port cavity is created during motor operation. The impinging port flow causes the inhibitor stub to bend in the downstream flow direction. Since a stiffer NBR inhibitor material would cause the inhibitor to bend less, it was necessary to know the difference in the bending of the original NBR material compared to the stiffer NBR material. The CELMINT CFD computer code was used to perform the fluid dynamic calculations of the motor flow field. The structural bending effect of the pressure loads from the CFD code was analyzed by ED28. Initially, the CELMINT code was used to determine the flow field and inhibitor pressure loads for unbent motor inhibitors. This pressure loading on the inhibitors was used by ED28 to generate the bending which would occur in the inhibitor. The computed bent inhibitor geometry was then used again by the CFD code to compute a new pressure loading on the inhibitors. This iterative computation between the CFD code and the structural analysis code was continued until convergence in the inhibitor bent geometry was achieved.

The CFD solution was then used to assess the effect of higher flow velocities and edge tone frequencies from the reduced inhibitor bending on the maximum oscillating pressure amplitudes that occur during resonance between the edge tones and the motor longitudinal modes. Also, a comparison of the difference in slag accumulation between the two NBR materials was also made to determine if the stiffer material increases slag collection in the field joints and the submerged nozzle cavity.

The coupled CFD/FEM structural analysis was successful in defining the effect of inhibitor stiffness on inhibitor geometry and the shift in edge tone frequencies. Also, the two-phase CFD analysis showed that there was a small increase in the rate of slag accumulation at the aft inhibitor; however, motor trajectory analyses of slag debris shed from the inhibitors showed that the debris would pass out the motor nozzle and therefore create no additional slag accumulation in the slag pool around the nozzle.

A COUPLED CFD/FEM STRUCTURAL ANALYSIS TO DETERMINE DEFORMED SHAPES OF THE RSRM INHIBITORS

Richard A. Dill
R. Harold Whitesides
ERC, Incorporated
Huntsville, Alabama

Thirteenth Workshop for CFD Applications in Rocket Propulsion
NASA Marshall Space Flight Center
Huntsville, Alabama
April 25-27, 1995

Background

- In October, 1994, Thiokol reported the use of NBR material in RSRM's with properties significantly different from the historical database.
- A 30% to 40% increase in modulus was reported.
- This increased stiffness had the potential to affect the amplitude of chamber pressure oscillations in the SRM:

  --By changing the inhibitor structural response

  --By indirectly changing the flow/acoustic interaction
- The slag accumulation in the field joints and submerged nozzle region might also be increased thereby increasing the potential for pressure and thrust perturbations.

ERC, Inc.

Objectives of Coupled CFD/FEM and Two-Phase CFD Analyses

- Determine deformed geometry of NBR inhibitors at the forward, center and aft joints for both nominal and stiff NBR materials using a coupled CFD/FEM analysis.
- Determine effect of inhibitor properties/geometry on inhibitor hole velocities to evaluate effect on hole edge tone (vortex shedding) frequencies.
- Determine effect of inhibitor properties/geometry on slag accumulation on both the inhibitor surfaces and underneath the nozzle nose.

ERC, Inc.

Coupled CFD/FEM Analysis Approach

1) Perform single-phase gas CFD analysis of entire RSRM port at 80 second burn time using straight inhibitor lengths from erosion analysis.

2) Perform FEM structural analysis on inhibitors to determine deformations using surface pressure distributions from CFD analysis.

3) Perform CFD analysis using deformed inhibitor geometries from step 2).

4) Repeat steps 2) and 3) until convergence of inhibitor geometry is achieved.

5) Provide velocity profile at each inhibitor location for both nominal and stiff inhibitors as input to flow/acoustic interaction analysis.

Two-Phase Flow CFD Methodology
CELMINT Code
(Combined Eulerian Lagrangian Multi-Dimensional Implicit Nonlinear Time-Dependent)

- **Navier-Stokes Solution**
  - Fully implicit, density-based, conservative, ensemble-averaged Navier-Stokes code
  - Low and high Reynolds number and wall injection $\kappa - \varepsilon$ models
  - Equilibrium and finite-rate chemistry for multi-species flows

- **Two-phase Flow Models**
  - Coupled Eulerian-Lagrangian for solid and liquid phases
  - Hermsen aluminum burn rate model for particle combustion
  - Specification of particle properties (density, size distribution)
  - Particle break-up based on Weber number
  - Agglomeration based on collisions between discrete phase particles and continuous phase smoke particles
  - Programmable for various particle capture criteria

ERC, Inc.

Propellant Thermochemical Properties and Motor Operating Conditions
RSRM 80 Second Burn Time

Propellant	TP-H1148
Pressure	625 psia
Total Temperature	6093° R
Molecular Weight	28.04
Dynamic Viscosity	6.189×10^{-5} bm/ft-sec
Ratio of Specific Heats	1.138
Flow Rate, Forward Segment	1555.9 lbm/sec
Flow Rate, Center Segment 1	2587.5 lbm/sec
Flow Rate, Center Segment 2	2578.6 lbm/sec
Flow Rate, Aft Segment	2849.0 lbm/sec
Flow Rate, Total	9571.0 lbm/sec
Throat Diameter	55.42 inches

ERC, Inc.

RSRM Motor Geometry

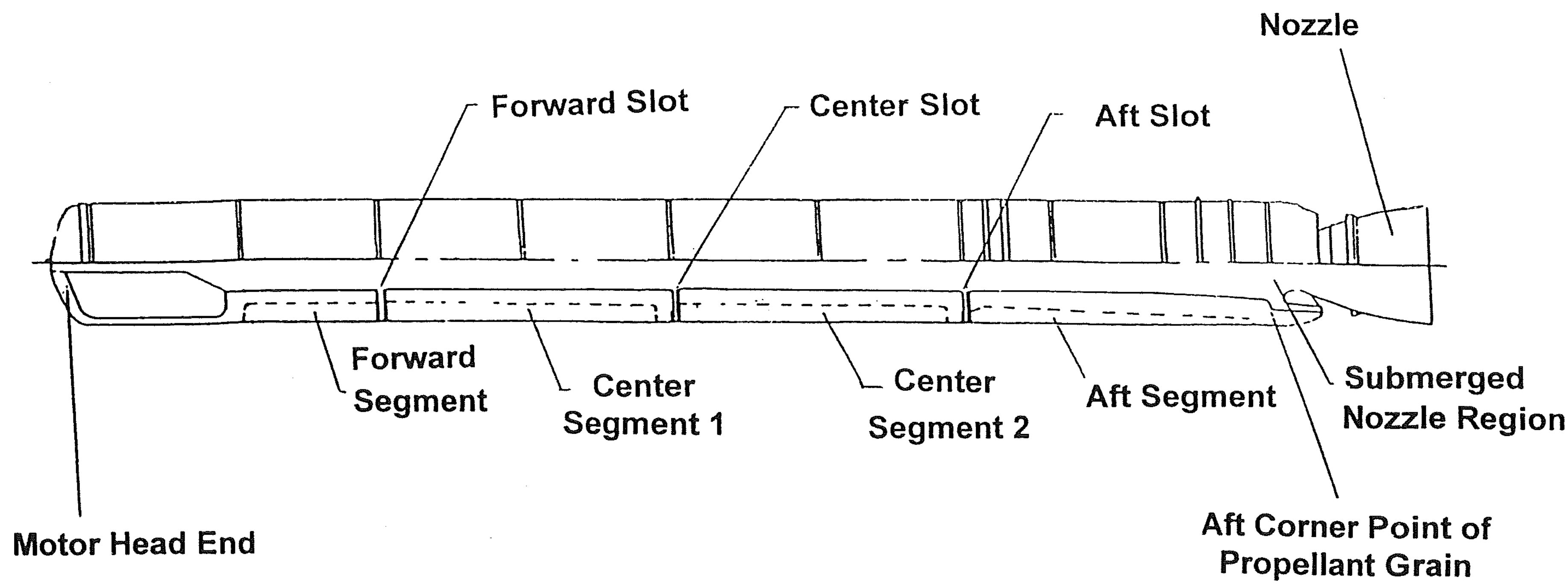

(Dashed Line Shows The 67 Second Burn Back)

Computational Grid Resolution

Port	400X50
Field Joints	30X20
Inhibitor Stub	4X20
Submerged Region	70X20
Overall Grid	488X70

ERC, Inc.

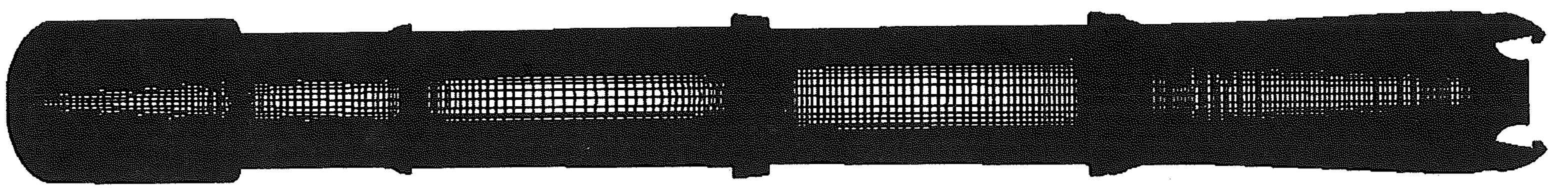

Computational Grid, Full Motor

RSRM 80 Second Stiff NBR Inhibitor

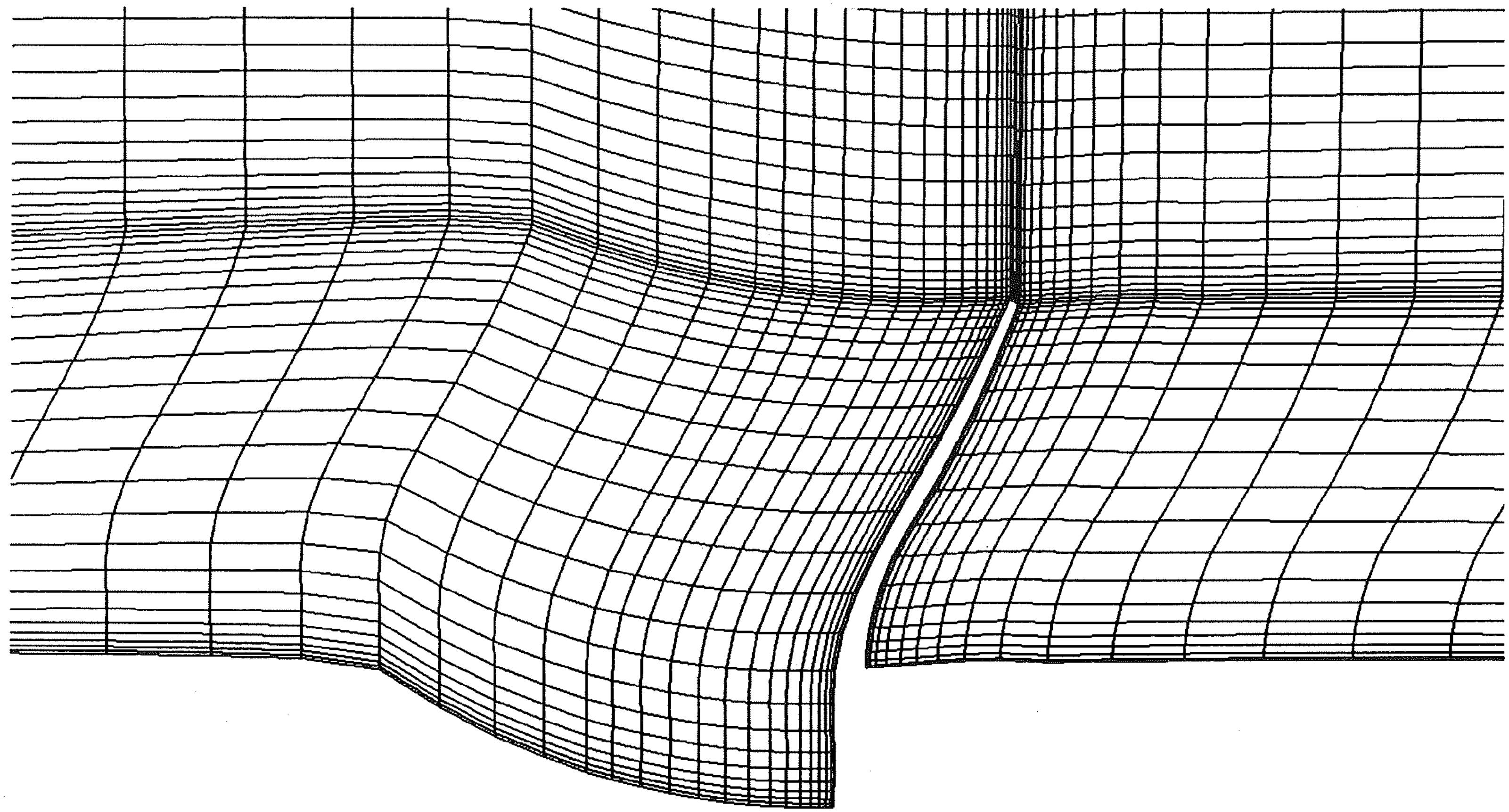

Computational Grid, Forward Slot

RSRM 80 Second Stiff NBR Inhibitor

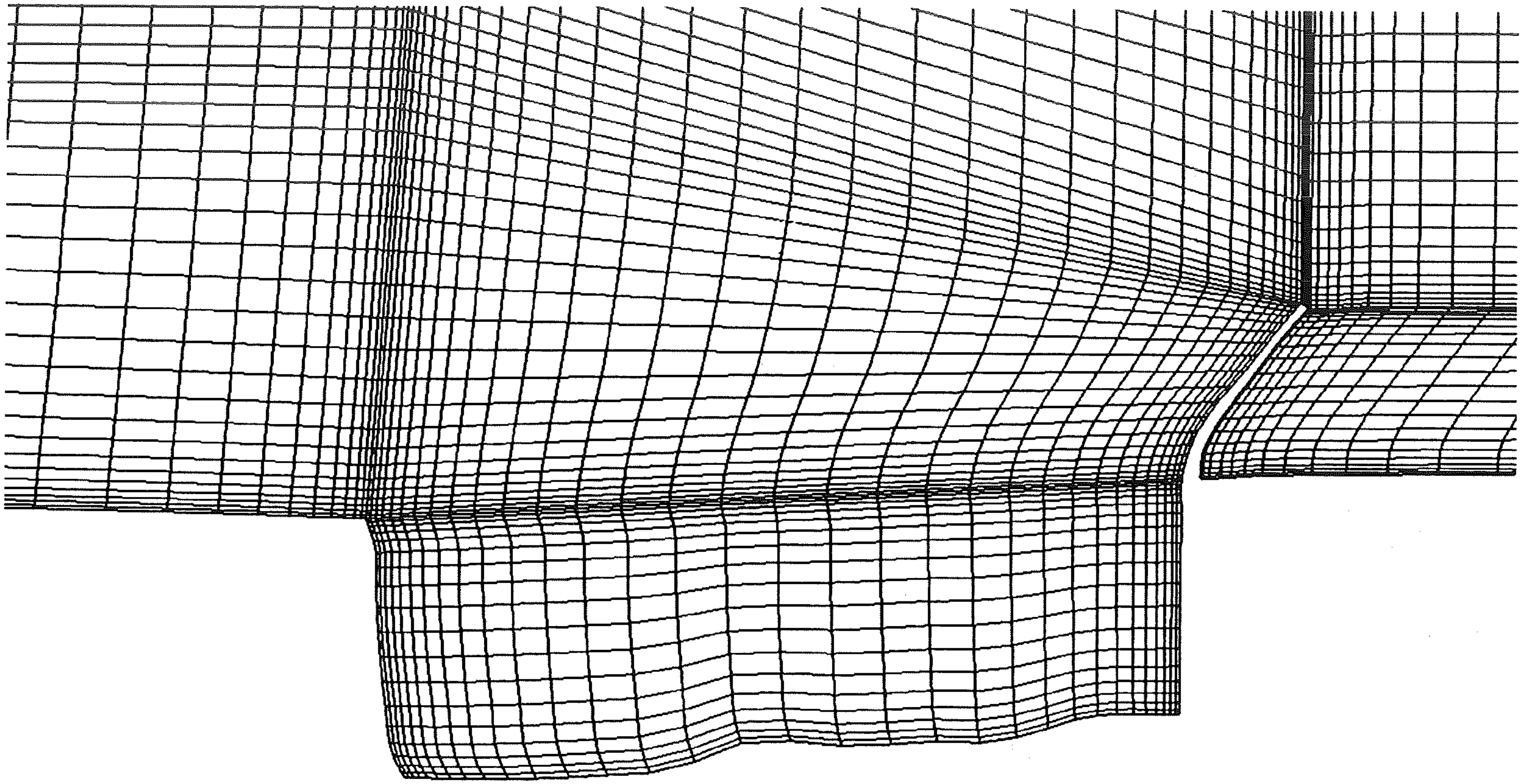

Computational Grid, Center Slot

RSRM 80 Second Stiff NBR Inhibitor

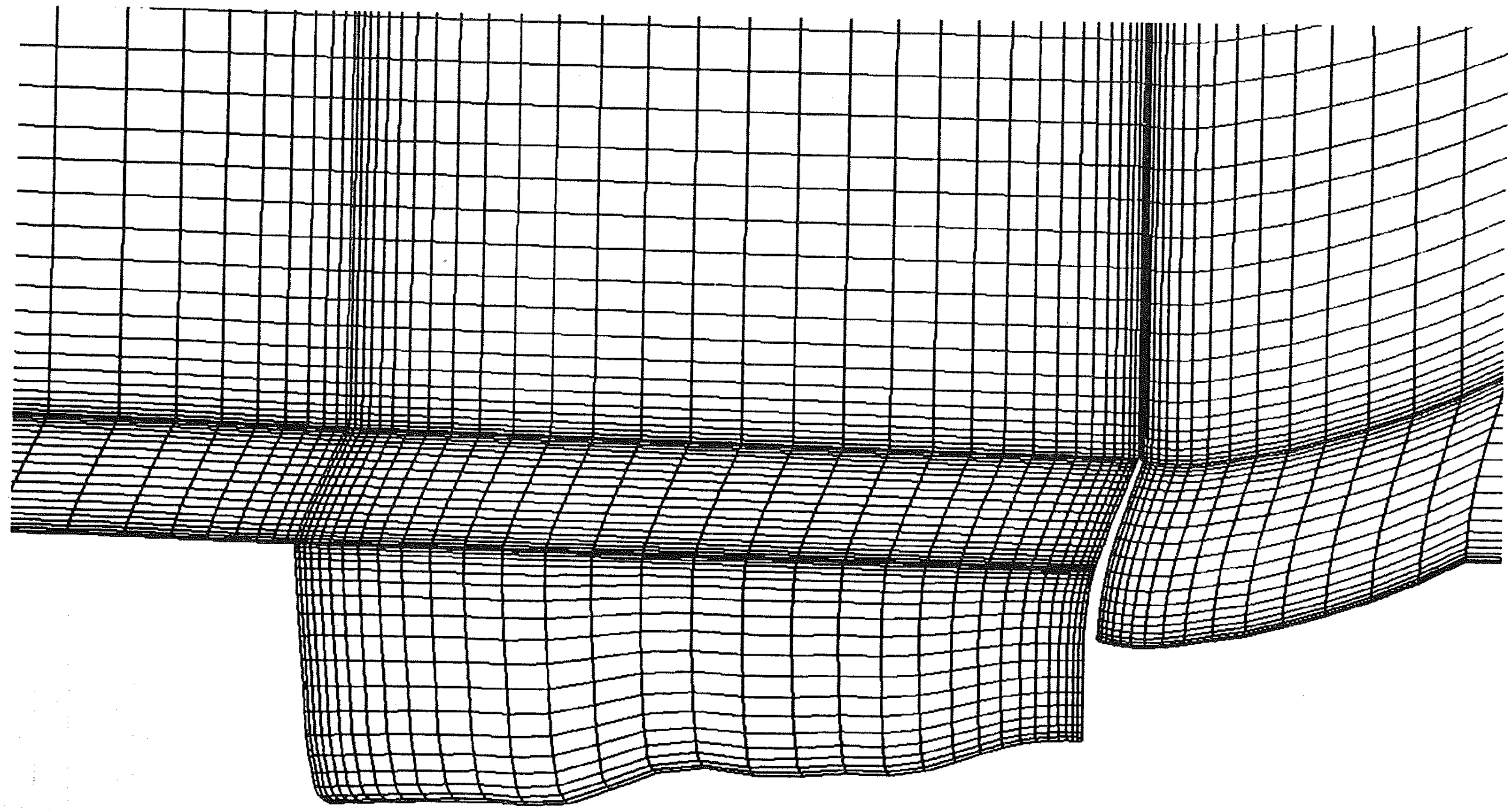

Computational Grid, Aft Slot

RSRM 80 Second Stiff NBR Inhibitor

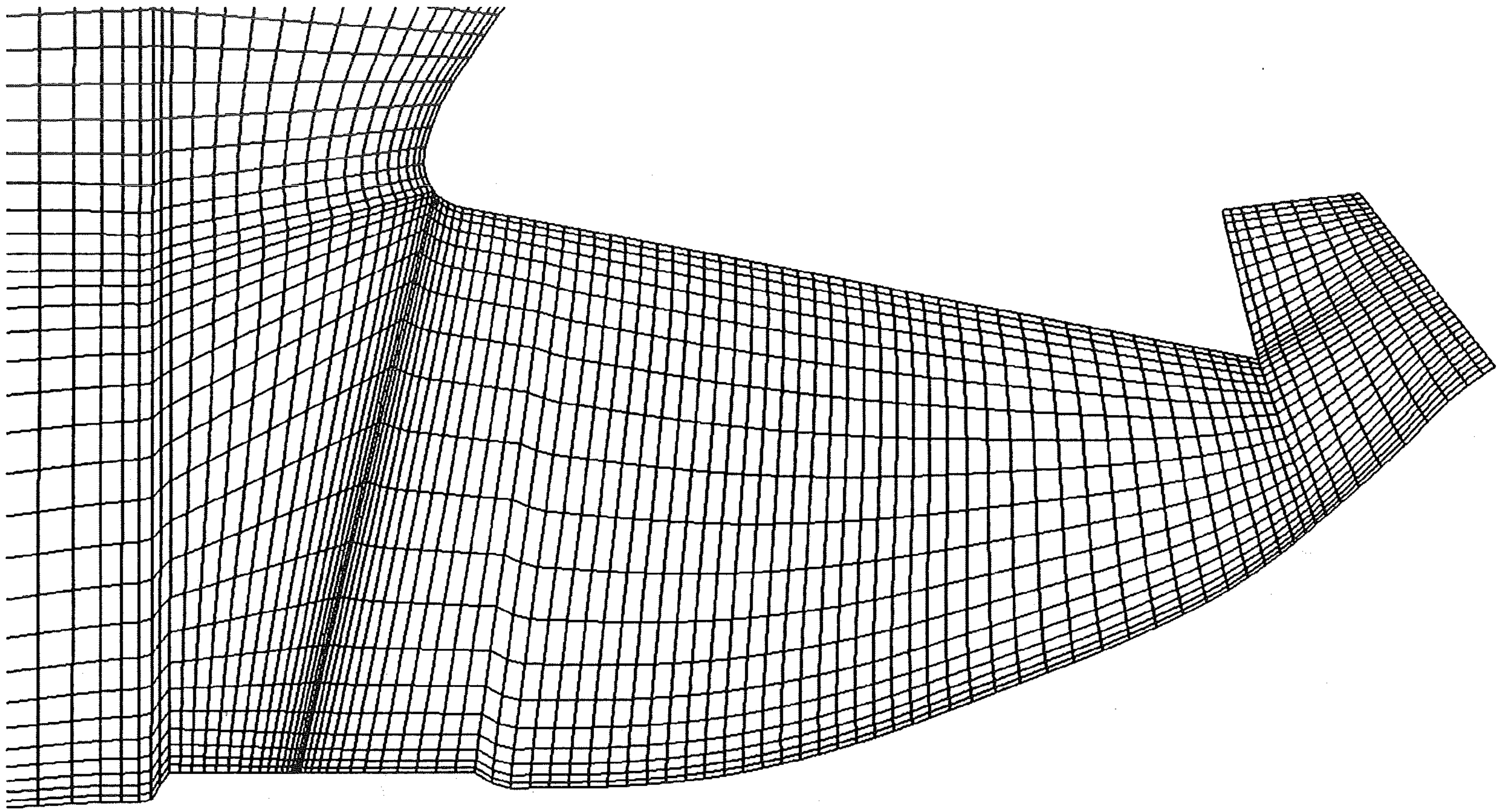

Computational Grid, Submerged Nozzle

RSRM 80 Second Stiff NBR Inhibitor

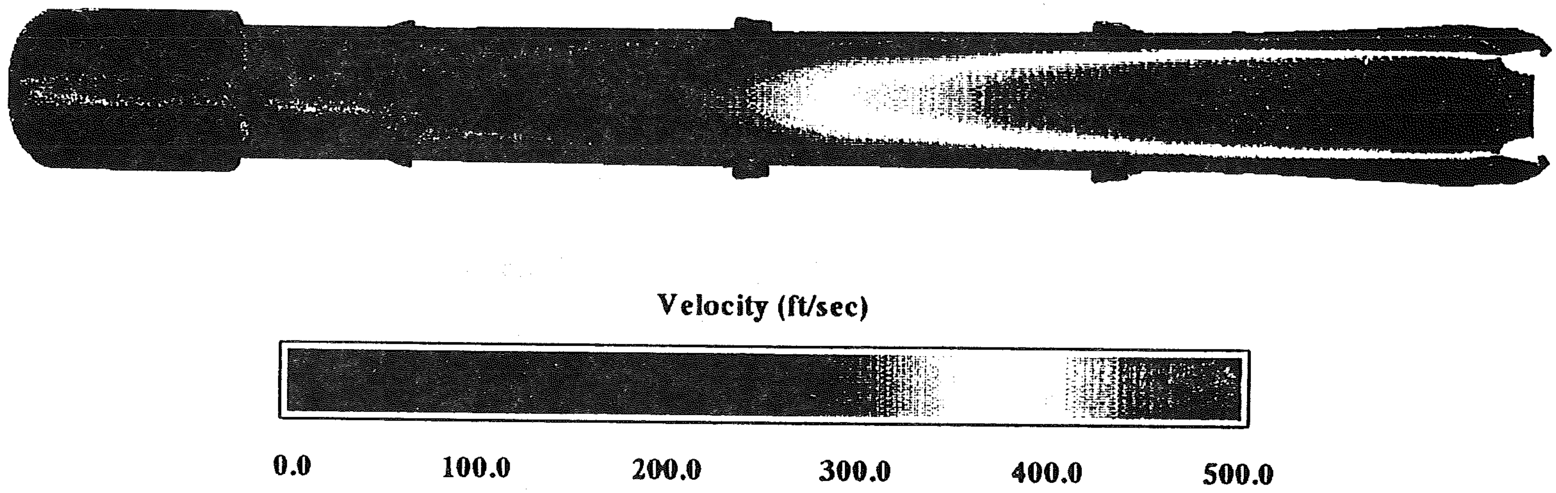

Flowfield Velocity Magnitude

RSRM 80 Second Stiff NBR Inhibitor

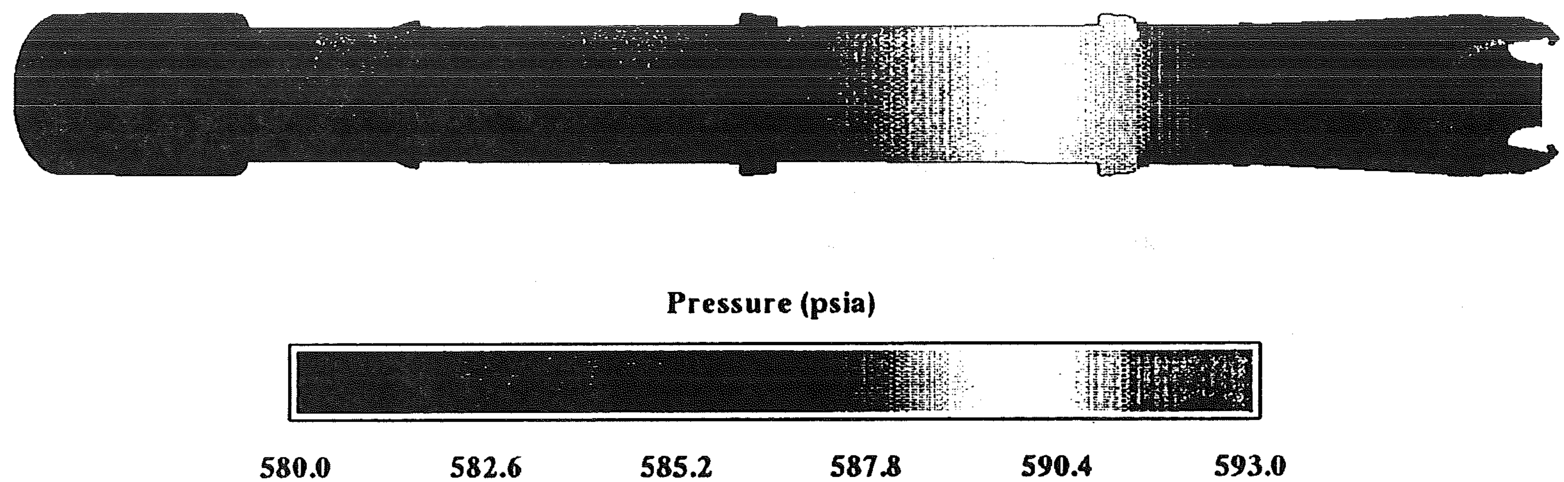

Flowfield Static Pressure

RSRM 80 Second Stiff NBR Inhibitor

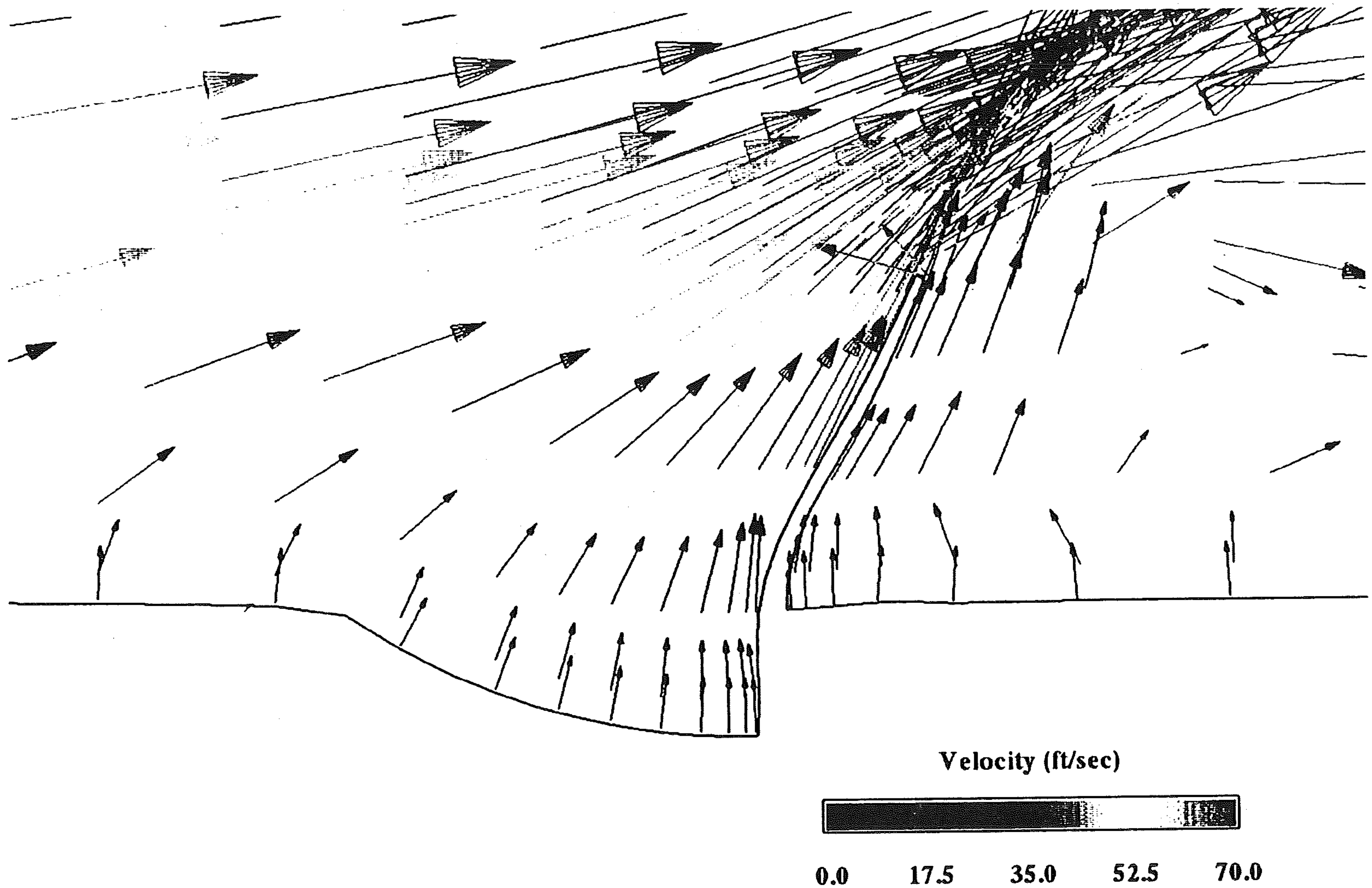

Velocity Vectors, Forward Slot

RSRM 80 Second Stiff NBR Inhibitor

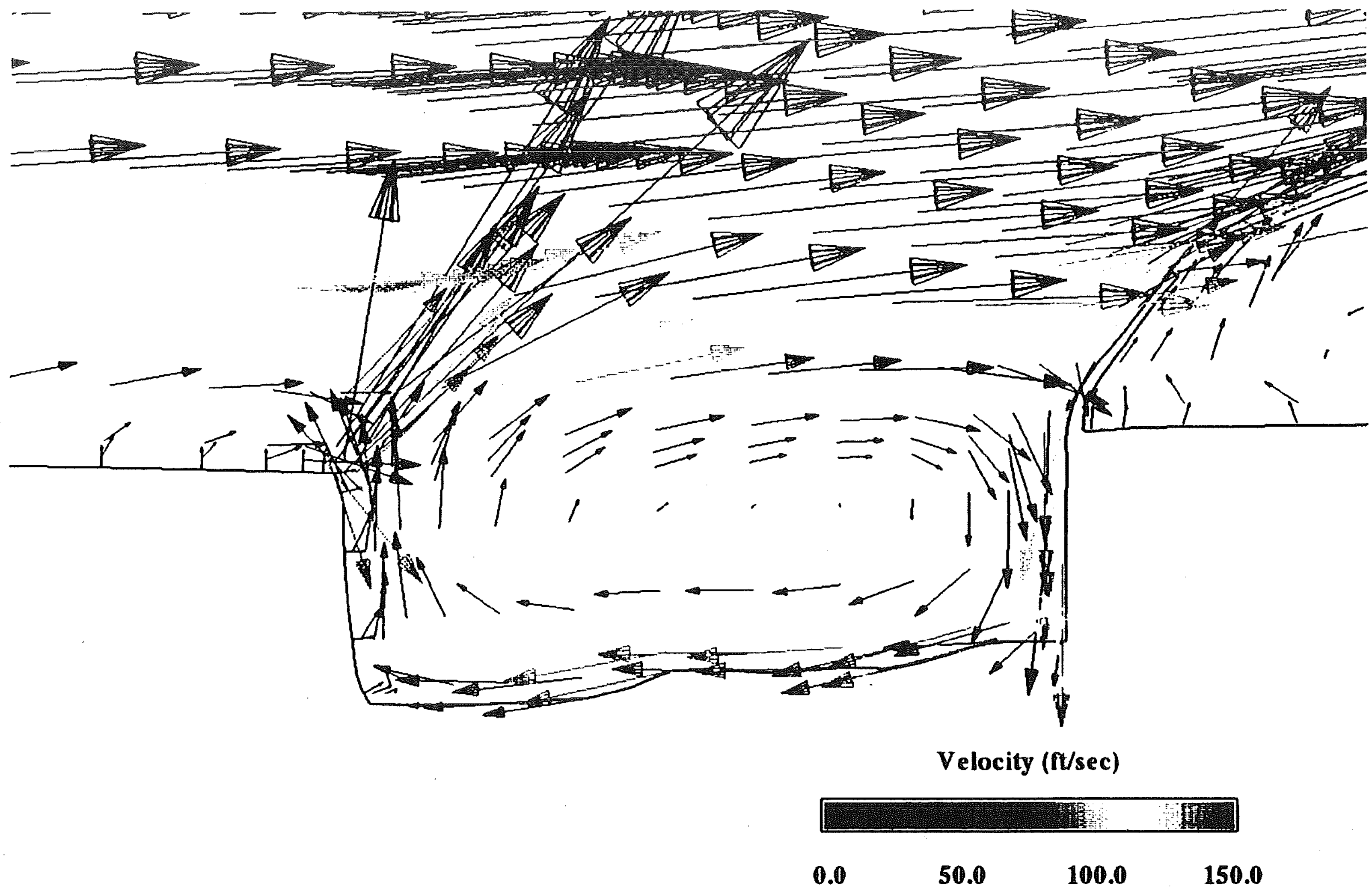

Velocity Vectors, Center Slot
RSRM 80 Second Stiff NBR Inhibitor

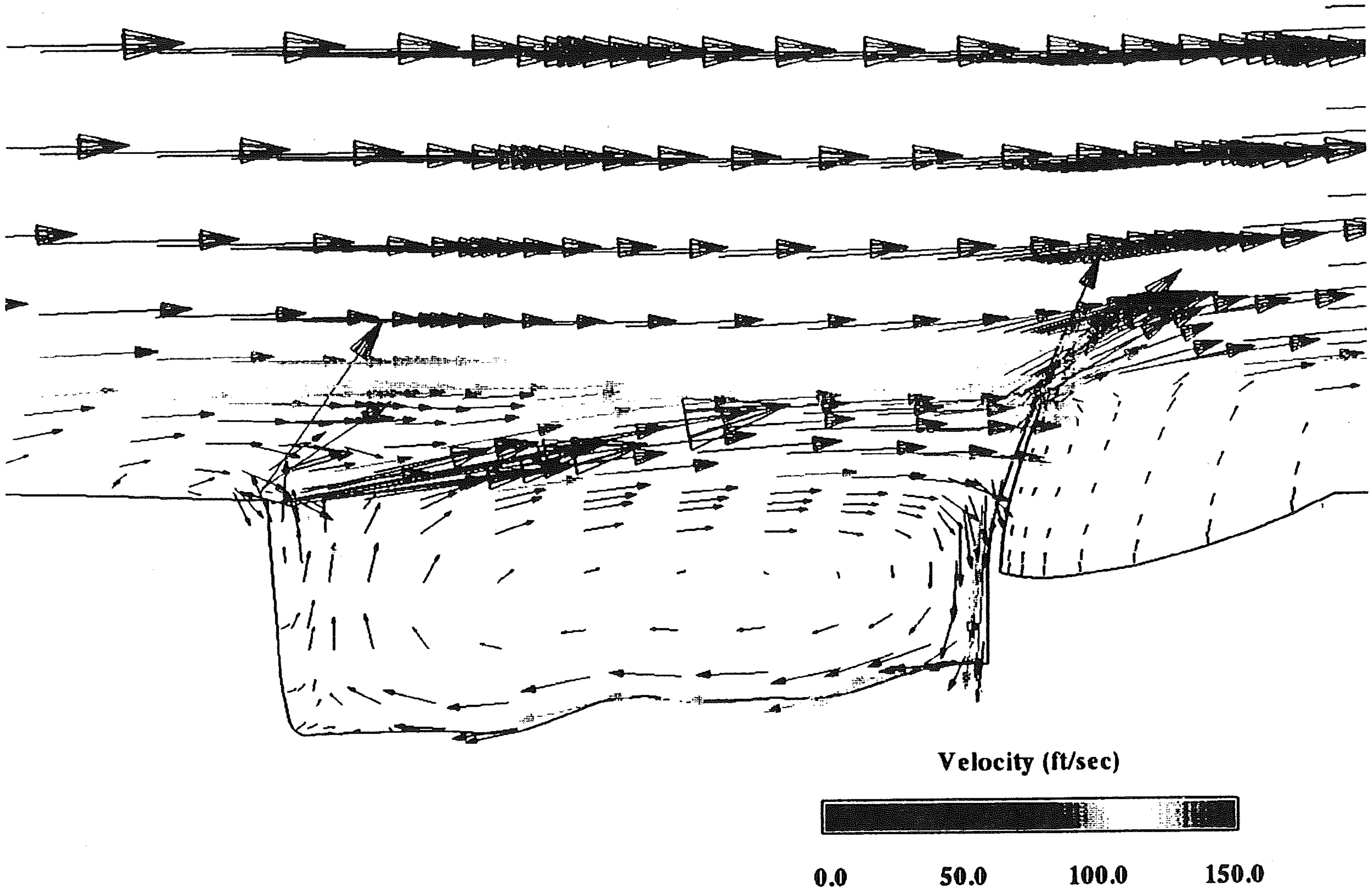

Velocity Vectors, Aft Slot

RSRM 80 Second Stiff NBR Inhibitor

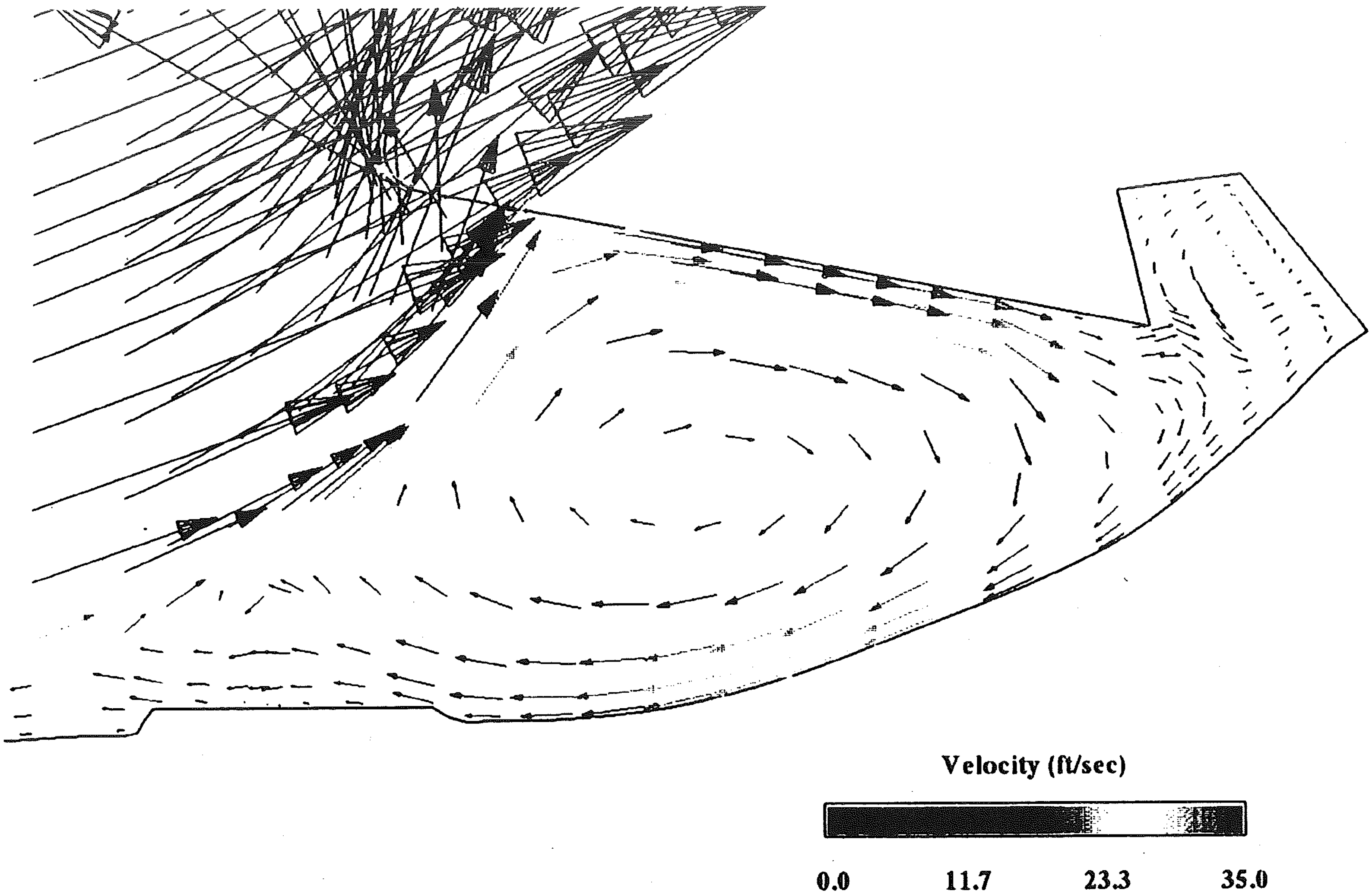

Velocity Vectors, Submerged Nozzle

RSRM 80 Second Stiff NBR Inhibitor

Forward Inhibitor Radial Pressure Distribution
RSRM 80 Seconds Burn Time
Stiff NBR

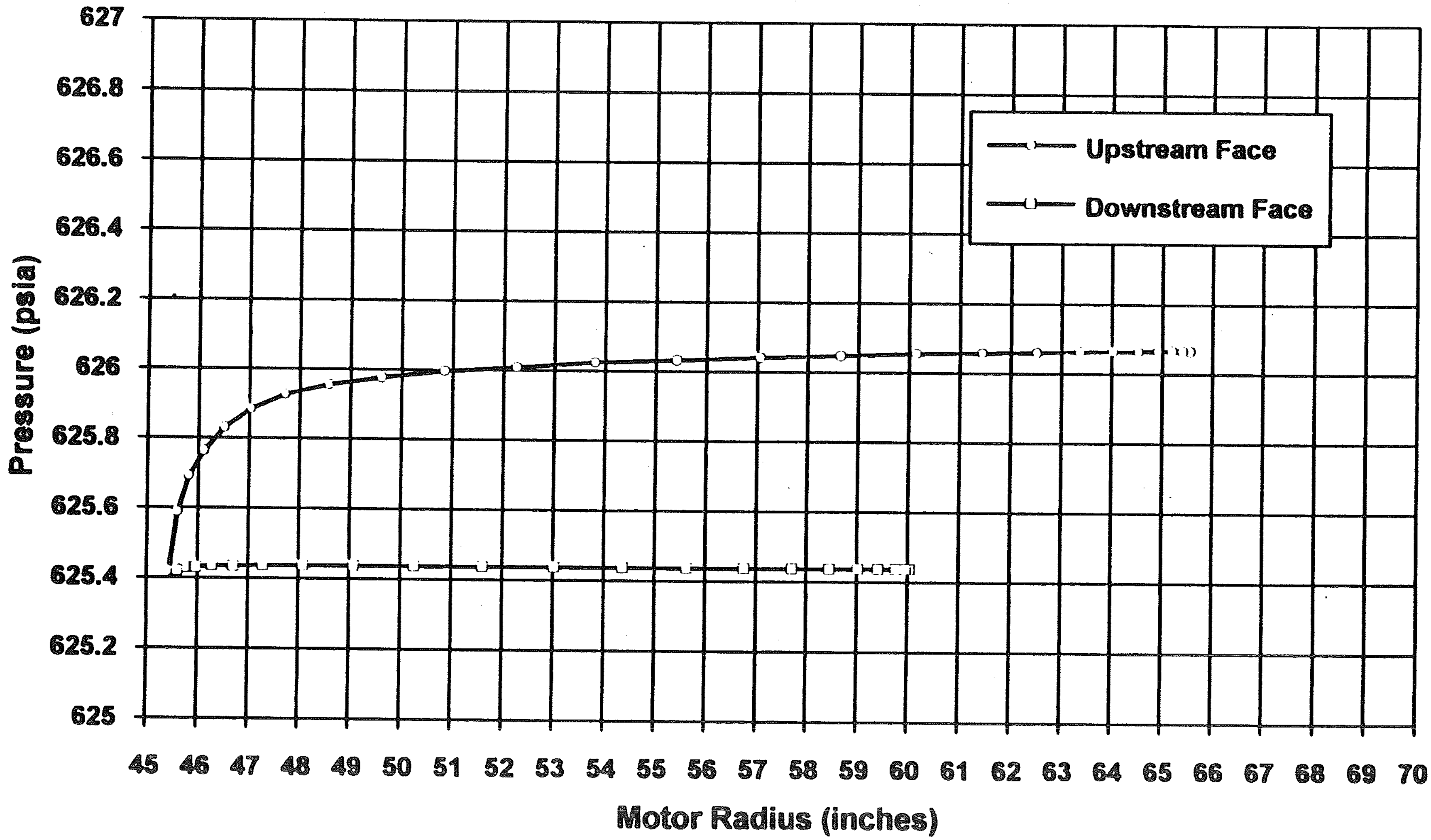

ERC, Inc.

Center Inhibitor Radial Pressure Distribution
RSRM 80 Seconds Burn Time
Stiff NBR

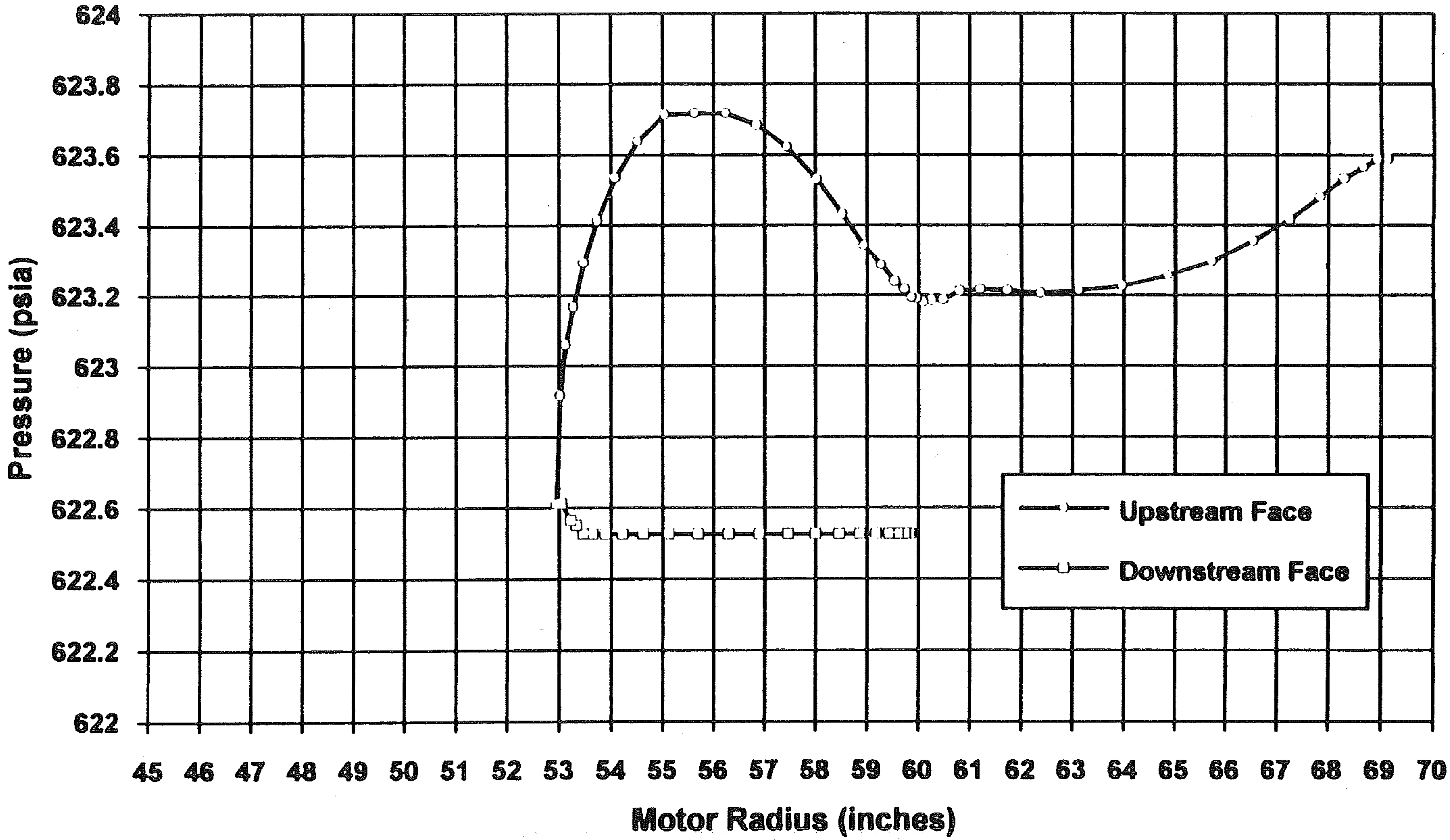

ERC, Inc.

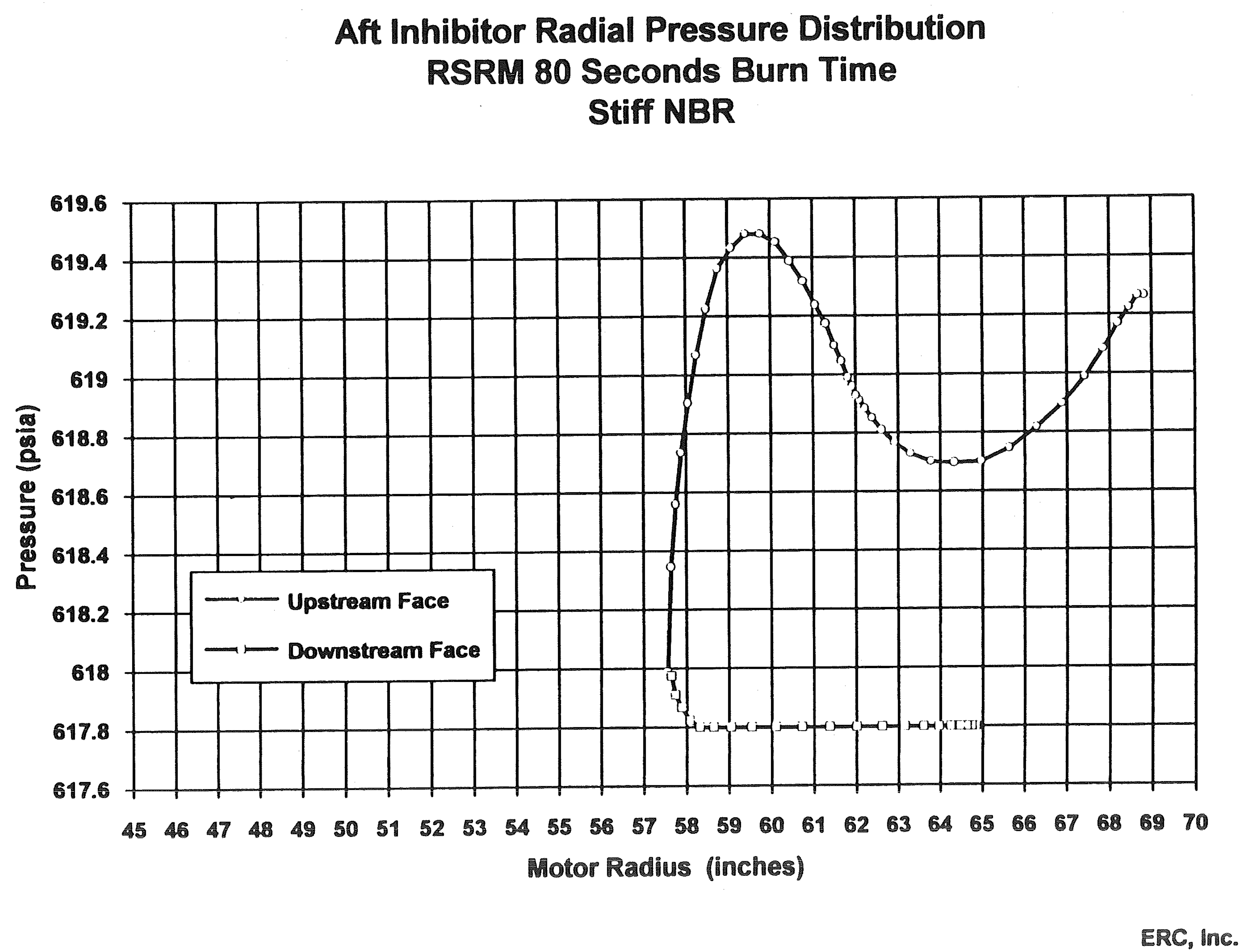

Aft Inhibitor Radial Pressure Distribution
RSRM 80 Seconds Burn Time
Stiff NBR
Pressure (psia)
619.6
619.4
619.2
619
618.8
618.6
618.4
618.2
618
617.8
617.6
Upstream Face
Downstream Face
45
46
47
48
49
50
51
52
53
54
55
56
57
58
59
60
61
62
63
64
65
66
67
68
69
70
Motor Radius (inches)
ERC, Inc.

Forward Inhibitor Deformation Iterations
Stiff NBR
RSRM 80 Seconds Burn Time

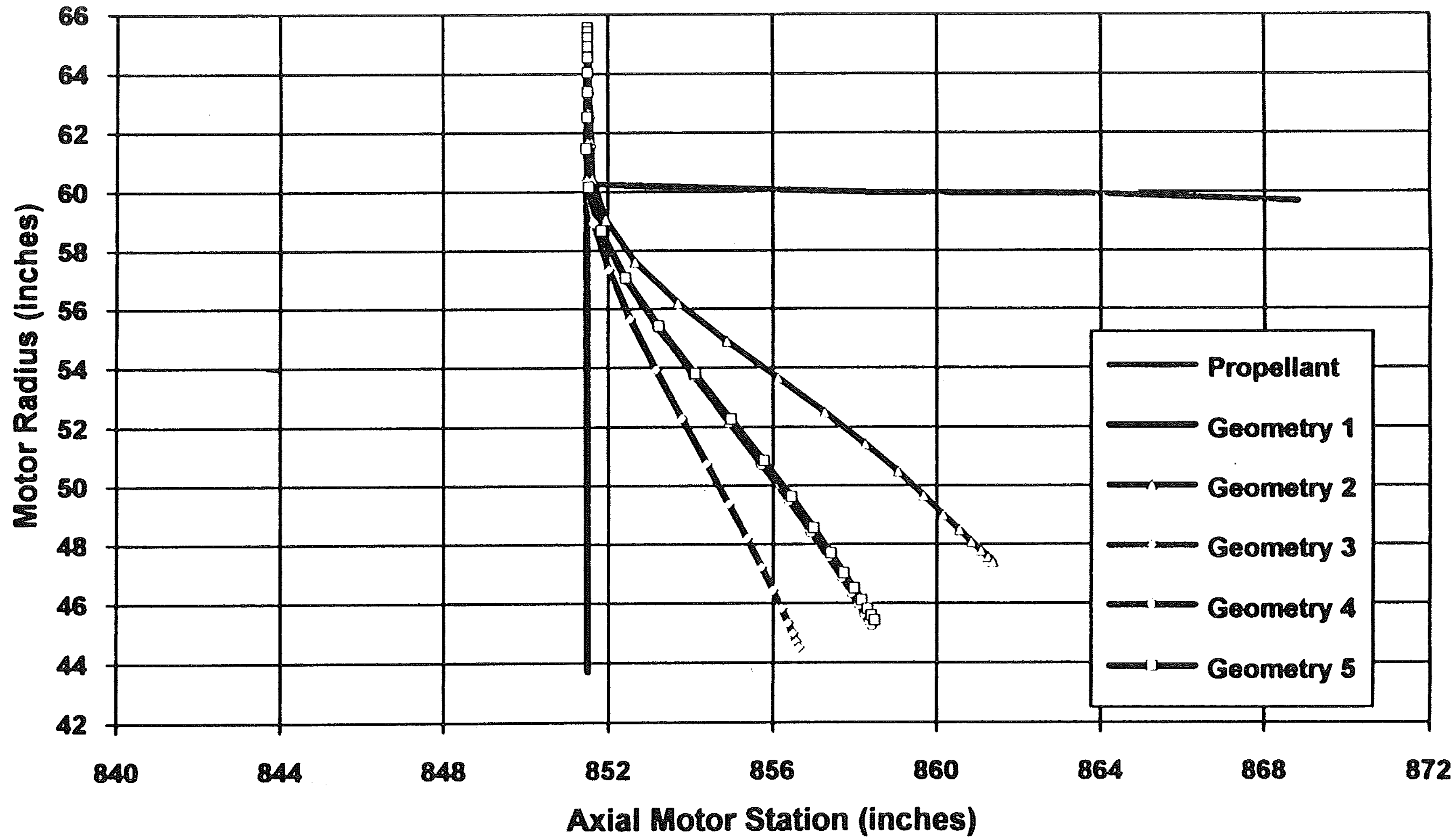

ERC, Inc.

Forward Inhibitor Deformations
Nominal and Stiff NBR
RSRM 80 Seconds Burn Time

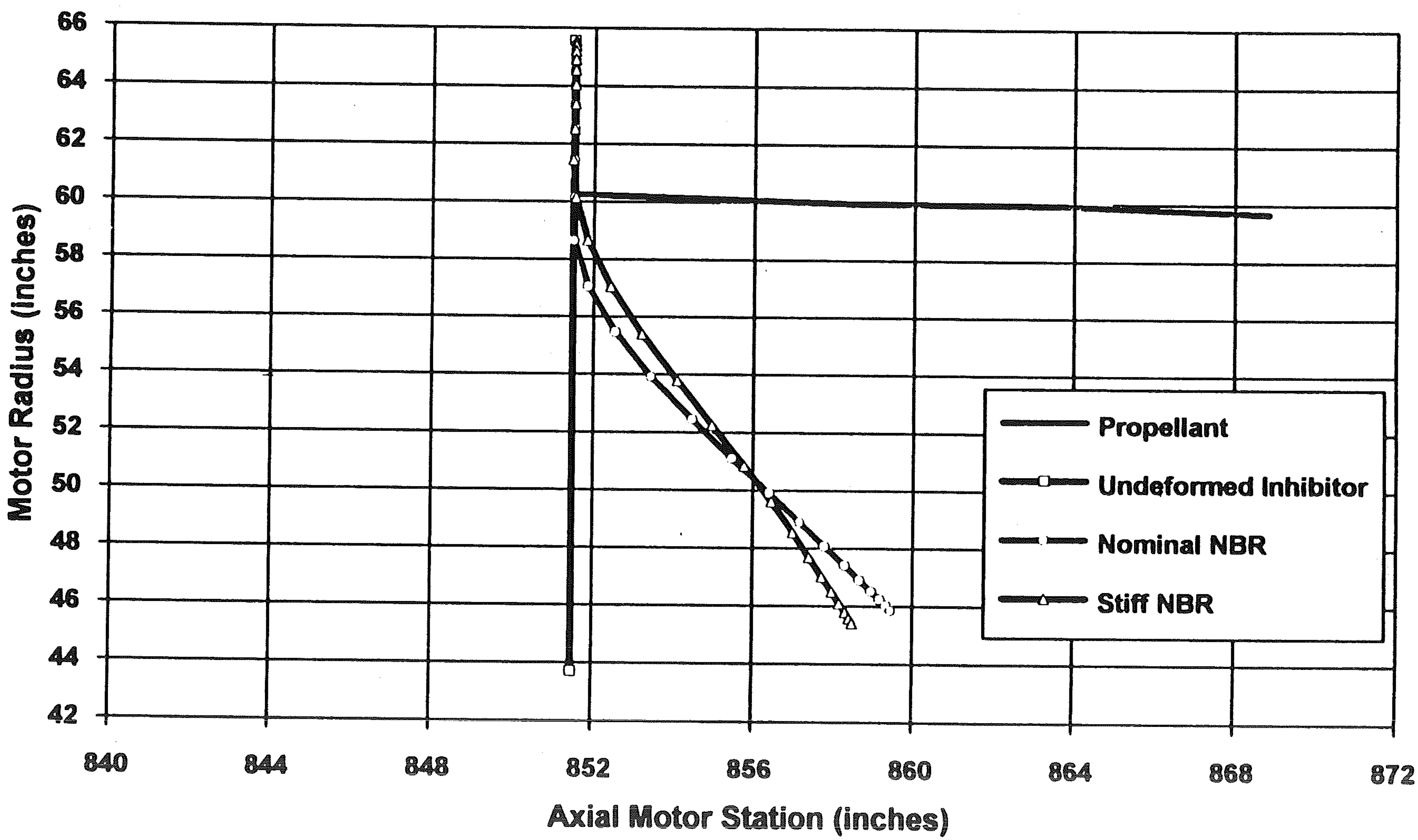

ERC, Inc.

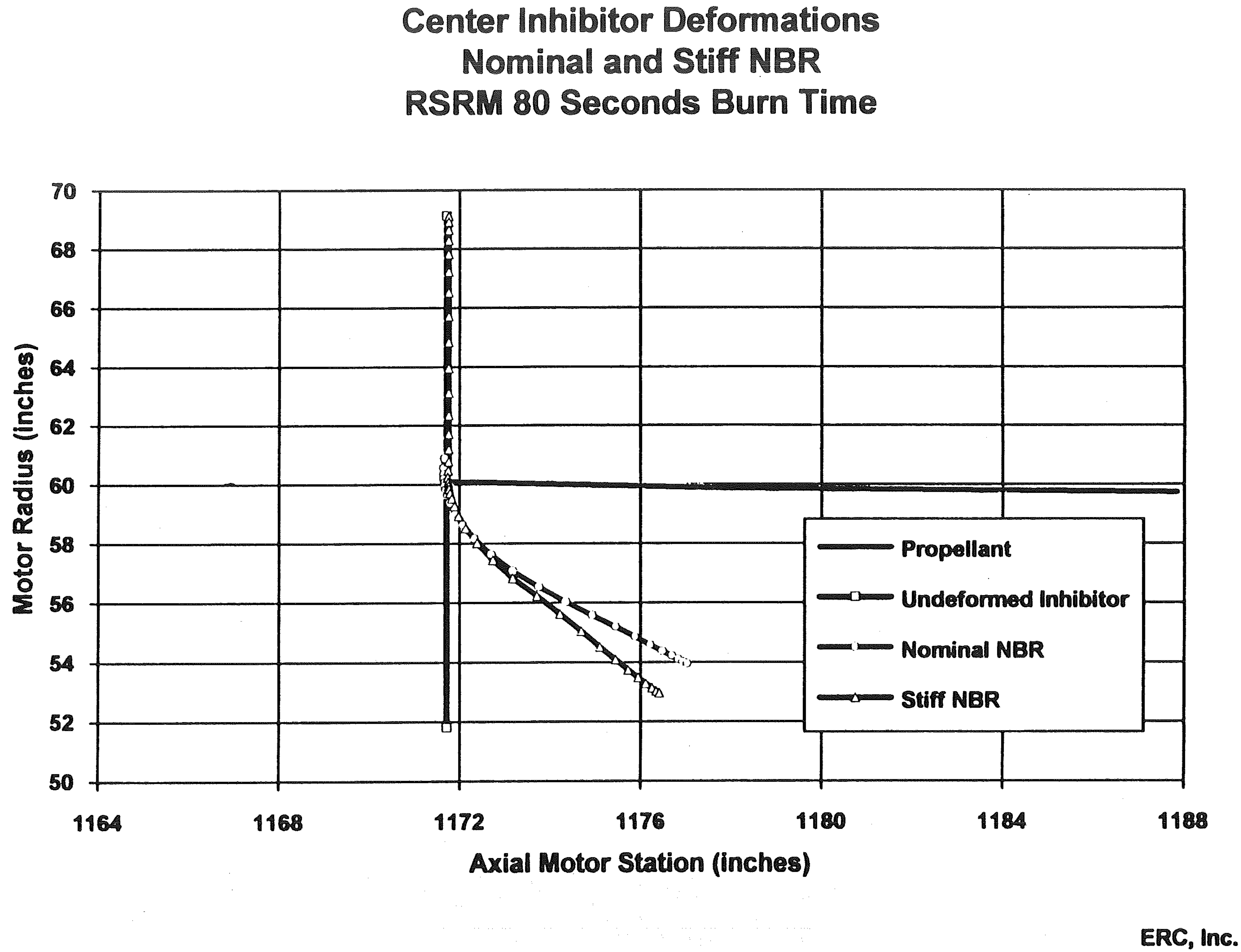
Center Inhibitor Deformations
Nominal and Stiff NBR
RSRM 80 Seconds Burn Time
Motor Radius (inches)
70
68
66
64
62
60
58
56
54
52
50
1164
1168
1172
1176
1180
1184
1188
Axial Motor Station (inches)
Propellant
Undeformed Inhibitor
Nominal NBR
Stiff NBR
ERC, Inc.

Aft Inhibitor Deformations
Nominal and Stiff NBR
RSRM 80 Seconds Burn Time

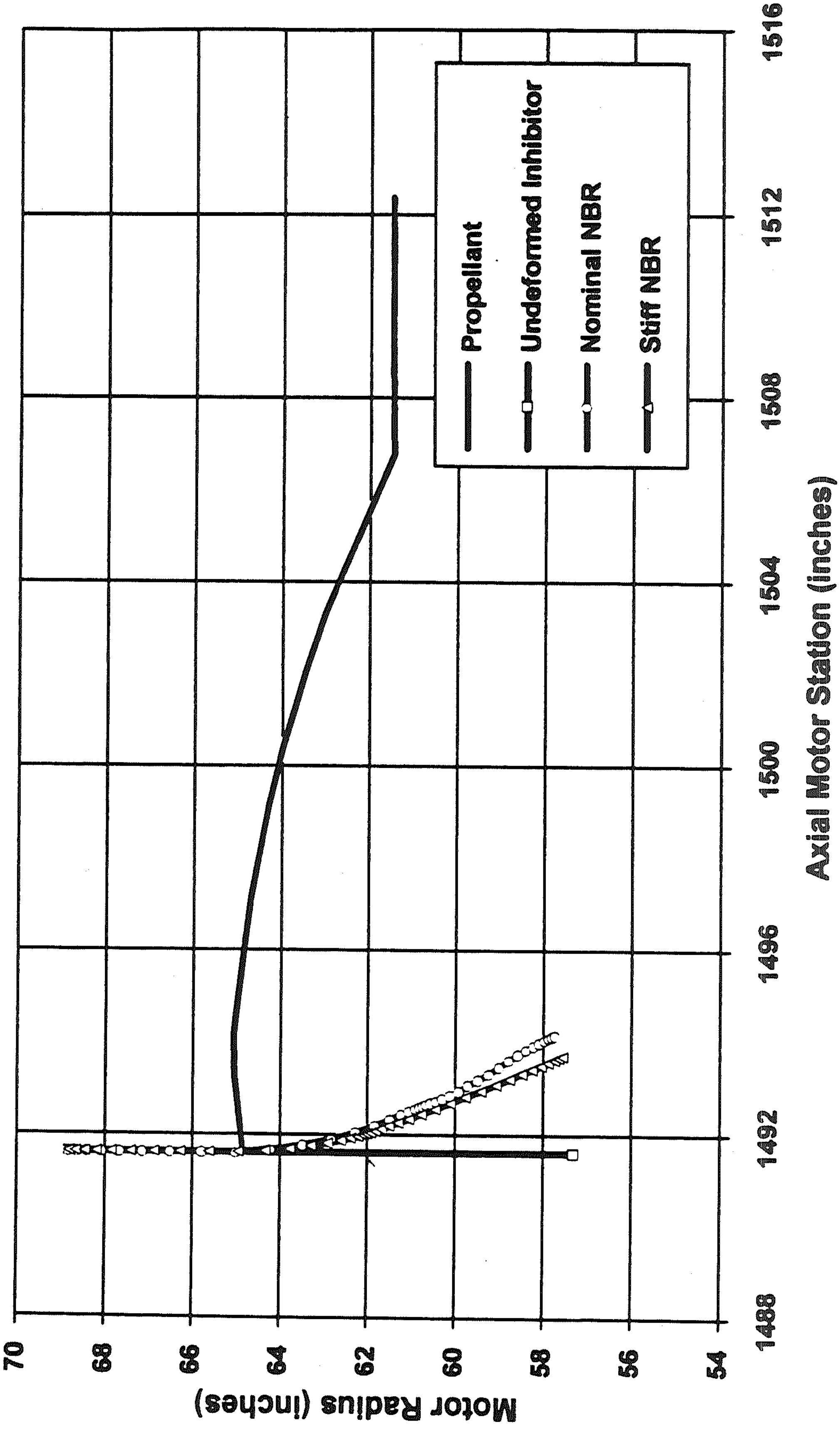

ERC, Inc.

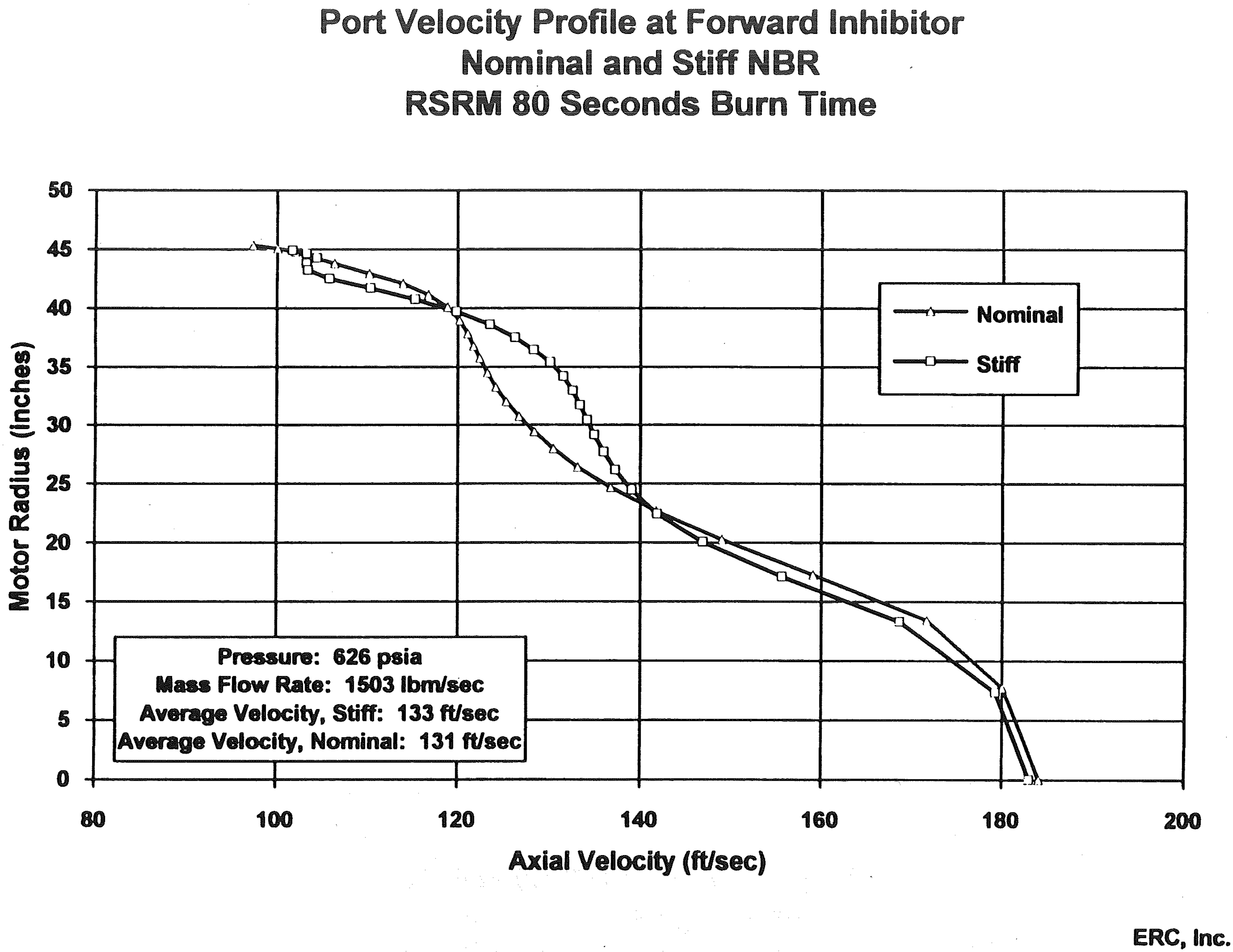

Port Velocity Profile at Forward Inhibitor
Nominal and Stiff NBR
RSRM 80 Seconds Burn Time
Motor Radius (Inches)
50
45
40
35
30
25
20
15
10
5
0
80
100
120
140
160
180
200
Axial Velocity (ft/sec)
Nominal
Stiff
Pressure: 626 psia
Mass Flow Rate: 1503 lbm/sec
Average Velocity, Stiff: 133 ft/sec
Average Velocity, Nominal: 131 ft/sec
ERC, Inc.

Port Velocity Profile at Center Inhibitor
Nominal and Stiff NBR
RSRM 80 Seconds Burn Time

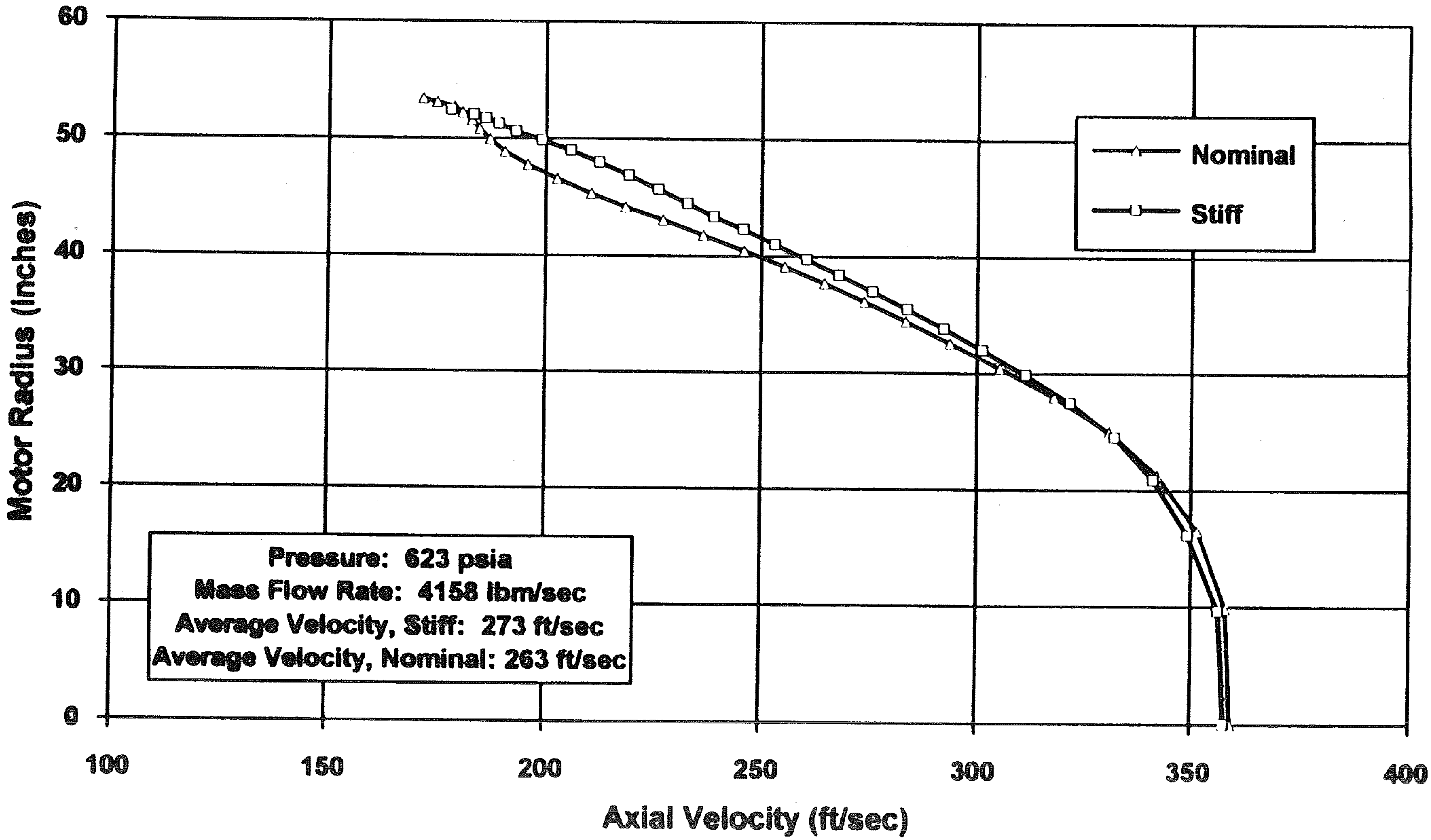

ERC, Inc.

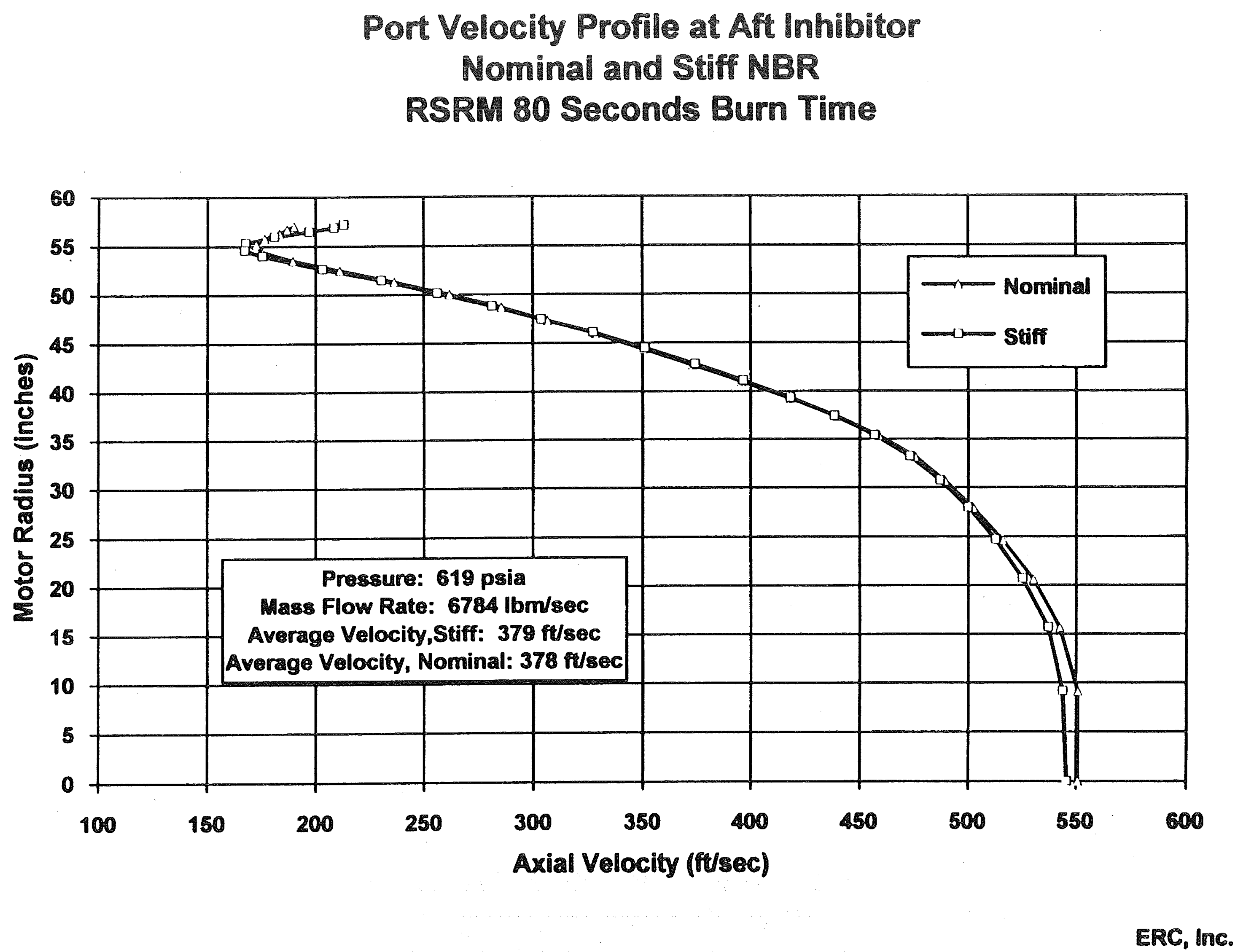
Port Velocity Profile at Aft Inhibitor
Nominal and Stiff NBR
RSRM 80 Seconds Burn Time
Motor Radius (inches)
60
55
50
45
40
35
30
25
20
15
10
5
0
100
150
200
250
300
350
400
450
500
550
600
Axial Velocity (ft/sec)
Nominal
Stiff
Pressure: 619 psia
Mass Flow Rate: 6784 lbm/sec
Average Velocity,Stiff: 379 ft/sec
Average Velocity, Nominal: 378 ft/sec
ERC, Inc.

Comparison of the Motor Port Velocity Profiles Immediately Upstream of Nozzle Nose RSRM 80 Seconds Burn Time

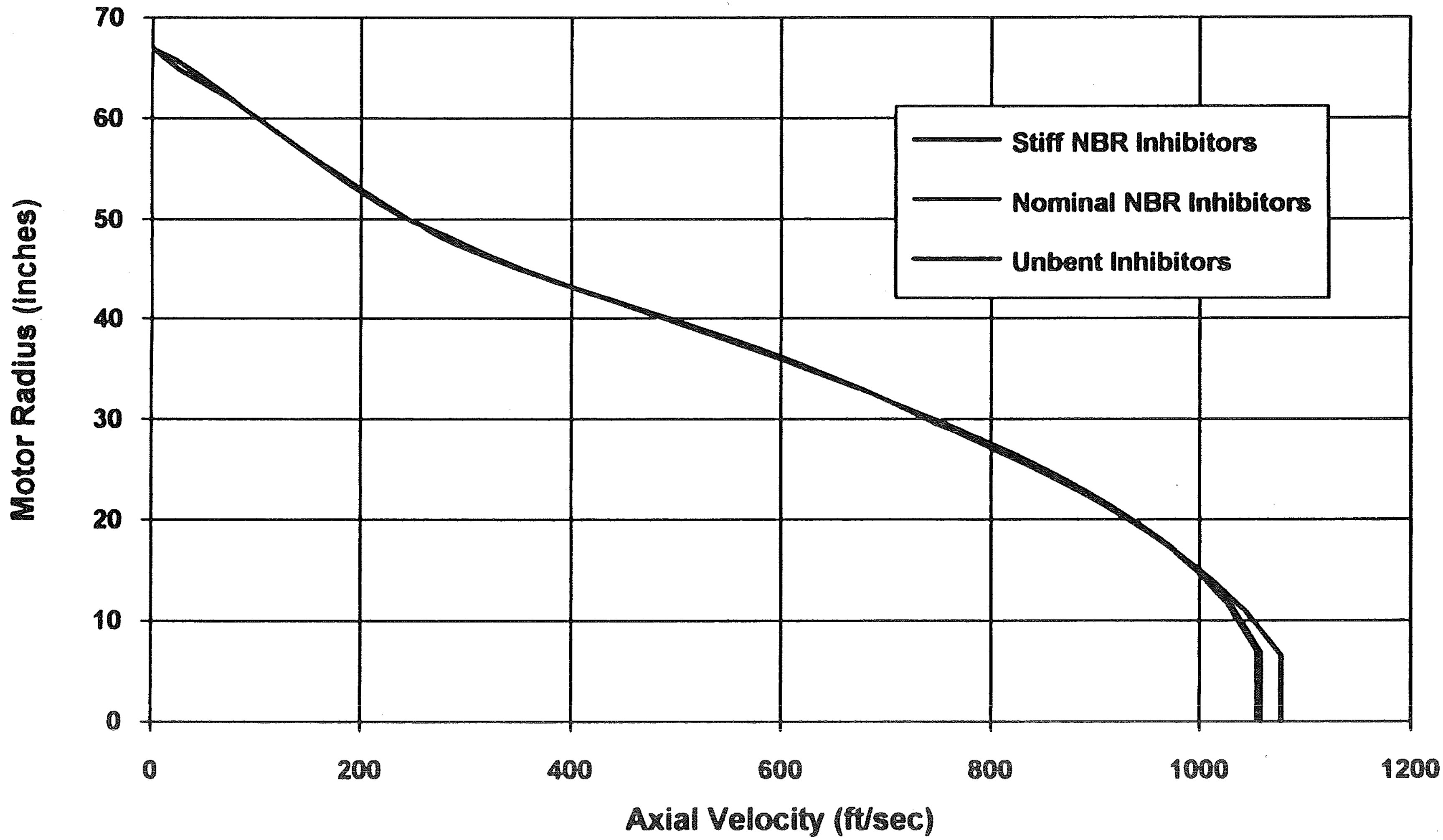

ERC, Inc.

Coupled CFD/FEM Analysis Conclusions

- The coupled CFD/FEM inhibitor structural analysis was successfully iterated to convergence to determined the deformed geometry of inhibitors at the forward, center and aft joints.
- The velocity through the inhibitor hole for the stiff inhibitors is somewhat higher which would increase the hole true frequency and delay tuning with the acoustic mode until a later burn time.
- The velocity profile at the nozzle entrance just upstream of the nose is not affected by the inhibitor stiffness/geometry and thus nozzle internal aerotorque would not be impacted.

ERC, Inc.

Two-Phase CFD Analysis Approach

- Perform two-phase CFD analysis of RSRM port at 80 second burn time using final deformed inhibitor geometries for both nominal and stiff inhibitors.
- Calculate slag captured on both nominal and stiff inhibitors at all three field joints.
- Perform trajectory analysis for slag debris shed from inhibitor tips for all above cases to determine whether it passes through nozzle or accumulates underneath nozzle nose.

RSRM Inhibitor Slag Accumulation
Nominal and Stiff NBR Inhibitors
80 Second Burn Time

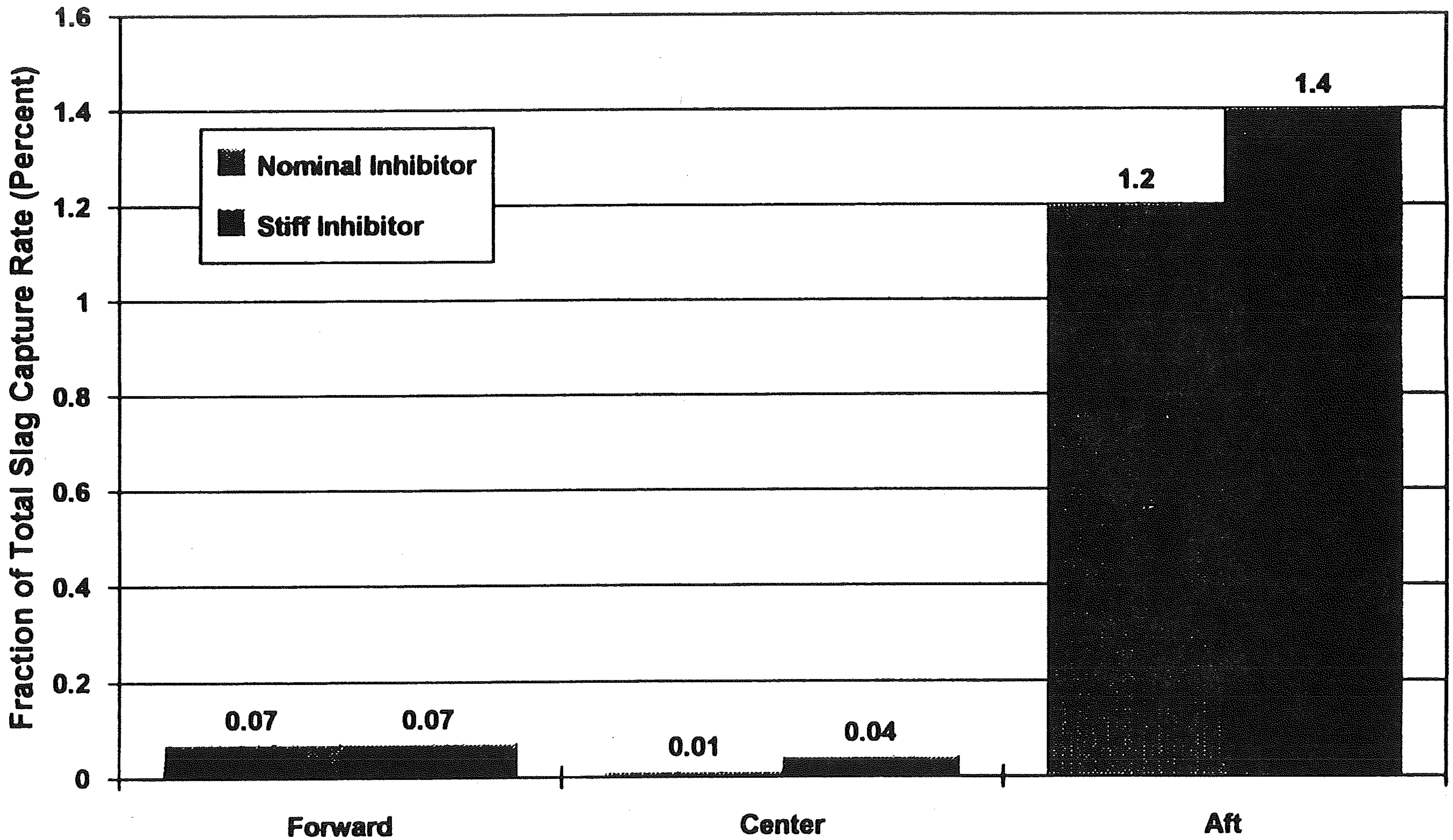

ERC, Inc.

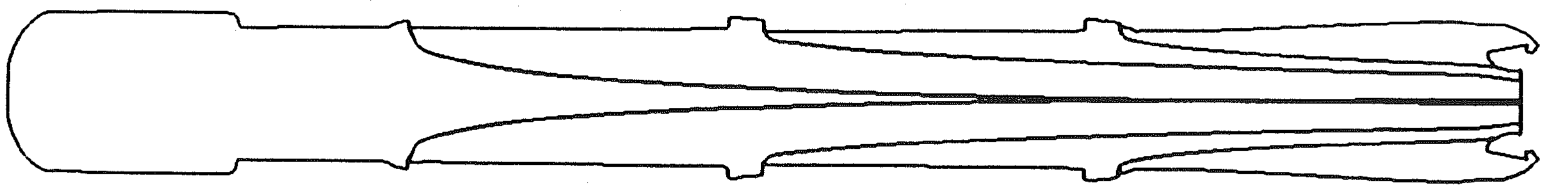

Slag Debris Trajectories

RSRM 80 Second Stiff NBR Inhibitor

Debris Diameter: 0.2 Inches

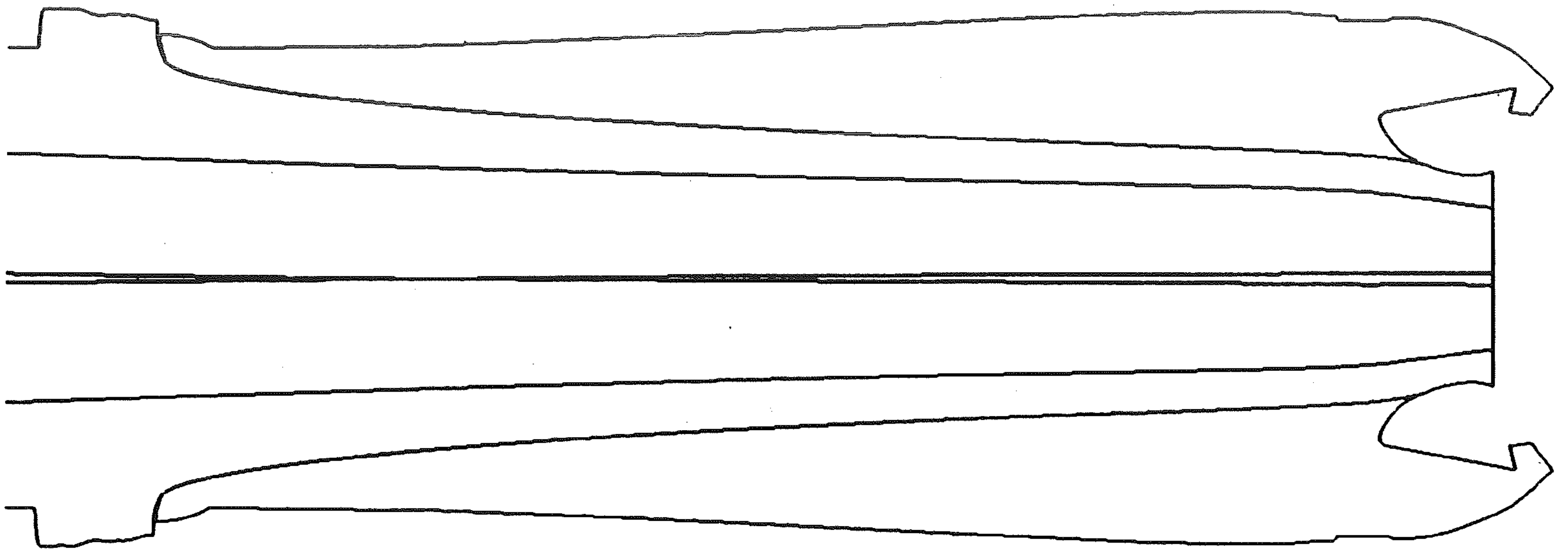

Slag Debris Trajectories

RSRM 80 Second Stiff NBR Inhibitor

Debris Diameter: 0.2 Inches

Slag Debris Trajectory Results
Nominal and Stiff NBR Inhibitors

Release Location	Debris Diameter			
	0.2 inches	0.4 inches	0.8 inches	1.6 inches
		Nominal NBR		
Forward	Exits Nozzle	Exits Nozzle	Exits Nozzle	Exits Nozzle
Center	Exits Nozzle	Exits Nozzle	Exits Nozzle	Exits Nozzle
Aft	Exits Nozzle	Exits Nozzle	Exits Nozzle	Nozzle Nose
		Stiff NBR		
Forward	Exits Nozzle	Exits Nozzle	Exits Nozzle	Exits Nozzle
Center	Exits Nozzle	Exits Nozzle	Exits Nozzle	Exits Nozzle
Aft	Nozzle Nose	Nozzle Nose	Nozzle Nose	Nozzle Nose

ERC, Inc.

1226

Two-Phase CFD Analysis Conclusions

- The rate of slag accumulation for both the nominal and stiff inhibitors at all joints is a very small percentage of the total motor slag accumulation rate.
- The rate of slag accumulation on the center inhibitor is approximately four times greater for the stiff NBR compared to the nominal NBR.
- Slag debris shed from the nominal inhibitors at all three joints exits the nozzle throat plane.
- Slag debris shed from the stiff inhibitors at the forward and center joints exits the nozzle throat plane. Slag from the aft joint stiff inhibitor impacts the nozzle entrance ramp.
- No excess slag collected on the stiff inhibitors is transported underneath the nozzle nose to add to the normal slag pool.

ERC, Inc.

CFD Flow Analysis and Code Validation for the MSFC Eight-Percent ASRM Cold Flow Model Part II

Thirteenth Workshop for CFD Applications in Rocket Propulsion
April 25-27, 1995

Jeff Lin

Ed Reske

NASA, Marshall Space Flight Center
Computational Fluid Dynamics Branch

OMIT TO
P 1245

CFD Flow Analysis and Code Validation for the MSFC Eight-Percent ASRM Cold Flow Model

Overview

- Introduction
  - purpose for code benchmarks
  - experimental results from the MSFC 8% ASRM Cold Flow Model
- Codes under Consideration
  - CELMINT
  - GASP
  - FDNS
- Physical and Geometrical Parameters
- Grid Issues
- Results
  - comparison between CFD and experiment
  - flow visualization
- Summary and Future Plans

Introduction

- Why a Code Benchmark is needed

  - To assure validity of CFD models used to predict

    -- motor performance
    -- internal nozzle aerodynamics (loads and hinge moments)
    -- heat transfer to the nozzle, insulation, and joints
    -- slag accumulation (and potential pressure spikes)
    -- chamber pressure oscillations

  - Potential problem areas

    -- flow field anomalies attributed to grid irregularities
      --- complex mappings
      --- skewness
      --- kinks
      --- zonal interfaces

    -- appropriate methodology?

CFD Flow Analysis and Code Validation for the MSFC Eight-Percent ASRM Cold Flow Model

Computational Fluid Dynamics Branch
Fluid Dynamics Division
Structures and Dynamics Laboratory
George C. Marshall Space Flight Center

- Experimental Results from the MSFC 8% ASRM Cold Flow Model
  - static wall pressures
  - velocity rakes
  - gimbal angles of 0, 4, and 8 degrees

Codes Under Consideration

- CELMINT (SRA)
  -benchmark complete for 0 and 8 degrees
- GASP (Aerosoft)
  -benchmark complete for 0 degrees
  -benchmark in progress for 4 and 8 degrees
- FDNS (MSFC and ESI)
  -benchmark complete for 0 degrees
  -benchmark in proress for 4 and 8 degrees

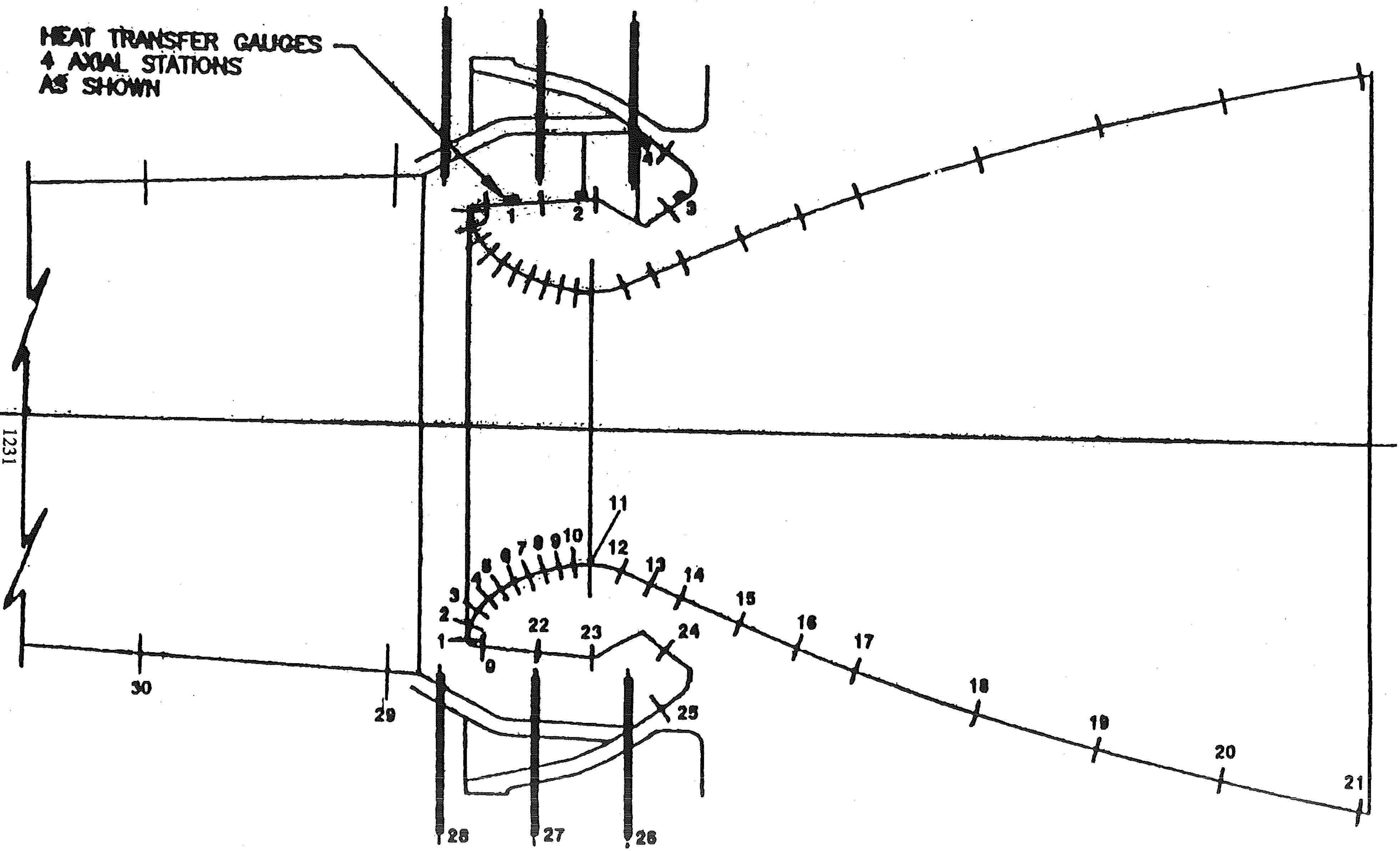

Note: Station 31 is the Gimbal Ring Vent Hole

ASRM Air Flow Model Inlet Velocity Profiles - Redesigned Velocity Profile Plate

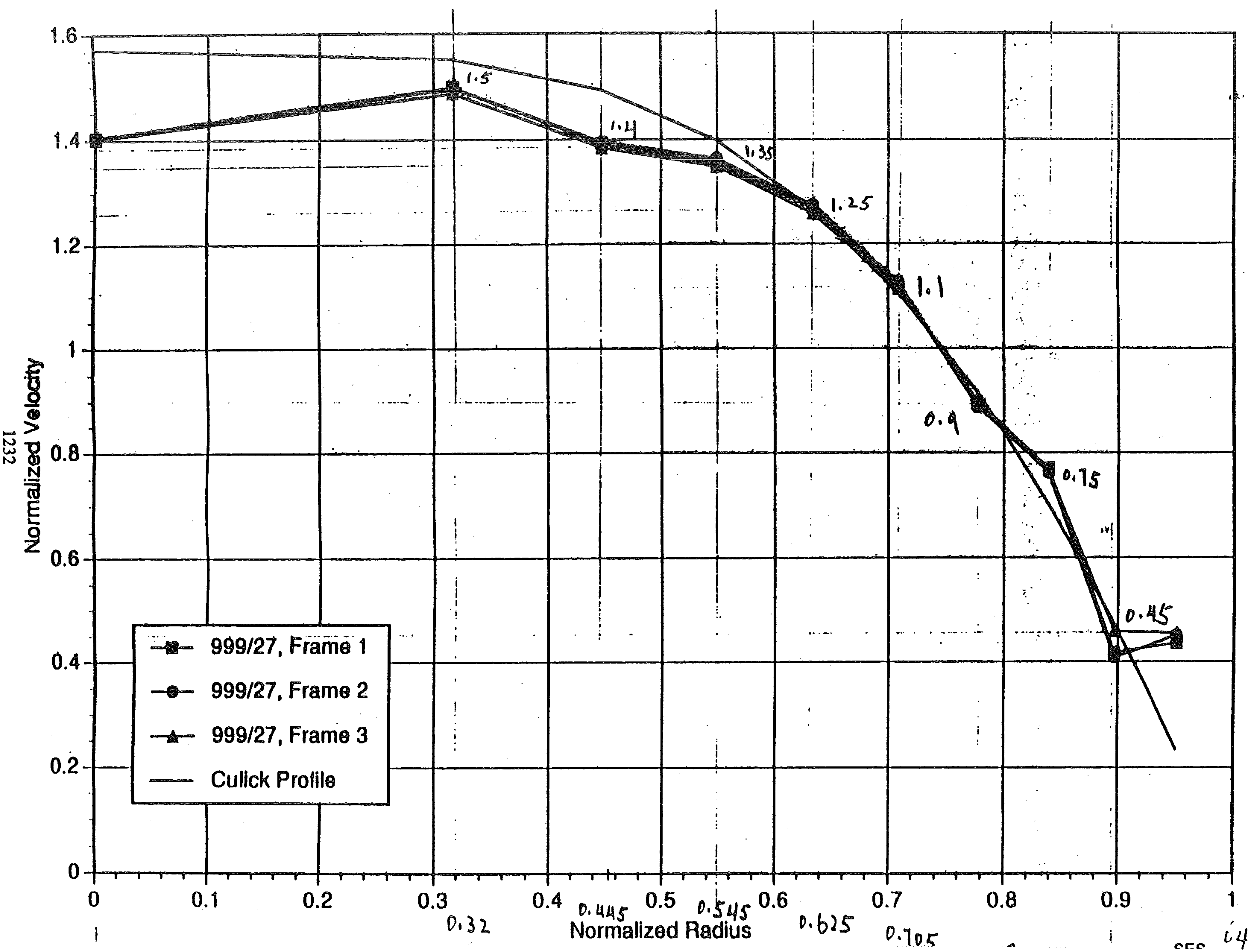

ASRM Aft Section/Nozzle Model

Boundary Conditions at the Probe Tip Axial Location

5-13-93

<u>1-D Conditions</u>

Throat Diameter	4.36 inches
T_o	530° R
P_o	572 psia
M_{wt}	28.97
Mach Number	.2125
Static Pressure	554.28 psia
Static Temperature	525.25°R
Mass Flow Rate	197.285 lbm/sec
Local Velocity	238.777 ft/s
Local Sonic Velocity	1123.4 ft/s
Local Density	2.8487 lbm/ft^3

Reynolds Number based on above conditions and viscosity equal to 1.8456 x 10^{-5} pa-s

R = 31.6 x 10^6

GEOMETRY

ASRM Cold Flow Model: 8/19/93

60x85	GRID 1
101x33	GRID 2
101x33	GRID 3

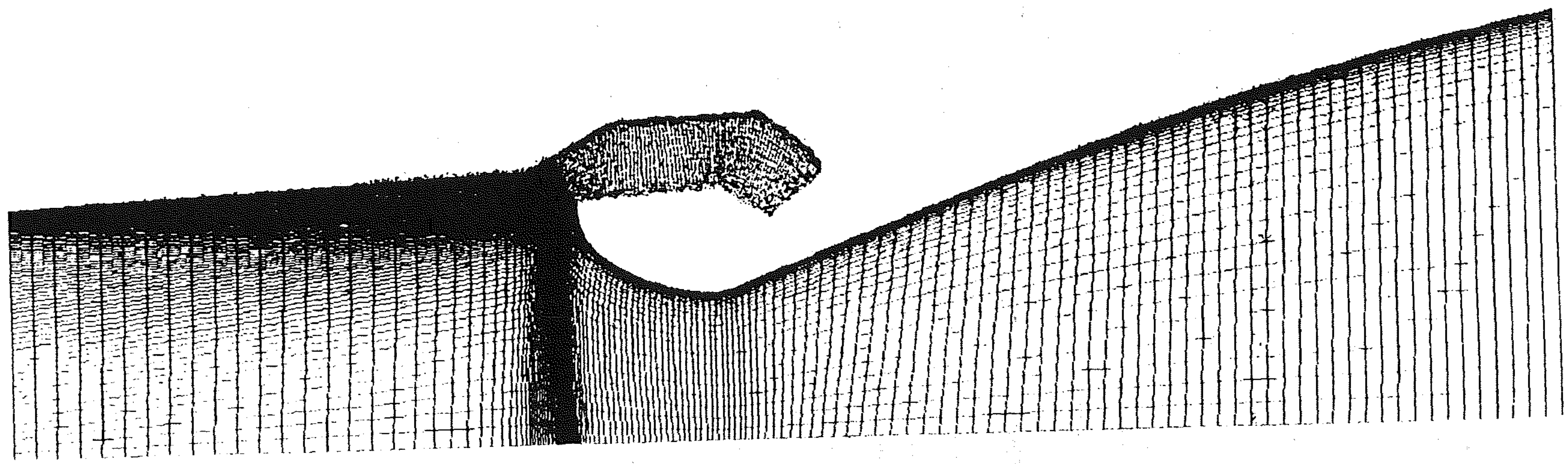

gridb.1.img

GEOMETRY

Grid for Cold Flow Benchmark

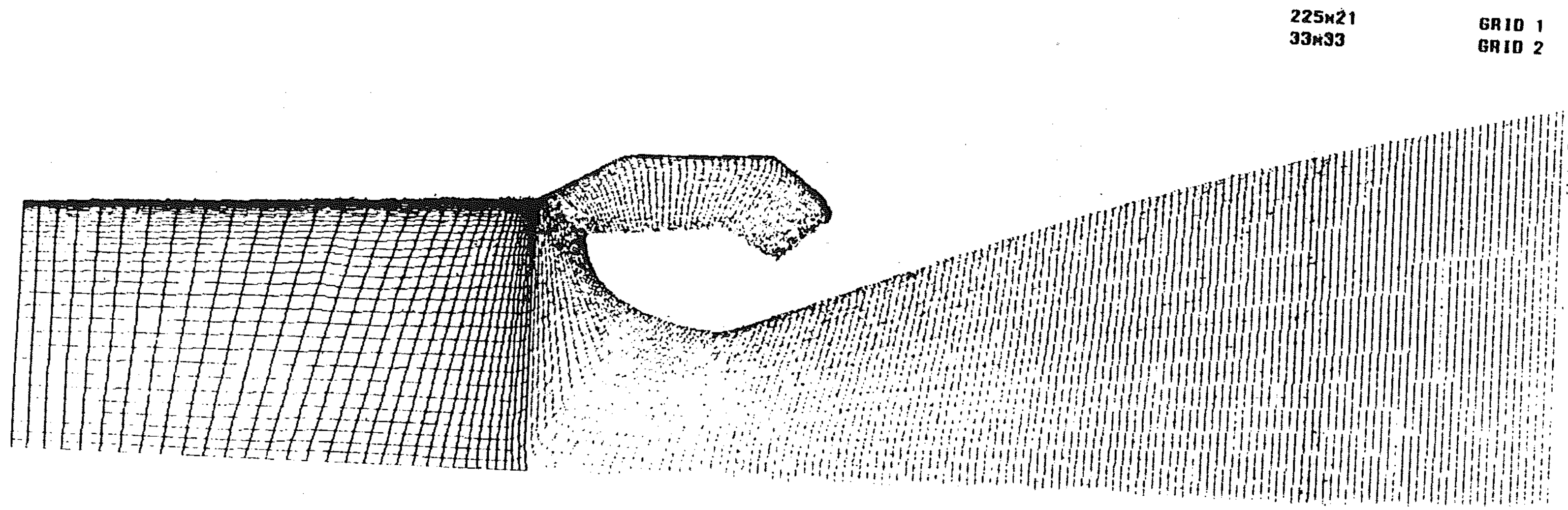

flow0.1.img

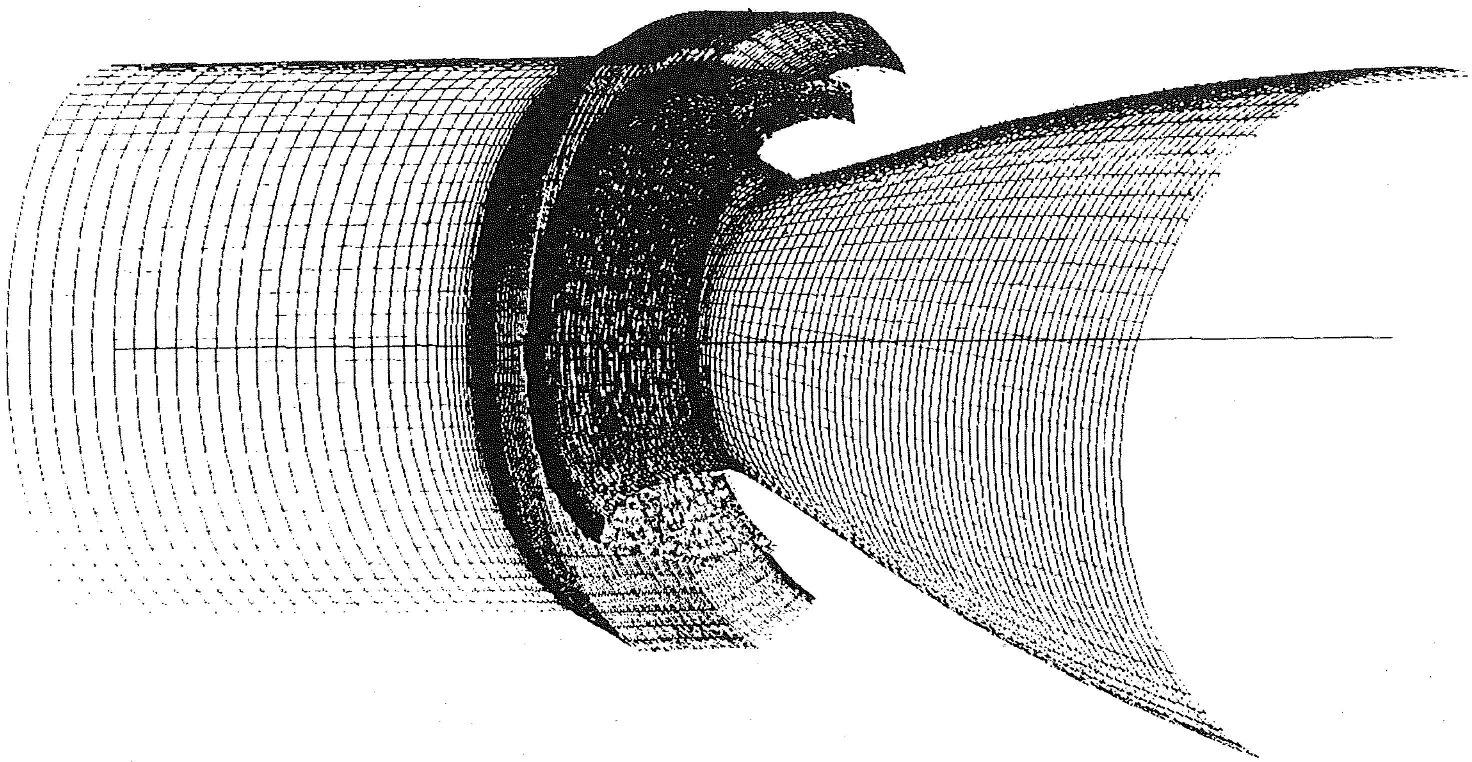
GEOMETRY
8% ASRM Cold Flow Model
with 8-degree gimbal angle
85x37x160
GRID
smoothd.1.img

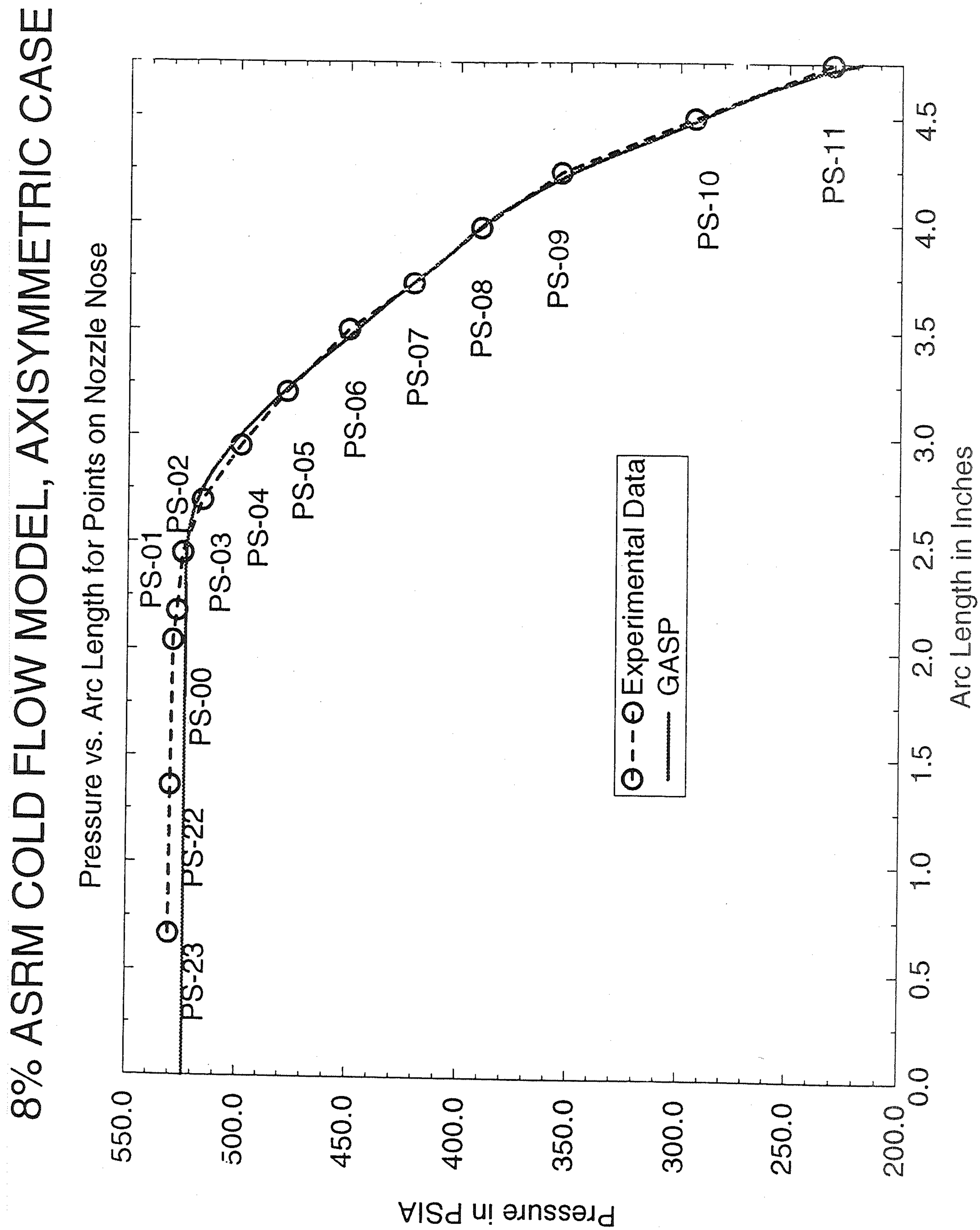

8% ASRM COLD FLOW MODEL, AXISYMMETRIC CASE
Pressure vs. Arc Length for Points on Nozzle Nose
Pressure in PSIA
Arc Length in Inches
550.0
500.0
450.0
400.0
350.0
300.0
250.0
200.0
0.0
0.5
1.0
1.5
2.0
2.5
3.0
3.5
4.0
4.5
PS-23
PS-22
PS-00
PS-01
PS-02
PS-03
PS-04
PS-05
PS-06
PS-07
PS-08
PS-09
PS-10
PS-11
Experimental Data
GASP

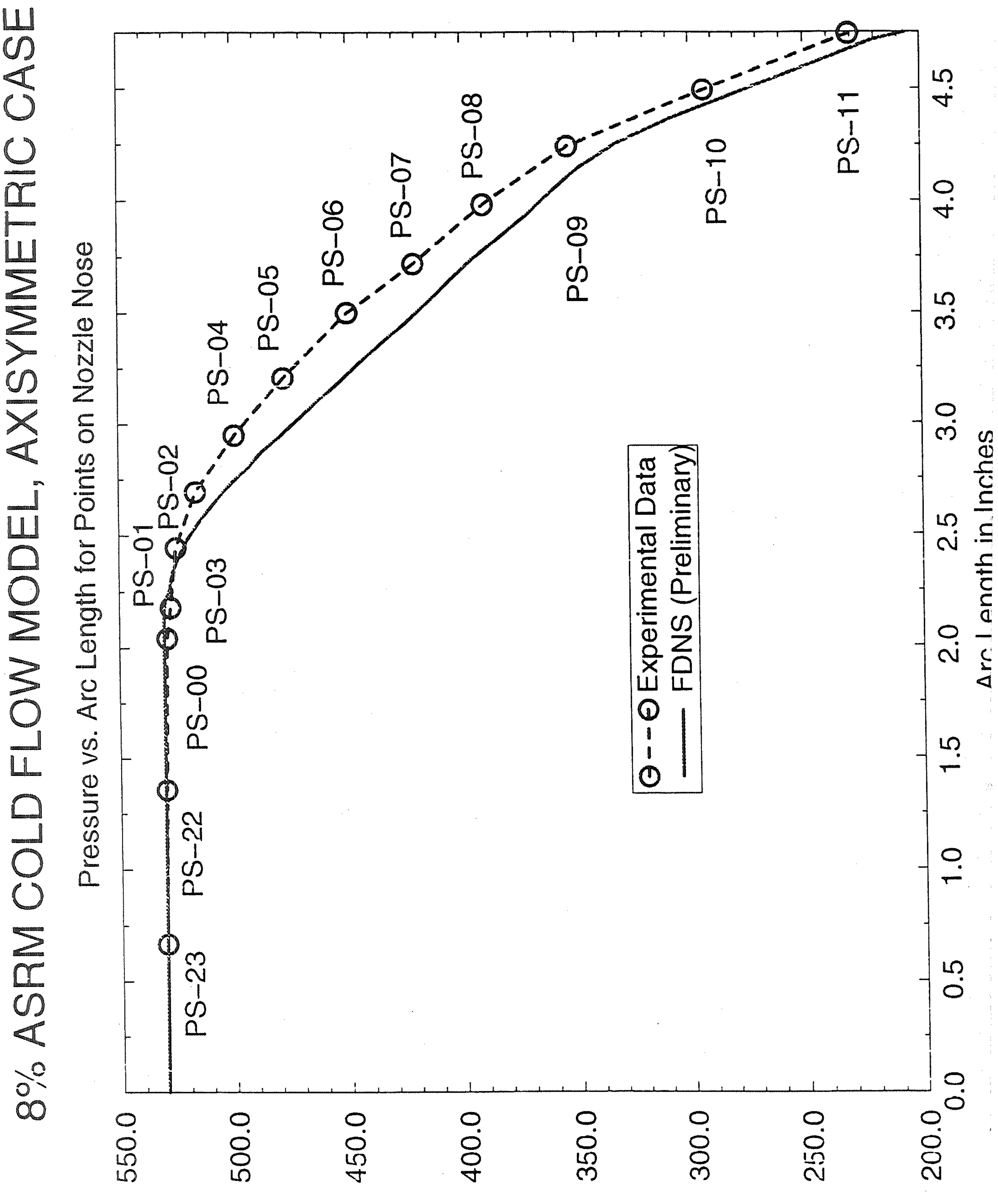
8% ASRM COLD FLOW MODEL, AXISYMMETRIC CASE
Pressure vs. Arc Length for Points on Nozzle Nose
Pressure in PSIA
Arc Length in Inches
550.0
500.0
450.0
400.0
350.0
300.0
250.0
200.0
0.0
0.5
1.0
1.5
2.0
2.5
3.0
3.5
4.0
4.5
PS–23
PS–22
PS–00
PS–01
PS–02
PS–03
PS–04
PS–05
PS–06
PS–07
PS–08
PS–09
PS–10
PS–11
Experimental Data
FDNS (Preliminary)

8% ASRM COLD FLOW MODEL, AXISYMMETRIC CASE

Pressure vs. Arc Length in Exit Cone from Throat to Exit Plane

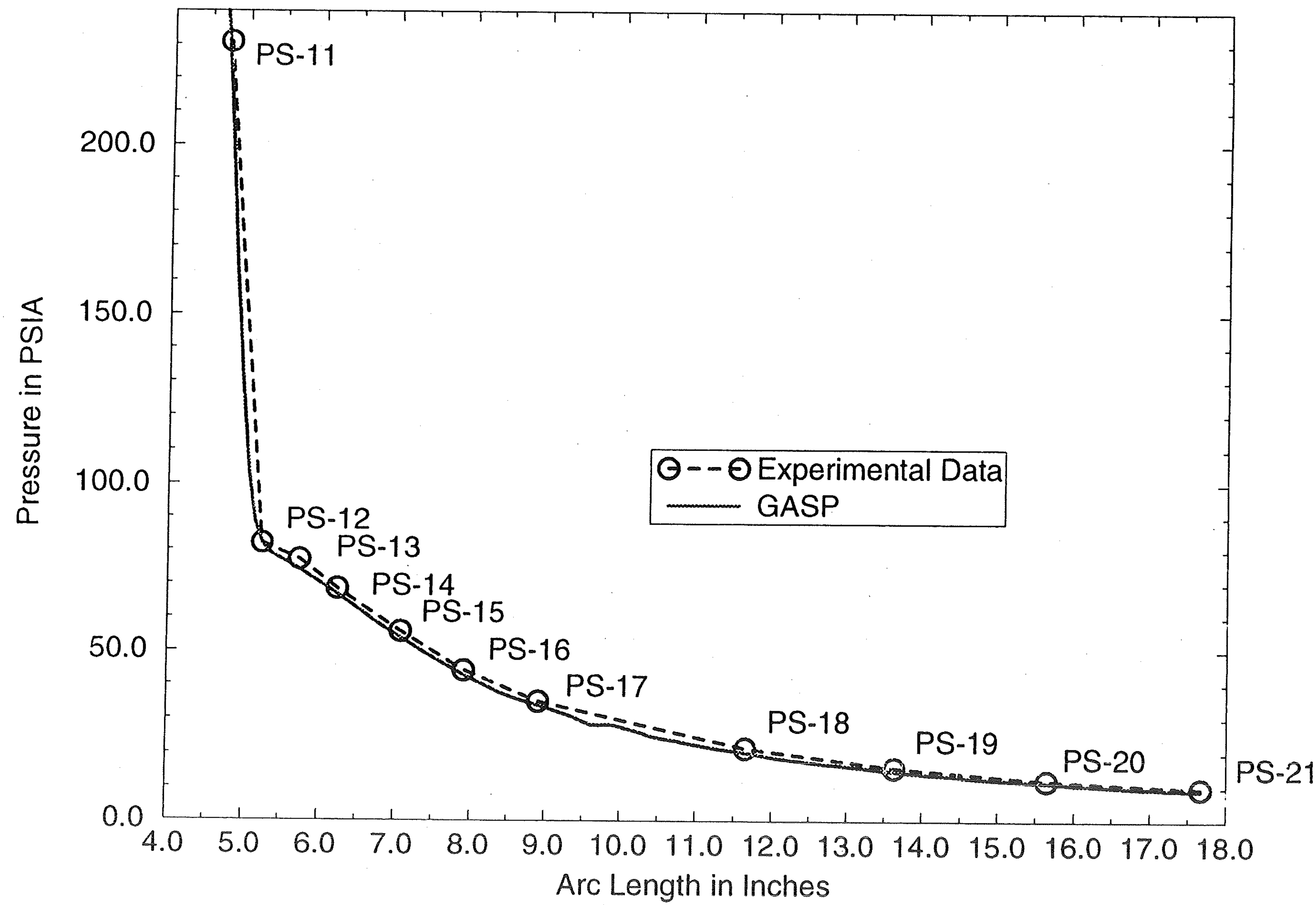

8% ASRM COLD FLOW MODEL, AXISYMMETRIC CASE

Pressure vs. Arc Length in Exit Cone from Throat to Exit Plane

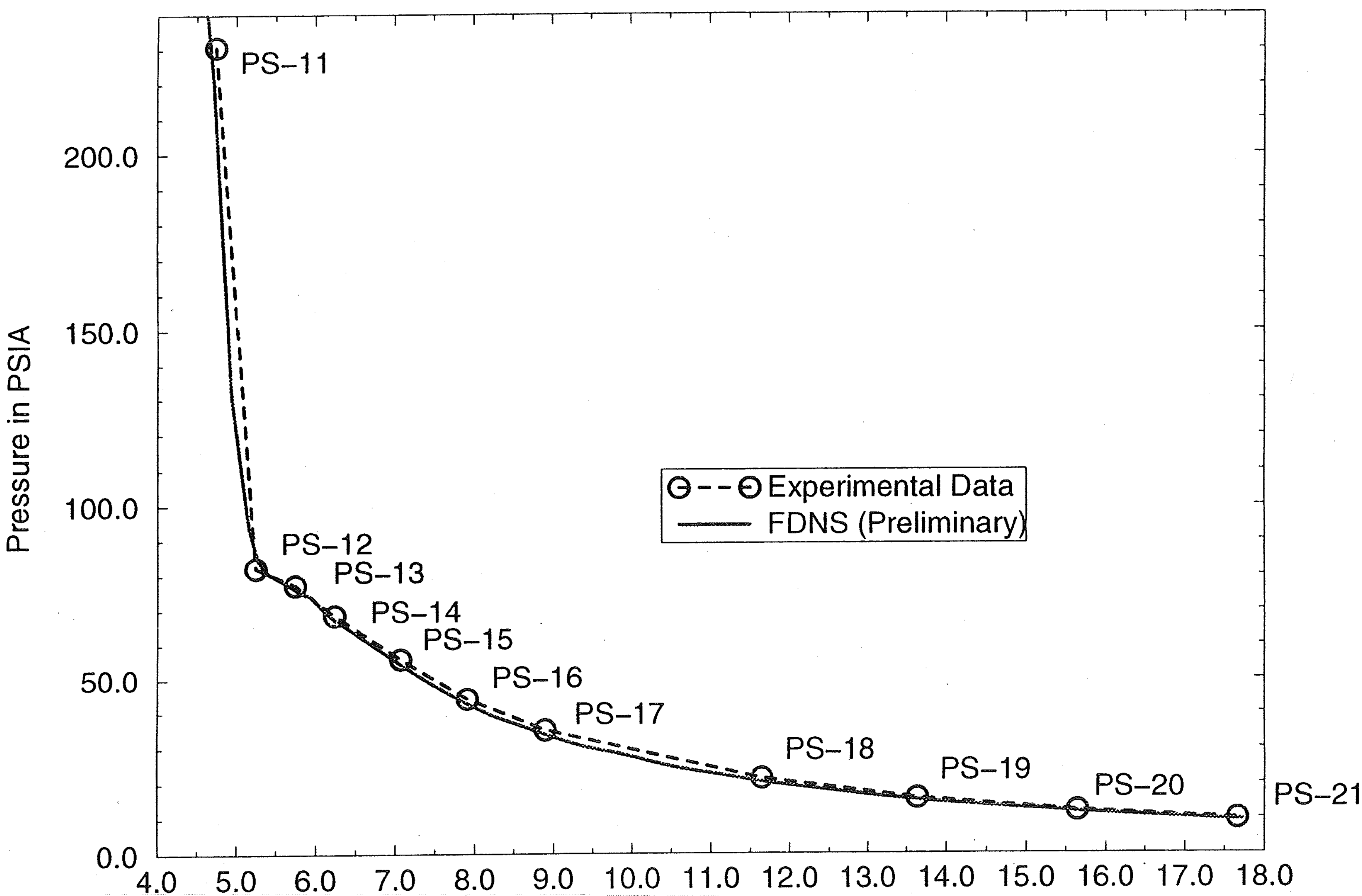

NORMALIZED PRESSURE

GASP Solution

Pressure in PSIA

CONTOUR LEVELS
12.5
25.0
37.5
50.0
62.5
75.0
87.5
100.0
112.5
125.0
137.5
150.0
162.5
175.0
187.5
200.0
212.5
225.0
237.5
250.0

1.000	MACH
0.00 DEG	ALPHA
1.0	Re
1.0	TIME
225x21	GRID 1
33x33	GRID 2

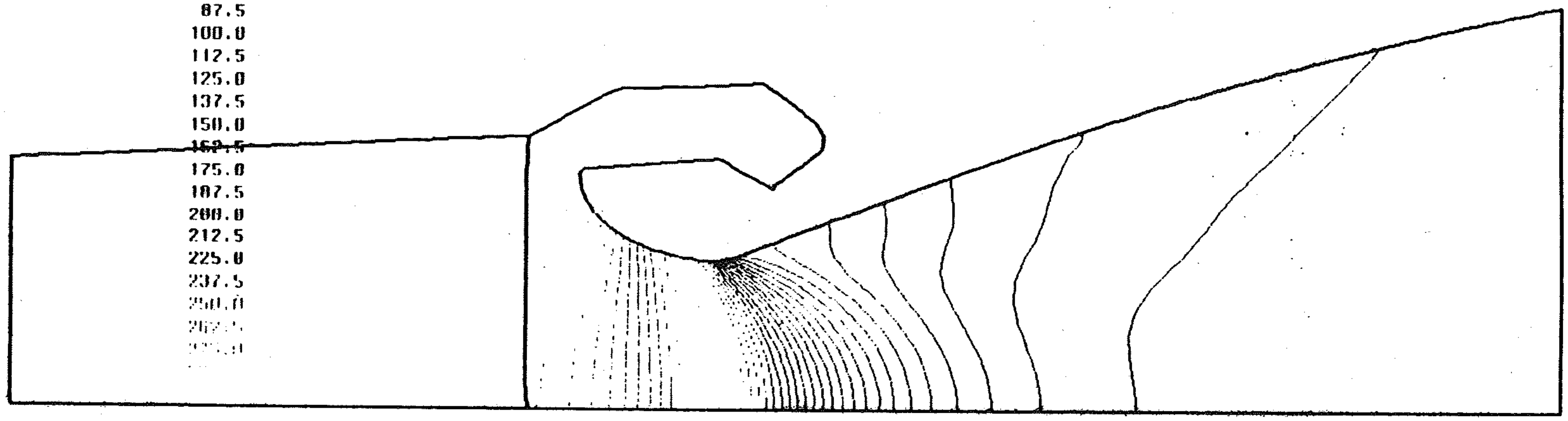

1241

flow0.2.img

U VELOCITY

GASP Solution

Velocities in ft./sec.

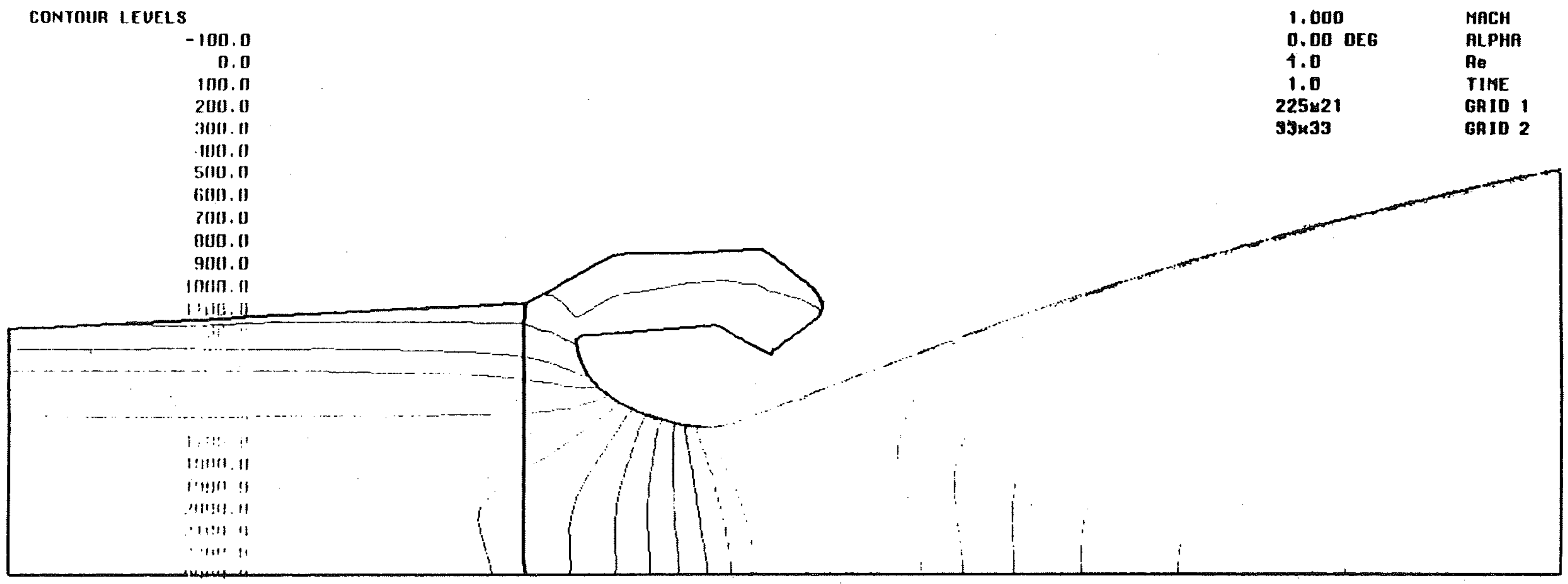

flow0.3.img

V VELOCITY

GASP Solution

Velocities in ft./sec.

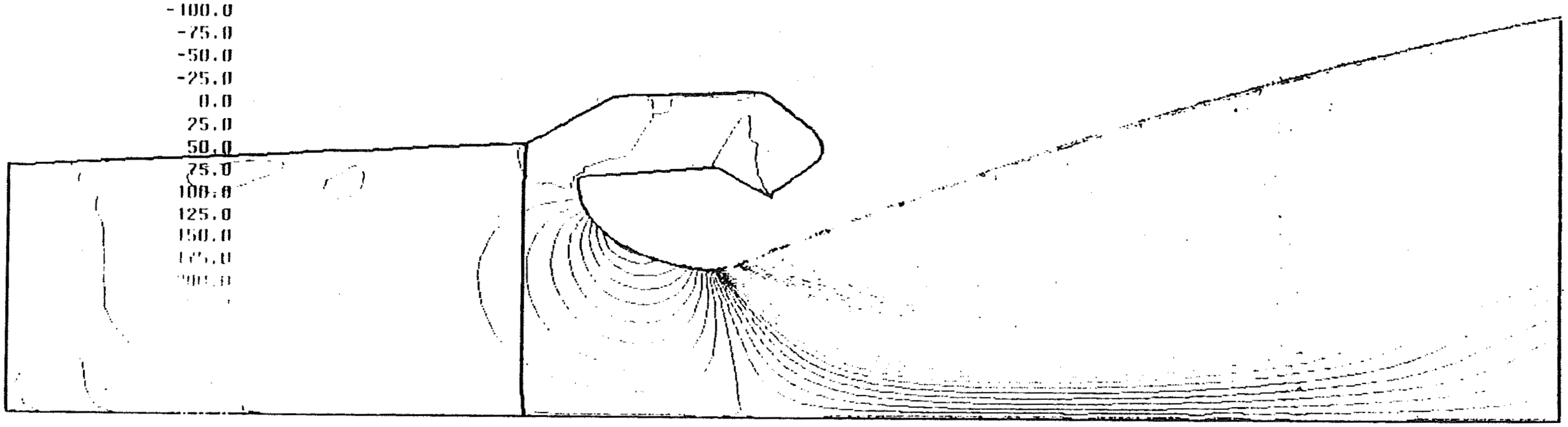

flowD.4.img

Summary and Future Plans

- Good agreement is attained for GASP at 0 degrees.
  - The 4- and 8-degree cases are in progress.
- The case for FDNS at 0 degrees will be readdressed.
  - The 4- and 8-degree cases will be attempted once the discrepancy is resolved.
- The final results from these benchmarks will be submitted for future publication.

522-34
57397
132119
48p

Application of Two-Phase CFD to the Design and Analysis of a Subscale Motor Experiment to Evaluate Propellant Slag Production

R. Harold Whitesides and Richard A. Dill
ERC, Incorporated, Huntsville, AL 35816

Abstract

The RSRM Pressure Perturbation Investigation Team concluded that the cause of recent pressure spikes during both static and flight motor burns was the expulsion of molten aluminum oxide slag from a pool which collects in the aft end of the motor around the submerged nozzle nose during the last half of motor operation. It is suspected that some motors produce more slag than others due to differences in aluminum oxide agglomerate particle sizes which may relate to subtle differences in propellant ingredient characteristics such as particle size distributions, contaminants, or processing variations.

In order to determine the effect of suspect propellant ingredient characteristics on the propensity for slag production in a real motor environment, a subscale motor experiment was designed to accomplish this objective. An existing 5 inch ballistic test motor was selected as the basic test vehicle due to low cost and quick turn around times. The standard converging/diverging nozzle was replaced with a submerged nozzle nose design to provide a positive trap for the slag which would increase both the quantity and repeatability of measured slag weights. CFD was used to assess a variety of submerged nose configurations to identify the design which possessed the best capability to reliably collect slag. CFD was also used to assure that the final selected nozzle design would result in flow field characteristics such as dividing streamline location, nose attach point, and separated flow structure which would have similitude with the RSRM submerged nozzle nose flow field. It was also decided to spin the 5 inch motor about its longitudinal axis to further enhance slag collection quantities. Again, CFD was used to select an appropriate spin rate along with other considerations, including the avoidance of burn rate enhancement from radial acceleration effects.

The CFD analyses were performed with the CELMINT code which is a two-phase Navier-Stokes coded employing an Eulerian/Lagrangian scheme, a low Reynolds number κ-ε turbulence model modified for wall injection, and both surface and distributed particle combustion models which include particle agglomeration and break-up. Aluminum oxide particle distributions were measured with RSRM propellant in a combustion bomb with particle quench capability. Predictions for slag weights and slag distribution patterns were compared with slag weight data from defined zones in the motor and nozzle. Various parameters were investigated to reconcile differences between CFD predictions and data. General comparisons were acceptable considering combustion bomb data on particle sizes was not available for each propellant sample. Confidence in using this methodology in the RSRM was enhanced by this successful subscale experiment.

Application of Two-Phase CFD to the Design and Analysis of a Subscale Motor Experiment to Evaluate Propellant Slag Production

R. Harold Whitesides
Richard A. Dill
ERC, Incorporated
Huntsville, Alabama

Thirteenth Workshop for CFD Applications in Rocket Propulsion
NASA Marshall Space Flight Center
Huntsville, Alabama
April 25-27, 1995

Background

- Flight and static test data for the Space Shuttle Reusable Solid Rocket Motors reveals roughness and small spikes in the pressure trace for some motors during the 65-75 second time period.

- An extensive investigation has determined that periodic expulsion of aluminum oxide slag is the cause of pressure perturbations.

- Excessive slag production by some motors is suspected as making these motors more susceptible to slag expulsion.

- Excessive slag production is related to propellant ingredient characteristics including but not limited to aluminum and ammonium perchlorate particle size distributions.

- A low cost, quick turn-around experimental method was needed to evaluate effects of subtle changes in propellant ingredient characteristics on the propensity for slag production.

ERC, Inc.

Experimental Program Objective and Approach

Objective:

Develop and employ a subscale rocket test motor capable of measuring relative slag production of propellants with subtle changes in ingredient characteristics.

Approach:

- Use an existing Thiokol 5-inch diameter ballistic test motor and static test spin stand.
- Modify existing converging/diverging nozzle entrance geometry by incorporating submerged nose to enhance slag capture and retention.
- Select motor operating pressure to match full scale motor pressure. Select spin rate to enhance slag capture but avoid propellant burn rate augmentation.
- Use CFD to determine overall viability of experiment, to aid in design of motor components, to support selection of test conditions, and to analyze test results.

ERC, Inc.

Specific CFD Analysis Tasks

- Evaluate candidate nozzle entrance designs for slag capturing characteristics.
- Select submerged nose nozzle geometry that qualitatively simulates the primary flow pattern and features relative to nozzle nose attachment and recirculation pattern in the RSRM.
- Determine viability of experiment design before hardware manufacture by evaluating sensitivity of slag capture weights to small changes in aluminum oxide particle size distribution.
- Determine effect of spin rate on slag capture weights to support final selection of test spin rate.
- Perform post-test analysis of data including parametric studies as required to validate and calibrate two-phase CFD model.
- Use analysis results to upgrade two-phase CFD model for RSRM slag predictions.

ERC, Inc.

FIVE INCH SPIN MOTOR ASSEMBLY

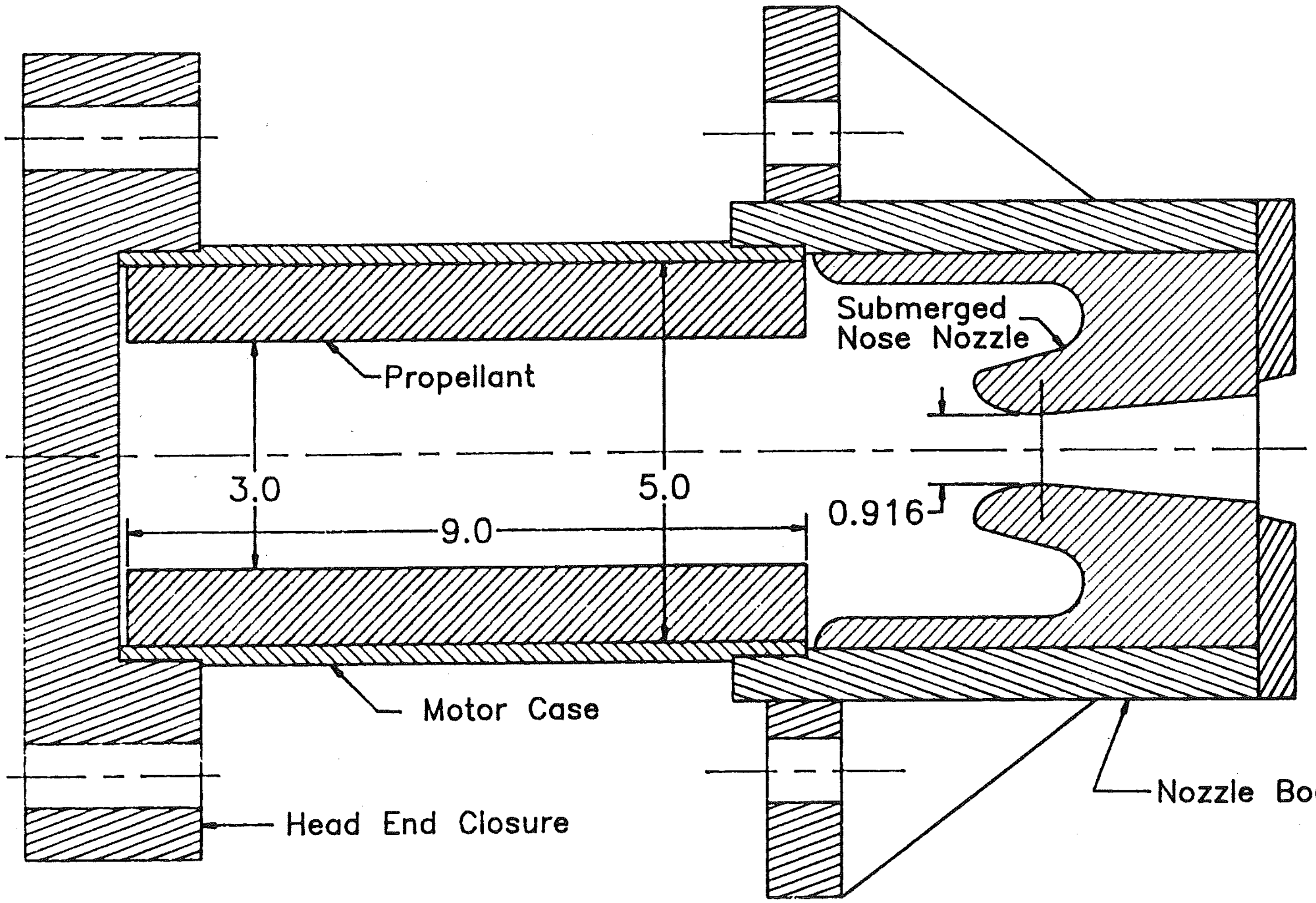

ERC, Inc.

FIVE INCH SPIN MOTOR NOZZLE
SLAG ZONES

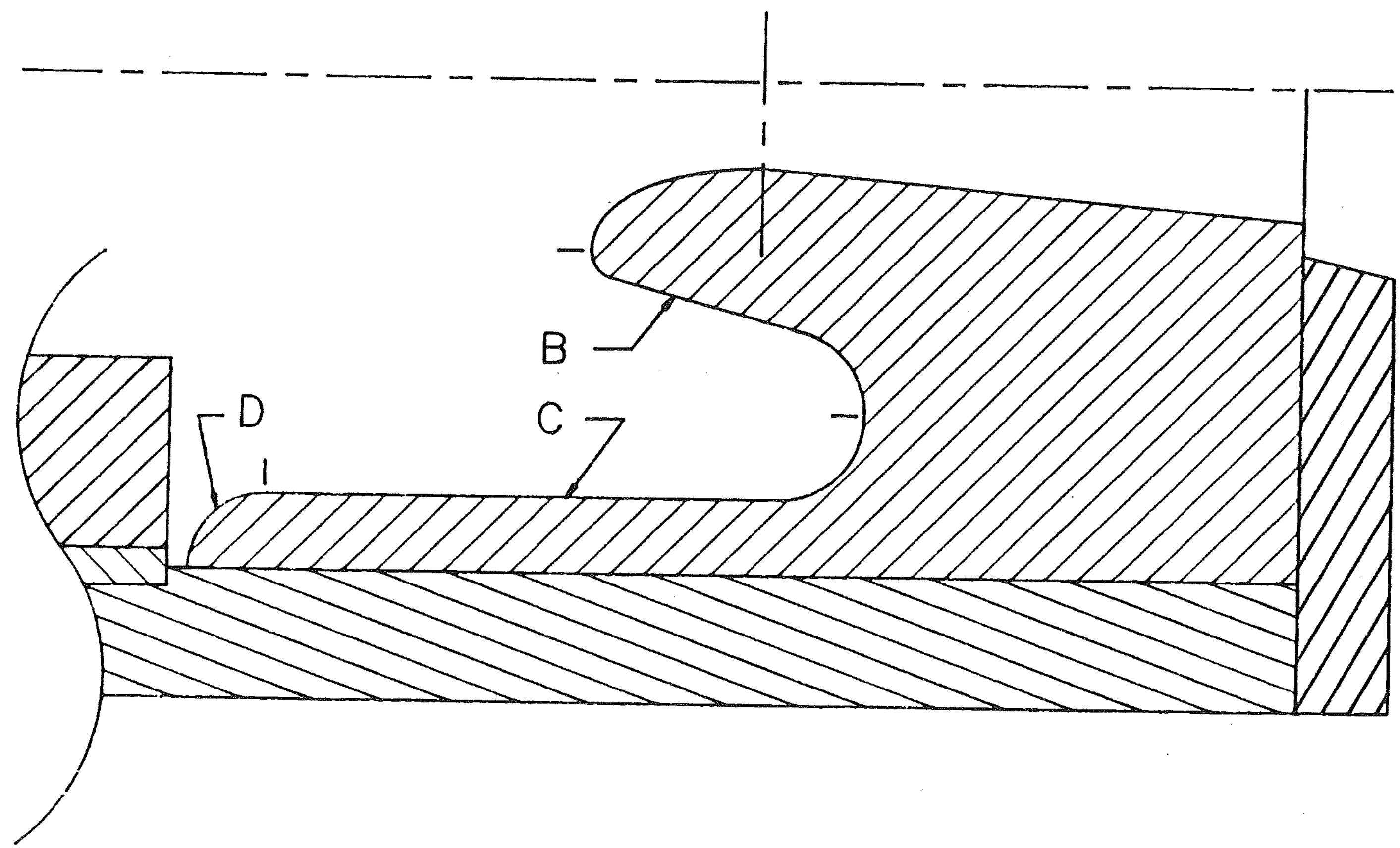

ERC, Inc.

FIVE INCH SPIN MOTOR NOZZLE
SLAG SUBZONES

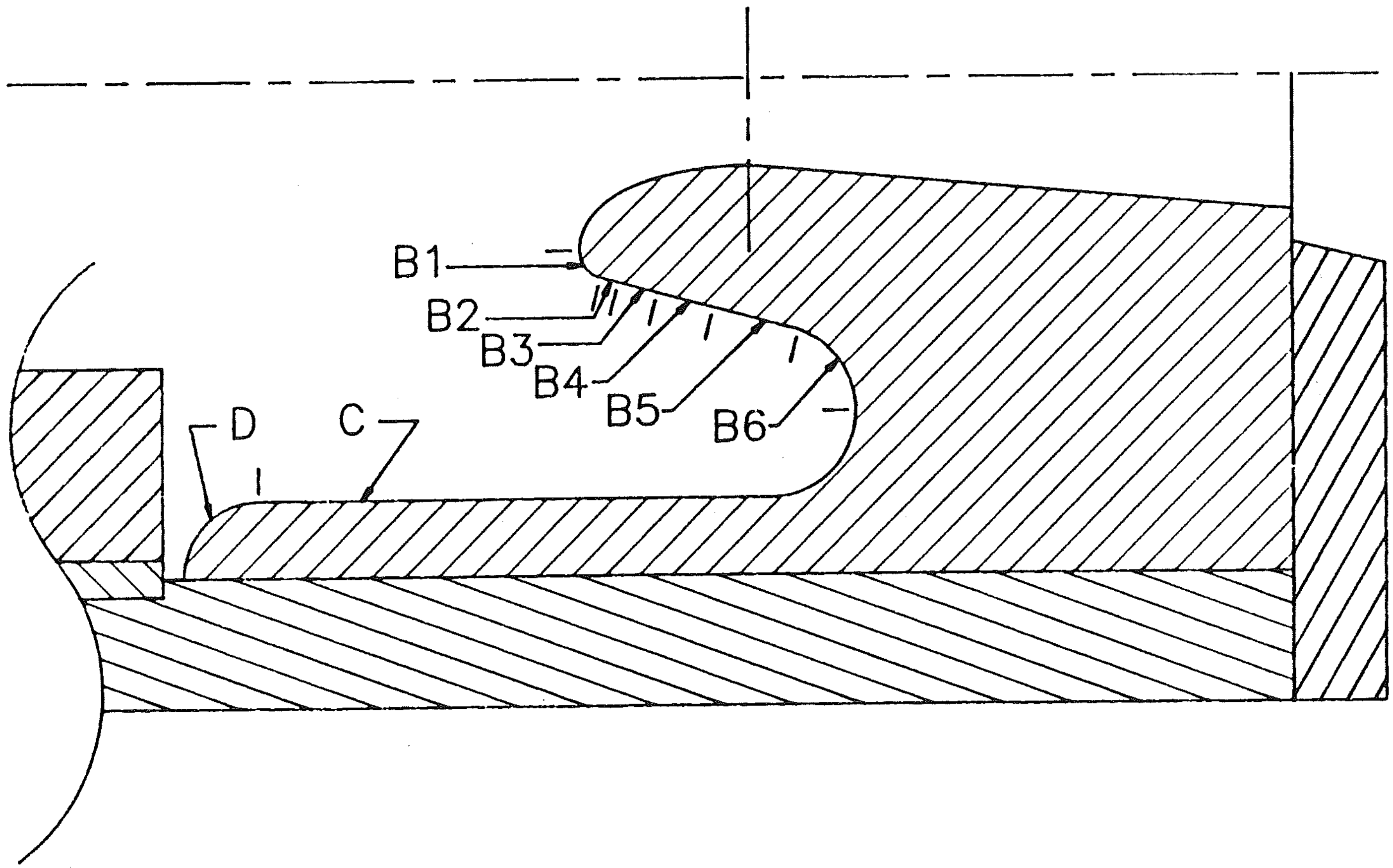

ERC, Inc.

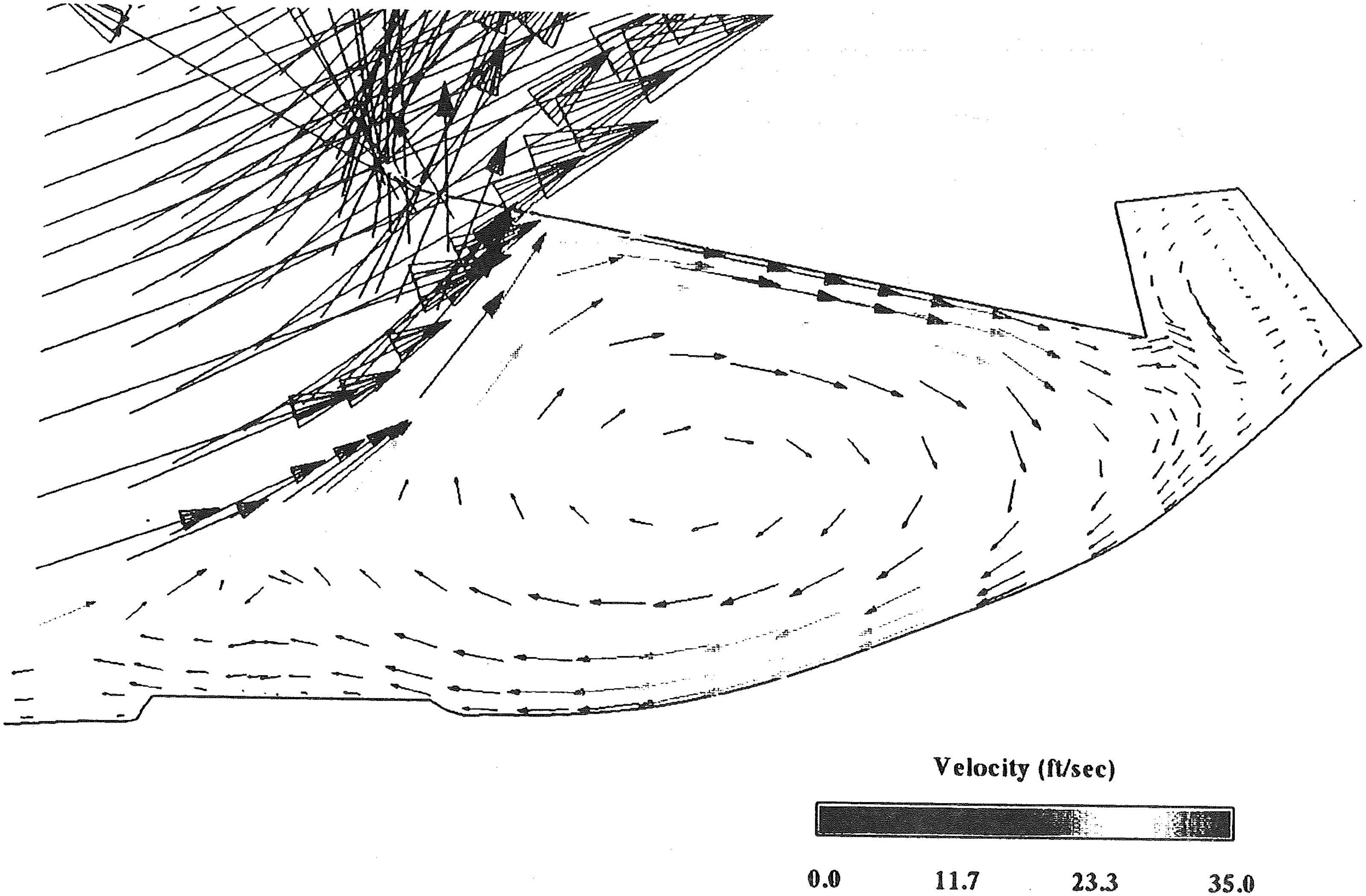

Velocity Vectors, Submerged Nozzle
RSRM 80 Second Stiff NBR Inhibitor

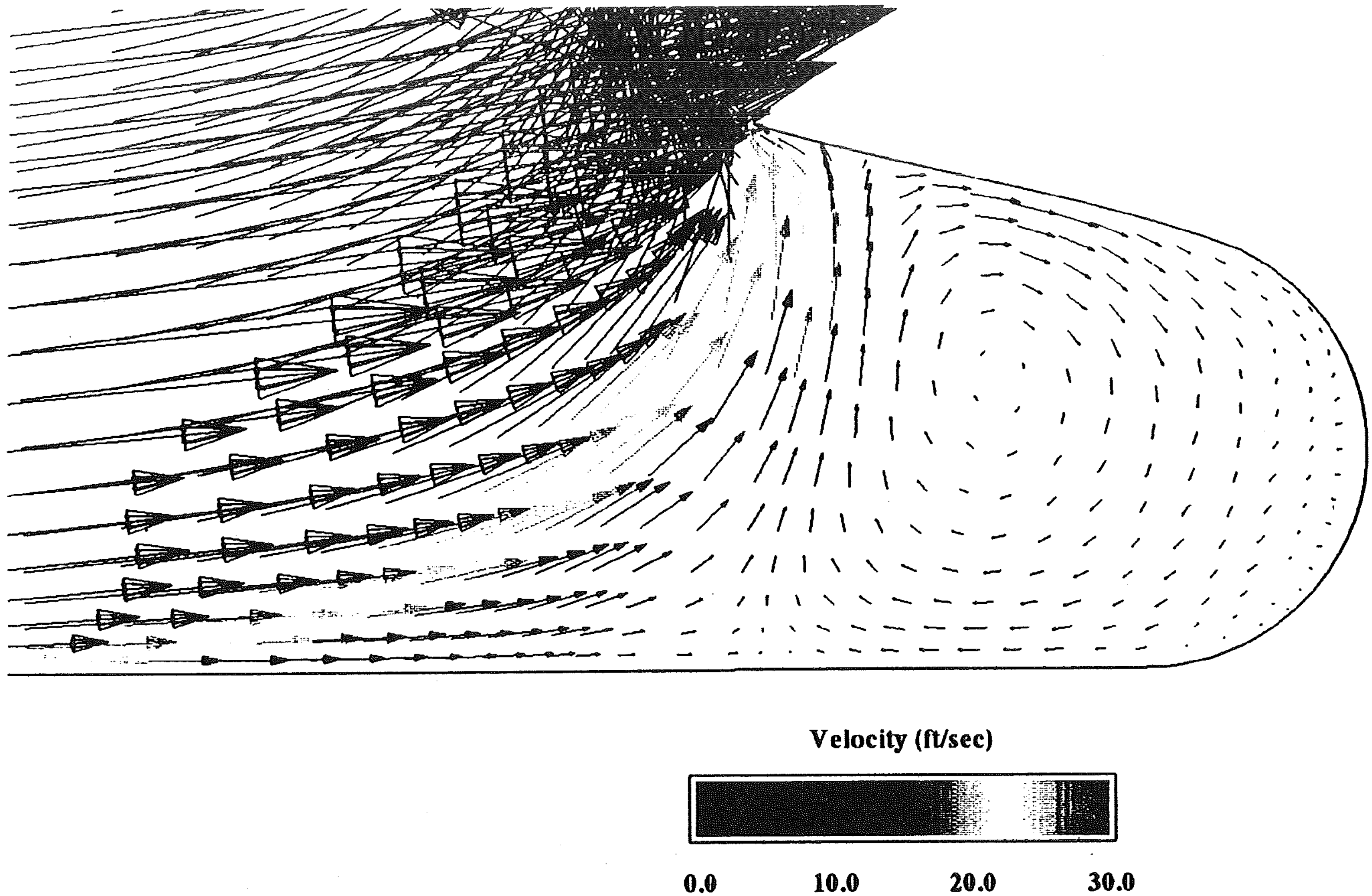

Velocity Vectors, Submerged Nozzle Spin Motor at 50% Web Time

Two-Phase Flow CFD Methodology
CELMINT Code
(Combined Eulerian Lagrangian Multi-Dimensional Implicit Nonlinear Time-Dependent)

- **Navier-Stokes Solution**
  - Fully implicit, density-based, conservative, ensemble-averaged Navier-Stokes code
  - Low and high Reynolds number and wall injection $\kappa-\varepsilon$ models
  - Equilibrium and finite-rate chemistry for multi-species flows

- **Two-phase Flow Models**
  - Coupled Eulerian-Lagrangian for solid and liquid phases
  - Hermsen aluminum burn rate model for particle combustion
  - Specification of particle properties (density, size distribution)
  - Particle break-up based on Weber number
  - Agglomeration based on collisions between discrete phase particles and continuous phase smoke particles
  - Programmable for various particle capture criteria

ERC, Inc.

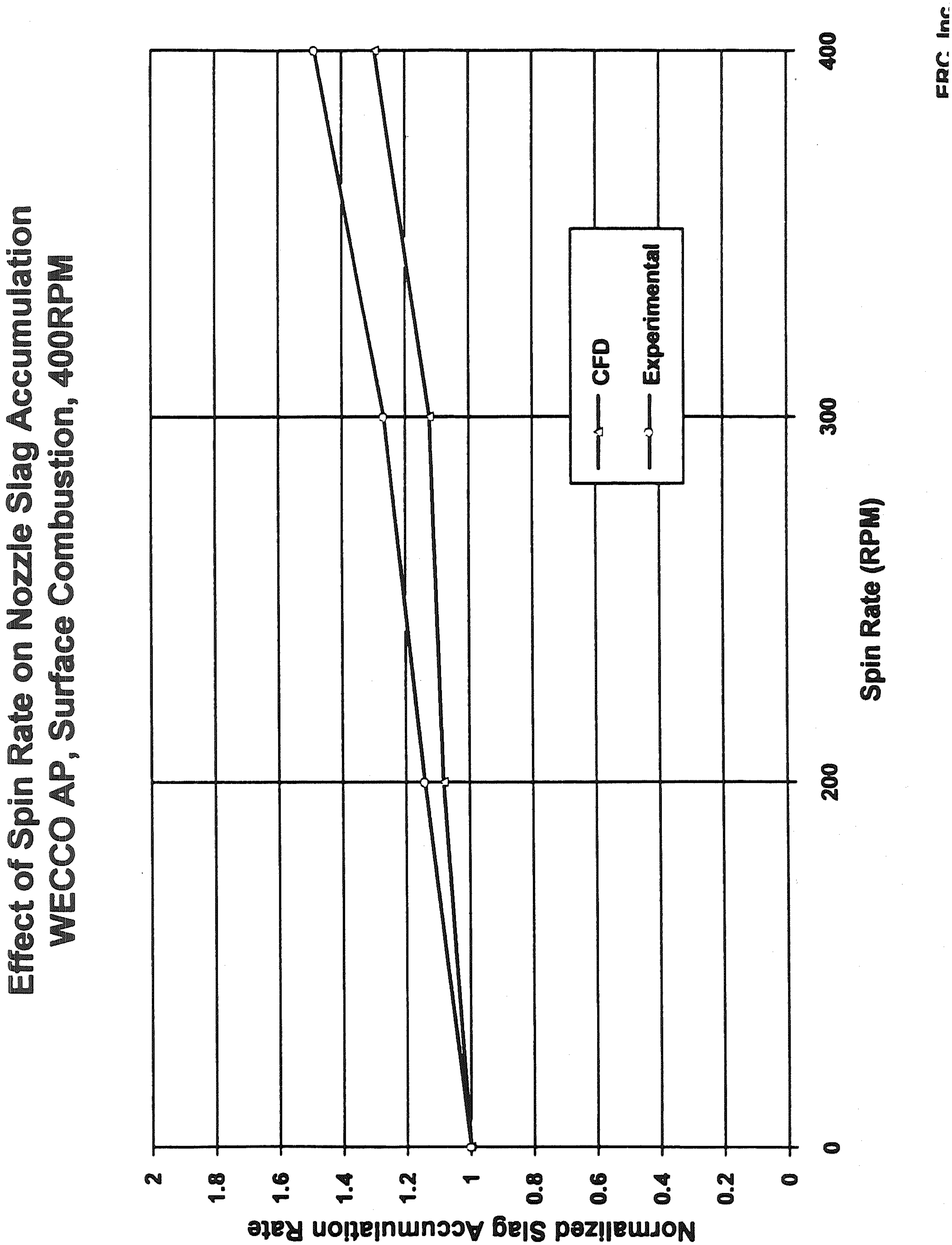

Effect of Spin Rate on Nozzle Slag Accumulation
WECCO AP, Surface Combustion, 400RPM
Normalized Slag Accumulation Rate
2
1.8
1.6
1.4
1.2
1
0.8
0.6
0.4
0.2
0
0
200
300
400
Spin Rate (RPM)
CFD
Experimental
ERC, Inc.

Computational Grid Resolution

Location	15% Web	50% Web	85% Web
Port	50X50	50X65	50X65
Nozzle Closure	105X85	110X95	115X80

ERC, Inc.

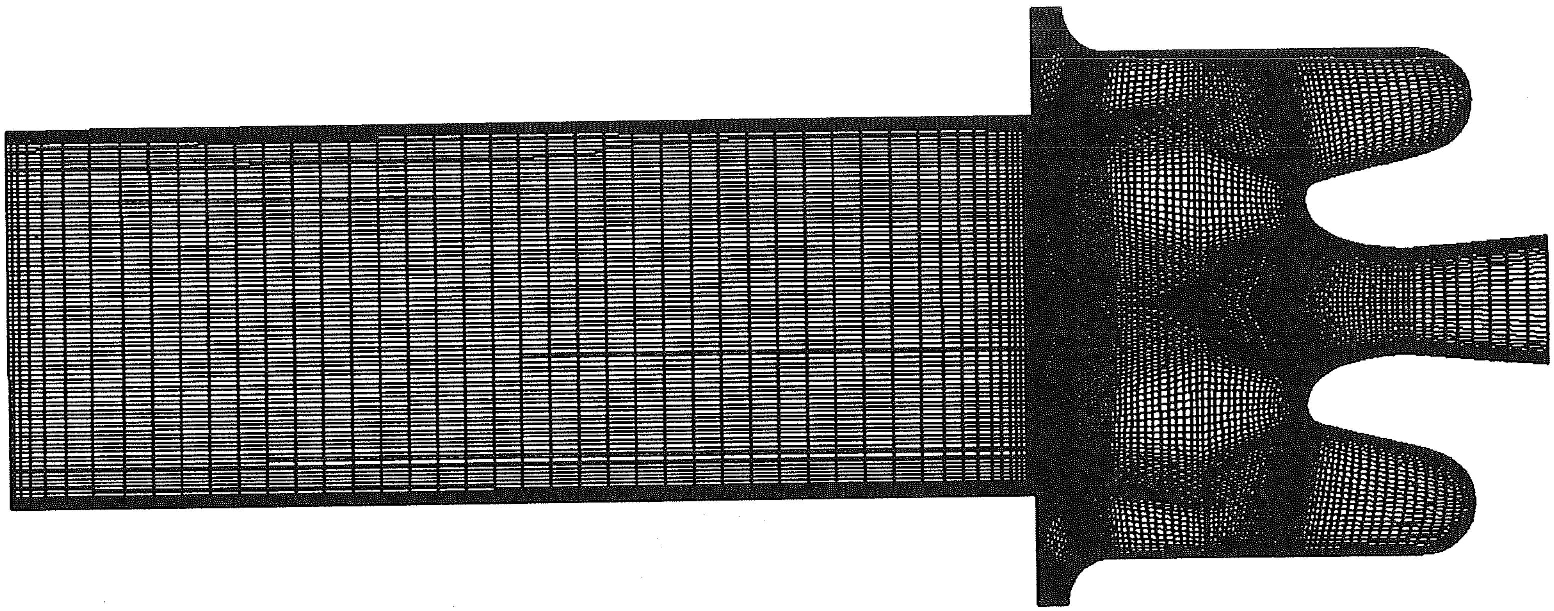

Computational Grid
Spin Motor At 15 % Web Time

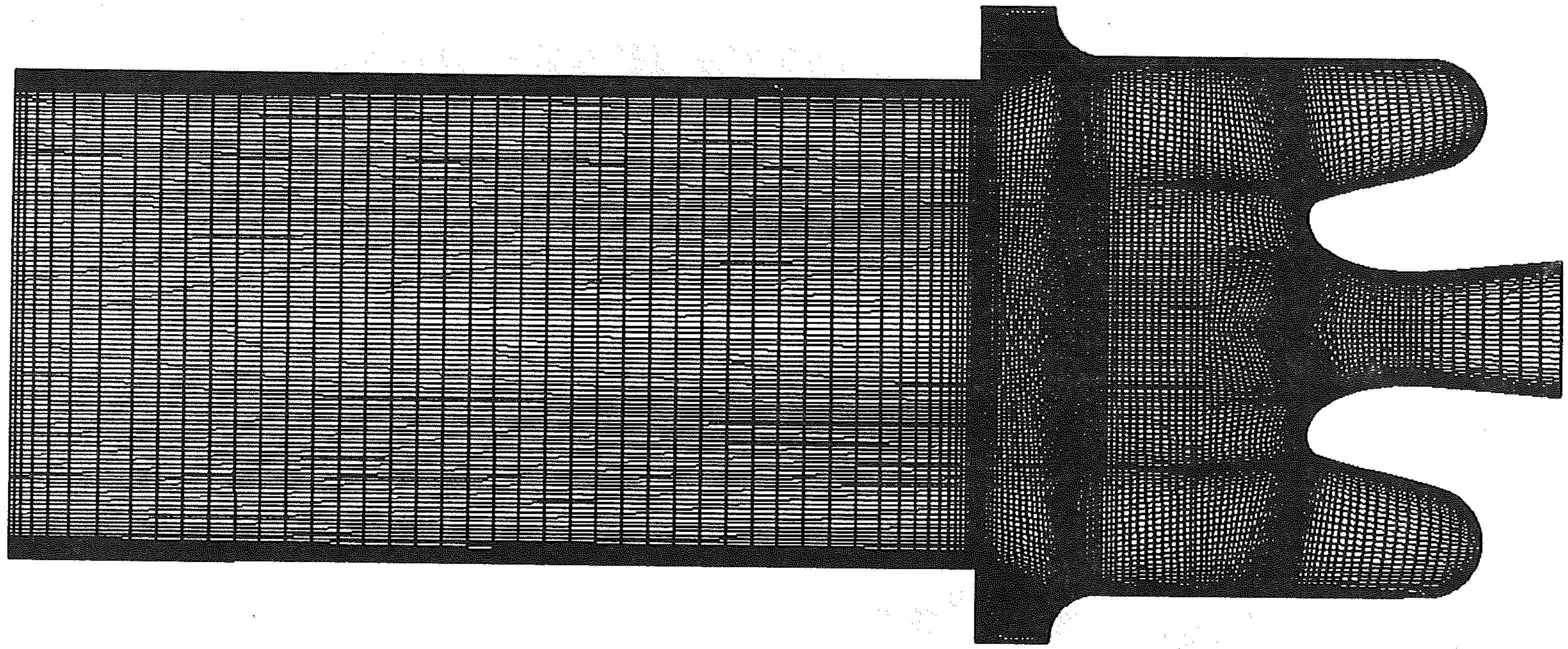

Computational Grid

Spin Motor At 50 % Web Time

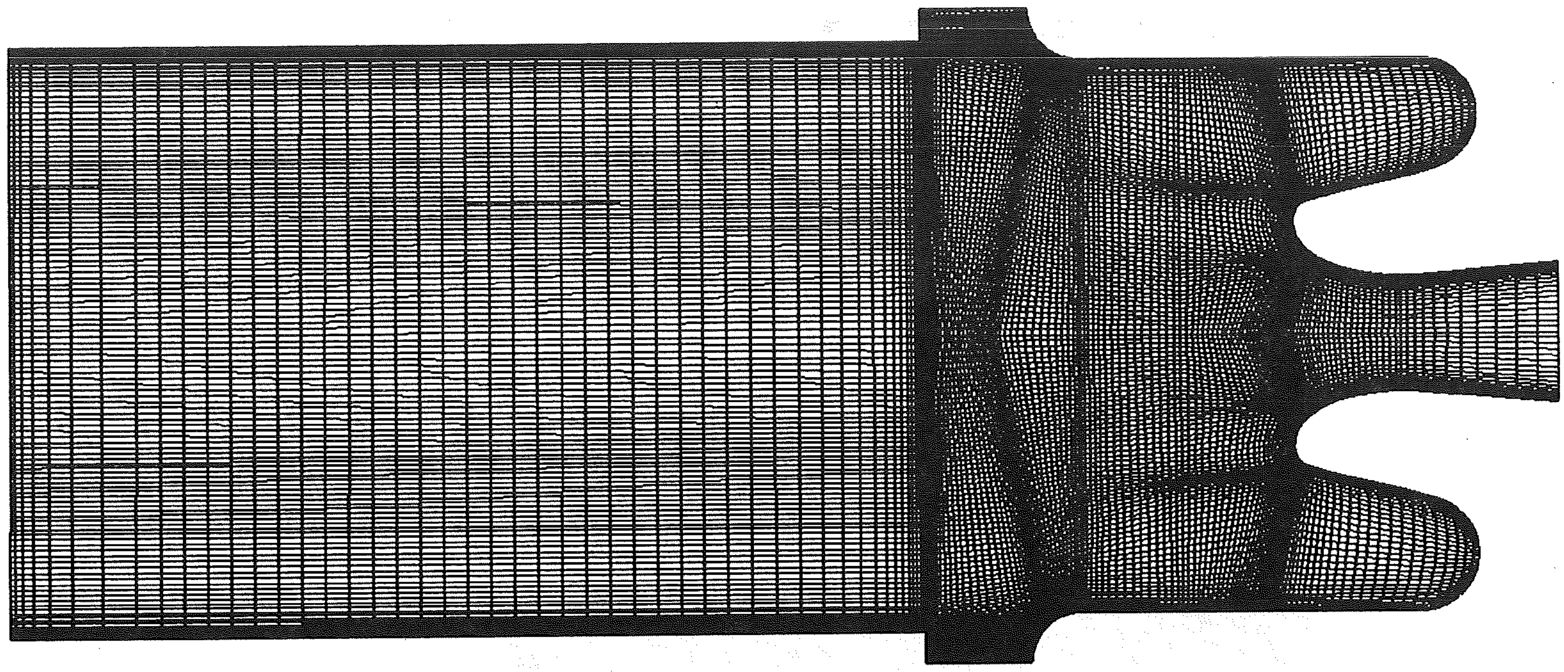

Computational Grid

Spin Motor At 85 % Web Time

RSRM Propellant Thermochemical and Nominal Particle Properties

Propellant	TP-H1148
Pressure	625 psia
Total Temperature	6093° R
Molecular Weight	28.04
Dynamic Viscosity	6.189×10^{-5} bm/ft-sec
Ratio of Specific Heats	1.138

Particle Distribution	Polynomial Fit to Wecco Quench Bomb Data
Particle Density	$60 lbm/ft^3$
Ratio of Initial Particle/Gas Velocity	1.0
Aluminum Oxide Caps Fraction (Discrete Phase)	28.33%

ERC, Inc.

Spin Motor Operation Conditions

Parameter	15% Web	50% Web	85% Web
Chamber Pressure:	610.6 psia	628.8 psia	610.6 psia
Mass Flow Rate:	2.613 lbm/s	2.691lbm/s	2.613 lbm/s
Propellant Burning Area:	115.47 in^2	114.67 in^2	112.35 in^2

Throat Diameter: .916 inches

Burn Time: 2.71 seconds

ERC, Inc.

Experimental Data and Curve Fit Distribution Functions
WECCO Quench Bomb Data- 500 psi
3-inch Quench Distance

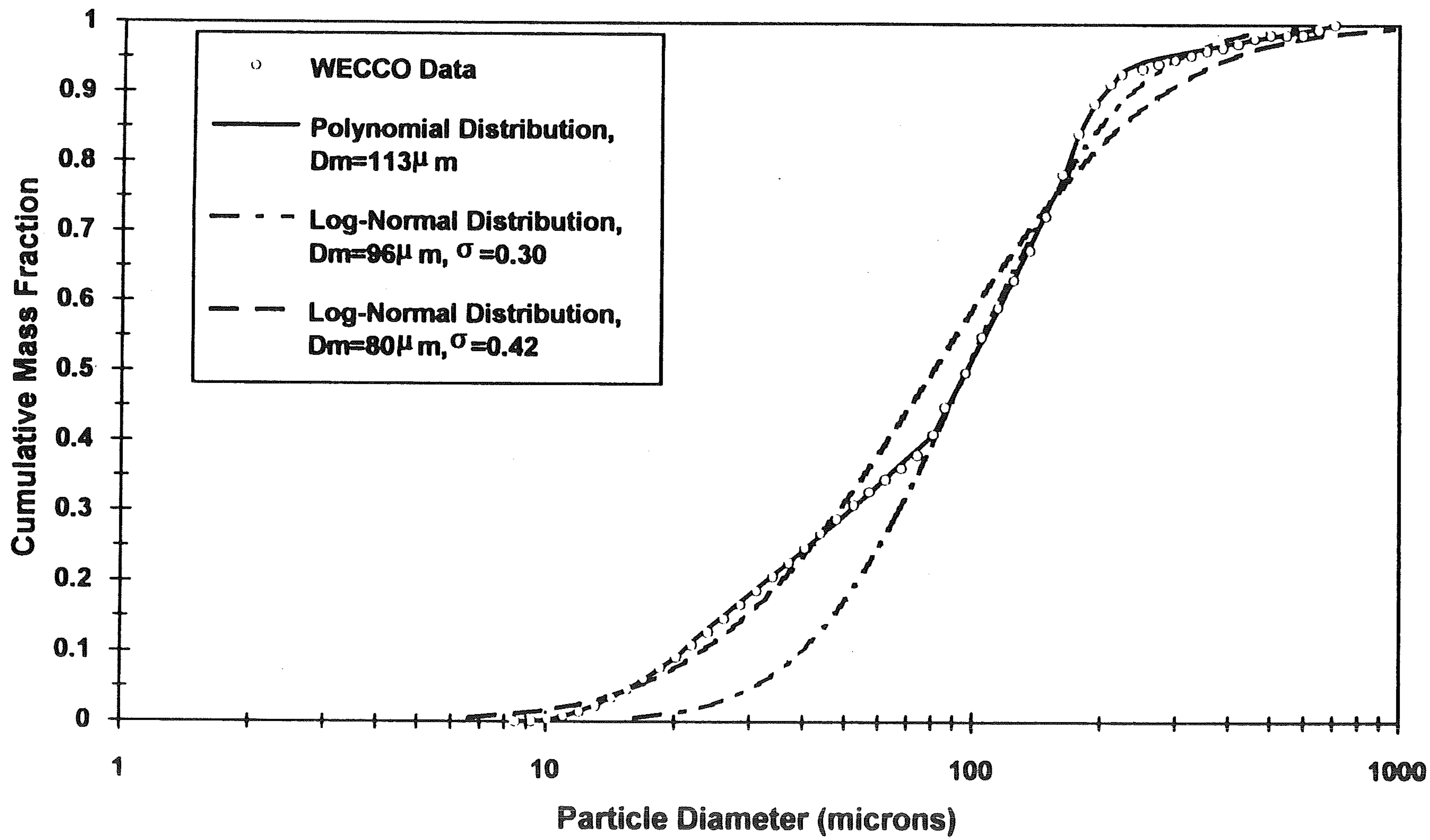

ERC, Inc.

Experimental Data and Curve Fit Density Functions
WECCO Quench Bomb Data- 500 psi
3-inch Quench Distance

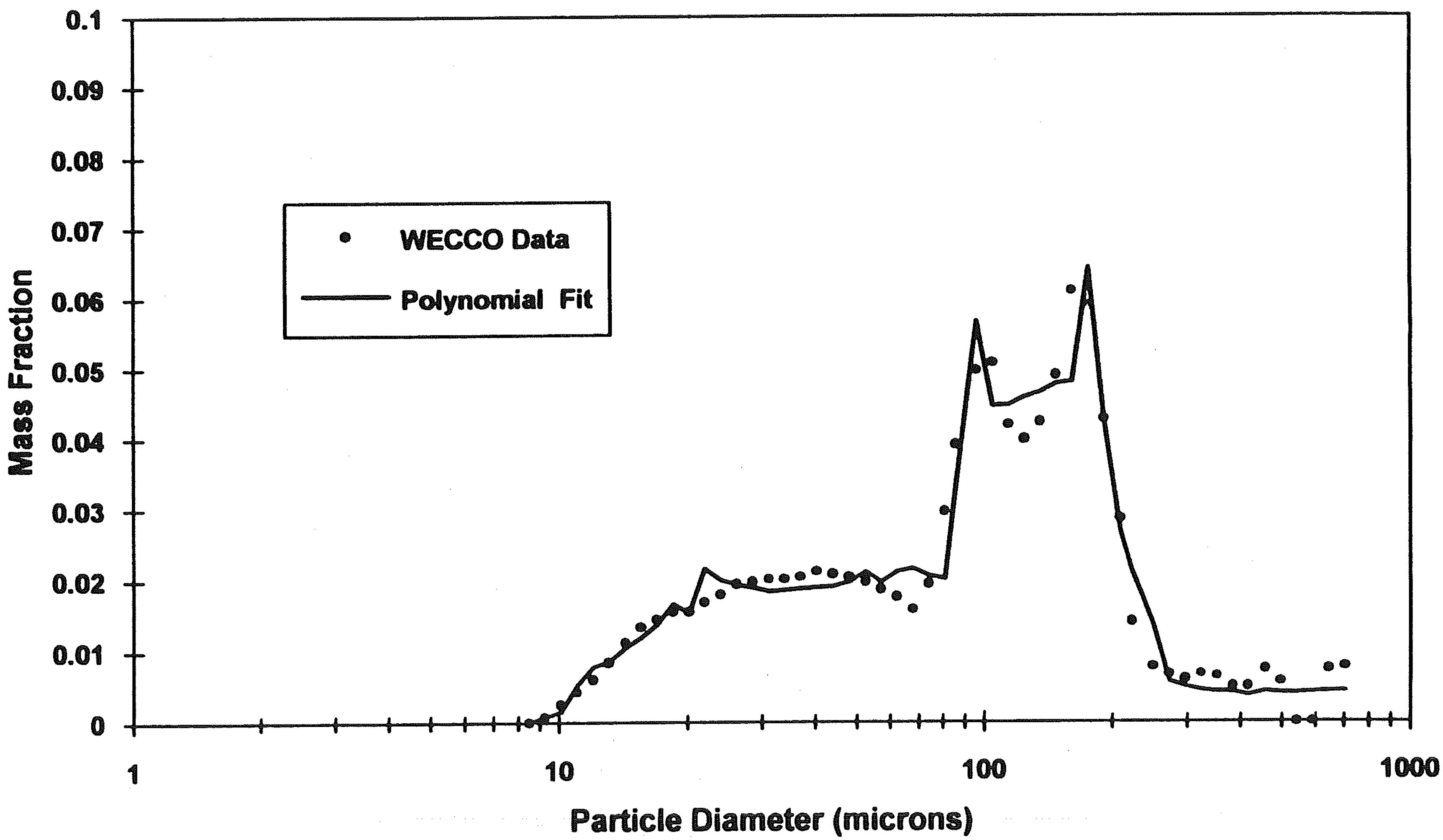

ERC, Inc.

Experimental Data and Curve Fit Distribution Functions
Kerr McGee Quench Bomb Data- 500 psi
3-inch Quench Distance

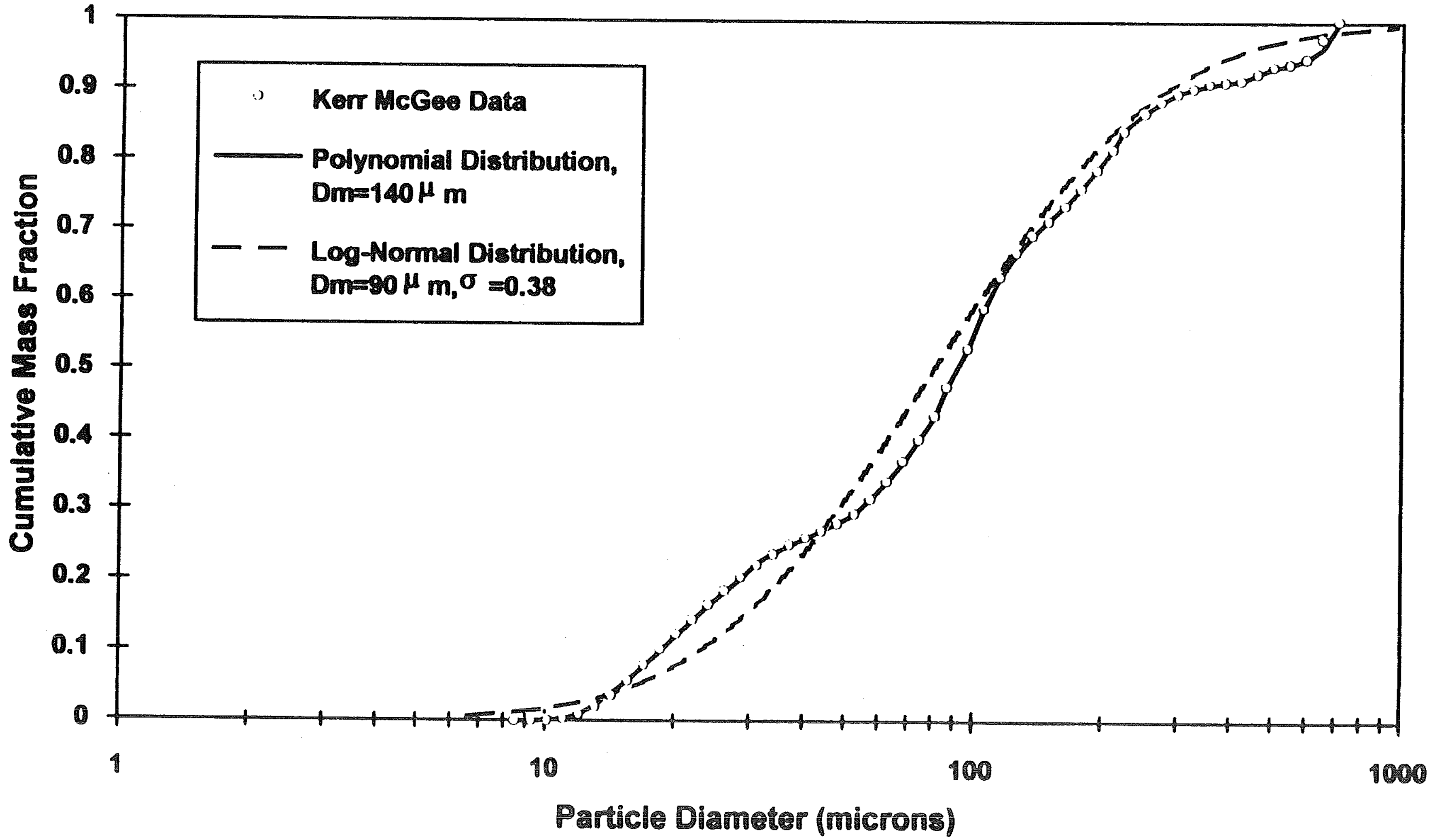

ERC, Inc.

Experimental Data and Curve Fit Density Functions
Kerr McGee Quench Bomb Data- 500 psi
3-inch Quench Distance

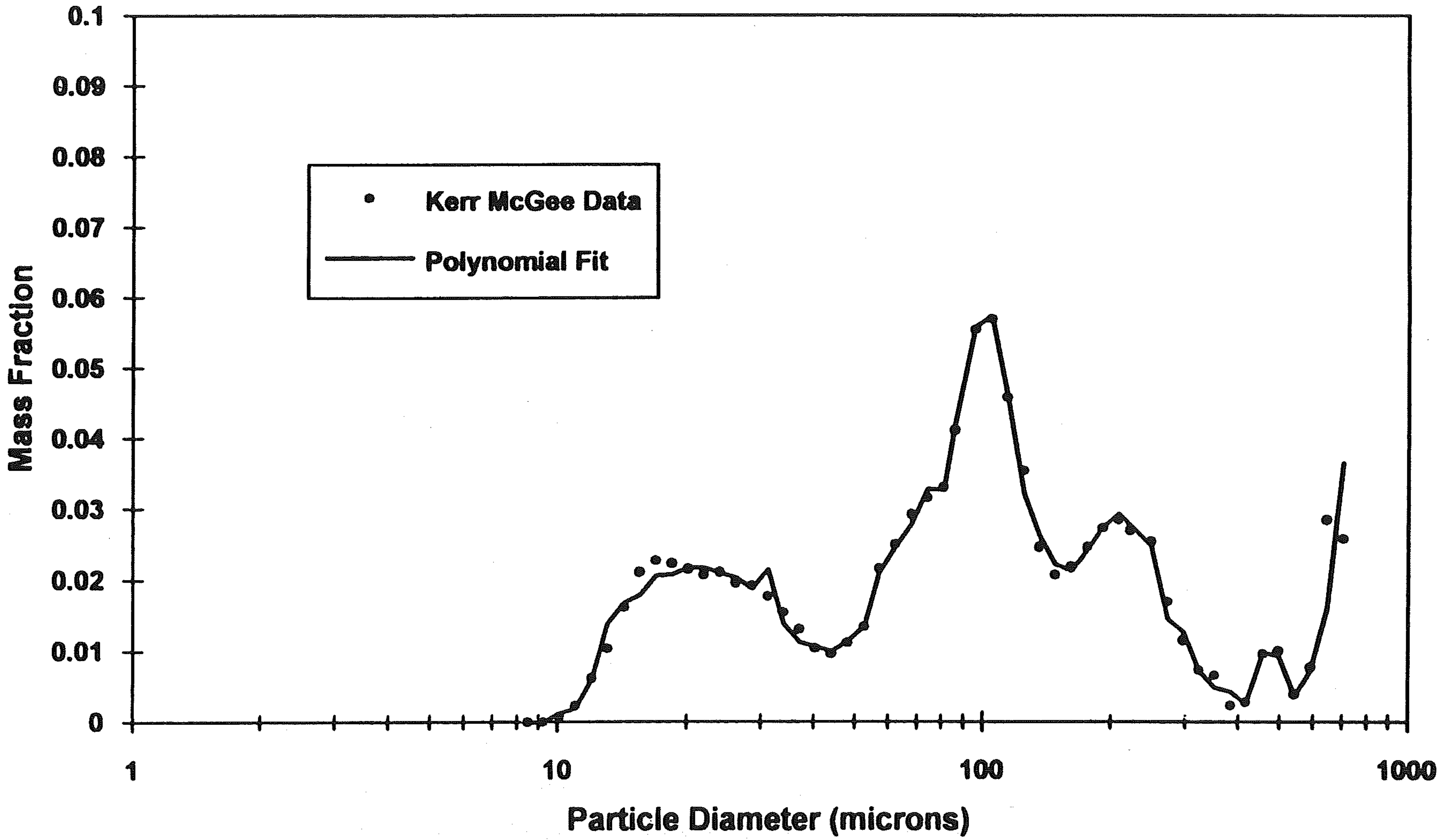

ERC, Inc.

Effect of Particle SIze Distribution on Slag Accumulation
WECCO AP, Surface Combustion, 400 rpm

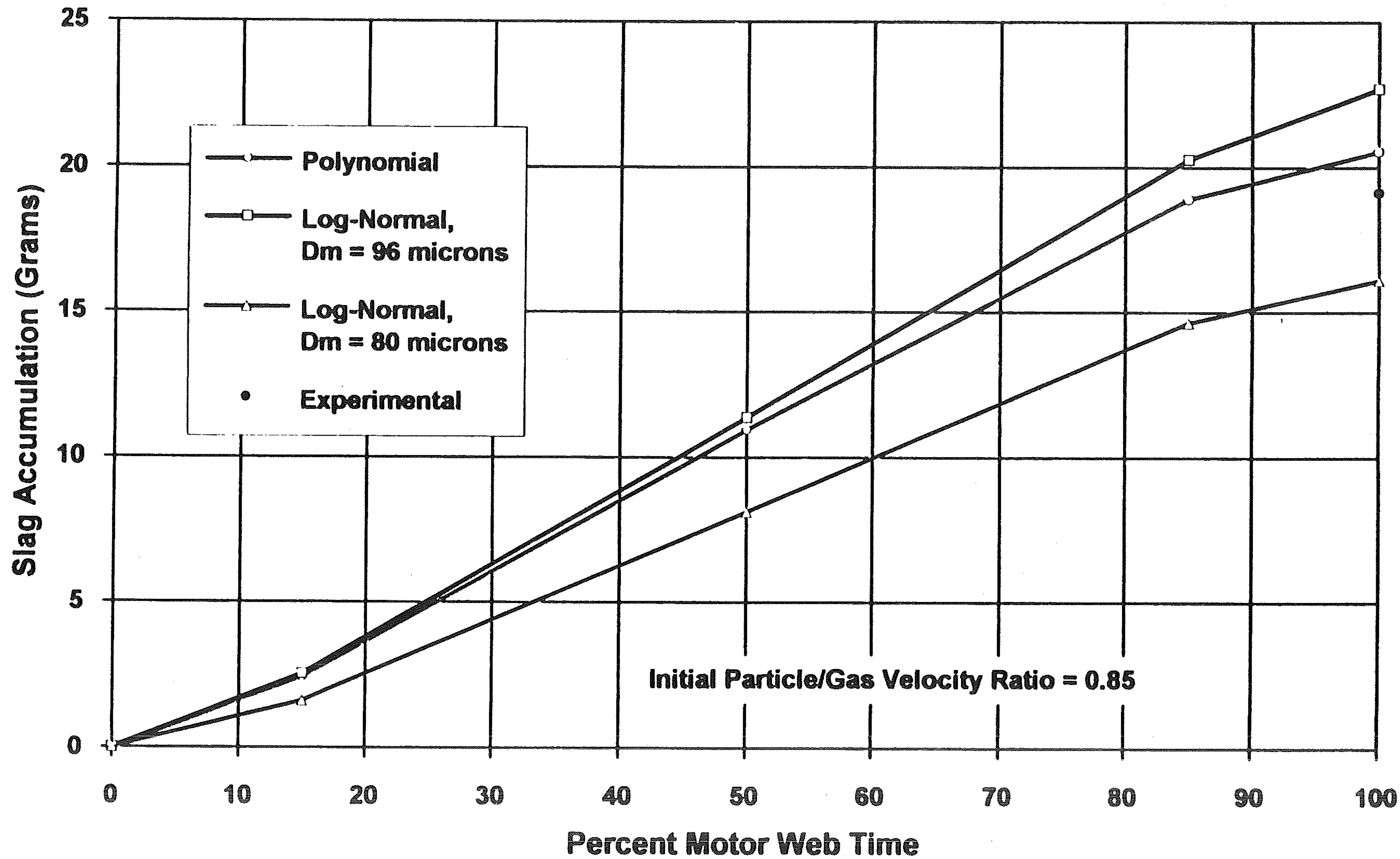

ERC, Inc.

Nozzle Slag Accumulation
WECCO and Kerr McGee AP
Surface Combustion, 400 RPM

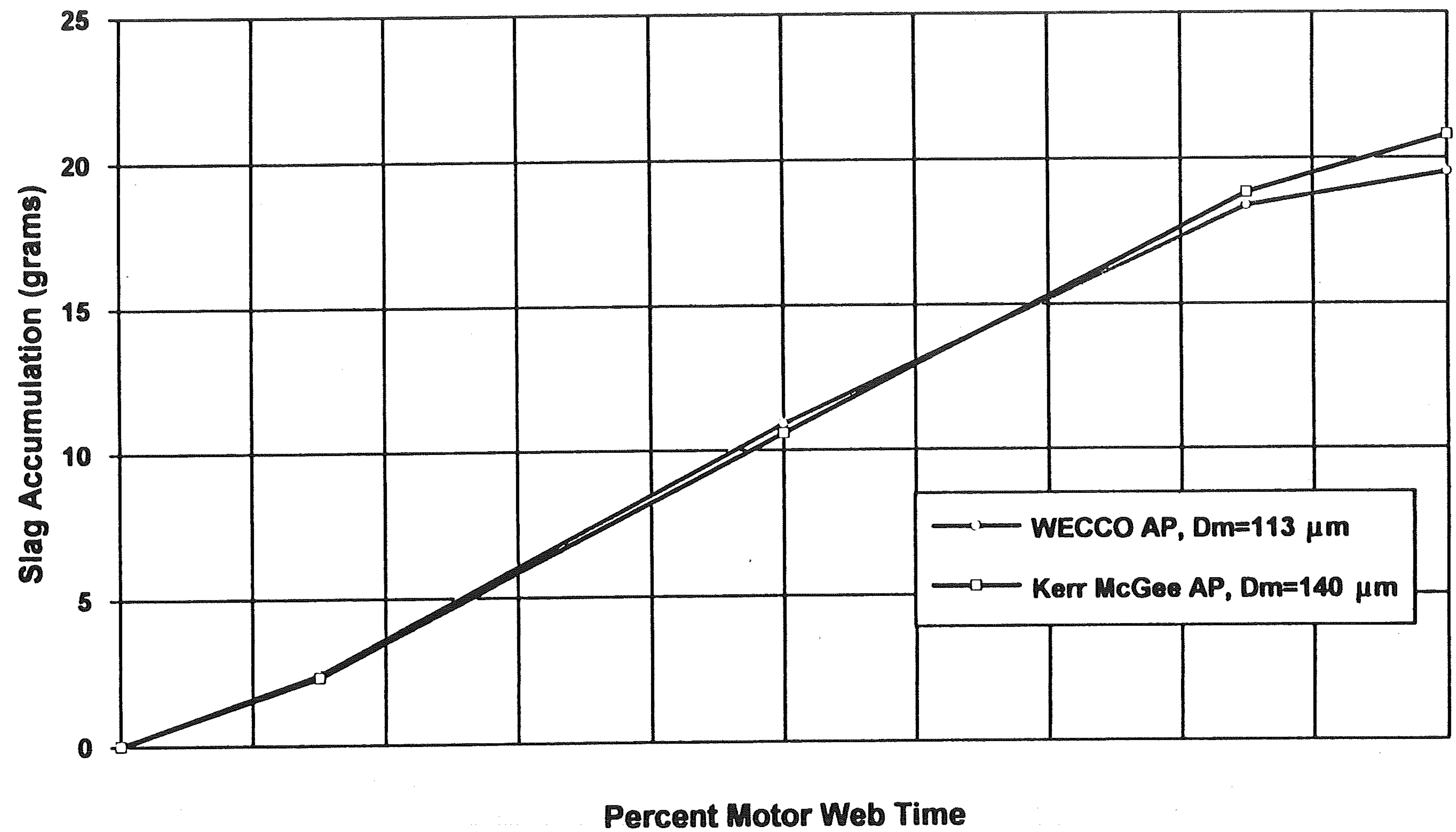

ERC, Inc.

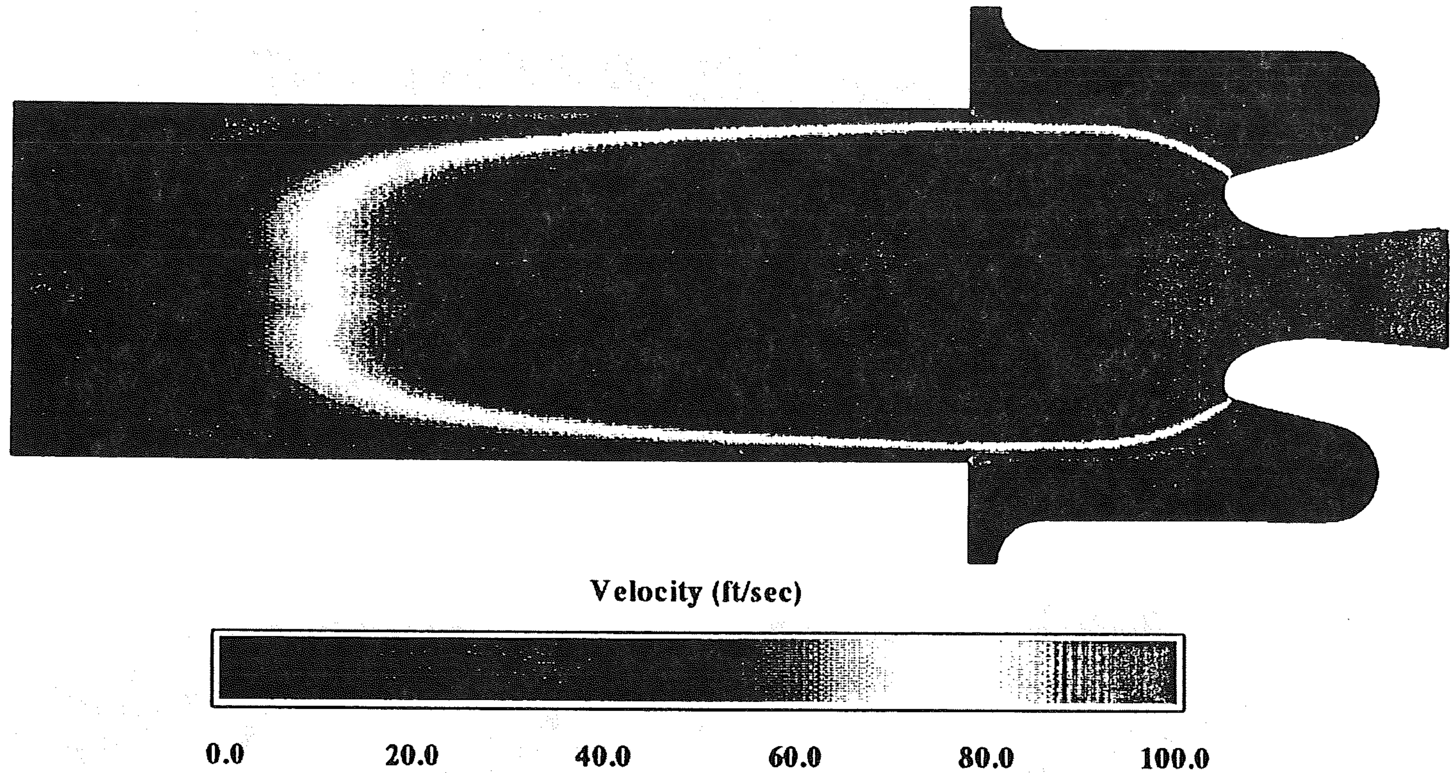

Velocity Magnitude

Spin Motor at 15% Web Time

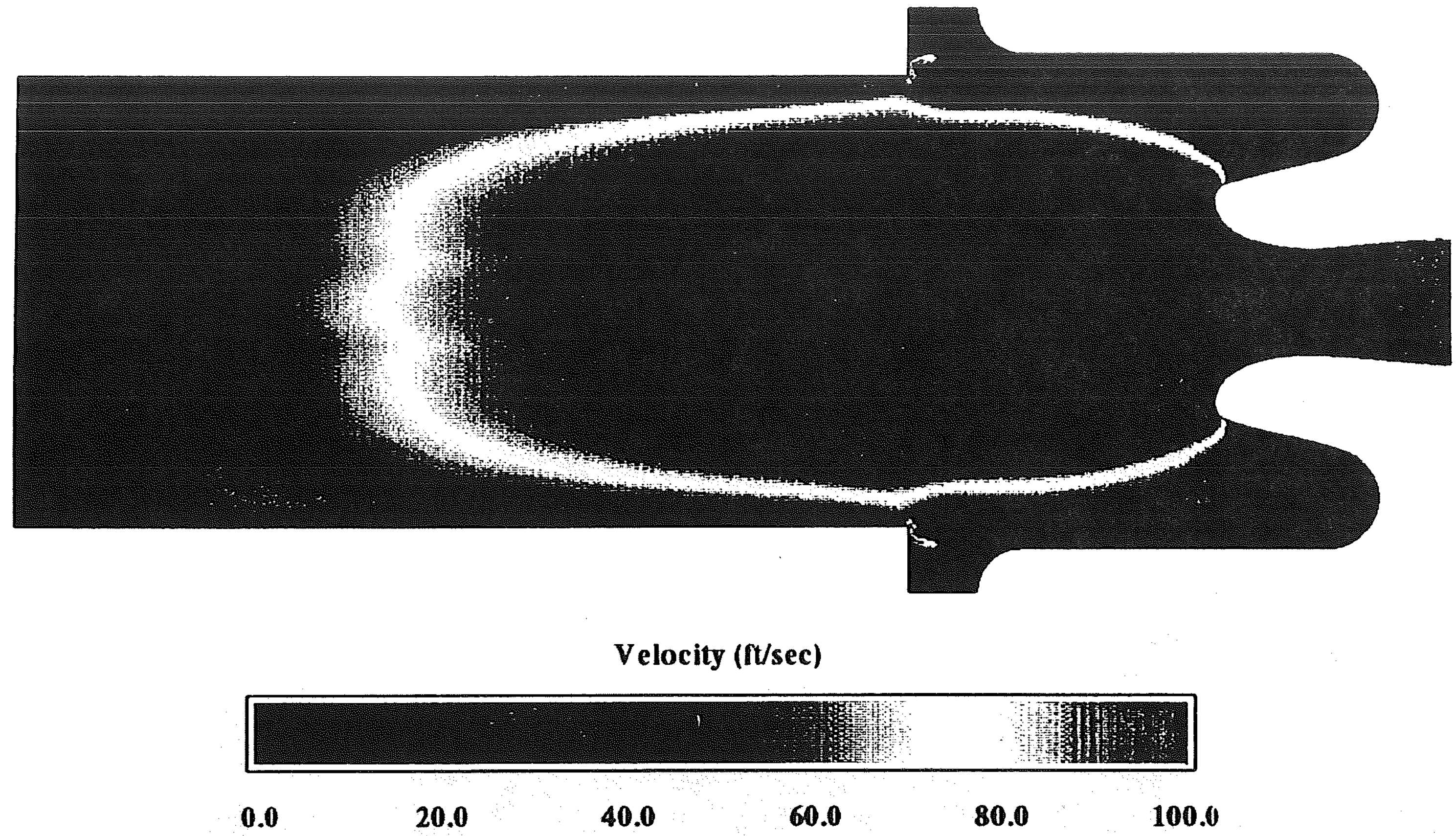

Velocity Magnitude

Spin Motor at 50% Web Time

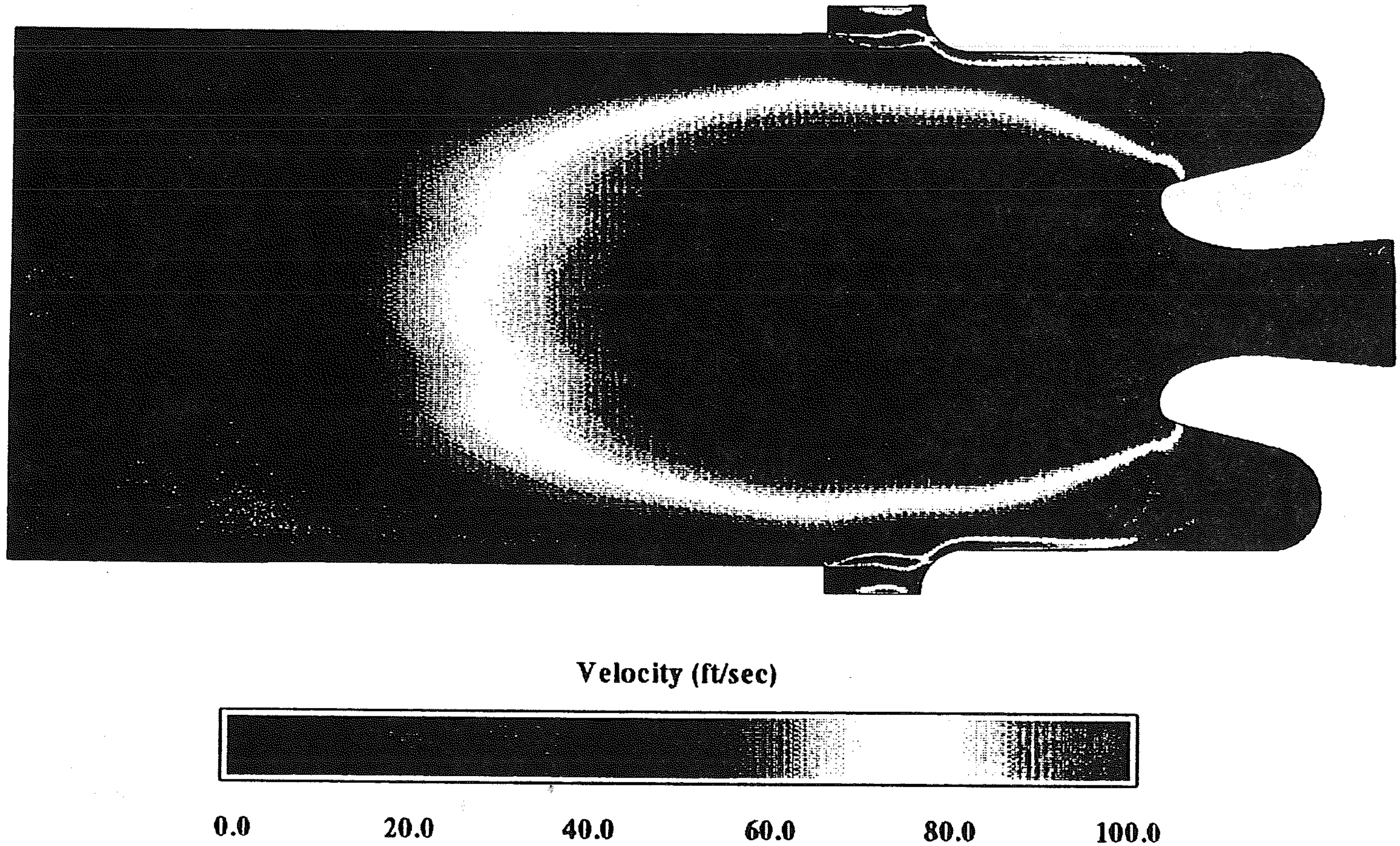

Velocity Magnitude
Spin Motor at 85% Web Time

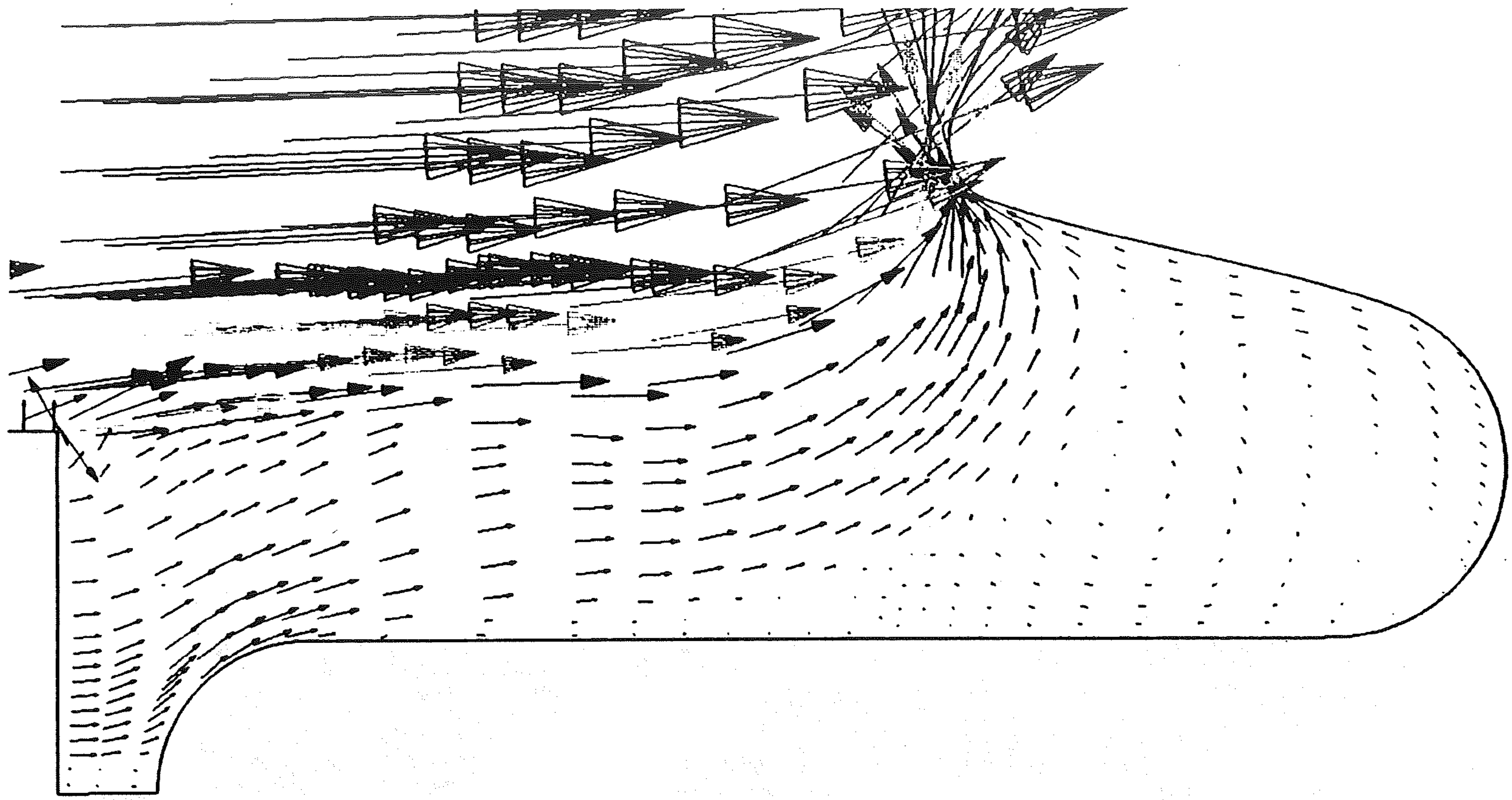

Velocity Field In The Submerged Nozzle Region

Spin Motor At 15 % Web Time

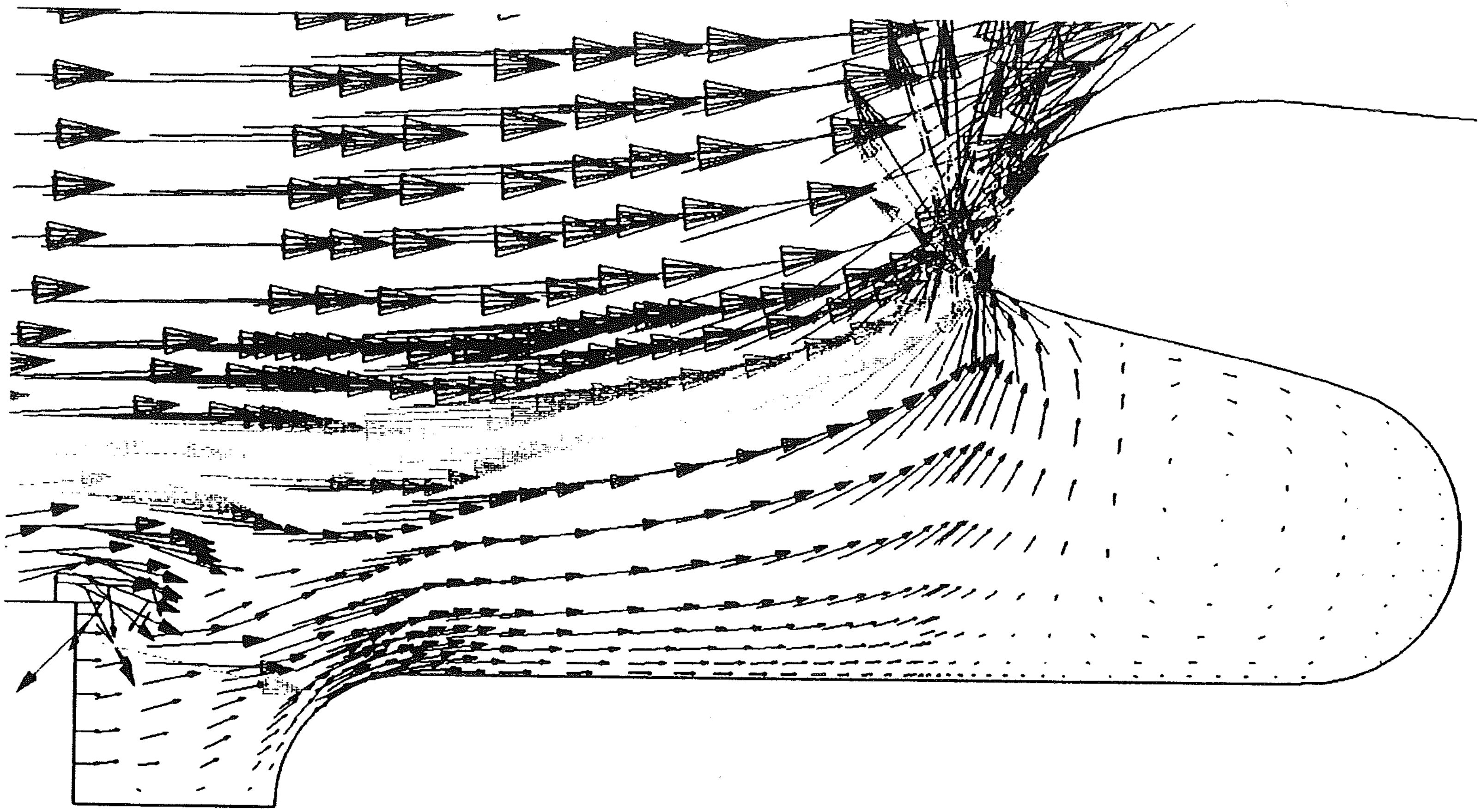

Velocity Field In The Submerged Nozzle Region

Spin Motor At 50 % Web Time

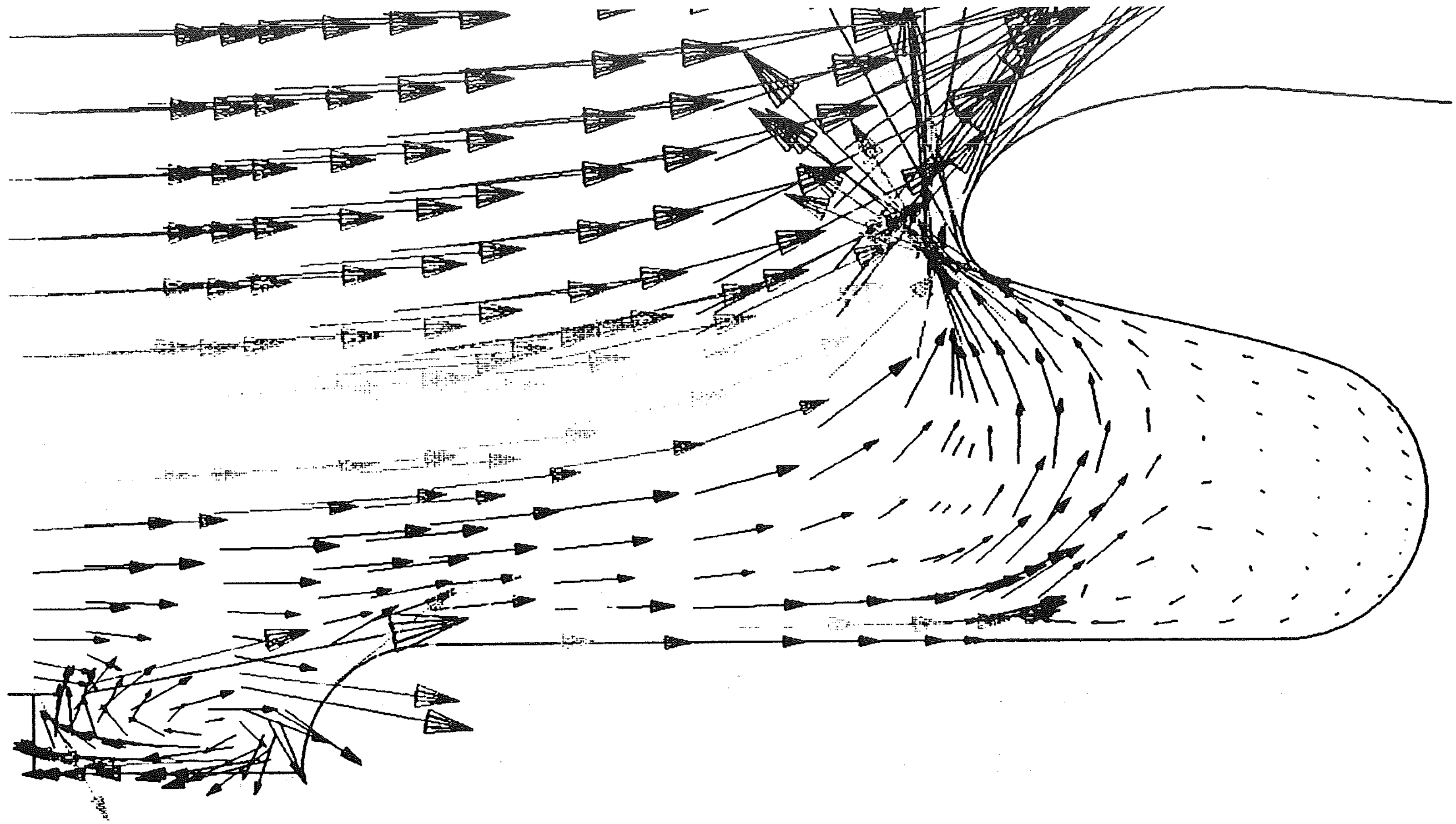

Velocity Field In The Submerged Nozzle Region

Spin Motor At 85 % Web Time

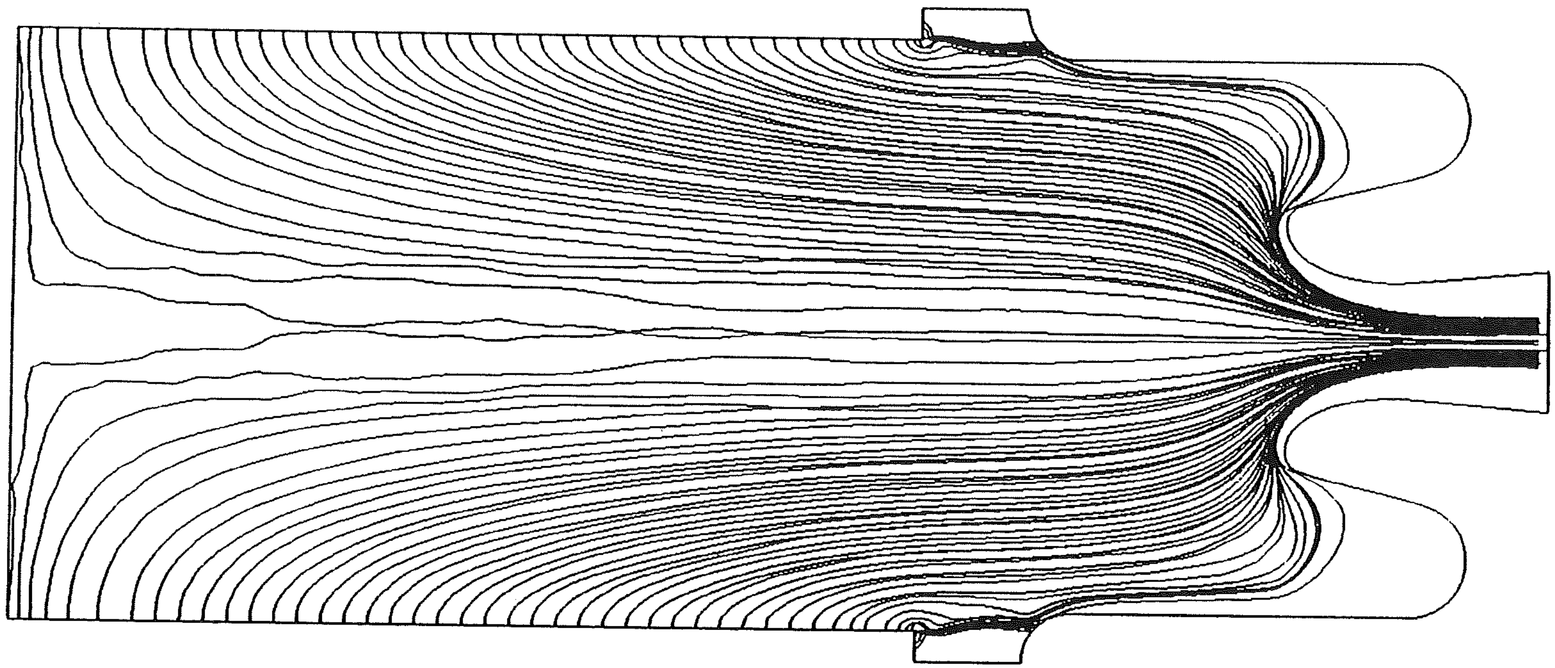

20 Micron Diameter Particle Trajectories

Spin Motor At 85 % Web Time

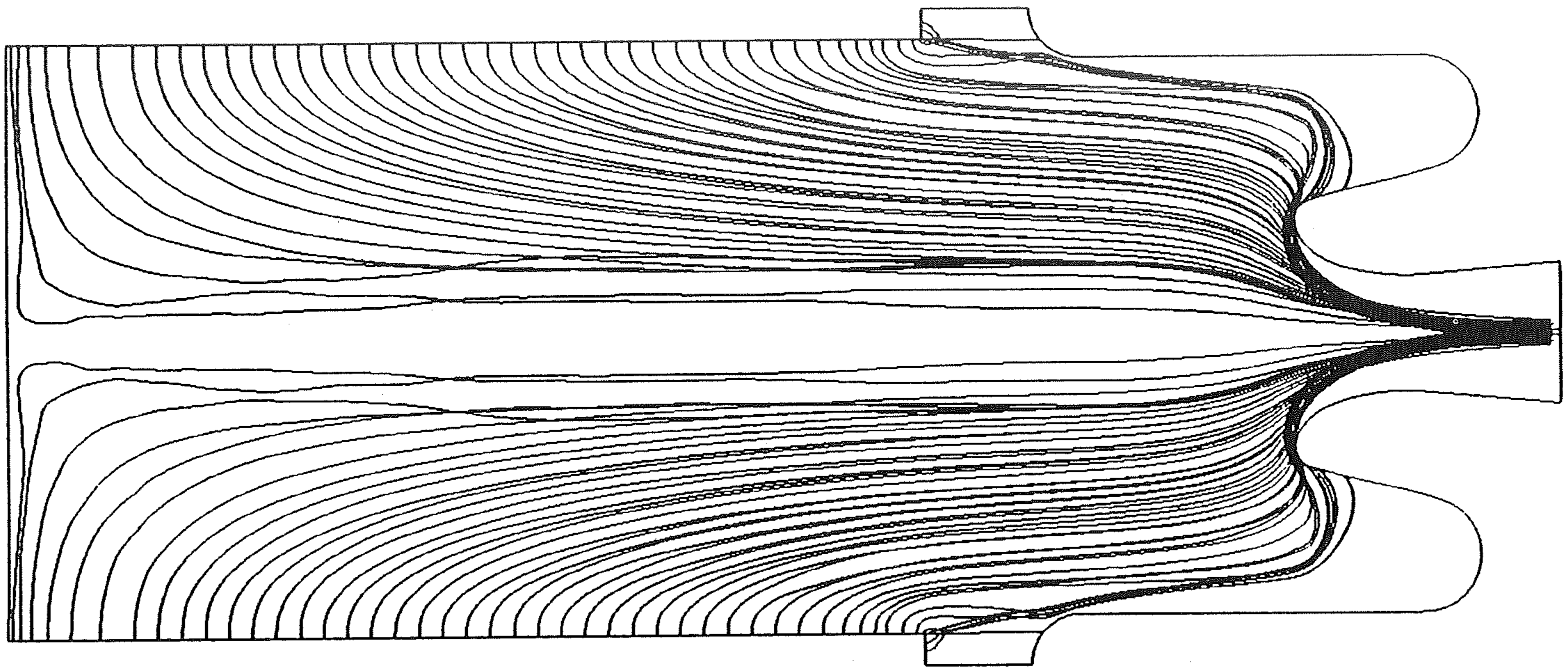

50 Micron Diameter Particle Trajectories

Spin Motor At 85 % Web Time

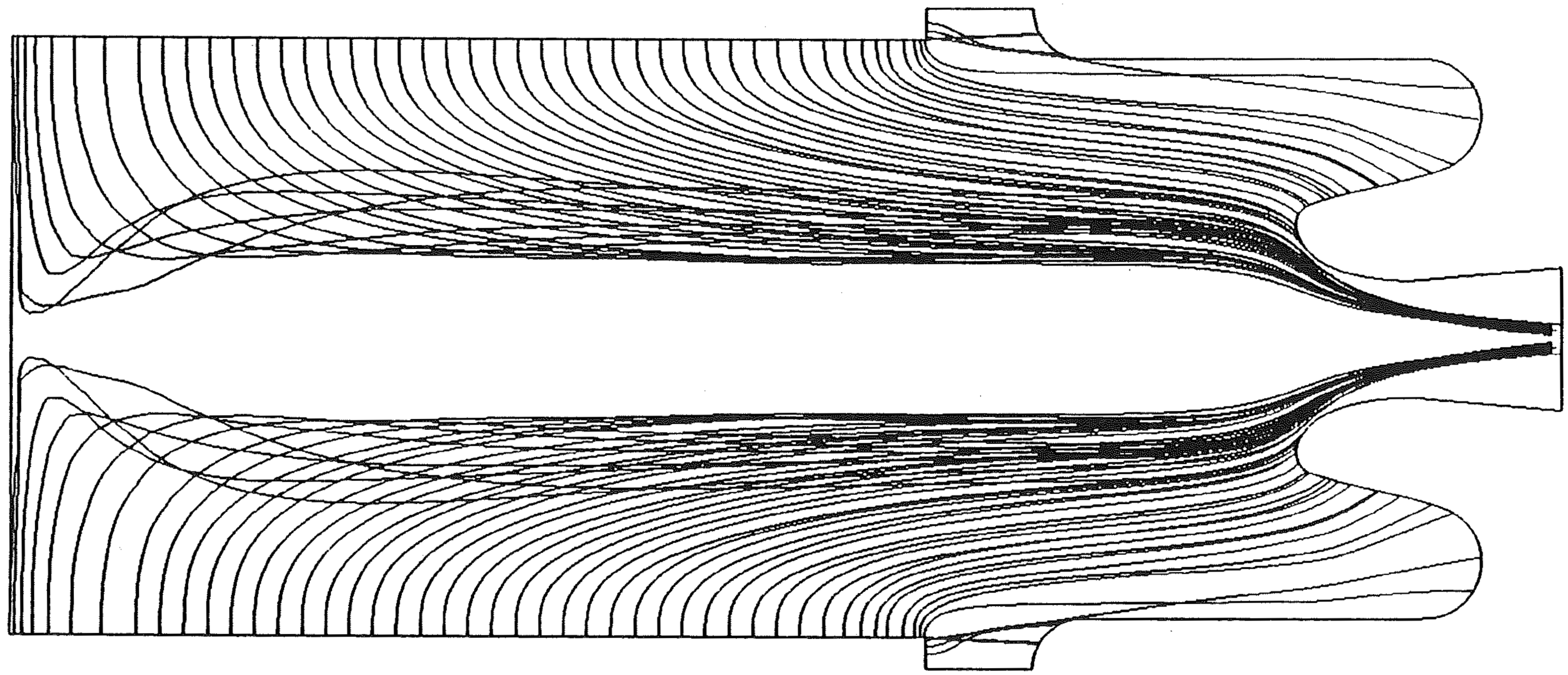

150 Micron Diameter Particle Trajectories

Spin Motor At 85 % Web Time

Spin Motor Circumferential Velocity
WECCO, Surface Combustion, 400 RPM
15% Web Time

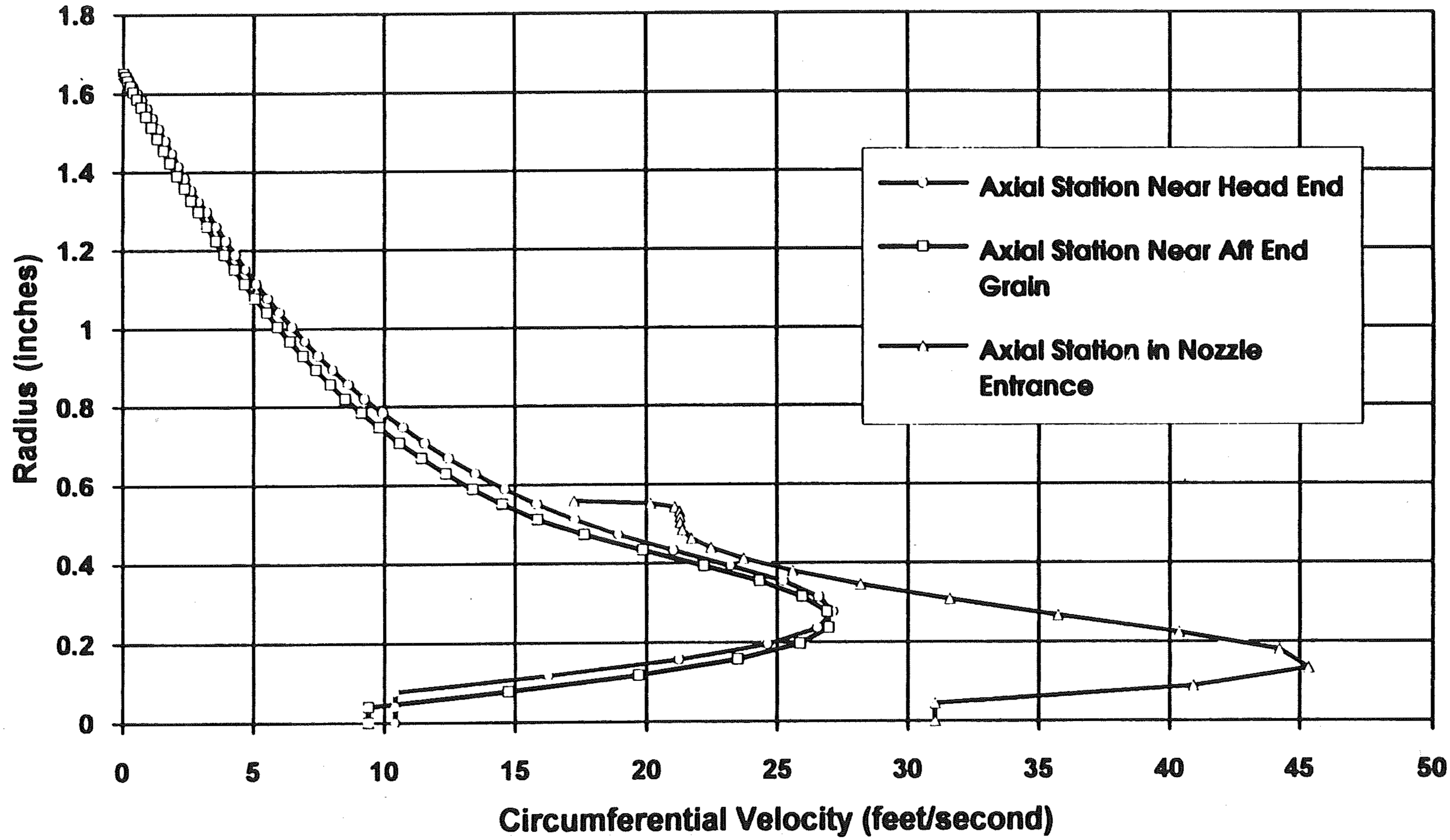

ERC, Inc.

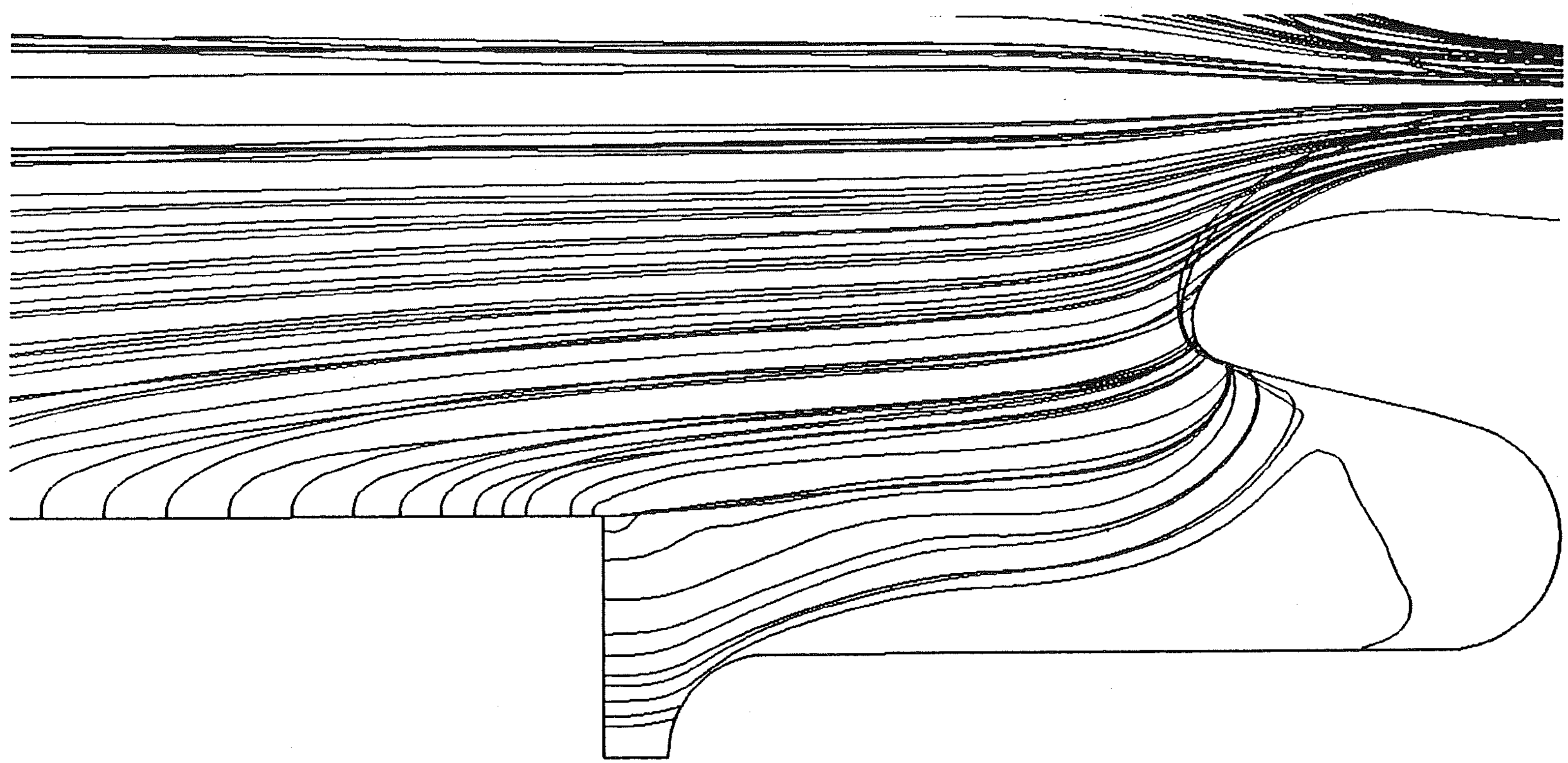

50 Micron Diameter Particle Trajectories
Spin Motor At 15 % Web Time

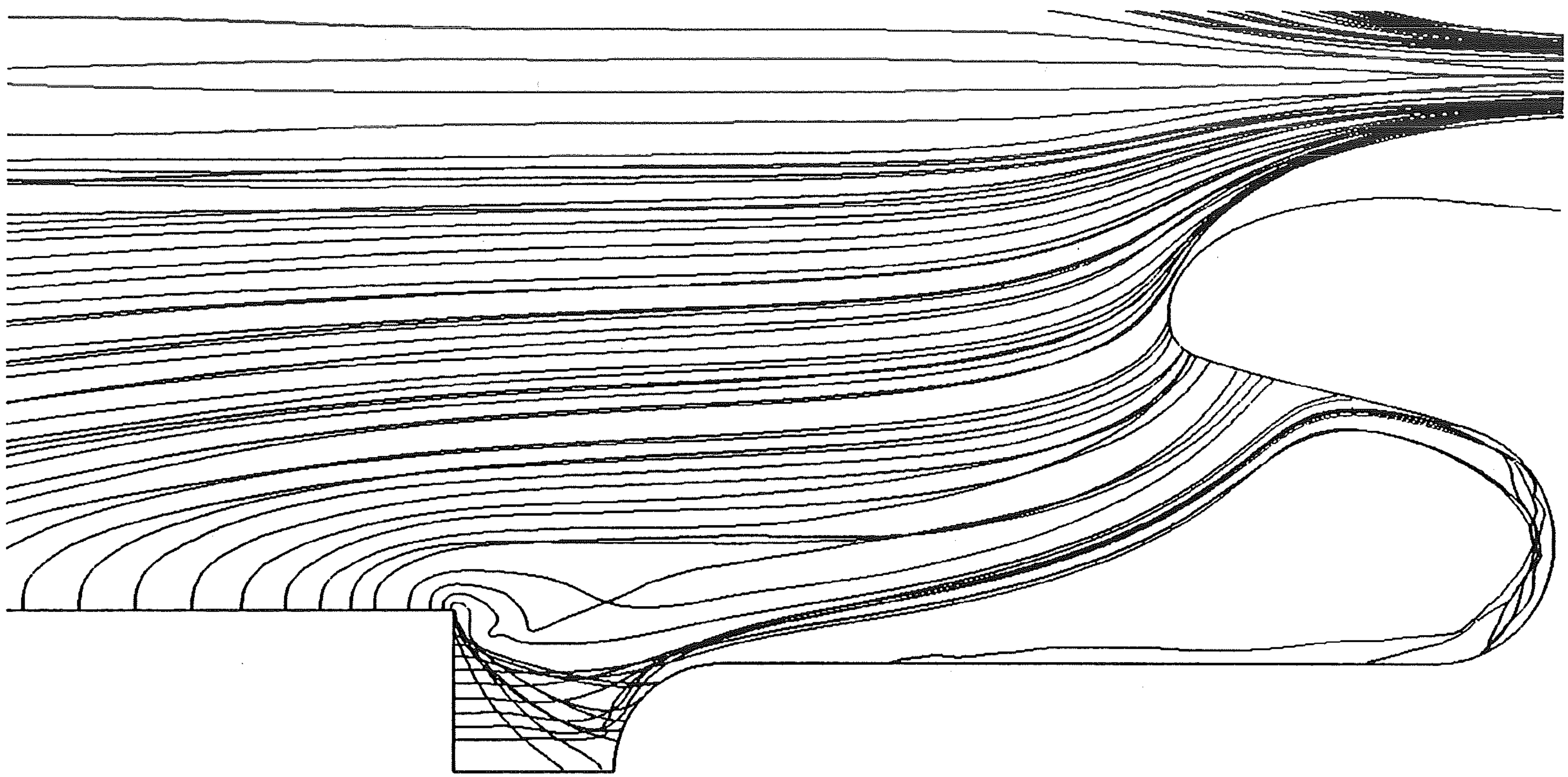

50 Micron Diameter Particle Trajectories

Spin Motor At 50 % Web Time

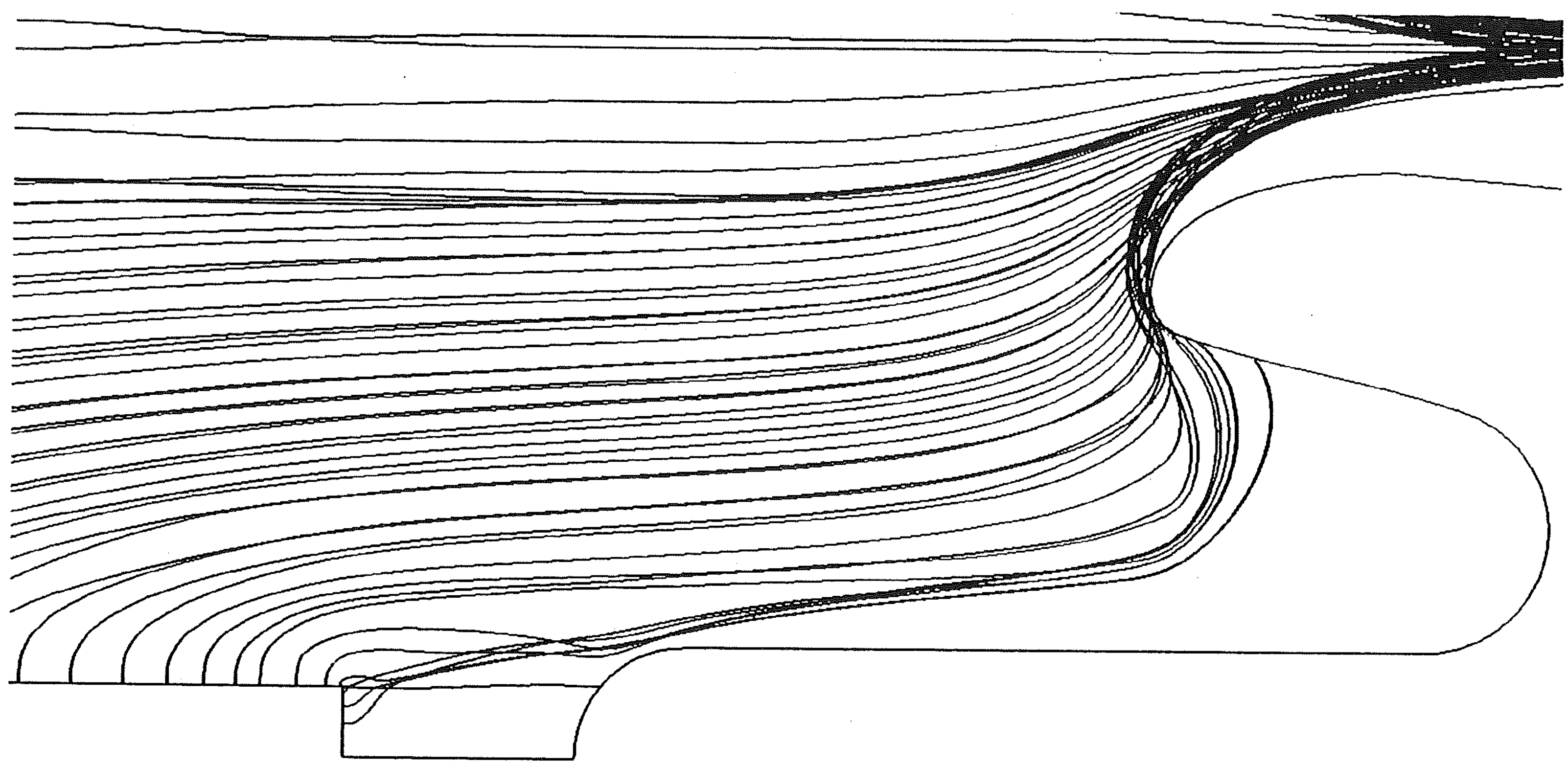

50 Micron Diameter Particle Trajectories

Spin Motor At 85 % Web Time

Nozzle Slag Accumulation Rate
WECCO AP, Surface Combustion, 400 rpm

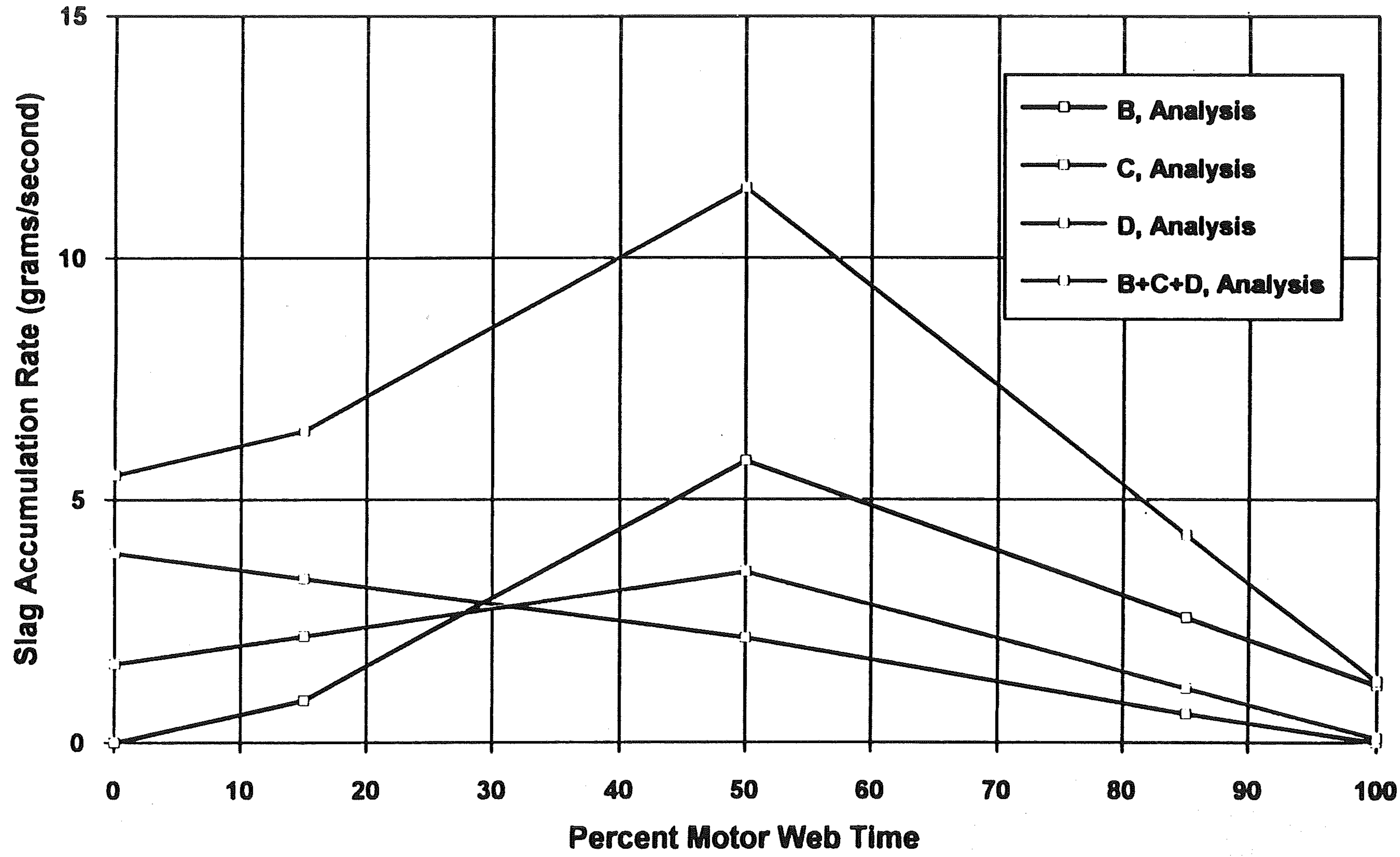

ERC, Inc.

Nozzle Slag Accumulation
WECCO AP, Surface Combustion, 400 rpm

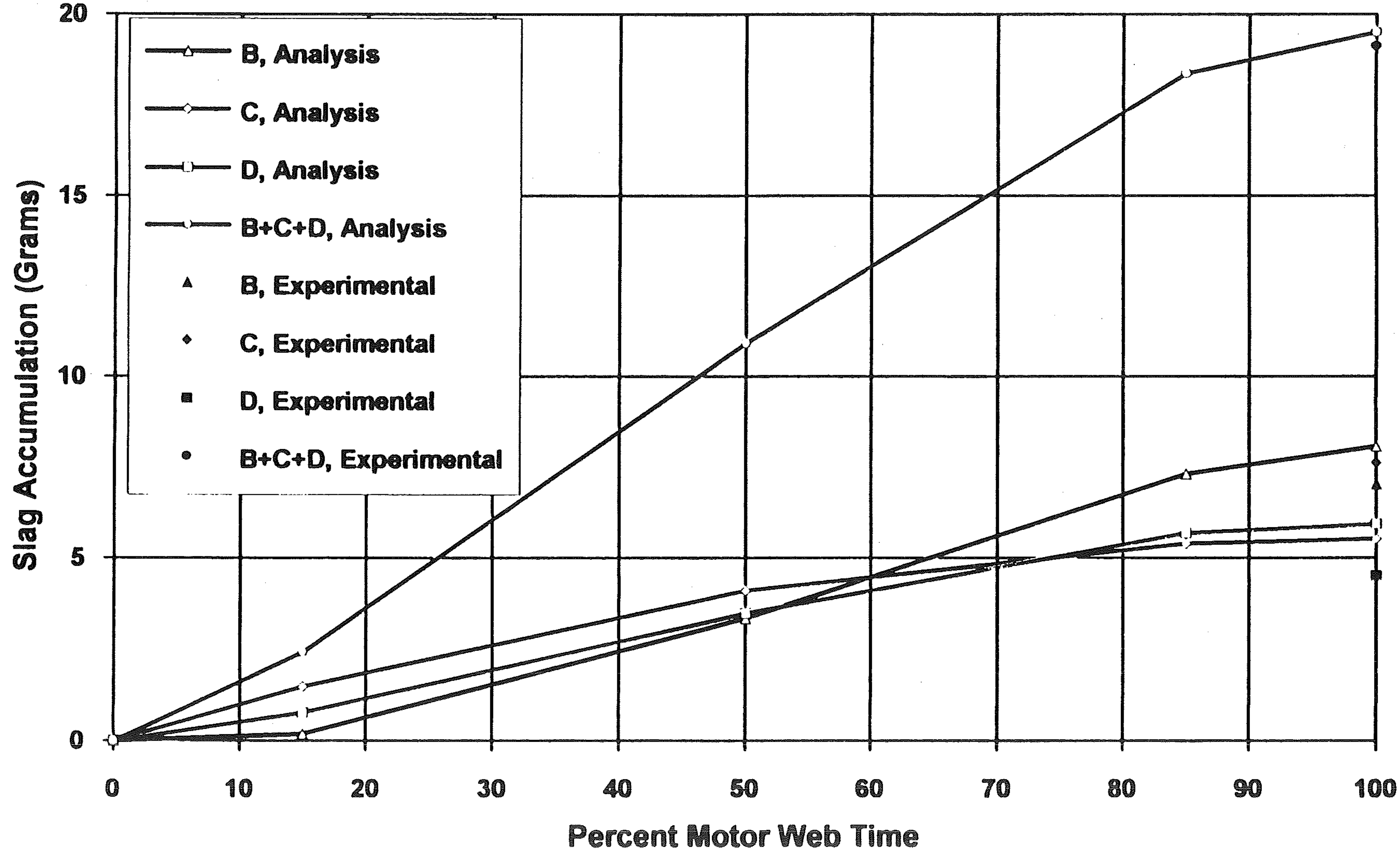

ERC, Inc.

FIVE INCH SPIN MOTOR SLAG DEPOSITS
CFD and Experimental

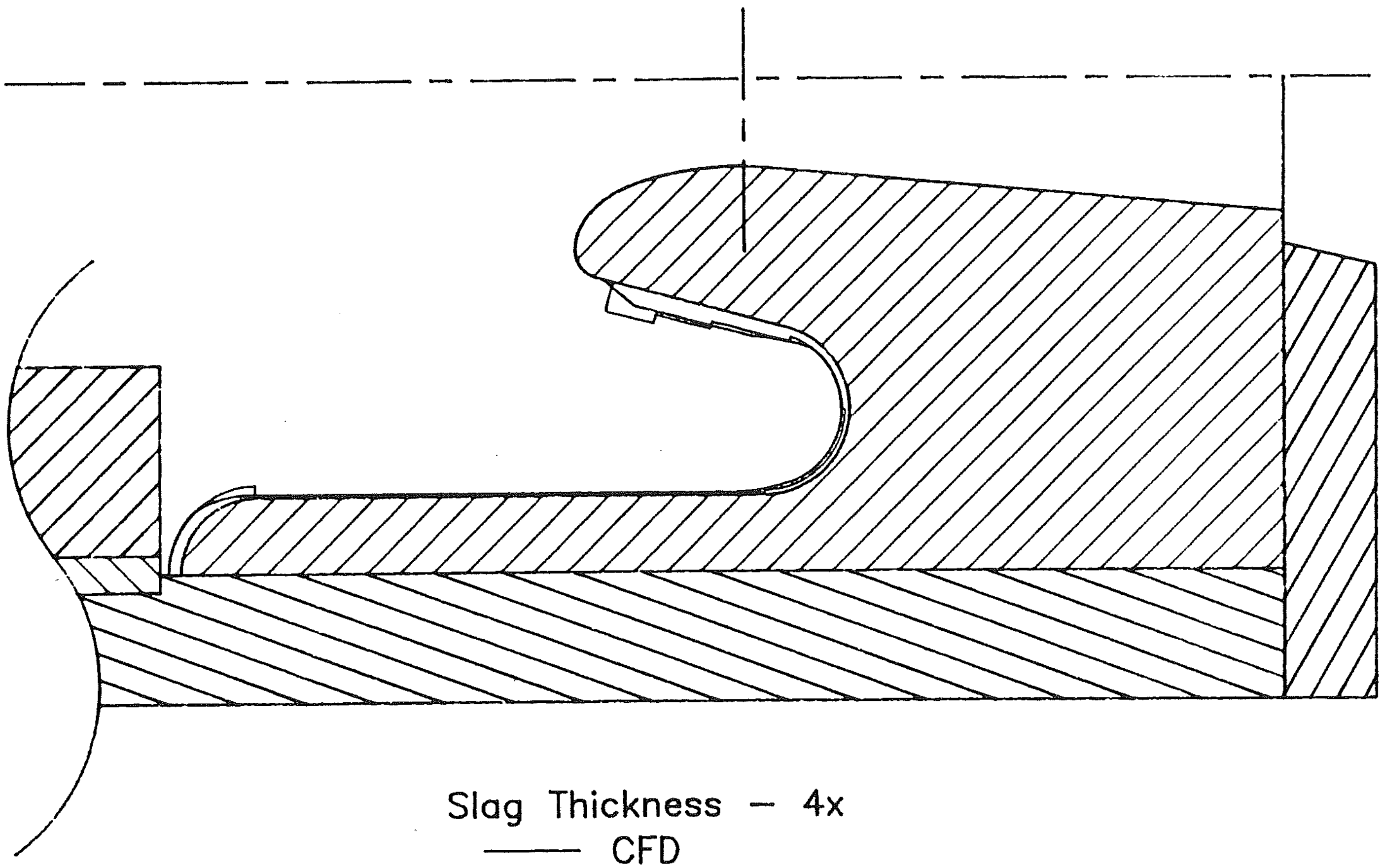

Slag Thickness — 4x
—— CFD
—— Experimental

ERC, Inc.

Slag Accumulation Per Unit Area Along The Nozzle
WECCO AP, Surface Combustion, 400 rpm

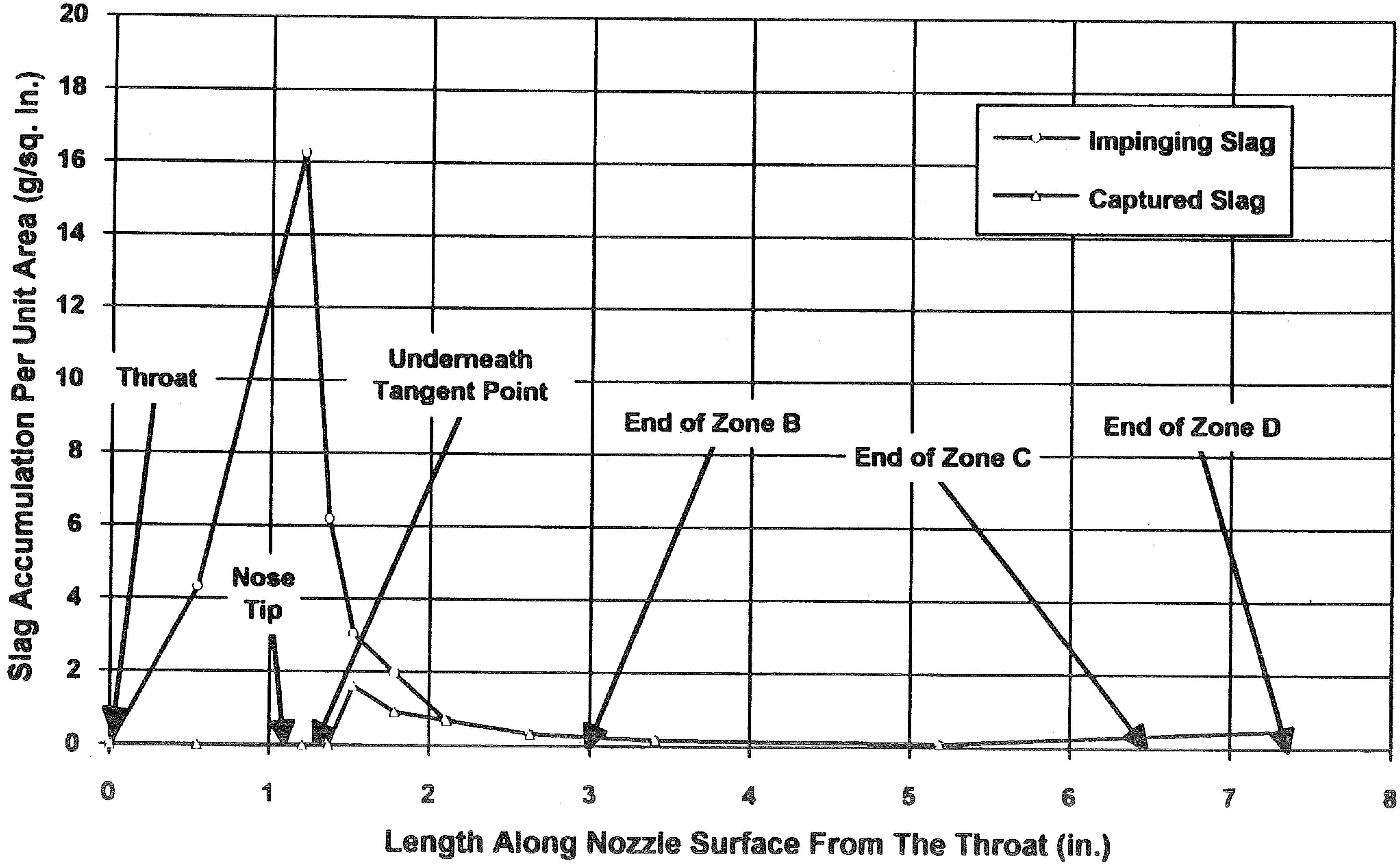

ERC, Inc.

NOZZLE NOSE SLAG DEPOSITS

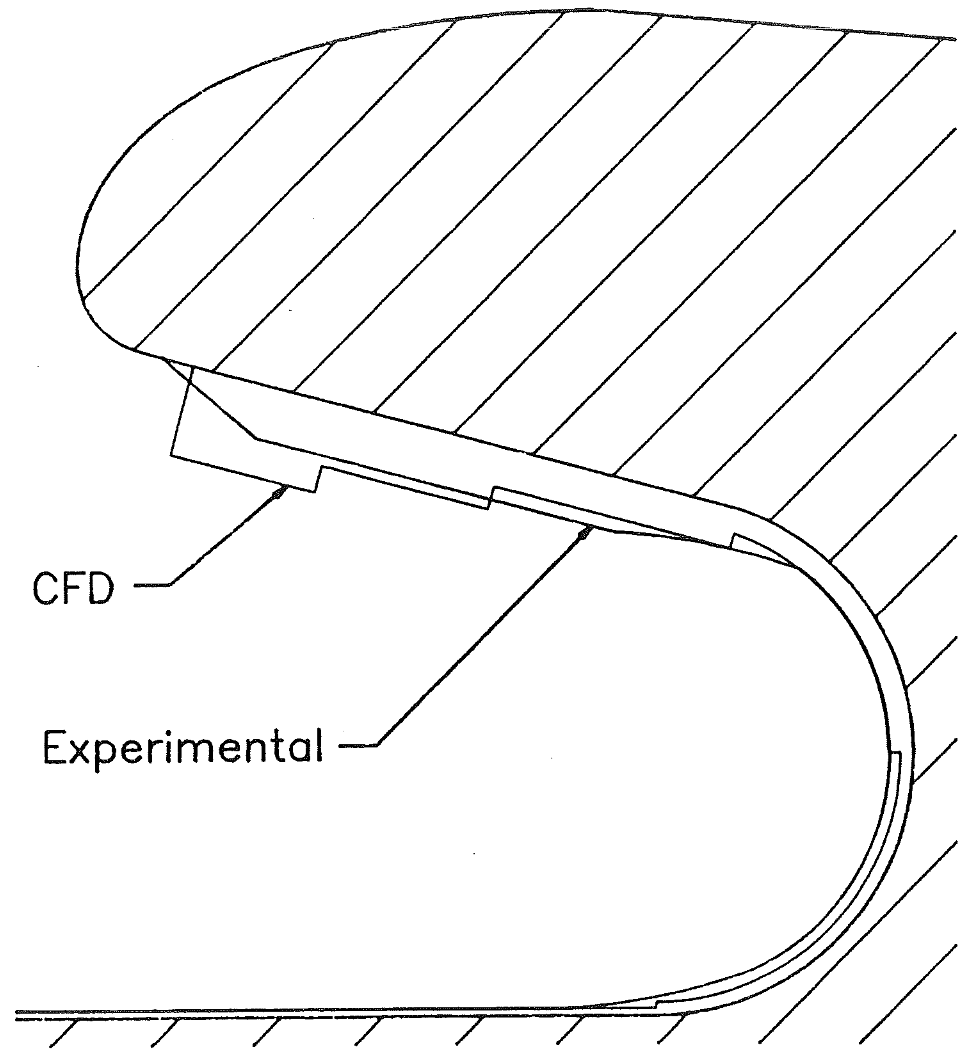

ERC, Inc.

NOZZLE FORWARD LIP SLAG DEPOSITS

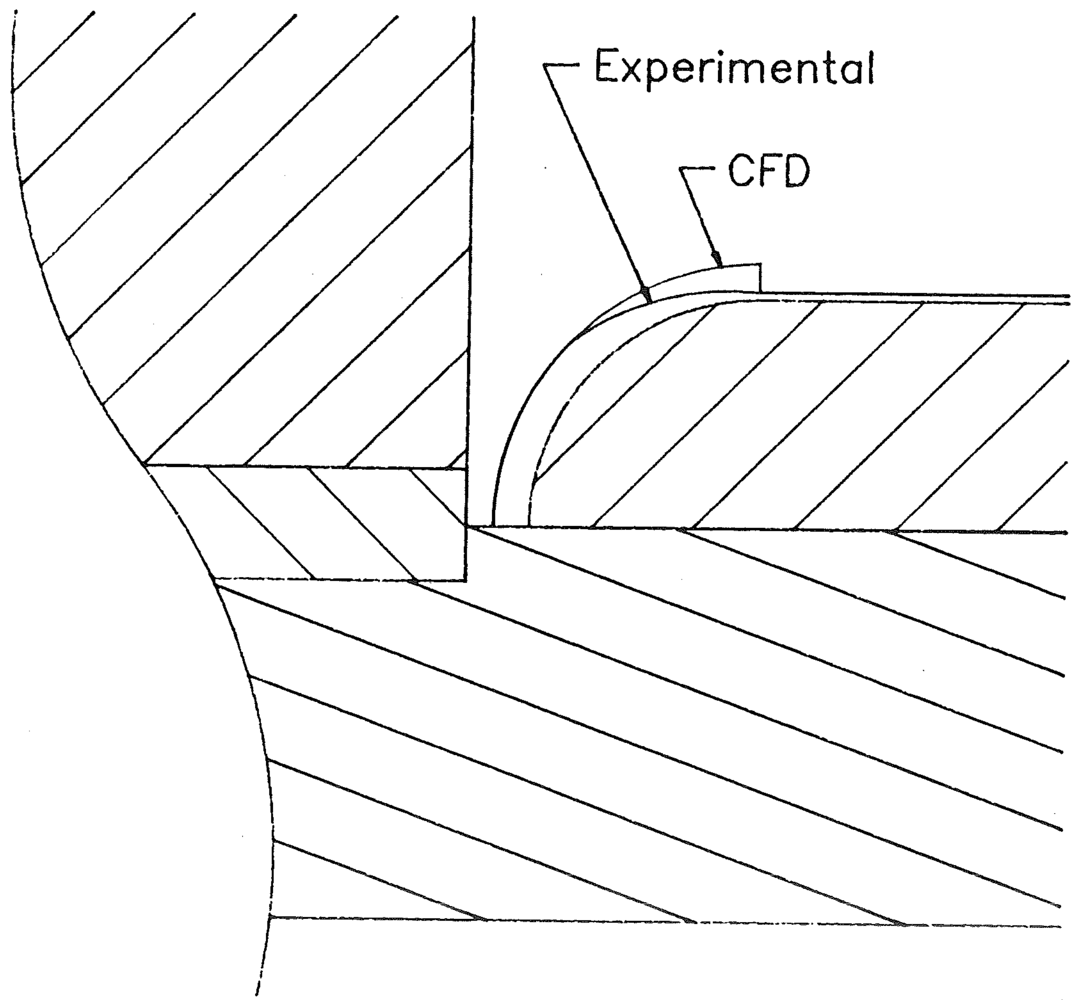

ERC, Inc.

Effect of Initial Particle Velocity on Slag Accumulation
WECCO AP, Surface Combustion, 400 rpm

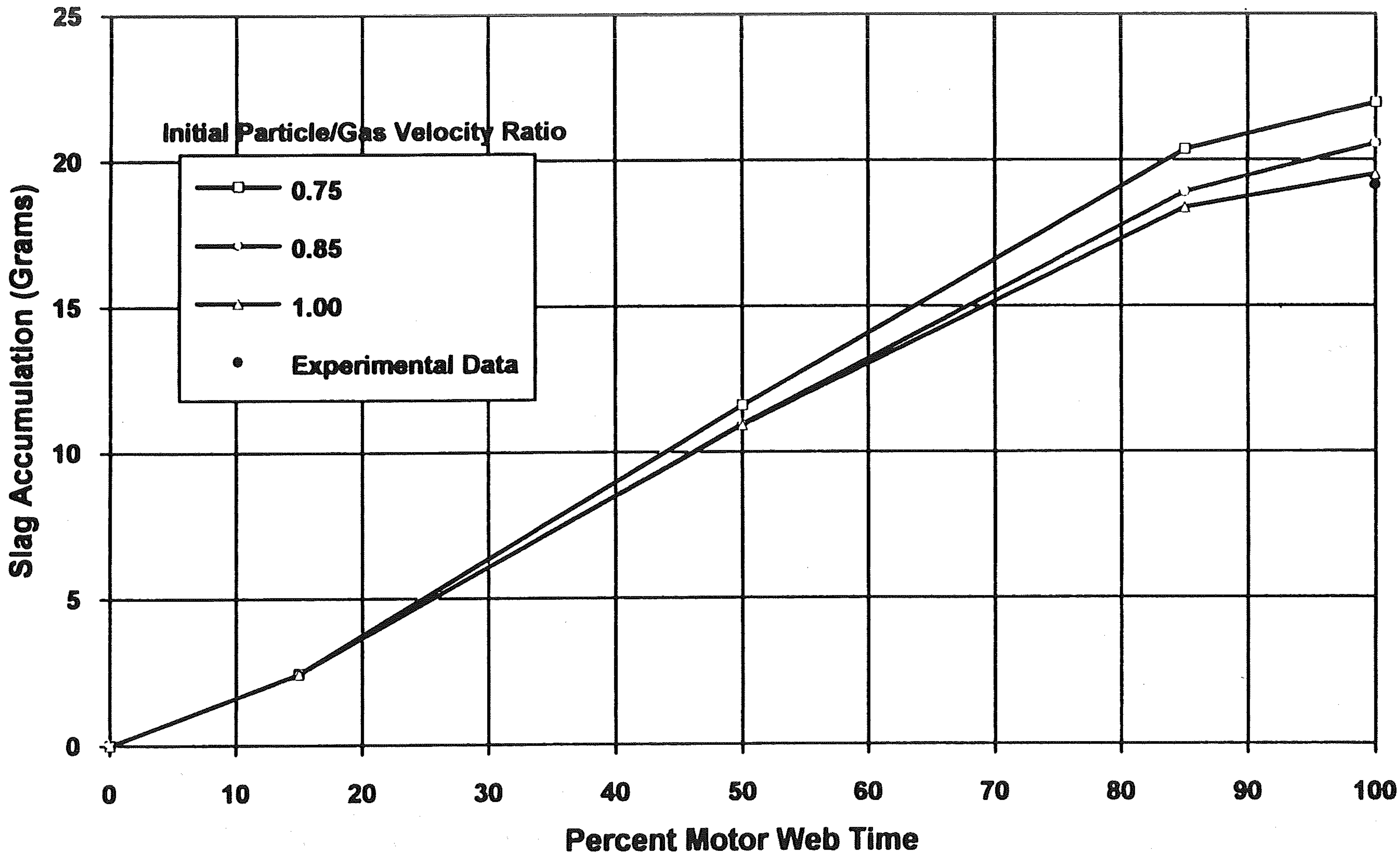

ERC, Inc.

Effect of Particle Density on Slag Impingement Rates
WECCO AP, Surface Combustion, 400 RPM
85% Web Time

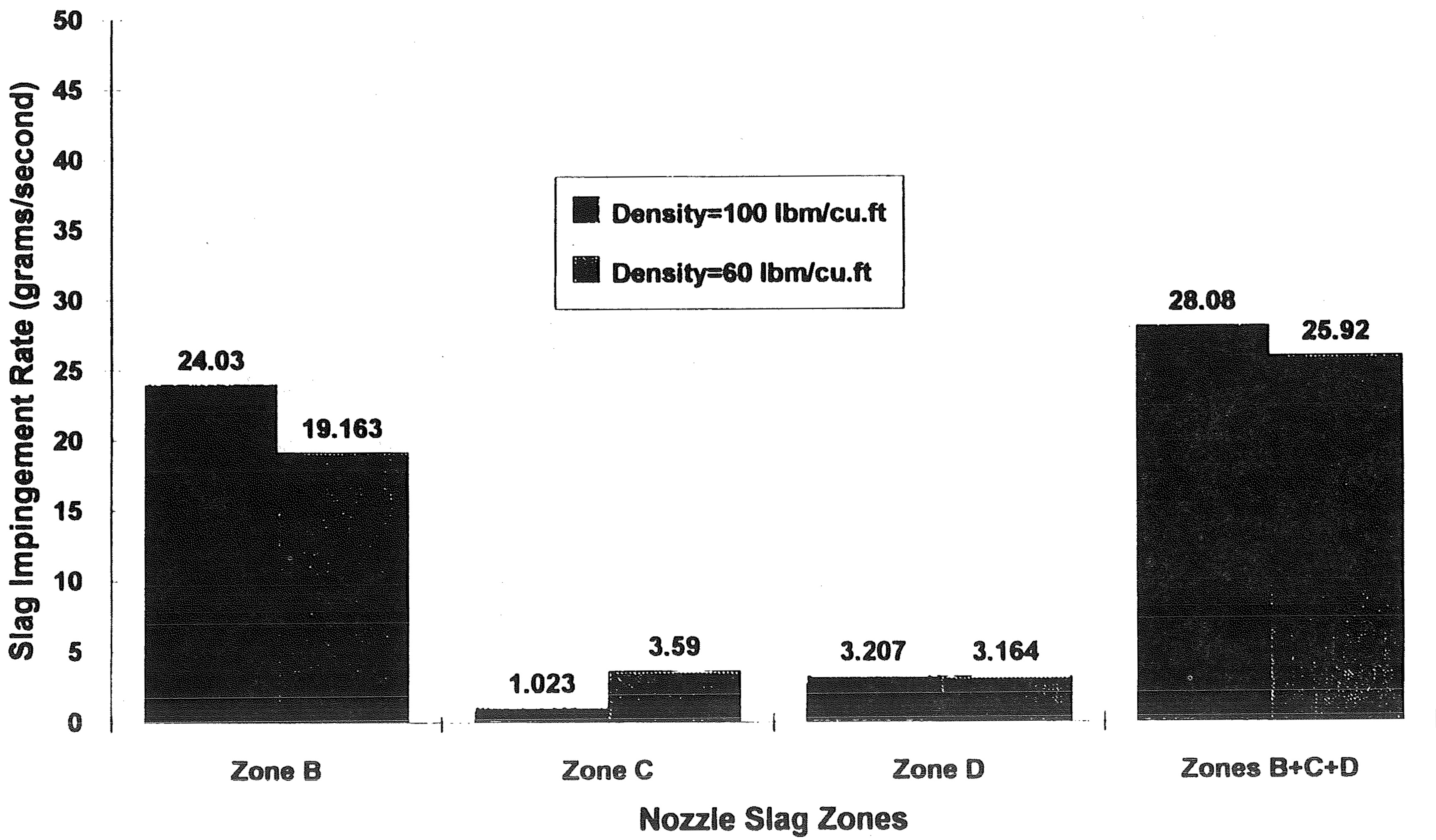

ERC, Inc.

Nozzle Slag Accumulation
WECCO AP, Distributed Combustion, 400 rpm

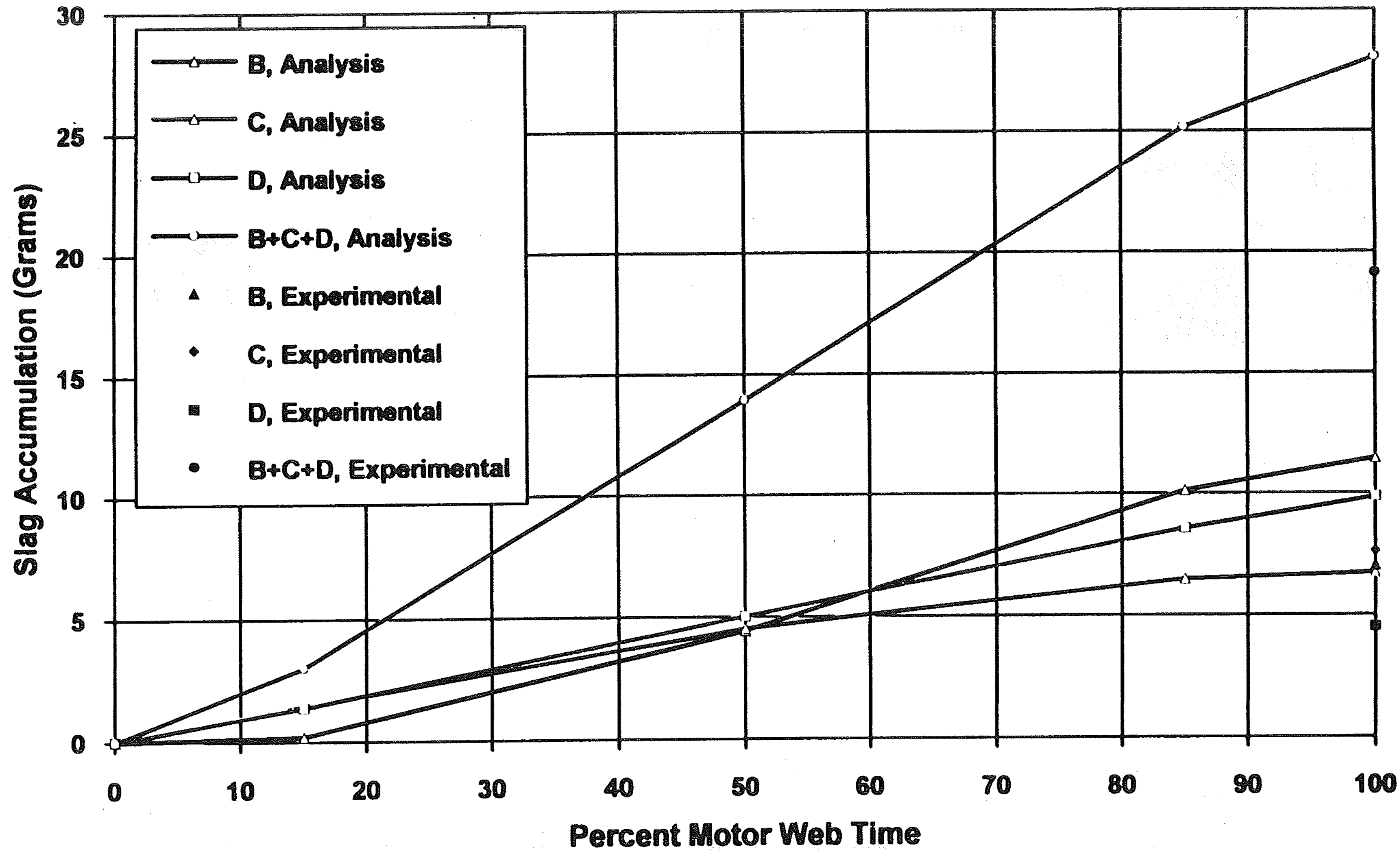

ERC, Inc.

Unburned Aluminum in Zone B
WECCO AP, Distributed Combustion, 400 rpm

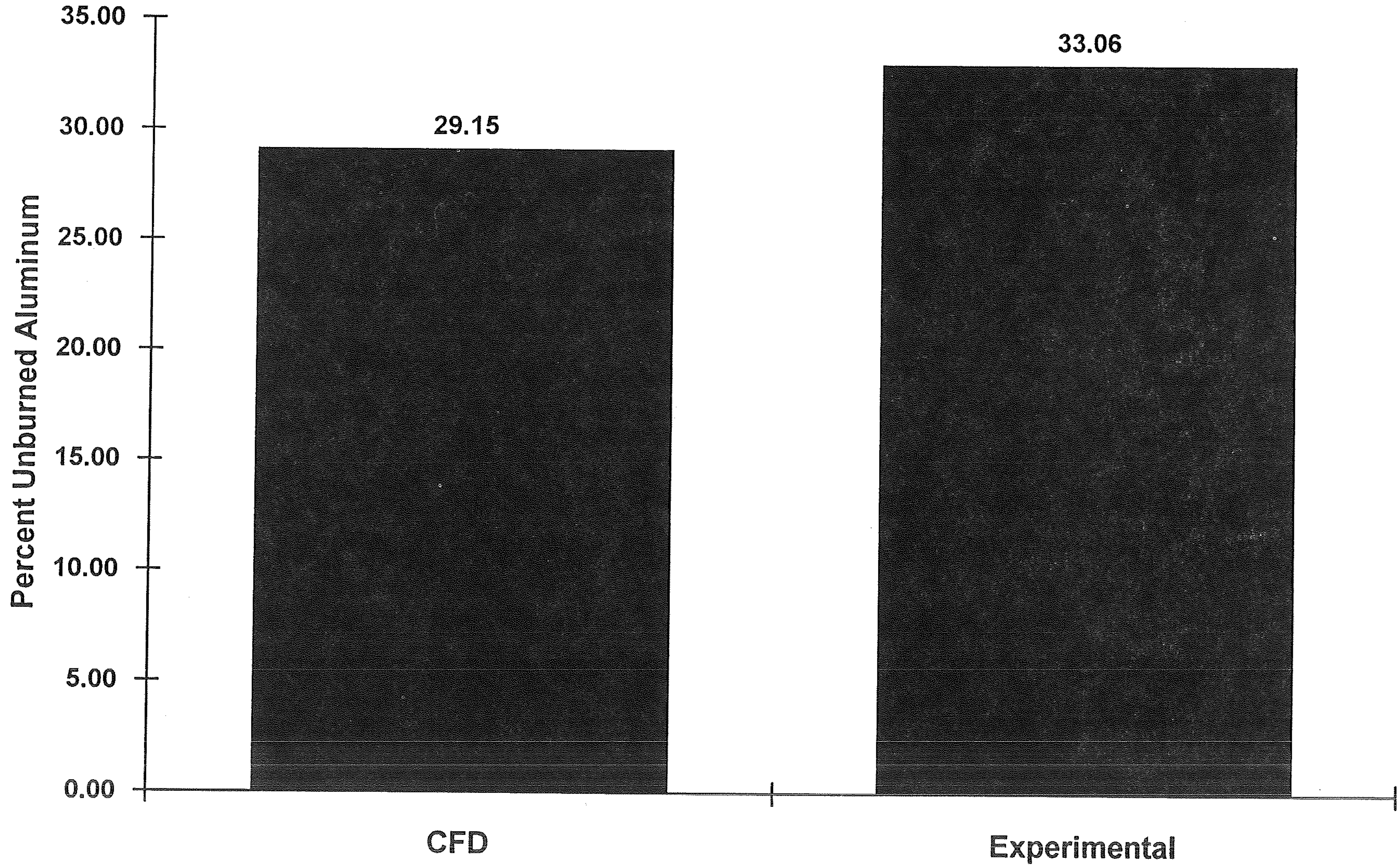

Conclusions

- The use of two-phase CFD analysis was highly successful indetermining in advance the viability of an experimental motor test program being designed to measure the propensity for slag production of propellants with various ingredient variations.
- A submerged nose nozzle design was successfully developed and motor test spin rate selected to maximize slag capture and retention weights using two-phase CFD.
- The two-phase CFD model for the 5-inch spin test motor proved to be a credible analysis tool in evaluation of the slag weight distributions in motor.
- The slag capture criteria is the most important factor in the prediction model for slag capture. Uncertainties in particle properties appear to be less important.

ERC, Inc.

Numerical Investigation of Slag Behavior for RSRM

P. Liaw ,Y-S Chen, H. Shang, amd M. Shih
Engineering Sciences, Inc., Huntsville, AL
and
D. Doran and E. Stewart
NASA MSFC, Huntsville, AL

S23-34
51398
132121
20p

ABSTRACT

It is known that the flowfield of the SRM (Solid Rocket Motor) is very complicated due to the complex characteristics of turbulent multi-phase flow, chemical reaction, particle combustion, evaporation, breakup and agglomeration etc. It requires multi-phase calculations, chemical reaction simulation, and particle combustion, evaporation, and breakup models to obtain a better understanding of thermophysics for the SRM design using numerical methods. Also, the slag buildup due to the molten particles is another factor affecting the performance of the SRM. Thus, a more realistic simulation is needed to provide a better design guide to improve the performance of SRM. To achieve this goal, the VOF (Volume Of Fluid) method is used to capture the free surface motion so as to simulate the accumulation of the molten particles (slag) of SRM. A Finite-rate chemistry model is used to simulate the chemical reaction effects. For multi-phase calculations, Hermsen combustion model is used for the AL particle combustion analysis and Taylor Analogy Breakup (TAB) model is used for the particle breakup analysis. An interphase mass-exchange model introduced by Spalding is used for the evaporation calculation. The particle trajectories are calculated using a one-step implicit method for several groups of particle sizes by which the drag forces and heat fluxes are then coupled with the gas phase equations.

The preliminary results predicted a reasonable physical simulation of the particle effects using a simple 2-D solid rocket motor configuration. It shows that the AL/AL2O3 particle sizes are reduced due to the combustion, evaporation, and breakup. The flowfield is disturbed by the particles. Mach number distributions in the nozzle are deformed due to the effect of particle concentrations away from the center line.

The RSRM (Redesigned Solid Rocket Motor) geometry at 67 seconds is employed to investigate the slag behavior in the aft-end cavity with the combustion, evaporation, and breakup models. The particulate phase was assumed to be aluminum oxide (AL2O3) for the preliminary study. It is assumed that the propellant grain of the aft-end cavity has burned out completely at 67 seconds. The geometry and mass flow rate information were provided by the NASA Marshall Space Flight Center. The slag may flow out of the cavity and enter the nozzle due to the accelerations. The molten particles entering the aft-end cavity merge with the slag. The volume of the slag will grow and affect the performance of the RSRM. This shows that the effects of particles and slag on the flowfield are very significant. From the caculation, a flow vortex exists in the aft-end cavity of the RSRM. A stagnation point on the wall is captured. This flow impingement may cause the erosion of the wall. The shape of the vortex is changed due to the slag. The particles entering the cavity may become slag and either flow into or out of the cavity depending on the temperature and the surface tension of the molten particles. An axial gravity force of 2.4g is assumed to simulate the RSRM flowfield at 67 seconds.

The flowfield analysis using the FDNS code in the present research using the proposed models should provide a design guide for the solid rocket motors. The obtained results can give the designer a basic guide line for the use of materials and the nozzle geometry to improve the performance of SRMs.

Numerical Investigation of Slag Behavior for RSRM

P. Liaw, Y. S. Chen, H. M. Shang, and M. Shih
Engineering Sciences, Inc.

and

D. Doran and E. Stewart
ED32, NASA Marshall Space Flight Center

13th Workshop for CFD Applications in Rocket Propulsion

April 25-27, 1995

OBJECTIVE

1. BACKGROUND AND GENERAL APPROACH
2. NUMERICAL METHOD
3. APPLICATION
4. CONCLUSIONS
5. FOLLOWING WORK

BACKGROUND & GENERAL APPROACH

- ACCUMULATED SLAG WAS FOUND IN THE AFT-END CAVITY AND NOZZLE.

  ==> WILL THIS AFFECT THE MOTOR PERFORMANCE DUE TO ITS EFFECT ON THE PRESSURE?

- WILL VOF METHOD WORK FOR THE ANALYSIS OF SLAG BEHAVIOR?

THE ASRM

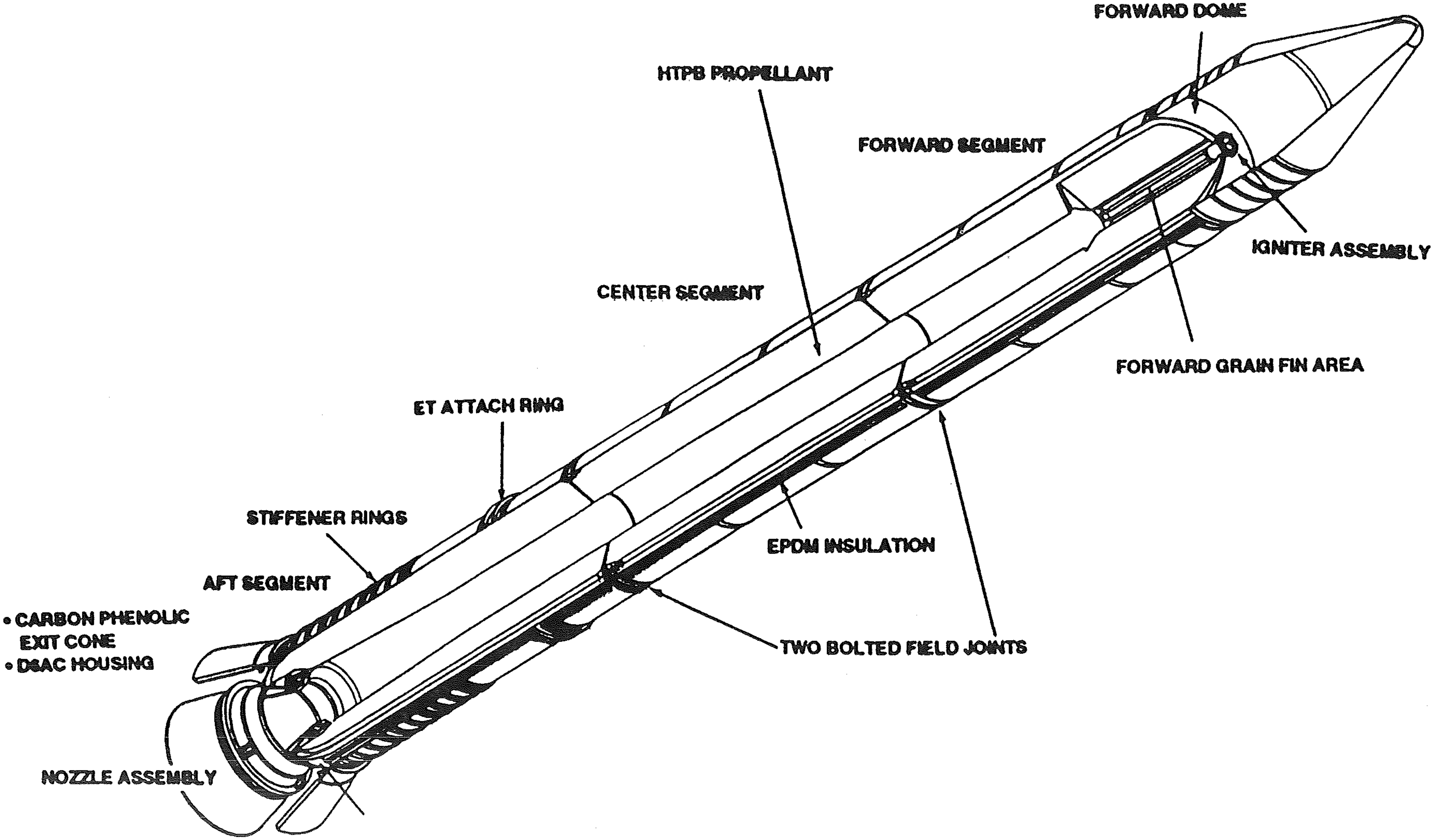

ESI Engineering Sciences, Inc.

VOF Model

The VOF transport equation is given below:

$$\frac{\partial \alpha}{\partial t} + \left(u - u_g\right)_i \frac{\partial \alpha}{\partial x_i} = S_\alpha$$

where α = 1 stands for liquid and α = 0 is for gas. The interface is located at 1 > α > 0. For a given solution of α field, equation (6) can be recast as:

for compressible gas:

$$\frac{\partial \rho_m \phi}{\partial t} + \frac{\partial \rho_m \left(u - u_g\right)_i \phi}{\partial x_i} = S_\phi \, , \alpha < 0.01$$

for incompressible gas:

$$\rho_m \frac{\partial \phi}{\partial t} + \rho_m \left(u - u_g\right)_i \frac{\partial \phi}{\partial x_i} = S_\phi \, , \alpha \geq 0.0$$

and

$$\rho_m = Max\left\{\rho_g , \alpha \rho_\ell\right\}$$

The interface α solution compression procedure is expressed as:

$$_{new} = Max\left\{0, Min\left[1, 0.5 + f\left(\alpha_{old} - 0.5\right)\right]\right\}$$

and

$$f = \frac{(Interface\ volume)_{new}}{(Interface\ volume)_{initial}}$$

The surface tension forces in the continuum surface force model is formulated as continuous body forces across the interface. These forces can be written as:

$$F_x = -\sigma\left(\nabla \hat{n}\right)\alpha_x$$

$$F_y = -\sigma\left(\nabla \hat{n}\right)\alpha_y + \left(\frac{|\alpha_y|}{y}\right), for\ 2D, axisymmetric\ case\ only$$

$$F_z = -\sigma\left(\nabla \hat{n}\right)\alpha_z, \quad for\ 3D\ case\ only$$

where

= surface tension constant

$$\nabla \hat{n} = \hat{\alpha}_{xx} + \hat{\alpha}_{yy} + \hat{\alpha}_{zz}$$

α is 0.5 for the free surface. The VOF method is used to represent the tracking of the free surface between the liquid and gas phase.

APPLICATIONS

SLAG BEHAVIOR ANALYSIS FOR RSRM CONFIGURATION AT 67 SECONDS

(1) NO PRE-ACCUMULATED SLAG IN THE AFT-END CAVITY
--- 2D AND 3D

(2) ASSUMED PRE-ACCUMULATED SLAG IN THE AFT-END CAVITY
--- 2D

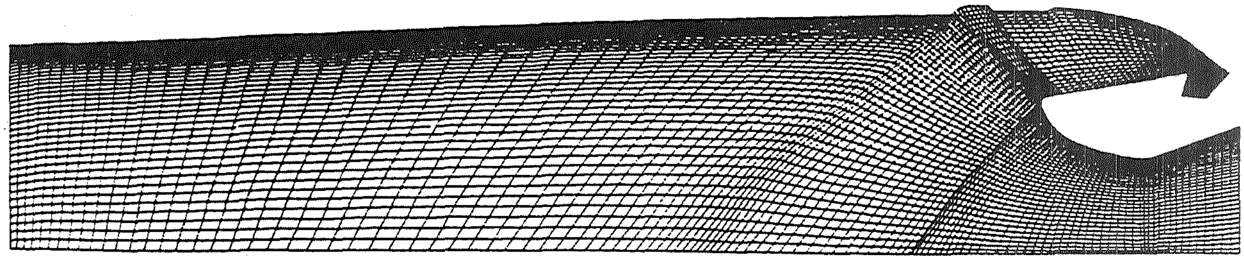

2D Grid system of RSRM configuration.

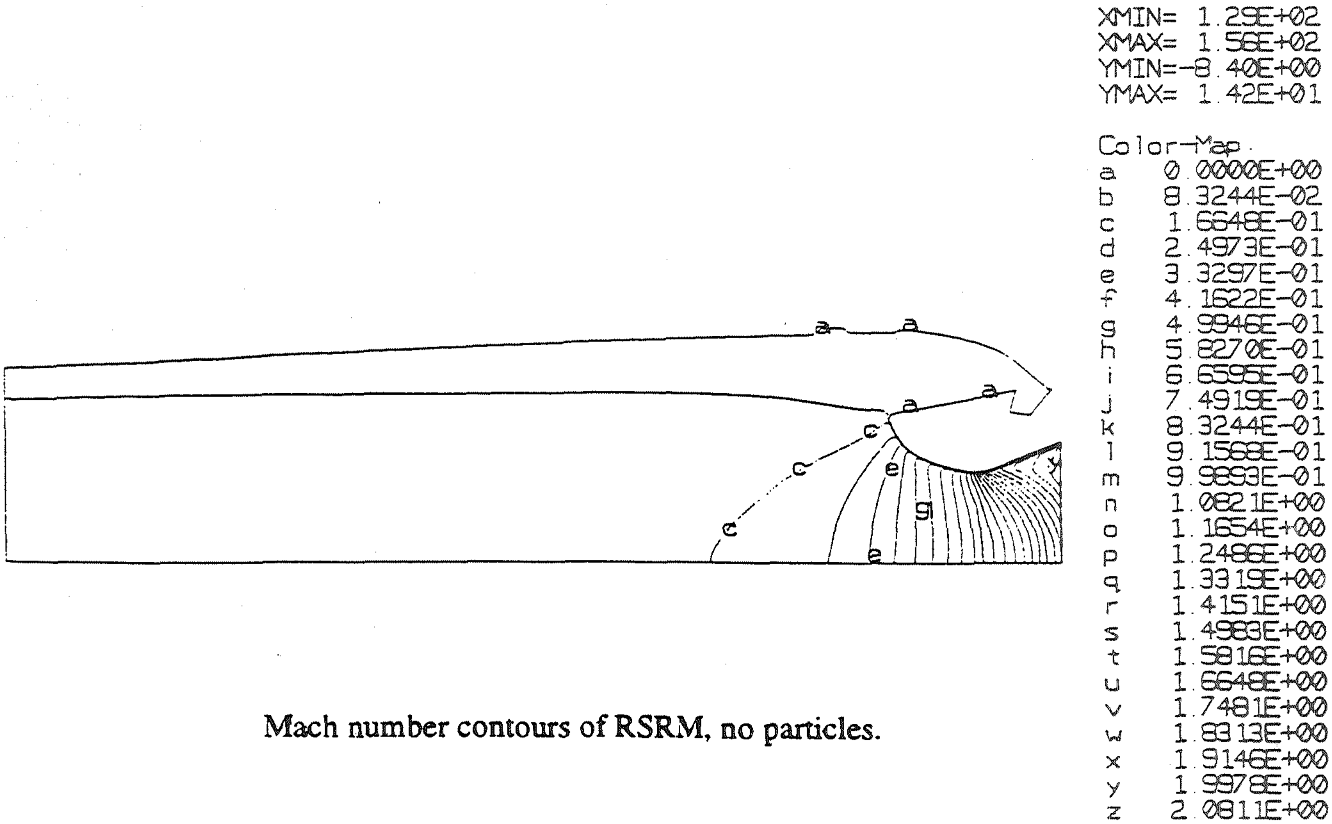

Mach number contours of RSRM, no particles.

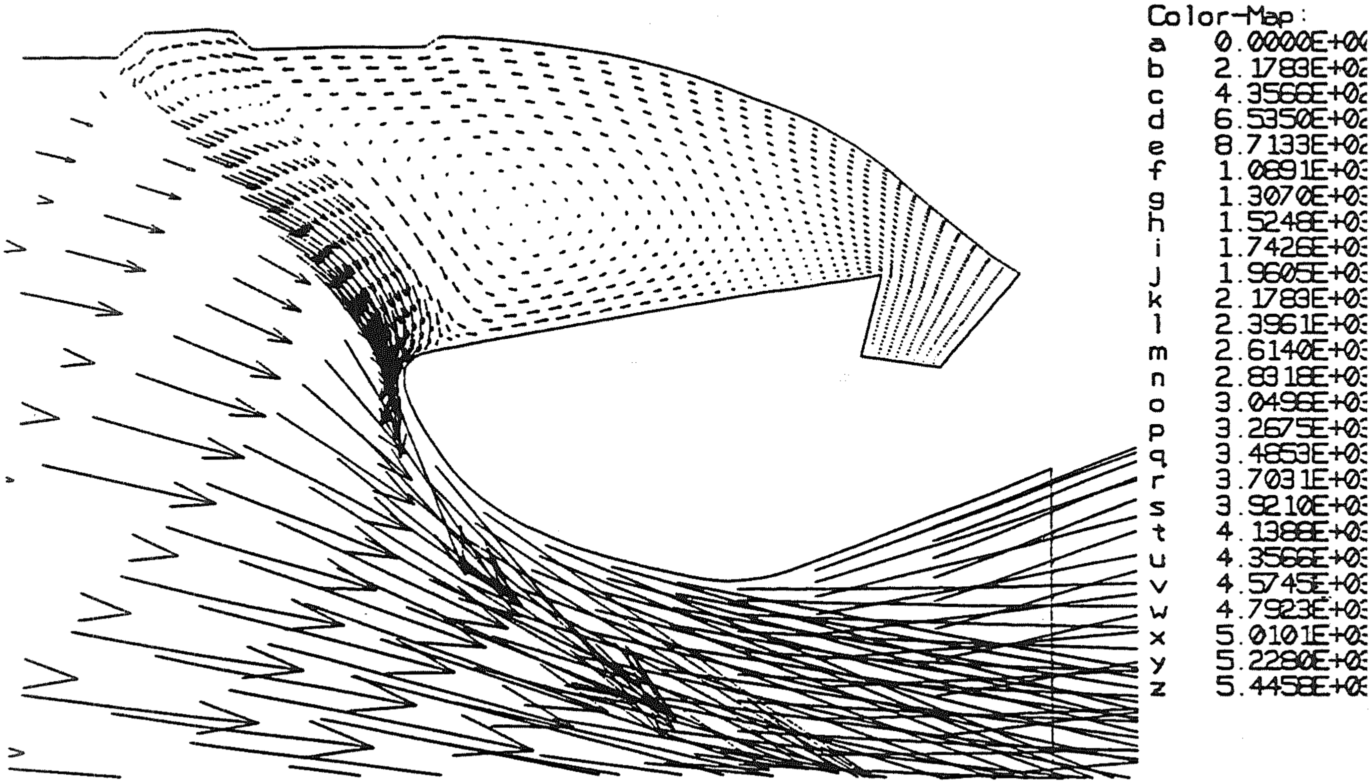

Velocity vectors near the aft-end cavity, no particles.

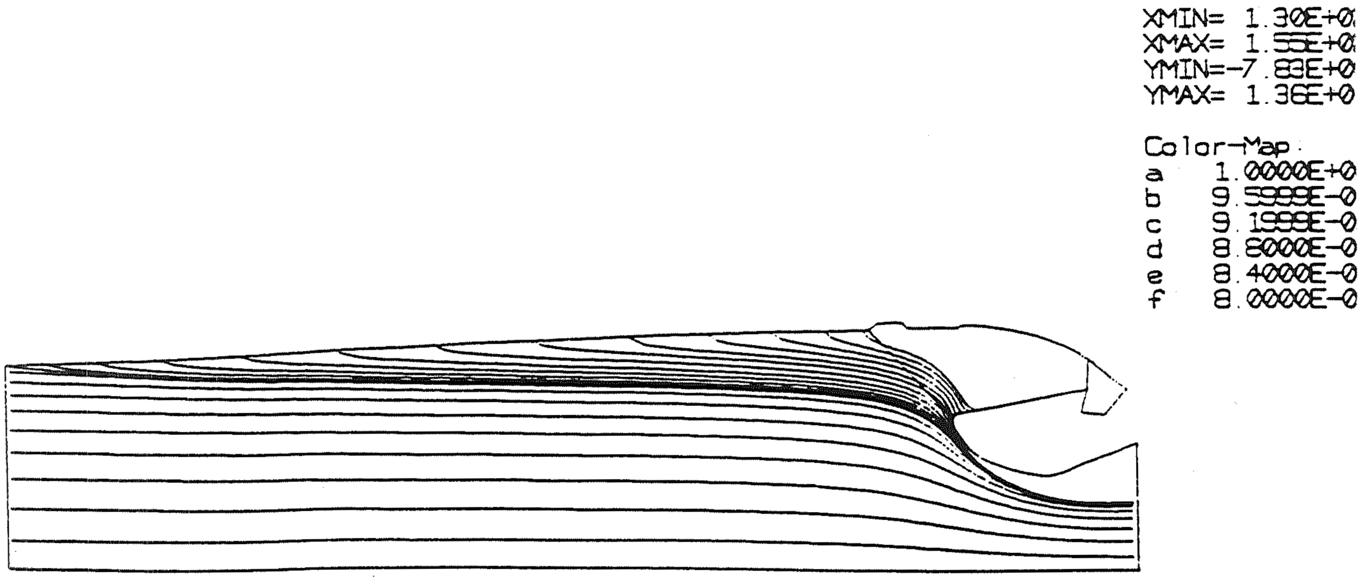

Particle trajectories.

Slag accunulation in the aft-end cavity

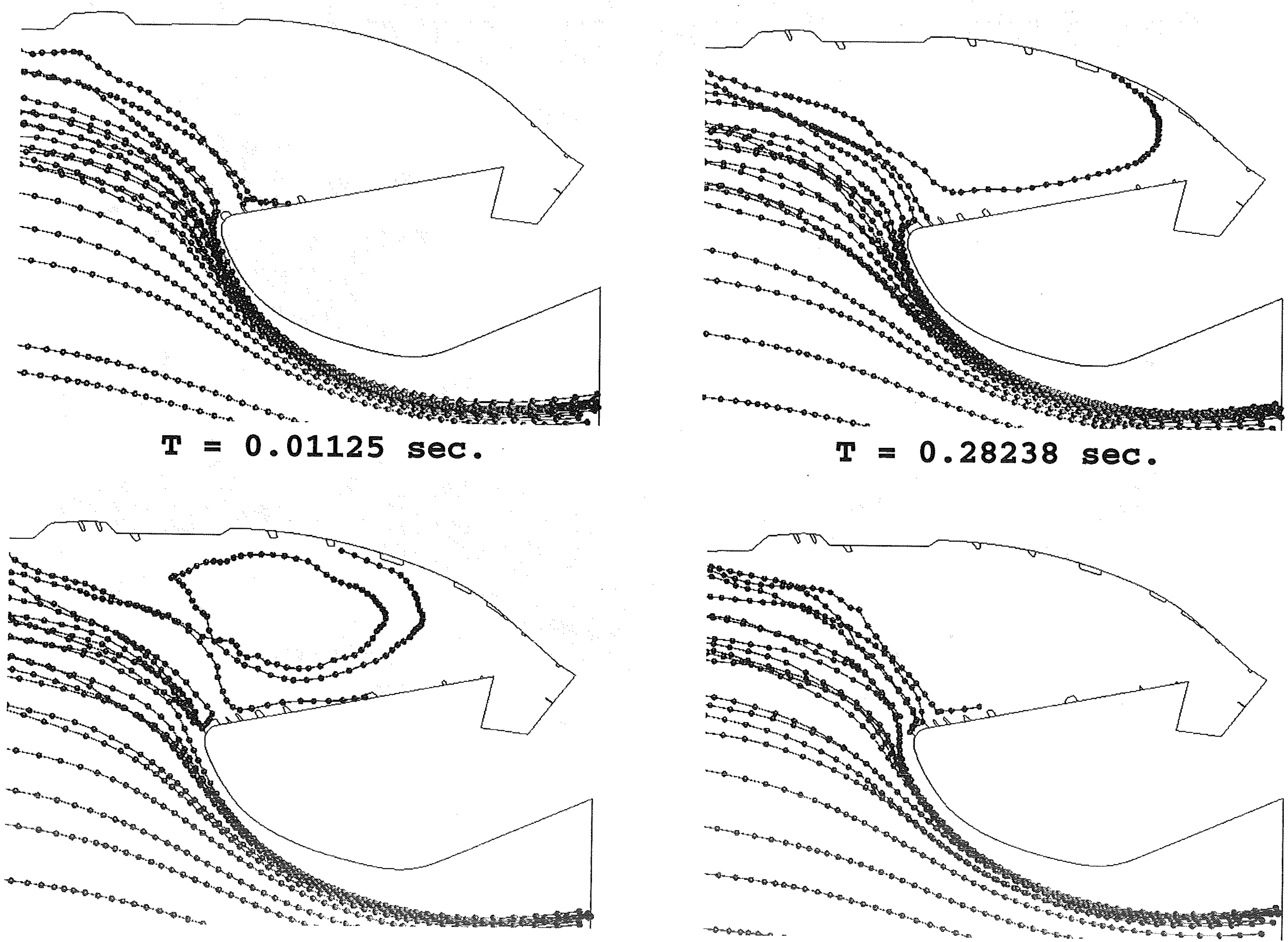

Slag accumulation at T = 2.3144 sec.

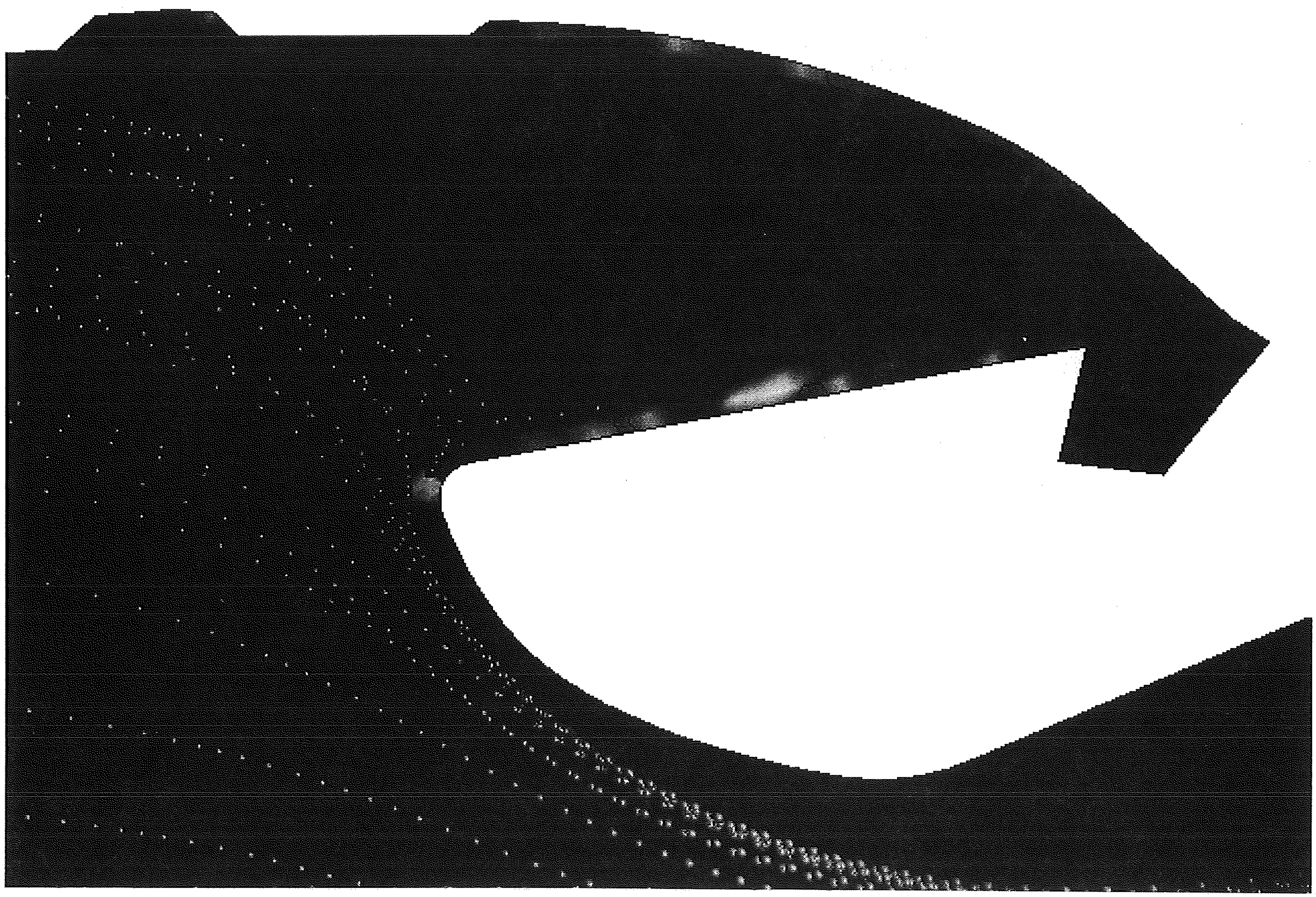

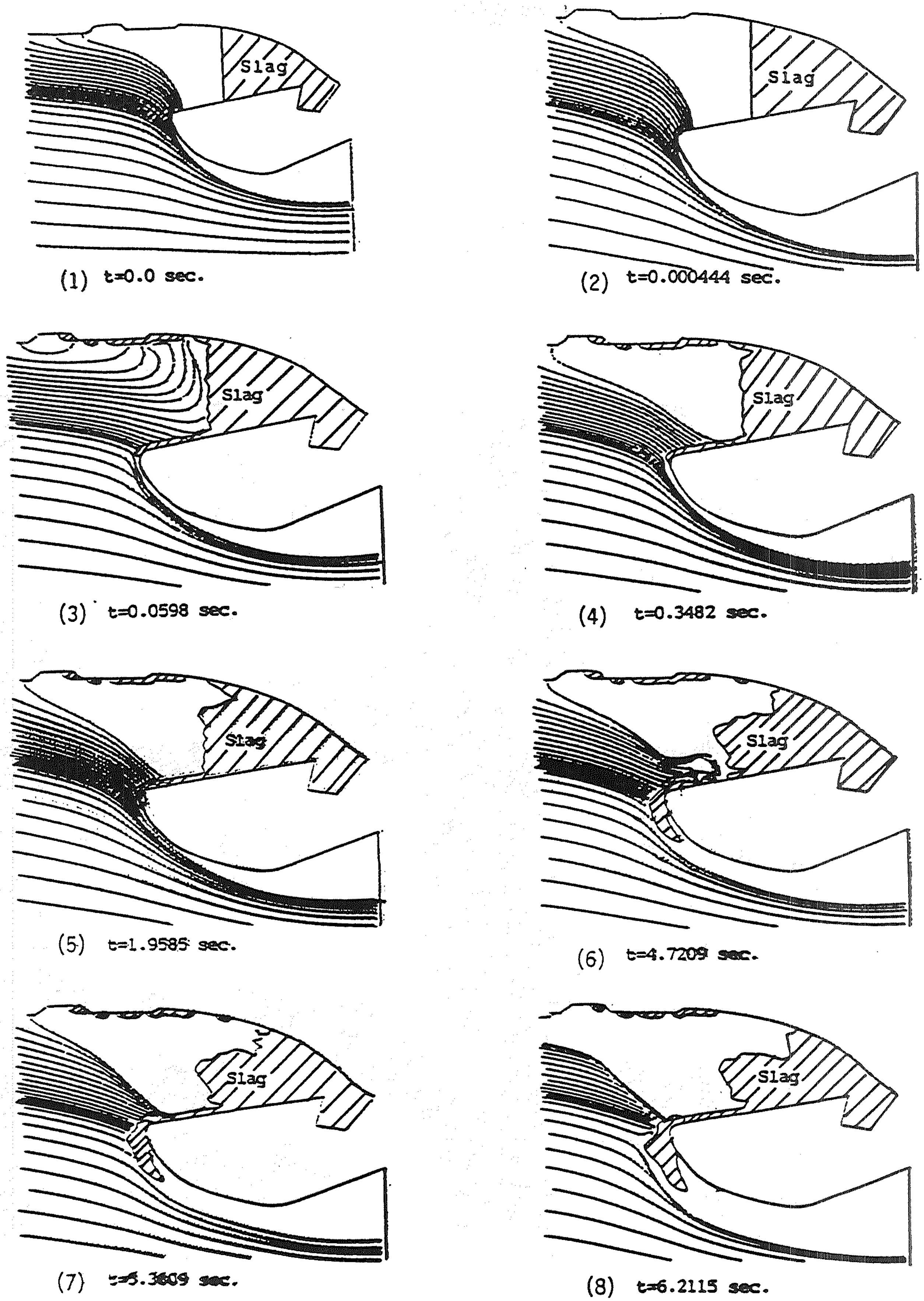

Slag buildup history in the aft-end cavity.

Slag Accumulation for 3D RSRM at T = 0.031687

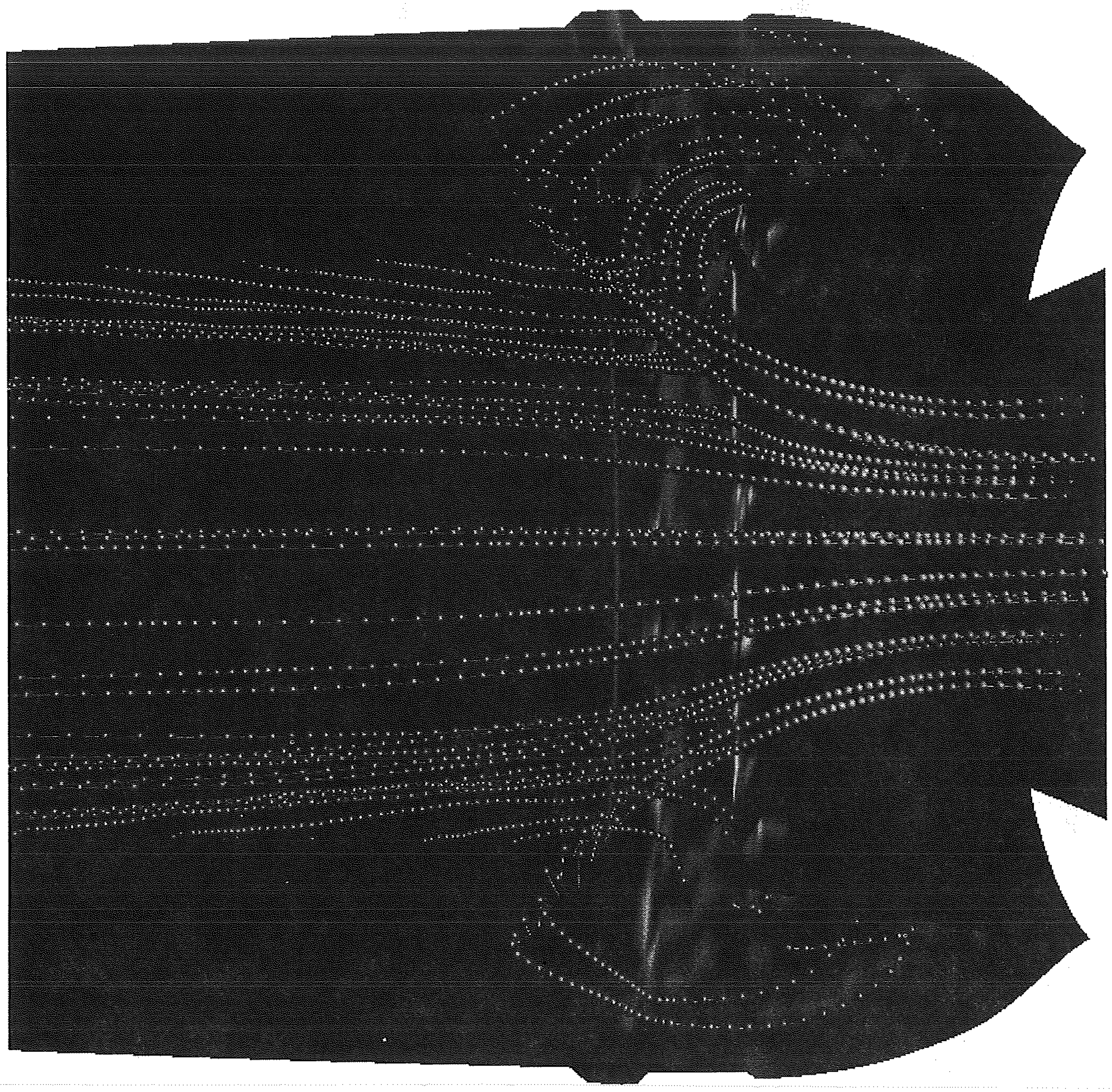

Slag Accumulation for 3D RSRM at T = 0.031687

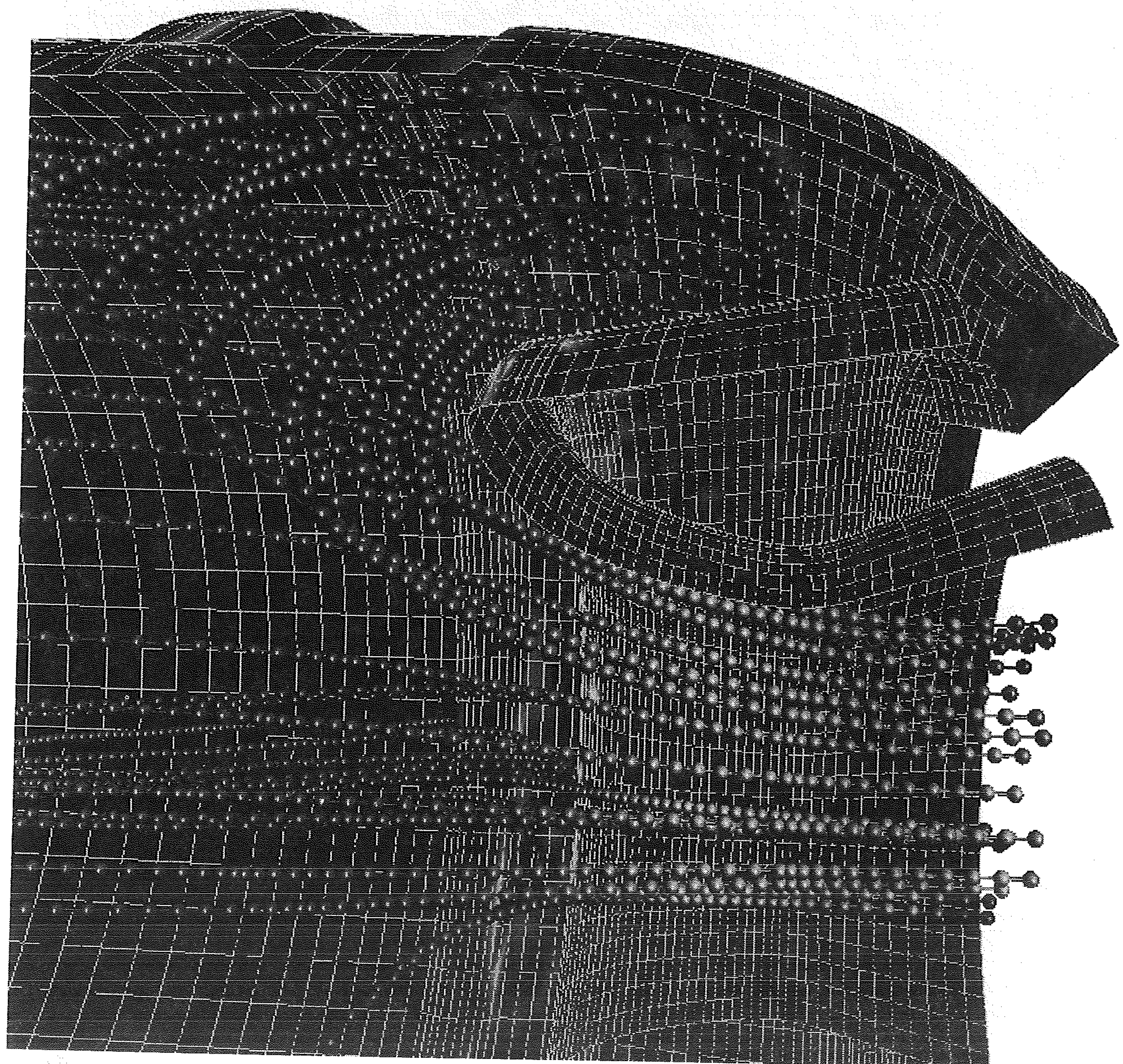

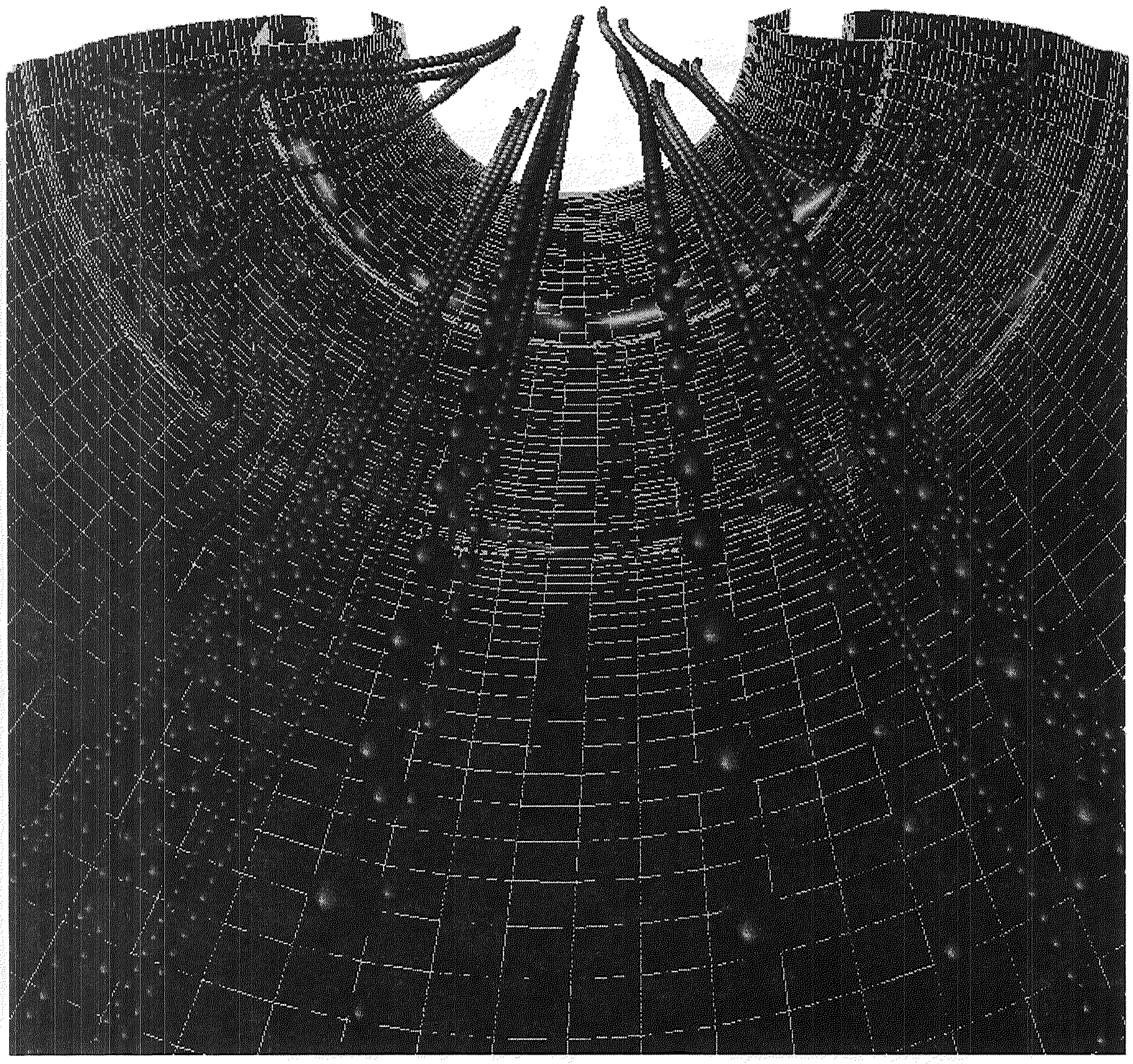

Slag Accumulation for 3D RSRM at T = 0.031687

Slag Accumulation for 3D RSRM at T = 0.031687

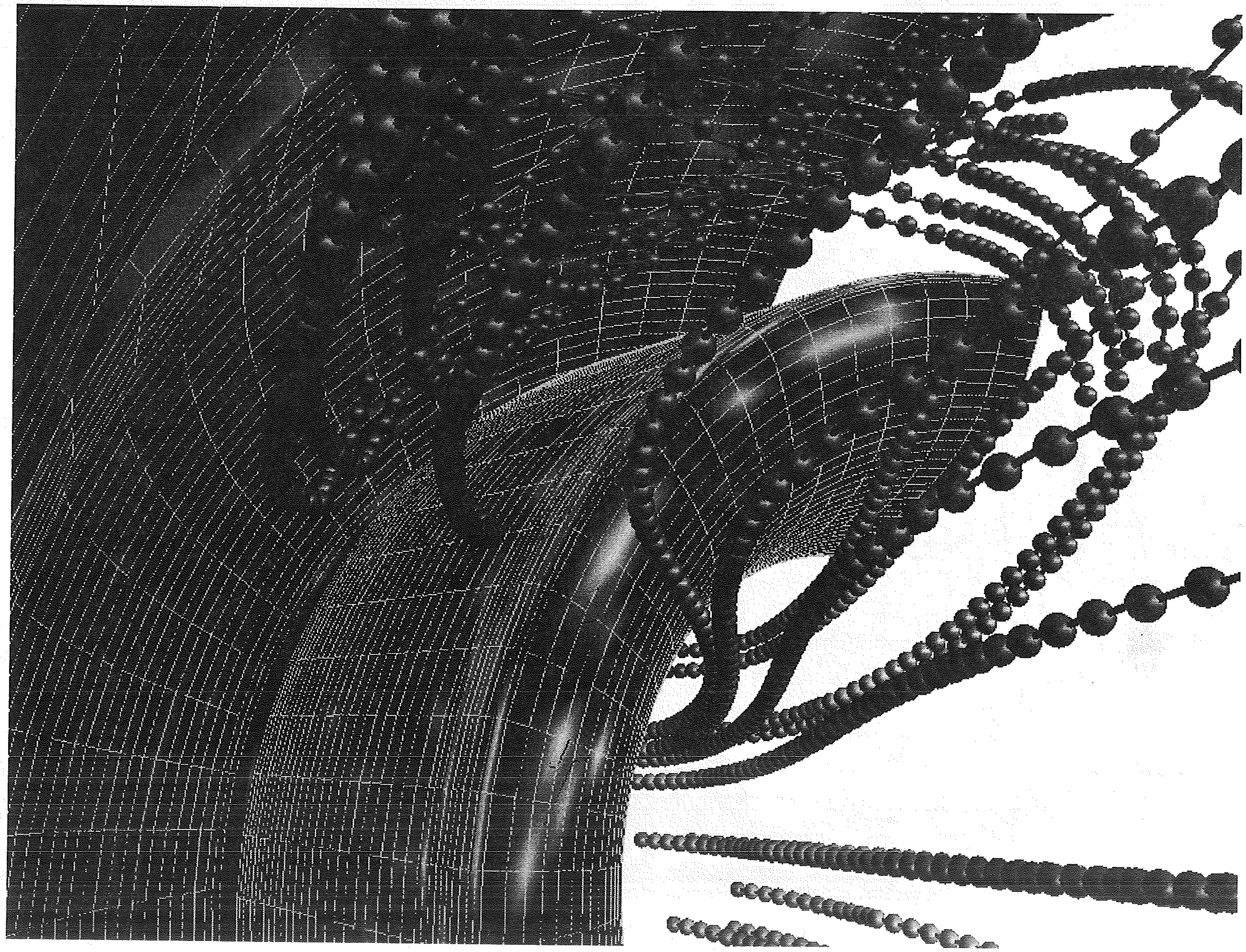

Slag Accumulation for 3D RSRM at T = 0.031687

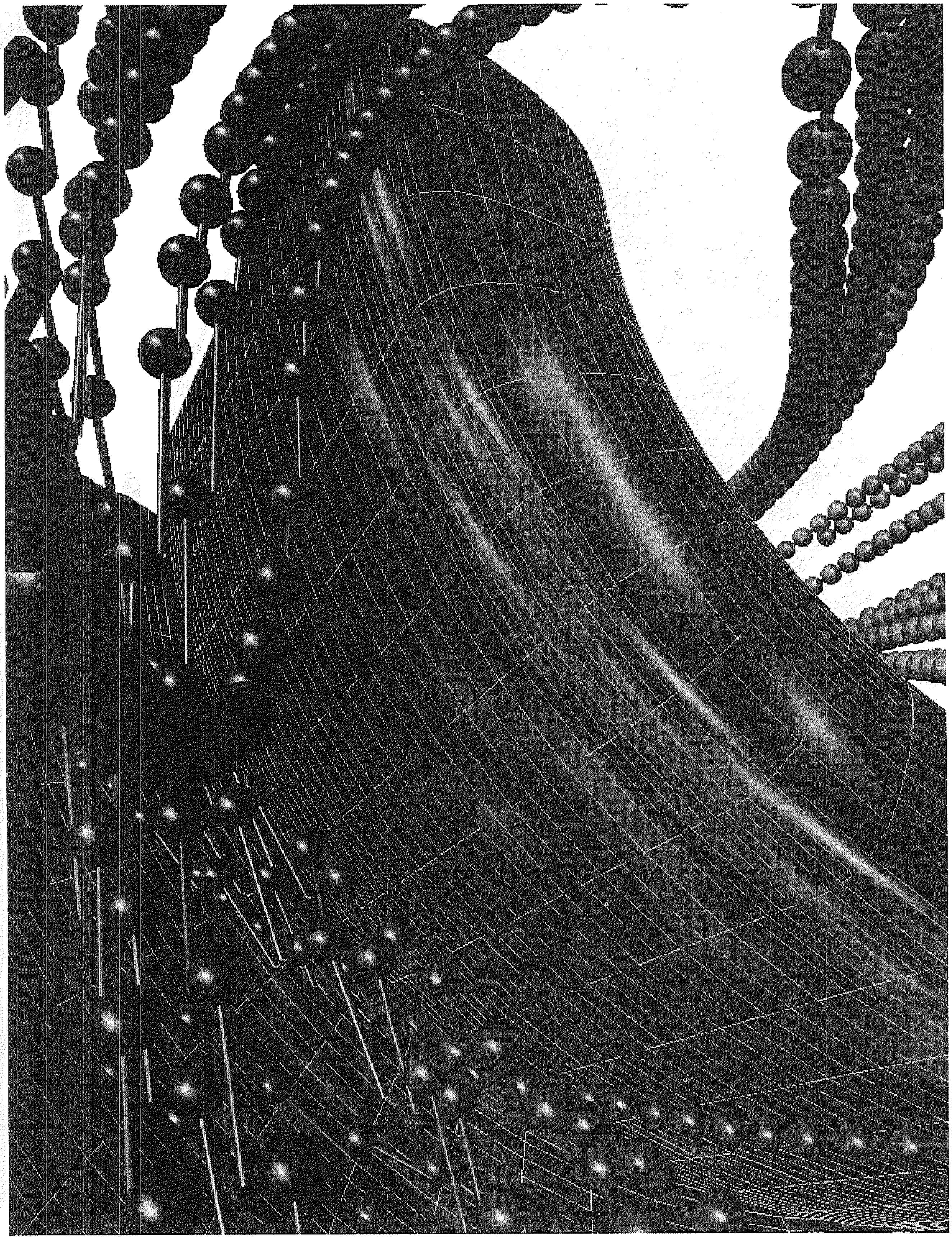

CONCLUSIONS AND RECOMMENDATIONS

- THE OBTAINED PRELIMINARY NUMERICAL RESULTS USING FDNS CODE SHOW THAT THE SLAG BEHAVIOR CAN BE PREDICTED NUMERICALLY. THE PREDICTED FLOW FIELD IS REASONABLE BASED ON THE PHYSICAL POINT OF VIEW.

- A DIRECT SIMULATION USING CHEMICAL REACTION, COMBUSTION/EVAPORATION/BREAKUP/AGGLOMERATION MODELS IS NECESSARY FOR A MORE ACCURATE NUMERICAL ANALYSIS OF SLAG BEHAVIOR.

Combustion Processes in Hybrid Rocket Engines

S. Venkateswaran and C. L. Merkle
Propulsion Engineering Research Center
The Department of Mechanical Engineering
The Pennsylvania State University
University Park, PA 16802.

S24-25
51399
132122
24p

In recent years, there has been a resurgence of interest in the development of hybrid rocket engines for advanced launch vehicle applications. Hybrid propulsion systems use a solid fuel such as hydroxyl-terminated polybutadiene (HTPB) along with a gaseous/liquid oxidizer. The perfomance of hybrid combustors depend on the convective and radiative heat fluxes to the fuel surface, the rate of pyrolysis in the solid-phase and the turbulent combustion processes in the gaseous-phase. These processes in combination specify the regression rates of the fuel surface and thereby the utilization efficiency of the fuel. In this paper, we employ computational fluid dynamic techniques in order to gain a quantitative understanding of the physical trends in hybrid rocket combustors.

The computational modeling is tailored to ongoing experiments at Penn State that employ a 2D slab-burner configuration. The co-ordinated computational/experimental effort enables model validation while providing an understanding of the experimental observations. Computations to date have included the full-length geometry with and without the aft-nozzle section as well as shorter-length domains for extensive parametric characterization. HTPB is used as the fuel with *1,3* butadiene being taken as the gaseous product of the pyrolysis. Pure gaseous oxygen is taken as the oxidizer. The fuel regression rate is specified using an Arrhenius rate reaction, while the fuel surface temperature is given by an energy balance involving gas-phase convection and radiation as well as thermal conduction in the solid-phase. For the gas-phase combustion, a two-step global reaction set is used. The standard $k - \epsilon$ model is used for turbulence closure. Radiation is presently treated using a simple diffusion approximation which is valid for large optical path lengths, representative of radiation from soot particles.

Computational results are obtained to determine the trends in the fuel burning or regression rates as a function of the head-end oxidizer mass flux, $G = \rho_e U_e$, and the chamber pressure. Furthermore, computations of the full slab-burner configuration have also been obtained for various stages of the burn. Comparisons with available experimental data from small-scale tests conducted by General Dynamics-Thiokol-Rocketdyne suggest reasonable agreement in the predicted regression rates. Future work will include: (1) a model for soot generation in the flame for more quantitative radiative transfer modeling, (2) parametric study of combustion efficiency and (3) transient calculations to help determine the possible mechanisms responsible for combustion instability in hybrid rocket motors.

Combustion Processes in Hybrid Rocket Engines

S. Venkateswaran and C. L. Merkle
Propulsion Engineering Research Center
The Pennsylvania State University
University Park, PA 16802

Presented at
The 13th Workshop for CFD Applications in
Rocket Propulsion, MSFC, April 25-27, 1995

Presentation Outline

- Introduction
  - Research Issues
  - Penn State Slab Burner Configuration
- Physical Modeling
  - Gas/Surface Coupling
  - Radiation
- Computational Results
  - Representative Solutions
  - Characterization of Regression Rates
- Conclusions

Introduction

- Advantages of Hybrid Propulsion
  - Reduced Cost
  - Safety
  - Improved Reliability
  - Thrust Tailoring
  - Environmentally Friendly
- Hybrids Development
  - Intermittent Testing Since 60's
  - JIRAD
  - AMROC
  - France & Japan
- Small-Scale Testing
  - JPL/Strand *et al.*
  - ONERA
  - UAH
  - Penn State

Research Issues

- Characterization of Fuel Surface Regression
  - — Fuel Pyrolysis and Surface Chemistry
  - — Heat Fluxes - Convection and Radiation
- Combustion Efficiency
- Combustion Instability
- Modeling Issue:
  - — Boundary Layer vs. Navier-Stokes

Schematic of Hybrid Rocket Motor

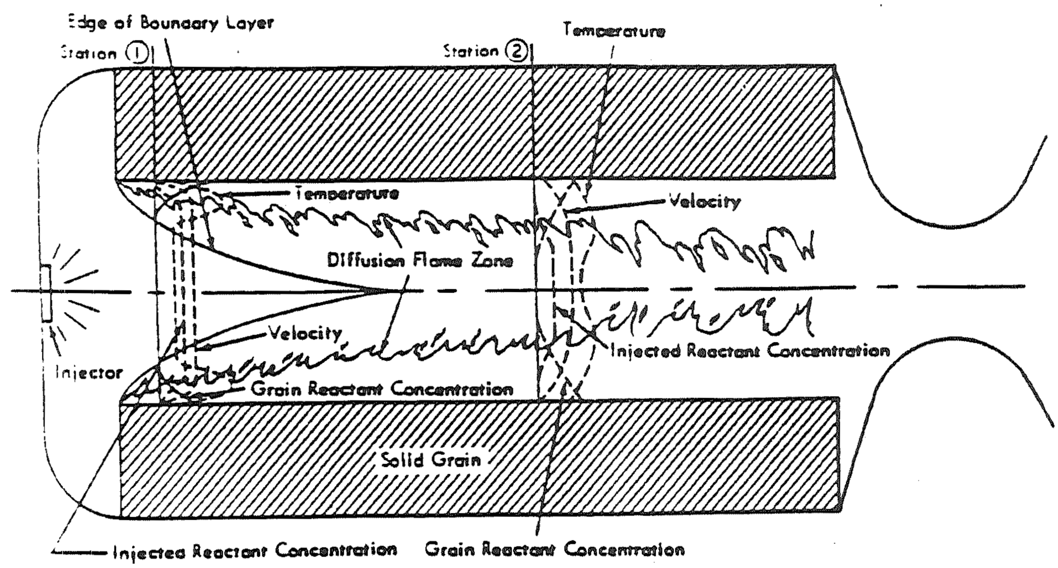

Experimental Configuration

Top View

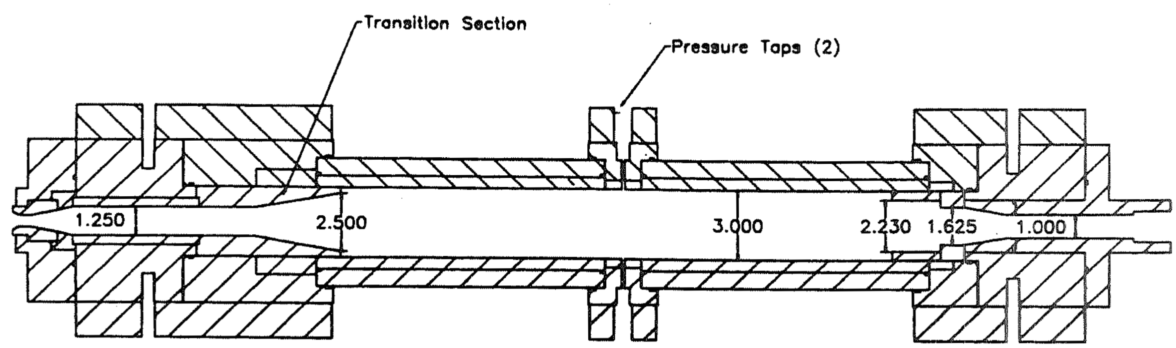

Profile View

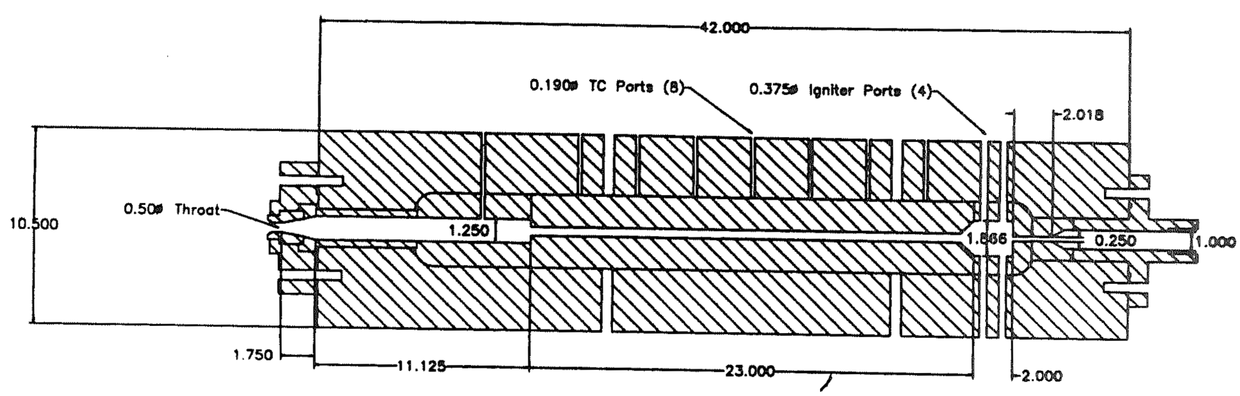

Experimental Configuration

- Test Conditions
  - Fuel - HTPB
  - Oxidizer - GOX
  - Pressures - 300 to 900 psi
  - GOX Flow Rates - 0.2 to 0.8 lbm/s
  - GOX Mass Flux $(G = \rho U)$ - ~~0.05~~ 0.1 to 0.5 $lbm/in^2 - s$

Physical Modeling

- Gas-Phase Navier-Stokes Equations
  — Standard $k-\epsilon$ Model
- Gas-Phase/Combustion Model:
  — Butadiene—Product of Pyrolysis
  — Two-Step Global Kinetics Model

$$C_4H_6 + 3.5O_2 \longrightarrow 4CO + 3H_2O$$

$$CO + 0.5O_2 \longleftrightarrow CO_2$$

- Solid-Phase/Pyrolysis:
  — Arrhenius Pyrolysis Rate

$$\rho_s r_b = A_s exp\left(\frac{-E_s}{R_u T_s}\right)$$

Solid/Gas Coupling

- Surface Mass Balance

$$\rho v = - \ \rho_s r_b$$

- Surface Energy Balance

$$-\lambda \frac{\partial T}{\partial y} \ + \ Q_{rad} \ + \ \rho v h \ - \ \sum_{i=1}^{N} \rho \mathcal{D}_{im} \frac{\partial Y_i}{\partial y} h_i \ = \ -\lambda_s \left(\frac{\partial T}{\partial y} \right)_s \ - \ \rho_s r_b h_s$$

Radiation Modeling

- Gaseous Molecular Radiation
  — Optically Thin Approximation

$$Q_{rad,k} = \sum_{i,j} \frac{4\sigma k_{i,j} T_{i,j}^4}{J_{i.j}} \mathcal{F}_{i,j\to k}$$

- Particulate (Soot) Radiation
  — Optically Thick Approximation

$$Q_{rad,k} = -\lambda_R \frac{\partial T}{\partial y}$$

where $\lambda_R = \frac{4}{3}\pi \frac{C}{k} T^3$

Representative Solution

Grid Geometry

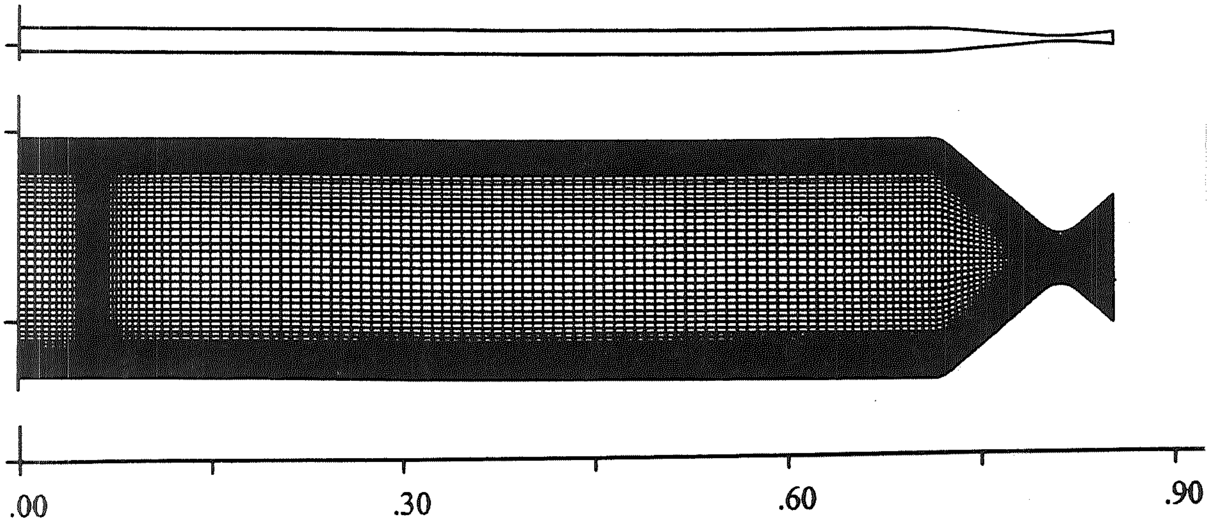

Temperature Contours

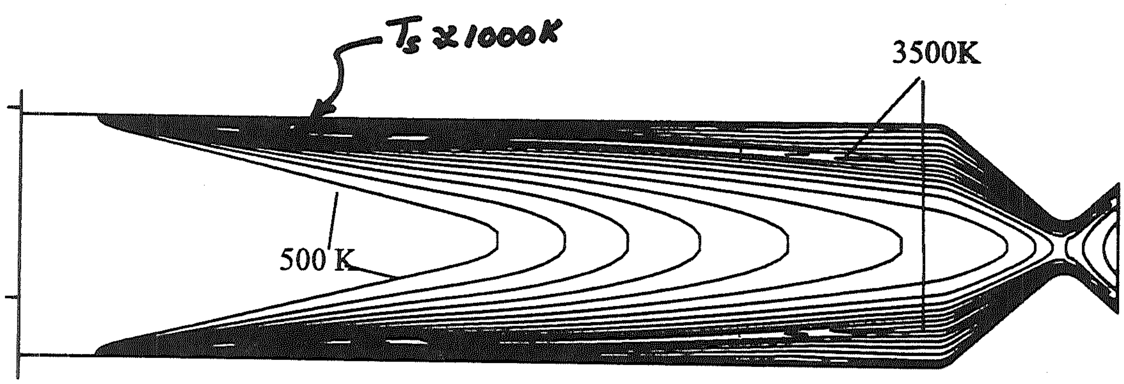

Representative Solution

Axial Velocity

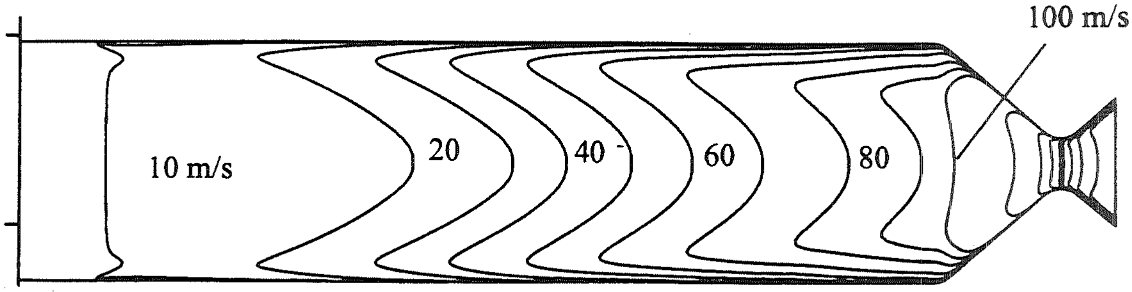

Mach Number Contours

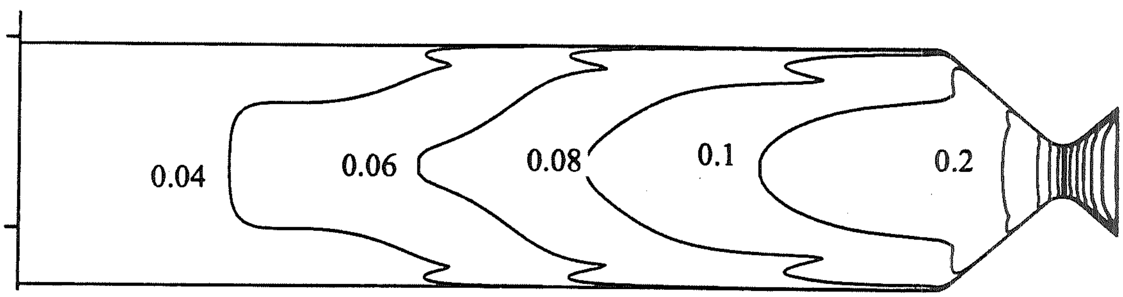

Representative Solutions

Carbon Dioxide Mass Fraction

GOX Mass Fraction

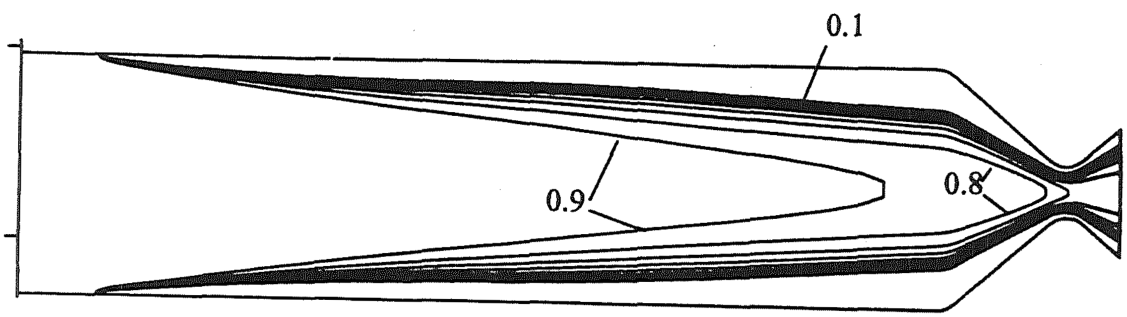

Representative Results

Centerline Variation of Mass Flux (G)

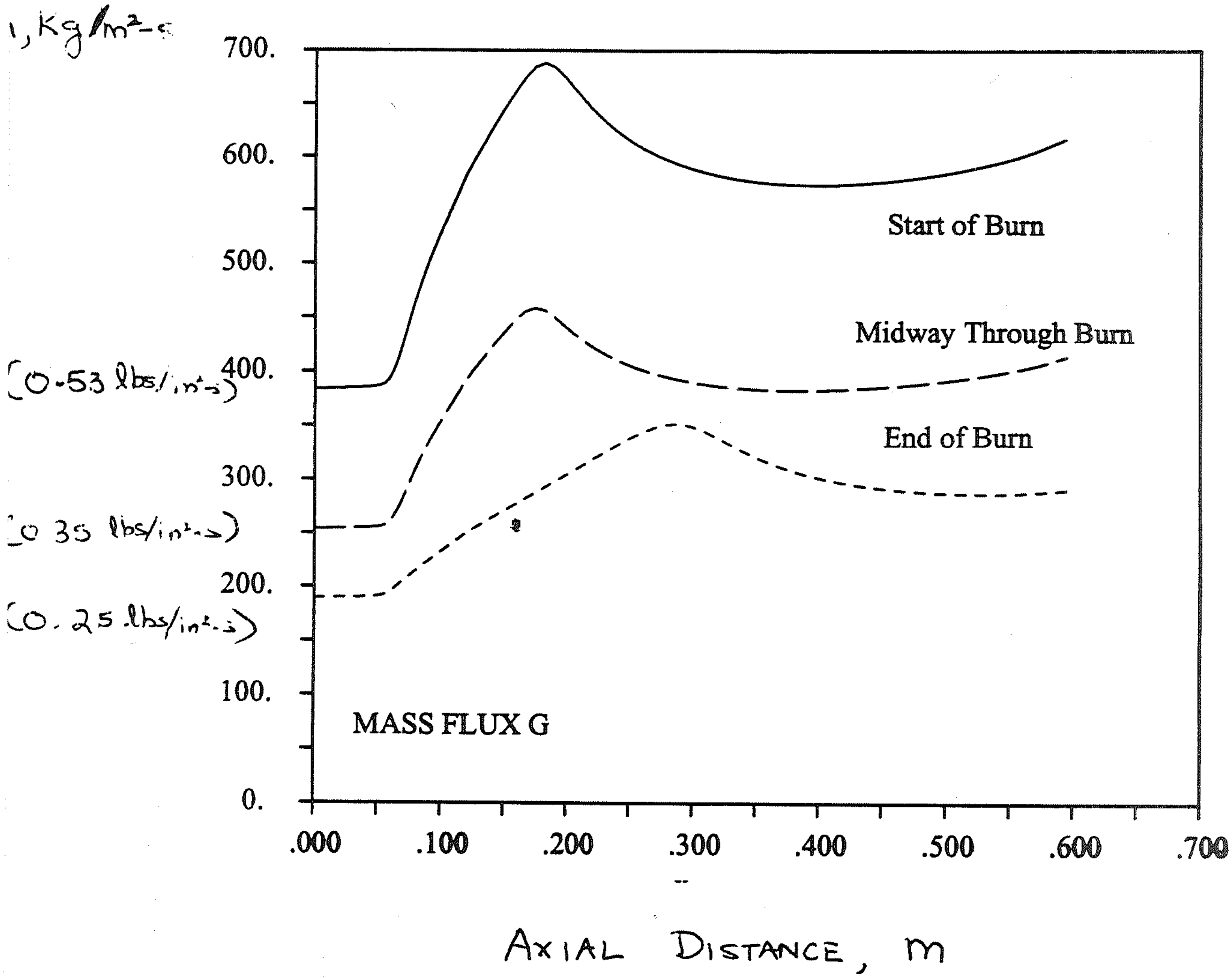

Representative Results

Surface Regression Rate

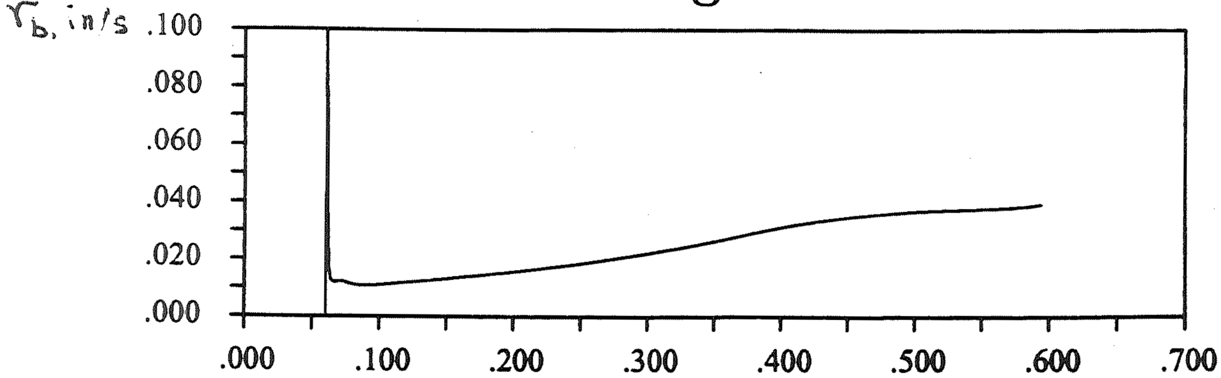

Fuel Surface Temperature

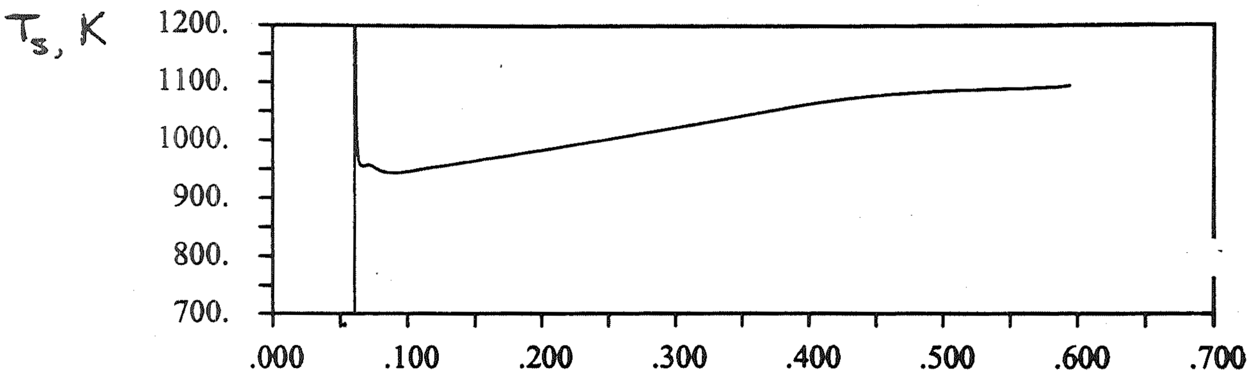

Wall Heat Fluxes

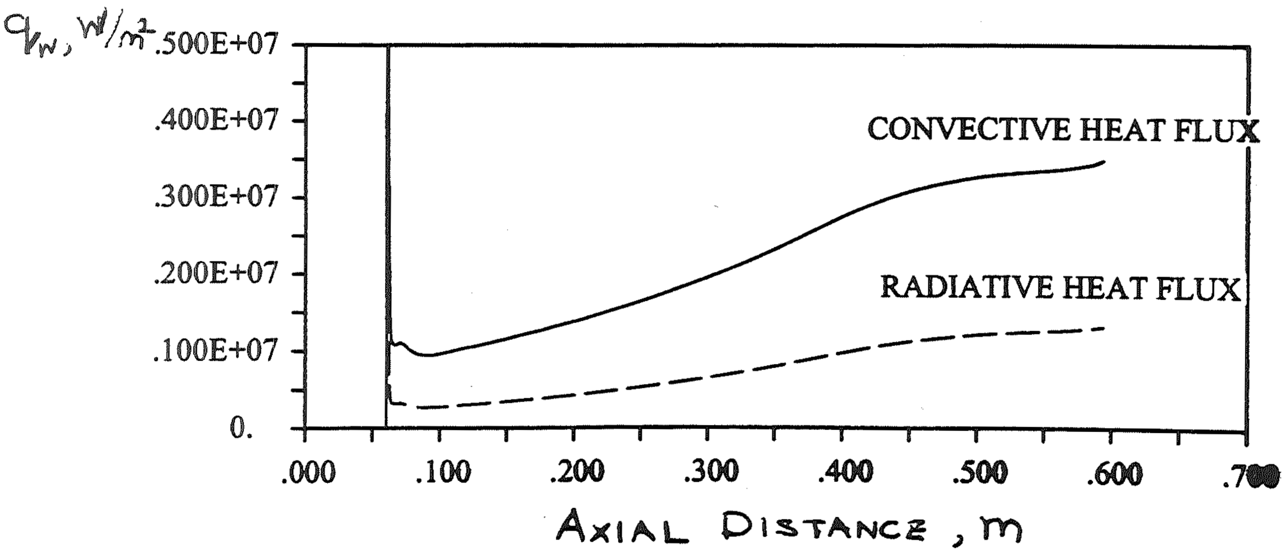

Parametric Studies
Different Stages in Burn

Start of Burn

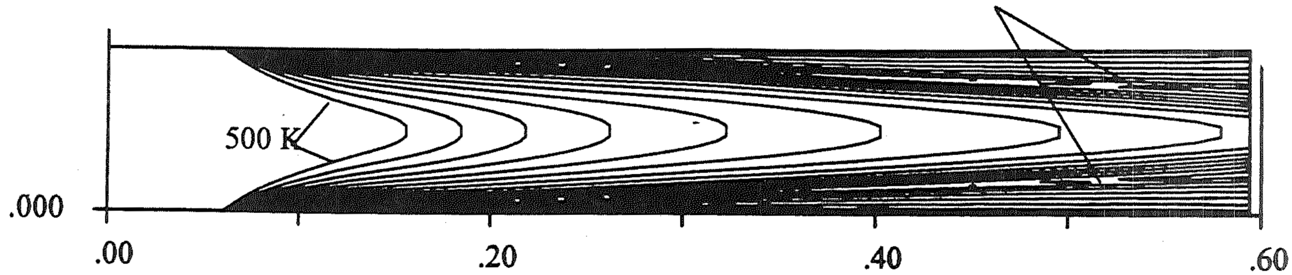

Midway Through Burn

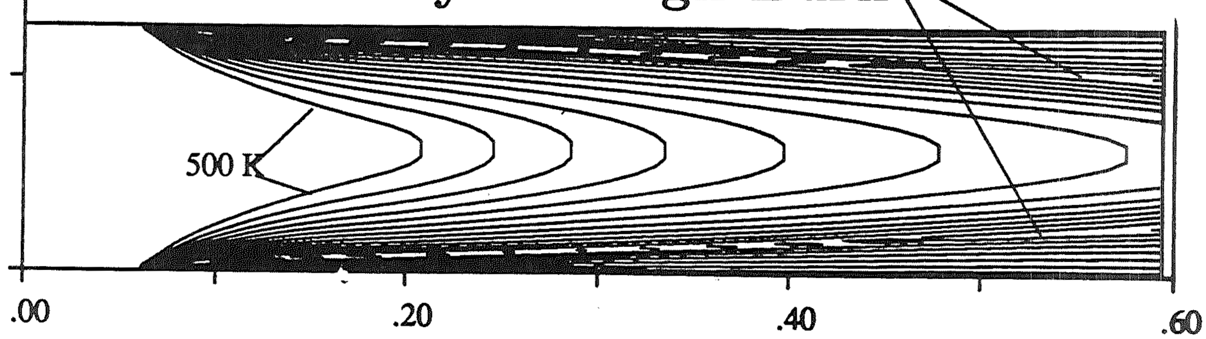

End of Burn

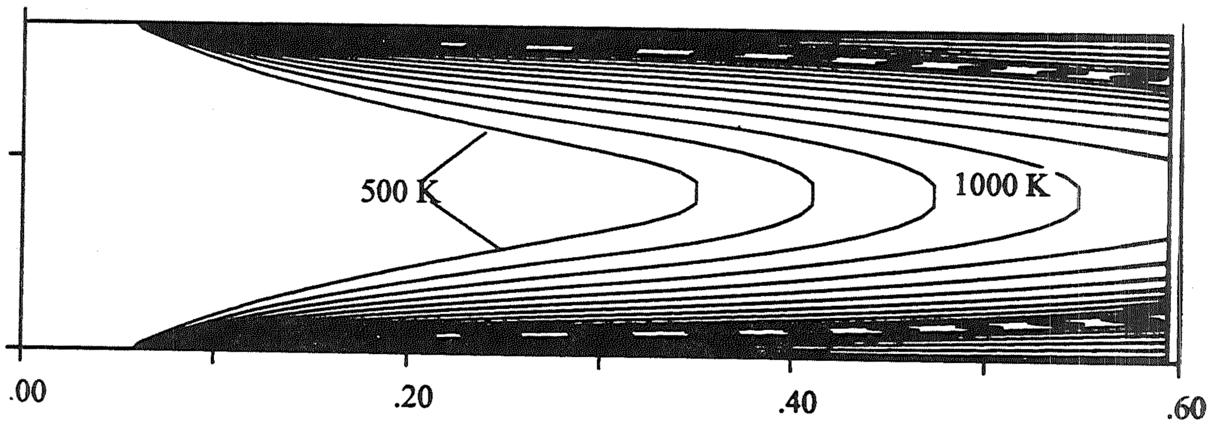

Parametric Studies
Different Stages in Burn

W/O Radiation

Surface Regression Rate

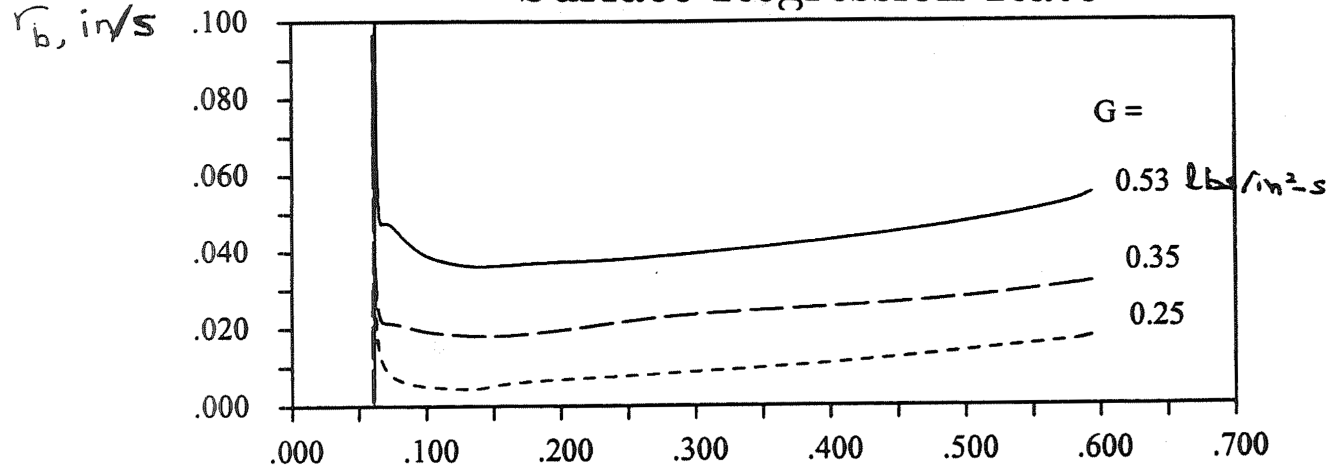

Convective Wall Heat Fluxes

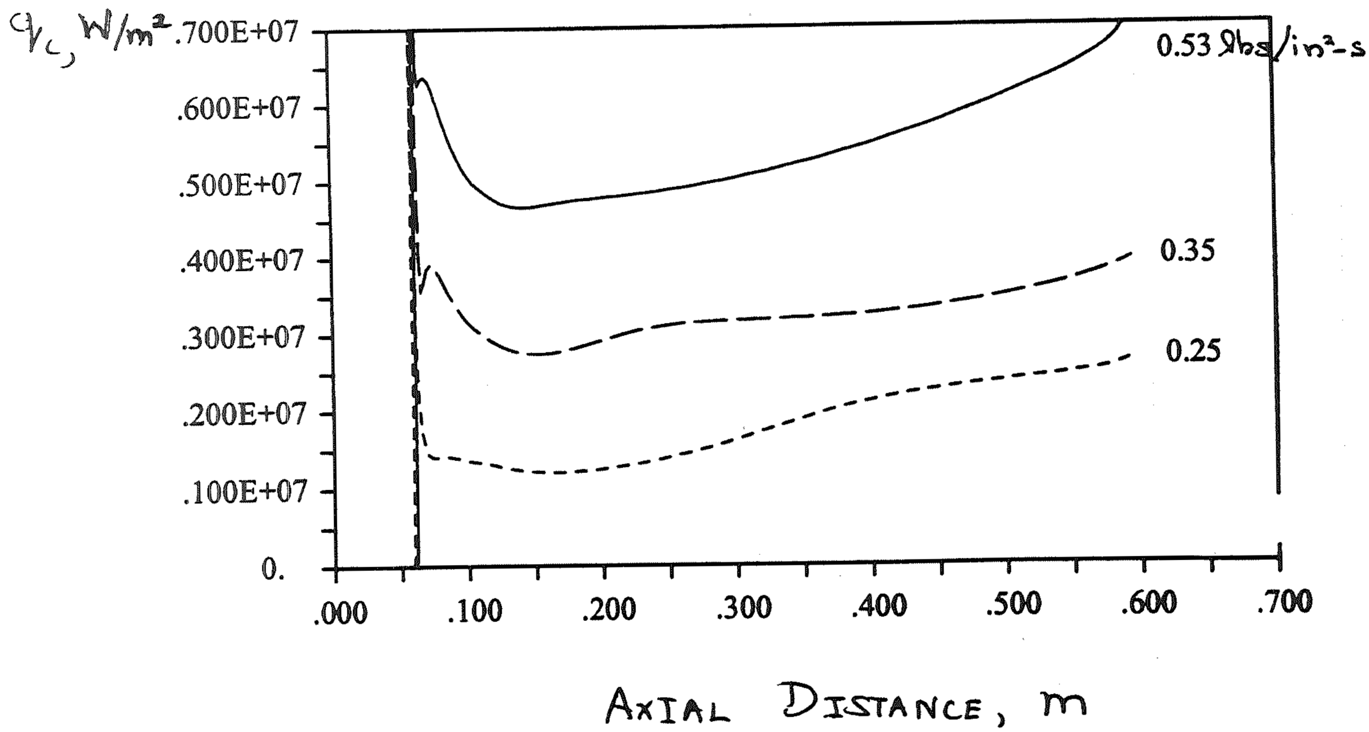

Parametric Studies
Different Stages in Burn

With Radiation/Optically Thick

Surface Regression Rate

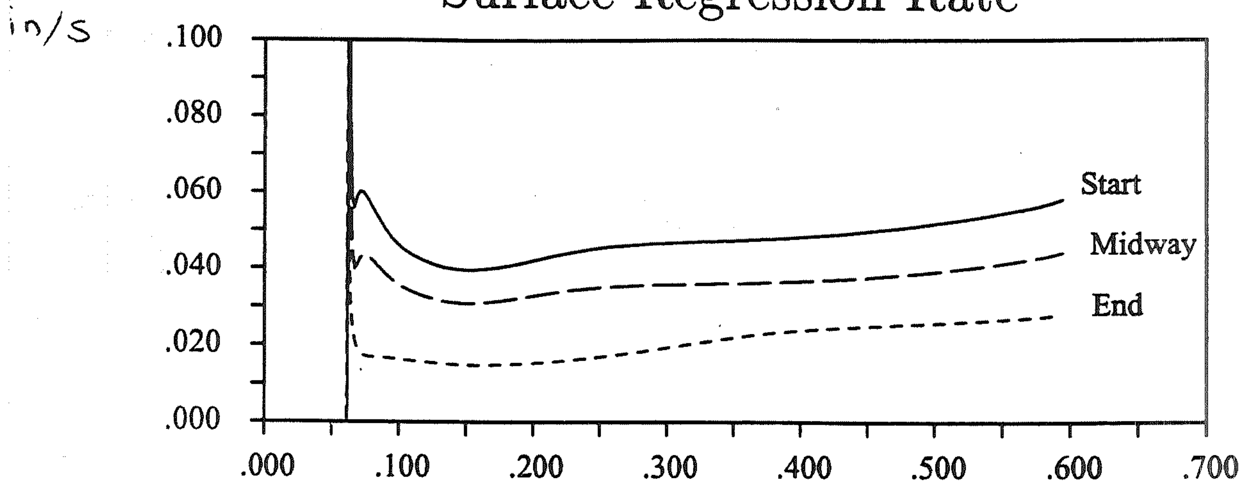

Radiative Wall Heat Fluxes

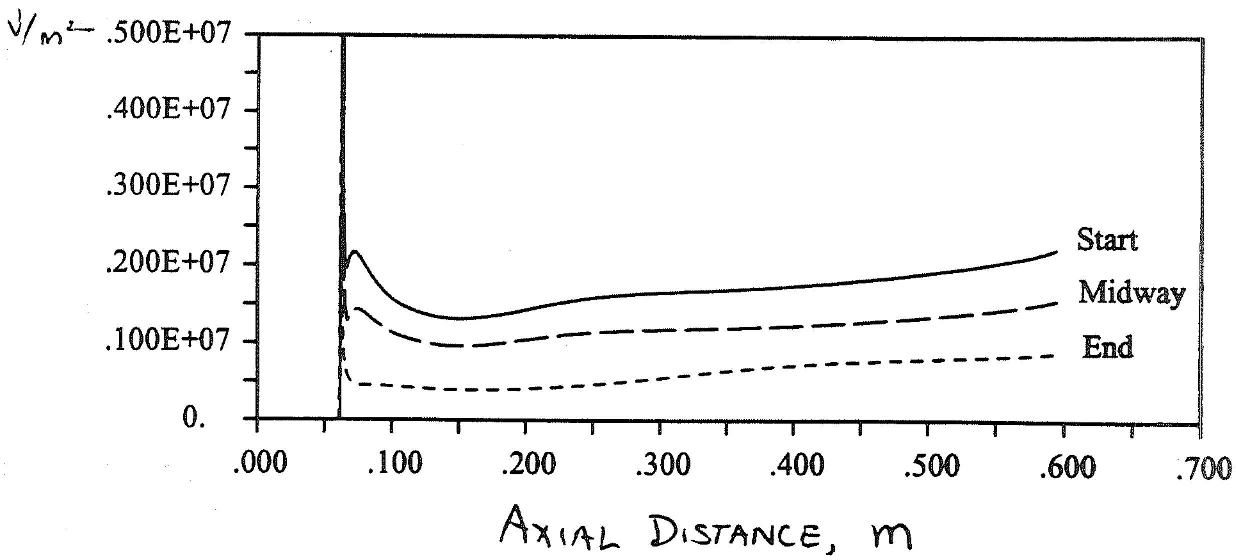

Parametric Studies
Effect of GOX Flow Rate

Temperature Contours

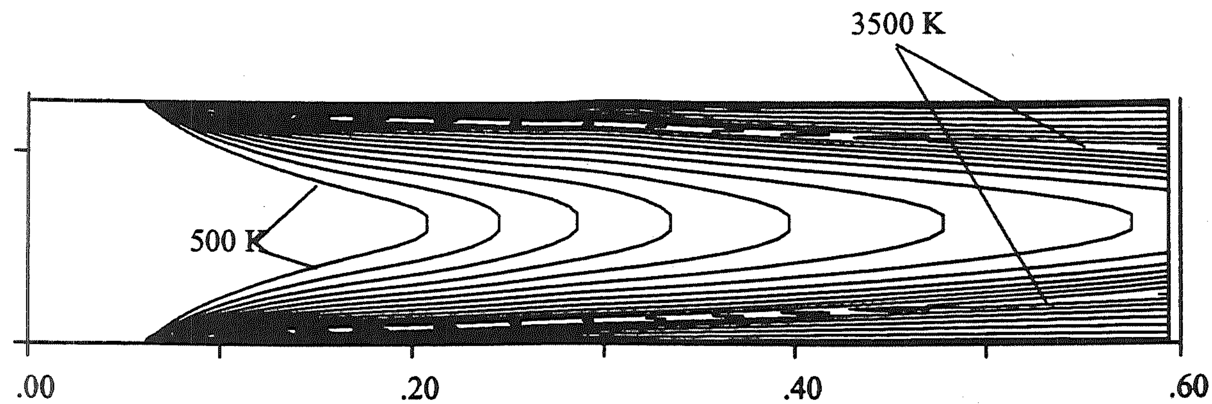

Temperature Profiles

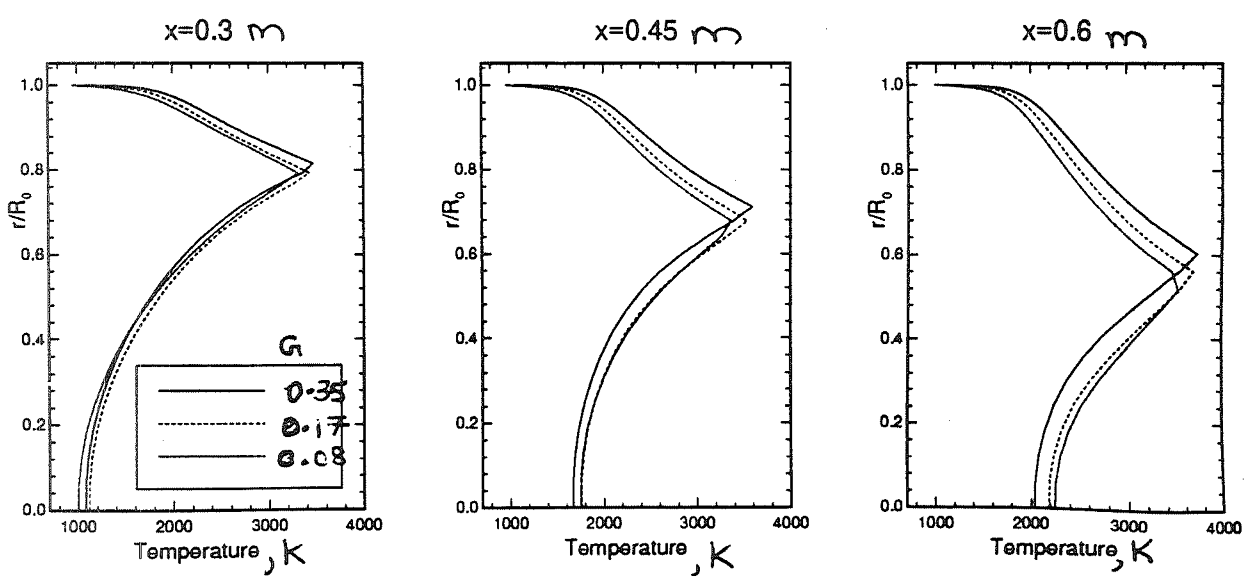

Parametric Studies
Effect of GOX Flow Rate

W/O Radiation

Surface Regression Rate

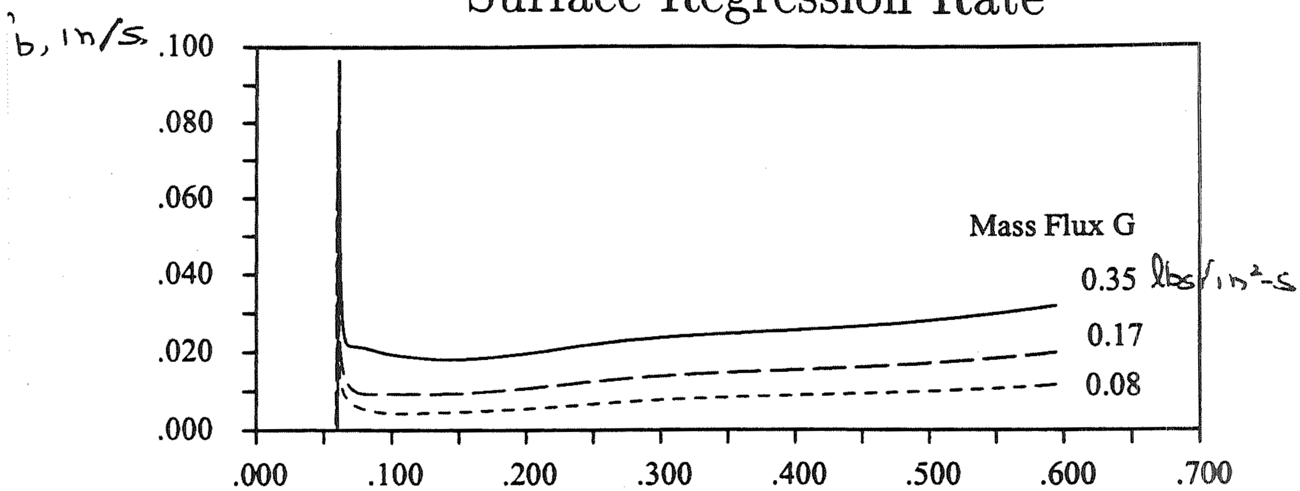

Convective Wall Heat Fluxes

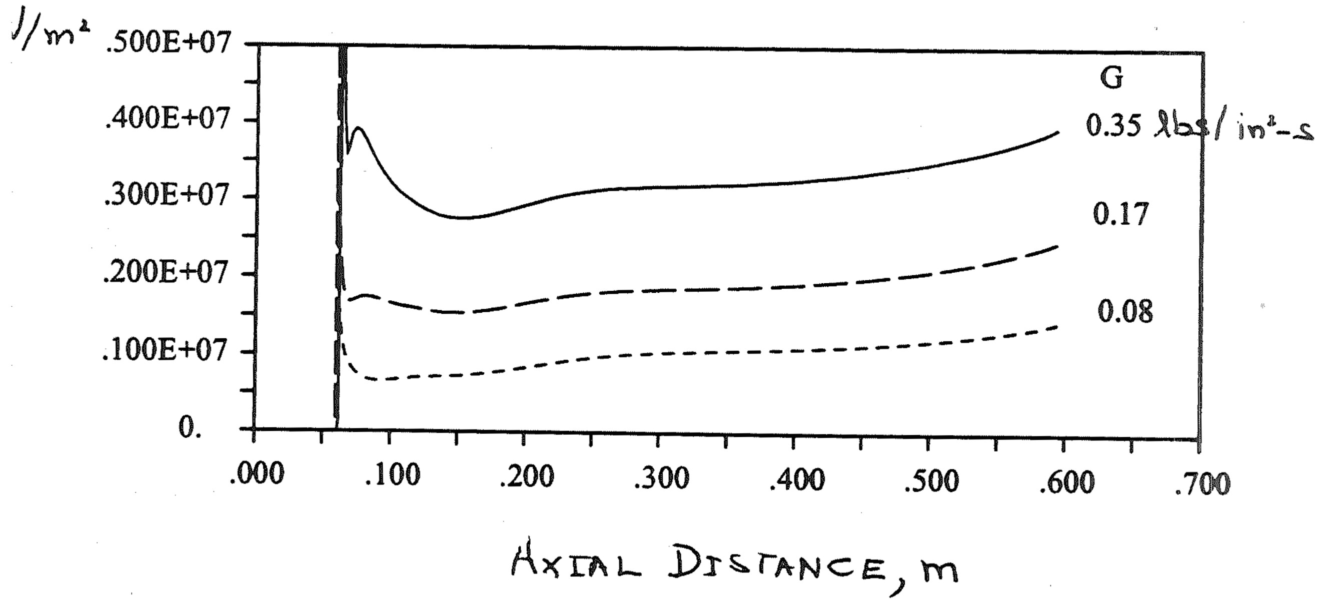

Parametric Studies
Effect of GOX Flow Rate

With Radiation/Optically Thick

Surface Regression Rate

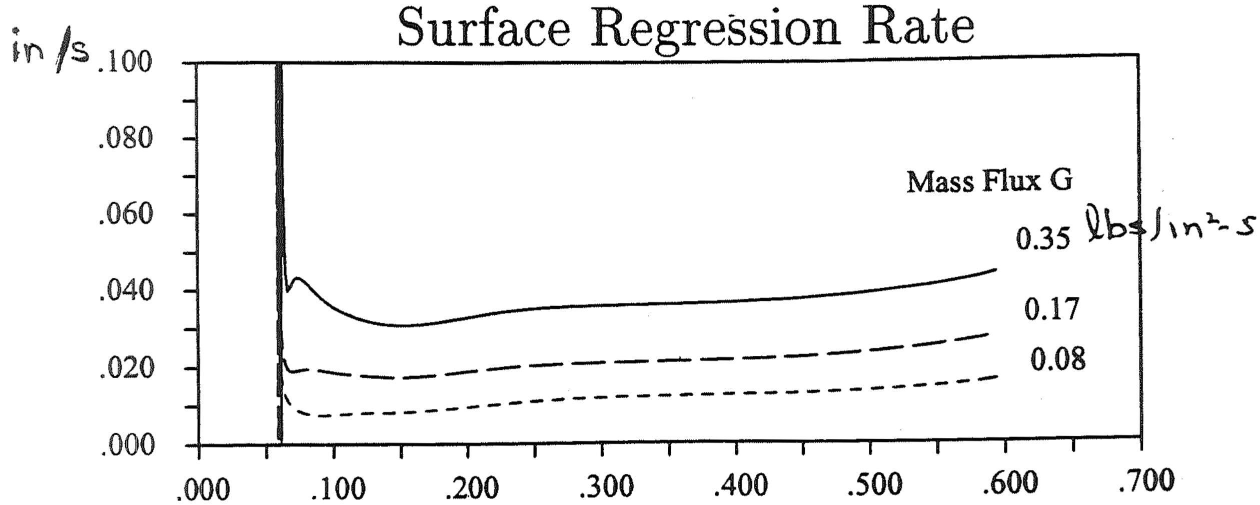

Radiative Wall Heat Fluxes

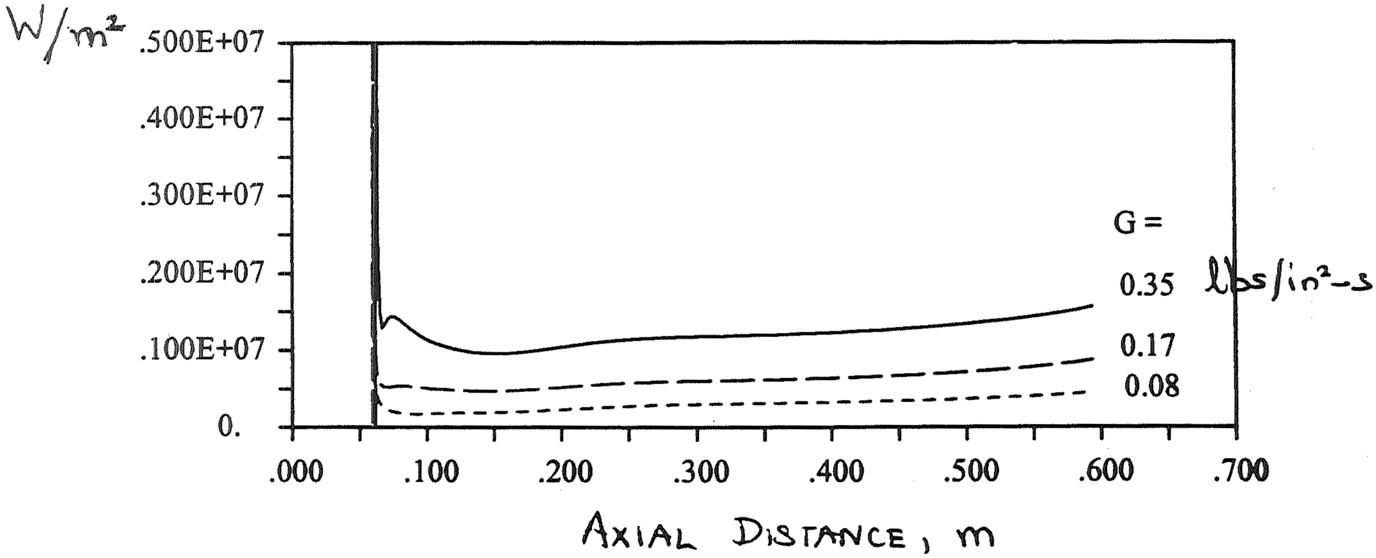

Parametric Characterization of Fuel Surface Regression

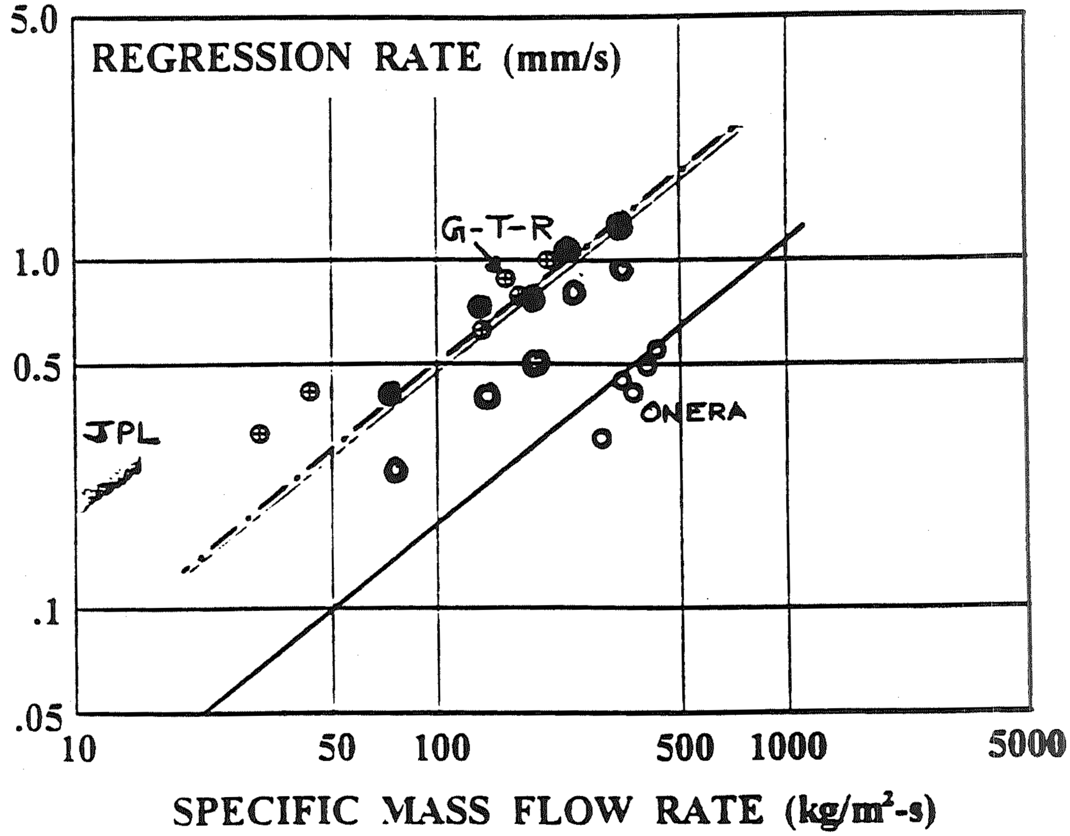

● Current Results With Radiation

○ Current Results W/O Radiation

Conclusions

- Navier-Stokes Analysis of Hybrid Motor
  - Planar Slab Burner Configuration
  - Arrhenius-Rate for Pyrolysis
  - Global Chemistry
  - Turbulence Model
  - 'Thick/Thin' Radiation Model
- Computational Results
  - Parametric Characterization
  - Fuel Surface Temperatures 900 to 1100 K
  - Regression Rates of 0.01 to 0.07 in/s
  - Radiative Fluxes - Significant Contribution
- Ongoing/Future Work:
  - Radiation Properties - Soot Concentration
  - Combustion Efficiency - Downstream Mixing
  - Combustion Instability - Transient Calculations

CFD ANALYSIS OF THE 24-INCH JIRAD HYBRID ROCKET MOTOR

Pak-Yan Liang, Ronald Ungewitter, Scott Claflin
CFD Technology Center
Rocketdyne Division, Rockwell International
Mail Code IB39, 6633 Canoga Avenue
Canoga Park, CA 91303

S25-34
51400
132123 16p

ABSTRACT

A series of multispecies, multiphase CFD analyses of the 24-inch diameter joint government/industry IR&D (JIRAD) hybrid rocket motor is described. The 24-inch JIRAD hybrid motor operates by injection of liquid oxygen (LOX) into a vaporization plenum chamber upstream of ports in the hydroxyl-terminated polybutadiene (HTPB) solid fuel. Injector spray pattern had a strong influence on combustion stability of the JIRAD motor so a CFD study was initiated to define the injector-end flow field under different oxidizer spray patterns and operating conditions. By using CFD to gain a clear picture of the flow field and temperature distribution within the JIRAD motor, it is hoped that the fundamental mechanisms of hybrid combustion instability may be identified and then suppressed by simple alterations to the oxidizer injection parameters such as injection angle and velocity.

The simulations in this study were carried out using the GALACSY (General ALgorithm for Analysis of Combustion SYstems) multiphase combustion codes. GALACSY consists of a comprehensive set of droplet dynamic submodels (atomization, evaporation, etc.) and a computationally efficient hydrocarbon chemistry package built around a robust Navier-Stokes solver optimized for low Mach number flows. Lagrangian tracking of dispersed particles describes a closely coupled spray phase.

The CFD cases described in this paper represent various levels of simplification of the problem. They include: (A) gaseous oxygen with noncombusting fuel vapor blowing off the walls at various oxidizer injection angles and velocities, (B) gaseous oxygen with combusting fuel vapor blowing off the walls, and (C) liquid oxygen with combusting fuel vapor blowing off the walls. The study used an axisymmetric model and the results indicate that the injector design significantly effects the flow field in the injector-end of the motor. Markedly different recirculation patterns are observed in the vaporization chamber as oxygen velocity and/or spray pattern is varied. The ability of these recirculation patterns to stabilize the diffusion flame above the surface of the solid fuel gives a plausible explanation for the experimentally determined combustion stability characteristics of the JIRAD motor, and suggests how combustion stability can be assured by modifications to the injector design. ~~Planned future activities to the submodels which allow for additional degree of realism will be discussed.~~ with The

CFD ANALYSIS OF 24 INCH JIRD HYBRID ROCKET MOTOR

Dr. Pak Liang , Ronald Ungewitter, Scott Claflin

Rocketdyne Div./ Rockwell International

Rockwell Aerospace

OVERVIEW

- ISSUE: SIGNIFICANT INCREASES IN PRESSURE OSCILLATION RECORDED DURING TESTING OF ANGLED AND STRAIGHT LOX INJECTORS

STRAIGHT

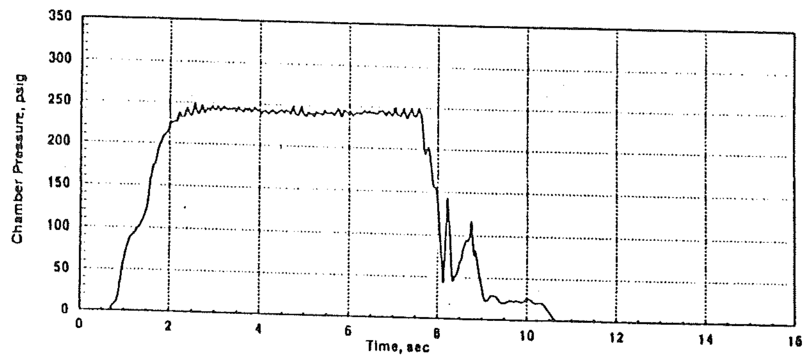

ANGLED

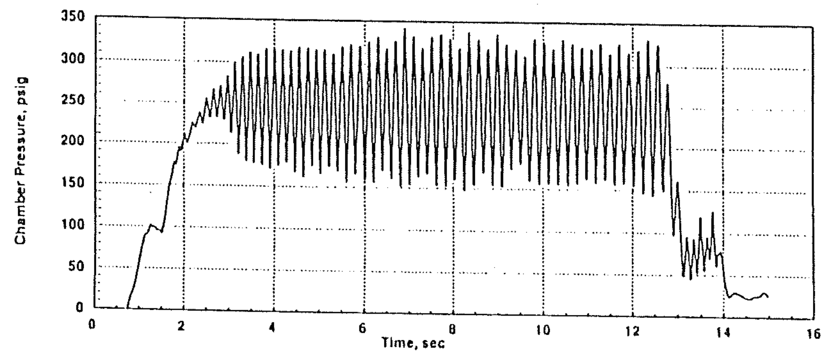

- GOAL: TO GAIN AN UNDERSTANDING OF THE PHYSICAL MECHANISMS OF HYBRID ROCKET MOTOR COMBUSTION AND THE CONDITIONS LEADING TO COMBUSTION OSCILLATIONS

HYBRID ROCKET MOTOR

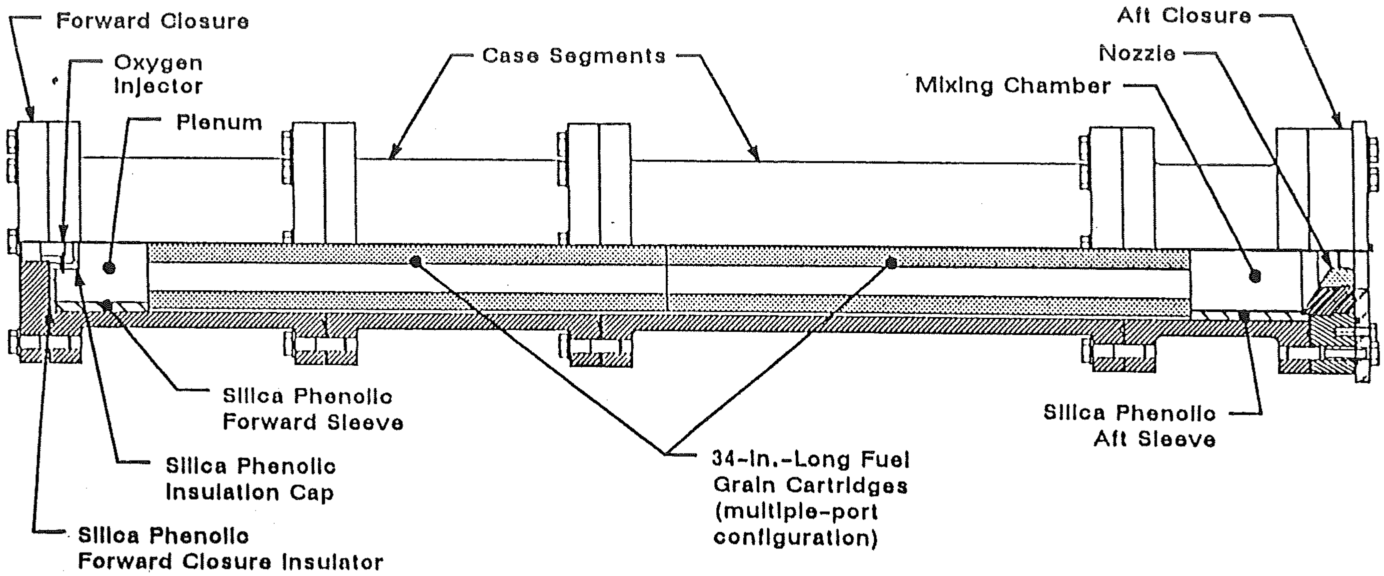

- LIQUID / GAS OXIDIZER INJECTED INTO VAPORIZATION CHAMBER
- SOLID FUEL SUBLIMATES WHICH THEN REACTS WITH OXIDIZER
- INJECTOR-END RECIRCULATION PATTERN DEEMED CRITICAL TO COMBUSTION STABILITY AND FLAME HOLDING MECHANISMS

Rockwell Aerospace
Rocketdyne

PLAN

APPROACH:

- USE GALACSY CFD COMBUSTION CODE FOR CFD ANALYSIS
- CONDUCT SERIES OF ANALYSES AT SEVERAL LEVELS OF SOPHISTICATION TO IDENTIFY BASIC FLUID DYNAMIC MECHANISMS

• MODEL

- TWO ZONE, AXISYMMETRIC (STEPS 1,2, & 3)
- WALL BLOWING FUEL REPRESENTING SUBLIMATION PROCESS
- O2/RP-1 CHEMISTRY

• PLAN:

- STEP 1 - THREE NON REACTING GOX FLOW CALCULATIONS WITH DIFFERENT INLET CONDITIONS (COMPLETED)
- STEP 2 - ANGLED AND STRAIGHT REACTING GOX CASES (COMPLETED)
- STEP 3 - LOX STREAM REPRESENTED AS FULLY ATOMIZED DROPS; STRAIGHT AND ANGLED FLOW (IN PROGRESS)
- STEP 4 - MULTI-PORT COMBUSTOR, STRAIGHT AND ANGLED FLOW

Rockwell Aerospace
Rocketdyne

CFD Technology Center

CFD-95-016-004/D1/RJU

GALACSY CODE

- PRESSURE-BASED, EXTENDED SIMPLE-S SEQUENTIAL SOLVER METHODOLOGY (REACT PLATFORM)
- LAGRANGIAN DROPLET TRACKING, "ONION SKIN" EVAPORATION MODEL
- EXPLICIT INTER-ZONAL COUPLING FOR MULTIZONE PROBLEMS
- GLOBAL FINITE RATE REACTION FOR HYDROCARBON FUEL PLUS H/O EQUILIBRIUM CHEMISTRY (VALIDATED FOR CH4)
    - RP1 (REPRESENTED AS $C_{12.449}H_{24.47}$) CHEMISTRY REQUIRES 10 SPECIES

Rockwell Aerospace
Rocketdyne

STEP 1 – NON REACTING RESULTS

CASE 1 RESULTS*

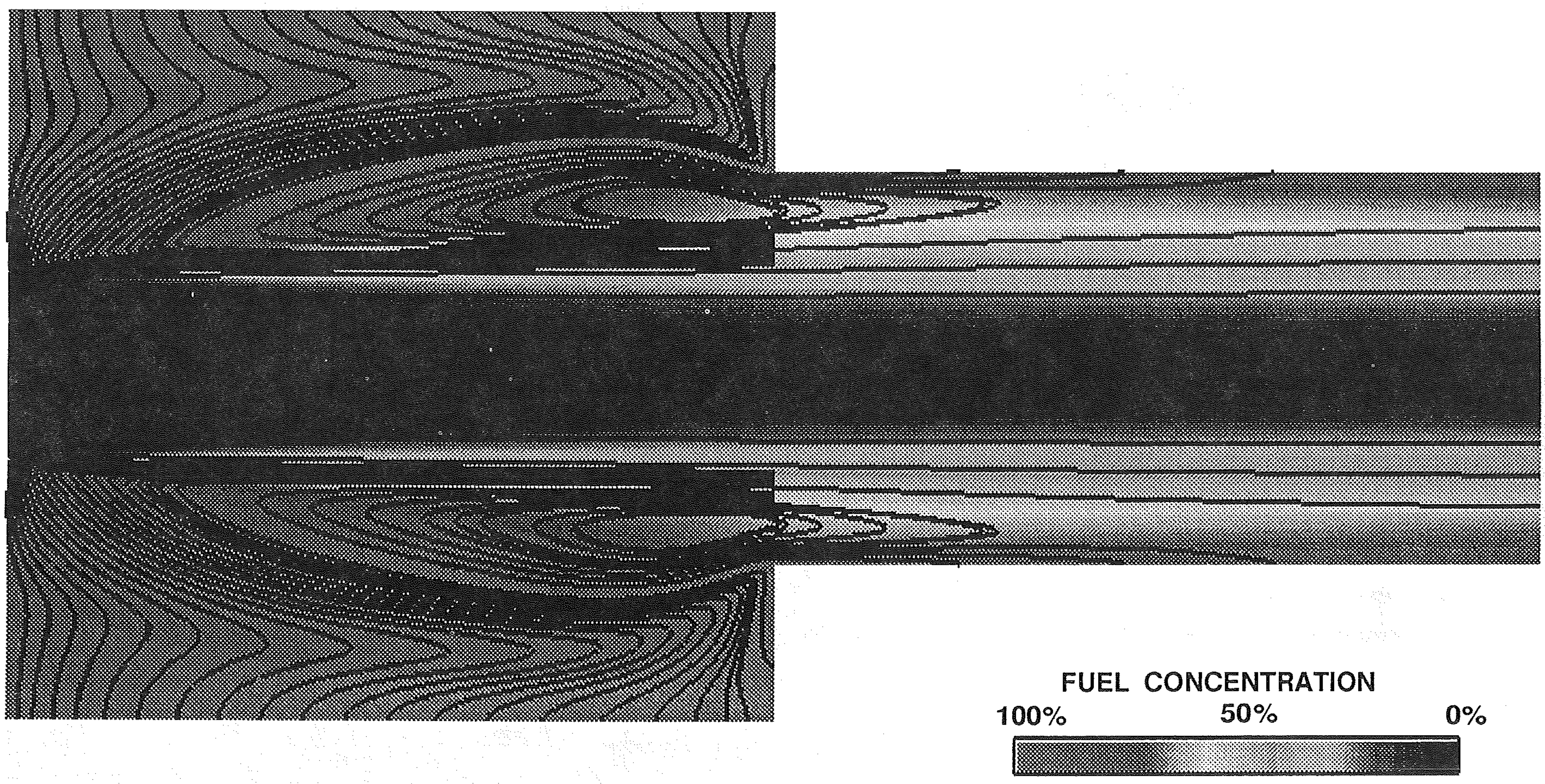

CONDITIONS: TWO ZONE: 90x40, 100x16

GOX, Tin=293^{O} K, Uin=47 m/s

* IMAGE TRUNCATES COMPUTATIONAL DOMAIN AND PARTICLE TRACES DO NOT MOVE BETWEEN ZONES

STEP 1 – NON REACTING RESULTS

CASE 2 RESULTS*

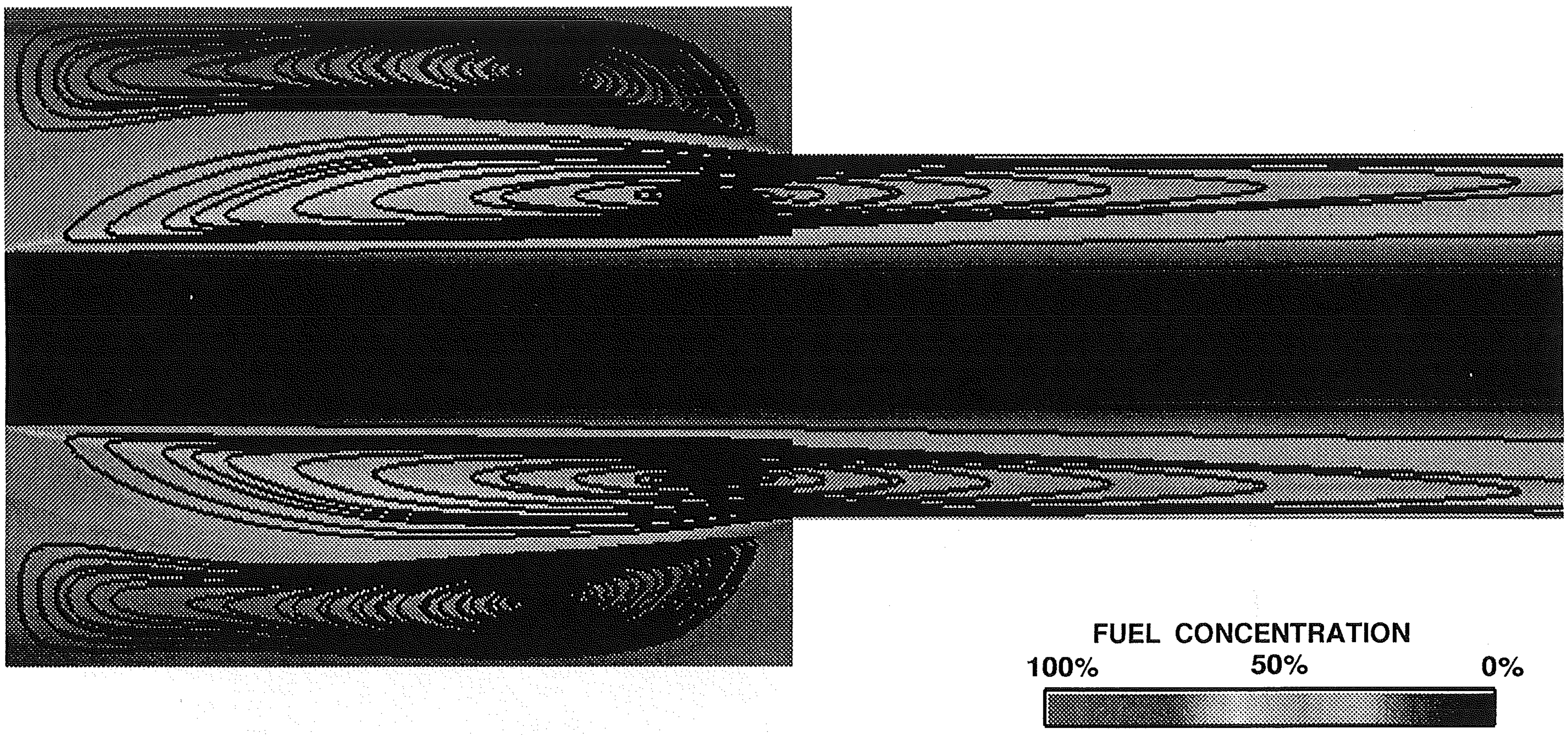

CONDITIONS: TWO ZONE: 90x40, 100x16

GOX, Tin=811^{O} K, Uin=132 m/s

* IMAGE TRUNCATES COMPUTATIONAL DOMAIN AND PARTICLE TRACES DO NOT MOVE BETWEEN

STEP 1 - NON REACTING RESULTS

CASE 3 RESULTS*

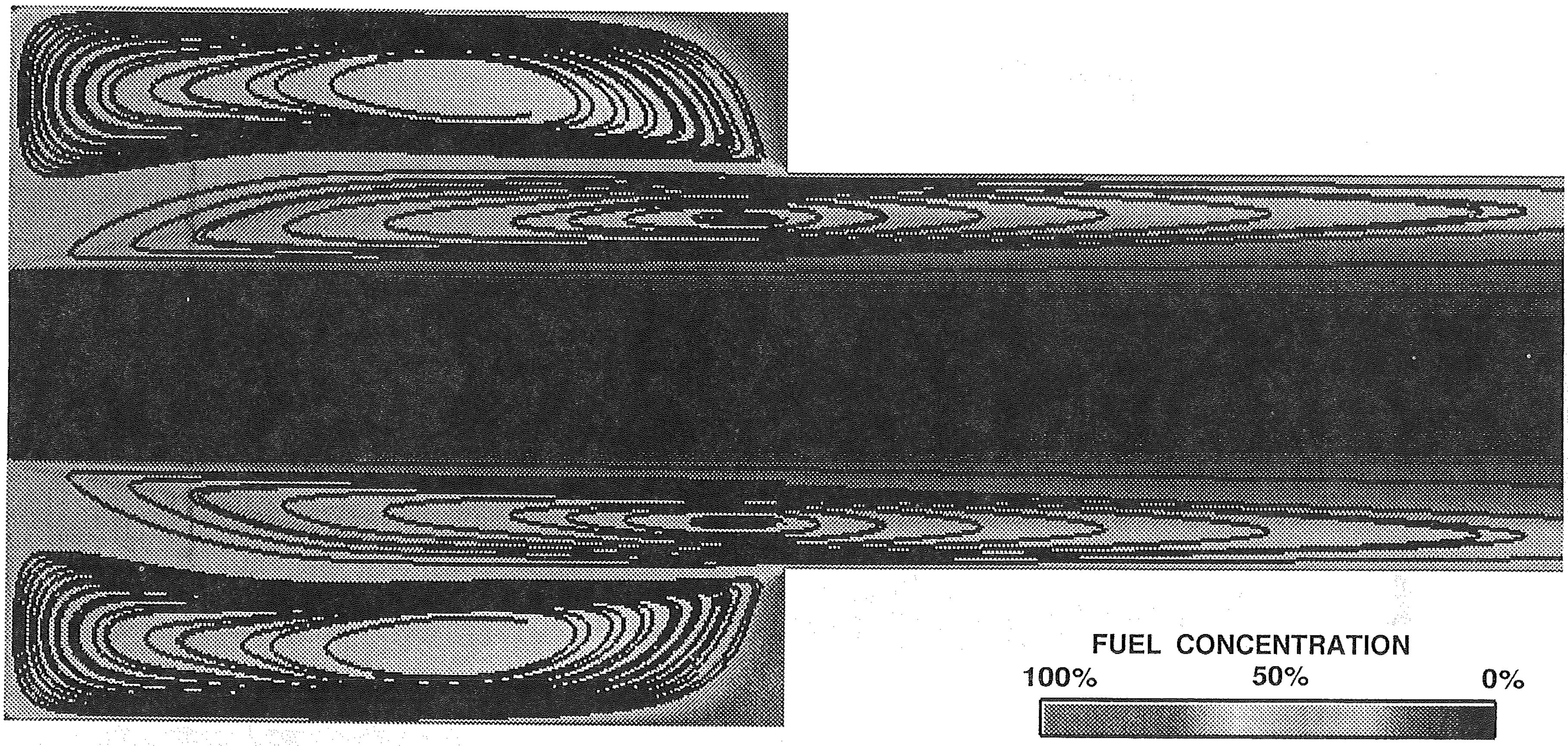

CONDITIONS: TWO ZONE: 90x40, 100x16

GOX, Tin=1810^{O} K, Uin=296 m/s

* IMAGE TRUNCATES COMPUTATIONAL DOMAIN AND PARTICLE TRACES DO NOT MOVE BETWEEN ZONES

STEP 2 - REACTING RESULTS

CASE 1 STRAIGHT FLOW*

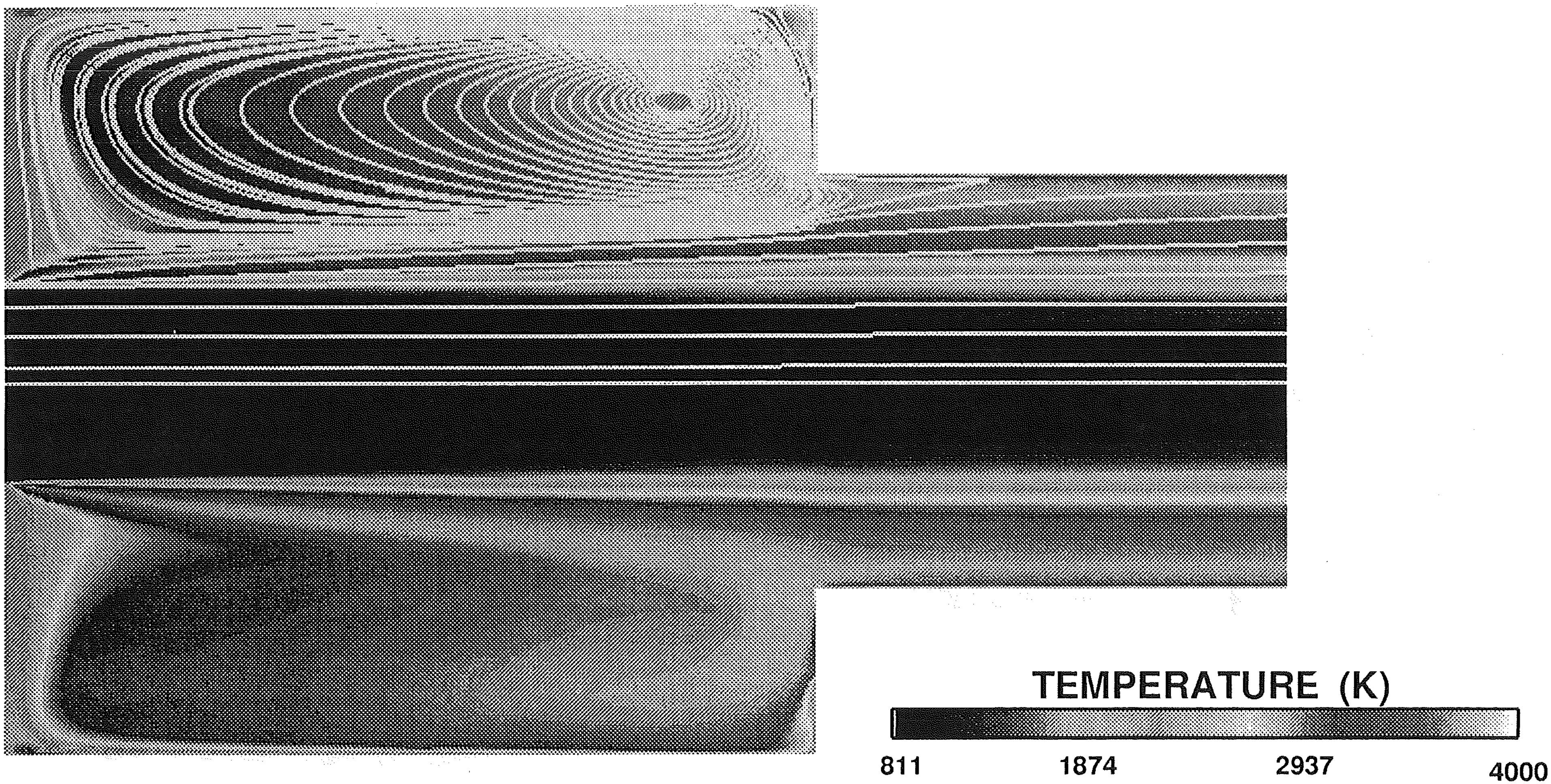

CONDITIONS: TWO ZONE: 90x40, 100x16

GOX, Tin=811^{O} K, Uin=132 m/s

* IMAGE TRUNCATES COMPUTATIONAL DOMAIN AND PARTICLE TRACES DO NOT MOVE BETWEEN

STEP 2 - REACTING RESULTS

CASE 2 ANGLED FLOW*

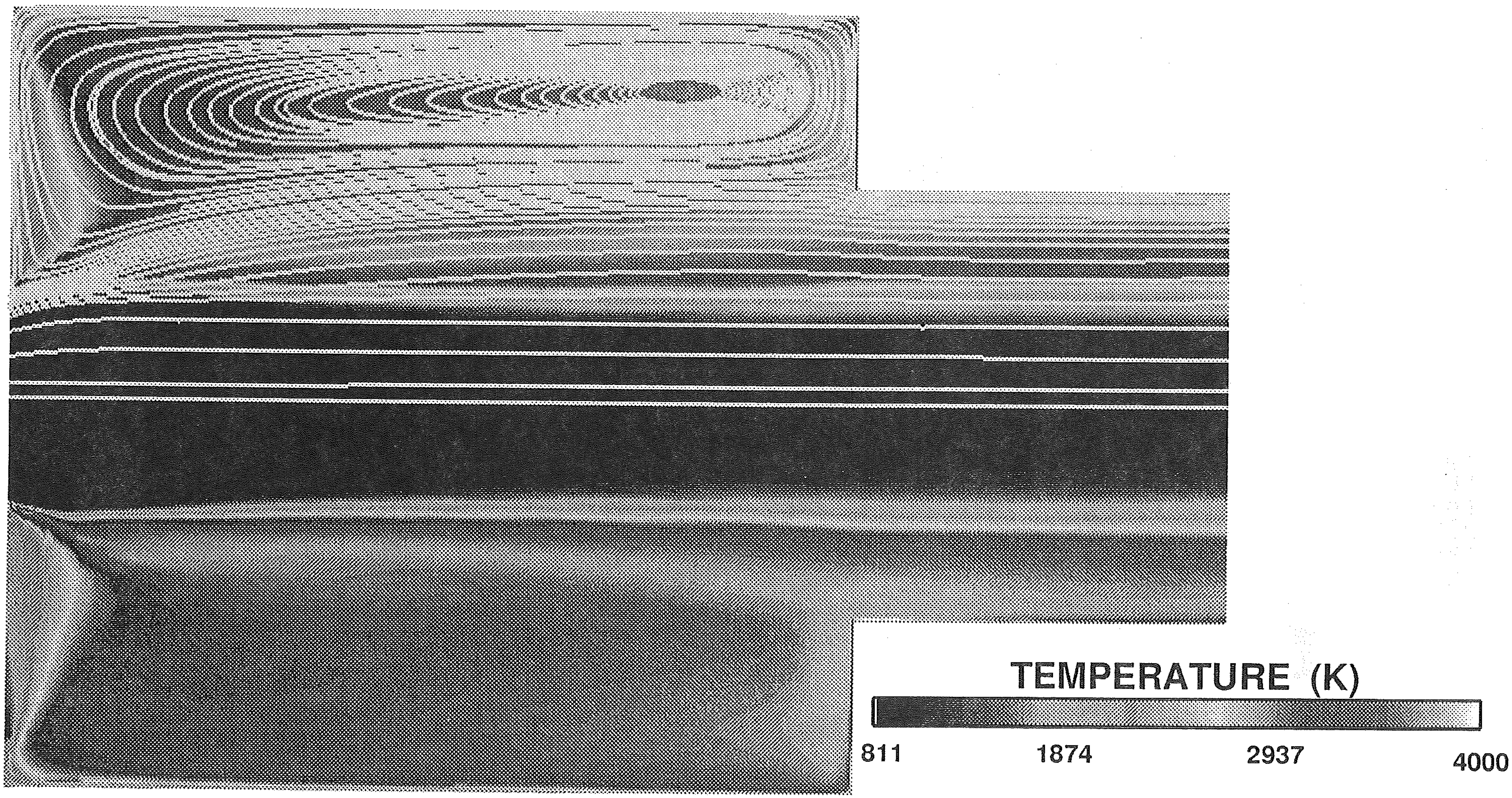

CONDITIONS: TWO ZONE: 90x40, 100x16

GOX, Tin=811^{o} K, Uin=132 m/s

* IMAGE TRUNCATES COMPUTATIONAL DOMAIN AND PARTICLE TRACES DO NOT MOVE BETWEEN ZONES

CONCLUSIONS

- **COMPLETED CASES CONSISTENT WITH SINGLE POINT TEST DATA**
- **RECIRCULATION PATTERN CAN CHANGE COMPLETELY DUE TO DIFFERENCES IN INJECTOR PATTERN**
- **CHEMISTRY PACKAGE NEED ADDITIONAL VALIDATION**
- **NEW CALCULATIONS (STEP 3) INDICATE PERFORMANCE DECREASE OF NUMERICAL SCHEME DUE TO DROPLET COUPLING AND INTERZONAL BOUNDARIES**
  - NEED ALGORITHMIC REFINEMENT TO INCREASE PERFORMANCE
  - POSSIBLE OPTION: REASSEMBLY OF MULTIZONE MATRICES BACK INTO SINGLE ZONE MATRIX BEFORE CALLING MATRIX SOLVER

Rockwell Aerospace
Rocketdyne

☆U.S. GOVERNMENT PRINTING OFFICE—1996—733-109/40024

REPORT DOCUMENTATION PAGE

Form Approved
OMB No. 0704-0188

1. AGENCY USE ONLY (Leave Blank)	2. REPORT DATE	3. REPORT TYPE AND DATES COVERED
	March 1996	Conference Publication

4. TITLE AND SUBTITLE

Thirteenth Workshop for Computational Fluid Dynamic Applications in Rocket Propulsion and Launch Vehicle Technology

5. FUNDING NUMBERS

6. AUTHOR(S)

R.W. Williams, Compiler

7. PERFORMING ORGANIZATION NAME(S) AND ADDRESS(ES)

George C. Marshall Space Flight Center
Marshall Space Flight Center, Alabama 35812

8. PERFORMING ORGANIZATON REPORT NUMBERS

9. SPONSORING/MONITORING AGENCY NAME(S) AND ADDRESS(ES)

National Aeronautics and Space Administration
Washington, DC 20546-0001

10. SPONSORING/MONITORING AGENCY REPORT NUMBER

NASA CP-3332
Volume II

11. SUPPLEMENTARY NOTES

Prepared by Structures and Dynamics Laboratory, Science and Engineering Directorate.

12a. DISTRIBUTION/AVAILABILITY STATEMENT

Unclassified-Unlimited
Subject Category 34

12b. DISTRIBUTION CODE

13. ABSTRACT *(Maximum 200 words)*

This conference publication includes various abstracts and presentations given at the 13th Workshop for Computational Fluid Dynamic Applications in Rocket Propulsion and Launch Vehicle Technology held at the George C. Marshall Space Flight Center April 25-27 1995. The purpose of the workshop was to discuss experimental and computational fluid dynamic activities in rocket propulsion and launch vehicles. The workshop was an open meeting for government, industry, and academia. A broad number of topics were discussed including computational fluid dynamic methodology, liquid and solid rocket propulsion, turbomachinery, combustion, heat transfer, and grid generation.

14. SUBJECT TERMS computational fluid dynamics, rocket propulsion, launch vehicle technology, liquid rocket, solid rocket, turbopump, turbomachinery, combustion, methodology, impeller, inducer, heat transfer, grid generation, nozzle, plume spray, injector

15. NUMBER OF PAGES 668

16. PRICE CODE A99

17. SECURITY CLASSIFICATION	18. SECURITY CLASSIFICATION OF THIS PAGE	19. SECURITY CLASSIFICATION OF ABSTRACT	20. LIMITATION OF ABSTRACT
Unclassified	Unclassified	Unclassified	Unlimited

NSN 7540 - 01 - 280 - 5500

Mac-Computer Generated

Standard Form 298 (Rev 2-89)
Prescribed by ANSI Std. 239-18

National Aeronautics and
Space Administration
Code JTT
Washington, DC
20546–0001

Official Business
Penalty for Private Use, $300

Postmaster: If Undeliverable (Section 158 Postal Manual), Do Not Return